Age-related performance of typical seal binders in South Africa

by

Francois Engelbrecht

Thesis presented in fulfilment of the requirements for the degree of Master of Engineering in Civil Engineering in the Faculty of Engineering at Stellenbosch University

Supervisor: Professor Kim Jenkins PrEng

SANRAL Chair in Pavement Engineering

Department of Civil Engineering

Co-supervisor: Mister Steph Bredenhann PrEng

Project Manager

SANRAL: Western Region

March 2018

Declaration

By submitting this thesis electronically, I declare that the entirety of the work contained therein is my own, original work, that I am the sole author thereof (save to the extent explicitly otherwise stated), that reproduction and publication thereof by Stellenbosch University will not infringe any third party rights and that I have not previously in its entirety or in part submitted it for obtaining any qualification.

March 2018

Summary

'*Learning never exhausts the mind.*'-Leonardo da Vinci

The age-related performance of typical seal binders in South Africa was studied to understand the behaviour of the binders as it ages.

The three main failure mechanisms for surfacing seals include surface cracking, ravelling and texture loss. These mechanisms shorten the life of the pavement exponentially. Various factors may be the cause of these failures. This study includes the analyses of the rate at which oxidation influences the performance of surfacing seals.

Rheology was used to analyse the age-related performance of the selected seal binders. Low and high temperature testing was conducted in the laboratory at various ages such as RTFO and PAV (20hr, 40hr and 80hr) which includes short-term ageing and long-term ageing of a binder. Several ageing parameters were used to analyse the results of each seal binder.

The South African Performance Grade Specification and the AASHTO M320 specification are established to set the required performance of asphalt binders. These specifications were used to compare the performance of surfacing seal binders to asphalt binders.

Results showed that ageing influences the modification within surfacing seal binders. It appears that the performance of the elastic component in the modifier decreases as the binders age. The low temperature results show that the difference between the unmodified and modified binders are minimal. The high temperature results indicate that the highly modified binders perform well considering the influence of ageing.

Opsomming

Die ouderdomsverwante gedrag van verskeie seël bindmiddels in Suid-Afrika is gebestudeer om die gedrag van die bindmiddels te evalueer soos wat die seëls verouder.

Die drie hoof faling meganismes van seëls sluit in oppervlak kraking, rafeling en tekstuur verlies (Gerber, 2016). Hierdie meganismes verkort die lewe van die pad eksponensieël. Verskeie faktore mag die oorsaak wees van hierdie falings. Hierdie studie behels die ontleding van die tempo waarteen oksidasie die gedrag van die seels beinvloed.

Reologie was gebruik om die ouderdomsverwante gedrag van die seël bindmiddels te analiseer. Lae en hoë temperatuur toetse was gedoen in ‘n laboratorium teen verskeie ouderdomme, soos ‘RTFO’ en ‘PAV’ (20ure, 40ure en 80ure) wat korttermynveroudering en langtermynveroudering van 'n bindmiddel insluit. Verskeie ouderdomsparamters was gebruik om die gedrag van die seël bindmiddels te analiseer.

Die Suid-Afrikaanse Prestasiegraadspesifikasie asook die ‘AASHTO M320’-spesifikasie is gestig om die gedragsvereistes van asfalt bindmiddels vas te stel. Hierdie spesifikasies was gebruik om die gedrag van seël bindmiddels te vergelyk met asfalt bindmiddels.

Die resultate het getoon dat veroudering wel ‘n invloed het op seël bindmiddels. Dit blyk dat die gedrag van die elastiese komponent in die modifiseerder afneem namate die bindmiddels verouder. Die lae temperatuur resultate toon dat die verskil tussen die ongemodifiseerde en gemodifiseerde bindmiddels minimaal is. Die hoë temperatuur resultate dui daarop dat die hoogs gemodifiseerde binders goed presteer met inagneming van die invloed van veroudering.

Acknowledgements

I would like to thank Professor KJ Jenkins and Mr S Bredenhann for acting as a study leader and mentor during my research.

I would also like to thank Dr J Gerber, Dr G Rowe and Mr G van Zyl for sharing their knowledge and experience with me.

I would like to acknowledge the laboratory managers i.e. Mr R Briedenhann, Mr C Brooks and Mr M Labuschagne for ensuring everything went well in the laboratories. Thanks to Stellenbosch University, Much Asphalt and Colas for the availability of the laboratories and equipment.

I am grateful for all the post graduate students for keeping me motivated and for the great atmosphere in die office.

I am thankful for my family and friends for their motivation and assistance.

Special thanks to the South African National Roads Agency for financing my studies.

Above all, I would like to thank God for standing by my side through the studies.

Contents

List of Tables

List of Figures

Chapter 1: Introduction

'Improvement makes strait roads: but the crooked roads without Improvement are roads of Genius' - William Blake

1.1 Background

The South African National Roads Agency (SANRAL) is currently busy with rheological research for the performance grading system of bitumen binders for both seals and asphalt. The Civil Engineering department of Stellenbosch University has a few master students, which fulfil each part of the required research that has to be done. This document entails research regarding the age-related performance of typical seal binders in South Africa.

Surfacing seals are used in South Africa for the resealing of existing bituminous pavements as well as for new constructed roads. Seals are used widely due to the fact that it is more cost effective and very effective on highways, rural roads and urban roads for light to heavy traffic loads (TRH 3, 2007).

Bituminous roads are known for their susceptibility to environmental factors such as the weather, which cannot be controlled. The physical properties of bituminous binders such as the viscosity, strain, stress and ageing are factors to consider to analyse in order to get the required performance in particular environments (Hunter, Self, & Read, 2015).

The physical properties of bituminous binders are known as the rheology of the binder. Rheology is defined as the science of the deformation and flow characteristics of materials. Rheology entails the elastic, viscous and plastic behaviour of materials. By analysing the rheological behaviour of bituminous materials at various ageing conditions ensure enough information to conclude the current and future problems in surfacing seals. The analyses entail laboratory tests on bituminous seal binders at the short-term and long-term age conditions.

1.2 Problem Statement

This report focuses on the analyses of the rheological as well as the ageing behaviour of the most used 'typical' seal binders in South Africa. The damage to seal binders in South Africa is particularly due to temperature change and continuous loadings.

Seal binders were identified and sourced from Colas in Cape Town and Johannesburg. Five seal binders were sourced from the refinery in Cape Town and three of them from the refinery in Johannesburg as well. The way in which the rheological properties and the ageing behaviour of these seal binders differ for each refinery were also evaluated.

The analysis of these binders was carried out at different levels of ageing, by using the following ageing apparatus:

- Original,
- Rolling Thin Film Oven (RTFO), and
- Pressure Aging Vessel (PAV).

The rheological properties of the binders were analysed with the Dynamic Shear Rheometer (DSR) and the Bending Beam Rheometer (BBR). The rheological parameters that were analysed and needed for developing Master Curves are as follows:

- Complex Modulus;

- Phase angle;
- Cross-over frequency;
- Non-recoverable creep compliance (J_{nr});
- G-R parameter;
- Viscoelastic transition (T_{VET}, G_{VET}), and
- ΔTc.

These rheological parameters are relative to the field performance of seal binders and will be analysed in such a way that it contributes to the research of the performance grading system of bitumen binders. The current Performance Grade (PG) specifications are currently set for only asphalt binders. This study will conclude the way in which the rheological properties of seal binders compare to asphalt binders.

1.3 Objectives

The primary objective is the analysis of the rheological properties of selected seal binders in their original condition and simulated ageing conditions. This primary objective can be subdivided into secondary objectives:

- Present a clear set of compliance criteria to ensure the optimal selection of bituminous binders for specific applications.
- The assessment of the rate of ageing of the seal binders using rheological parameters, and
- The evaluation of typical seal binder properties using rheological parameters and indices as well as their correlation with the current South African Performance Grade Specifications for asphalt binders and the Texas Surface Performance Graded (SPG) specification.

1.4 Scope and Limitations

This report includes the theory and analyses of the rheological aspects of typical used bituminous seal binders in South Africa. It forms part of a greater project for SANRAL which entails rheological research for the performance grading system of bitumen binders for seals. The information gathered from this study will be compared to the current PG specifications which is compiled for asphalt binders.

Eight seal binders were selected to be analysed. Five of the eight binders are sourced from two refineries where the rheological properties are compared with one another. The amount of time to complete this project was limited as well as the quantity of seal binders available at the refineries.

1.5 Report Overview

Chapter 2 focus on the literature of several aspects such as bitumen, modified bitumen, seals, rheology of bitumen, ageing of bituminous binders, rheological testing and rheological modelling.

Chapter 3 includes the research design and methodology that was used in this study. The entire experimental procedure and inputs are discussed in this section of the report.

Chapter 4 entail the analysis procedures that were followed to evaluate the behaviour of each seal binder.

Chapter 5 focus on the comparison of the results for all the seal binders with their ages.

The conclusions and recommendations are presented in Chapter 6.

Chapter 2: Literature Review

'I have not failed. I've just found 10,000 ways that won't work'-Thomas A. Edison

Seals consist mainly of aggregates and bitumen. This thesis focusses strongly on the bitumen within a seal. This thesis also includes the factors which may influence bitumen and the performance of seals simultaneously.

2.1 Surfacing seals in South Africa

The process of seal construction entails a layer of aggregate that is covered with a layer of bituminous binders onto a required road surface. Aggregate comprises of stone particles or sand particles. A typical surface seal consists of an aggregate layer on top of a bituminous layer. The roller compacts the aggregate particles into the bituminous layer ensuring good adhesive bonds and minimising voids between the binder and the aggregate. The Technical Recommendations for Highways (TRH 3) states that the process is finalised with the action of the traffic upon the surfacing seal (TRH 3, 2007).

When the aggregate is applied to the binder sprayed road surface, the so-called seal provides a durable surfacing with the following functions (Webb, 2010):

- Increases resistance to air and water intrusion;
- Improves an existing road surface;
- Delivers a skid-resistant surface;
- Delivers a uniform-appearing surface;
- Offers the required surface texture, and
- Improves the surface, which shows signs of distress.

The aggregate and binder mixture ensure a new wearing course and provides a waterproof seal. The function of the aggregate is to increase the friction of the pavement surface (for skid resistance), to resist traffic abrasion and to transmit the wheel loads of the vehicles.

The TRH 3 (2007) provides a list of various seals commonly used in South Africa, namely single seals, double seals, Cape seals, slurry seals and sand seals. Other types of seals are such as inverted double seals, geotextile seals, split seals, graded aggregate seals and choked seals. The seals which are commonly used in South Africa, are illustrated in Figure 1.

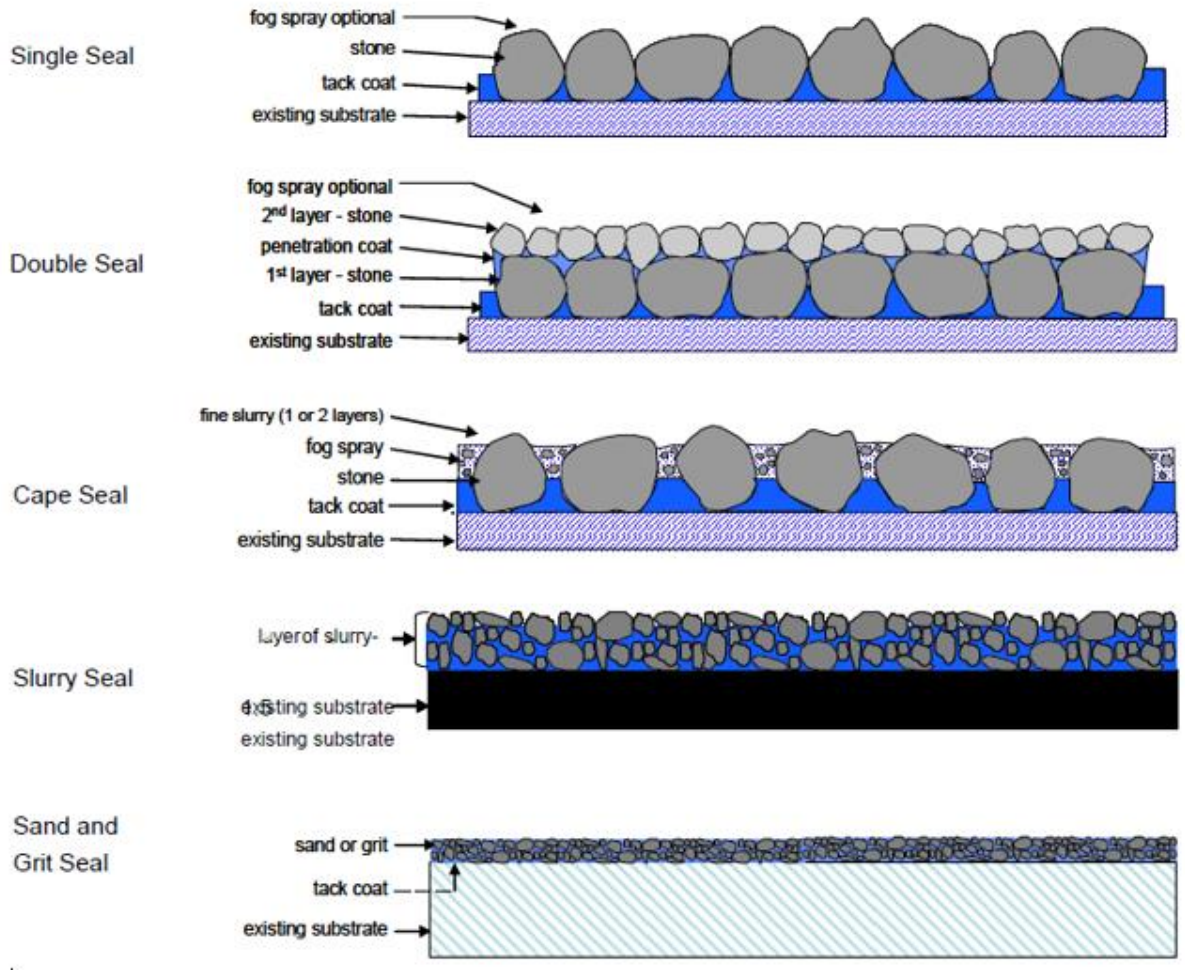

Figure 1: Schematic illustration of various seals (TRH 3, 2007)

2.2 Factors affecting surface seal performance

This section will focus on some of the factors which may influence the performance of seals. This section also includes a discussion on the components within the seal composition.

The performance of surfacing seals depends on numerous factors. These factors entail short- and long-term effects on the performance of the seals, as outlined below:

- Pavement structure and condition;
- Traffic;
- Design;
- Road geometry, and
- Materials.

The factors mentioned above are the primary factors that influence the performance of seals, but the list is not exhaustive.

2.2.1 Pavement structure and condition

The performance of a surface seal is largely reliant on the layers within a road structure. The surface seal acts as a wearing course for moving traffic and prevents water from entering the structural layer.

According to the TRH 3 (2007) and Abrahams (2015), the degree of penetration of the aggregate into the base layer is dependent on the materials within the base and the degree of compaction of the layer. This embedment of the aggregate into the base layer minimises voids within the seal and can lead to bleeding of the surface (Abrahams, 2015).

The flexural characteristics of pavements is another consideration. The way in which pavements deflect with several load repetitions may cause fatigue in the layers and surfacing. The degree of cracking is dependent on the temperature, chemical reactions, the level of stress or strain and the amount of load repetitions on the surface. It is thus very important to select the appropriate seal and binder type for the pavement behaviour characteristics (TRH 3, 2007).

2.2.2 Traffic

TRH 3 (2007) states that the number, type and combination of vehicles have a tremendous effect on the performance of seals. Heavier axles have a much greater effect than lighter vehicles. The volume of the vehicles is also a very important factor to consider. High volume traffic causes wearing within the seal, which minimises voids and results in loss of skid resistance.

Heavier vehicles cause more embedment of the stone into the surface than lighter vehicles. The speed of the traffic is also an important factor to consider. The horizontal forces on the surface of the road are much smaller with fast moving vehicles in comparison to lighter vehicles. The traction on the surface of the road when a heavy vehicle brakes may cause a lot of damage to the seal.

2.2.3 Design

The pre-design investigation is very important and determines the way in which the seal will perform. The design process entails the identification of the required structure type and material type for each layer in the pavement structure. The objective of the design process is to construct a pavement that can withstand the required traffic demand and weather conditions within the region.

2.2.4 Road geometry

The geometry of the road is an important aspect as it influences the performance of a seal in numerous ways. The road geometry may lead to surface water following a flow path on the road. This may limit the speed of vehicles and the gradient of the surface influences the magnitude of the pressure of wheel loads. The type of stresses applied on a road with sharp curves may differ for each vehicle type and size as well as vehicle volumes. These stresses have a tremendous effect on the surface as well as on the layers of the pavement structure (Read & Whiteoak, 2003).

2.2.5 Materials

The materials within a seal are also an important factor to consider. This section discusses these materials such as aggregates and binders, as well as how they influence the performance of seals. The next section discusses bitumen, which is also one of the materials to consider within seals.

2.2.5.1 Aggregates

Seal construction mostly consists of single size aggregates. Nominal size aggregates consist of aggregates sieved with various sieve sizes. In South Africa the following sieve sizes are used: 19 mm, 13.2 mm, 9.5 mm and 6.7 mm (Gerber, 2016).

According to the TRH 3 (2007), aggregate has the following main functions:

- Ensures resistance to the friction of the wheel loads;
- Spreads wheel loads through the pavement structure;
- Provides skid-resistance to the surface;
- Provides a structure to ensure that the viscoelastic bituminous binder stays in position, and
- Protects the bituminous binder from the ultraviolet rays of the sun.

The following material related aspects affect the performance of seals (TRH 3, 2007):

- The shape and size of the aggregate;
- Spread rate;
- Embedment;
- Adhesion characteristics;
- Strength, and
- Porosity and bitumen absorption.

Size and Shape

The size and shape of the aggregate are two of the factors, which dictate the strength of the interlocking in the layer. For example: an aggregate with a more angular shape will have much better interlocking characteristics in comparison to an aggregate which has a round shape. Single-sized aggregates provide more friction between the tyres and the surface of the road. More friction ensures that the stone resists polishing and gives good skid-resistance over a long period (TRH 3, 2007).

Spreading

The aggregate spreading procedure is very important during the construction period. The aggregates have to be packed together in a single layer and in a tightly knit pattern (Abrahams, 2015).

The spreading of the aggregate and embedment, discussed below, are closely associated. Embedment can also be explained as the result of the way in which spreading occurs.

Embedment

Embedment includes the loss in texture depth of a pavement. The embedment phases are illustrated in Figure 2.

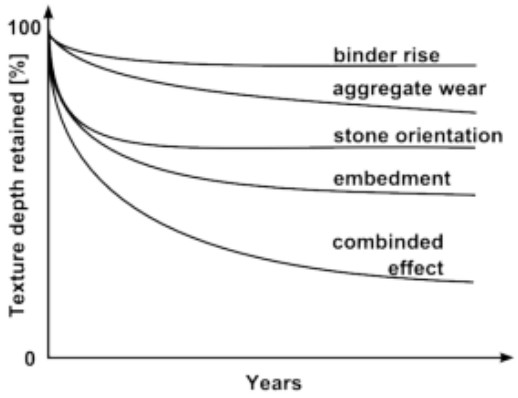

Figure 2: Phases of texture loss in a pavement (Gerber, 2016)

The orientation of the stones within a pavement structure occurs during the construction of the pavement. The rest of the orientation of the aggregate takes place when the road is open for traffic. The orientation of the aggregate ensures an increase in the binder height. The texture loss occurs when the binder height increases (Gerber, 2016).

The term 'punching' occurs when the aggregate penetrates through the tack coat film and into the top of the base. This can occur during construction or during trafficking. According to Gerber (2016), the larger aggregate particles have more texture loss potential compared to smaller aggregates.

Adhesion

The adhesion properties between the binder and the aggregate, is susceptible to dust, surface tension, porosity, moisture, etc. The intrusion of dust and/or water may result in a tremendous loss in aggregate (TRH3, 2007).

During the adhesion process, the road experiences aggregate loss, which shortens the life of the pavement. Section 1.3.2.3 includes a detailed discussion regarding adhesion.

Strength

The seal aggregates need to be able to withstand the impact and friction of moving wheel loads. Another important characteristic of aggregates is to withstand the impact of the rollers during the compaction process of road construction. The overall purpose of aggregates within the surface is to minimise the rate of disintegration and to maximise the stability of the compacted layer (Tarrer & Wagh, 1991).

Porosity and Binder Absorption

Porosity is the ratio of the volume of the pores to the total volume of the particle. The existence of pores within the aggregate are believed to be the result of binder absorption. Binder absorption is determined by the total porosity, the continuity of the pores and the pore size distribution and may also affect the following (Tarrer & Wagh, 1991):

- Strength of the aggregate;
- Surface texture;
- Bonding capabilities;
- Abrasion resistance, and
- Resistance to freezing.

2.2.5.2 Bitumen

Section 1.3 includes a brief discussion on bitumen technology.

2.3 Bituminous binders

Bitumen, obtained from crude oil, is one of the most common asphaltic binders. Crude oil is a complex mixture of hydrocarbons which has to be separated, purified, blended and chemically/ physically changed before it can be used (Read & Whiteoak, 2003).

Bitumen is a dark brown/black viscoelastic material obtained naturally or as a residue of petroleum distillation. The flow of crude oil through a refinery is indicated in Figure 3. Figure 3 illustrates the process of fractional distillation. It should also be noted that bitumen is last to be obtained from the primary refinery tank (Rowe, 1996).

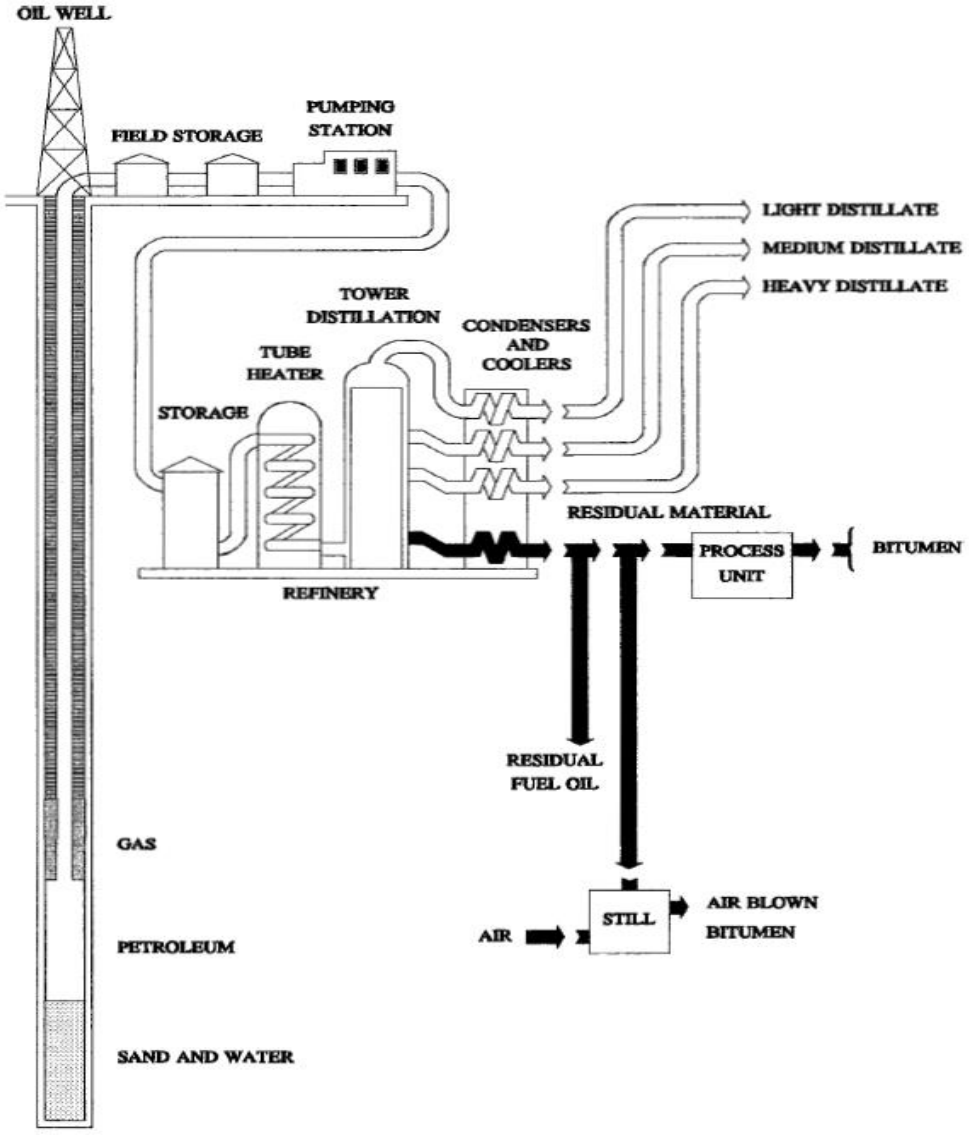

Figure 3: Asphaltic binder (Bitumen) production (Rowe, 1996)

Heating the crude oil in the refinery ensures the separation of the lighter and heavier oil fractions from one another. The fractions with the higher boiling points are then transferred to a vacuum distillation

column where the residues are then used to manufacture several grades of bitumen (Refined Bitumen Association, 2016).

2.3.1 Chemical composition

The chemical composition of bitumen is extremely complex. It varies for each source of crude oil. Furthermore, according to Read and Whiteoak (2003), it is impossible to do a complete analysis of the chemical composition of bitumen. The composition of bitumen is important to analyse to understand the various changes in bitumen rheology. It is possible to separate bitumen into two chemical groups such as maltenes and asphaltenes (Romberg *et al*, 1959). Figure 4 indicates the maltenes and asphaltenes and can be subdivided into various groups.

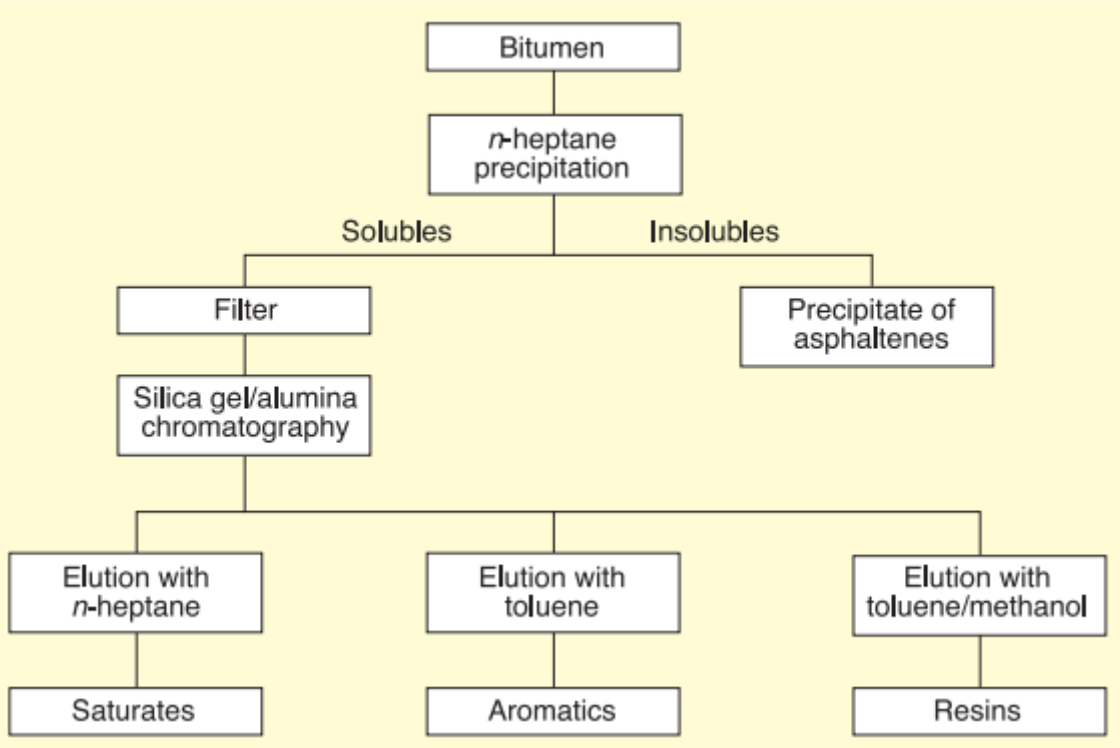

Figure 4: Chemical composition of bitumen (Read & Whiteoak, 2003)

There are various methods for separating bitumen into these fractions, as seen in Figure 4. The discussion of the separation process is not relevant for this thesis. The chemical composition of bitumen as well as the molecular structure of bitumen is very important in terms of the viscoelastic behaviour of various binders. Maltenes comprises of saturates, aromatics and resins. A brief description of the four main components such as saturates, aromatics, resins and asphaltenes follows below.

2.3.1.1 Saturates

Bitumen contains 5 - 20 % saturates. The chemical structure of saturates consists of aliphatic hydrocarbons, alkyl-naphthalenes and some alkyl-aromatics. The chemical structure consists of straight and branch chains between the chemicals mentioned earlier (Milne, 2004; Read & Whiteoak, 2003).

2.3.1.2 Aromatics

Aromatics comprise 40 - 60 % of bitumen with a dark brown colour and with a viscous behaviour. The chemical structure comprises of non-polar carbon chains where the unsaturated ring systems (aromatics) dominate (Read & Whiteoak, 2003). Figure 6 indicates the structure of aromatics.

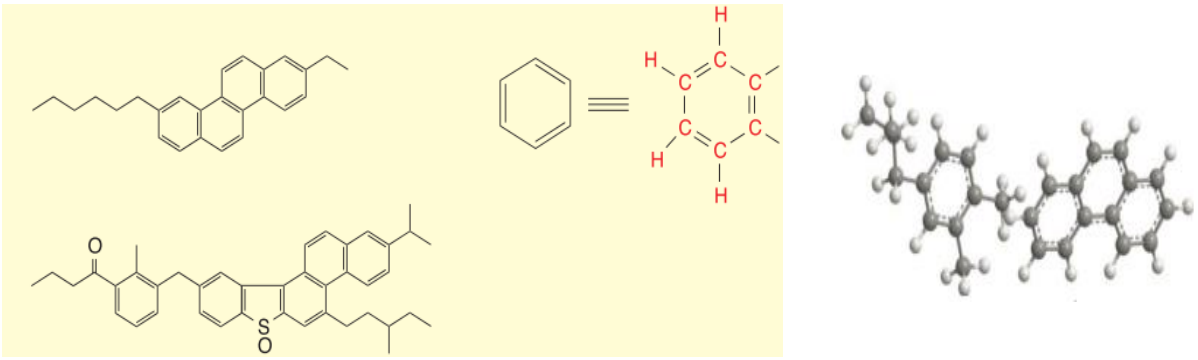

Figure 5: Chemical structure of aromatics (Paliukaitė *et al*, 2014; Read & Whiteoak, 2003)

2.3.1.3 Resins

Resins consist of hydrogen, carbon, small amounts of oxygen, sulphur and nitrogen just like asphaltenes. Resins are dark brown in colour with strong adhesive characteristics and behave as a solid or semi-solid in a highly polar manner. The chemical structure consists mostly of stacked rings (Milne, 2004; Read & Whiteoak, 2003). Figure 7 indicates the structure of resins.

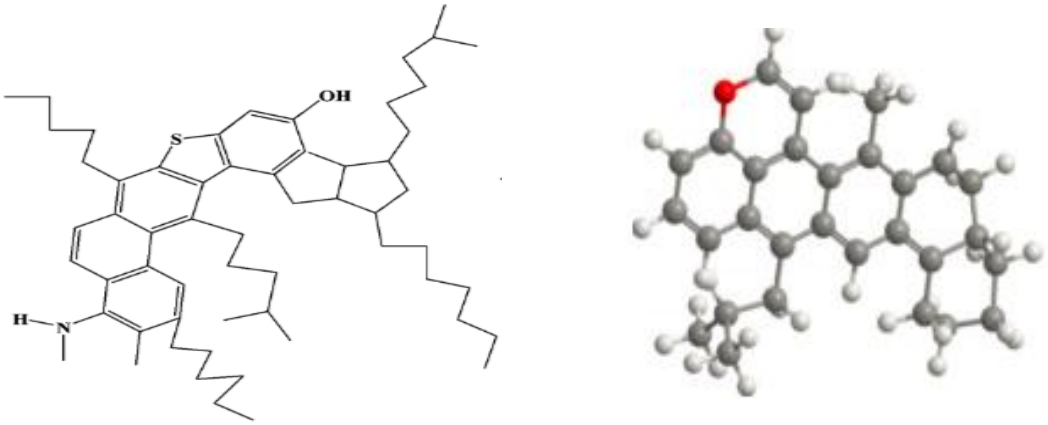

Figure 6: Chemical structure of resins (Lin *et al*, 2015; Paliukaitė *et al*, 2014)

2.3.1.4 Asphaltenes

Asphaltenes are dark black and comprise 5 - 25% of bitumen. Asphaltenes are polar and contain aromatic materials with high molecular weight. Asphaltenes have a major impact on the rheological properties of bitumen. Increasing the asphaltene content can affect characteristics like the stiffness, viscosity, penetration and softening point of bitumen (Milne, 2004; Read & Whiteoak, 2003). Figure 8 illustrates the structure of asphaltenes.

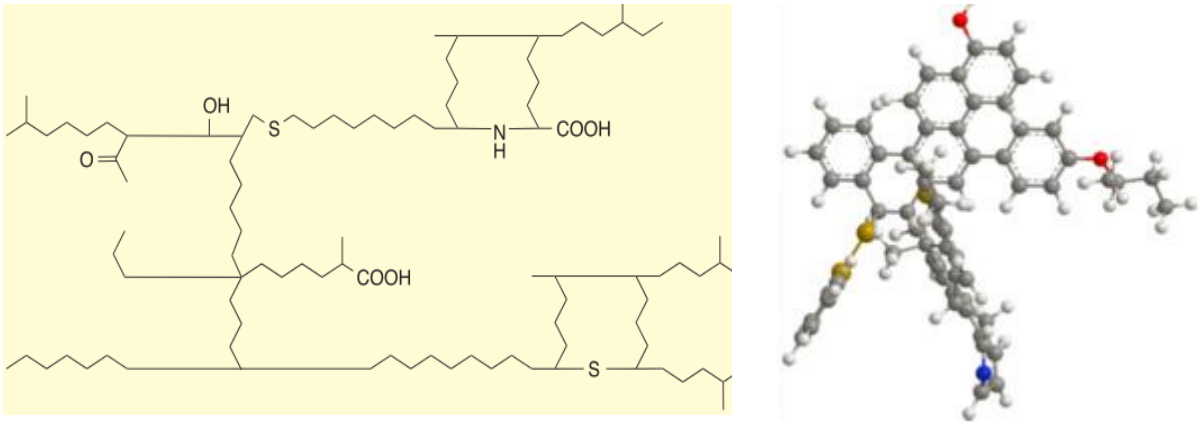

Figure 7: Chemical structure of asphaltenes (Paliukaitė *et al*, 2014; Read & Whiteoak, 2003)

2.3.2 Physical characteristics

The physical characteristics of bitumen are determining factors with respect to its durability and lifespan. Bitumen should act as a 'glue' when it encounters aggregates to ensure a stable surface that can withstand the environmental conditions to which it may be exposed. This section will discuss characteristics and failure mechanisms such as rheology, visco-elastic behaviour, cohesion, cohesive failure, adhesion, adhesive failure and binder ageing.

2.3.2.1 Rheology (General Discussion)

The term 'rheology' includes the theory regarding the flow and deformation behaviour of materials. Bituminous materials display elastic and viscous behaviour. The viscoelastic behaviour of bituminous binders includes both creep and relaxation properties when subjected to loadings. Creep contributes to the deformation of a material with time. Relaxation can be described as the decrease in the stress within a material with a constant load over a period of time (Woldekidan, 2011). The different types of deformation in a continuum are summarised in Table 1.

Table 1: Different types of deformation of a material adapted from (Poulikakos & Partl, 2012)

Type of deformation	Characteristics	Molecular level
Elastic	Time independent. Deformation occurs the instant stress is applied or released. Reversible. Energy is not dissipative (recoverable).	Deformation due to change in bond length of atoms. Long molecular chains are frozen in position.
Plastic	Time independent irreversible. Energy dissipative. Yield stress.	Atoms rearrange permanently.
Viscoelastic	Instantaneous elastic strain. Viscous time dependant strain. Elastic recoverable strain upon release.	Same as elastic with time dependence.
Viscoplastic	Time dependant irreversible. Energy dissipative.	Atoms rearrange permanently.
Viscous flow	Deformation is not instantaneous. Time dependant. Not reversible upon release. Energy dissipative.	Chain motion intensifies. Chain segments vibrate and rotate independently of one another.

The behaviour of bitumen under loadings can be categorised into two divisions. Under a small load, bitumen behaves in a linear viscoelastic manner. During larger loadings, bitumen behaves in a nonlinear form.

Note: Section 1.7 entails a detailed discussion regarding the rheology of bituminous materials.

2.3.2.2 Cohesion

The term 'cohesion' is derived from the tensile stresses that are needed within bituminous materials to break the bond between the molecules (Asphalt Academy, 2007). Cohesive binder strength i.e. crack resistance within the binder-aggregate mixture is strongly influenced by the rheology of the binder (Little & Jones, 2003). Plastomeric modified binders may not increase the tensile strength within the molecules of the binder, but the stiffness (Asphalt Academy, 2007). The increase in stiffness may result in a brittle behaviour under repetitive loadings (Rowe, 1997).

Cohesive failure

Cohesive failure occurs when cracks are formed within the bituminous binder (Mo, 2010). Figure 9 illustrates the cohesive failure mechanisms within the binder-aggregate mixture.

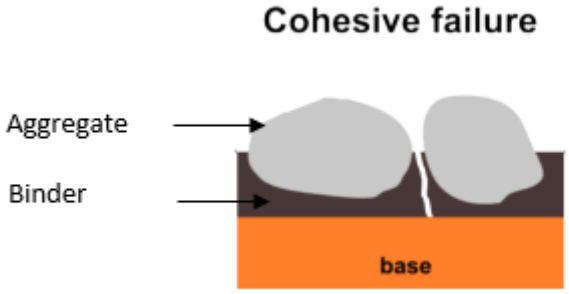

Figure 8: Cohesive failure within the binder adapted from (Gerber, 2016)

Cohesive failure, as seen in Figure 8, may occur due to numerous factors such as mechanical loadings, temperature, binder hardening (ageing), etc. These factors may cause fatigue cracking which results in cohesive failure (Gerber, 2016). After several tests, Rowe *et al*. (2014) concluded that both mechanical and thermal related (environmental) cracking could be associated with cohesive failure. According to Little & Jones (2003), moisture influences seals and asphalt mixtures tremendously. Moisture influences the cohesive and adhesive bond strength of both seals and asphalt mixtures.

2.3.2.3 Adhesion

Adhesion defines the measure of the stresses which occur within the bitumen-aggregate bond. The adhesion properties of a mixture are largely dependent on the physical chemistry and the chemical nature of the aggregate type and bituminous material (Asphalt Academy, 2007).

Adhesive failure

Adhesive failure occurs between the aggregate and the bituminous binder within the mixture (TRH3, 2007). Figure 10 illustrates adhesive failure between aggregates and bituminous binders.

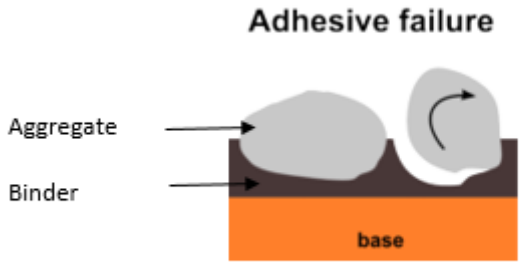

Figure 9: Adhesive failure between aggregates and bituminous binders adapted from Gerber (2016)

The sensitivity of the bitumen-aggregate bond depends mostly on factors such as aggregate size, aggregate spreading and the position of the binder (Gerber, 2016). The following factors may cause adhesive failure within the bitumen-aggregate mixture (Asphalt Academy, 2007):

- Aggregate which is moist and filled with dust;
- The percentage of modification within a binder influences the rheological behaviour of the binder, and
- Road and air temperature.

The type of failure (cohesive and/or adhesive) is strongly dependant on the binder film thickness and the nature of the binder. Figure 11 illustrates cohesive and adhesive failure in relation to the film thickness of the binder.

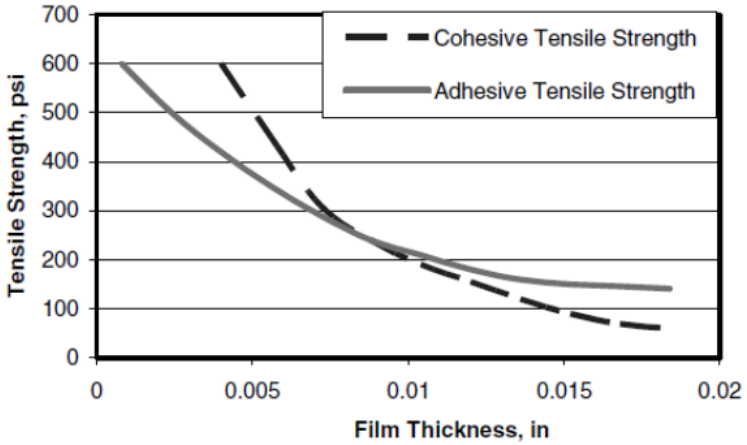

Figure 10: Cohesive and adhesive failure in relation to binder film thickness (Little & Jones, 2003)

As seen in Figure 11, the tensile strength of the bond between the aggregates and the binder (adhesive) increases as the binder film thickness decreases. The same result occurs regarding the bond strength between the molecules of the binder itself.

2.3.2.4 Ageing and Durability

Bitumen ageing, also known as hardening/curing, occurs primarily with the presence of oxygen, ultraviolet radiation and by variation in temperature. The above-mentioned factors cause an increase in the material stiffness and the load spreading capabilities of the structure while decreasing the elastic properties of the material (Read & Whiteoak, 2003). The hardening of bitumen can negatively influence the surface course of the pavement structure. Cracking may occur on the surface due to a high increase in stiffness of the material.

Bitumen hardening also takes place during the hot storage and transportation of the binders. These factors also influence the rheological behaviour of the binder, but at a lower extent in comparison to the primary factors mentioned earlier (Read & Whiteoak, 2003).

Several ageing test methods were proposed over the years, for both asphalt and surfacing seal binders, and the most utilised tests are as follows (Mastrofini & Scarsella, 2000):

- Rolling Thin Film Oven Test (RTFOT, ASTM D2872 / TG1 MB3), and
- Pressure Ageing Vessel (PAV, ASTM D6521).

Section 2.4 entails a detailed discussion regarding the above-mentioned test methods. The RTFOT simulates the short-term ageing (STA) of the binder. STA entails the extraction of oxidation and volatiles within the bituminous binder during the construction phase. Oxidation describes the reaction of oxygen with the binder. Volatilisation describes the loss of light fractions from the binder and is mainly dependent on the temperature. The initial ageing of the bituminous binder for surfacing seals occurs at the facility during the heating process for constructional purposes. The RTFO method evaluates the variation in the viscosity, penetration and softening point of the binder (Hagos, 2008).

The mechanisms for the reactions during short-term ageing are as follows (Hagos, 2008):

<u>Loss of volatiles</u>

The loss of volatiles is due to evaporation and indicates the instability of the binders. More stable binders will undergo minimal loss in volatiles and will indicate a smaller change in their rheological properties.

Oxidation

Several types of chemical reactions take place during the oxidation process. More stable bituminous binders experience minimal loss of volatiles. This behaviour indicates that the binder is less susceptible to oxidation which ensures a lower extent of hardening.

The PAV method simulates the long-term ageing (LTA) of bituminous binders. LTA entails mostly oxidation of the bituminous binder during the service life of the surfacing seal. In this test the effect of ageing and ageing itself is determined by dynamic rheological analysis and evaluated by means of the complex modulus and the phase angle of the binder(s) (Mastrofini & Scarsella, 2000).

Section 2.8 discusses the construction of a master curve and black space diagram as well as the way in which ageing is analysed. Figure 12 is only an indication of the effect that ageing has on the stiffness of a bituminous binder. It indicates the complex modulus against the phase angle (Black Space diagram) as well as the Glover-Rowe cracking constraint curves.

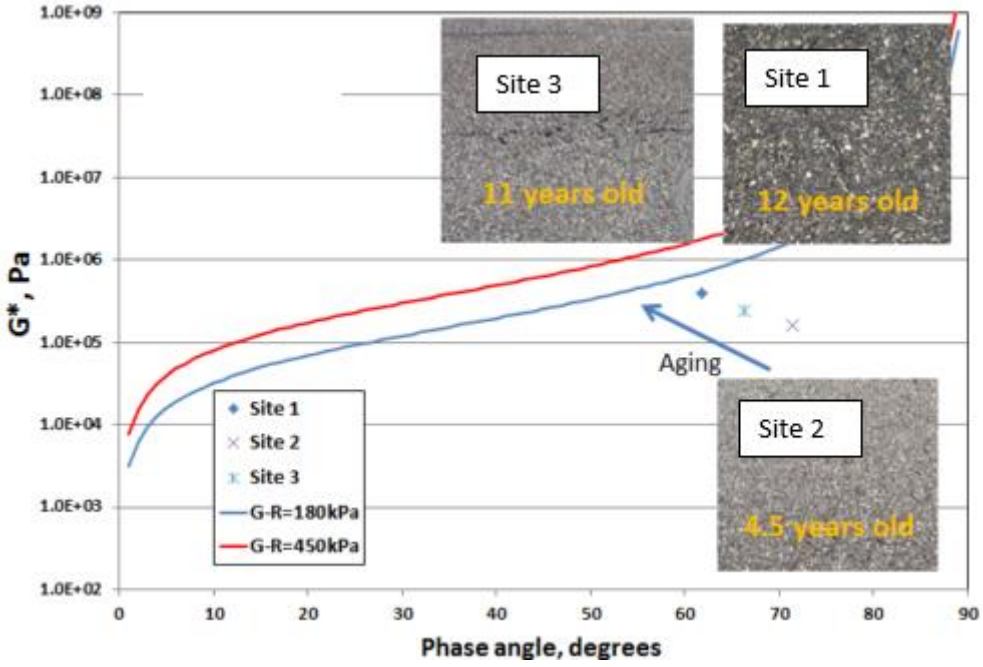

Figure 11: Increase in ageing increase the chances of surface cracking (G. Rowe, 2014)

Figure 12 illustrates how the complex modulus increases as the age of a bituminous binder increases. The blue line indicates crack initiation and the red line indicates severe cracking. The Glover-Rowe parameter moves closer to the severe cracking curve as the oxidation and loss of volatiles increase.

Viscosity is an important factor to consider during the ageing of a binder. Viscosity is analysed through the ageing index of a binder. Equation 1 indicates how the ageing index is calculated (Mastrofini & Scarsella, 2000).

$$A.I = \left(\frac{\eta_{0\,(after\ RTFO)} - \eta_{0\,(Original)}}{\eta_{0\,(Original)}} \right) \times 100 \qquad (1)$$

Where:

$A.I$ = Ageing index

η_0 = Zero shear viscosity

It is known that as the film thickness of the asphalt mixture and surfacing seals increases, the ageing index decreases (Read & Whiteoak, 2003). Figure 12 indicates the behaviour of the ageing index as the binder hardens through each stage of its life span.

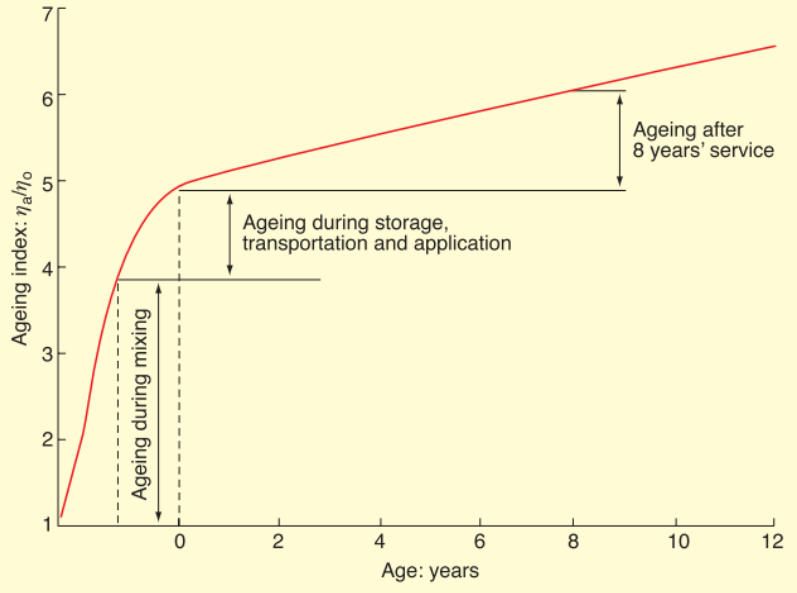

Figure 12: The change in the ageing index during the ageing process of a typical bitumen binder (Read & Whiteoak, 2003)

The trend of the curve shown in Figure 13 illustrates the change in the ageing ratio (viscosity ratio of the aged to un-aged binder) during the production and service period of typical bituminous binders. Figure 13 indicates the importance of ageing during the mixing period with the sudden increase in the ageing index. After ageing during the mixing process, the curve flattens off which indicates minimum variation in the data.

Temperature susceptibility

The temperature susceptibility of bituminous binders depends on the variation in the stability of the binder during the variation in temperature. The change in the fragility point at a low temperature and the softening point at high temperatures regulate the stability of the binder. Below the fragility point one may experience some cracks and above the softening point one may experience bleeding. The service temperature of a binder is the range in the temperature between the fragility point and the softening point. The crude source of the binder as well as the grade of the binder are factors that influence the service temperature of the binder. Figure 14 indicates the behaviour of a typical bitumen binder over its working temperature and indicates the range at which the binder may be unworkable and experience distresses.

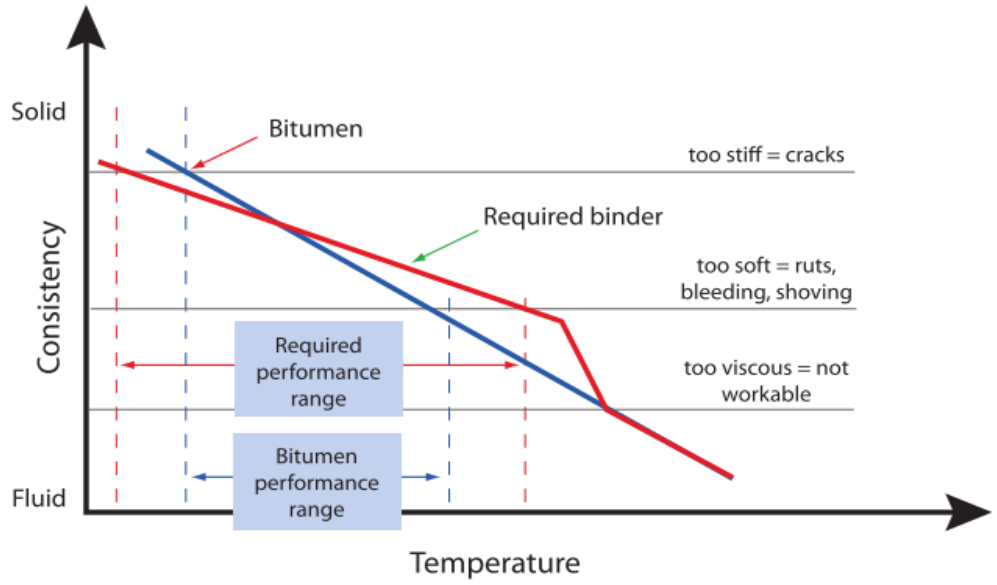

Figure 13: The typical behaviour of a binder over its working temperature (Asphalt Academy, 2007)

Figure 14 illustrates that as binders reach temperatures above the softening point, distresses such as bleeding and/or rutting may occur. Cracking may occur at the lower temperatures where the binder meets its fragility point.

The service temperature of bituminous binders may widen by adding polymers to modify binders. Section 1.5 and 1.6 discuss various modification techniques on bituminous binders. It is important to monitor the temperature of modifiers such as SBS, SBR and rubber due to their sensitivity to oxidation and degradation(Asphalt Academy, 2007).

Effect of ageing on low temperature performance of bituminous binders

Hagos (2006) performed Direct Tension Tester (DTT) tests on an unaged and long term aged binder at 0˚C, -5˚C and -10˚C. The data was shifted to a reference temperature of -5˚C to form master curves. Figure 14 show that the material strength increases as the loading rate increases until a maximum is reached, after which the failure stress starts to decrease. After the maximum stress of the binder is reached it is very brittle due to the high stiffness and high frequency load. This behaviour is common for low temperature performance of bitumen due to the binder becoming more brittle at low temperatures and higher frequency loadings.

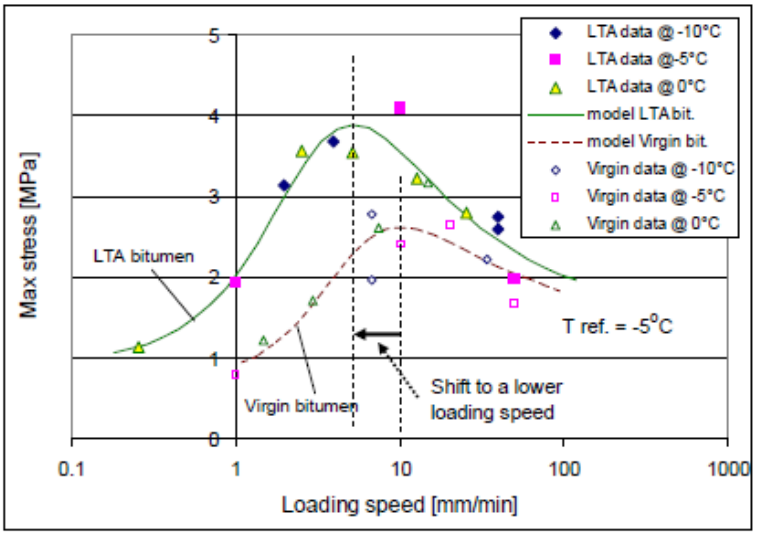

Figure 14: Unaged and long term aged binder failure master curve from DTT tests, T_{ref} = -5˚C (Hagos, 2006)

Observations were made by Hagos (2006) regarding the behaviour of the binders in Figure 14.

- The long term aged binder reached a maximum failure stress at a lower loading speed compared to the unaged binder. This indicates the hardening of the long term aged binder and can be described as the transition to brittle behaviour.
- The long term aged binder experience higher stresses that develop because of a temperature drop compared to the unaged binder. This behaviour may cause thermal cracks in the long term aged binder and reduce the fatigue life.
- The analysis of failure master curves provides important information regarding the effect of ageing on the low temperature performance of bituminous binders.

2.4 Ageing apparatus

The way in which bitumen reacts during the stages of the production process is very important and should be analysed. Numerous ageing tests simulate the resistance of bitumen hardening. The main aim of these tests is to simulate the effect of oxidation on bitumen during its service life. The Shell Bitumen Handbook (Sixth Edition) as well as Section 1.3.2.4 discuss the two most used ageing apparatus worldwide, which is the PAV and RTFO ageing apparatus.

2.4.1 RTFO

In 1963, the Highway Division of the State of California Department of Public Works, developed an ageing apparatus (Rolling Thin Film Oven test) which simulates the short-term ageing behaviour of bituminous binders (Hunter et al., 2015). Figure 16 indicates the short-term conditioning apparatus.

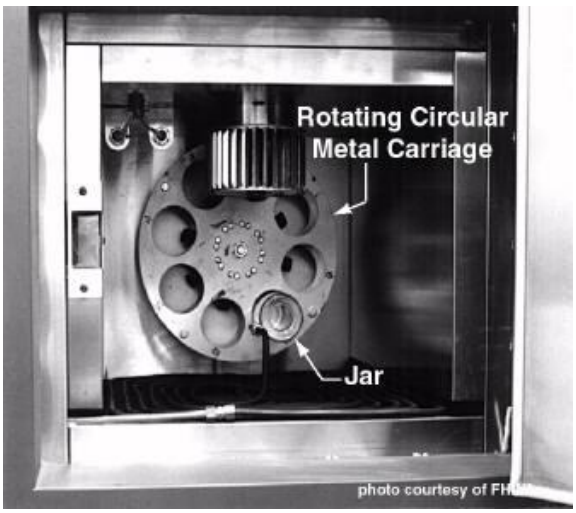

Figure 15: The Rolling Thin Film Oven apparatus (Pavement Interactive, 2012)

This test entails eight cylindrical glass containers filled with 35g of bitumen. Figure 16 indicates the containers with a vertical rotating metal carriage. During the testing, bitumen flows around the inner surface of each container in a thin film. The preheated air within the oven is then blown onto the bitumen in each jar as the shelf rotates, which ensures that all the bitumen is exposed to heat and air (Hunter, Self & Read, 2015a). The testing temperature and the period in which the test is performed is as described in the ASTM D2872 (ASTM D 2872-04, 2004).

The way in which bitumen ages in practice is clearly not the same, but according to Hunter, Self, & Read (2015) experience has shown that the results obtained from practice correlates with the results that are obtained from the RTFO apparatus.

2.4.2 PAV

The simulation of long-term ageing has proven to be extremely difficult due to numerous factors which influence bitumen long-term ageing. Factors such as void content, aggregates, mixture type, etc influnce the way in which a binder ages over time (Hunter et al., 2015). The Pressure Ageing Vessel, as seen in Figure 17, was identified as an accelerated ageing technique and the preferred apparatus to analyse the long-term ageing of bituminous binders (Anderson A *et al*., 1994).

Figure 16: Pressure Ageing Vessel (Pavement Interactive, 2012)

The PAV tests entails bitumen samples to be placed within the vessel at a pressure of 2.1 MPa. The testing periods are 20 hours (standard), 40 hours (2x std) and 80 hours (4 x std). The temperature at which the test is performed is normally between 90˚C and 110˚C (ASTM D 6521 - 08, 2008).

The RTFO test is used for the initial ageing of the samples. The PAV test is used for the long-term ageing of the samples. After the samples are aged the DSR device is used to evaluate the way in which oxidation influences the rheological properties of bitumen, in other words simulating the in-service ageing of the binders.

2.5 Modified Binders

Modifiers are known for improving the physical properties of bituminous binders (Alatas & Yilmaz, 2013). Modifiers improve the following properties of bitumen (Asphalt Academy, 2007; Zieli ski, 2008):

- Reliability;
- Resistance to temperature variation;
- Cohesion properties;
- Adhesion properties;
- Flexibility and toughness, and
- Resistance to in-service ageing.

However, it is important to note that the aggregate particles, quality and mixture are also factors to consider during the evaluation of pavement failures and distresses. The flexibility and toughness of a pavement depends a lot on the bituminous binder. Figure 18 indicates the load distribution of a flexible pavement and a rigid pavement.

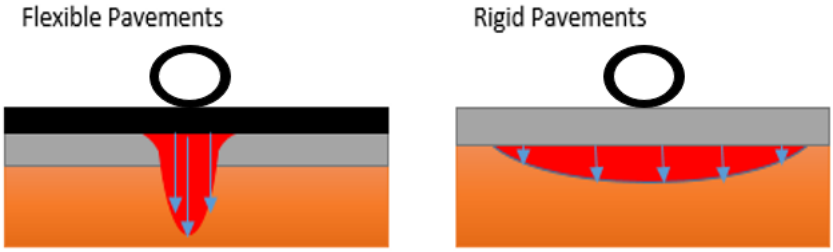

Figure 17: The load distribution of Flexible and Rigid pavements

Pavements with a lot of flexibility may fail due to rutting. Too rigid pavements may fail due to thermal cracking. The use of modified binders ensures a safer load distribution to increase the service life of a pavement.

Modified binders consist of two compositional groups. The two compositional groups are as follows (Asphalt Academy, 2007):

- Homogenous binders, and
- Non - homogenous binders.

Homogenous binders consist of polymers and bituminous material where the material behaves as a single-phased material from a localised viewpoint. Non-homogenous binders, e.g. bitumen rubber, consist of two detectable phases where the properties are dependent on the testing stage.

The homogenous polymer modifiers that are typically used in bitumen modification are as follows (Asphalt Academy, 2007):

- Styrene-Butadiene-Styrene (SBS), Elastomeric;
- Synthetic styrene-Butadiene-Rubber (SBR), Elastomeric;
- Natural rubber, Elastomeric;
- Ethylene-Vinyl-Acetate (EVA), Plastomeric, and
- Bitumen rubber.

2.5.1 Styrene-Butadiene-Styrene (SBS)

SBS is a thermoplastic elastomer with a crosslinking bond between the particles, which contributes to its high elastic properties. SBS results in much higher viscosities and softening points in comparison to other elastomers making it more difficult to mix with bitumen. The block copolymer (SBS) consists of mainly saturates and aromatics which ensure interaction with bitumen (Collins, 2006).

The SBS modification process entails the absorption of maltenes in the bitumen, forming a continuous molecular network in the bitumen phase, which make up a substantial portion of the bitumen's volume. An increase in the SBS concentration results in a dramatic increase in the softening point of bitumen (Asphalt Academy, 2007). Figure 18 indicates the way in which the softening point increases as the SBS content increases.

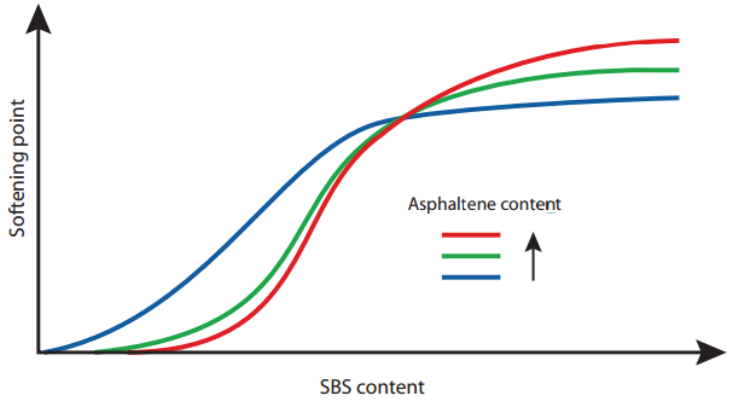

Figure 18: Effect of SBS on the softening point of bitumen with different asphaltene content (Asphalt Academy, 2007)

SBS displays higher softening points and higher elastic recovery properties in comparison to other modifiers at lower temperatures. The addition of SBS increases the flexibility properties of bitumen which decreases the probability of cracking and increases the binders' resistance to cracking (Collins, 2006).

The ageing of polymers results in an increase in the polymer weight, an increase in the content of polymer oxygen containing molecules as well as an increase in the molecular weight of bitumen. The way the rheological properties of the aged-modified binder changes is dependent on the polymer degradation and oxidation of the binder. According to several studies the aged-modified binders display much greater results in comparison to the unaged modified binders (Lu & Isacsson, 1998).

2.5.2 Styrene-Butadiene-Rubber (SBR)

SBR is an emulsification of styrene butadiene and approximately 50% solids, depending on the grade of the binder. The butadiene contributes to the elastic component of the modifier and improves the flexibility properties of the binder while the styrene ensures an increase in the stiffness and strength of the binder (Asphalt Academy, 2007).

SBR has very similar mechanical bonding mechanisms and chemistry to that of SBS. Both hot and cold modified binders typically consist of SBR latex. It is important to keep in mind that anionic emulsions use anionic latex and that cationic emulsions uses cationic latex. Hot modified SBR are currently commonly used for seals and to a smaller extent in asphalt mixtures (Asphalt Academy, 2007).

2.5.3 Natural rubber

Natural rubber latex comprises of polymerised isoprene monomers, which contributes to the elastic component of binders. Cold modified binders typically consist of natural rubber due to its sensitivity to high temperatures. Natural rubber is commonly used in the sealing of small cracks with a width smaller than 3 mm (Asphalt Academy, 2007).

2.5.4 Ethylene Vinyl Acetate (EVA)

EVA, a thermoplastic material, comprises of the copolymerisation of ethylene and vinyl-acetate. The characteristics of EVA lies between those of low-density polyethylene, semi-rigid translucent and transparent rubbery materials (Panda *et al*, 1999).

The above-mentioned monomers detach from one another when the temperature increases above the material's glass transition point. The polarity of the copolymers and the maltenes from bitumen will determine the adhesion properties of the binder. The properties of EVA are controlled by the following (Asphalt Academy, 2007):

- Molecular weight: The greater the melt flow index (MFI), the lower the molecular weight and viscosity, and
- Vinyl-Acetate (VA) content: An increase in the VA content will increase the flexibility and decrease the stiffness of the binder. The flexibility increases due to an increase in the rubbery regions.

EVA modified binders increase the resistance of the binder to rutting and improve the compatibility and workability compared to SBS and SBR modifiers. The properties of EVA are less tangible with the fluctuation in temperature during storage compared to SBS and SBR (Asphalt Academy, 2007).

2.5.5 Bitumen rubber

Bitumen rubber, a non-homogenous binder, comprises of rubber crumbs and bitumen. Mixing bitumen rubber at high temperatures ensures a complex two-phase product. The elastic and stiffness characteristics for bitumen rubber is virtually the same as tyre rubber. After the mixture is cooled down, the rubber network with bitumen contributes to the improved cohesion, elasticity, flexibility and strength of the material (Asphalt Academy, 2007).

2.6 Modified Binder Classification

The Technical Guideline 1 provides a clear description regarding the need for binder classification. The classification provides a binder blind system, where the focus is set on the end-property performance requirements of the binder. The modified binders are thus classified according to their application type, temperature, polymer used and a numerical value (Technical Guideline 1, 2016).

The application types are as follows:

- Seal (S);
- Asphalt (A), and
- Crack sealant (C).

For emulsions, the letter 'C' indicates the binder type. No letter indicates the binder type for hot applied mixtures.

The type of modifiers are as follows:

- Rubber (R);
- Plastomer (P);
- Elastomer (E), and
- Hydrocarbon (H).

The level of modification entails the degree of the softening point of the binder. The higher the numerical number the higher the softening point. If a binder has a higher softening point in comparison to other binders, it does not directly imply greater overall physical properties. Table 2 on the following page indicates the modified binder classification system.

Table 2: The modified binder classification system (Asphalt Academy, 2007)

Modified Binder Class	**Application – Surface Seal**
S – E1	Surface seal – hot applied elastomer modified
S – E2	Surface seal – hot applied elastomer modified
S – R1	Surface seal – hot applied bitumen rubber
SC – E1[1]	Surface seal – emulsion elastomer modified
SC – E2[1]	Surface seal – emulsion elastomer modified
Modified Binder Class	**Application – Premixed Asphalt**
A – E1	Hot mix asphalt – elastomer modified
A – E2	Hot mix asphalt – elastomer modified
A – P1[2]	Hot mix asphalt – plastomer modified
A – H1	Hot mix asphalt – hydrocarbon modified
A – H2[2]	Hot mix asphalt – hydrocarbon modified
A – R1	Hot mix asphalt – bitumen rubber
AC – E1	Microsurfacing – emulsion elastomer modified
AC – E2	Microsurfacing – emulsion elastomer modified
Modified Binder Class	**Application – Crack Sealant**
C – E1	Crack sealant – hot applied elastomer modified
CC – E1	Crack sealant – emulsion elastomer modified
C – R1	Crack sealant – hot applied bitumen rubber

Notes

1. These emulsions have the option of being made with or without cutters depending on their application.
2. Some of the modifiers in these generic classification classes are also capable of imparting fuel resistant properties.

2.7 Rheology of bituminous binders

Section 1.3.2.1 entails the basic description of rheology in general. This section will discuss the flow behaviour of bituminous binders by means of applied shear stress and shear rate. The way in which linear viscoelastic behaviour is modelled will be discussed. A detailed discussion regarding the viscoelastic parameters of bituminous materials follows below.

2.7.1 Newtonian and Non-Newtonian fluids

Newtonian fluids indicate a linear relationship between the stresses and shear/strain rate, as seen in Figure 19. Figure 20 indicates the constant slope of a Newtonian fluid and gives the viscosity of the fluid.

A non-newtonian fluid entails the response of a fluid under a certain shear stress and the shear rate. Unlike a newtonian fluid a non-newtonian fluid can be categorised by a non-linear relationship between the applied shear stress and the rate of shear (Partal & Franco, 2010). The slope of the curves, as seen in Figure 20, defines the viscosity. The viscosity of a non-Newtonian fluid is not constant, as seen in Figure 21.

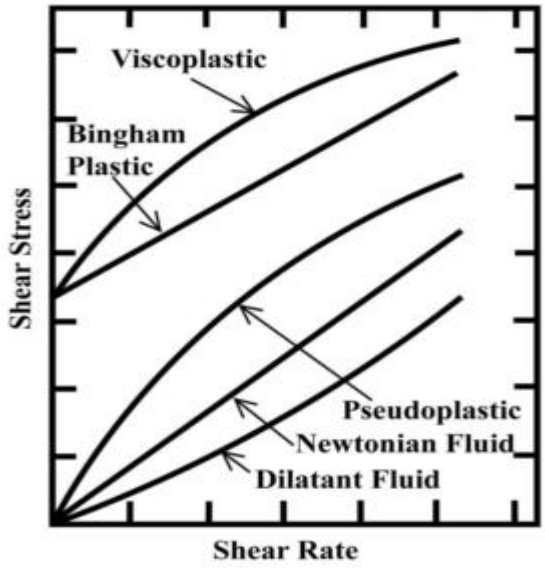

Figure 19: Flow curves indicating various fluid behaviours (Chhabra, 2010)

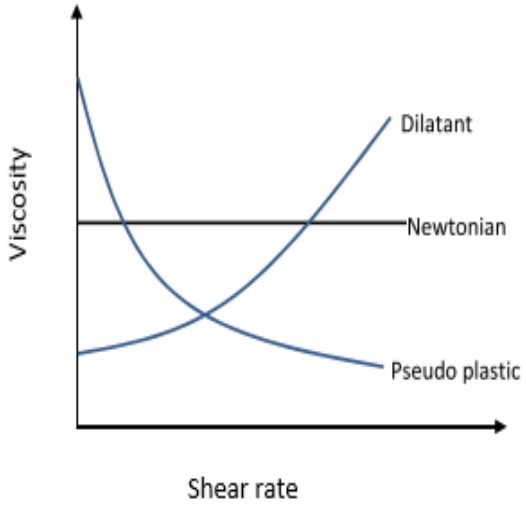

Figure 20: Change in viscosity of non-newtonian fluids (Kashaya, 2013)

Previous studies have shown that normal penetration grade bitumen typically behaves as a newtonian fluid while modified binders behave as non-newtonian fluids (Van De Ven, 2001). Results have shown that at a high temperature SBS modified bitumen exhibited shear thinning. Bitumen emulsions with a bitumen content of higher than 50% act as non-newtonian fluids and exhibit shear thinning. However, normal penetration grade binders tend to behave as non-newtonian fluids at low temperatures (Kashaya, 2013).

The difference between shear thinning and shear thickening materials depends on the following:

- The alignment of neighbouring macromolecules;
- Degree of their entanglement, and
- Concomitant immobilisation.

2.7.1.1 Shear-Thickening fluids

Shear-thickening or dilatant behaviour occurs when the viscosity of a material increases as the shear rate increases, as seen in Figure 20. This behaviour has one similarity to pseudo-plastic materials namely the fact that they have no yield stress. It is thus not yet possible to say whether these materials achieve the limiting ranges of viscosity ($\dot{y} \to 0 \; and \; \dot{y} \to \infty$) (Chhabra, 2010).

2.7.1.2 Shear-Thinning fluids

Shear-Thinning is possibly the most common type of time-independent non-newtonian fluid behaviour (Partal & Franco, 2010). Shear thinning occurs when the viscosity of a material decreases as the shear rate increases. The viscosity, which is defined as the shear stress over the shear rate, can describe this behaviour ($\sigma/\dot{y}$), that decreases as the shear rate increases. Zero shear viscosity can be described through Equation 2 and occurs with very low shear rates (Chhabra, 2010).

$$\lim_{\dot{y}\to 0} \frac{\sigma}{\dot{y}} = \eta_0 \qquad (2)$$

Where:

σ = Shear stress

$\dot{y}$ = Shear Rate

η_0 = Zero shear viscosity

The infinite shear viscosity occurs as the shear rate becomes infinite through very high shear rates. The infinite shear rate can be described through Equation 3 (Chhabra, 2010).

$$\lim_{\dot{y}\to \infty} \frac{\sigma}{\dot{y}} = \eta_\infty \qquad (3)$$

Where:

σ = Shear stress

$\dot{y}$ = Shear Rate

η_∞ = Infinite shear viscosity

Shear-thinning occurs with the pseudo-plastic behaviour as seen in Figure 20. The material behaviour of bitumen can be seen as shear-thinning (Macosko, 1994).

2.7.2 Viscoelastic Modelling

Linear viscoelastic springs and dashpots can describe the behaviour of bituminous binders. Three common systems that are typically used is the Maxwell model, the Kelvin-Voigt model and the Burgers' model. These are derived from the Hooke and Newton models.

2.7.2.1 Hooke's Model

The spring represents the elastic element in the model by obeying Hooke's law regarding an ideal solid. The Hooke model can be seen in Equation 4 with '*m*' as the elastic modulus (Mainardi & Spada, 2011).

$$\sigma(t) = m\epsilon(t) \quad (4)$$

Where:

$\sigma(t)$ = Stress as a function of time

m = Elastic modulus

$\epsilon(t)$ = Deformation as a function of time

In this case, the relaxation and creep response is zero, as indicated by Figure 21. Deformation will take place as a stress is applied over a certain period of time. The result will thus be that the material will recover fully as the stress unloads.

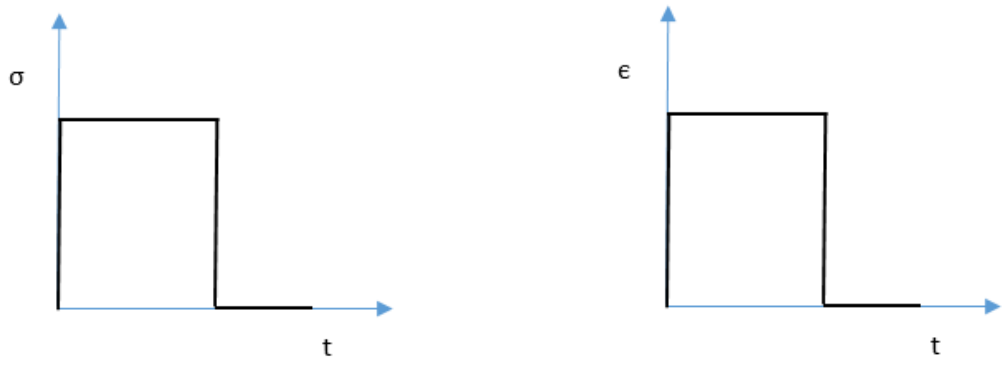

Figure 21: The elastic behaviour of the spring under a stress over time

2.7.2.2 Newton Model

The dashpot represents the viscous element in the model. The Newton model obeys the law of Newton (Ideal liquid) with the force being proportional to the rate of extension. Newtonian fluid behaviour is the same as the law of Newton in that there is a linear relationship between the shear rate and the shear strain. The behaviour of a Newtonian fluid is illustrated in Figure 22 above. Equation 5 indicates the Newton model with the $'b_1'$ as the viscosity coefficient (Mainardi & Spada, 2011).

$$\sigma(t) = b_1 \times \frac{d\epsilon}{dt} \quad (5)$$

Where:

$\sigma(t)$ = Stress as a function of time

b_1 = Viscosity coefficient

$\epsilon(t)$ = Deformation as a function of time

Deformation of the material will take place. The creep and relaxation behaviour will be visible. This behaviour can be illustrated with Figure 22.

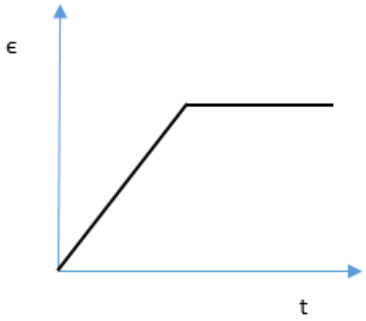

Figure 22: Viscous behaviour of a material

Figure 22 illustrates the deformation of a material as a load is applied over a certain period of time. As the load unloads the material experiences permanent deformation. Without the elastic part of the model the material won't be able to obtain its initial form.

2.7.2.3 Kelvin-Voigt and Maxwell Models

The Kelvin-Voight and Maxwell models comprise of a spring and dashpot in parallel and series, respectively. The Maxwell model illustrates a uniform distribution of stress in the system where the stress in the dashpot is equal to the stress in the spring. The total deformation (strain) within the system is thus the sum of the strain in the dashpot and spring (Gerber, 2016). The Maxwell model can be illustrated with Equation 6 (Mainardi & Spada, 2011).

$$\sigma(t) + a_1 \times \frac{d\sigma}{dt} = b_1 \times \frac{d\epsilon}{dt} \qquad (6)$$

Where:

a_1, b_1 = Creep/Relaxation coefficients

Linear deformation will take place as a load is applied to a material. As the load unloads, the material will recover slightly, but not fully due to permanent viscous deformation. Figure 24 indicates the behaviour of a material according to the Maxwell model.

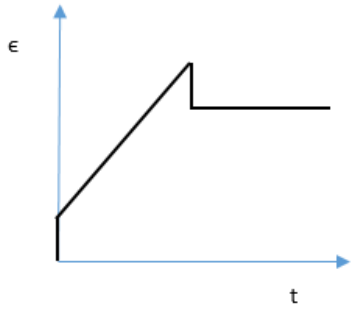

Figure 23: The Maxwell model material behaviour

The Kelvin-Voight model illustrates a uniform distribution of strain where the strain in the dashpot and spring are equal and the stress of the spring and dashpot are added together. Equation 7 represents the Kelvin-Voight model (Mainardi & Spada, 2011).

$$\sigma(t) = m\epsilon(t) + b_1 \times \frac{d\epsilon}{dt} \quad (7)$$

The Kelvin-Voight model illustrates a non-linear response as a material experiences an applied load. As the load unloads, permanent deformation will occur. Figure 24 illustrates the above-mentioned statements.

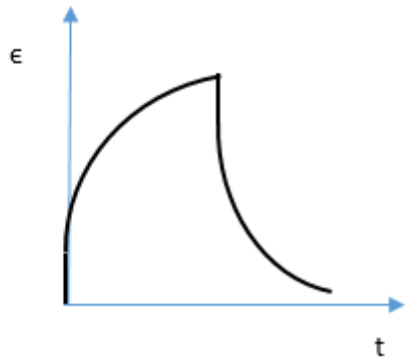

Figure 24: The Kelvin-Voight model material behaviour

The above-mentioned models are summarised in Figure 25 below.

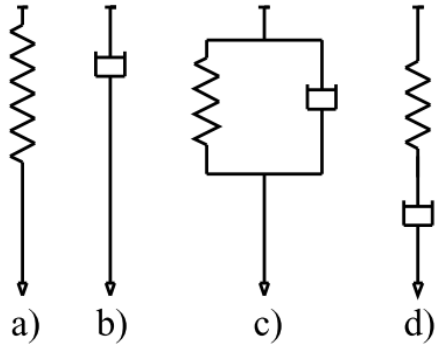

Figure 25: Demonstration of the mechanical models: a) Hooke's spring, b) Newton's dashpot, c) Kelvin - Voight model, d) Maxwell model (Mainardi & Spada, 2011)

The Kelvin-Voight model has limitations when modelling the relaxation of a material. The Maxwell model on the other hand simulates stress decay and models the relaxation of a material, but lacks regarding the creep analysis of a material. The above-mentioned models are not sufficient for analysing the behaviour of bituminous materials (Woldekidan, 2011). This phenomenon was solved by combining the above-mentioned models in series and parallel, which is known as the Burgers' model.

2.7.2.4 Burgers' Model

The Burgers' model is commonly known for analysing the behaviour of a bituminous material (Woldekidan, 2011). The Burgers' model comprises of two mechanical representations. The creep representation of the Burgers' model is devised by adding a Kelvin-Voight element in series with a Maxwell element, as seen in Figure 27 (a). The relaxation representation is devised by adding two Maxwell elements in parallel, as seen in Figure 27 (b).

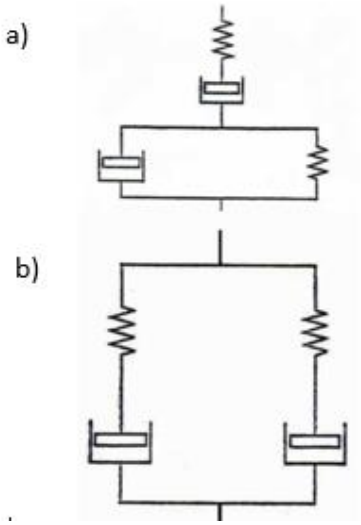

Figure 26: Two mechanical representations of the Burgers' model: a) Creep representation, b) Relaxation representation adapted from (Mainardi and Spada, 2011)

The Burgers' model is commonly used for analysing the behaviour of bituminous materials and for describing the elastic, viscous and viscoelastic components of the material. Bituminous materials' behaviour comprises of all three responses mentioned above. The disadvantage of this model is the fact that it analyses the behaviour of a material only for a limited frequency range (Woldekidan, 2011). The Burgers' model can be described with Equation 8 below, with the four parameters (a_1 , a_2, b_1, b_2).

$$\left[1 + a_1\frac{d}{dt} + a_2 \times \frac{d^2}{dt^2}\right]\sigma(t) = \left[b_1\frac{d}{dt} + b_2 \times \frac{d^2}{dt^2}\right]\epsilon(t) \quad (8)$$

Where:

a_1 , a_2, b_1, b_2 = Creep/Relaxation coefficients

2.7.3 Rheological testing

In October 1987, the Strategic Highway Research Program (SHRP) in the U.S.A analysed a few new testing methods for bituminous materials. The result of this study was a new binder specification, named Superpave (Superior Performing Pavements). The new binder specification focuses on the use of performance-based criteria for bituminous binders as well as climate considerations in the utilisation of bitumen. The specification focuses on the following distresses regarding bituminous binders (Skoglund & Peltonen, 2002):

- Low-temperature cracking of bituminous binders;
- High-temperature permanent deformation (rutting) of bituminous binders, and
- Long-term fatigue cracking of bituminous binders.

Rheological testing is done to analyse the rheological behaviour of materials and/or fluids. The viscoelastic properties of bituminous materials will be analysed in this report. Rheological testing is commonly done with the following devices (Zipf, 2016):

- Dynamic Shear Rheometer (DSR, ASTM D7175 & D7405), and

- Bending Beam Rheometer (BBR, ASTM D6648 & D7643).

The purpose of these devices is to replace the normal viscosity, penetration and ductility tests respectively (Skoglund & Peltonen, 2002). These devices measure the stresses and strains within a material, at various temperatures and frequencies, by rotating and bending material specimens. The relaxation and creep behaviour of a material can then be analysed with the results obtained from these devices.

The ageing devices that are discussed earlier, also form part of the rheological testing and analyses of bituminous binders. The Superpave performance graded (PG) binders were developed to withstand the average 7-day highest pavement temperatures in summer and the lowest measured temperatures in winter. The Superpave is thus used in order to determine the quality of the binders to resist permanent deformation and fatigue cracking (Skoglund & Peltonen, 2002).

2.7.3.1 DSR testing

This section includes the description of a typical DSR device, the most common tests done on bituminous specimens and a few results of typical seal binders.

2.7.3.1.1 Apparatus

As mentioned earlier, the DSR device, as seen in Figure 28, measures the engineering properties of a binder at various frequencies and temperatures. The frequencies at which tests are performed symbolises the travel speed of vehicles on the road (Skoglund & Peltonen, 2002). For example, one of the common frequencies to test on is at 10 rad/s which symbolises a travel speed of 80km/h.

Figure 27: Dynamic shear rheometer (Anton Paar, 2016)

The DSR device typically consists of three major parts, namely the rheometer, the controller and the computer. The rheometer includes a frame, a motor to apply the required stresses and strains on the specimen, a transducer to measure the behaviour of the specimen and a temperature control and measurement system. The controller in the rheometer is the link between the computer and the rheometer which transfers the data of each test to the computer. The computer is used to control the rheometer and to analyse the data, which is obtained from the rheometer (Skoglund & Peltonen, 2002).

2.7.3.1.2 Tests

The DSR test includes two parallel plates where the top plate rotates, and the bottom plate is stationary. The DSR rotational behaviour can be seen in Figure 29, which results in a sinusoidal form.

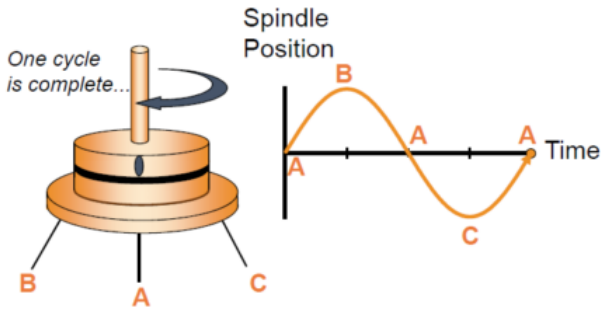

Figure 28: DSR rotation for one cycle (Technical Guideline 1, 2016)

According to the ASTM D 7175-08 (2013), the gap between the parallel plates is most commonly fixed at 1mm and 2mm. The most frequently used sizes for the parallel plates are 8mm and 25mm. The 8mm plates with a gap size of 2mm is used to determine the binder behaviour at low temperatures which typically ranges between 0˚C and 40˚C. The 25mm plates with a 1mm gap are used for testing at higher temperatures of above 40˚C (Skoglund & Peltonen, 2002). The above-mentioned temperature ranges may differ depending on the DSR characteristics.

The DSR testing at temperatures below 5˚C indicates significant compliance errors in the results of the storage modulus and loss modulus. Errors were experienced on the 8mm plates when performing low temperature testing. The SHRP developed the BBR device to evaluate the rheological properties for bituminous binders at temperatures below 5˚C. The 4mm DSR parallel plate was initially developed to test the behaviour of bituminous binders at low temperatures. After a few tests conclusions were made, based on limited data, that the data from the 4mm parallel plates can be related to the results obtained by the BBR device. Compliance errors in DSR results are not only experienced based on the type of parallel plates that are used but also in the way the sample is trimmed. Trimming of the specimen is very important during the preparation of the sample. The specimen needs to be trimmed to exactly the size of the required parallel plate before testing, otherwise it will result in inaccurate results (Farrar *et al*., 2015).

There are two types of rheometers, namely controlled stress and controlles strain rheometers. The controlled stress concept entails that the upper plate of the rheometer is set at a fixed torque to generate the oscillatory motion between points A and B, as seen in Figure 29. Controlled strain rheometers apply a sinusoidal varying strain on a speciman and the magnitude of the resulting stress is measured afterwards.

The stress and strain distribution of a bituminous sample within the DSR device can be seen in Figure 30.

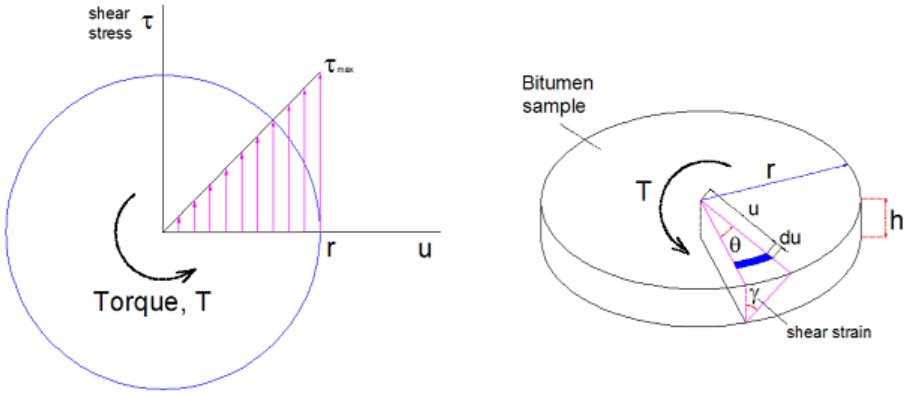

Figure 29: The stress and strain distribution of a bituminous binder sample in the DSR

The maximum shear stress is calculated as $\tau_{max} = \frac{2T}{\pi r^3}$. The maximum shear strain is calculated as $\Upsilon_{max} = \theta \frac{r}{h}$. The complex modulus is decribed as the resistance that a material has to deformation under shear load pulses. The complex modulus is to some extent an indication of the stiffness of the material and can be calculated as seen in Equation 9 (Macosko, 1994).

$$G^* = \frac{\tau_{max}}{\Upsilon_{max}} \tag{9}$$

Where:

G^* = Complex modulus

τ_{max} = Maximum applied shear stress

Υ_{max} = Maximum resulting shear strain

The complex modulus consists of two components, namely the storage modulus (G') and loss modulus ($G^{"}$). The complex notation of the above-mentioned statement can be seen in Equation 10 (Zipf, 2016).

$$G^* = G' + iG^{"} \tag{10}$$

Where:

G^* = Complex modulus

G' = Storage modulus

$G^{"}$ = Loss modulus

i = Imaginary number ($\sqrt{-1}$)

The storage modulus, also known as the elastic component, illustrates the stress-strain relationship that is in phase. The loss modulus is the out-of-phase component which is also known as the viscous component (Skoglund & Peltonen, 2002). This relationship can also be described with a graph as seen in Figure 31.

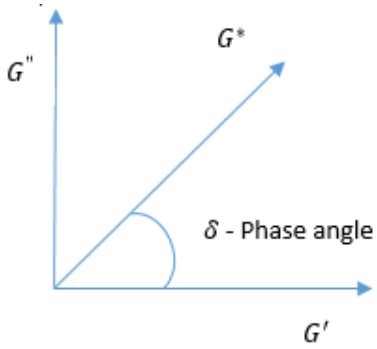

Figure 30: Viscoelastic behaviour

The phase angle is an indication of the recoverable and non-recoverable deformation of a material (Somwangthanaroj, 2010). The applied stress is proportional to the strain for an elastic solid material and for viscous liquids the stress is proportional to the rate of the strain. The phase angle of 90˚ describes an out-of-phase relation for the applied stress and strain which is known as viscous behaviour. The in-phase relation (δ = 0˚) for the applied stress and strain is known as elastic material behaviour. Bituminous materials act as a viscoelastic material where the applied stress is in and out of phase with the strain. Thus, both solid-like and liquid-like behaviour is observed and the phase angle ranges between 0˚ and 90˚ (Zipf, 2016). The phase angle can be calculated as seen in Equation 11.

$$\delta = \tan^{-1}\left(G^{"}/_{G'}\right) \tag{11}$$

Where the symbols are as descibed above.

The desciption above regarding the phase angle is illustrated in Figure 32 for a conceptual description.

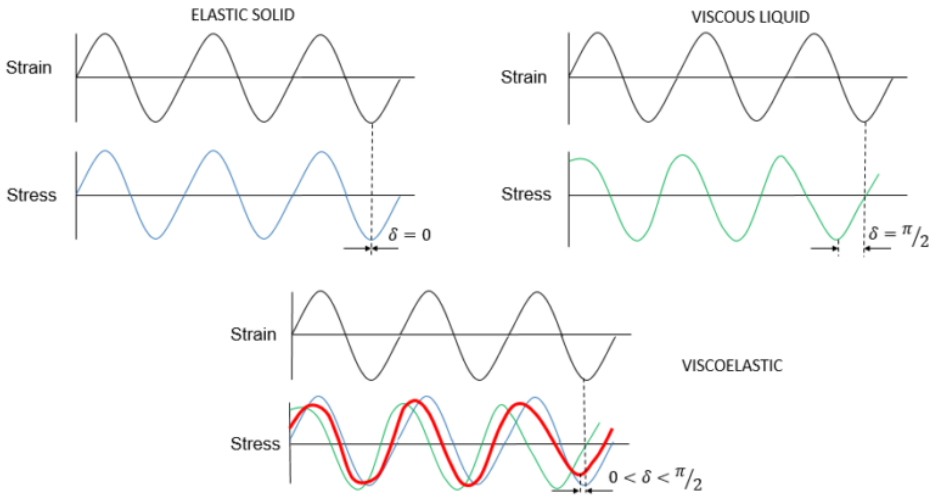

Figure 31: The phase angle for an elastic solid, viscous liquid and viscoelastic material behaviour (Zipf, 2016)

The above-mentioned parameters are obtained, as mentioned earlier, by carrying out tests on the DSR device. Tests typically done on the DSR device are as follows:

- Strain sweep test;
- Frequency sweep test, and
- Creep recovery test.

Strain sweep tests

Strain sweep tests are done to analyse the linear viscoelastic range (LVE) of bituminous binders. The LVE range indicates the strain range at which the complex modulus is 95% or more of the initial strain value (ASTM D 7175-08, 2013). In other words, the LVE range ensures a "safe region" in strain levels for further testing. Testing within the LVE range of a binder ensures accurate results. Testing on the edge of the LVE range results in too high strains and the specimen may break. The tests that follow, namely frequency sweep tests and creep recovery tests, should obey the LVE conditions by using strain values within the LVE range.

These tests can be carried out by constructing Master Curves, which will be explained in Section 1.8, with the complex modulus against various strain percentages. The testing temperature depends on the testing that needs to be done. The analyses of high, medium and low regions require testing to be done at temperatures ranging from -22˚C to 70˚C, according to the PG Binder specifications.

Frequency sweep tests

These tests should be done within the LVE range. Selecting the controlled strain option on the DSR device will ensure that the tests are done within the LVE range. The strain range depends on the type of binder, the testing temperature and the age of the binder.

The results obtained from this test ensure that a Master Curve and black diagram can be constructed for each bituminous binder at each testing temperature. The rheological parameters as described above are used to construct a Master Curve. The oscillatory loading frequency ranges typically between 1 and 160 Hz (ASTM D 7175-08, 2013). The frequency range may also influence the accuracy of the construction of the Master Curve. The typical frequency range is between 2 decades on a log-scale graph. The above-mentioned statement will be discussed in further detail in section 2.8.

Creep Recovery tests

The Multiple Stress Creep and Recovery (MSCR) test is used to determine the elastic behaviour of a bituminous binder under shear creep and recovery. This test indicates the recovery potential of bituminous binders at high temperatures to analyse the rutting on the surface of a pavement. The creep recovery test is done at two stress levels at the required testing temperature. The testing temperature will be the upper (higher) temperature for PG binders (ASTM D 7405, 2012).

Creep recovery testing is done for the following reasons (Gierhart, 2011):

- It ensures the possibility for performance-related binder specifications that are blind to modification type;
- It evaluates the rutting performance of bituminous binders, and
- It allows for a much more economical use of polymers to improve performance.

The MSCR test entails that a sample is loaded for 1sec under a constant stress of 0.1kPa followed by a constant stress of 3.2kPa for 9sec. During this time, the sample experiences properties such as relaxation and recovery. The results obtained from the MSCR test ensure that the non-recoverable creep compliance (J_{nr}) can be calculated. J_{nr} is calculated as seen in Equation 12.

$$J_{nr} = \frac{Average\ un-recovered\ strain}{Applied\ stress\ during\ creep} \qquad (12)$$

According to Gierhart (2011), it has been seen in numerous laboratories that it is possible to reduce rutting by reducing J_{nr}. Figure 33 indicates the behaviour of a creep recovery test for one cycle.

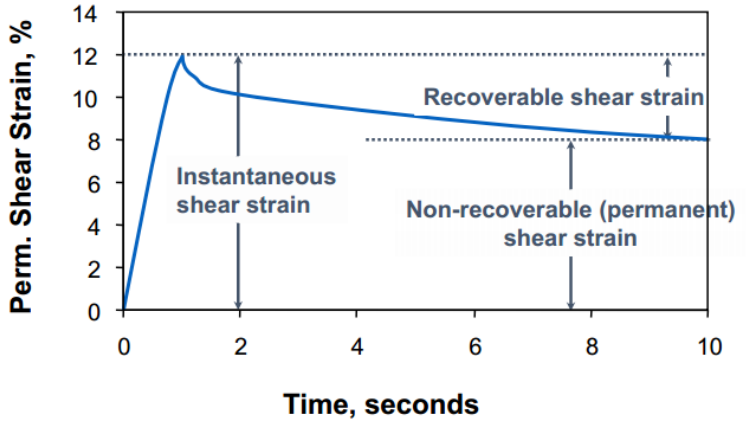

Figure 32: Creep recovery test for one cycle (Anderson, 2014)

2.7.3.2 BBR testing

The bending beam rheometer is used for rheological testing at low temperatures ranging from -36˚C-0˚C. The results obtained from the BBR test are used to analyse the susceptibility of bituminous binders to cracking at low temperatures. The bitumen specimens are moulded into a beam shape. The standard sizes and type of moulds are as discussed in the ASTM D 6648-08.

The BBR tests evaluate the flexural creep stiffness (S) and the logarithmic creep velocity (m-value) of the bituminous binders.

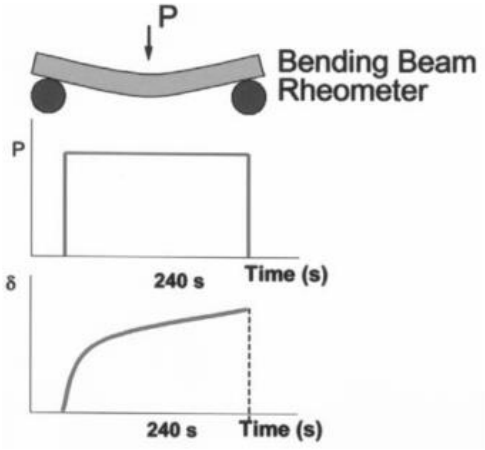

Figure 33: The deformation principle of the BBR (Sybilski, Vanelstraete, & Partl, 2004)

A constant 100g load is applied on a bitumen beam for 240s, as illustrated in Figure 34. The flexural creep stiffness ($S_{(t)}$) of the bituminous beam is measured as seen in Equation 13.

$$S(t) = \frac{P\ x\ l^3}{4\ x\ b\ x\ h^3\ x\ \delta(t)} \qquad (13)$$

Where

$S(t)$ = Creep stiffness at time t (MPa)

P = Applied constant load, 0.981 (N)

l = Distance between beam supports (mm)

b = Beam width (mm)

h = Beam thickness (mm)

$\delta(t)$ = Deflection at time t (mm)

The deflection is measured at 8, 15, 30, 60, 120, and 240 sec. The determination of the S- and m values are as described in Figure 34. The value m(t) represents the slope of the stiffness-time curve in a double logarithmic diagram. Both the S- and m values are calculated at 60sec, as illustrated in Figure 34 (ASTM D 6648-08, 2012).

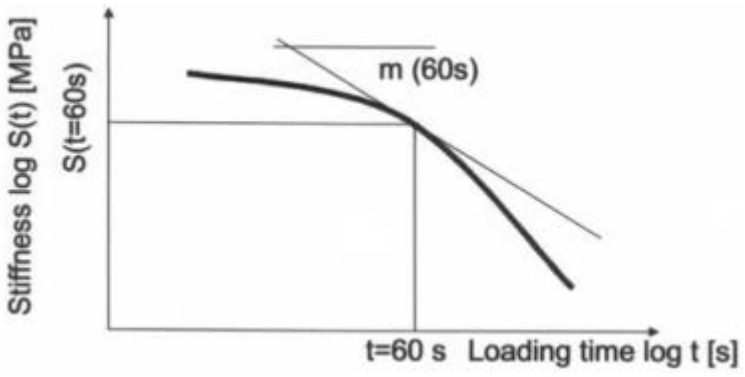

Figure 34: Determination of the S- and m values from the BBR test (Sybilski *et al*., 2004)

The mean values of S(60s) and m(60s) are used to determine the critical low temperature of the binder corresponding to S(60s) = 300MPa and m(60s) = 0.3MPa/s. The low temperature cracking specifications indicate that S must be smaller than 300 MPa and m has to be greater than 0.3 to prevent low temperature cracking (Harrigan, Leahy & Youtcheff, 1994; Rowe, 1997). Figure 36 illustrates an example of the low, medium and high chances of low temperature cracking.

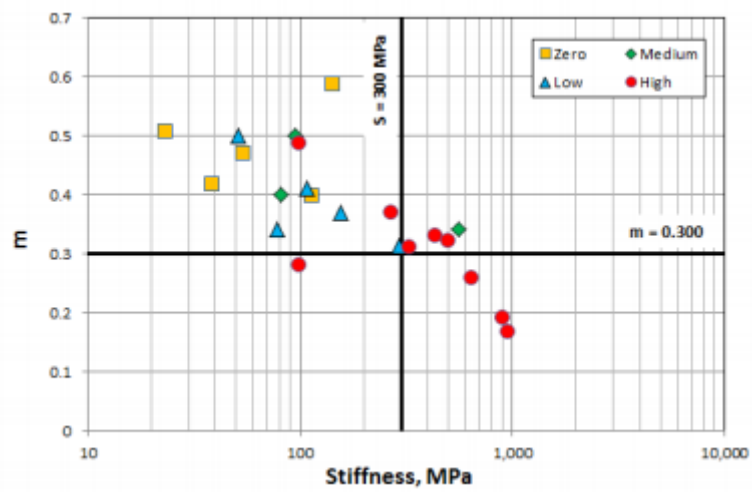

Figure 35: Low temperature cracking regions for BBR data (Rowe, 2014)

Rowe (2014) show the BBR results of several binders and temperatures. The red dots indicate a high chance of cracking for that specific binder. Some of the red dots are in the “safe zone” which show that the binder may not experience cracking at higher temperatures i.e. higher m-value and lower stiffness.

2.8 Rheological Modelling

Rheological modelling entails the study and analysis of rheological characteristics of materials. Viscoelastic materials will be analysed in this study. The data obtained from the rheological testing should be used in a way that it can be represented in a useful form. The most commonly used

mathematics and diagrams are used in this section to represent the behaviour of various bituminous materials (Claxton, 1996).

2.8.1 Master curves

Master curves are compiled with the analysis of rheological data. Master curves can be developed due to the thermorheologically simple behaviour of bituminous binders. The time-temperature superposition principle is used to construct master curves. Master curves are used to analyse the behaviour of bituminous binders at various temperatures and frequencies. The complex modulus indirectly describes the stiffness of bituminous binders.

Master curves can be constructed in either the time or temperature domain as well as from dynamic and transient loading tests. Master curves consist of the complex shear modulus versus the frequency plots (isotherms) at different temperatures along the logarithmic frequency axis (Hunter et al., 2015). The isotherms are then manually shifted to the reference temperature (T_{ref}) where the shift factor (a_T) is one, to produce a smooth master curve. Figure 37 illustrates the shifting principle of the isotherms.

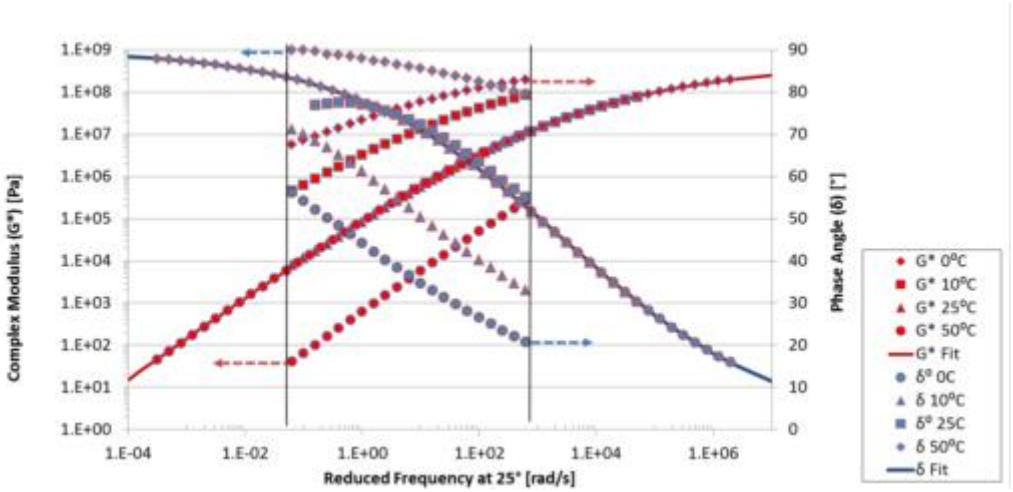

Figure 36: Master curve (Complex modulus and phase angle) example for bituminous binders where T_{ref} = 25˚C (Mukandila, 2016)

Shift factors are used to shift the isotherms to the reference isotherm. Various shift factors are developed to ensure the perfect shift of the isotherms to obtain a smooth master curve. Various shift factor methods as well as a detailed discussion regarding each, are listed below.

The frequency scale used on the logarithmic frequency axis in a master curve is known as the reduced frequency scale. The reduced frequency scale is calculated as illustrated in Equation 14 (Hunter et al., 2015).

$$\log f_r = \log f + \log a(T) \qquad (14)$$

Where,

f_r = Reduced frequency (Hz)

f = Frequency (Hz)

$a(T)$ = Shift factor

To determine the temperature susceptibility of bituminous materials the shift factor needs to be determined. Master curves are based on the time-temperature superposition principle, which can be illustrated through Equation 15 (Yusoff, 1997).

$$G(\omega, T) = G(\omega a(T), T_r) \quad (15)$$

Where,

G = Modulus (such as G', G'' *or* G^*)

ω = Loading frequency

T = Temperature

T_r = Reference temperature

The shift factor can be determined in various ways, depending on which shift factor law is used. It is important to keep in mind that the temperature dependency, which is indicated by the shift factor, does not correspond with the temperature susceptibility of bituminous materials. Temperature susceptibility is based on the change in the hardness of bituminous materials due to temperature change.

2.8.1.1 Shift factor analysis

Several researchers have found that these shift factor equations are widely used all over the world (Hunter et al., 2015; Rowe & Sharrock, 2011; Yusoff, 1997):

- Arrhenius equation;
- William, Landel and Ferry (WLF) equation;
- Kaelble equation, and
- Modified Kaelble equation.

The Arrhenius equation can be used to describe the relationship between the shift factors and relatively lower temperatures. Research done by Rowe & Sharrock (2011), by using the Arrhenius shift factor equation, illustrated that the master curve data indicated less scatter in the lower temperatures of the master curve than in the higher temperatures, therefore Arrhenius is usually applied in the low temperature range. The Arrhenius equation can be described as follows (Yusoff, 1997):

$$\log a_T = C\left(\frac{1}{T} - \frac{1}{T_{ref}}\right) = \frac{0.4347\ x\ E_a}{R}\left(\frac{1}{T} - \frac{1}{T_{ref}}\right) \quad (16)$$

Where,

a_T = Shift factor

C = A constant

T = Temperature (K)

T_r = Reference temperature(K)

E_a = Activation energy (J/mol),

R = Ideal gas constant, 8.314 (J/mol.K)

In literature, different values were reported for the constant (C). These constants are binder specific and temperature dependant. These constants may change and were reported by the following researchers regarding their results as:

i. 7680 K (Jacobs, 1995)

ii. 10920 K (Francken & Clauwaert, 1987)
iii. 13060 K (Lytton *et al.*, 1993)

The WLF equation is an alternative to describe the relationship between the shift factors and higher temperatures. Based on several DSR tests performed by Rowe & Sharrock (2011), the results obtained from master curves indicated that less scatter occurred in the data within the higher temperature region, therefor the WLF equation is normally applied in the higher temperature region. The WLF equation can be described as follows (Medani, Tech & Huurman, 2003):

$$\log a_T = \frac{C_1(T - T_{ref})}{C_2 + T - T_{ref}} \quad (17)$$

Where,

C_1, C_2 = Empirical constants

and the other variables are as defined previously.

The empirical constants need to be solved, for example within Excel. Several researchers have solved these constants and came to the following conclusions:

i. C_1 = 19 and C_2 = 92 (Lytton *et al.*, 1993)
ii. C_1 = 9.5 and C_2 = 95 (Sayegh, 1967)

These constants may change for each type of binder and need to be solved during the data analysis. The conclusions made above were from results that were obtained from the above-mentioned researchers.

Rowe & Sharrock (2011) researched in more depth how the shift factors behave and how they correlate with one another. The Kaelble equation resulted in a small change in the WLF equation. The Kaelble equation can be described as follows (Rowe & Sharrock, 2011):

$$\log a_T = \frac{C_1(T - T_d)}{C_2 + |T - T_d|} \quad (18)$$

Where,

T_d = Defining temperature (K)

The other variables are as defined previously.

The magnitude term within the Kaelble equation ensures an inflection point at the defining temperature. Due to the inflection point the shape of the hyperbolic curve changes to a sigmoidal curve (Christensen, 1992). The defining temperature is binder specific which can be calculated or solved with Microsoft Excel. Christensen (1992) discuss the method for evaluating the defining temperature.

Figure 36 indicates that the Kaelble equation is almost identical to the WLF below the inflection point. At a certain low temperature, as seen in Figure 38, the WLF function increases rapidly. The small change in the WLF equation ensures that rapid increases do not occur. The only problem with the Kaelble equation, as seen in Equation 18, is that it will be difficult to apply to data due to the reference temperature that must be taken as the defining temperature. This problem is solved by modifying the Kaelble equation by adding a constant term, which is related to the reference temperature (Rowe & Sharrock, 2011). The modified Kaelble equation can be described as seen in Equation 19 (Rowe & Sharrock, 2011):

$$\log a_T = -C_1\left(\frac{T - T_d}{C_2 + |T - T_d|} - \frac{T_{ref} - T_d}{C_2 + |T_{ref} - T_d|}\right) \quad (19)$$

The modification ensures that the root mean square error is reduced from 0.8872 % to 0.2367%, which is a much better fit in comparison to the other shift factor equations (Rowe & Sharrock, 2011).

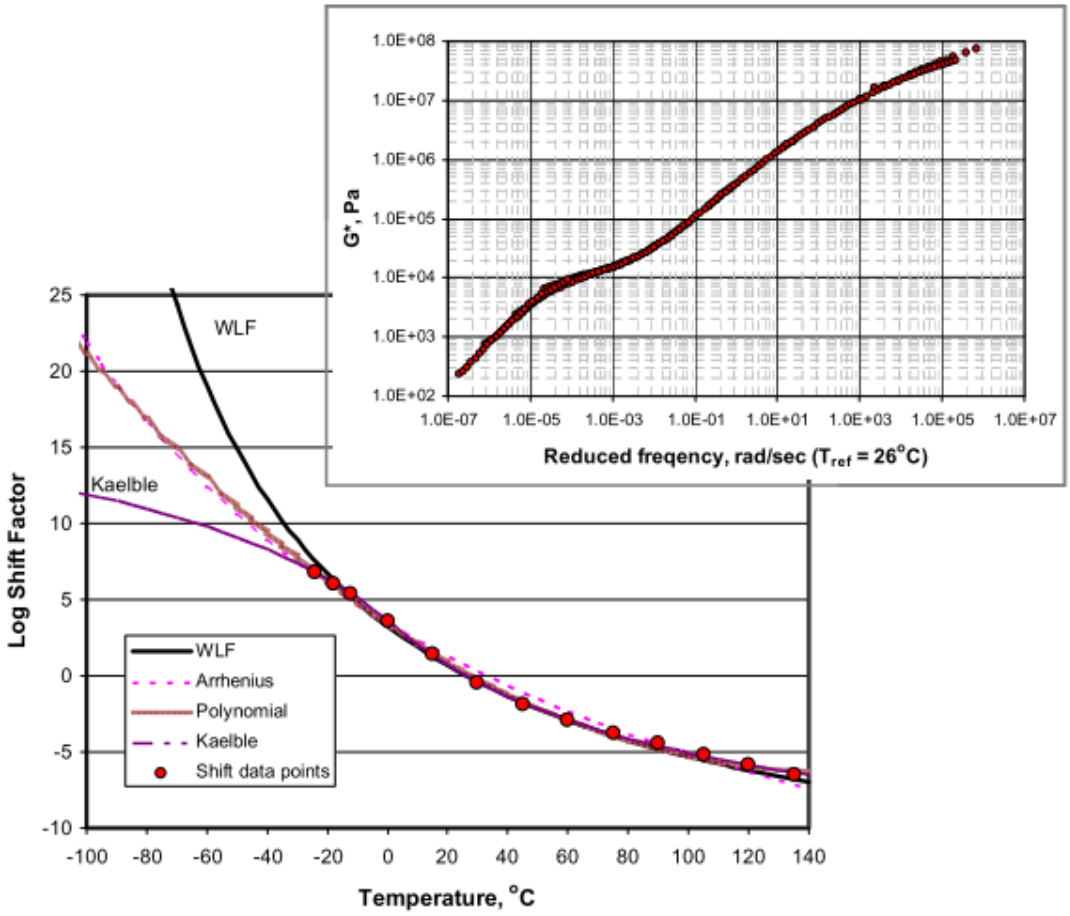

Figure 37: The modified Kaelble equation compared to the WLF and Arrhenius equations for a SBS binder at a reference temperature of 26˚C (Rowe & Sharrock, 2011)

2.8.1.2 Mathematical models

Models are widely used as a tool to describe the rheological properties of bituminous binders. During the 1960s, Van der Poel nomographs were used to analyse the rheological behaviour of bituminous binders (Shell Bitumen, 1995). Due to insufficient data accuracy, mathematical and mechanical models are developed (Yusoff *et al.*, 2010).

Mathematical and mechanical models are interdependent. The mechanical models make use of springs and dashpots, as discussed in section 1.6.2, to illustrate the linear viscoelastic properties which result in mathematical models (Yusoff *et al.*, 2010).

A few mathematical models will be discussed in the following section, which entails models on bituminous materials.

Christensen and Anderson (CA) Model

Christensen and Anderson developed this mathematical model by analysing 8 SHRP binders. They discovered that the following parameters are needed to fully characterise the properties of any bitumen (Christensen *et al.*, 1992):

- Steady-state viscosity (η_o): Coefficient of viscosity under linier flow conditions.
- Glassy modulus (G_g): The value of the complex modulus at high frequencies and low temperatures. The glassy modulus is binder and temperature dependant and ranges between 0.6 and 1.5 GPa for most bituminous binders. A glassy modulus value of 1 GPa can be assumed for most engineering purposes.
- Crossover frequency (ω_c): The frequency at the point where the loss and storage moduli are equal and tan δ = 1. The crossover frequency can be associated with a stiffness parameter where the consistency of a binder is measured at a selected temperature and is binder specific.
- Rheological index (R): The difference between the dynamic shear complex modulus and the glassy modulus at the crossover frequency and is proportional to the broadness of the relaxation spectrum.

The above-mentioned parameters are summarised visually in Figure 39.

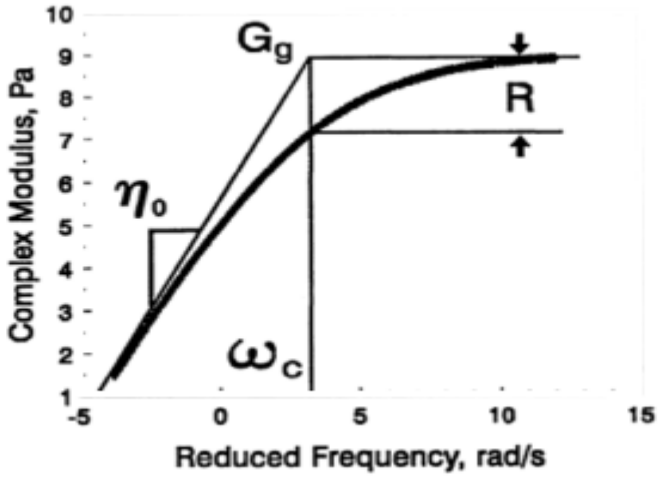

Figure 38: The definition of the CA Model (Anderson *et al*., 2008)

For the CA model the following mathematical function, Equation 20, is used to illustrate $|G^*|$: (Yusoff *et al*., 2010)

$$|G^*| = G_g \left(1 + \left(\frac{\omega_c}{\omega}\right)^{\frac{(\log 2)}{R}}\right)^{-\frac{R}{\log 2}} \quad (20)$$

Where the parameters are as defined earlier. The phase angle can be represented as follows in Equation 21:

$$\delta = \frac{90}{\left(1 + \left(\frac{\omega_c}{\omega}\right)^{\frac{(\log 2)}{R}}\right)} \quad (21)$$

Where the parameters are as defined earlier. The combination of Equation 20 and 21 define the R - value as seen in Equation 22 (Anderson et al., 2011a):

$$R = \frac{(\log 2) x log\left(\frac{|G^*|}{G_g}\right)}{log\left(1 - \frac{\delta}{90}\right)} \quad (22)$$

Where the parameters are as defined earlier. Equation 22 was found to be very useful, but the data was difficult to obtain at a phase angle of 90˚. The R-value is a measure to indicate the cracking behaviour of a binder. The Rheological Index correlates well with the Glover-Rowe (G-R) parameter as well, which will be explained later in this report.

It was found by several researchers that the use of the CA model resulted in a lack in the fit of the master curve, as seen in Figure 40, at high and intermediate temperatures. That said, the CA model is more suitable for unmodified binders with an s-shaped master curve than it is for polymer modified binders (PMB) (Asgharzadeh *et al.*, 2013). The CA model is therefore recommended for applications in the stiffness (G*) range greater than 100kPa.

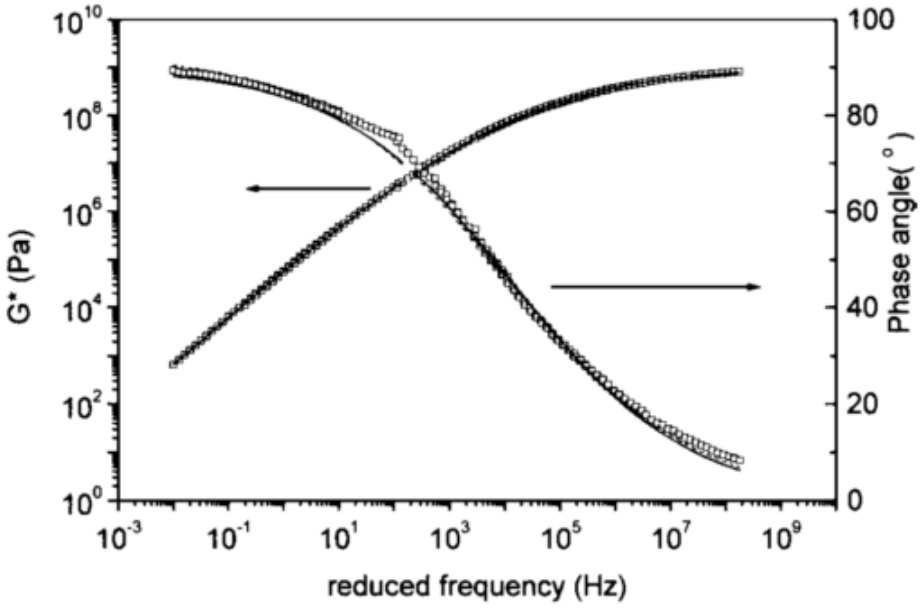

Figure 39: Master curve construction with the use of the CA model (AC - 1 with linear SBS binder) (Da Silva *et al.*, 2004)

Christensen, Anderson and Marasteanu (CAM) model

In 1999, Marasteanu and Anderson experimented with the variables of the CA model to improve the fitting of the master curve, at higher and lower temperatures, for a variation of binders. The improved CA model, known as the CAM model, attempts to improve the fitting of the master curve for both modified and unmodified binders. By combining the Havriliak and Nagami Model with the CA model the complex modulus can know be defined as seen in Equation 23 (Da Silva *et al.*, 2004; Yusoff *et al.*, 2010):

$$|G^*| = G_g\left(1 + \left(\frac{\omega_c}{\omega}\right)^v\right)^{-\frac{w}{v}} \quad (23)$$

Where v = log2/R and the other parameters are as defined earlier. The parameter 'w' depends on the converging tempo of the G* data and the asymptotes, which include the 45˚ asymptote and the G_g asymptote. The phase angle in the CAM model is defined as seen in Equation 24 (Yusoff *et al*., 2010):

$$\delta = \frac{90w}{\left(1 + \left(\frac{\omega_c}{\omega}\right)^{v}\right)} \qquad (24)$$

Where the parameters are as defined earlier.

Marasteanu and Anderson (1996) evaluated the difference between the CA and the CAM model by looking at the rheological change in 38 modified and unmodified binders. The difference in the data between the two models was between 10 and 35 percent (Yusoff *et al*., 2010). Theoretically, the CAM model provides a better fit in comparison to the CA model. Silva *et al*. (2004) also analysed the difference between the CA and CAM model, as seen in Figure 41.

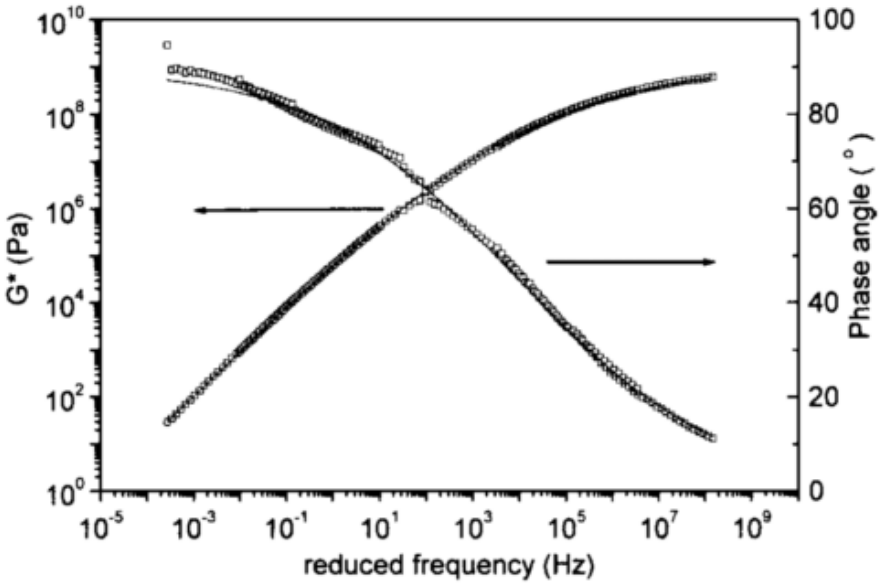

Figure 40: Modelling by using the CAM model (Da Silva *et al*., 2004)

The complexity of bituminous materials can be seen in Figure 41, which includes the same binder as seen in Figure 41. The behaviour of the modified binder at a high temperature is very complex. Figure 41 indicates that the fit of the master curve is not smooth at the lower temperatures and lower frequencies due to the complexity of modified binders.

Generalised Logistic Sigmoidal (GLS) Model

The Sigmoidal Model was initially developed to analyse the rheological behaviour of asphalt mixtures. Rowe *et al*. (2008) modified the Sigmoidal Model and generalised the model to get a more accurate description of the properties of asphalt mixtures. The generalised model is also known as the Richards Model. The GLS model is also applicable to bituminous binders (Rowe *et al*., 2008). The parameters within the GLS Model are described in Figure 42.

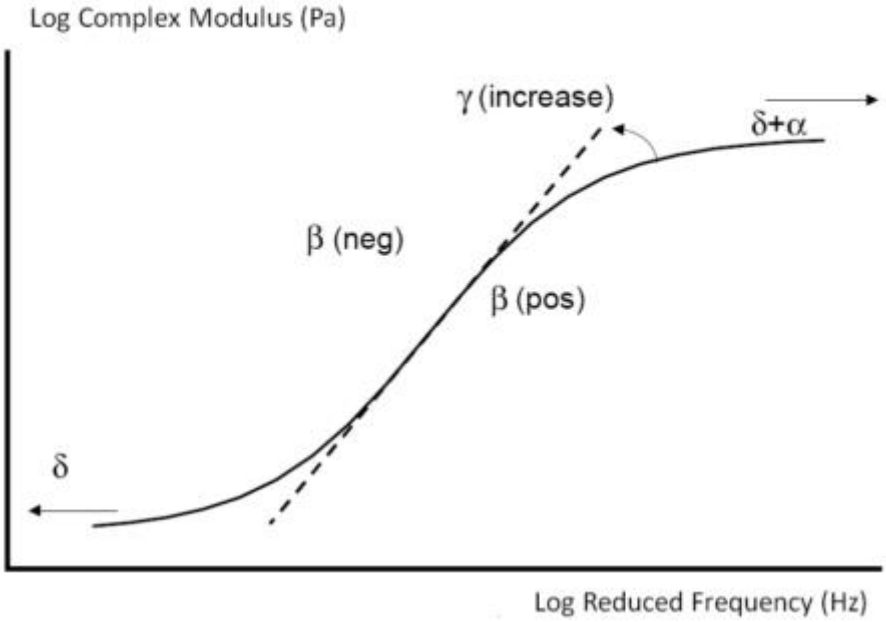

Figure 41: Parameter description of the GLS Model (Yusoff *et al*., 2010)

The 'β' and 'γ' describe the shape of the curve between the position of the inflection point and the asymptotes. The inflection point can be determined from $10^{(\beta/\gamma)}$. The 'α' indicates the distance between the asymptotes, as seen in Figure 42. The complex modulus is defined in Equation 25 in accordance to the GLS Model (Rowe *et al*., 2008):

$$log|G^*| = v + \frac{\alpha}{\left([1 + \gamma e^{(\beta+\gamma(\log(\omega)))}]^{1/\gamma}\right)} \quad (25)$$

Where the parameters are as defined earlier. As mentioned earlier, the 'γ' describes the shape of the master curve and when 'γ' results in the value one, the GLS model becomes the standard Sigmoidal Model as seen in Equation 26 (Rowe *et al*., 2008):

$$log|G^*| = v + \frac{\alpha}{(1 + e^{(\beta+\gamma(\log(\omega)))})} \quad (26)$$

Where the parameters are as described earlier.

2.8.2 Black Space Diagram with the Glover-Rowe (G-R) parameter

The Black Space diagram is used to analyse various material properties and for the evaluation of pavement cracking. Transverse cracking and block cracking are the two most common types of damage due to thermal cracking. Transverse cracking mostly occurs during seasonal change, early in the winter. Block cracking is difficult to predict and is believed to occur in older pavements where the binder is highly oxidised (Rowe *et al*., 2005).

The Black Space diagram is described by compiling a graph with the Complex Shear Modulus (G*) and the Phase angle (δ), as discussed in Section 1.6.3. An example of a Black Space diagram can be seen in Figure 43.

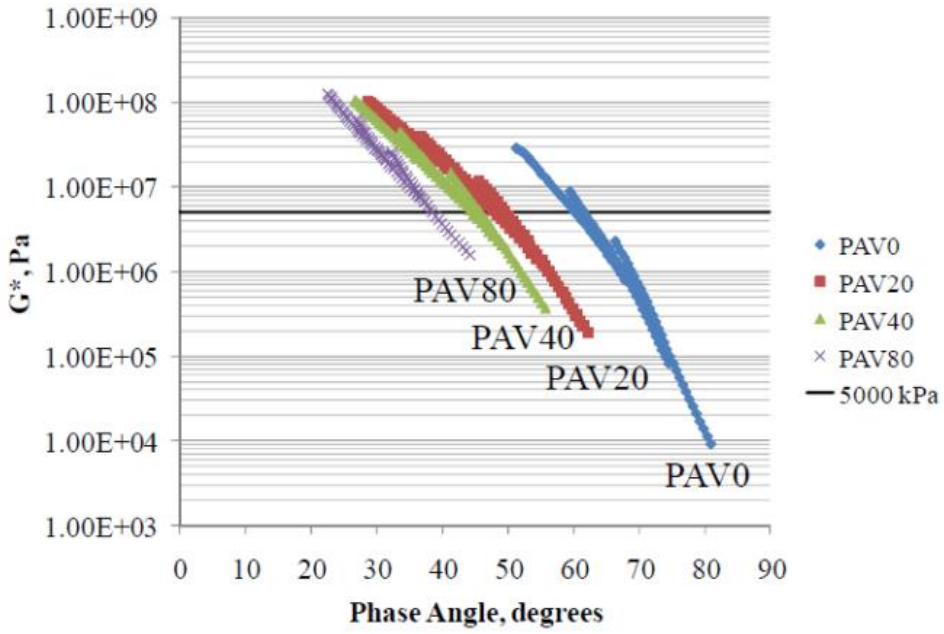

Figure 42: Black Space Diagram of a PAV aged PG 64 - 28 binder of 0, 20, 40 and 80 hours (Zvirblis *et al.*, 2014)

Figure 43 indicates the way in which the elastic behaviour of a binder increases as it ages. At a G* value of 5000 kPa, a stiffer binder will result in a lower phase angle (Zvirblis *et al.*, 2014).

The DSR parameter $\left(G'/(^{n'}/_{G'})\right)$ can be calculated with the use of the complex modulus (G*) and the phase angle (δ). Rowe showed in a prepared discussion that the DSR parameter can be expressed as $G^{*}(\cos(\delta)^{2}/\sin(\delta))$. The DSR parameter is generally measured at a temperature of 15˚C and a frequency of 0.005 rad/s. Several researchers experienced that the slow loading rate influenced the simplicity of the testing procedure (Anderson et al., 2011). The researchers suggested that the same values could be obtained by taking the measurement at 44.7˚C at a frequency of 10 rad/s.

The age of the binder increases as the DSR parameter increases. The above-mentioned behaviour results in a decrease in the ductility of a binder. The limiting values of the G-R parameter on the Black Space diagram is as follows (Rowe *et al.*, 2017):

- A G-R parameter of 180 kPa indicates damage onset, and
- A G-R parameter of 600 kPa indicates significant cracking.

The above-mentioned theory can be summarised by plotting a Black Space diagram. These limits are based on results from previous research done on bituminous binders for asphalt. The limits for seal binders are not defined yet and may differ for research done on seal binders. Figure 44 illustrates the Black Space diagram with the G-R cracking limits as well as the direction of the G-R result as binders age.

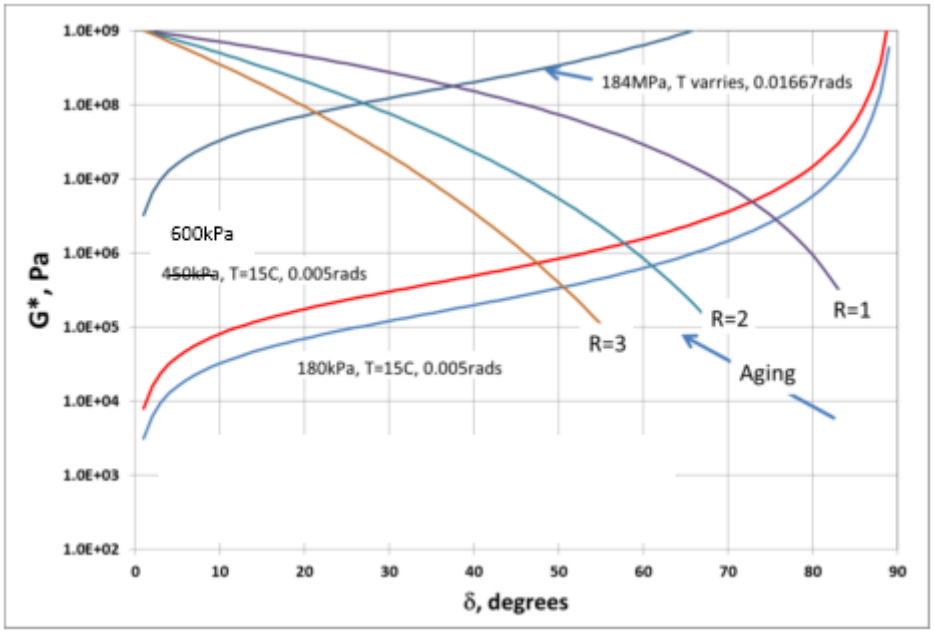

Figure 43: Black Space diagram with the G-R cracking limits (G. Rowe, 2014)

The G-R parameter data of the complex modulus and the phase angle at a reference temperature of 15˚C and a frequency of 0.005 rad/s can easily be obtained from DSR tests. Figure 43 show the direction of the G-R parameter as the binders age. This behaviour is observed by Rowe (2017) and many other researchers for asphalt binders. The results for seal binders is limited and more research has to be done to come to a conclusion for seal binders in terms of the G-R parameter.

2.8.3 The ΔT_c Parameter

The ΔT_c parameter is determined from the BBR testing procedure, as discussed in Section 2.7.3.2, and is temperature independent (Anderson et al., 2011a). ΔT_c comprises of the difference between the critical temperature where S (60) = 300MPa ($T_{c,S}$) and the critical temperature where m (60) = 0.3 ($T_{c,m}$). The ASTM D 6648-08 is used to determine the stiffness's and m-values for each binder.

The result of the ΔT_c parameter indicates if the binder is S-controlled or m-controlled. S-controlled behaviour occurs when $T_{c,S}$ result is larger than the $T_{c,m}$ result and the other way around for m-controlled behaviour. S-controlled behaviour result in a positive ΔT_c value which generally indicate better performance.

According to Anderson *et al*. (2011), it is sufficient using multiple temperatures with interpolation rather than extrapolation to determine the critical temperatures. The ductility of a binder decreases as ΔT_c increases. Figure 44 indicates the way in which ΔT_c is influenced after the ageing procedure.

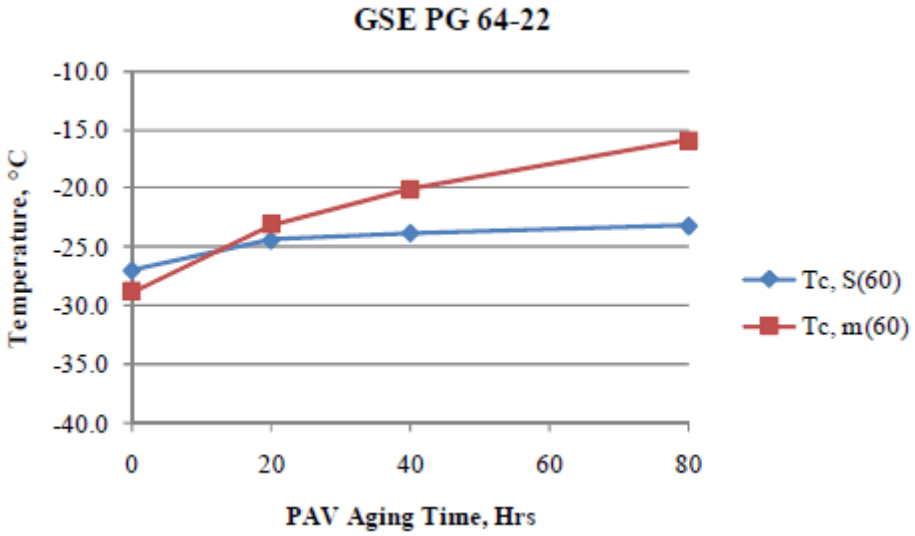

Figure 44: The effect of PAV ageing at critical temperatures (Anderson et al., 2011a)

Figure 45 indicates that the critical temperatures increase as the ageing time increases. It is noticeable that $T_{c,m}$ increases more rapidly, in comparison to $T_{c,S}$, which represents a loss in the relaxation properties of the asphalt binder.

Anderson *et al*. (2011) observed, through his research, that the G-R parameter correlates well with ΔT_c. The Texas A&M research identified a cracking boundary for the G-R parameter corresponding to 3cm ductility for the 600kPa limit and 5cm ductility for the 180kPa limit. The G-R parameter resulted in 9.0E-04 and 3.0E-03 MPa/s corresponding to the cracking boundary values at 15 °C and 0.005 rad/s. Figure 46 illustrates the above-mentioned statements and show that as the G-R parameter increases the ΔT_c temperature increases.

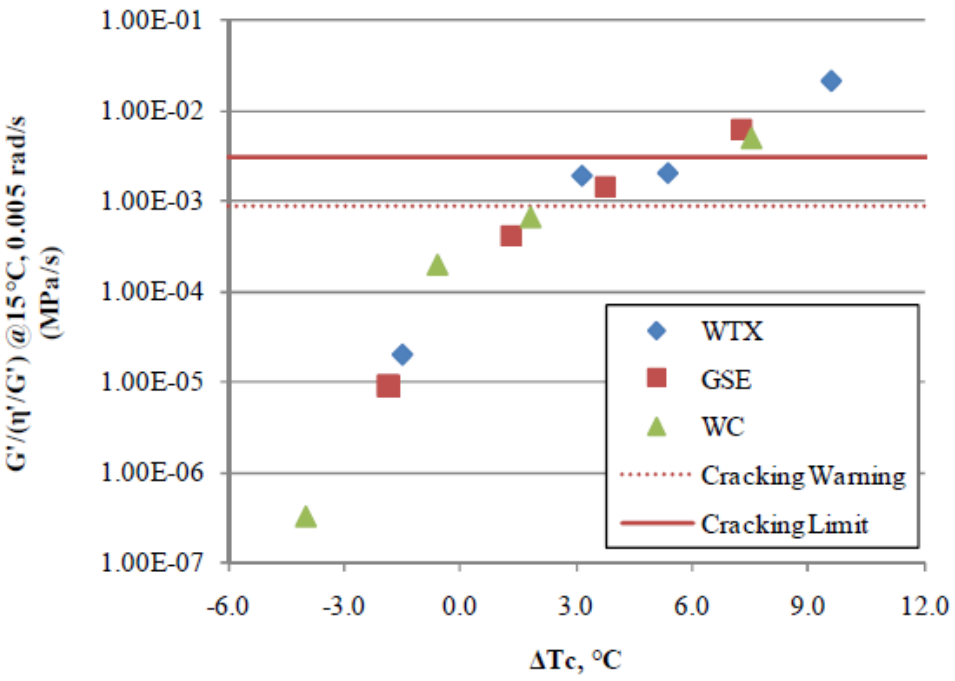

Figure 45: The relationship between the G-R parameter and ΔT_c (Anderson et al., 2011a)

2.8.4 Viscous to Elastic Transition (VET) Temperature

The VET temperature (T_{VET}) is defined at the point where the elastic component (G') of the complex shear modulus is equal to the viscous component (G") i.e. $\delta = 45^{o}$ (Migliori *et al.*, 1999). Widyatmoko (2005) states that the higher penetration grade binders result in lower VET temperatures compared to the lower penetration grade binders. The lower the VET temperature the more viscous the binders are at low temperatures. French researchers discovered, after several site observations in France, that a phase angle of 45^{o} is related to surface cracking (Widyatmoko, 2005).

Widyatmoko *et al*. (2002) reported after a series of laboratory assessments that the complex modulus can be determined from the VET temperature i.e. G^*_{VET} at a frequency of 0.4Hz. A frequency of 0.4Hz is commonly used in the UK as specified in SHW clause 956 for DSR testing which simulates slow moving traffic (Standards for Highways, 2008). The trend between G^*_{VET} and T_{VET} was found to be unique for bituminous binders at various ageing conditions (Widyatmoko *et al.*, 2004). This was found to be a useful tool to evaluate changes in the properties of bituminous binders at different ageing conditions.

Widyatmoko (2005) evaluated the change in the bituminous properties for a 15pen and 50pen binder by plotting G^*_{VET} against T_{VET}. The ageing conditions entailed the Rolling Thin Film Oven (RTFO) and the High-Pressure Ageing Test (HiPAT).

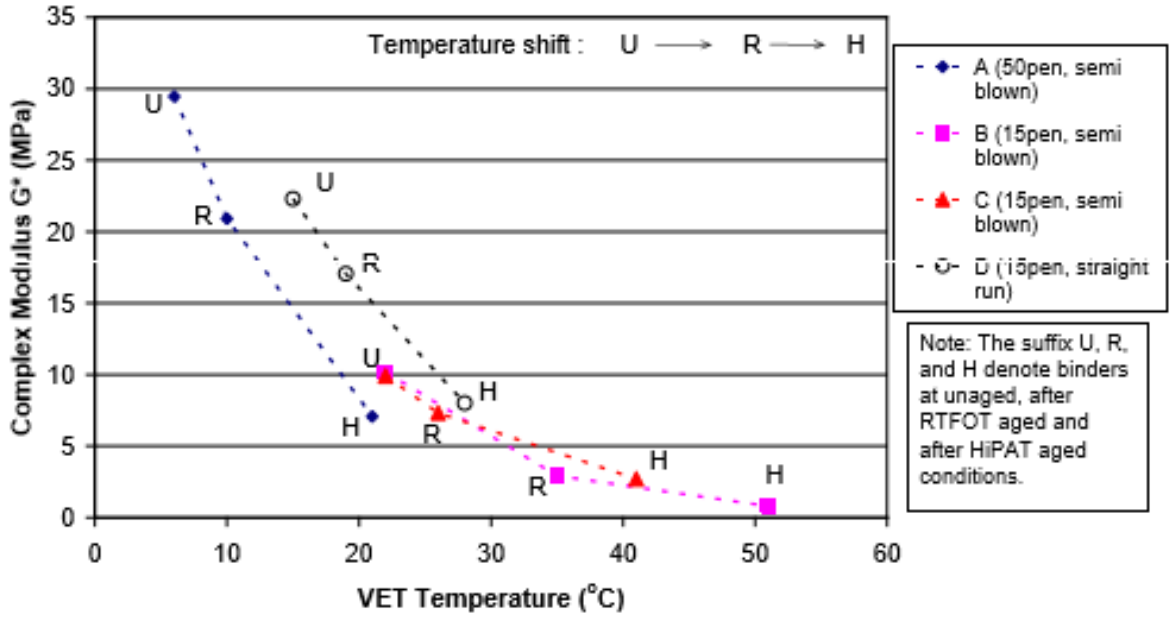

Figure 46: G*VET at 0.4Hz for different ageing conditions (Widyatmoko, 2005)

The results in Figure 46 show that as the age of the binders increase T_{VET} increases and G^*_{VET} decreases. It was found that as the binders age the plot of each binder moves from the left to the right axis. Widyatmoko (2005) found that higher grade binders show high T_{VET} values and low G^*_{VET} values. The viscous to elastic transition principle is binder grade dependent. The binders which result in a low G^*_{VET} value and high T_{VET} value generally indicates poorer performance. Widyatmoko (2005) states that for UK conditions the lower low VET temperatures and High G^*_{VET} values indicate a greater resistance to cracking and ageing.

Widyatmoko (2005) concluded that with the available data it was possible to compile a tentative specification for bituminous binders to minimise the crack susceptibility of the binders. The tentative specification is as follows:

- 15pen binders: VET temperature (0.4 Hz) < 35˚C and G*VET (0.4 Hz) > 5 MPa, and
- 50pen binders: VET temperature (0.4Hz) < 20˚C and G*VET (0.4 Hz) > 10 MPa.

Widyatmoko (2005) suggests that further work has to be done to validate the above specification.

2.8.5 BBR data to DSR data

The conversion of BBR data to DSR data is essential to evaluate the change in the rheological characteristics of bituminous binders over the entire temperature range (very low to high temperatures). Rowe *et al* (2011) investigated advanced techniques to develop master curves from BBR data.

The relaxation modulus, $E_{(t)}$, must be determined to correlate the data with DSR data. Firstly, the $S_{(t)}$ master curve must be compiled before the relaxation modulus can be determined (Yusoff *et al*., 2010). The CAM model indicated the best results, compared to the other mathematical models, by using two sets of BBR data (Rowe *et al*, 2011).

The relaxation modulus can be determined by using the Hopkins and Hamming (1957) method. This method provides a numerical solution to the convolution integral to convert BBR creep compliance to the relaxation modulus. Firstly, the compliance $D_{(\xi)}$ $\left(D_{(\xi)} = {}^{1}/_{S_{BBR\,(\xi)}}\right)$ must be calculated with the CAM model. The convolution integral can be calculated as follows (Rowe *et al*, 2011):

$$\int E_{(\xi)} D(t - \xi) dV = 1 \tag{29}$$

Where the integral starts at zero, $E_{(\xi)}$ is the relaxation modulus at reduced time (ξ) and 't' is the physical loading time. The Hopkins and Hamming method is illustrated in Equation 30.

$$E(t_{n+\frac{1}{2}}) = \frac{t_{n+1} - \sum_{i=0}^{n-1} E\left(t_{n+\frac{1}{2}}\right)[f(t_{n+1} + t_i) - f(t_{n-1} - t_{i+1})}{f(t_{n+1} - t_n)} \tag{30}$$

Where

$$f(t_{n+1}) = f(t_n) + \frac{1}{2}\,[D(f(t_{n+1}) + D(t_n)][t_{n+1} - t_n]$$

The $f(t)$ time at zero is set to zero. The relaxation modulus is then solved with Equation 29 and 30. This method is complex but by taking the inverse and using it as the relaxation modulus may cause inaccurate results. Figure 47 indicates the relevance of the statement mentioned above. The error in the results of the inverse compliance increases when the material becomes more viscous (Rowe *et al*, 2011).

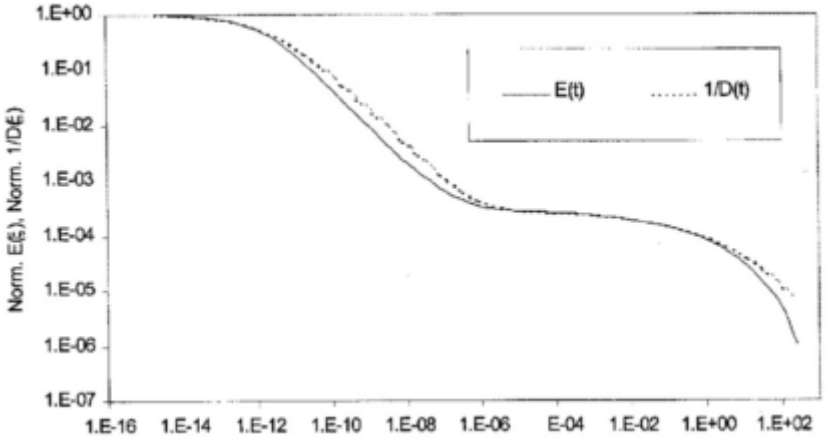

Figure 47: A comparison of the inverse compliance to the relaxation modulus of polyisobutylene (Rowe *et al*, 2011)

2.9 Summary and conclusions

The PG binder specifications are currently compiled for bituminous binders. The focus of this study is to evaluate the performance of seal binders and to evaluate the results with the current specifications for asphaltic binders.

Seals in general consist of bituminous binder and aggregate. The bituminous binder provides the viscoelastic properties in surfacing seals. The environmental forces and traffic loadings influence the performance of seals. The performance within the seal structure decreases due to damage that is mostly caused by the ageing of the binder and moisture on the seal surface. The damage within seals is known as loss of stone (adhesive failure) and cracking (cohesive failure).

The literature review discusses the fundamental concepts regarding the characterisation of bituminous seal binders in detail. These concepts are also summarised as follows:

Composition of seals: A seal consists mainly of bituminous binder and aggregate. The bitumen binds the aggregate together and ensures waterproofing. The viscoelastic properties of the bituminous binder ensure that the seal can withstand the repetitive loadings of traffic as well as environmental factors. The characteristics of the binder such as the complex modulus and phase angle are tested with the DSR and BBR device to evaluate the response of the seal.

Factors affecting seals: The volumes of traffic, the speed and weight of each type of axle together are considered factors that have an influence in the performance of seals. The design of the pavement structure is another factor to consider. The type of material and pavement structure need to be designed according to the environmental conditions and traffic type for each environment. The type of binder and aggregate are then chosen to satisfy the design constraints.

Ageing of seals: Bitumen ageing occurs due to changes in temperature and weather conditions. One of the reasons for the loss in cohesion properties of bituminous binders is due to binder ageing. The simulation of binder ageing is divided into two phases namely long-term ageing and short-term ageing. Short-term ageing occurs during the construction phase and long-term ageing during the pavement life. Short-term ageing represents the loss of volatiles and long-term ageing represents the oxidation process of bituminous binders. The short-term ageing is done on the RTFO device and long-term ageing on the PAV device.

The short-term ageing procedure is normally done on asphalt binders as they experience plant ageing. Seals do not experience plant ageing and short-term ageing is thus not necessary/applicable. This report will cover the short-term aged behaviour of seals for research purposes.

Rheology of bituminous binders: Several studies have shown that modified bitumen behaves as a non-newtonian fluid and exhibits shear thinning behaviour. One of the reasons for this behaviour is due to the alignment of the neighbouring macromolecules within the binder. Shear thinning occurs when the viscosity of a material decreases as the shear rate increases. The characteristics of bituminous binders such as the complex modulus and phase angle are measured with the DSR device.

Rheological modelling of bituminous binders: The modelling of bituminous material entails the construction of master curves using the thermorheologically simple behaviour of bituminous materials. Master curves are based on the Time Temperature Superposition (TTS) principle. The master curves are constructed with the use of shift factors and mathematical models. Based on the results of various researchers, as mentioned in Section 1.8, the Kaelble shift factor indicates the lowest percentage error by constructing master curves over the temperature range of -30˚C and 70˚C. Together with the Kaelble shift factor the CAM model is used to minimise the percentage error of the data. Minimal research has been done to indicate which mathematical model satisfies which condition the best, but for the PG specifications it was decided to use the CAM model.

The data obtained from the BBR device must be analysed to construct a master curve. To obtain a complete master curve, with the above-mentioned temperature range, the BBR data must be converted to the corresponding parameters obtained by the DSR device.

Chapter 3: Research Methodology

'*The journey of a thousand miles begins with one step*'-Lao Tzu

3.1 Introduction

The rheological properties of selected seal binders require analyses in their original condition and simulated ageing conditions. Bituminous seal binders were selected from various refineries to evaluate the susceptibility of the binders to ageing. Bituminous specimens were prepared at the bitumen workshop of Stellenbosch University. The testing and conditioning of the specimens were done at various laboratories in the Western Cape, based on the availability of testing equipment. Equipment from the following institutions was used:

- Stellenbosch University;
- Much Asphalt, and
- Colas.

This chapter includes the following details related to the laboratory testing:

- The type of tests that had to be done for this study;
- The testing procedures and equipment that were used, and
- The steps that were under taken to analyse the variables pertinent to this study.

3.2 Materials used for this study

The selection process regarding seal binders for this study, was carefully considered, given the range of binders used in seal technology. The seal binders for this study include the most used seal binder in each region in South Africa. The selection of the seal binders was done by the collective input of Stellenbosch University, SANRAL and industry. The bituminous binders, refineries and regions that were used for this study are as follows:

Penetration Grade bitumen:

- 70/100 from Colas in the Western Cape, sourced from Chevron refinery;
- 70/100 from Colas in KwaZulu - Natal, sourced from Sapref refinery;

Polymer modified bitumen:

- S-E1 (SBS) from Colas in the Western Cape, sourced from Chevron refinery;
- S-E1 (SBS) from Colas in Gauteng, sourced from Natref refinery;
- S-E1 (SBS) from Tosas in Gauteng, sourced from Natref refinery;
- S-E2 (SBS) from Bituguard in KwaZulu-Natal, sourced from Sapref refinery;
- S-E2 (SBS) from Tosas in Gauteng, sourced from Natref refinery;
- Recovered SC-E1 (SBR) from Colas in the Western Cape, sourced from Chevron refinery.

3.3 Testing and conditioning devices

The testing devices that were used for this study are as follows,

- The Anton Parr MCR 302 Dynamic Shear Rheometer (DSR), and
- The Cannon Thermoelectrically-cooled Bending Beam Rheometer (TE - BBR).

The DSR device is used to analyse the rheological properties of the selected bituminous binders at intermediate temperatures. The BBR device is used to analyse the stiffness of the bituminous binders at various low temperatures.

The conditioning devices used in this study are as follows:

- Rolling Thin Film Oven (RTFO), and
- Pressure Ageing Vessel (PAV).

The conditioning devices are used to age the binders to present the rheological properties for short- and long-term ageing, in other words, the age during the construction process of the binder and the age of the in-service life of the binder. The RTFO device is used for the short-term ageing process and the PAV device for the long-term ageing process. Although there is no RTFO ageing for seals the standard procedure was followed as required by the ASTM.

Chapter 2 includes a detailed description on all the devices mentioned in this section.

3.4 Experimental design

The experimental design of this study includes the objectives of the testing procedure, the materials used as well as the testing and conditioning devices. The experimental design flow chart is included to summarise the steps taken to test and condition the bituminous specimens, as indicated in Figure 48.

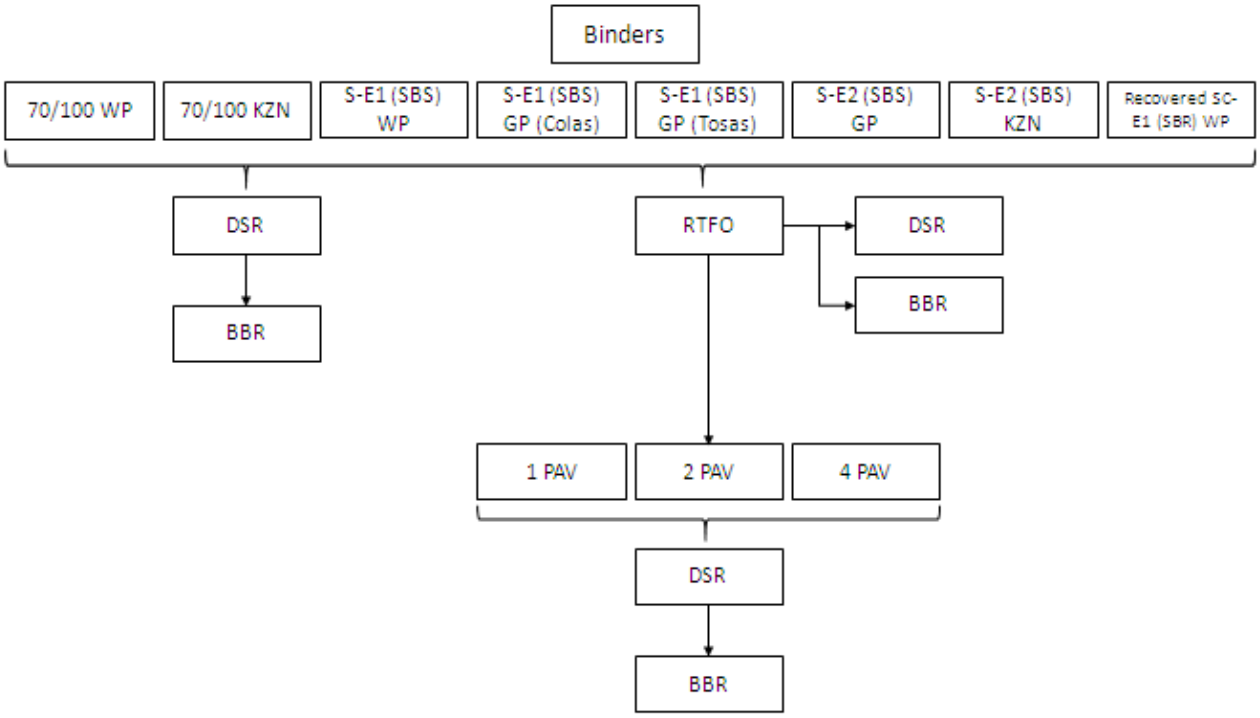

Figure 48: The experimental flow chart

The rheological terminology and testing devices that are mentioned in this section are briefly explained in Chapter 2 of this report.

3.4.1 Objectives of the testing procedure

The primary objective of this report is to analyse the rheological properties of the selected seal binders to evaluate the susceptibility of the binders to ageing, as mentioned in Section 3.2. The original condition and simulated ageing conditions of the seal binders are analysed to investigate the effect of the degree of ageing on the rheological properties of seal binders. The results are analysed to identify realistic limits that will provide the necessary performance properties. These findings are compared to the current Performance Grade specifications of South Africa to get a correlation between the seal binder performance and the asphalt binder performance.

The objective of this analysis can be subdivided into the following:

- The presentation of a clear set of compliance criteria to ensure the optimal selection of bituminous binders for specific applications.
- The assessment of the rate of ageing of the seal binders using rheological parameters, and

- The evaluation of typical seal binder properties using rheological parameters and indices as well as their comparative reliability in determining performance, linked to their correlation with the current Performance Grade Specifications for asphalt binders.

3.5 Test procedure

The test procedure included the preparation of the bituminous samples. As soon as the samples were prepared the laboratory ageing of the binders could be performed. After the binders were aged the DSR testing and BBR testing could be performed. This section is summarised in Figure 49:

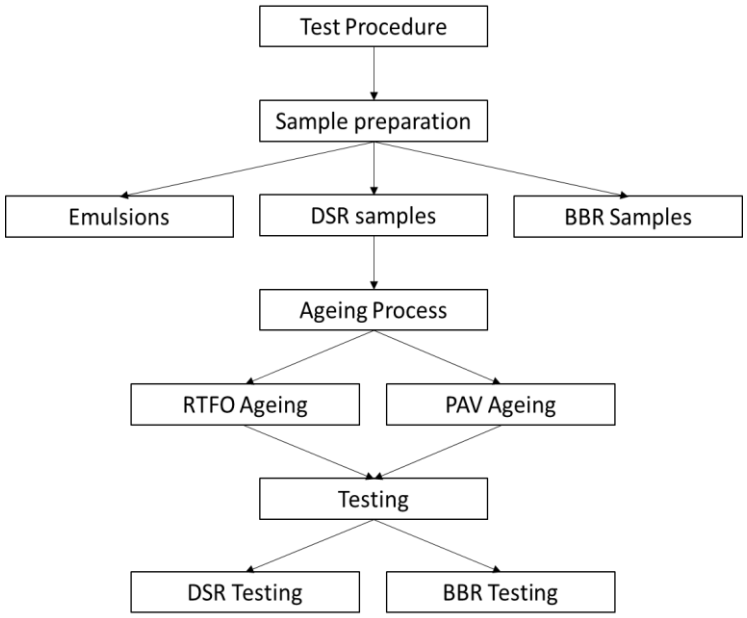

Figure 49: Test procedure diagram

3.5.1 Sample Preparation

The bituminous binders used for this project were obtained from refineries all over South Africa. The binders were procured in 5 litre drums, as seen in Figure 50. To decrease the number of times the binders were heated in an oven, small glass containers were bought, as presented in Figure 50. The unmodified bituminous binders were heated once at 160˚C for an hour and a half. The modified binders were heated at 170˚C for an hour and a half and then poured into the small glass containers. The glass containers were then used as needed and were only heated once after it was poured from the 5 litre drums.

Figure 50: Bituminous binder drums and small glass containers

3.5.1.1 Emulsions

One of the binders used for the PG binder research was, as mentioned earlier, the emulsion SC-E1 with SBR from the Western Cape region. The recovery procedure used to obtain the binder residue from the emulsion in this study, was sourced from the Netherlands (Dzwig, 2011). During the study, after the recovery of binder from the emulsion, an update on the recovery of bituminous binders occurred (Dzwig, 2011). The recovery procedure entailed the following:

- The recovery plates with a minimum surface area of 0.04 m^2.
- The binder height, within the steel plates, with a maximum interval of 35mm.
- The recovery procedure including a 24h recovery at a temperature of 65°C.

During the recovery process, the binder height of 35mm was used and the bitumen formed a layer on the surface which decreased the rate of evaporation. An interval height of 10mm was tested afterwards, which ensured no layer to form on the surface. Figure 51 indicates the recovery process the oven.

Figure 51: Bituminous emulsion during the recovery process

After the recovery process, the binder needed to follow a stabilisation process. This process entailed a further 24 hours in the oven at 85°C. Figure 52 shows the preparation of the recovered and stabilised binder in the glass containers.

Figure 52: The recovered and stabilised bituminous binder in glass containers

3.5.1.2 DSR samples

The DSR testing for this study entailed the use of the 8mm and 25mm parallel plates. The selected parallel plates were sufficient for the type of binder and testing temperatures of this study. Firstly, the DSR sample moulds were prepared, as seen in Figure 53. The rubber mould mix was left to dry for 24 hours before the binder samples were prepared.

Figure 53: DSR sample mould preparation

Once the DSR moulds have set sufficiently, the binders could be poured into the moulds and left to cool to room temperature before being tested in the DSR device, as seen in Figure 53.

3.5.1.3 BBR beams

BBR beams can be prepared in two different ways. The BBR beams can be prepared in aluminium moulds and silicone rubber moulds (ASTM D 6648-08, 2012). In this study both preparation methods were used.

Before the BBR beams could be made, the binders had to be conditioned with the short-term ageing simulation process, namely RTFO. The ageing process will be explained in the next section. After the RTFO conditioning the short term aged binders were then poured into the glass containers. Only 20ml of binder was poured into the glass containers to ensure minimal heating of the binder. One BBR beam could be made from one glass container containing 20ml of RTFO residue. Some sort of short-term ageing takes place each time the binder is heated which influences the performance of the binder. Figure 54 indicates the two preparation methods for the BBR beams.

Figure 54: BBR silicon rubber and aluminium moulds

The silicon rubber mould was used for seven of the eight binders used in this study. The aluminium mould had to be used for the SC-E1 (SBR) recovered emulsion. The recovered residue had very large particles, even after it was heated, which cooled down too fast for a beam to form in the silicon rubber mould, as seen in Figure 55.

Figure 55: Recovered SC-E1 (SBR) binder in the silicon rubber mould

The aluminium mould was then used to prepare the BBR beams for the recovered emulsion SC-E1 (SBR). The ASTM D6648 states that after the binder is poured into the aluminium mould, the top part of the mould, with the overfilled binder, must be trimmed. Figure 56 indicates the trimming of the binder with a heated spatula as well as the result after trimming.

Figure 56: SC-E1 (SBR) during and after the trimming process

After the bituminous binder is poured into the moulds the binder must be allowed to cool to room temperature for between 45 and 60 minutes. Prior to testing the BBR beams in the BBR device the moulds containing the binder must be placed into a cold chamber for no longer than 5 minutes. After 5 minutes in the cold chamber the beams should be taken out of the moulds. Checking of the physical measurements was done before the beams are placed into the BBR device. The ASTM D6648 provides interior dimensions for each beam i.e. 6.35 ± 0.05mm wide and 12.7 ± 0.05mm deep. The beams are then placed into the BBR device for between 45 and 60 minutes at the testing temperature, as seen in Figure 57.

Figure 57: BBR beams in the BBR device

3.5.2 Ageing process

The ageing process entailed the preparation of the DSR samples and BBR beams for five ageing conditions. The binders used in this study were tested, for both the DSR samples and BBR beams, at original state, RTFO conditioning, 20hr PAV conditioning, 40hr PAV conditioning and 80hr PAV conditioning. The ageing apparatus used in this study is as explained in Chapter 2.

3.5.2.1 RTFO

The short-term ageing of the binders differs for unmodified and modified binders. The unmodified binders' procedure entailed the usage of glass containers whereas the modified binders entailed the usage of brass containers, as seen in Figure 58. The glass containers were filled up to 50 grams of unmodified binder each and the brass containers were filled up to 35 grams each for the modified binders. The binder amount for both the modified and unmodified binders in the containers guarantees a film thickness which ensures the binders' contact with the airflow. The procedure for the RTFO conditioning for both the modified and unmodified binders differs (ASTM D 2872-04, 2004).

Figure 58: The glass and brass containers used for the short-term ageing process

3.5.2.2 PAV

The PAV conditioning consists of two procedures as explained in the ASTM D6521. The PAV consists of a pressurising unit and a degassing unit, as seen in Figure 59.

Figure 59: The PAV and degassing unit

The PAV procedure entails the filling of steel plates for each of the binders, as seen in Figure 60. Each plate may not contain more than 50 grams of bituminous binder. The PAV device holds up to 10 steel plates.

Figure 60: The PAV steel plates filled with bituminous binder

After the 20hr, 40hr and 80hr PAV conditioning the binders must be degassed. The steel plates containing the bituminous binder must be heated to 168˚C before it can be poured into the degassing cups, as seen in Figure 61. The degassing of the bituminous binders is done at 168˚C for 30 minutes. After the binders are degassed the DSR samples and BBR beams can be made.

Figure 61: Steel cup of the degassing unit

3.5.3 Testing

The testing procedures for both the DSR and BBR devices are summarised in this section of the report.

3.5.3.1 DSR testing

The testing procedure for this study entailed testing on the DSR and BBR device. The DSR testing carried out in this study is as summarised in Figure 62 for all five ages of the bituminous binders mentioned in Section 3.2. The DSR testing was done according to the ASTM D7175.

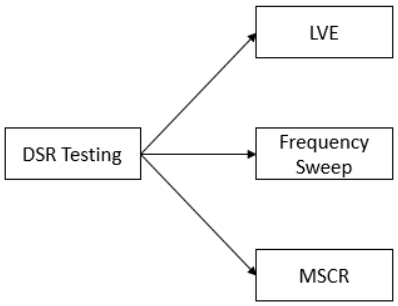

Figure 62: DSR testing procedure

The strain sweep (LVE) testing was done as summarised in Table 3. The temperatures at which the LVE range of the binders were tested were sufficient for the unaged and RTFO samples. The higher temperature testing allows the LVE range of the binders to be achieved without a problem. At the lower temperature, all the ages of all the binders applied to the requirements of the ASTM. The strain curves for the Unaged and RTFO binders show good results within the 1% to 4% strain region. The PAV1, PAV2 and PAV4 binders have a smaller LVE range and showed good results within the 1% to 2% strain region. The low temperature strain sweep data can be seen in Annexure A.

Table 3: LVE testing conditions

LVE		
Parallel Plate (mm)	8	25
Temperature (˚C)	10	70
Frequency (rad/s)	10	
Strain (%)	1 - 12	

The frequency sweep tests were done for all the binders mentioned in Section 3.2. The frequency sweep tests were done as specified in Table 4.

Table 4: Frequency Sweep testing conditions

Frequency Sweep							
Parallel Plate (mm)	8		8 & 25		25		
Temperature (˚C)	10	15	25	35	45	60	70
Frequency (rad/s)	0.251; 0.316; 0.398; 0.501; 0.63; 0.794; 0.999; 1.26; 1.58; 1.99; 2.51; 3.16; 3.98; 5.01; 6.3; 7.94; 9.99; 12.6; 15.8; 19.9; 25.1						
Strain (%)	1						

The selected temperature range for the frequency sweeps for this study included the low, intermediate and high temperature for the PG Binder specifications. The frequency sweep testing for the 8mm parallel plate and the 25mm plate overlap at temperatures 25 ˚C and 35 ˚C. The overlapping of the data ensures that the data can be correlated to one another.

The testing frequency range was selected to ensure data over a maximum of two decades. The frequency range was as specified in the current SANRAL specifications and the data in this range can be related to research done in the past.

The strain at which the frequency sweeps were done is binder specific and may differ for each long-term ageing condition. The strain at which the unaged and RTFO binders were tested is as specified in Table 4.

The Multiple Stress Creep and Recovery (MSCR) tests are done at the high temperatures of the PG Binder Specifications (ASTM D 7405, 2012). The temperatures used for this study are as indicated in Table 5. The MSCR test is done to determine the elastic and viscous components' response of a binder under shear creep and the recovery of the binder at the stresses mentioned in Table 5. The MSCR test is useful to identify the susceptibility of a binder to permanent deformation under repetitive loadings. The result of this test identifies the creep compliance of each binder at each ageing condition. The creep compliance can then be correlated with the results obtained by the frequency sweeps and BBR testing.

Table 5: MSCR testing conditions

MSCR			
Parallel Plate (mm)	25		
Temperature (˚C)	58	64	70
Shear Stress (kPa)	0.1/3.2		

3.5.3.2 BBR testing

Firstly, before testing, the BBR temperature and load calibration needed to be done to ensure accurate results. After the beams of the BBR device were prepared, they were placed in the BBR cooling bath for between 45min and 60min, as mentioned in Section 3.5.1.3. The BBR beams were tested at temperatures ranging from -6˚C to -30˚C with -6 ˚C intervals.

As explained in Chapter 2, after the test was completed the deflection, stiffness and m value were given at certain time intervals, as seen in Figure 63. The results were then used in RHEA and Excel to analyse the data.

Project :	Francois	Target Temp (°C) :	-12.0	Conf Test (GPa) :	217
Operator :	FE	Min. Temp (°C) :	-12.0	Conf Date :	05/03/2017
Specimen :	70100 KZN--12C	Max. Temp (°C) :	-12.0	Force Const (mN/bit) :	0.152
Test Time :	02:55:01 PM	Temp Cal Date :	05/03/2017	Defl Const (µm/bit) :	0.161
Test Date :	05/03/2017	Soak Time (min) :	60.0	Cmpl (µm/N) :	6.77
File Name :	17050313	Beam Width (mm)	12.70	Cal Date :	04/26/2017
BBR ID :	3833-A1816	Thickness (mm) :	6.35	Software Version :	BBRw 1.25

t Time (s)	P Force (mN)	d Deflection (mm)	Measured Stiffness (MPa)	Estimated Stiffness (MPa)	Difference (%)	m-value
8.0	984	0.262	303	302	-0.330	0.315
15.0	985	0.325	244	245	0.410	0.352
30.0	984	0.420	189	189	0.000	0.393
60.0	**986**	**0.558**	**142**	**142**	**0.000**	**0.433**
120.0	986	0.765	104	104	0.000	0.474
240.0	987	1.082	73.6	73.7	0.136	0.515

A = 2.71 B = -0.193 C = -0.0675 R^2 = 0.999982

Force (t=0.0s) = 34 mN Deflection (t=0.0s) = 0.000 mm
Force (t=0.5s) = 976 mN Deflection (t=0.5s) = 0.124 mm

Max Force Deviation (t=0.5 - 5.0s) = -10, +0 mN
Max Force Deviation (t=5.0 - 240.0s) = -2, +2 mN

Average Force (t=0.5 - 240.0s) = 986 mN
Maximum Force (t=0.5 - 240.0s) = 988 mN
Minimum Force (t=0.5 - 240.0s) = 976 mN

Figure 63: Example template of the BBR test result

During testing it was recognised that some of the unaged and RTFO beams failed before the BBR test was completed. The beam did not break physically, but deflected more than 5mm. The BBR software is written in a way that it does not give any results for a sample beam that deflects more than 5mm. Figure 64 indicates the behaviour of a BBR beam during testing and after testing. The binder used in Figure 64 was an unaged binder at -6 ˚C with more than 5mm deflection which is a failed test.

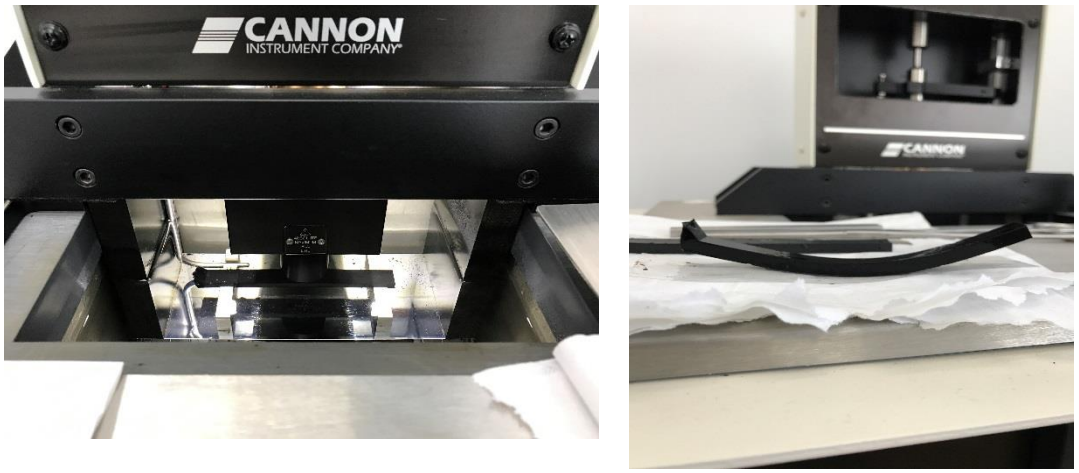

Figure 64: (Left) BBR beam during testing (Right) BBR beam after testing with 5mm deflection

3.6 Data analyses

The data obtained from the DSR and BBR devices were analysed on the Abatech RHEA software and Microsoft Excel. This section can be subdivided into the following phases, as illustrated in Figure 65:

i. Phase 1: A detailed discussion regarding the results of the rheological properties of typical seal binders obtained from the laboratory testing.
ii. Phase 2: Descriptive information regarding the RHEA software used for both the BBR data analyses and DSR data analyses. Microsoft Excel is used to analyse the merged data of the BBR and DSR data by using mathematical models.
iii. Phase 3: A description and illustration of the viscous and elastic component of the seal binders used in this study.
iv. Phase 4: The analysis procedure for the creep and recovery behaviour of the seal binders.
v. Phase 5: Descriptive and visual content regarding the influence of ageing on the Glover -Rowe parameter for typical seal binders.

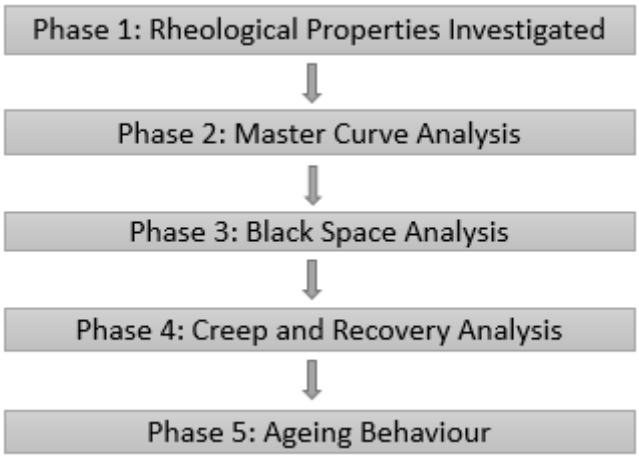

Figure 65: Section organisation

3.6.1 Rheological properties investigated

The rheological properties analysed for this study are according to the South African Performance Grade Bitumen Specifications (2016). The testing entailed the rheological properties for all binder ages (Unaged, RTFO, 20hr PAV, 40hr PAV and 80hr PAV) to investigate the age-related performance of seal binders. The investigated rheological properties are as follows:

- Storage Modulus (G');
- Loss Modulus (G");
- Complex Modulus (G*);
- Phase Angle (δ);
- Non - recoverable creep compliance (J_{nr});
- Glover-Rowe Parameter (G-R);
- Viscoelastic transition (T_{VET}, G_{VET}), and
- ΔT_cParameter.

3.6.2 Master Curve Analysis

Master Curves indicate the way in which the stiffness of each binder reacts at a certain frequency and temperature range. The visco-elastic behaviour of bituminous binders ensures that as temperature decreases the stiffness increases.

The conversion of the BBR data to the complex shear modulus was done through the RHEA software. The software uses the method of Hopkins and Hamming, as discussed in Chapter 2. The RHEA software makes use of the free-shift method, as discussed by Gordon and Shaw, to shift each isotherm to a required refence temperature (Gordon & Shaw, 1994). The reference temperature was chosen as 15˚C to ensure that the Glover-Rowe parameter can be calculated.

Chapter 4 discusses the master curve analysis of the BBR data and DSR data separately as well as the combined master curve of both the BBR and DSR data. The mathematical models (CA, CAM, CAS and DS Model) were used to plot a function through the master curve to ensure that any required data point can be calculated within the master curve temperature range. The mathematical models were compared to one another to ensure the best fit to the master curve for each bituminous binder. The mathematical models were analysed with Excel due to the limiting models of the RHEA software.

3.6.3 Black Space Analysis

The data for the Black Space diagram were obtained from the RHEA software for the combined Master curve of both the BBR and DSR data. The Black Space diagram as well as the plot of the loss modulus against the storage modulus (Cole-Cole Diagram) indicates the viscous and elastic behaviour of the binders. The amount of modifier and the age of the binder are two of numerous mechanisms that effects the binder behaviour for each property.

3.6.4 Creep and Recovery Analysis

The creep and recover data analysis were done in Excel. The creep and recovery behaviour of a binder is analysed with the non-recoverable creep compliance as well as the percentage recovery. The behaviour of each binder was analysed and compared to one another.

3.6.5 Ageing behaviour

The way in which the age of the binders influences their performance are analysed with the following:

- Master Curves;
- Black Space diagrams;
- Creep and Recovery behaviour;
- ΔT_cParameter;
- Viscoelastic transition (T_{VET}, G_{VET}), and
- Glover-Rowe parameter.

Multiple plots will be shown in Chapter 4 to indicate and compare the ΔT_cParameter and the Glover-Rowe parameter for all the binders.

3.7 Limitations

The methodology of this study had the following limitations:

i. The recovery of the emulsion in the steel plates with a binder depth of 35mm was unsuccessful. The binder in the emulsion formed a layer on the surface of the sample which limited the rate of the evaporation process in the oven. The problem was solved by carrying out the recovery with a binder depth of 10mm.

ii. During the preparation of the BBR beams it was observed that the aged binders needed to be heated to a higher temperature. The beams of the unaged binders were heated up to 160 ˚C. The aged binders heated to 160 ˚C solidify inside the BBR beam mould before the beam formed. The problem was solved by heating the aged binders to 170 ˚C before pouring it into the BBR beam moulds.

iii. After a few trial and error runs with the BBR device it was observed that the rubber moulds influence the thickness of the BBR beams. As soon as the bituminous binder set within the rubber mould the rubber mould seems to change its shape. The thickness of the BBR beams that were prepared within the rubber moulds was measured multiple times and the thickness of the beams was out of specification most of the time. With this said, it is thus important that the BBR beams must be measured when the rubber moulds are used to ensure that the thickness of the beam is within the limits of the specification.

iv. The beam measurements for the rubber moulds ranged between 6.3mm and 6.32mm compared to the measurements of the steel moulds between 6.38 and 6.4. The measurements were on the upper and bottom boundary of the specification limits.

v. The devices used for this study are not very common in South Africa. This required three different testing centres to be used for this research.

3.8 Summary

The laboratory tests were carried out as part of the PG Binder research to analyse the behaviour of surfacing seals. The current South African Performance Grade specifications summarise the requirements that asphalt binders must satisfy. The results from the tests are used to evaluate the susceptibility of the seal binders to ageing. The performance properties of the seal binders can then be used to enhance the South African Performance Grade specification limits and at the same time investigate the correlation between asphalt binders and seal binders.

The most used seal binders in South Africa were therefore used for the laboratory testing of this study. Several dummy runs were done during the DSR and BBR testing to ensure results that correlate well with one another, as shown in Chapter 4.

Chapter 4 follows which discusses the results and their interpretation.

Chapter 4: Results and Interpretation

'*The secret of getting ahead is getting started*'-Mark Twain

4.1 Introduction

This chapter covers the results and interpretation of the rheological testing done for the performance grading system of seven bituminous seal binders. The aim of this study is to investigate the age-related performance of typical bituminous seal binders in South Africa. This chapter contains the following phases:

vi. Phase 1: A detailed discussion regarding the BBR results of the seal binders obtained from the laboratory testing as well as the conversion from BBR data to DSR data.
vii. Phase 2: Provision of descriptive information regarding the RHEA software used for both the BBR data analysis and DSR data analysis. Microsoft Excel is used to analyse the merged BBR and DSR data with mathematical models.
viii. Phase 3: Description and illustration of the rheological characteristics i.e. viscous and elastic components of the seal binders used in this study.
ix. Phase 4: The analysis procedure for the creep and recovery behaviour of the seal binders.
x. Phase 5: Development of Black Space diagrams which describe the influence that ageing has on the G-R parameter and various other parameters for seal binders.

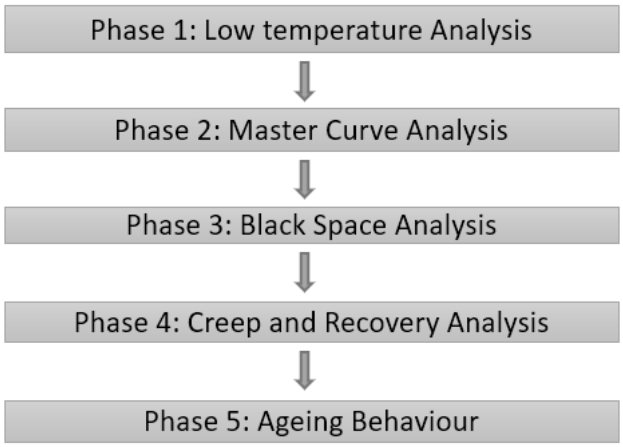

Figure 66: Chapter organisation

Chapter 4 entails the analysis of the results of only one binder. The 70/100 from the Western Cape (WP) is used to indicate the analysis procedure that is followed for all binders. The low temperature results for the emulsion that was recovered is unexplainable. It was decided that only the MSCR data for the recovered SC-E1 binder will be used. Chapter 5 discusses the comparison of the results of all seven binders.

4.2 Low Temperature Analysis

Thermal cracking is an important factor to consider when looking at the degradation of a pavement. Studies have shown that temperatures below zero cause thermal cracking that deteriorates a pavement tremendously (Clyne & Marasteanu, 2004).

The low temperature analysis was done on the BBR device. Each of the seven binders were tested at 5 ages (Unaged, RTFO, PAV1, PAV2 and PAV4) and temperatures ranging from -6˚C to -30˚C, with increments of 6˚C.

After testing the results were copied into Excel. The raw BBR results entail the degree to which a binder deflects over the testing period. Figure 67 shows the deflection over time curves of the 70/100 WP PAV1 binder at each temperature.

Figure 67: The deflection curves for the unaged 70/100 WP PAV1 binder.

The deflection curves, illustrated in Figure 67, indicate deflection behaviour as expected. As the temperature of a viscoelastic material decreases it becomes stiffer. Thus, the deflection at -24˚C must be more than the deflection at -30˚C. During the testing procedure some of the binders experienced deflections of more than 5mm due to the softness of the binder. The BBR device does not export data with deflections more than 5mm and indicates the condition of the result as failed. This may occur in the case of unmodified and unaged binders. The deflection curves of all the binders with their ages are summarised in Annexure B.

The ASTM D6648-08 describes the methods to convert the deflection to the stiffness (S) and m-value of a beam at a certain temperature. This conversion was done in Excel where the m-value and stiffness at 60 seconds for each temperature and age were summarised. With the known S and m-value at 60 seconds the ΔTc can be calculated at S = 300 MPa and m = 0.3 with interpolation. Table 6 summarises the stiffness and m-value at 60 seconds as well as the interpolated ΔTc values for each age of the 70/100 WP binder. The S(60), m(60) and ΔTc results for the rest of the binders can be seen in Annexure C. All stiffness values seen in Table 6 are in MPa.

Table 6: S(60), m(60) and ΔTc results for 70/100 WP

Unaged		
TEMP (˚C)	S60 (MPa)	m60
-6	Deflection > 5mm	
-12	218	0.378
-18	473	0.266
-24	937	0.181
-30	1285	0.104
Tc,S	-14.471	
Tc,m	-16.191	
ΔTc	1.719	

RTFO		
TEMP (˚C)	S60 (MPa)	m60
-6	Deflection > 5mm	
-12	238	0.343
-18	556	0.255
-24	858	0.185
-30	1347	0.120
Tc,S	-13.647	
Tc,m	-14.931	
ΔTc	1.284	

PAV1		
TEMP (˚C)	S60 (MPa)	m60
-6	105	0.388
-12	252	0.309
-18	488	0.231
-24	868	0.174
-30	1104	0.114
Tc,S	-13.593	
Tc,m	-12.659	
ΔTc	-0.933	

PAV2		
TEMP (˚C)	S60 (MPa)	m60
-6	118	0.347
-12	288	0.271
-18	518	0.210
-24	858	0.166
-30	977	0.126
Tc,S	-12.425	
Tc,m	-9.692	
ΔTc	-2.734	

PAV4		
TEMP (˚C)	S60 (MPa)	m60
-6	120	0.312
-12	289	0.257
-18	472	0.205
-24	918	0.167
-30	1025	0.126
Tc,S	-12.453	
Tc,m	-7.274	
ΔTc	-5.180	

DATA SUMMARY		
AGE	Tc,S (˚C)	Tc,m (˚C)
Unaged	-14.471	-16.191
RTFO	-13.647	-14.931
PAV1	-13.593	-12.659
PAV2	-12.425	-9.692
PAV4	-12.453	-7.274
AGE	ΔTc (˚C)	
Unaged	1.719	
RTFO	1.284	
PAV1	-0.933	
PAV2	-2.734	
PAV4	-5.180	

The stiffness values increase as the age of the binder increases. The m-value decreases as the temperature decreases which indicates a loss in the relaxation properties of the binder (Clyne & Marasteanu, 2004). The binders are very stiff at the lower temperature region (-18˚C, -24 ˚C and -30 ˚C) which influences the relaxation properties due to the brittleness of the binder. The slight decrease in the m-value at a certain temperature, for each age, indicates the influence that ageing has on the relaxation properties of the binder. A decrease in the m-value indicates a steeper slope, which is also an indication of the loss in the relaxation properties of the binder.

The S-controlled behaviour of the Unaged and RTFO binders ensure a positive ΔTc, which indicates that the relaxation properties of the binder are still in a good state and chances of thermal cracking are slight. The m-controlled behaviour occurs at PAV 1, 2 and 4. At this stage the relaxation potential of the binder is much less in comparison with the Unaged and RTFO binders. According the South African Performance Grade Specifications a ΔTc of larger than -5 is acceptable for a PAV1 binder. ΔTc = -5 correlates well with the 180kPa crack initiation boundary of the G-R parameter (Anderson et al., 2011b). This research indicates that the 70/100 WP binder will start forming cracks at the PAV4 state.

The correlation between the ΔTc parameter, cross-over frequency, J_{nr} and the G-R parameter can be seen later in this chapter.

4.3 Master Curve Analysis

This section entails the master curves of the converted BBR data to DSR data and the merged DSR and BBR master curves of the 70/100 WP binder. The analyses of several mathematical models are presented on each master curve for each age of the binder.

4.3.1 BBR data

The data obtained by the BBR device entails a conversion to stiffness and the m-value, as stated earlier. The stiffness-time curves were free-shifted with the Gordon and Shaw method by using the RHEA software. Figure 68 shows the stiffness-time isotherms that are free-shifted by using the RHEA software.

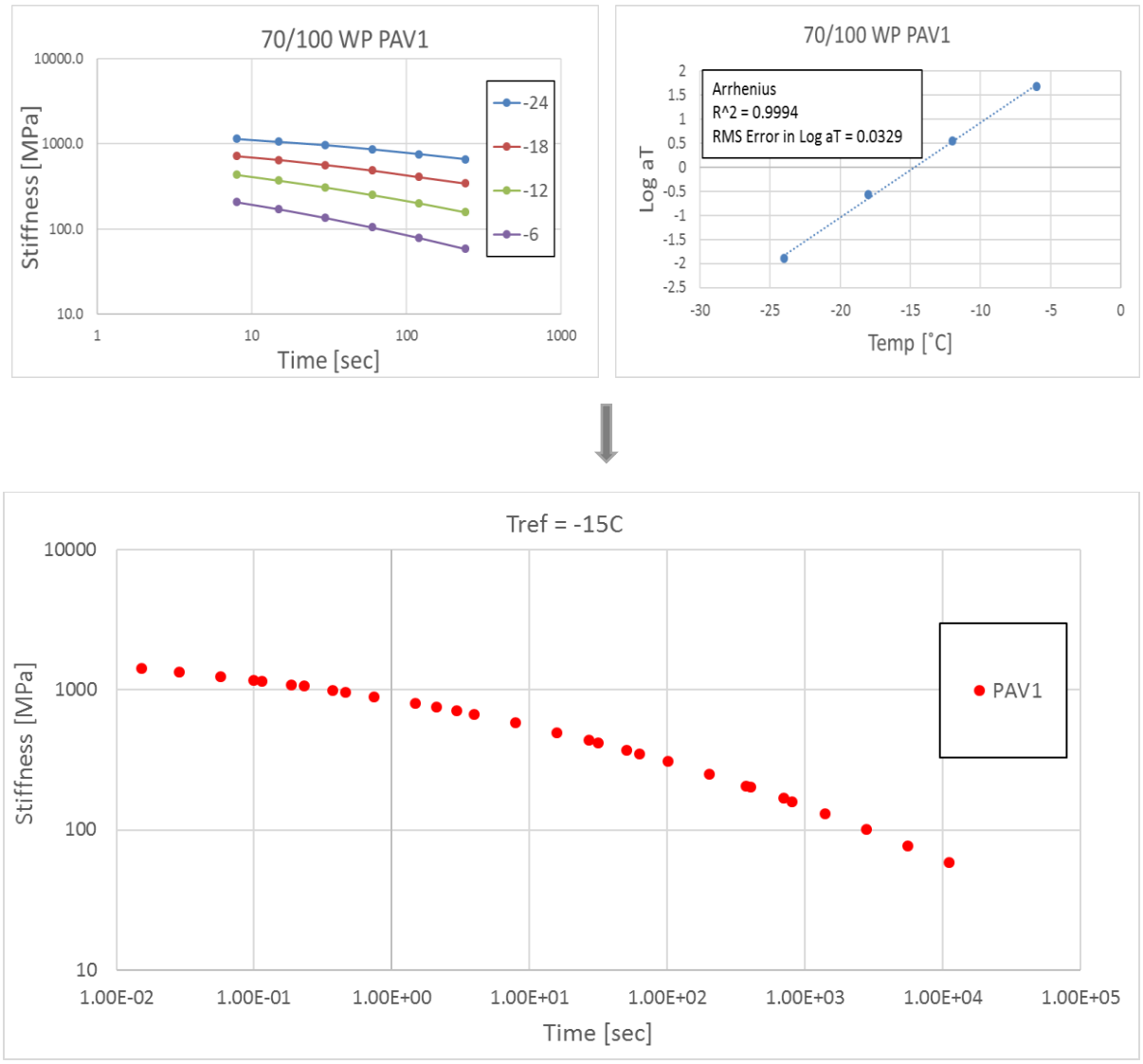

Figure 68: Free shifted stiffness isotherms for the 70/100WP PAV1 binder

The stiffness isotherms of the 70/100 WP PAV1 binder are shifted to a reference temperature of -15˚C. A reference temperature of -15˚C was chosen as it was the average of all the isotherms in most of the cases. The data for most of the binders at a temperature of -30˚C indicated inaccurate results which made the data impractical. The RHEA software fits a discrete spectrum of springs and dashpots as Maxwell models through the shifted isotherms to represent the shape of the curve. The discrete spectra model ensures that any temperature can be selected within the test temperature range.

Figure 69 indicates the shifted stiffness curves for all 5 ages of the 70/100 WP binder between the temperatures of -6˚C and -30˚C with increments of 6. Figure 70 indicates the Arrhenius fit of the BBR data for the Unaged, RTFO, PAV2 and PAV4 ages of the 70/100 WP binder. The shift-factor curve for the PAV1 data is as illustrated in Figure 68. The shifted stiffness curves for the other 6 binders can be seen in Annexure D.

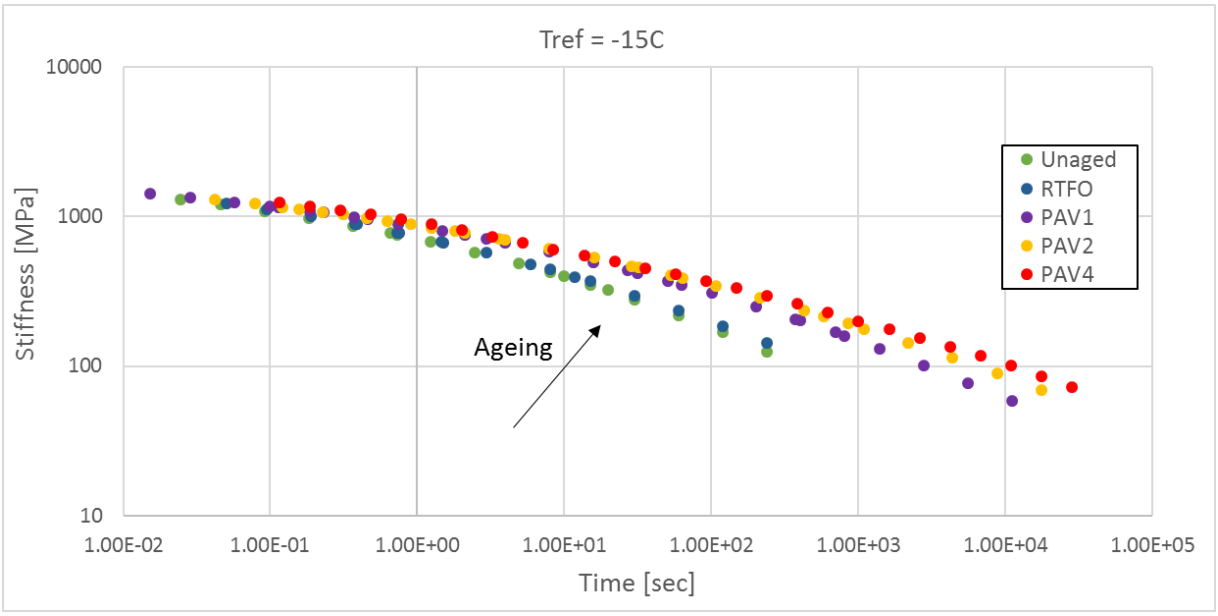

Figure 69: Free shifted stiffness curves for all ages of the 70/100 WP binder

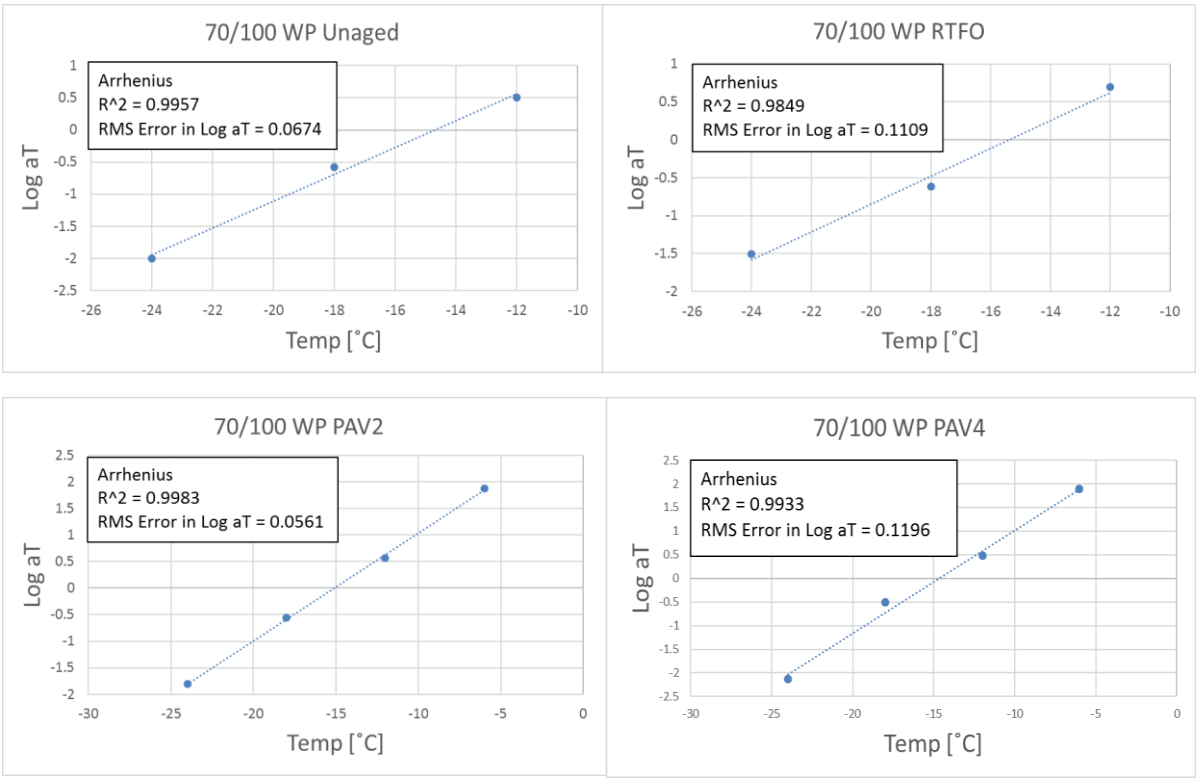

Figure 70: Shift-factor graphs that indicate the fit of the data to the Arrhenius shift-factor

The stiffness curves show the susceptibly of the binder to ageing. As the age of the binder increases the stiffness of the binder increases and the slope of the curves becomes flatter (m-value increases). The stiffness increases due to ageing that cause the binder to become stiffer and more brittle. The

slope of the curves flattens off as the age of the binder increases due to ageing that influences the relaxation properties of the binder. The binder is thus less resilient (recovery potential) after a few years in comparison to the construction period of the binder in a pavement. Figure 69 shows the point of convergence at more or less a stiffness of 3000 MPa which correlates with the glassy modulus between 0.6 GPa and 1.5 GPa of bituminous binders (Christensen *et al*., 1992).

For a master curve to be constructed with BBR and DSR data the stiffness values of the BBR data should be converted to G*. The RHEA software was used to convert the stiffness values to G* values with the use of the Hopkins and Hamming (1957) method.

4.3.2 Merged data

The merged data section entails the merged BBR and DSR data to construct master curves. The RHEA software was used to combine the BBR data and the DSR data.

The LVE range tests were done for each binder, as described in Chapter 3. The DSR tests were done at 1% strain for both the 8mm and 25mm parallel plate. The 1% strain was within the LVE range for all the binders and their ages at 10˚C, which was the coldest DSR test temperature. Figure 71 indicates the unshifted BBR and DSR data for the 70/100 WP PAV1 binder.

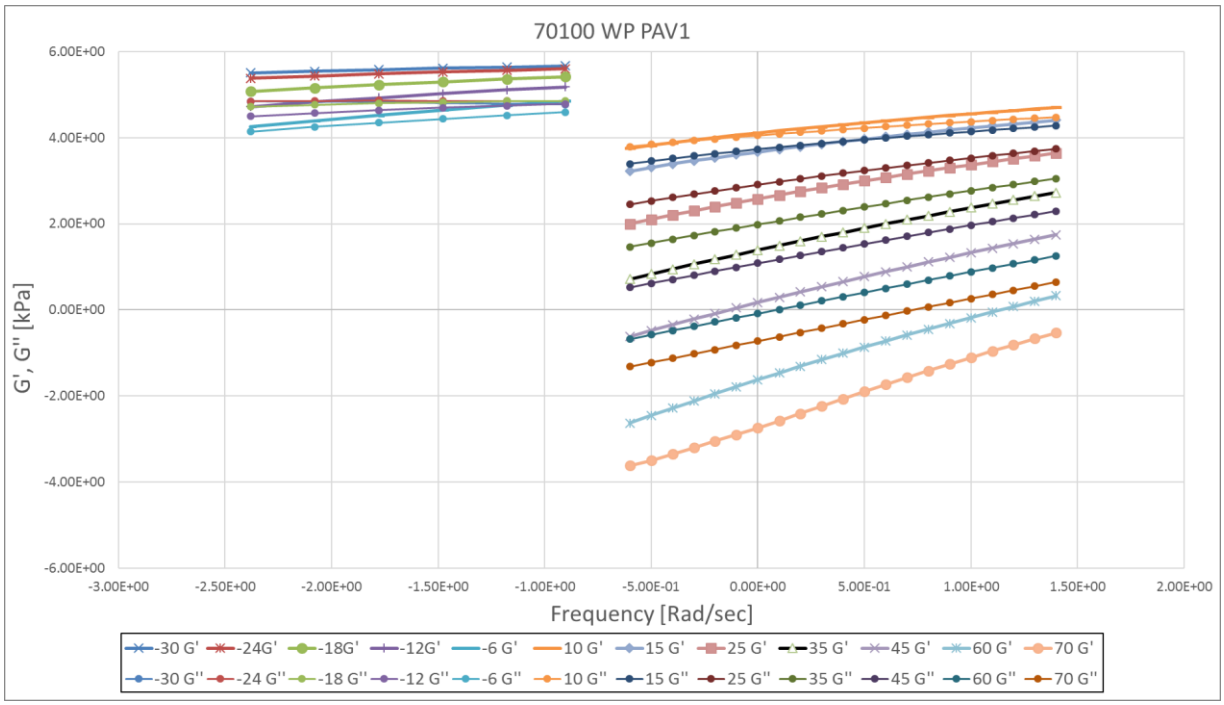

Figure 71: Unshifted isotherms of the 70/100 WP PAV1 binder

The combined master curves were shifted with the RHEA software to a reference temperature of 15˚C. This is chosen to calculate the G-R parameter at a frequency of 0.005 rad/sec from the master curve data. RHEA uses the storage and loss modulus to calculate the complex shear modulus. Figure 72 shows the shifted storage and loss modulus curves which have been converted to G*.

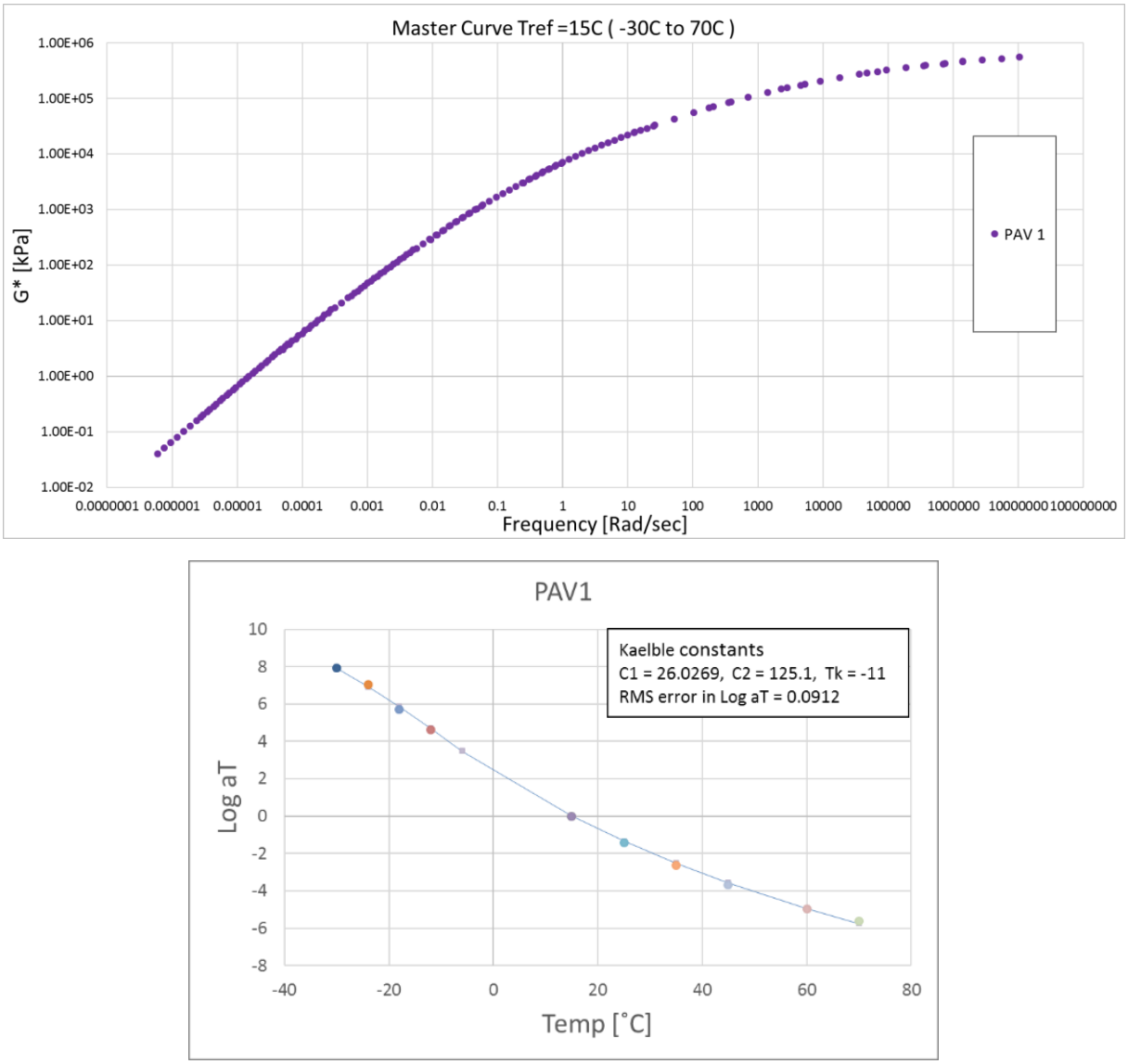

Figure 72: Master curve and Kaelble shift-factor curve of the 70/100 WP PAV1 binder

It seems that the master curve represented in Figure 7 strives to the glassy modulus of between 0.6 GPa and 1.5 GPa, as expected for bituminous materials. This statement will be proved later in the modelling of master curves section. The Kaelble shift-factor represents this set of data the best as the WLF and Arrhenius shift-factor equations indicate a RMS error in Log aT above 0.29. The effect that ageing has on the binder can also be seen from the master curves of all the ages of the 70/100 WP binder. Figure 73 indicates the master curves in complex shear modulus space of all the ages of the 70/100 WP binder. The master curves for the other 6 binders can be seen in Annexure E.

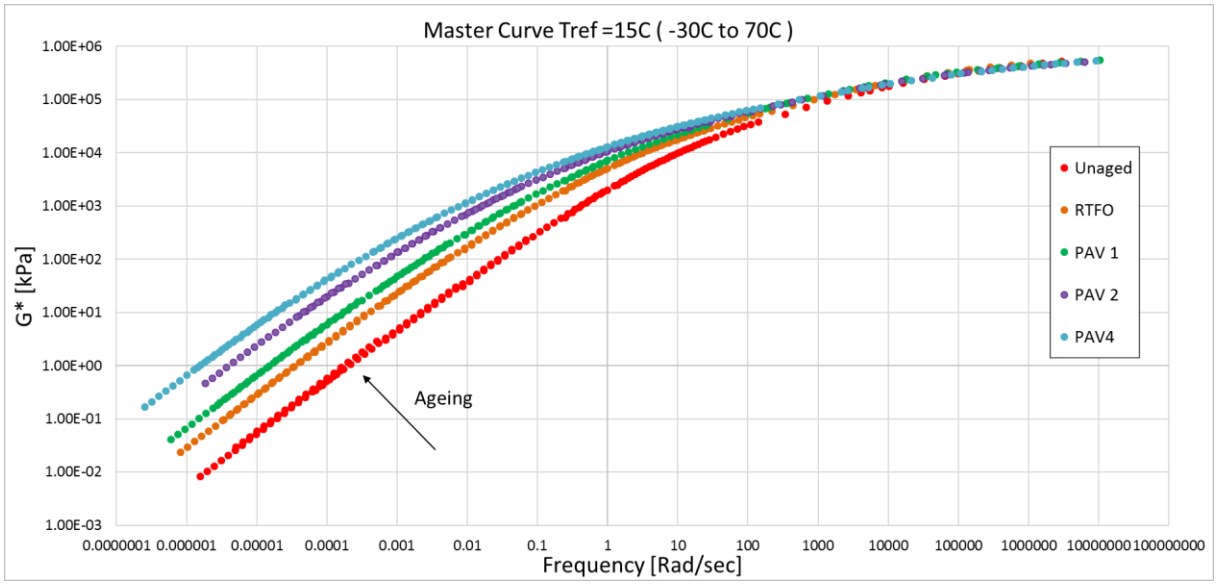

Figure 73: The master curves of all the ages of the 70/100 WP binder

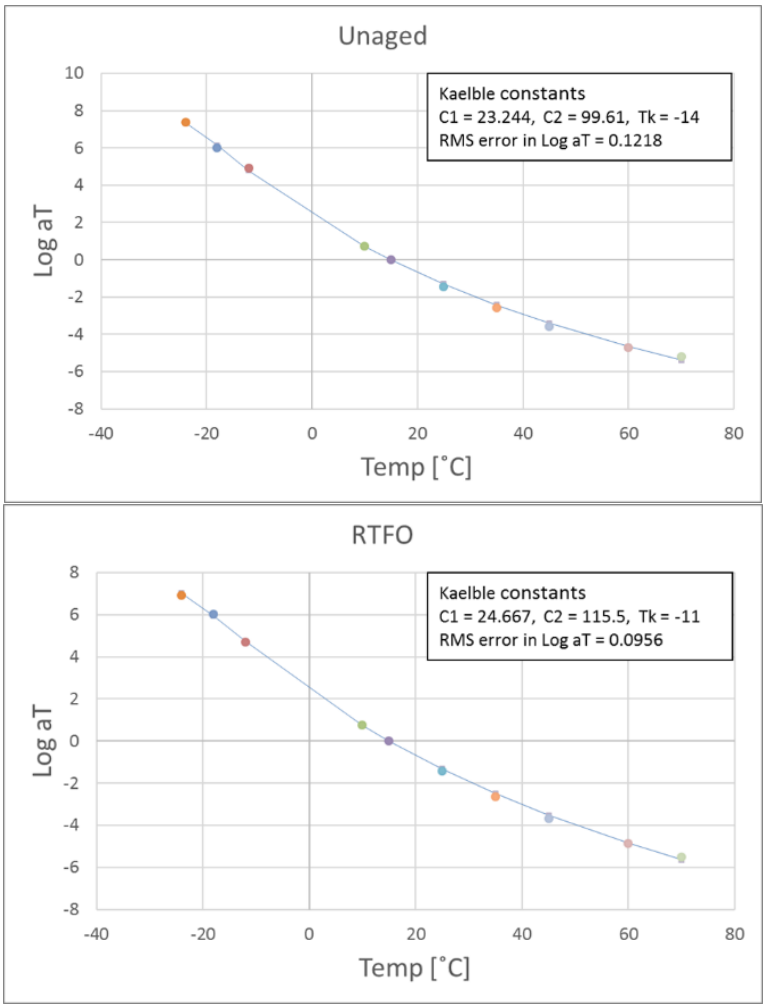

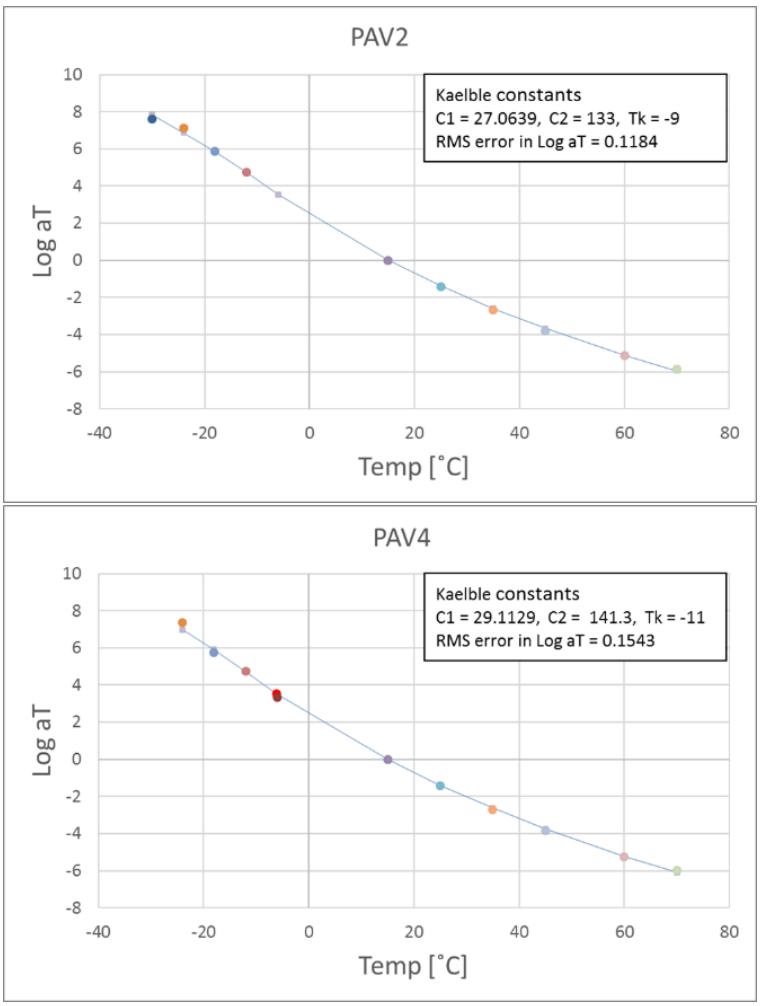

Figure 74: The Kaelble shift-factor curve for the ages of the 70/100 WP binder

Figure 73 indicates the way in which oxidation and temperature variation influence the 70/100 WP binder. As the binder ages, the stiffness of each master curve increases, and the slope becomes flatter. The slope of each master curve becomes steeper due to the binder becoming stiffer which results in a loss in the relaxation properties of the binder. At a frequency of 0.005 rad/sec the G* for the unaged binder is 20.4 kPa and for the PAV4 binder at the same frequency the G* is 754.6 kPa, which indicates the magnitude of the influence that ageing has on the 70/100 binder. This behaviour indicates that the slope of the binder becomes flatter. As the binder ages the gradient of each master curve becomes smaller. This indicates a loss in the relaxation properties of the binder as it ages.

All the master curves converge at the same point (Glassy modulus), which will be between 0.6 GPa and 1.5 GPa (Christensen *et al*., 1992). The glassy modulus will be analysed in the next section where various mathematical models will be applied to the master curves.

The PAV2 binder has a shorter master curve as shown in Figure 73. This is due to bad data that has been taken out from the isotherms during the shifting of the isotherms. Bad data includes outliers that do not form part of the curve. This data should be taken out to ensure that no errors occur during the analysis of the data.

The Kaelble shift-factor equation fits the merged BBR and DSR master curves the best. Figure 74 indicates the RMS error in log aT for all the ages which is close to 10% if one takes the average of all the errors. The shift-factor error is determined using the RHEA software as well as Microsoft Excel and the difference was evaluated each time with the combination of the G', G'' and G*. The differences between the shift-factors calculated with the RHEA software and Microsoft Excel were less than 3%.

The results from these master curves are acceptable for the parameters used to evaluate the susceptibility of the binders to ageing i.e. cross-over frequency, G-R parameter and J_{nr}.

The cross-over frequency is an important factor to consider when analysing the susceptibility of a bituminous binder to ageing. The cross-over frequency for the 70/100 WP binder is summarised in Table 7.

Table 7: Cross-over frequency and G_c* for the 70/100 WP binder

	70/100 WP				
	Unaged	RTFO	PAV1	PAV2	PAV4
Cross-over frequency (rad/sec)	106.049	16.476	6.597	1.260	0.408
Gc* (kPa)	32404	21998	18223	11760	8695

Table 7 shows the susceptibility of the 70/100 WP binder to ageing with a decrease in the cross-over frequency and complex modulus at the cross-over frequency as the binder ages. At the very low frequency and high temperature region the binders become more viscous which result in lower stiffness's. The cross-over frequency decreases at a magnificent rate between the unaged and RTFO state of the binder in comparison to the long-term aged conditions. This indicates that the binder is more susceptible to short-term ageing than long-term ageing. This statement will be analysed in detail in Chapter 5 by comparing all the seal binders with one another.

4.3.3 Mathematical Model Comparison

This section covers the goodness of fit between the data and the mathematical models for the unaged 70/100 WP binder. The analyses of the models for the rest of the binders with their ages can be seen in Annexure F. The parameters of the models as well as the root mean square error is indicated on the graphs in this section. The shift-factor curves are as seen in section.

The mathematical models used to evaluate the master curves of all 7 binders are as follows:

- Christensen and Anderson (CA) model,
- Christensen, Anderson and Marasteanu (CAM) model,
- Generalised Logistic Sigmoidal (GL) Model, and
- Discrete Relaxation Spectrum (Generalized Maxwell Model).

The parameters needed within the mathematical models to evaluate the data were calculated using the RHEA software and Microsoft Excel. The glassy modulus (Gg) was back calculated with the RHEA software and Microsoft Excel. The crossover frequency (w_0) was determined with excel by calculating the point of intersection between the storage and loss modulus. A glass transition temperature (T_g) of -20˚C was assumed for bituminous binders (Baglieri *et al*., 2012). This glass transition temperature was applied to the RHEA software for further analyses.

Each model is represented with a master curve in G*-space followed by one in δ-space. Thus, the RMS error depends on the goodness of fit of both the G*-space and the δ-space master curves. Figure 75 show the fit of the CA model on the G*-space master curve.

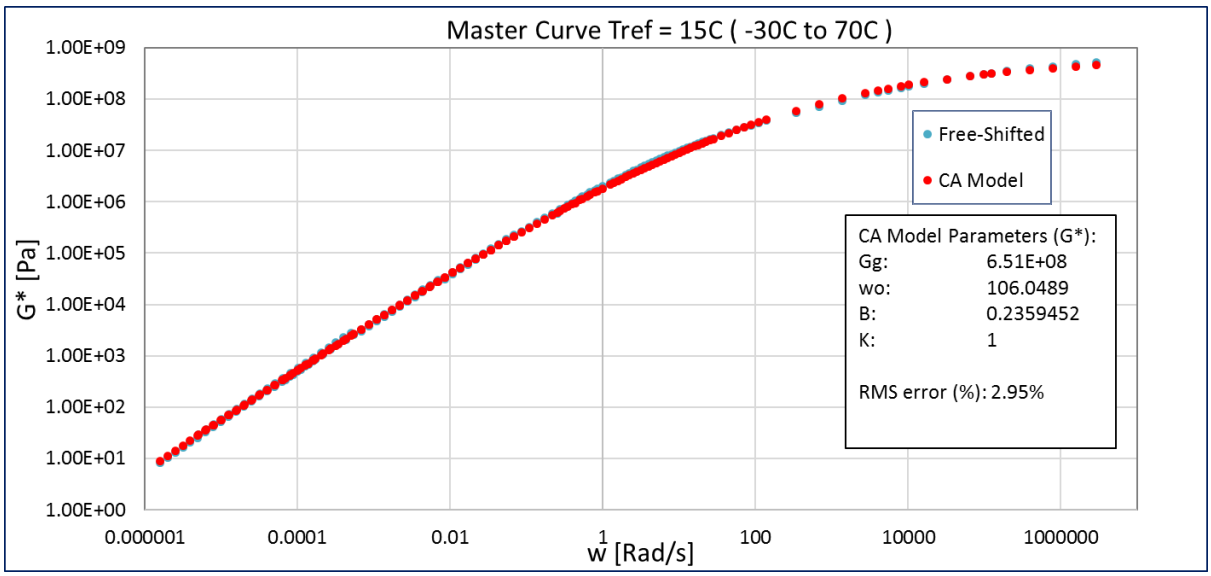

Figure 75: G*-space master curve of the unaged 70/100 WP binder with the CA model fit

The CA model appears to provide a good fit to the G* master curve of the unaged 70/100 WP binder with a RMS error percentage of 2.95. In the top right corner of Figure 75 the model has a flatter trend than the data, which influence the value of the glassy modulus. Figure 76 show the CA-model on the unaged 70/100 WP binder data in phase angle space.

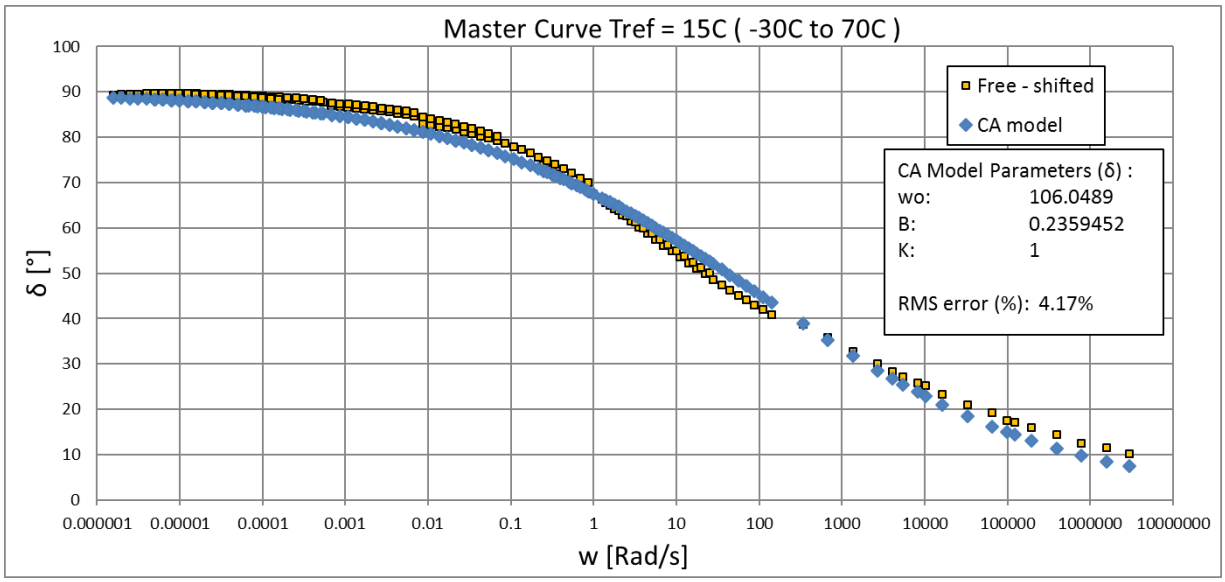

Figure 76: δ-space master curve of the unaged 70/100 WP binder with the CA model fit

The fit of the CA-model does not appear to be accurate, but the RMS error is 4.17% which is acceptable. The RMS error is not the only variable to look at during the analysis of data. Through inspection the CA model does not fit the phase angle master curve very well. The difference between the model and the data at 0.005rad/sec is remarkably large. The total error for the fit of the CA model to the unaged 70/100 WP binder is 7.12%. Figure 77 indicates the CAM model fit to the unaged 70/100 WP binder in G*-space.

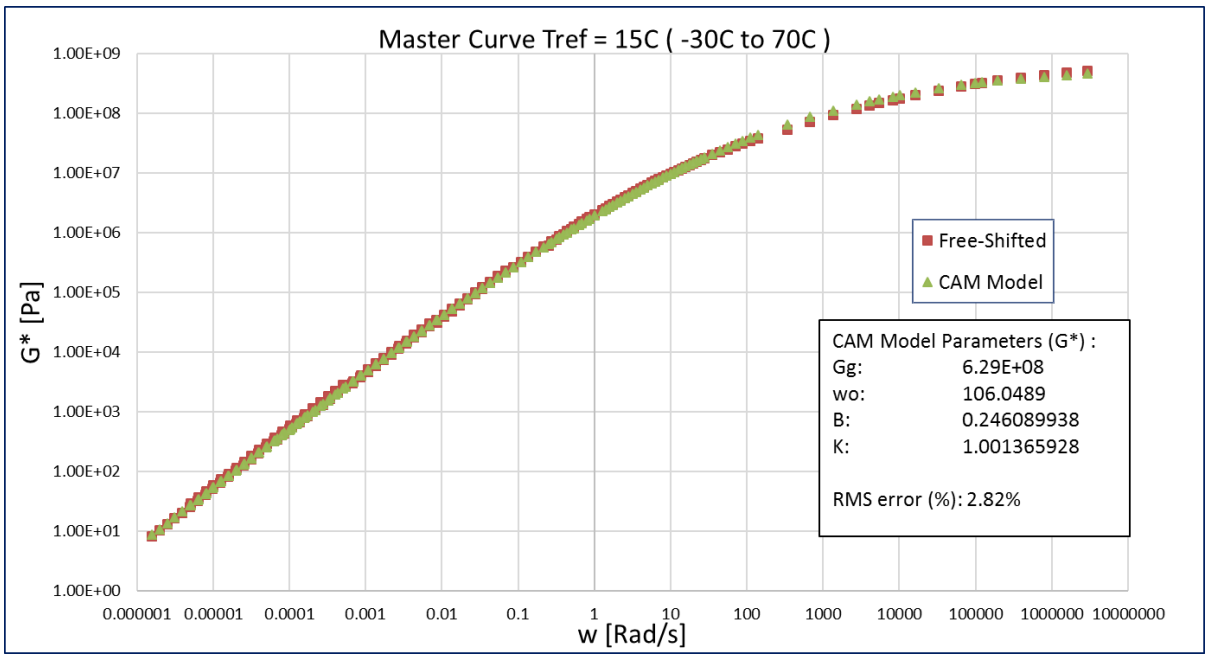

Figure 77: G*-space master curve of the unaged 70/100 WP binder with the CAM model fit

The CAM model indicates a better fit in comparison with the CA model. The 'K-value' for the CAM model is not a constant and was solved with Excel. It is observed that the 'K-value' is very close to the constant 'K-value' of 1 in the CA model. Figure 78 indicates the phase angle space for the fit of the CAM model.

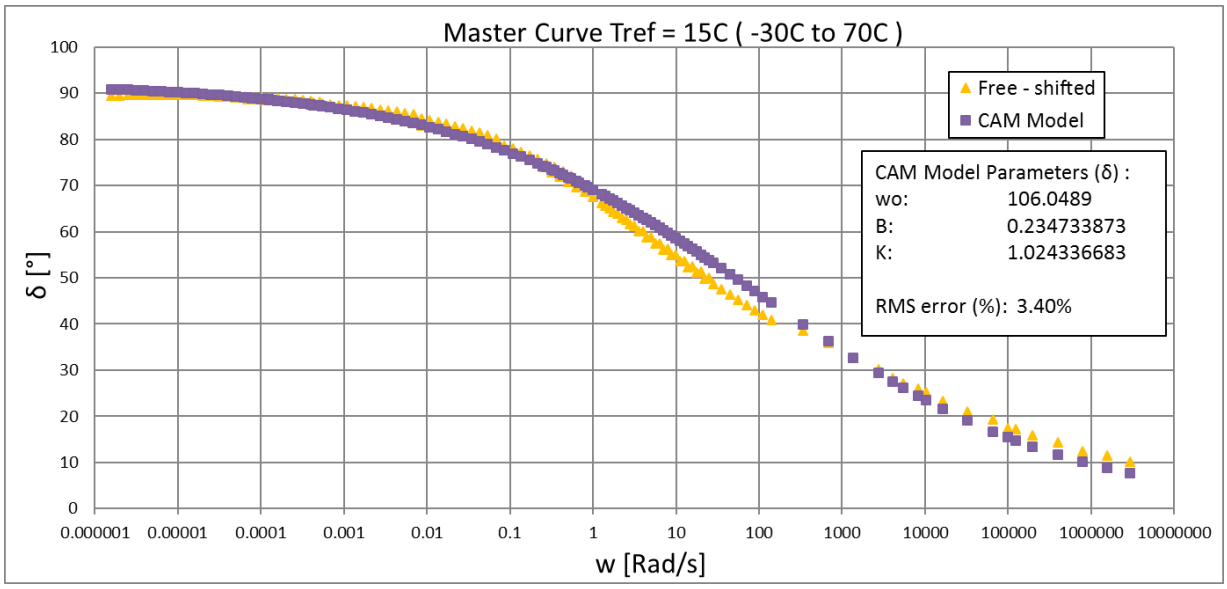

Figure 78: δ - space master curve of the unaged 70/100 WP binder with the CAM model fit

The fit of the CAM model in phase angle space is better in comparison with the CA model. The CAM model indicates a good fit at a frequency of 0.005 rad/sec in comparison with the CA model. The total RMS error for the CAM model fit is 6.22% which is slightly lower than that of the CA model fit.

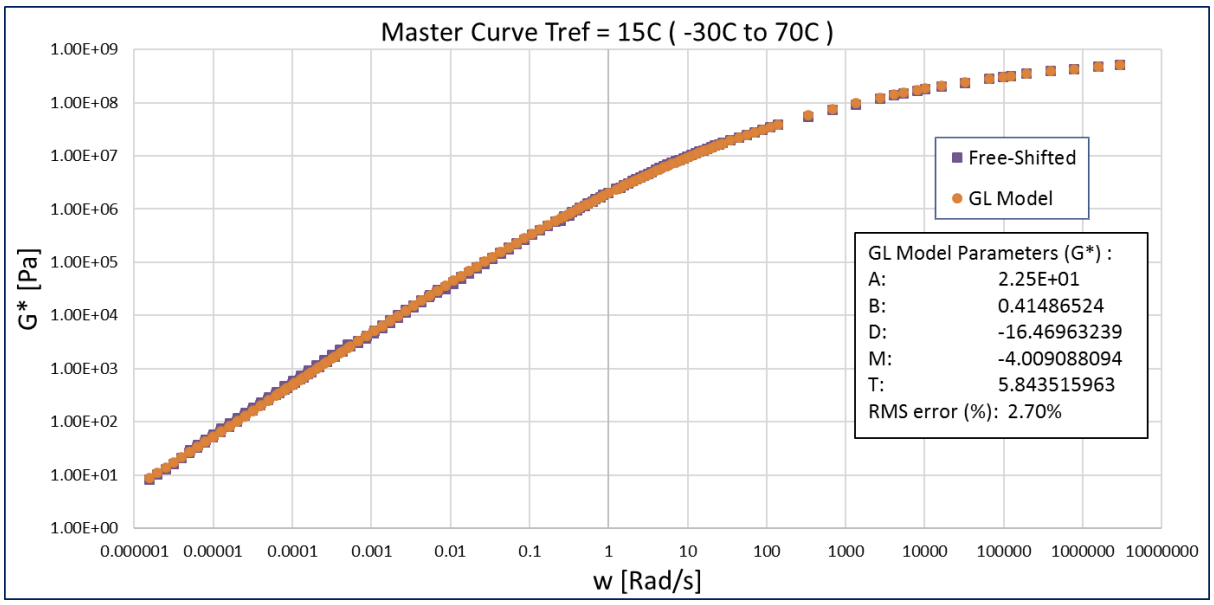

Figure 79: G*-space master curve of the unaged 70/100 WP binder with the GL model fit

The model parameters in Figure 79 differ from the parameters discussed in Chapter 3 and are as follows A = α, B = β, D = *δ,* M = γ and T = ʎ.

The GL model has a very good fit of 2.7%. Through inspection, in Figure 79, is it observed that this model evaluates the glassy modulus very well. Figure 80 indicates the GL model fit for the phase angle master curve for the unaged 70/100 WP binder.

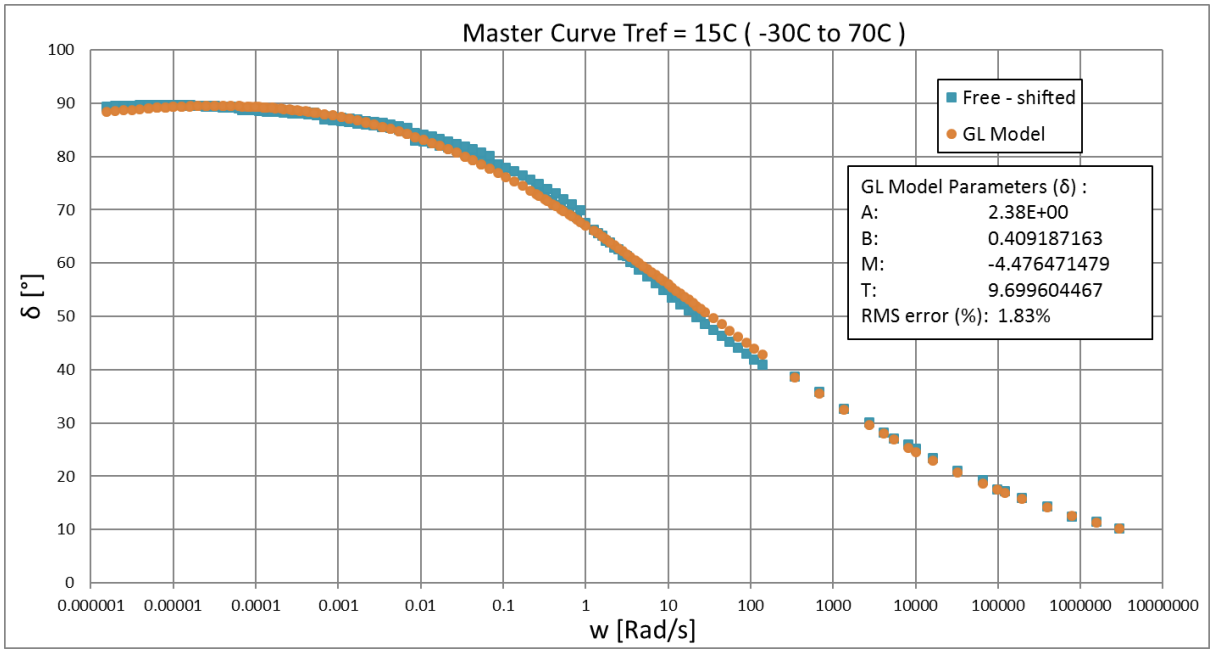

Figure 80: δ-space master curve of the unaged 70/100 WP binder with the GL model fit

The GL model analysis the phase angle master curve very well in comparison with the CA and CAM model. The phase angle at a frequency of 0.005rad/sec for the G-R parameter will be accurate within an error of 1.83%. The total RMS error for the GL model on the master curves of the unaged 70/100 WP binder is 4.3%.

Figure 81 shows the fit of the discrete spectrum on the complex modulus fit for the unaged 70/100 WP binder. Table 8 indicates the strength and relaxation for each mode of the complex modulus and phase angle master curves of the unaged 70/100 WP binder. The modes where obtained by using the RHEA software and processed in Excel for further analyses.

Table 8: The strength and relaxation parameters for each mode of the master curves

Mode Number, i	Mode Strength gi, kPa	Mode Relaxation Time ʎt, sec
1	7.66E+04	1.23E-07
2	1.67E+05	1.31E-06
3	1.37E+05	1.59E-05
4	9.90E+04	1.49E-04
5	5.19E+04	1.17E-03
6	2.54E+04	7.97E-03
7	1.02E+04	4.77E-02
8	3.41E+03	2.64E-01
9	5.84E+02	1.43E+00
10	1.31E+02	6.98E+00
11	1.20E+01	5.06E+01
12	1.05E+00	3.05E+02
13	1.32E-01	1.76E+03
14	5.18E-03	1.83E+04
15	7.37E-05	5.53E+05

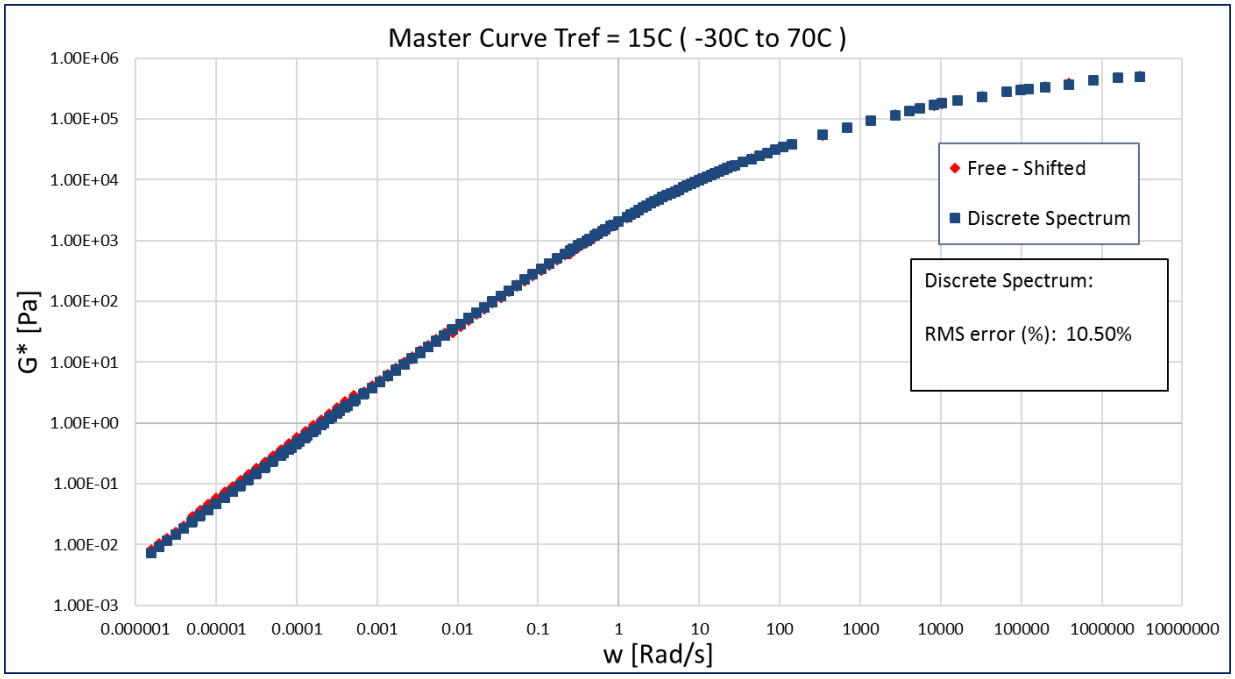

Figure 81: G*-space master curve of the unaged 70/100 WP binder with the discrete spectrum fit

The RMS error of 10.5% is the total RMS error for both the G* and δ-space master curves based on the discrete spectrum model using the RHEA software. The discrete spectrum seems to fit the G*-pace master curve very well with a slight deviation at the higher temperatures in the bottom left corner of Figure 81.

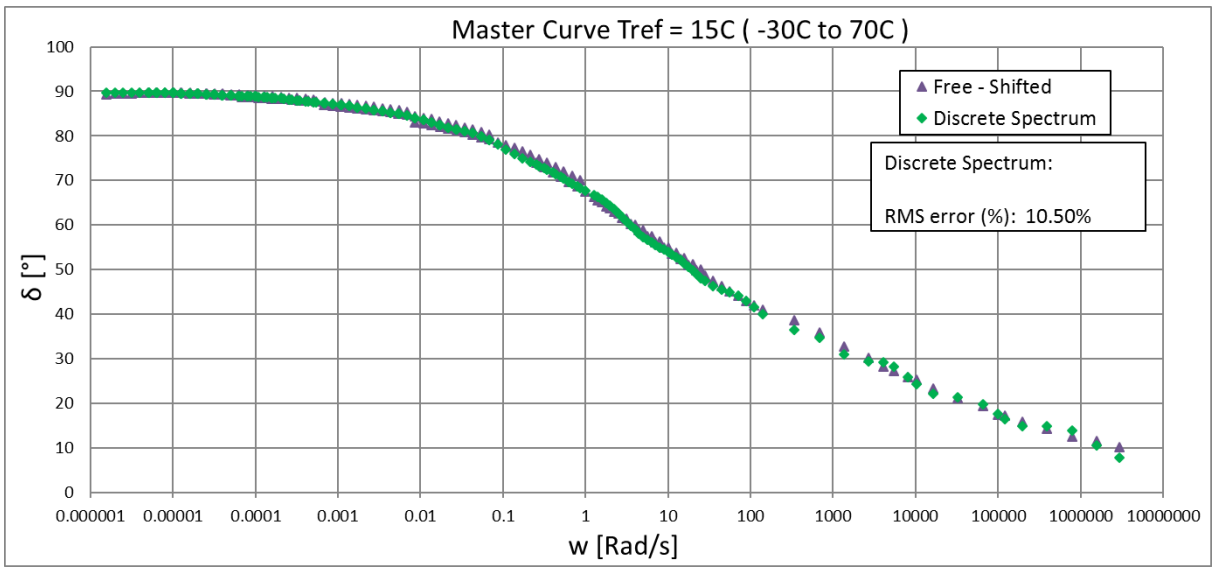

Figure 82: δ-space master curve of the unaged 70/100 WP binder with the discrete spectrum fit

For the higher temperatures, the discrete spectrum phase angle master curve fits the data well. The model does not fit the data smoothly in the lower temperature region. This may be the reason for the RMS error being larger than the error of the other 3 models. The discrete spectrum fits the data of both master curves very well at the required frequency of 0.005 rad/sec.

Only one model was chosen to determine the variables for the G-R parameter. Although the discrete spectrum had the highest RMS error for the unaged 70/100 WP binder, it was this model that provided the most accurate data at a frequency of 0.005 rad/sec throughout the analyses of all the seal binders. The discrete spectrum was chosen to evaluate the properties of the seal binders.

Figure 83 shows one of the largest differences between the discrete spectrum and the GL model in phase angle space. The binder of which the data is seen in Figure 83 is the S-E2 KZN PAV2 binder. The GL model was used to be compared to the discrete model in Figure 83 because the GL model had the best fit in comparison with the CA and CAM models.

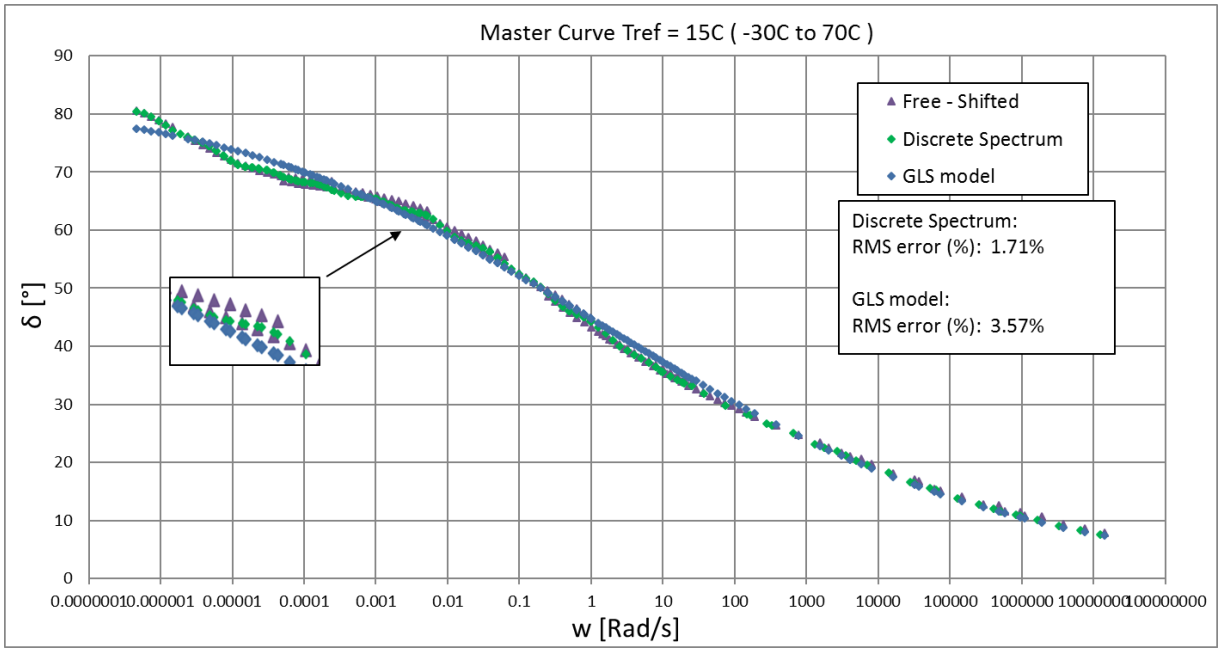

Figure 83: δ-space master curve of the S-E2 KZN PAV2 binder with the Discrete spectrum and GL model fit

The phase angles for these two models i.e. 60˚ for the GL model and 62˚ for the discrete spectrum, yield 2˚ difference. This might not seem to be a significant difference, but the RMS error also affects the G*-value. The G-R parameter for these two models differ more than 10 kPa.

4.4 Black Space Analysis

The black space diagrams were prepared from the merged DSR and BBR data. This section covers the Black space diagrams for all the ages of only the 70/100 WP and S-E1 WP binder. The black space diagrams for the rest of the binders can be seen in Annexure G.

The test temperature range for the black space diagrams is between -30˚C and 70˚C for all the ages of the 70/100 binder. The black space diagram for the 70/100 WP binders is analysed at a refence temperature of 15˚C. Figure 84 indicates the way in which ageing effects the viscous and elastic component of the 70/100 WP binder.

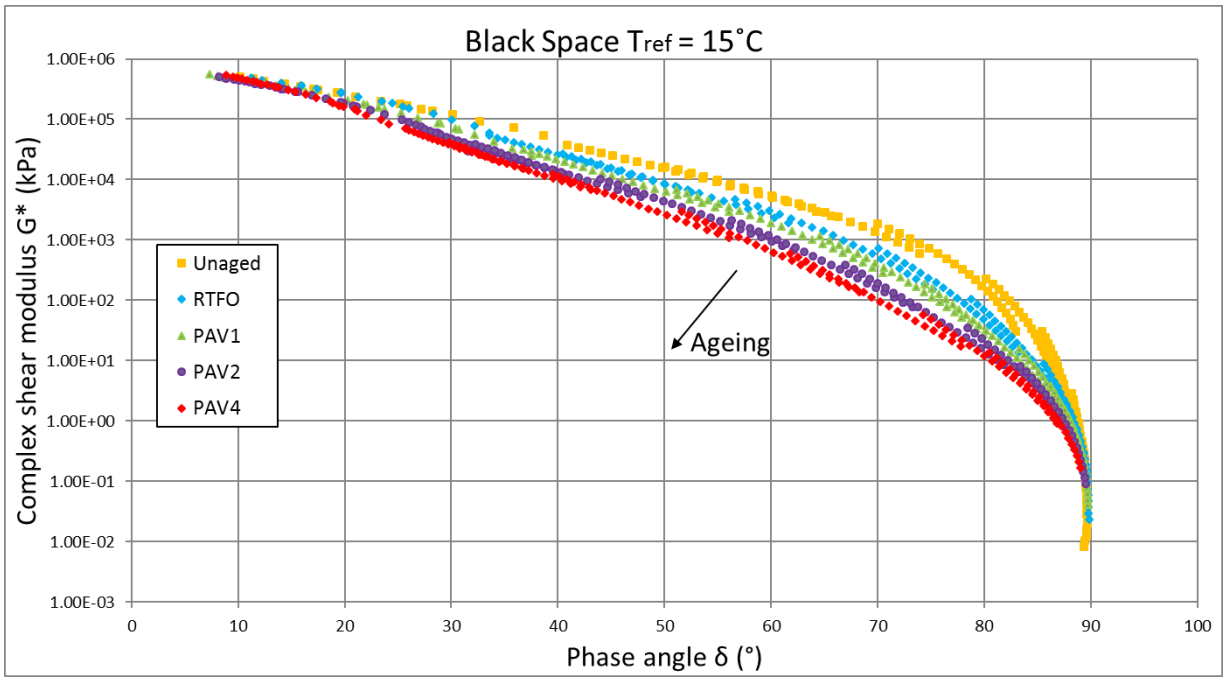

Figure 84: The black space diagram for all the ages of the 70/100 WP binder

Figure 84 shows that the black space diagrams for the 70/100 binder converge at a phase angle of 7˚ and 90˚. Theory states that a binder is fully elastic or glassy at a phase angle of 0˚and a complex modulus between 0.6GPa and 1.5 GPa for most bituminous binders. It is thus true that the exact point of convergence in this case is not necessarily at 7˚, but as illustrated in Figure 84 the black diagrams are very close to their point of convergence at a phase angle of 7˚. At a phase angle of 90˚ the binder is completely viscous.

The black space diagram for the 70/100 WP binder indicates the way in which the elastic component increases as the binder ages. The 25˚C isotherm for the unaged 70/100 binder has a phase angle of 78˚ in comparison with the 52˚ of the PAV1 70/100 binder. As the binder ages the stiffness increases and the elastic component at each temperature increases. This is true just before each black space diagram reaches the fully viscous and fully elastic state.

Through the analysis procedure it was observed that the ageing process influences the modification of the binder. Figure 85 shows the black space diagrams of the S-E2 KZN binder.

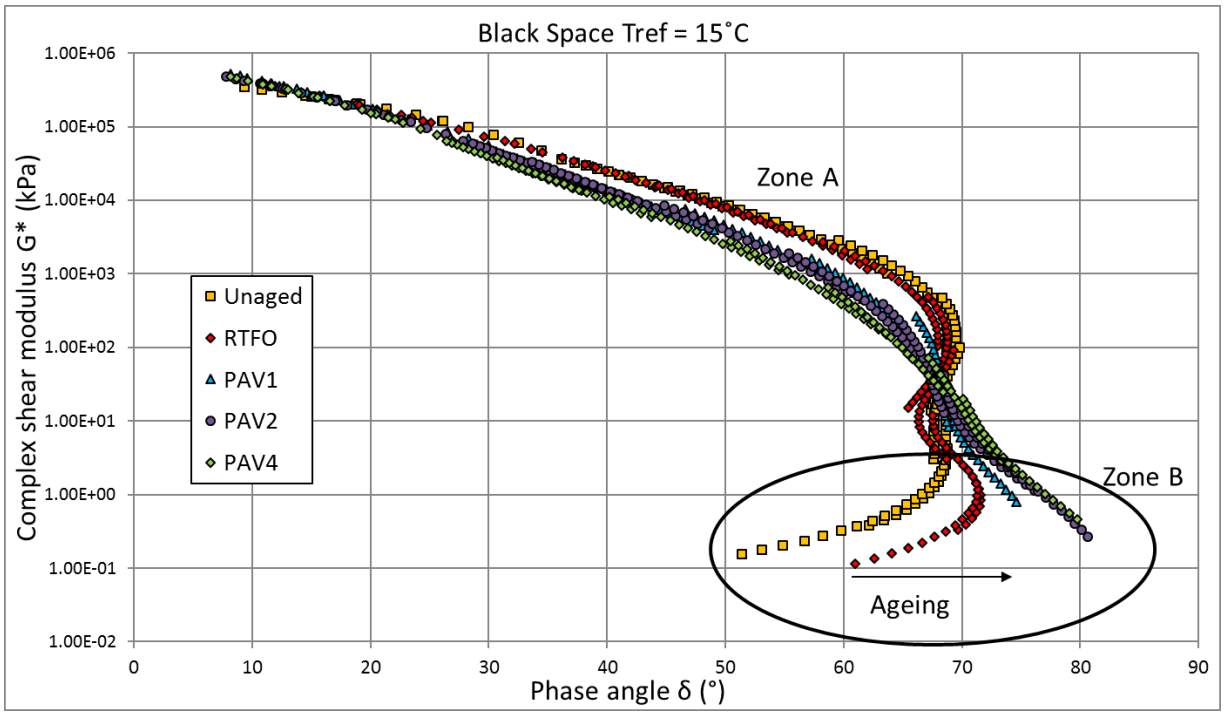

Figure 85: The black space diagram for all the ages of the S-E2 KZN binder

The S-E2 KZN binder indicates that the black diagrams do not converge at the viscous region in comparison with the 70/100 binder. This behaviour is due to modification within the binder. The S-E2 binder is modified with SBS and crosslinking agents, which begins to dominate the binder behaviour at sufficiently low viscosity and high phase angle i.e. in the high temperature range.

Analysis of the difference in the unaged and RTFO black diagrams shows that the binder becomes more viscous as it ages in Zone B (High temperature region). It appears as if the modification is less effective in Zone B. Zone A show the opposite where less viscous behaviour occurs as the binder ages. The black diagrams of the long-term aged S-E2 KZN binder do not even show any sign of modification. It is as if there is no effective modifier left within the binder after the long-term ageing process. This behaviour may be due to rupture and detachment of modification particles from one another as the binder ages, although no explicit proof of this mechanism has been obtained. This observation was not made only in the case of the S-E2 KZN binder but for all the modified binders, as indicated in Annexure G.

4.5 Creep and Recovery Analysis

The creep and recovery properties of bituminous binders include the analyses of the J_{nr} and percentage recovery. This section includes the creep and recovery behaviour for all the ages of the 70/100 WP binder. The creep and recovery data for the rest of the binders can be seen in Annexure H. The MSCR results for the recovered SC-E1 binder can be seen in Annexure H.

The plot of strain percentage against time curves of the 70/100 WP binder is provided in Figure 86, tested at 58˚C and 70˚C. Figure 86 includes the results for both the 0.1kPa and 3.2kPa shear stresses.

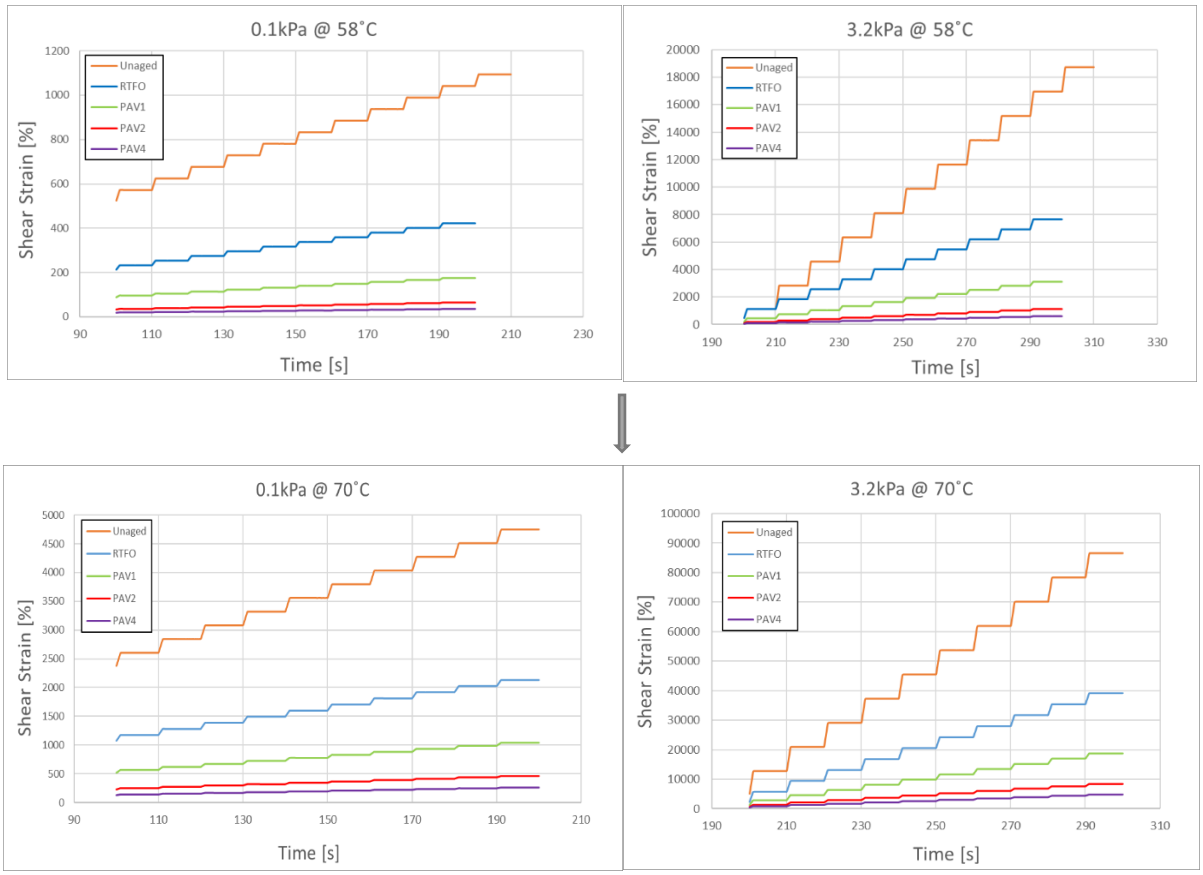

Figure 86: Percentage strain curves for all the ages of the 70/100 WP binder at 58˚C and 70˚C

Figure 86 illustrates that the percentage shear strain for the 70/100 WP binder tested at 70˚C is five times larger than the shear strain at 58˚C. This is an indication of the susceptibility of the 70/100 WP binder to temperature. The increase in the shear strain as the temperature increases is due to the binder behaving in a more viscous manner. As the temperature increases the recovery properties of the binder decreases. The non-recoverable creep compliance (J_{nr}) of the binder increases as the recovery properties of the binder decreases.

The influence of ageing on the creep and recovery properties of a binder is unavoidably large. The shear strain decreases as the age of the binder increases. Table 9 summarises the results of the creep and recovery behaviour of the 70/100 WP binder.

Table 9: Creep and recovery summary for all ages of the 70/100 WP binder

		0.1kPa		3.2kPa	
	Tmax (°C)	JNR (1/kPa)	Recovery (%)	JNR (1/kPa)	Recovery (%)
Unaged	58	5.066	0.000	5.066	0.000
	64	11.449	0.000	11.449	0.000
	70	24.431	0.000	24.431	0.000
RTFO	58	1.912	1.500	2.049	0.000
	64	4.594	0.000	4.903	0.000
	70	9.923	0.000	10.809	0.000
PAV1	58	0.779	3.831	0.820	1.275
	64	1.475	21.631	2.000	3.464
	70	4.749	0.000	5.102	0.000
PAV2	58	0.279	11.051	0.291	7.595
	64	0.812	5.309	0.868	1.640
	70	2.072	1.669	2.240	0.000
PAV4	58	0.145	18.839	0.151	15.343
	64	0.434	9.836	0.463	5.387
	70	1.177	4.573	1.282	0.885

Table 9 shows that the percentage recovery of the unmodified binder increases as the age of the binder increases. This is due to ageing that increases the elastic component of the binder which increases the percentage recovery. The J_{nr} on the other hand decreases as the age of the binder increases. The behaviour of the 70/100 WP binder indicates that as the binder ages the percentage recovery increases, and the percentage unrecovered strain decreases which causes the J_{nr} to decrease. This behaviour may be due to ageing that effects the resilient behaviour of the particles within the binder i.e. saturates, aromatics and resins. The South African Performance Grade Specifications state that for a RTFO aged binder the J_{nr} must be smaller than 4.5 for an applied shear stress of 3.2kPa to conform to minimum requirements for standard traffic classes set for asphalt binders. This 70/100 WP binder is just outside the J_{nr} range for the South African Performance Grade Specification.

The Asphalt institute (AI) constructed a curve which assesses the delayed-elastic response of bituminous binders with the AASTHO 320 specification which form part of the ASTM D7405 – 10a for MSCR testing (Asphalt Institute, 2010). Equation 31 illustrates the formulation of this curve (Asphalt Institute, 2010). The curve analyses the relationship between the percentage recovery and the J_{nr} of a binder. The results for the shear stress of 3.2kPa are used in Table 9 to evaluate the creep and recovery behaviour of the 70/100 WP binder in Figure 87. The orange line in Figure 87 indicates the boundary for the percentage recovery against the J_{nr}.

$$\%Recovery = 29.37(J_{nr})^{-0.263} \quad (31)$$

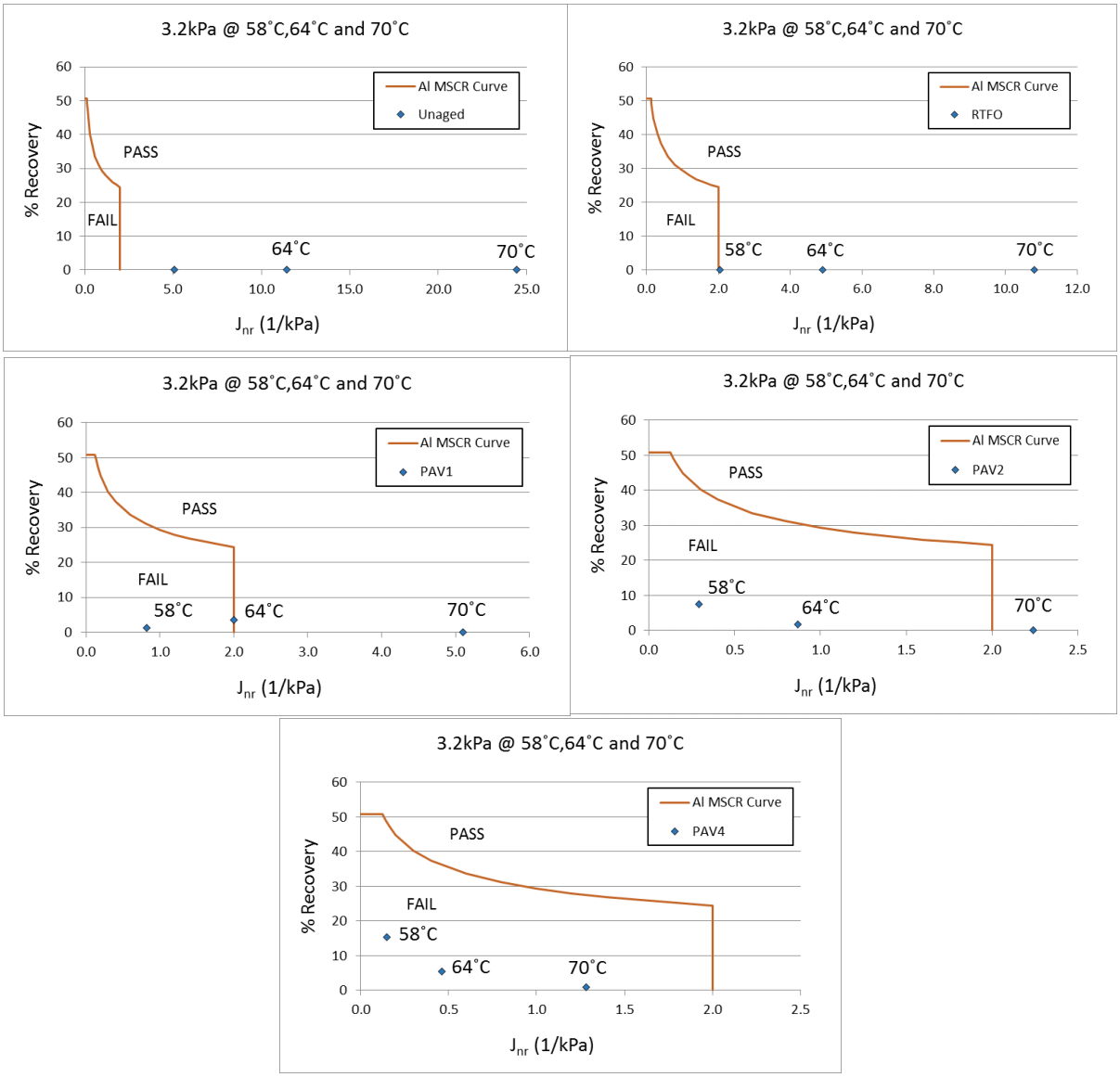

Figure 87: Asphalt institute percentage recovery against J_{nr} analyses for all ages of the 70/100 WP binder

Figure 87 shows how the percentage recovery increases and the J_{nr} decreases as the age of the binder increases. As the age of the binder increases the creep compliance moves closer to the failure zone for all three temperatures.

The results of the RTFO binder from Figure 87 show that the data at 64˚C and 70˚C do not meet the ASTM D7405 – 10a specification curve. By looking at the J_{nr} results of the RTFO binder from Table 9 it is ones again the 64˚C and 70˚C data that does not meet the South African Performance Grade Specification limit for the J_{nr}. The South African Performance Grade Specification limit for the J_{nr} is focused on the results from asphalt binders and only the RTFO condition of the binder. Only the RTFO results is thus compared to the ASTM D7405 – 10a specification curve.

In the case of the PAV2 binder it is only the results at 58˚C that satisfy the ASTM D7405 – 10a specification curve. The J_{nr} results for all three temperatures of the PAV4 binder do not satisfy the specification.

4.6 Ageing behaviour (G-R parameter)

This section describes the ageing behaviour for all the ages of the 70/100 WP binder in terms of the G-R parameter. The data from the discrete spectrum is used as discussed in Section 4.3.3. The results of the other binders will be compared with one another in Chapter 5.

The summary of the G-R parameter includes the complex modulus and phase angle at a reference temperature of 15˚C and a frequency of 0.005rad/sec for all the ages of the binder.

Table 10: G-R parameter and rheological index summary for all the ages of the 70/100 WP binder

	Unaged	RTFO	PAV1	PAV2	PAV4
Complex modulus, G* [kPa]	20.483	97.146	183.073	448.007	754.654
Phase angle, δ [˚]	85.0	77.4	72.2	64.7	58.7
G-R parameter [kPa]	0.156	4.748	18.031	90.195	237.828
Rheological index, R	1.303	1.447	1.571	1.750	1.894

Table 10 shows that the complex modulus increases as the binder ages. As the stiffness of the binder increases with age the phase angle decreases, which is intuitive. This behaviour indicates that the binder becomes more elastic and stiffer at the same time. As the binders age the rheological index increases. This behaviour is due to the cross-over frequency that decreases and the stiffness that increases as the binder ages. Figure 88 indicates the increase in the G-R parameter as the age of the binder increases. The direction in which the G-R parameter increases is also shown in Figure 88.

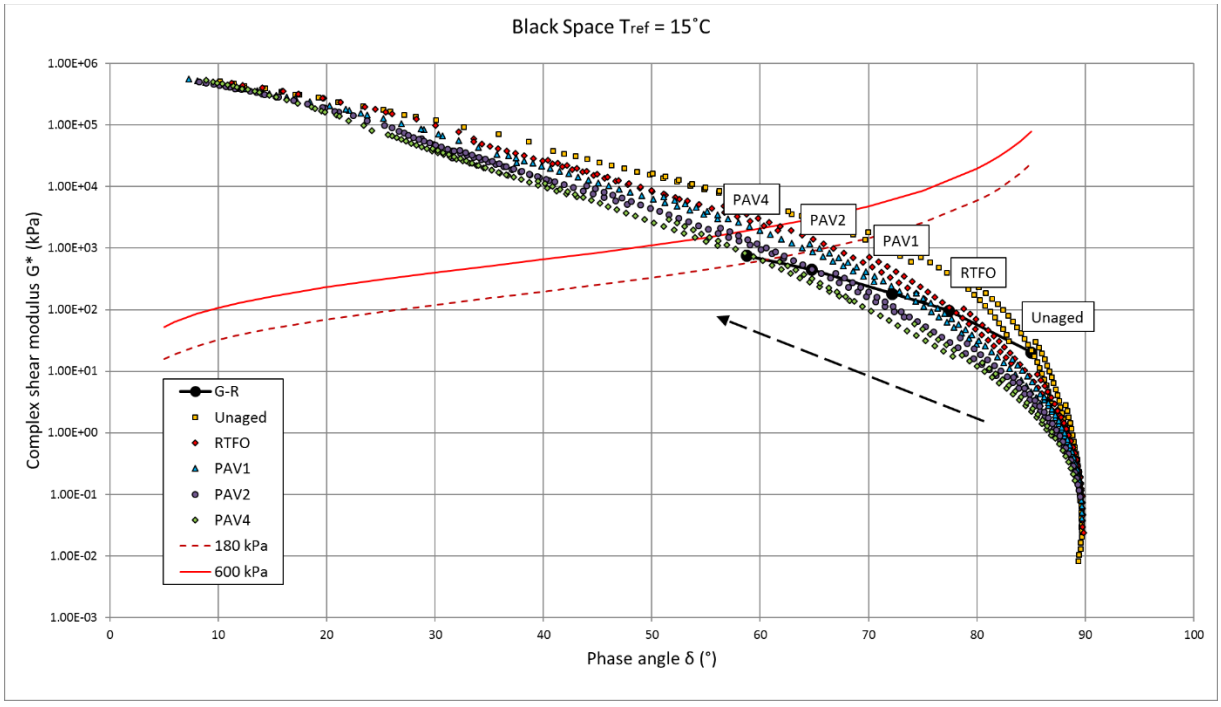

Figure 88: The black space diagram with the G-R parameter for all the ages of the 70/100 WP binder

The G-R parameter limits are indicated with red lines in Figure 88. The G-R parameter of the PAV4 70/100 WP binder exceeds the cracking initiation limit. This graph infers that this binder will start to form some cracks 7 to 10 years after construction.

The G-R parameter indicates the cracking resistance of a binder at high temperatures and the ΔTc parameter at low temperatures. By analysing the results of the cracking resistance at low temperatures it was clear that the binder indicates a ΔTc of smaller than -5 at the PAV 4 aged binder. The G-R parameter results and the ΔTc parameter correlate well with one another in this case. Figure 89 show the relationship between G-R and ΔTc as well as with the rheological index.

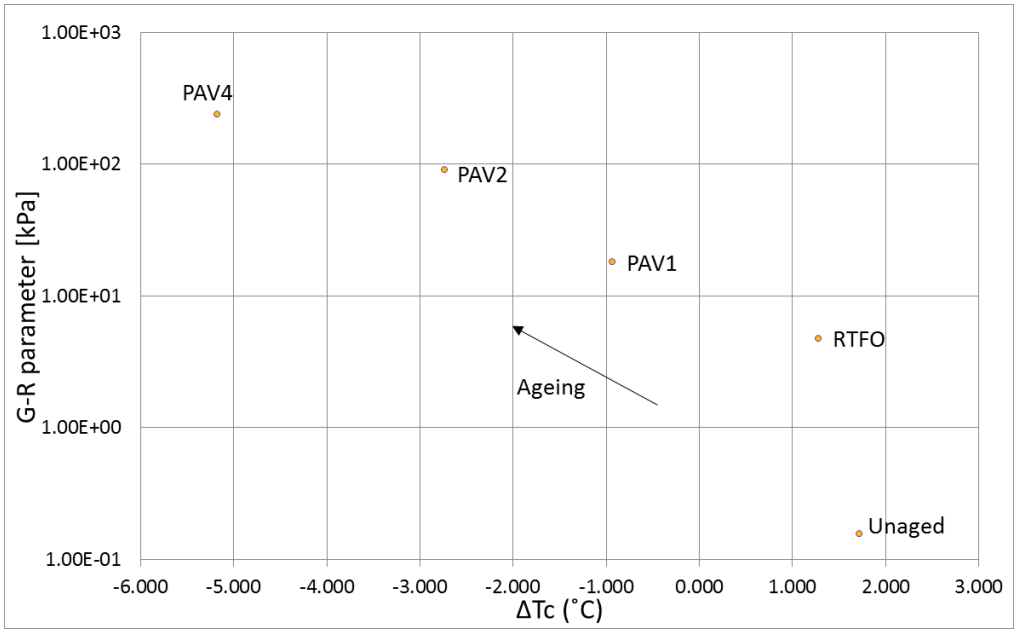

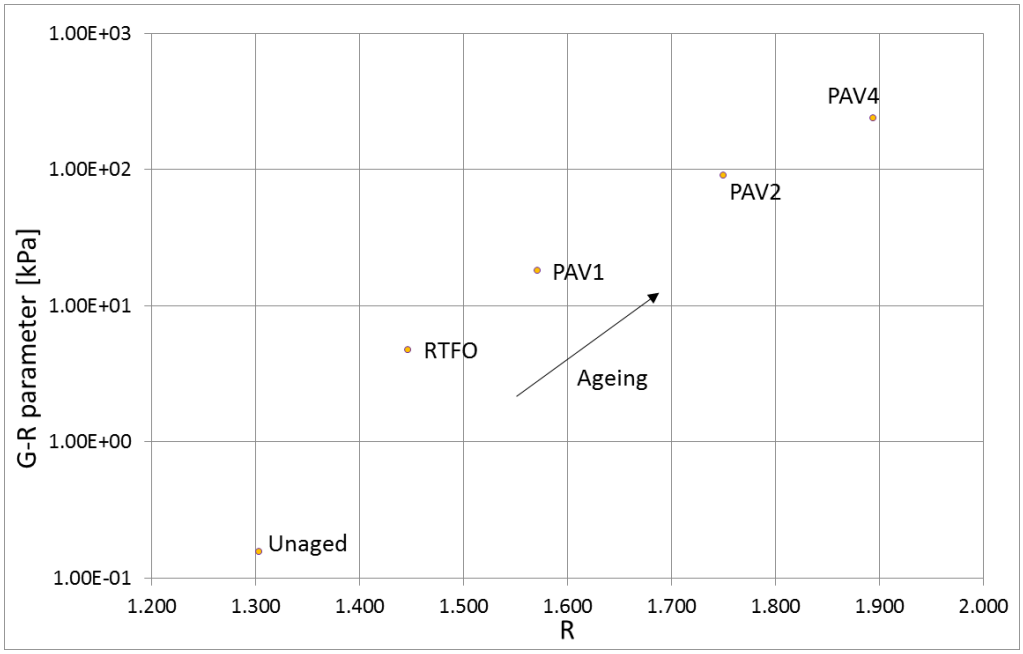

Figure 89: Relationship between G-R, ΔTc and R for the 70/100 WP binder

The relationship between the three cracking parameters seems to correlate well with one another as expected. Figure 89 show how the shape of the G-R against ΔTc and G-R against R curves are similar. Both curves have the same shape as the age of the binder increases. The ΔTc parameter decrease as the G-R parameter increase which show how the binder strives to the crack initiation zone as it ages.

The viscous to elastic transition (VET) temperature is another parameter that evaluates the ageing rate of the seal binders as well as their susceptibility to cracking. T_{VET} and G^*_{VET} is calculated for all the ages of the 70/100 WP binder. Figure 90 and Table 11 show the T_{VET} and G^*_{VET} values for all the ages of the 70/100 WP binder.

Table 11: VET data for all the ages of the 70/100 WP binder

		Unaged	RTFO	PAV1	PAV2	PAV4
FT111	T_{VET} (˚C)	6.574	12.087	14.420	19.730	23.770
	G^*_{VET} (kPa)	22266.033	14555.624	12821.166	7985.428	5593.780

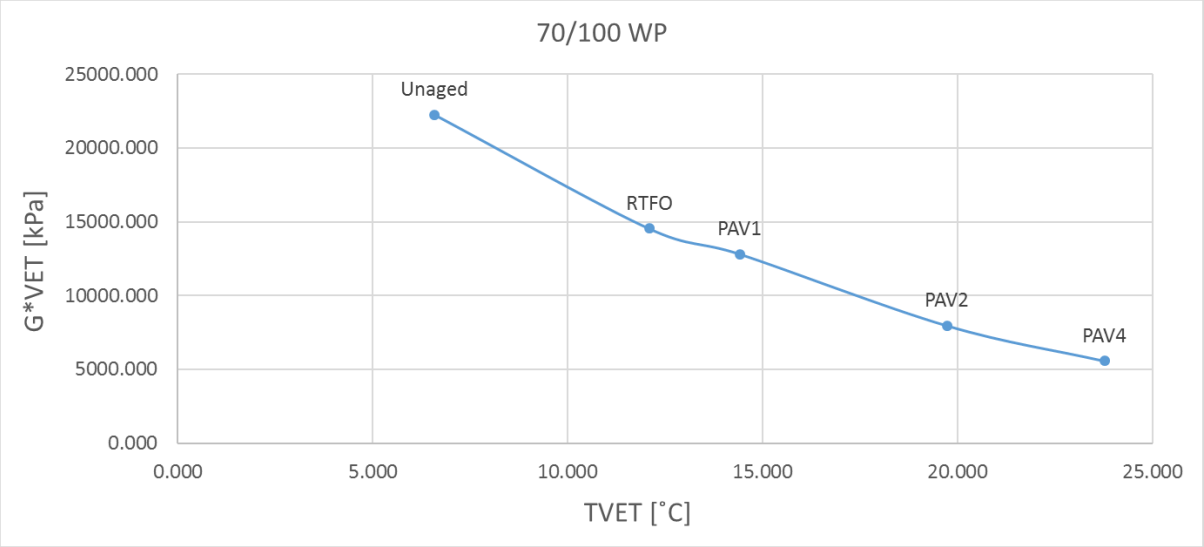

Figure 90: VET temperatures for all the ages of the 70/100 WP binder

As stated by Widyatmoko (2005) for a 50pen bituminous binder the tentative specification is T_{VET} < 20˚C and G^*_{VET} > 10 MPa. By comparing the 70/100 binder with this specification the T_{VET} limit will decrease and the G^*_{VET} limit will increase. With this said the Unaged, RTFO and PAV1 state of the 70/100 WP binder indicates a good resistance to ageing and cracking. The PAV2 and PAV4 age condition of this binder may indicate thermal cracking a few years after the construction period.

In the next Chapter the ageing behaviour of all the binders will be discussed and compared to one another.

4.7 Summary

The focus of this chapter was to indicate the analyses procedure for the age-related performance of typical seal binders in South Africa by using the results of the 70/100 WP binder. The results for the rest of the binders are compared with one another in Chapter 5 and provided in the Annexures.

The results of the 70/100 WP binder including the ΔTc, crossover frequency, G* at the crossover frequency, J_{nr}, R and G-R parameter were analysed and compared to the South African Performance Grade Specification. The ΔTc result for the PAV1 aged 70/100 WP binder satisfy the specification limit of -5˚C with a value of -0.933˚C.

The crossover frequency of the 70/100 WP binder show that the binder is highly influenced by ageing from the unaged to RTFO condition with a 16% decrease in the cross-over frequency. The long-term aged conditions for the 70/100 binder show a 6% decrease from the PAV1 to PAV4 condition. This indicates that the binder is more susceptible to ageing during short-term ageing. As the crossover frequency of the binder decreases as the binder ages the stiffness at the crossover frequency decreases. This is due to the binder becoming more viscous in the low frequency and high temperature range.

After the mathematical model analyses of all the binders it was decided that the discrete spectrum will be used for further analyses. The discrete spectrum does not have the best fit compared to the other models, but it has the best fit at the required frequency of 0.005 rad/sec. This appears to be the case for the modified and unmodified binders.

The high temperature analysis of the 70/100 binder show that the J_{nr} at 3.2kPa apply to the MSCR limits of the AI at the unaged and RTFO condition. At the PAV1 state of the binder the J_{nr} at 58˚C enters the failure zone of the AI MSCR curve. The J_{nr} for the PAV2 condition fails at 58˚C and 64˚C and for the PAV4 state at 58˚C, 64˚C and 70˚C.

The G-R parameter results for the unaged, RTFO, PAV1 and PAV2 aged 70/100 WP binder apply to the limits set by researchers. The G-R result for the PAV2 condition is 90.195 kPa which is not even close to the crack initiation limit of 180 kPa. The PAV4 condition of the 70/100 WP binder exceeds the crack initiation limit a result of 237.828 kPa. The overall creep and recovery results for the seal binders appear to correlate well with the current specification for asphalt binders, but further testing is required to make final conclusions.

The R value increase as the binder age which indicates how the binder strives to the cracking limit of the binder. The relationship between the G-R parameter with R and ΔTc is noticeable. The shape of the curves is very similar as the age of the binder increases.

The VET data for the 70/100 WP binder satisfy the tentative specification of Widyatmoko (2005) at the Unaged, RTFO and PAV1 state of the binders. The crack and age resistance of the binder at these ages are still in a good state. During the PAV2 and PAV4 age condition some thermal cracks may occur.

Chapter 5 focuses on the comparison of the results of all seven seal binders tested.

Chapter 5: Synthesis

'*Education is the most powerful weapon which you can use to change the world*'-Nelson Mandela

5.1 Introduction

This chapter provides a synthesis of the rheological testing carried out for the performance grading system of seven bituminous seal binders. This chapter contains the following phases:

xi. Phase 1: A detailed discussion regarding a comparison of the BBR results of the seal binders obtained from the laboratory testing.
xii. Phase 2: Provision of descriptive information regarding the comparison of the mathematical model fit on the seven seal binders.
xiii. Phase 3: Description and illustration of the comparison between the rheological characteristics i.e. viscous and elastic components of the seven seal binders used in this study.
xiv. Phase 4: A comparison of the creep and recovery behaviour of the seven seal binders.
xv. Phase 5: Brief discussion and comparison regarding the influence that ageing has on various parameter for the seal binders.

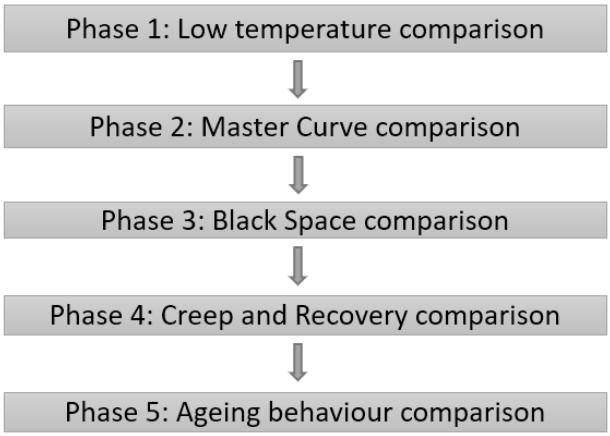

Figure 91: Chapter organisation

The abbreviations used to describe the comparison of the seal binders are as follows:

- FT111: 70/100 from Colas in the Western Cape;
- FT131: 70/100 from Colas in KwaZulu–Natal;
- FT211: S-E1 (SBS) from Colas in the Western Cape;
- FT221: S-E1 (SBS) from Colas in Gauteng;
- FT222: S-E1 (SBS) from Tosas in Gauteng;
- FT322: S-E2 (SBS) from Tosas in Gauteng, and
- FT333: S-E2 (SBS) from Bituguard in KwaZulu–Natal.

The fourth and final numeral indicates the age of the binder. The FT111 binder is used as an example:

- FT111**1** indicates the unaged binder;
- FT111**2** indicates the RTFO binder;
- FT111**3** indicates the PAV1 binder;
- FT111**4** indicates the PAV2 binder, and
- FT111**5** indicates the PAV4 binder.

5.2 Low Temperature comparison

This section entails a comparison of the results obtained from the BBR tests. Annexure C contains the stiffness and m-value for all the ages of the seven seal binders. The ΔTc parameter for all the ages of the seal binders is summarised in Table 12. Table 12 indicates the manner in which the age of the binder influences the low temperature performance and how the performance of the binders compare to one another.

Table 12: ΔTc comparison for all the ages of the seven seal binders

ΔTc (˚C)						
Binder	Type	Age				
		Unaged	RTFO	PAV1	PAV2	PAV4
FT111	Unmodified	1.719	1.284	-0.933	-2.734	-5.180
FT131	Unmodified	2.429	2.071	0.235	-2.734	-6.457
FT211	Modified (3% SBS)	-0.415	-0.802	-2.212	-4.565	-5.238
FT221	Modified (3% SBS)	2.423	1.981	-0.693	-1.491	-3.189
FT222	Modified (3% SBS)	-1.264	-2.159	-4.869	-5.934	-8.316
FT322	Modified (5% SBS)	-3.445	-3.125	-4.738	-6.580	-8.003
FT333	Modified (5% SBS)	-0.852	-1.115	-2.673	-4.457	-5.475

The unmodified binders i.e. FT111 and FT131 and modified FT221 binder yield a ΔTc parameter of more than 0˚C in their unaged and RTFO aged conditions. The FT131 binder is the only binder that has a ΔTc above 0˚C after the PAV1 ageing. A ΔTc above 0˚C indicates S-controlled behaviour, which shows that the relaxation properties of the binders at this stage are still in a good condition. Except for the modified FT221 binder, both the unmodified binders show more resistance to thermal cracking in comparison with the rest of the modified binders in the Unaged, RTFO and PAV1 age region. The FT131 is the only binder that indicates S-controlled behaviour after the PAV1 ageing condition. The FT111 and FT221 binders are just inside the m-controlled region after the PAV1 ageing condition, which means the binders become more susceptible to thermal cracking during the PAV2 and PAV4 age.

Table 12 shows that the FT211, FT222, FT322 and FT333 binders do not have S-controlled behaviour at any stage of ageing. There is no indication that these binders will experience thermal cracking at low temperatures during the Unaged, RTFO or PAV1 condition. These results indicate a susceptibility to thermal cracking. The South African Performance Grade Specification states that an asphalt binder must have a ΔTc above -5˚C after PAV1 conditioning. The results in Table 12 show that all the binders satisfy the specification at PAV1.

It was observed that the FT222 and FT322 binders are the only two binders that are just inside the specification boundary. At PAV2 and PAV4 these two binders indicate much lower ΔTc values in comparison with the rest of the binders. These results show that the FT222 and FT322 binders are more susceptible to thermal cracking at low temperatures. These two binders may exhibit some degree of cracking between a pavement life of 3 and 10 years, which is represented by the PAV2 and PAV4 age condition. The other 4 binders, except for the FT221 binder, satisfy the specification at the PAV2 condition but will start forming some cracks during the PAV4 state.

The FT221 binder showed the best results for this study in terms of the ΔTc parameter. With a ΔTc = -3.189˚C at PAV4 it indicates that the relaxation properties of the binder are more resistant to ageing than the other 6 binders. This binder conforms to the specification at the PAV4 state, which means this binder may retain its relaxation properties for 7 - 10 years of pavement life.

5.3 Master Curve Analysis

This section covers the individual and combined BBR and DSR master curve comparison for all the binders. The data for the PAV1 aged binders is used to evaluate the comparisons between the BBR results of the binders. Lastly, a clear discussion will follow regarding the mathematical model fit on each of the binders.

5.3.1 BBR data

The raw BBR data, which entails the deflection and time data, was converted with the RHEA software to stiffness and time as discussed in Chapter 4. With the known stiffness the Gordon and Shaw free-shifting method could be applied to the data. The PAV1 aged data for each binder is represented in Figure 92. The difference in the stiffness curves for the unaged, RTFO, PAV2 and PAV4 aged binders is comparable to the results seen in Figure 92. Figure 93 show the Arrhenius shift of the PAV1 aged binders. The comparisons for the other ages can be seen in Annexure D.

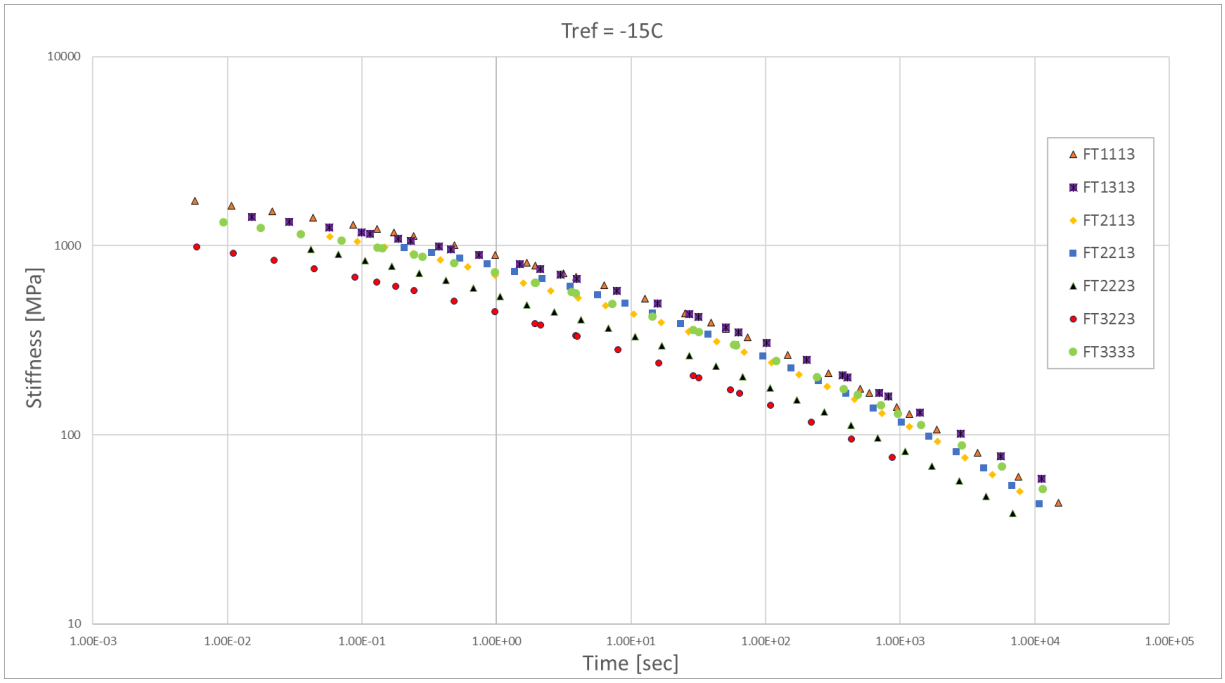

Figure 92: The stiffness-time diagrams for the PAV1 aged binders

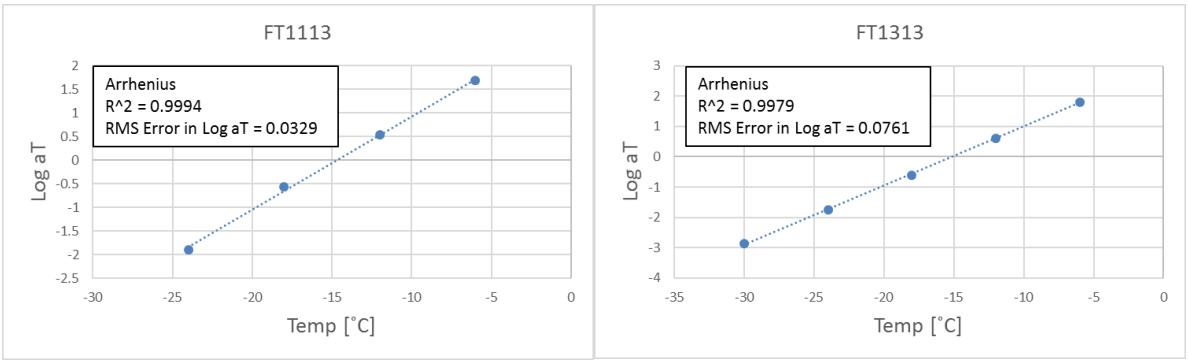

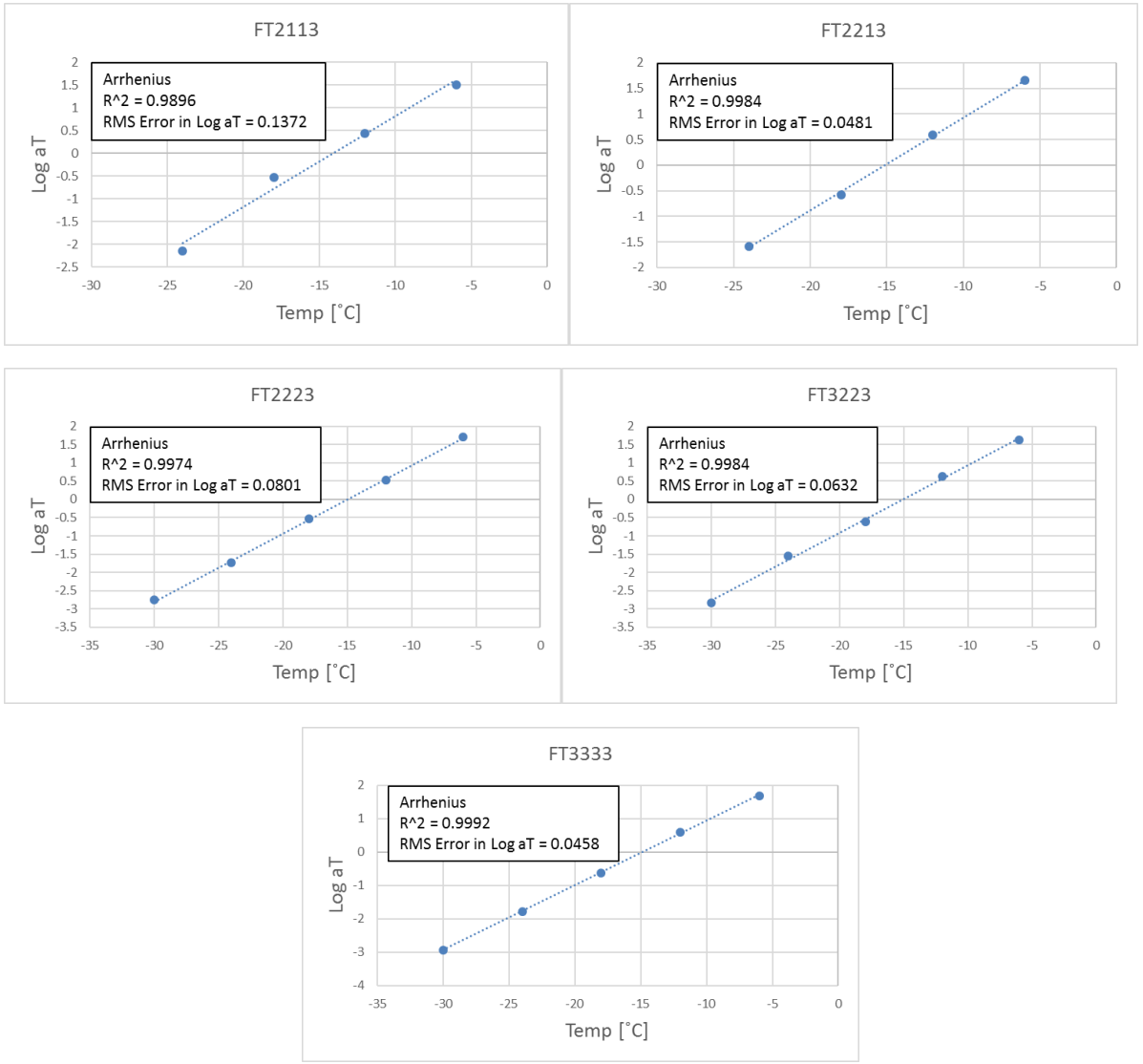

Figure 93: Shift factor graphs for the PAV1 aged binders indicating the fit of the Arrhenius shift factor

Figure 92 shows the shifted stiffness-time curves for all the seal binders at their PAV1 conditioning state. The stiffness curves for the Unaged, RTFO, PAV2 and PAV4 state are summarised in Annexure D. Except for the FT1313 and FT3333 binders, it appears as if the trend of the stiffness curves for each binder decreases consistently as time increases in comparison with one another. The trends of the stiffness curves for FT1313 and FT333 are slightly flatter in comparison with the rest of the binders. These binders indicate more resistance to deformation as the stiffness decreases at a slower rate as time increases.

The FT2223 and FT3223 binders exhibited the lowest stiffness in comparison with the rest of the binders at the field ageing condition (PAV1). These two binders indicated the highest ΔTc value, as seen in the previous section. With lower stiffness at the PAV1 state these two binders are the closest to the South African Performance Grade specification for the ΔTc limit of >-5. The reason for this may be due to the preparation of the binders i.e. the percentage modification of SBS and/or the influence of the crosslinking agent.

The effect that ageing has on only the BBR data for each binder is indicated in Annexure C. The effect of ageing at lower temperatures is small in comparison with the effect at higher temperatures. This behaviour is due to the binders becoming increasingly glassy at the same point. By following the trends of these stiffness curves all of the binders have the potential to reach a stiffness of 3000MPa that

correlates with the Glassy Modulus for bituminous binders (Christensen *et al*., 1992). The difference in the effect that ageing has on these binders will be illustrated in section 4.3.2.

5.3.2 Merged data

The merged BBR and DSR data was analysed with the RHEA software and Microsoft Excel to correlate the results. The cross-over frequency was determined with the raw BBR and DSR data by taking the point of intersection between the loss and storage modulus. The results were correlated with the RHEA software and the difference was negligibly small. Table 13 indicates the susceptibility of the cross-over frequency to ageing.

Table 13: The influence of ageing on the cross-over frequency and G* at the cross-over frequency for T_{ref} = 15˚C

		Unaged	RTFO	PAV1	PAV2	PAV4
FT111	wo (rad/sec)	106.049	16.476	6.597	1.260	0.408
	Gc* (kPa)	32403.937	21998.207	18223.250	11759.750	8694.658
FT131	wo (rad/sec)	260.227	123.586	15.481	3.310	0.661
	Gc* (kPa)	35880.150	30106.440	19983.919	13940.256	9151.018
FT211	wo (rad/sec)	43.260	17.381	5.213	1.188	0.148
	Gc* (kPa)	18429.041	14863.955	11675.210	8116.024	4696.008
FT221	wo (rad/sec)	268.920	186.139	5.569	3.523	3.064
	Gc* (kPa)	33282.914	28216.390	12376.510	11414.707	10105.750
FT222	wo (rad/sec)	25.672	19.900	1.424	0.396	0.325
	Gc* (kPa)	12447.185	9768.173	6028.117	4873.415	4634.608
FT322	wo (rad/sec)	67.103	15.927	1.107	0.284	0.183
	Gc* (kPa)	8831.662	8672.750	4299.118	3003.290	2267.759
FT333	wo (rad/sec)	15.800	12.104	0.873	0.675	0.224
	Gc* (kPa)	11855.605	11186.726	7747.294	7125.404	5660.008

As the age of a bituminous binder increases the binder oxidizes and hardens. During the oxidation process the cross-over frequency of the binder decreases (G. M. Rowe, Eng, & Ph, 2014). Table 13 shows how the cross-over frequency of each binder decreases as the age of the binder increases. The rate at which the cross-over frequency decreases for each binder differs. As the cross-over frequency decreases as the age of the binders increase the complex modulus at the cross-over frequency decreases for each binder age. This behaviour is due to the binders becoming more viscous at the higher temperatures and lower frequencies.

The FT111, FT131 and FT221 binders have the highest cross-over frequency at their unaged condition in comparison with the rest of the binders. The FT111 binder was mostly susceptible to the short-term ageing process as the cross-over frequency between the unaged and RTFO state decreased dramatically. The FT131 and FT221 binders were more susceptible to the long-term ageing process as their cross-over frequency had a rapid decrease between the RTFO and PAV1 state.

The FT221 binder had a rapid decrease in the cross-over frequency between the unaged and long-term aged conditions. Furthermore, the cross-over frequency experienced a slight decrease as the binder went through the PAV2 and PAV4 state. This behaviour indicates that the binder was more resistant to the ageing procedure in comparison with the rest of the binders.

The FT333 binder had the smallest cross-over frequency at the unaged state in comparison with the other six binders. The rate at which the cross-over frequency decreased as the age of the binder increased was much slower in comparison with the rest of the binders. This does not say that the

binder was less affected by the ageing process. This may be due to the binder being highly modified. At the PAV4 state the cross-over frequency of the FT333 binder is close to those of the FT322 and FT211 binders.

As the binders age the stiffness of the binders increase. The highest difference in the stiffness values of the binders occur at higher temperatures. Table 14 indicates the complex modulus values at a frequency of 0.00001rad/s which include the 70˚C isotherm results for all the ages of all seven binders. Figure 94 show the comparison of the complex modulus values of all the binders with their ages as summarised in Table 14.

Table 14: The influence of ageing on the Complex Shear Modulus at T_{ref} = 15˚C

	G*(Pa) @ 0.00001rad/s				
	Unaged	RTFO	PAV1	PAV2	PAV4
FT111	46.652	270.697	623.833	2317.837	5559.635
FT131	20.929	41.362	299.621	1301.452	4363.723
FT211	150.914	354.833	802.900	2386.334	9400.012
FT221	50.694	57.949	866.006	1196.070	1324.304
FT222	159.394	313.430	1817.253	4546.353	5232.012
FT322	470.287	465.589	1783.909	4126.684	4922.065
FT333	496.814	583.240	3102.069	3572.757	7334.146

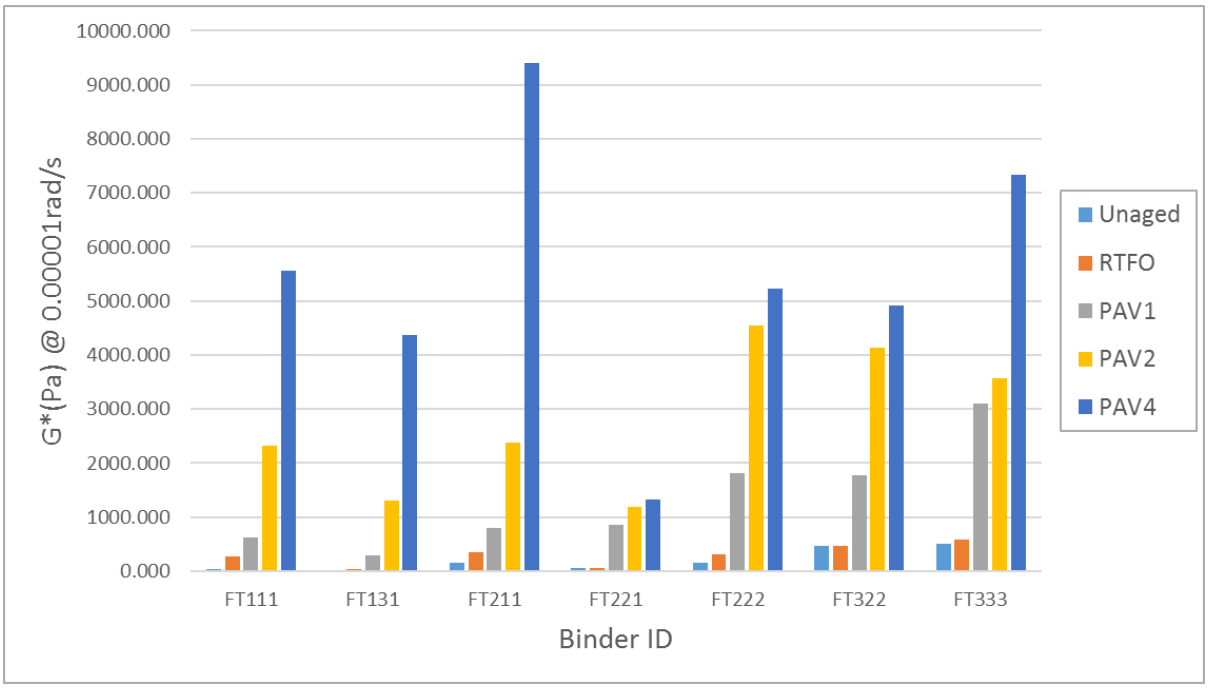

Figure 94: Complex Shear Modulus data from Table 14

By comparing the results in Table 13 and Table 14, the binders that had the higher cross-over frequencies had the lowest complex modulus. The FT111, FT131 and FT221 binders had a complex modulus of less than 100 Pa in their unaged state in comparison with the other 4 binders that had a smaller cross-over frequency and thus a higher complex modulus. The susceptibility of the FT111 and FT131 binders to ageing caused the binders to result in a high complex modulus at their PAV4 state. The FT211 binder indicated the highest complex modulus and the lowest cross-over frequency at the PAV4 state in comparison with the rest of the binders. This binder is highly susceptibility to ageing and the relaxation properties of the binder may be damaged. The FT221 binder showed the lowest complex modulus at the PAV2 and PAV 4 state in comparison with the rest of the binders. This behaviour may be due to the binder being more resilient to the ageing process.

The rapid change in the cross-over frequency of the binders correlate well with the rapid change in the results of the complex modulus of the binders at the specified position. By looking at the FT111 binder the complex modulus increased from 46.652 to 270.697 between the unaged and RTFO state. The large increase in the complex modulus may be explained by the sudden decrease in the cross-over frequency of the binder between the unaged and RTFO state. These results indicate how ageing influences the performance of the seal binders.

5.3.3 Mathematical Model Comparison

This section covers the mathematical model comparison for all the ages of the seven seal binders. The CA, CAM, GL and DS models were analysed to evaluate the goodness of fit to the data.

Table 15 summarises the RMS error percentage for the fit of the master curve data of the seal binders to the models. The RMS error includes the total "goodness of fit" of the complex modulus master curve and the phase angle master curve. Annexure F shows the fit of each model to the data of the seal binders with their ages.

Table 15: RMS error fit of the models to the master curves of all 7 seal binders

Binder	Age	Model (RMS error [%])			
		CA	CAM	GL	DS
FT111	Unaged	7.12	6.21	4.53	10.50
	RTFO	7.45	6.50	2.32	4.94
	PAV1	8.24	7.89	2.02	3.68
	PAV2	8.98	8.91	1.83	2.96
	PAV4	9.97	9.86	1.63	2.65
FT131	Unaged	4.60	3.84	3.07	14.31
	RTFO	4.91	3.87	2.56	9.00
	PAV1	7.33	6.29	1.55	5.55
	PAV2	9.21	8.76	1.73	2.72
	PAV4	10.15	10.01	1.32	4.90
FT211	Unaged	17.63	14.94	3.35	3.14
	RTFO	10.08	9.84	3.45	2.52
	PAV1	5.59	5.49	3.06	3.29
	PAV2	4.03	4.01	3.20	2.85
	PAV4	4.21	3.85	1.67	2.36
FT221	Unaged	9.35	7.33	3.24	5.73
	RTFO	8.73	8.74	3.22	4.37
	PAV1	2.74	2.67	2.49	2.50
	PAV2	2.05	1.94	2.62	2.09
	PAV4	3.81	3.72	3.69	2.14
FT222	Unaged	7.48	5.46	2.31	4.57
	RTFO	4.01	3.06	2.39	4.42
	PAV1	3.23	3.02	1.81	3.08
	PAV2	4.67	4.47	1.34	3.33
	PAV4	4.07	3.79	1.24	2.48
FT322	Unaged	21.67	19.44	4.28	3.67
	RTFO	14.96	14.92	3.71	3.55
	PAV1	2.54	2.42	2.47	1.68
	PAV2	2.94	2.84	2.51	2.13
	PAV4	3.64	3.54	2.94	2.24
FT333	Unaged	14.96	14.92	3.71	3.55
	RTFO	12.00	11.76	3.80	3.65
	PAV1	4.74	4.69	2.85	1.99
	PAV2	3.67	3.67	2.85	1.71
	PAV4	2.59	2.58	2.16	2.33

It appears in

Table 15 that the GL and DS models have the lowest RMS error percentage in comparison to the CA and CAM model. The RMS error results may not necessarily indicate which model is the best or which model gives the better fit. The RMS error may differ for each binder and age as well as with repeatability of the data.

The RMS error analysed the data in such a manner that the area above the model is compared to the area below the model. By analysing the fit of the CA model to the unaged FT333 binder the fit appears to be unacceptable, but the RMS error is 14.96% which is not extremely high.

The CA and CAM model appear to analyse the unmodified FT111 and FT131 binders acceptably well during all the ages of the binders. The CA and CAM models do not fit the modified models very well in the unaged and RTFO state. As the modified binders age the master curves become flatter and the RMS error for the CA and CAM models appear to decrease due to an increase in the goodness of fit of the models to the master curves.

Table 15 shows that there is a slight difference in the fit of the models in the PAV1, PAV2 and PAV4 state of the binders. With all this said, the DS model was chosen to analyse the parameters needed to evaluate the susceptibility of the seal binders to ageing. The DS model may not appear to be the best model to use in terms of the RMS error, but the model is the most accurate at the required positions. For example, the DS model is the best fit at a frequency of 0.005rad/sec where the G-R parameters need to be analysed.

The RMS error for the phase angle master curves is much larger than the error of the complex modulus. Most of the RMS error percentages, in

Table 15, is due to the fit of the model to the phase angle master curve. The fit of the models to the complex modulus master curve vary between 0% and 2% compared to the fit of the phase angle master curves which vary between 3% and 15%. The phase angle was determined for all the binders with their ages at 0.005 rad/sec with each model. Figure 95, Figure 96 and Figure 97 show the difference in the phase angle at frequency of 0.005 rad/sec between the models for each age of the FT131, FT211 and FT322 binders. The comparisons of the FT111, FT221, FT222 and FT333 binders can be seen in Annexure F.

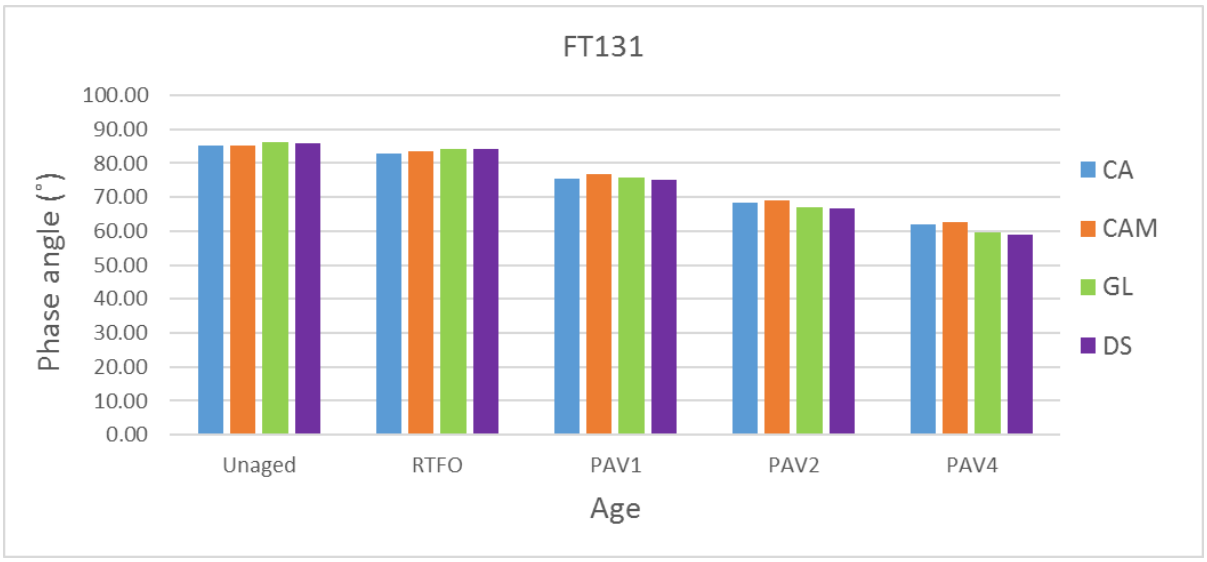

Figure 95: Phase angles of FT131 at 0.005 rad/sec and T_{ref} = 15˚C for all the ages and models

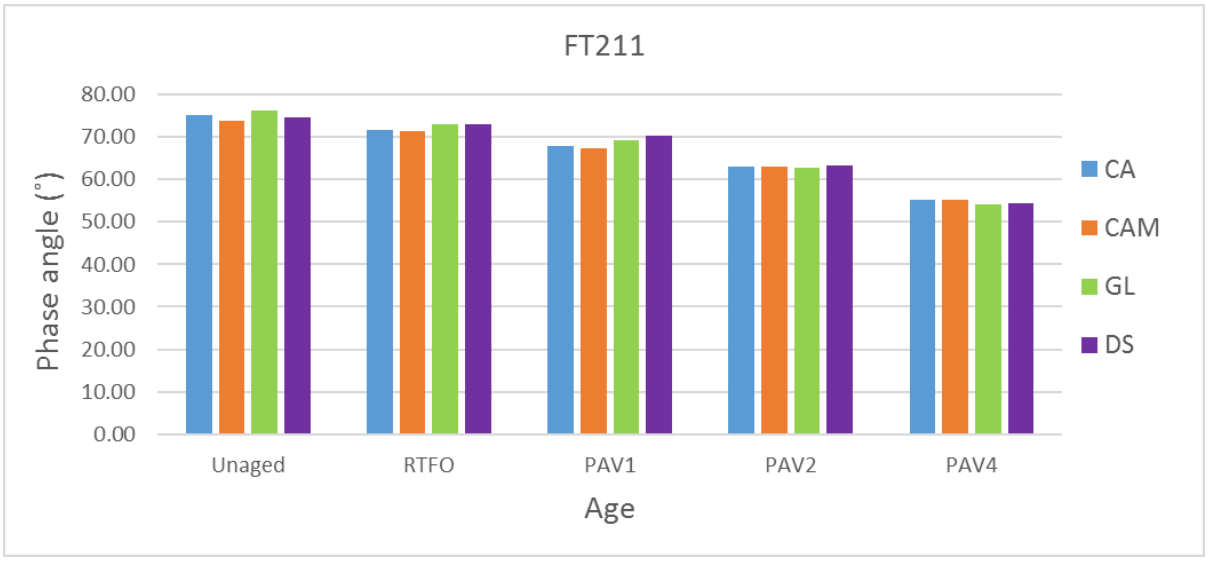

Figure 96: Phase angles of FT211 at 0.005 rad/sec and T_{ref} = 15˚C for all the ages and models

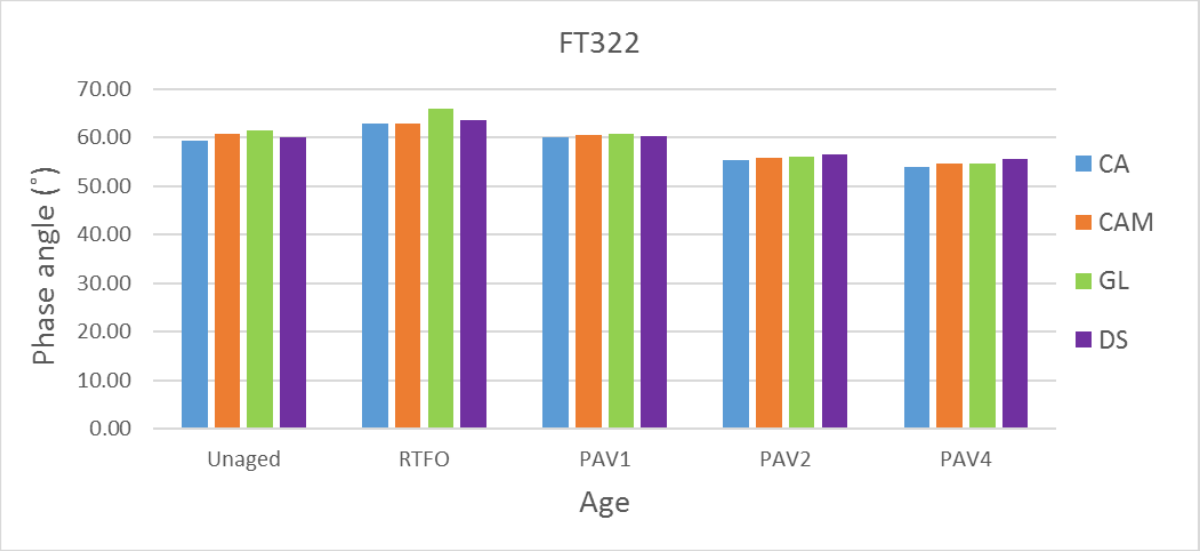

Figure 97: Phase angles of FT322 at 0.005 rad/sec and T_{ref} = 15˚C for all the ages and models

Figure 96 and Figure 97 show a decrease in the difference between the phase angles for each model as the binders age. This is clearer for the modified binders compared to the unmodified binders. As the modified binders age the shape of the phase angle master curve flattens out and starts to assume a shape similar to that of the unmodified binders. This explains the slight difference in the phase angle values for each model at the PAV2 and PAV4 state of the modified binders.

5.4 Black Space Analysis

This section discusses the comparisons between an unmodified 70/100 binder, 3% SBS modified 70/100 binder and a 5% SBS modified 70/100 binder. The FT131, FT 211 and FT322 binders are compared with one another to analyse how ageing affects the binder and the modification.

The Black Space diagrams are analysed at a reference temperature of 15˚C. The temperature range for each Black Space diagram is between -30˚C and 70˚C. The shift factor curves for each of the binders and their age can be seen in Annexure G. Figure 98 shows the behaviour of an unmodified binder in its unaged, RTFO, PAV1, PAV2 and PAV4 state in black space.

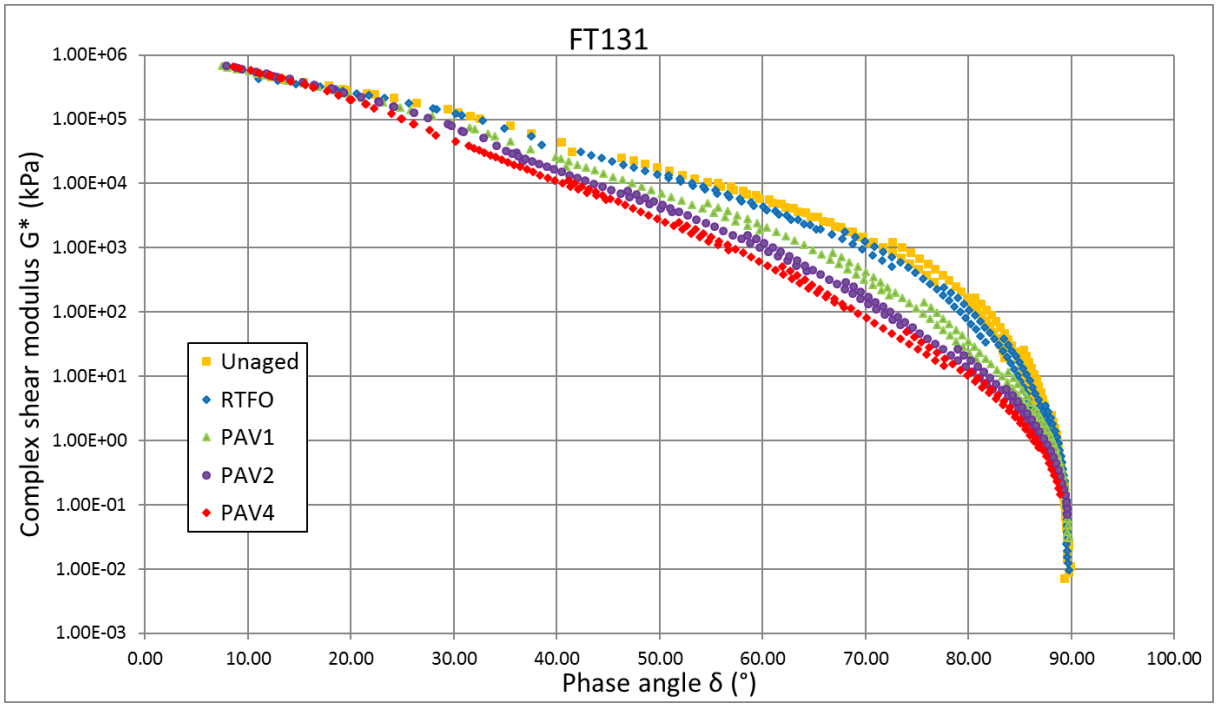

Figure 98: The Black Space diagram for all the ages of the FT131 binder, Tref = 15˚C.

The Black Space diagrams for the FT131 binder in the colder region appear to converge at the completely glassy point between 0.6 GPa and 1.5 GPa, as expected for bituminous materials. The unmodified behaviour of the FT131 binder can be seen with the point of convergence in the warmer region at a phase angle of 90˚. At 70˚C all ages of the FT131 binder experience completely viscous behaviour with a phase angle of 90˚.

Figure 98 shows the influence that the oxidation process has as the binder ages. The phase angle for each temperature isotherm decreases as the binder ages. It appears that between the completely viscous and completely elastic state as the binder ages it becomes stiffer and more elastic simultaneously.

Figure 99 illustrates the behaviour of a 3% modified S-E1 binder with crosslinking agents and 70/100 as the base binder. The behaviour of the FT211 binder is compared to the behaviour of the FT131 binder in black space.

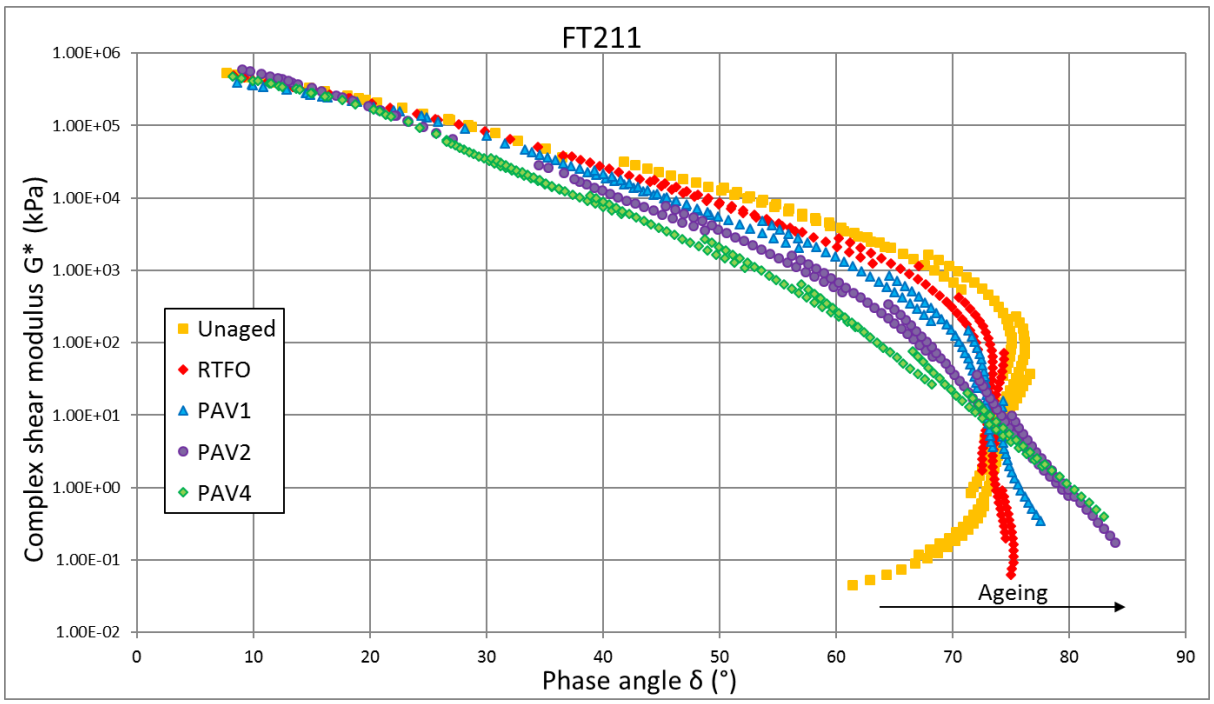

Figure 99: The Black Space diagram for all the ages of the FT211 binder, Tref = 15˚C.

Figure 99 shows that the ages of the FT211 binder converge well at the high viscosity and low phase region i.e. low temperature range. At the higher temperature and high phase angle region the Black Space diagrams do not converge at a phase angle of 90˚ in comparison with the results of the FT131 binder due to the presence of the modifier in the FT211 binder. The shape of the unaged Black Space diagram for the FT211 binder changes at a phase angle of 75˚ which indicates the position where the modifier improves the elastic component of the binder. As the age of the binder increases the shape of the Black Space diagrams for the FT211 binder becomes comparable to those of the FT131 binder. By analysing the shape of the Black Space diagram for the RTFO and PAV1 state of the FT211 binder, it appears that the rate at which the modification improves the elastic component of the binder decreases. The PAV2 and PAV4 Black Space diagrams of the FT211 binder strive to the completely viscous state at a phase angle of 90˚. The behaviour of the PAV2 and PAV4 aged FT211 binder appears to match the behaviour of the unmodified FT131 binder.

It appears that the modification of the FT211 binder becomes less effective as the binder ages (Lu, Sandman & Redelius, 2007). It is noticeable that something changes within the particle bonds of the modifier as the oxidation process continues. This behaviour is observed in die higher temperature region where the binder is more viscous. As the binder ages the elastic network of the modifier may experience some deterioration and the higher temperatures may cause the network of the aged binders to detach.

Figure 100 illustrates the Black Space diagram for each age of the FT322 binder. This binder is highly modified SBS and contains crosslinking agents.

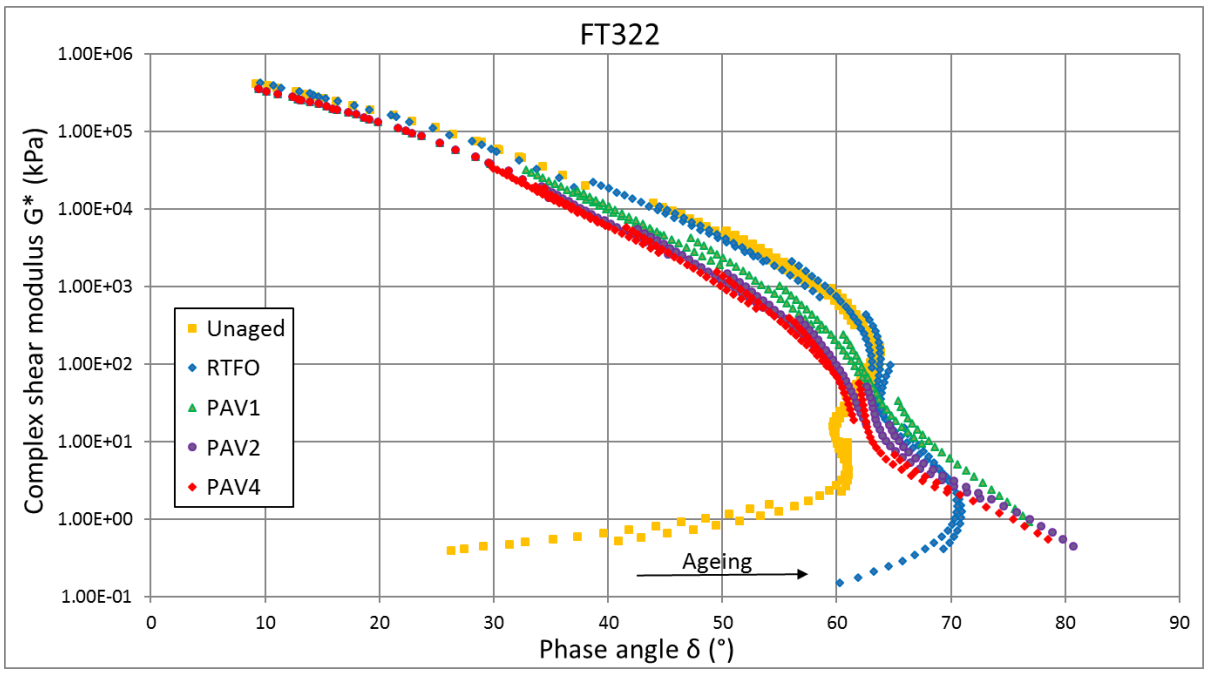

Figure 100: The Black Space diagram for all the ages of the FT322 binder, Tref = 15˚C.

Once again, it appears that the Black Space diagram for all the ages of the FT322 binder will converge at the glassy state of bituminous binders between 0.6Gpa and 1.5GPa. However, due to the high modification percentage, the appearance at the low viscosity and high phase angle region differs in comparison to those illustrated in Figure 98 and Figure 99.

The shape of the Black Space diagram for the unaged FT322 binder changes at a phase angle of 63˚ in comparison with the 75˚ of the FT211 binder. The difference in the percentage of modification between these two binders is only 2% and the phase angle decreases with 13%. By comparing the other 3% modified SBS binders with the other 5% SBS modified binder the difference is not as large as with the FT211 and FT322 binders but still above 8%.

The RTFO aged FT322 binder indicates that some of the modification is still present within the binder with a small change in the shape of the curve at a phase angle of 70˚. The Black Space diagram for the PAV1 aged FT211 binder shows that some modification is still present, but by comparing this result to the behaviour of the FT322 binder it differs. The PAV1 aged Black Space diagram of the FT322 binder shows that the binder has no modification left to increase the performance of the elastic component within the binder as the curve has no change in shape. Table 16 show the points at which the shape of the black space diagrams changes for all the ages of the binders.

Table 16: Summary of the phase angle curvature points

		Phase Angle (˚)				
		Unaged	RTFO	PAV1	PAV2	PAV4
FT111	Unmodified	Converge at 90				
FT131	Unmodified					
FT211	Modified (3% SBS)	75	72	70	No bend , strives to 90	
FT221	Modified (3% SBS)	76	74	No bend, strives to 90		
FT222	Modified (3% SBS)	77	65	No bend, strives to 90		
FT322	Modified (5% SBS)	62	70	Slight bend, strives to 90		
FT333	Modified (5% SBS)	68	66	Slight bend, strives to 90		

The unmodified binders have no curvature point and the black space diagrams strive to 90˚ due to no modification. It appears that the curvature points of the 3% modified binders occur at 75˚ for the

unaged state of the binders. The results for the RTFO aged condition are between 72˚ and 74˚. During the long-term age condition of the 3% modified binders there is no bend in the curve.

The highly modified binders i.e. FT322 and FT333 show a point of curvature between 62˚ and 68˚ for the unaged state of the binders. This is due to the modification that starts to improve the elastic properties of the binder. As the age of the highly modified binders increase a slight bend is still visible. The point of curvature of the black space diagram is thus dependant on the amount of modification within the binder.

5.5 Creep and Recovery Analysis

The MSCR results entail data at temperatures 58˚C, 64˚C and 70˚C for all the ages of the binders. Two stress conditions were analysed according to the procedures of the ASTM D7405 which incorporates the AASHTO M320 specifications.

The individual results for each binder are summarised in Annexure H. The results for the comparison of the seal binders can be seen in Annexure H.

The J_{nr} and percentage recovery results in Table 17 and Table 18 show the susceptibility of the seal binders to temperature and ageing at the lowest (58˚C) and highest test temperature (70˚C). The results in Table 17 and Table 18 were obtained at a stress of 3.2kPa.

Table 17: MSCR results for all the ages of each binder at 3.2kPa and 58˚C

		Unaged	RTFO	PAV1	PAV2	PAV4
FT111	Jnr (1/kPa)	5.066	2.049	0.820	0.291	0.151
	Recovery (%)	0.000	0.000	1.275	7.595	15.343
FT131	Jnr (1/kPa)	3.999	3.033	1.162	0.374	0.170
	Recovery (%)	0.000	0.000	0.637	6.156	15.091
FT211	Jnr (1/kPa)	0.466	0.428	0.319	0.156	0.049
	Recovery (%)	68.641	49.219	43.531	37.691	50.623
FT221	Jnr (1/kPa)	2.653	1.007	0.344	0.197	0.253
	Recovery (%)	12.276	19.257	25.031	28.761	25.799
FT222	Jnr (1/kPa)	0.397	0.014	0.137	0.051	0.063
	Recovery (%)	50.873	97.419	38.754	47.184	42.609
FT322	Jnr (1/kPa)	0.138	0.388	0.107	0.028	0.035
	Recovery (%)	78.481	39.743	50.569	74.279	69.507
FT333	Jnr (1/kPa)	0.243	0.278	0.103	0.078	0.040
	Recovery (%)	64.891	56.221	59.376	54.438	60.461

Table 18: MSCR results for all the ages of each binder at 3.2kPa and 70˚C

		Unaged	RTFO	PAV1	PAV2	PAV4
FT111	Jnr (1/kPa)	24.431	10.809	5.102	2.240	1.282
	Recovery (%)	0.000	0.000	0.000	0.000	0.885
FT131	Jnr (1/kPa)	23.268	18.399	7.297	2.851	1.448
	Recovery (%)	0.000	0.000	0.000	0.000	0.754
FT211	Jnr (1/kPa)	3.940	3.008	2.273	1.292	0.496
	Recovery (%)	27.430	19.658	16.247	9.901	16.007
FT221	Jnr (1/kPa)	12.799	5.566	2.274	1.511	1.848
	Recovery (%)	0.000	1.958	4.122	4.862	3.868
FT222	Jnr (1/kPa)	3.979	5.531	1.175	0.516	0.610
	Recovery (%)	15.667	0.000	12.275	12.951	10.492
FT322	Jnr (1/kPa)	1.382	2.149	0.870	0.361	0.402
	Recovery (%)	51.189	20.910	22.427	32.226	30.367
FT333	Jnr (1/kPa)	1.441	1.464	0.770	0.811	0.397
	Recovery (%)	47.384	44.796	37.942	17.824	31.873

The J_{nr} results in Table 17 and Table 18 are visually represented in Figure 101 and Figure 102. Only the 58 and 70 results were used to evaluate the temperature and age susceptibility of the binders.

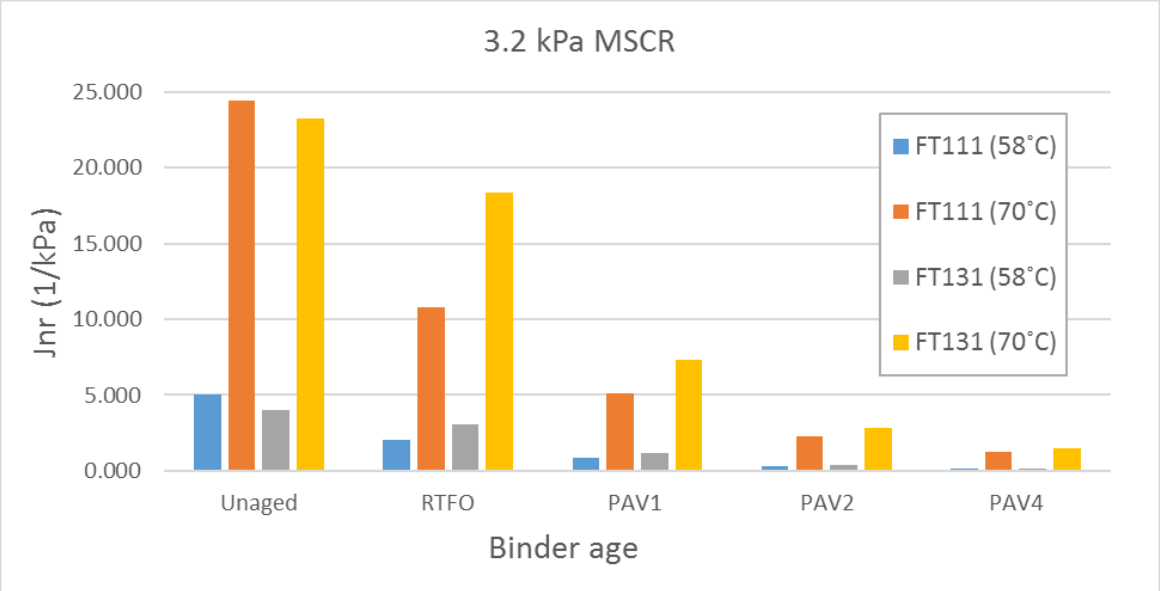

Figure 101: The J_{nr} results for the unmodified binder at 3.2kPa

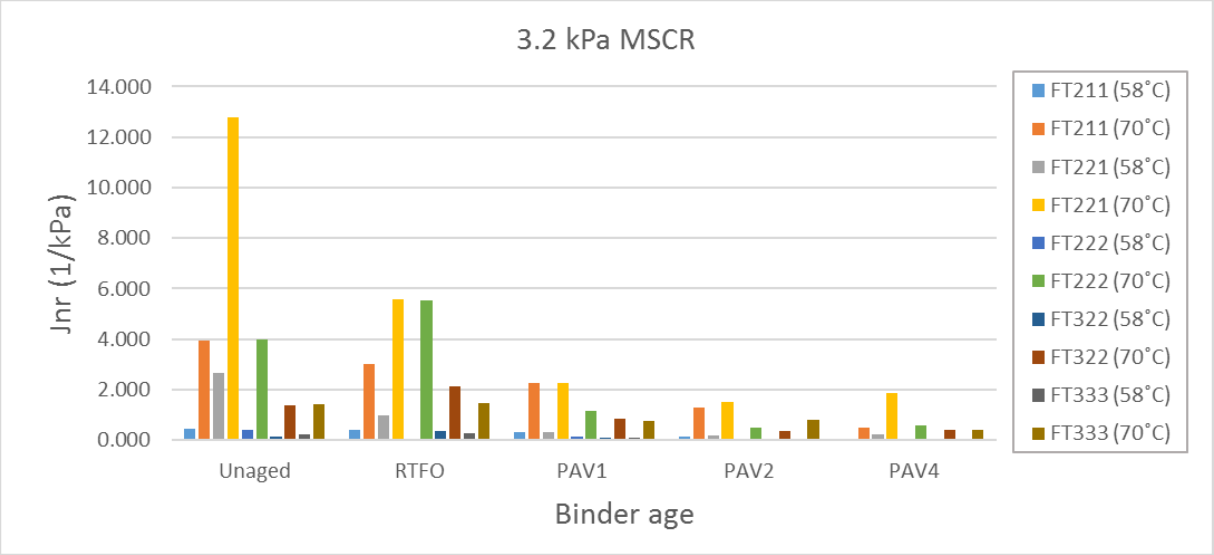

Figure 102: The J_{nr} results for the modified binder at 3.2kPa

By comparing the MSCR results of each binder in Table 17 and Table 18 with one another the temperature susceptibility is remarkably large in terms of the J_{nr} and percentage recovery. The J_{nr} results increase as the test temperature increases. This is due to the increased viscous behaviour resulting in an increase in unrecovered strain. The binder becomes more viscous as the temperature increases and the binder loses its ability to recover. Table 17 and Table 18 show that the percentage recovery of each binder and age decreases as the temperature increases due to the loss in the recovery properties of the binders.

The J_{nr} results of each binder appear to decrease as the age of the binder increases. The J_{nr} is thus highly susceptible to temperature and age. It appears that the J_{nr} and percentage recovery results for all the binders are very close to one another at the PAV2 and PAV4 state. By looking at the combined master curves of these binders it appears that as the binders reach the PAV2 and PAV4 state the ageing rate decreases, which means the binders do not experience a high property change between these two ages. The results in Table 17 and Table 18 are thus as expected at the PAV2 and PAV4 state. It is important to remember that the results should be more accurate by repeating the test procedure several times for each binder and age.

As expected, the unmodified binders (FT111 and FT131) show very low percentage recovery results. The J_{nr} results of these binders are two of the highest at all the ages in comparison with the modified binders. This behaviour is due to the binder not having any recovery properties.

The results of the FT221 binder are the closest to the unmodified binders with may be due to the binder having less than 3% modification. The highly modified binders indicate the highest percentage recovery results. This behaviour is as expected due to the FT322 and FT333 binders having the highest percentage of modification. These binders have very low J_{nr} values due to the percentage unrecovered strain that is minimal. The modification within the binders increases the elastic component of the binders which increases the recovery properties of the binders.

Figure 104, Figure 105, Figure 106 and Figure 107 show the results of the J_{nr} and percentage recovery for all the ages of the binders. Figure 107 data includes the results at 58˚C, 64˚C and 70˚C and at a stress of 3.2kPa. The Asphalt Institute (AI) document was used to analyse the data which contains the procedures of ASTM D7405 specifications.

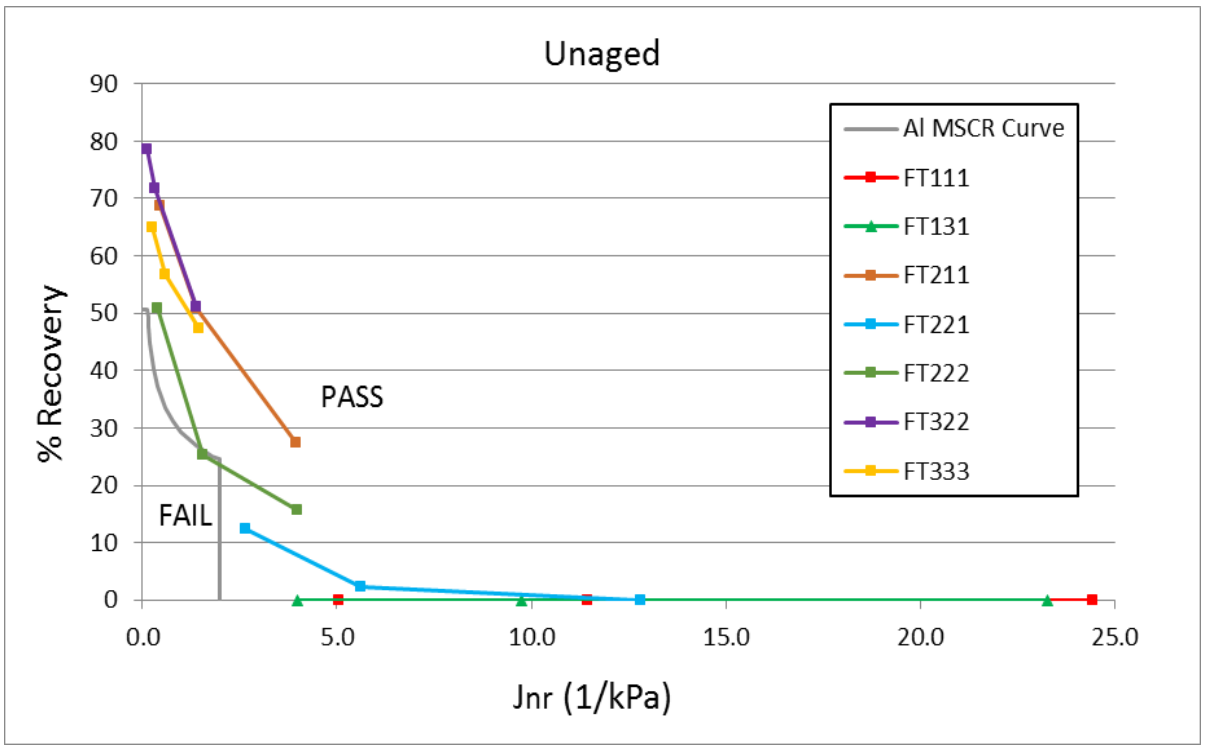

Figure 103: MSCR data for the unaged binders at 3.2kPa and temperatures of 58˚C, 64˚C and 70˚C

Figure 107 shows the magnitude of the susceptibility of the seal binders to ageing. During the unaged state the binders satisfy the MSCR boundary of the AI. The 64˚C point of the FT222 binder is just inside the failure zone at the unaged state. Figure 104 show the behaviour of the RTFO aged binders.

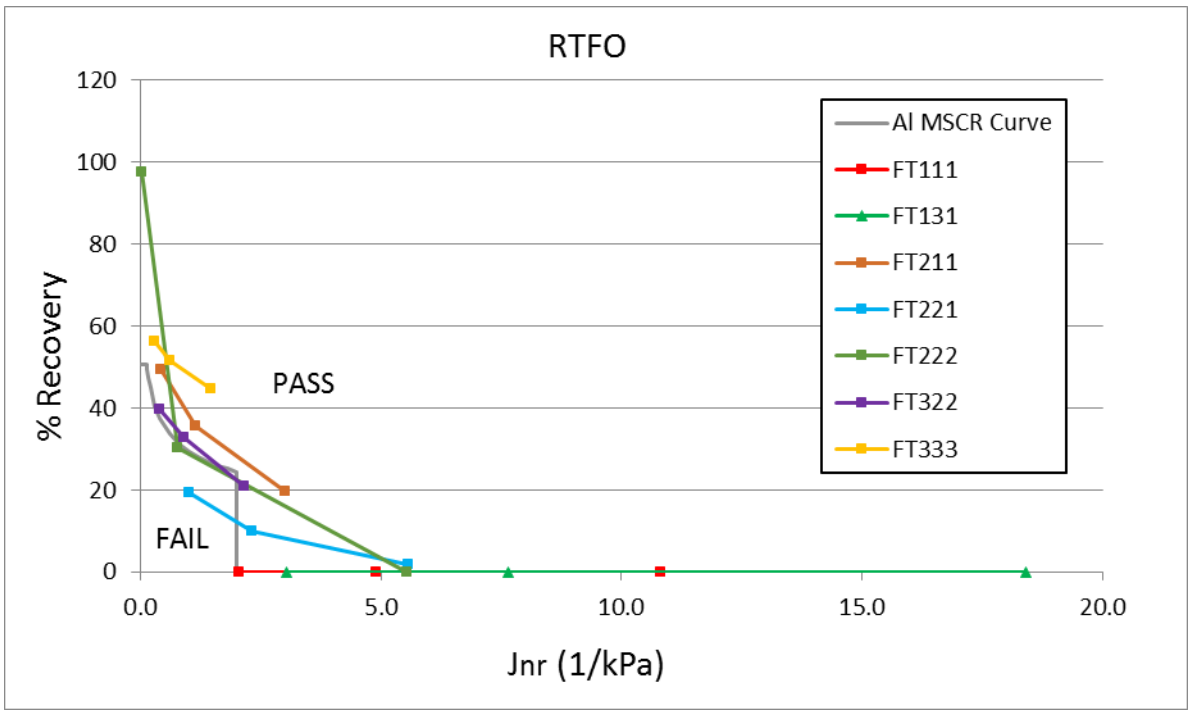

Figure 104: MSCR data for the RTFO aged binders at 3.2kPa and temperatures of 58˚C, 64˚C and 70˚C

At the RTFO state the binders start to move closer to the failure zone. The 58˚C point of the FT221 binder moves inside the failure zone. The 58˚C point of the FT111 binder is on the edge of the ASTM D7405 specification MSCR curve. The FT222 binder shows that the MSCR data for 64˚C is inside the failure zone. The 58˚C, 64˚C and 70˚C data of the FT322 binder is on the edge of the failure zone. Figure 105 shows the behaviour of the PAV1 aged binders.

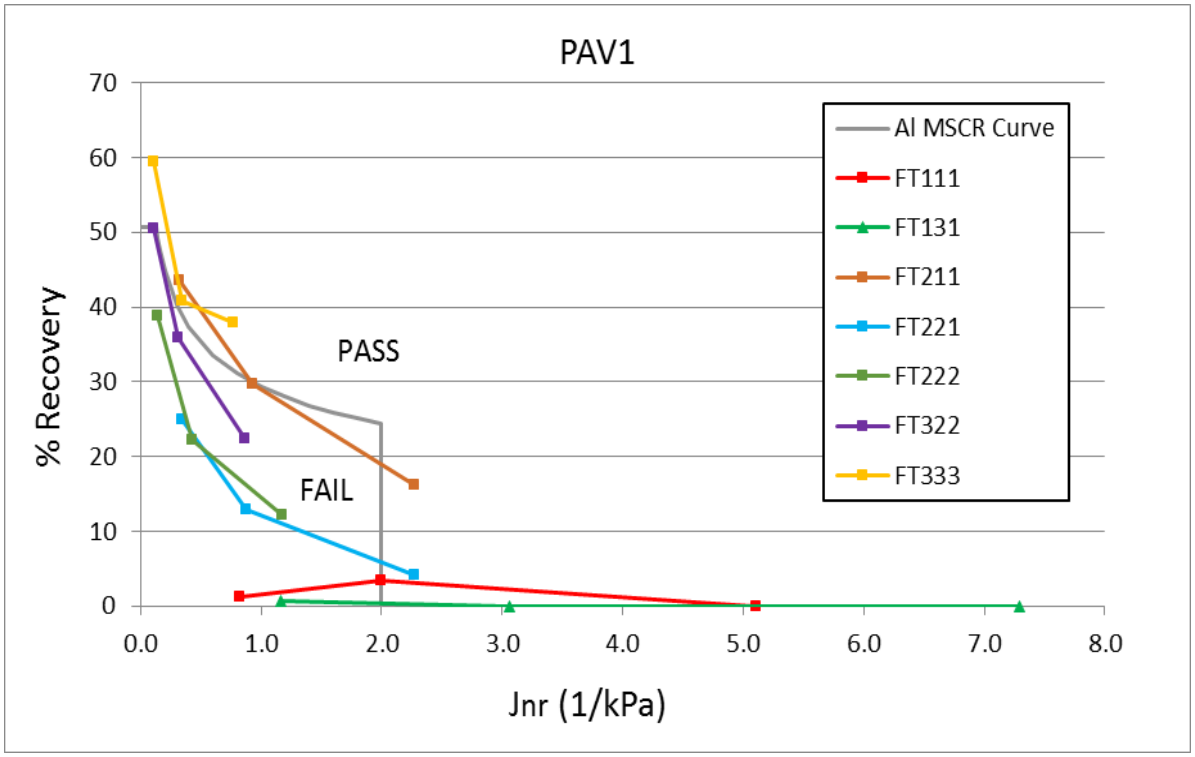

Figure 105: MSCR data for the PAV1 aged binders at 3.2kPa and temperatures of 58˚C, 64˚C and 70˚C

The PAV1 age results show that the FT222 binder is completely inside the failure zone. The 70˚C data for the FT111, FT131, FT211 and FT221 binders satisfy the ASTM D7405 specifications. The FT211

binder is the only 3% modified binder that satisfy the MSCR results at 58˚C and 64˚C for the PAV1 aged condition. Figure 106 shows the behaviour of the PAV2 aged binders.

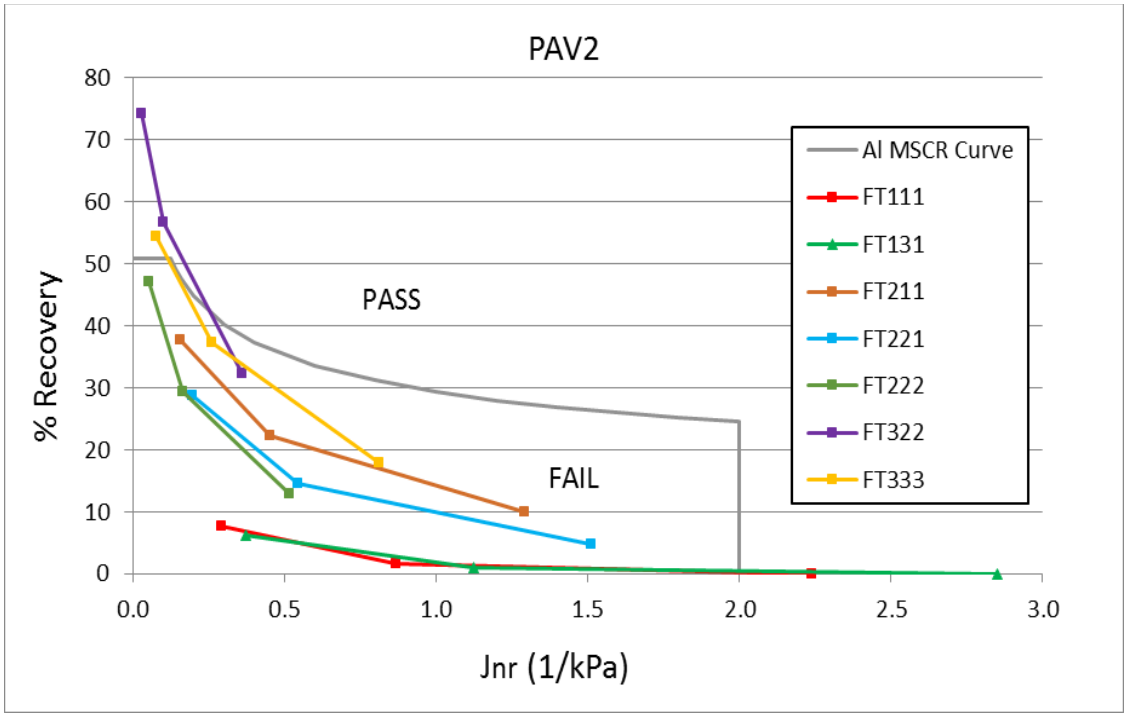

Figure 106: MSCR data for the PAV2 aged binders at 3.2kPa and temperatures of 58˚C, 64˚C and 70˚C

The PAV2 age results show that the unmodified binders satisfy the ASTM D7405 specifications at 70˚C and the highly modified FT322 and FT333 binders at 58˚C. This is due to the unmodified binders having a large J_{nr} and a low percentage recovery. The highly modified binders indicate acceptable results at the 58˚C point due to the percentage recovery of the binder that is above 50%. At the PAV2 state all the 3% modified binders are completely inside the failure zone.

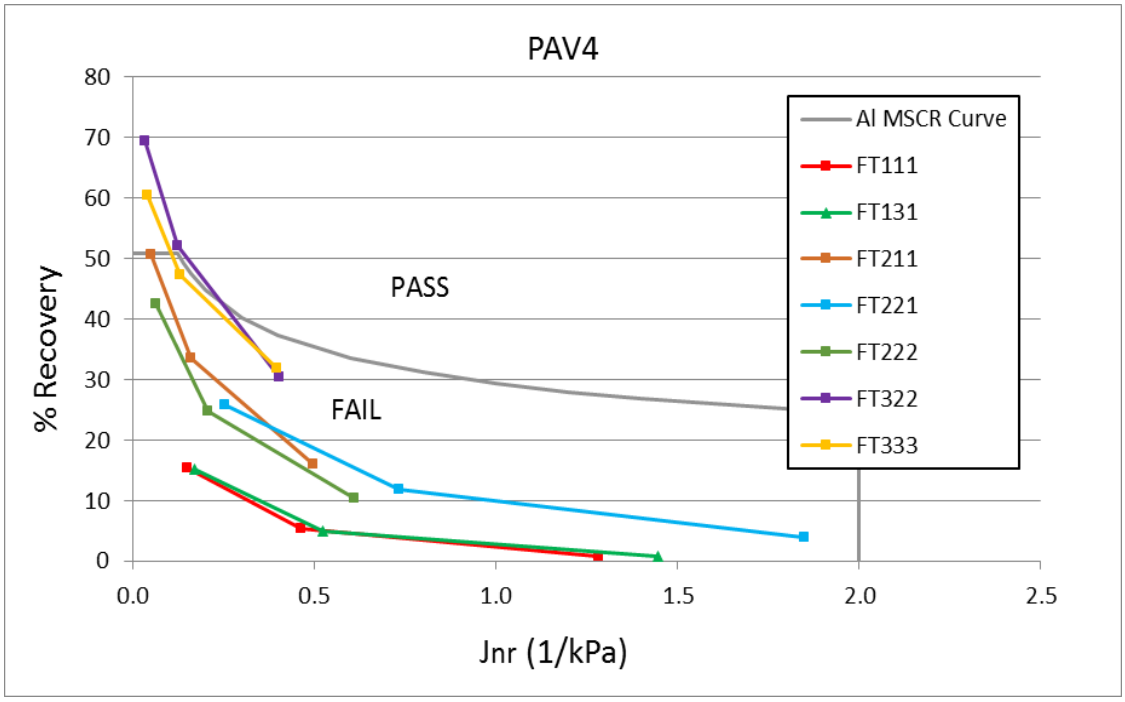

Figure 107: MSCR data for the PAV4 aged binders at 3.2kPa and temperatures of 58˚C, 64˚C and 70˚C

The 58˚C results for the FT322 and FT333 binders are the only ones that satisfy the ASTM D7405 specifications at the PAV4 state. The rest of the binders are highly susceptible to long-term ageing and do not satisfy the AI specification. It appears that the modification within the modified binders leads to them experiencing a loss in their recovery properties as the binder ages. As the modified binders age the percentage recovery decreases which influences the performance of the binder. It appears that the modification particles experience some rupture and detachment during the ageing process.

5.6 Ageing behaviour (G-R parameter)

This section discusses the comparison of the G-R results of all the binders and ages with each other as well as with the Rheological index and ΔTc. The Discrete Spectrum (Generalised Maxwell Model) was used to analyse the data at a temperature of 15˚C and a frequency of 0.005rad/s.

Table 19 contains a summary regarding the complex modulus and phase angle results for all the ages of the binder as well as the G-R parameter results at a temperature of 15˚C and a frequency of 0.005rad/s. The rheological index for all the binders with their ages can also be seen in Table 19.

Table 19: Summary of the G-R and R results for all the ages of all seven binders

		Unaged	RTFO	PAV1	PAV2	PAV4
FT111	Complex modulus, G* [kPa]	20.483	97.146	183.073	448.007	754.654
	Phase angle, δ [˚]	85.0	77.4	72.2	64.7	58.7
	G-R parameter [kPa]	0.156	4.748	18.031	90.195	237.828
	Rheological Index, R	1.303	1.447	1.571	1.750	1.894
FT131	Complex modulus, G* [kPa]	9.299	18.076	100.826	281.862	605.600
	Phase angle, δ [˚]	85.8	84.2	75.1	66.6	58.9
	G-R parameter [kPa]	0.050	0.189	6.945	48.498	189.200
	Rheological Index, R	1.318	1.342	1.568	1.833	1.995
FT211	Complex modulus, G* [kPa]	22.481	51.259	124.731	306.784	746.672
	Phase angle, δ [˚]	74.4	73.0	70.3	63.3	54.4
	G-R parameter [kPa]	1.682	4.604	15.000	69.107	310.802
	Rheological Index, R	1.533	1.742	1.829	2.020	2.318
FT221	Complex modulus, G* [kPa]	11.108	12.759	138.399	182.667	196.602
	Phase angle, δ [˚]	76.7	76.4	67.6	65.9	65.5
	G-R parameter [kPa]	0.602	0.726	21.756	33.281	37.177
	Rheological Index, R	1.589	1.628	1.919	1.951	2.001
FT222	Complex modulus, G* [kPa]	45.485	53.840	213.304	422.959	450.541
	Phase angle, δ [˚]	68.9	69.4	61.2	56.6	56.4
	G-R parameter [kPa]	6.306	7.106	56.478	153.685	165.795
	Rheological Index, R	1.987	2.210	2.214	2.327	2.367
FT322	Complex modulus, G* [kPa]	21.135	50.768	171.600	284.433	312.807
	Phase angle, δ [˚]	60.2	63.5	60.3	56.4	55.7
	G-R parameter [kPa]	6.034	11.271	48.532	104.327	120.310
	Rheological Index, R	2.148	2.175	2.339	2.588	2.685
FT333	Complex modulus, G* [kPa]	52.972	63.648	333.109	370.171	657.631
	Phase angle, δ [˚]	67.4	67.0	63.5	62.3	57.1
	G-R parameter [kPa]	8.445	10.538	74.094	90.156	230.631
	Rheological Index, R	1.994	2.013	2.036	2.077	2.176

The complex modulus of each binder increases as the age of the binder increases. This behaviour is due to the oxidation process that hardens the binders. This is true for both modified and unmodified binders. On the other hand, the phase angle decreases. The results obtained in Table 19 explain the complexity of the behaviour of bituminous binders. The results for both the unmodified and modified binders show that as the stiffness of the binder increases the binders become more elastic with the phase angle that decreases.

The crack initiation limit for the G-R parameter is 180kPa. Four of the seven binders enter the crack initiation zone at their PAV4 state. The FT111, FT131 and FT333 binders are just inside the crack

initiation limit and may show some cracks at a pavement life of 7 to 10 years if it was only dependant on the binder. The FT211 binder also exceeded the crack initiation limit boundary with the highest G-R parameter of 310.802kPa. The FT221 binder has the lowest G-R result at the PAV4 ageing condition of 37.177kPa. This means this binder still has a long way to go to reach the crack initiation limit.

The rheological index values for all the binders increase as the age of the binders increases. This behaviour is due to the cross-over frequency that decreases and the stiffness's that increase as the binders age. It is interesting to see in Table 19 that it is only the unmodified binders that have a R value of less than 2 at the PAV4 condition. The modified binders have a R value above 2 at the PAV4 condition. The larger the R value the higher the chances for surface cracking in a pavement.

Figure 108 illustrates the black space diagram with only the G-R parameter results for all the binders with their ages. The arrow on the graph indicates the direction in which the G-R parameter increases as the age of the binder increases. Figure 109 show the G-R results for all the binders with their ages and the crack initiation limit of 180 kPa.

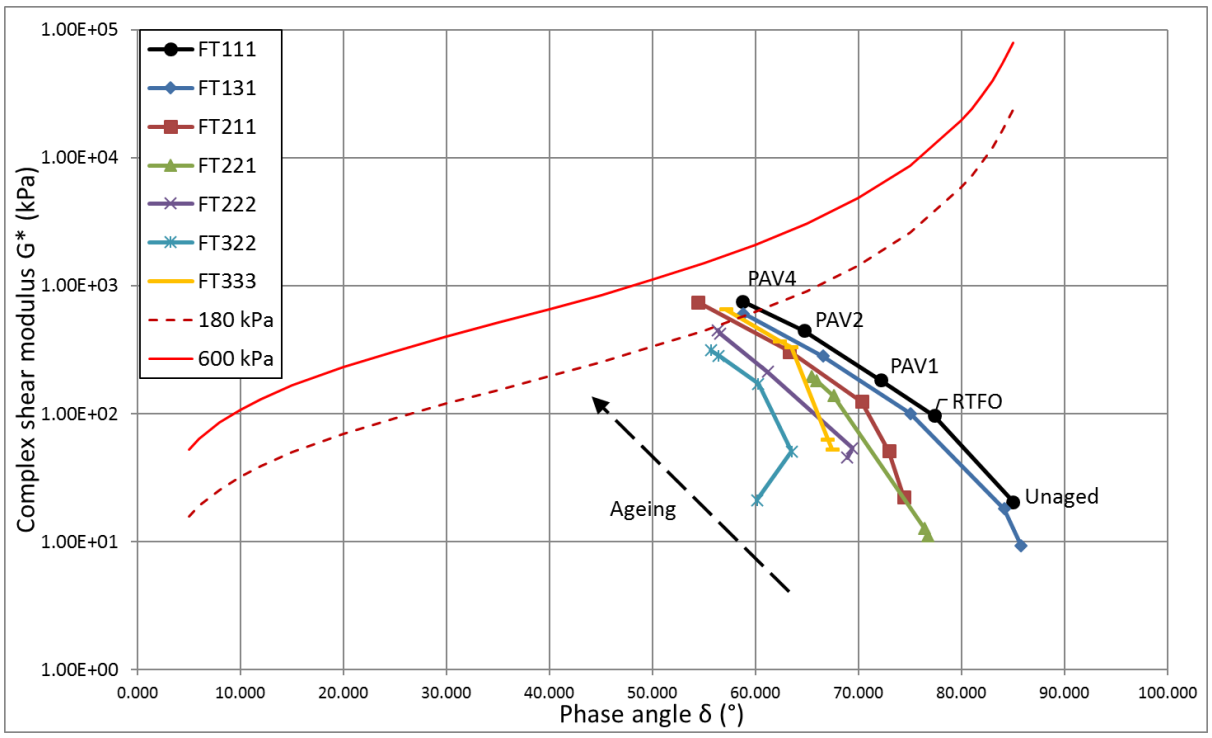

Figure 108: Black Space diagram which summarises the G-R curves for all the binders

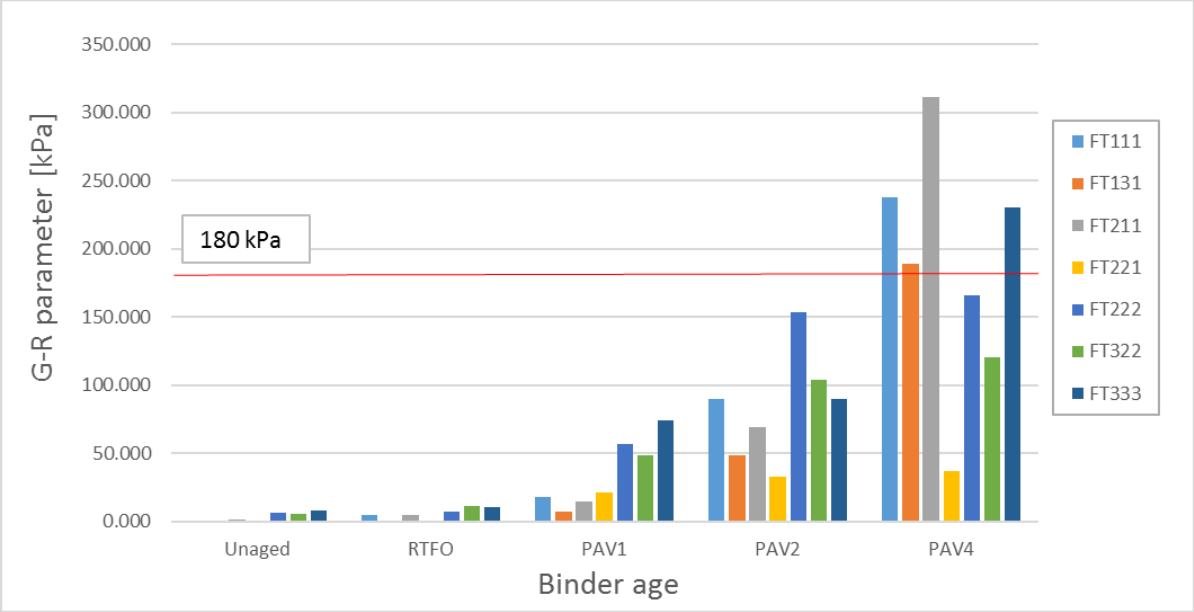

Figure 109: G-R results for all the binders with their ages

Figure 108 and Figure 109 show that the G-R parameter results for the PAV4 condition of binders FT111, FT131, FT211 and FT333 exceed the crack initiation limit of the G-R parameter. The FT222 binder is very close to the crack initiation boundary while binders FT221 and FT322 satisfy the G-R parameter limit theory for bituminous binders.

It is noticeable that the shape of the unmodified FT111 and FT131 binders are smoother in comparison with the modified binders. The results of the G-R parameter for each age of the unmodified binders are spaced out more consistently on the graph. This behaviour is due to the consistent effect that oxidation has on the binders as is ages. The shape of the curves for the 3% SBS modified binders i.e. FT211, FT221 and FT222 have a slight bend at the Unaged, RTFO and PAV1 age condition. The shape of the curves for the highly modified binders i.e. FT322 and FT333 have a slightly larger bend at the unaged, RTFO and PAV1 age condition. This behaviour is due to the modifier that ensures more elastic behaviour within the bituminous binders. As the modified binders reach the PAV2 and PAV4 age condition the shape of the G-R curves becomes a straight line, which is an indication of the modification that no longer influences the elastic properties of the modified binders.

Figure 110 show the correlation between the G-R parameter and ΔTc. The G-R crack initiation limit of 180kPa is illustrated on the graph as well as the South African Performance Grade Specification for ΔTc > -5. Figure 111 show how the G-R parameter correlates with the rheological index.

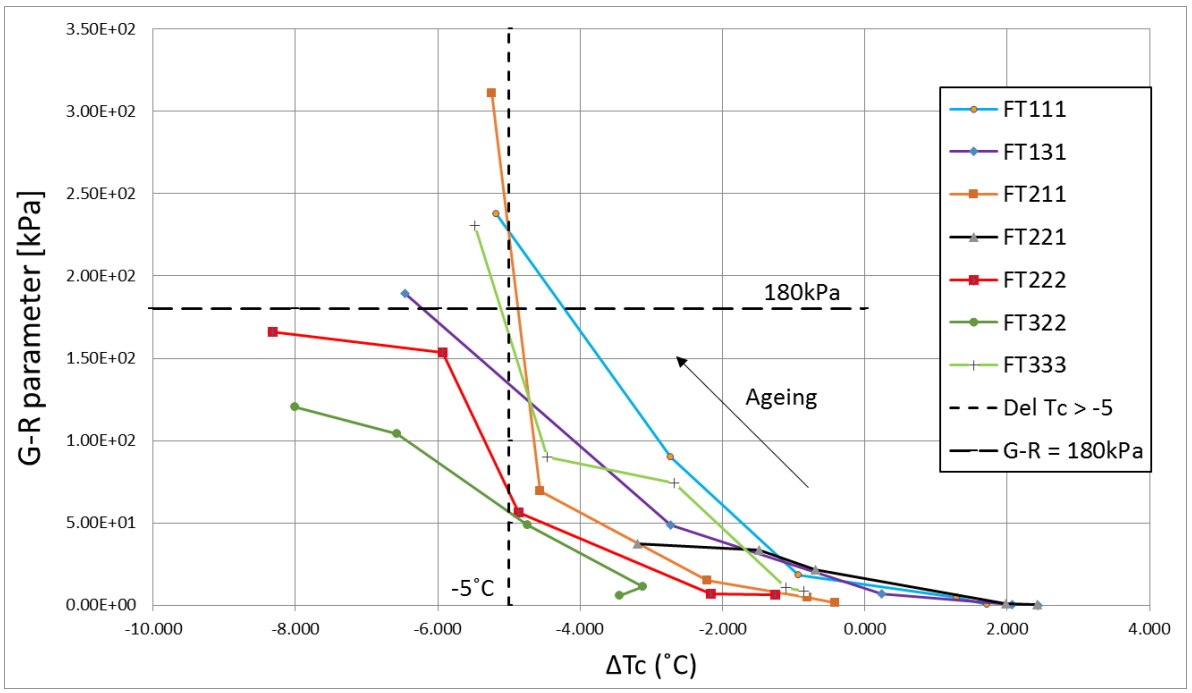

Figure 110: Correlation between the G-R parameter and ΔTc

Figure 110 gives enough information to identify which age of which binder is susceptible to thermal cracking. The PAV4 condition of FT111, FT131, FT211 and FT333 are the binders that exceeds the boundary for the G-R parameter and ΔTc. FT221 is the binder that performs the best according to Figure 110. Binders FT222 and FT322 exceeds the ΔTc boundary of -5 but do not exceed the G-R parameter crack initiation boundary.

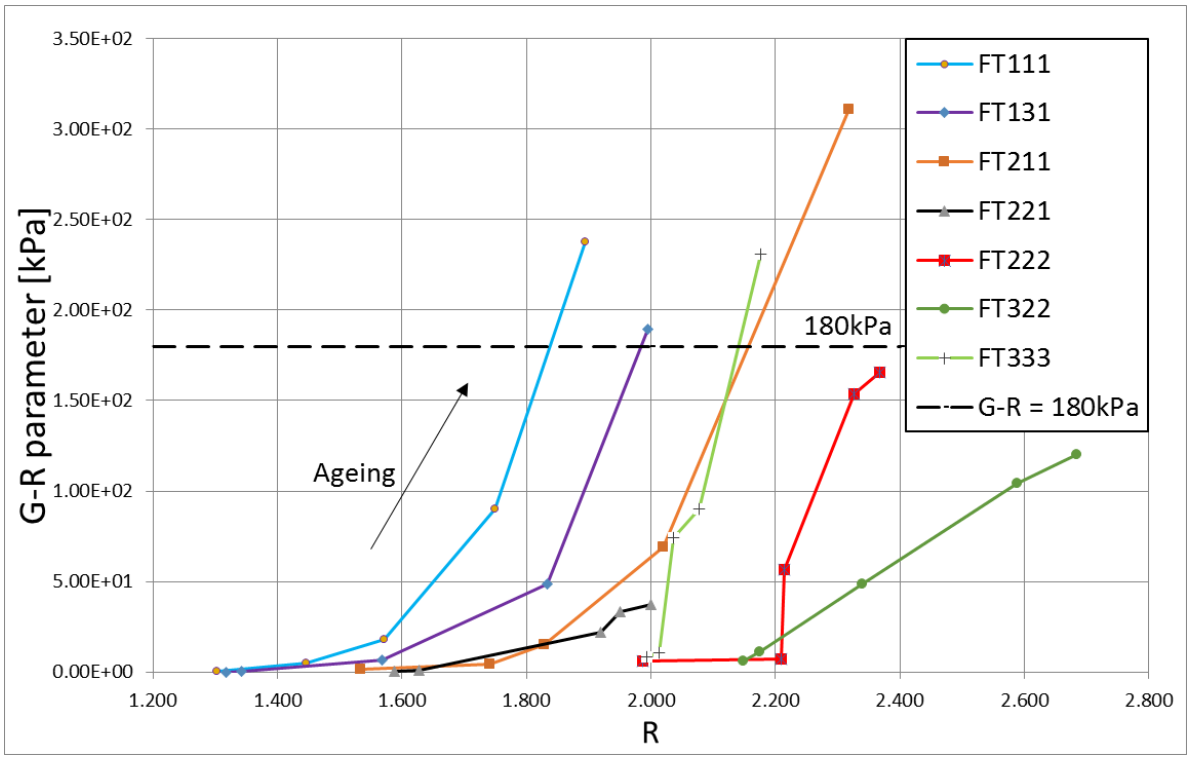

Figure 111: Correlation between the G-R parameter and R

Figure 111 indicates that R correlates well with the G-R parameter with the smooth increase in the curves as the binders age. The binders that exceed the G-R crack initiation boundary can be seen in Figure 111. By comparing Figure 110 and Figure 111 a conclusion can be made that a larger R value

may be more susceptible to thermal cracking. The results from Figure 110 can be used to estimate an acceptable R value for seal binders. A R value of 2.1 appears to be a good boundary for seal binders by looking at which binder exceeds the G-R parameter and ΔTc cracking boundary.

The viscous to elastic transition (VET) temperatures of all the binders with their ages are summarised in Table 20 and Figure 112.

Table 20: T_{VET} and G^*_{VET} data for all the binders with their ages

		Unaged	RTFO	PAV1	PAV2	PAV4
FT111	TVET (˚C)	6.574	12.087	14.420	19.730	23.770
	G*VET (kPa)	22266.033	14555.624	12821.166	7985.428	5593.780
FT131	TVET (˚C)	3.233	5.436	11.484	17.259	22.394
	G*VET (kPa)	25631.236	21108.922	14460.672	8641.568	5728.033
FT211	TVET (˚C)	6.389	8.606	13.498	18.129	25.869
	G*VET (kPa)	17968.560	16154.619	10374.516	7214.840	3687.611
FT221	TVET (˚C)	1.233	2.790	12.652	14.324	15.348
	G*VET (kPa)	29811.769	24717.206	12048.781	10186.485	9135.995
FT222	TVET (˚C)	9.732	9.087	17.395	22.732	23.105
	G*VET (kPa)	8620.230	8767.490	5546.930	4031.807	4003.927
FT322	TVET (˚C)	4.964	9.464	16.585	21.813	22.925
	G*VET (kPa)	8638.013	8193.737	5093.290	3017.610	2715.186
FT333	TVET (˚C)	9.169	9.786	18.149	19.033	23.485
	G*VET (kPa)	13637.704	11059.071	8032.983	7375.992	5259.226

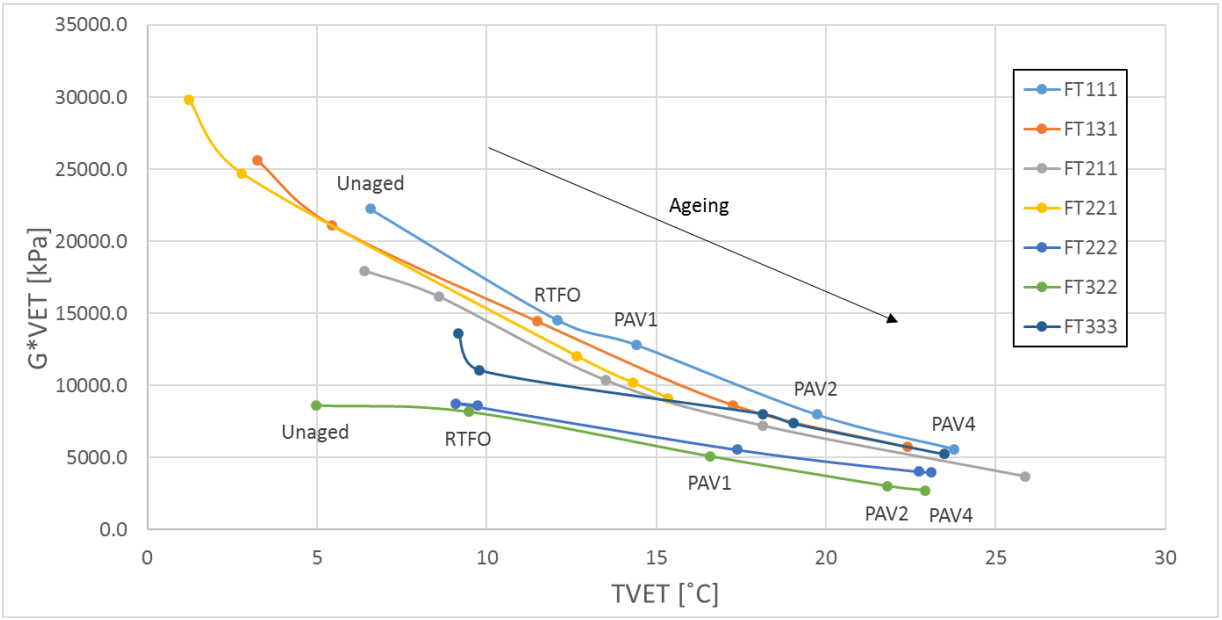

Figure 112: VET data for all the binders with their ages

As mentioned in Chapter 2 the tentative VET specification for bituminous binders are as follows (Widyatmoko, 2005):

- The lower pen binders (15) pen the VET temperature must be smaller than 35˚C and G^*_{VET} greater than 5 MPa, and
- The higher pen binders (50) pen the VET temperature must be smaller than 20˚C and G^*_{VET} greater than 10 MPa.

The FT111 and FT131 are the two unmodified 70/100 binders. The results of these two binders indicate that the Unaged RTFO and PAV1 state of the binders are still in a very good condition in terms of the tentative VET specification. The PAV2 age condition of the FT131 binder may be within this specification if there were one for a 70/100 pen binder. By looking at the change in the specification as the pen of the binder increase a lower VET temperature and higher G^*_{VET} value indicates binder properties with a high resistance to ageing and cracking.

The FT221 binder indicates the best results with the highest resistance to thermal cracking and ageing with the highest G^*_{VET} values and the lowest VET temperatures. The VET limits for a modified binder will not be the same as specified by Widyatmoko (2005). With this said by looking at Figure 112 the FT222 and FT322 binders show minimal resistance to thermal cracking and ageing due to the low G^*_{VET} values.

As mentioned by Widyatmoko (2005), there are still a lot of testing to be done to compile a VET specification for seal and asphalt binders.

5.7 Summary

This chapter provides an analysis of the rheological data procured in the study. It motivates the selection of shift-factors and mathematical models, as well as representativeness of the different ageing parameters

The low temperature analysis shows that the ΔTc for the FT222 and FT322 is the lowest for each age in comparison with the rest of the binders. This may be due to the modification and/or the crosslinking agents within the binders. These two binders are just inside the South African Performance Grade Specifications at the PAV1 state with a ΔTc of higher than -5˚C. The FT222 and FT322 binders may experience some thermal cracking at a pavement life of between 3 and 10 years. The FT221 binder had the highest ΔTc value of -3.189˚C at the PAV4 state of the binder. The other four seal binders do not satisfy the South African Performance Grade Specifications for the ΔTc parameter and may experience some thermal cracking at the PAV4 state.

The cross-over frequencies of the merged master curve data for all the binders with their ages indicate the susceptibility if the binders to ageing very well. As the binders age the cross-over frequencies decrease for each binder at its own rate. The stiffness's at each cross-over frequency decrease as the cross-over frequency decreases. This is due to the binders becoming more viscous due to the high temperature and low frequency conditions. The unmodified binders show high cross-over frequencies at the unaged state of the binders in comparison with the modified binders. At the PAV4 state of the binders it appears that the cross-over frequencies of all the binders differ slightly. The FT221 binder appears to have the highest cross-over frequency at the PAV4 state in comparison with the other binders. By comparing the results of Table 12 and Table 13 it appears that there is a slight relation between the ΔTc parameter and the cross-over frequency. The binders that have the highest ΔTc value have the highest cross-over frequency.

The comparison of the models in terms of the RMS error shows that the CA and CAM models have a better fit to the unmodified binders in comparison with the modified binders at the unaged and RTFO state. As the binders age the RMS error of the CA and CAM decreases due to the master curves of the modified binders that flattens off. The overall RMS error for the GL and DS models is acceptable for all the ages of the binders. The DS model was the most suitable model in terms of accuracy at the required positions where further analyses were done.

It appears that the Black Space diagrams of all the binders with their ages converge at the expected glassy modulus between 0.6 GPa and 1.5 GPa at the high viscosity and low phase angle region. By comparing the Black Space diagrams of the unmodified, 3% SBS modified and 5% SBS modified binders the following conclusions were formulated:

- The unmodified binders converged at the low viscosity and high phase angle region at 90˚ as expected. The unaged and RTFO aged 3% modified binders experienced a change in the shape of their Black Space diagrams between 70˚ and 80˚, due to the improvement of the modifier to the elastic part of the binders. The highly modified binders at the unaged and RTFO state experienced a change in the shape of their Black Space diagrams between 60˚ and 70˚.
- As the binders age the Black Space diagrams of the modified binders flatten off. This may be due to the particles within the modifier that detach and rupture as the binders age.

The MSCR curve of the AI was used to analyse the high temperature behaviour of the binders. The MSCR results showed that as the age of the binders increased the J_{nr} of the unmodified binders decreased and the percentage recovery for the modified binders decreased. As the age increased the binders entered the failure zone in terms of the J_{nr} and percentage recovery. At the unaged state of the binders all the binders applied to the boundaries of the AI at 58˚C, 64˚C and 70˚C. The results for

the PAV4 state of the binders showed that only the lower temperature data (58˚C) of the FT322 and FT333 binders applied to the AI specifications with a high percentage recovery and a low J_{nr}.

The G-R parameter results for all the binders showed that as the binders age the complex modulus increased and the phase angle decreased. This behaviour is due to the binder that becomes stiffer and more elastic at the same time. The G-R parameter for the FT111, FT131, FT211 and FT333 enters the crack initiation zone of 180 kPa at their PAV4. The FT211 binder had the highest G-R value at the PAV4 state of 310.802 kPa. All the ages of the FT221, FT222 and FT322 binders satisfy the G-R parameter limits. The FT221 binder showed the best results in terms of the G-R parameter with the lowest G-R value at the PAV4 state of 37.177 kPa.

The R value seem to increase as the age of the binders increase. This behaviour is due to the cross-over frequency that decreases as the binders age and the distance between the glassy modulus and the stiffness of each age of the binders at the cross-over frequency becomes larger as the age of the binders increase. From the data analysed an R value of 2.1 appears to satisfy the results obtained by the G-R parameter and ΔTc.

In terms of the VET data the FT111, FT131, FT211 and FT221 were the binders that showed the best resistance to thermal cracking and ageing at the Unaged, RTFO and PAV1 condition. The FT221 binder indicated the best results with all of the ages of the binder within the tentative specification of Widyatmoko (2005). It is thus difficult to conclude what the specification limits will be for modified binders. More testing has to be done to compile a sensible specification for seal and asphalt binders.

Chapter 6: Rheological Performance Requirements for Seal Binders

6.1 Introduction

This chapter entails an evaluation of the rheological performance of surfacing seal binders. The current South African Performance Grade Specification is compiled for asphalt binders and not for seal binders. In Texas a surface performance graded (SPG) specification was developed for surface binders. The development of this specification formed part of previous projects namely the Texas Department of Transportation (TxDOT) and National Cooperative Highway Research Program (NCHRP) (Vijaykumar, 2012).

The SPG specification was found to be practical in terms of binder selection to ensure adequate surface performance. Vijaykumar (2012) did further research and compared the field performance of several seal binders to develop additional criteria in the SPG specification.

6.2 SPG specifications

Table 21 show the Modified SPG Specification developed by Hoyt *et al*. in 2010. Researchers recommended that the SPG specification developed by Hoyt *et al*. (2010) needed further field validation in regions other than Texas before it can be used at a national level.

The development of the SPG specification was adapted from the standard PG binder testing process. The difference between the PG system and the SPG specification is that for the SPG specification the high and low pavement temperatures were calculated at the surface to reflect the critical conditions for surface treatment binder performance. From these results temperature increments of 3˚C were utilised.

The binders are evaluated at the unaged and 20h PAV conditions to account for the critical first year of surface binder performance. The low temperature testing was done on the PAV aged binders. The binder stiffness at low temperatures was measured at a loading time of 8s using the BBR device to simulate critical traffic loading conditions. The actual test temperature was used to determine the low temperature SPG grade.

Table 21: Modified SPG Specification (Hoyt et al, 2010)

Only three SPG grades are shown, but the grades are unlimited and can be extended in both directions of the temperature spectrum using 3 ° and 6°C increments for the high temperature and low temperature grades, respectively.	Performance Grade											
	SPG 64				SPG 67				SPG 70			
	-12	-18	-24	-30	-12	-18	-24	-30	-12	-18	-24	-30
Average 7-day Maximum Surface Pavement Design Temperature, °C	<64				<67				<70			
Minimum Surface Pavement Design Temperature, °C	>-12	>-18	>-24	>-30	>-12	>-18	>-24	>-30	>-12	>-18	>-24	>-30
Original Binder												
Dynamic Shear, AASHTO T 315/ASTM D7175 $\frac{G^*}{Sin\,\delta}$, Minimum: 0.65 kPa Test Temperature @10 rad/s, °C	64				67				70			
Shear Strain Sweep % strain @ $0.8G_i^*$, Minimum: 25 Test Temperature @10 rad/s linear loading from 1-50% strain, 1 sec delay time with measurement of 20-30 increments, °C	25				25				25			
Pressure Aging Vessel (PAV) Residue (AASHTO PP1)												
PAV Aging Temperature, °C	100				100				100			
Creep Stiffness, AASHTO T 313/ASTM D6648 S, Maximum: 500 MPa m-value, Minimum: 0.240 Test Temperature @ 8s, °C	-12	-18	-24	-30	-12	-18	-24	-30	-12	-18	-24	-30
Shear Strain Sweep G_i^*, Maximum: 2.5 MPa Test Temperature @10 rad/s linear loading at 1% strain and 1 sec delay time, °C	25				25				25			

Vijaykumar (2012) validated the SPG system with additional tests to develop a reliable performance-based specification for surface treatments. Table 22 show the Modified SPG Specification after the additional testing of Vijaykumar (2012).

Table 22: Modified SPG Specification by Vijaykumar (2012)

Only three SPG grades are shown, but the grades are unlimited and can be extended in both directions of the temperature spectrum using 3°C increments for the high temperature and low temperature grades.	Performance Grade											
	SPG 64				SPG 67				SPG 70			
	-13	-16	-19	-22	-13	-16	-19	-22	-13	-16	-19	-22
Average 7-day Maximum Surface Pavement Design Temperature, °C	<64				<67				<70			
Minimum Surface Pavement Design Temperature, °C	>-13	>-16	>-19	>-22	>-13	>-16	>-19	>-22	>-13	>-16	>-19	>-22
Original Binder												
Dynamic Shear, AASHTO T 315/ASTM D7175 $G^*/\sin\delta$, Minimum: 0.65 kPa Test Temperature @10 rad/s, °C	64				67				70			
Shear Strain Sweep % strain @ $0.8G_i^*$, Minimum: 15 Test Temperature @10 rad/s linear loading from 1-50% strain, 1 sec delay time with measurement of 20-30 increments, °C	25				25				25			
Pressure Aging Vessel (PAV) Residue (AASHTO PP1)												
PAV Aging Temperature, °C	100				100				100			
Creep Stiffness, AASHTO T 313/ASTM D6648 S, Maximum: 500 MPa m-value, Minimum: 0.21 Test Temperature @ 8s, °C	-13	-16	-19	-22	-13	-16	-19	-22	-13	-16	-19	-22
Shear Strain Sweep G_i^*, Maximum: 2.5 MPa Test Temperature @10 rad/s linear loading at 1% strain and 1 sec delay time, °C	25				25				25			

In the study of Vijaykumar (2012) most of the samples tested did not meet the exisiting m-value limit of 0.24. Based on the field and laboratory results of Vijaykumar (2012) it is suggested that the m-value limit decrease to 0.21. Vijaykumar (2012) state that there is currently no existing limit for the J_{nr} at 0.1kPa and 3.2kPa for surface binders. The Emulsion Performance Grade (EPG) specification formed part of the project done in 2011 namely NCHRP 9-50. The EPG specification covers the high temperature requirements of an emulsion but not for seals and will not be analysed in this section.

6.3 Low temperature seal binder evaluation (Stiffness and m-value)

This section includes the BBR results of all 7 seal binders at the PAV1 (20h) state of the binders. The data are analysed according to the SPG specification for only the 20h PAV data. The stiffness's and m-values are analysed after 8s of testing and temperatures ranging from -13˚C and -22˚C with increments of 3˚C. Table 23 show the stiffness results of 7 seal binders according to the SPG specification.

Table 23: Low temperature stiffness according to SPG specifications

Time 8 sec, Frequency 0.01 Hz, Stiffness (Mpa)					
Binder	Type	PAV1			
		-13˚C	-16˚C	-19˚C	-22˚C
FT111	Unmodified	481.277	626.903	786.784	919.134
FT131	Unmodified	576.424	742.626	942.306	1164.250
FT211	Modified (3% SBS)	416.941	558.255	717.700	911.683
FT221	Modified (3% SBS)	413.218	560.936	705.700	907.877
FT222	Modified (3% SBS)	279.979	372.290	480.786	604.099
FT322	Modified (5% SBS)	253.157	360.316	470.315	571.567
FT333	Modified (5% SBS)	393.984	532.729	687.522	844.841

The SPG specification states that the binder stiffness has to be less than 500MPa after 8sec of testing at -13˚C, -16˚C, -19˚C and -22˚C. The BBR results for the 7 South African seal binders are summarised in Table 23 above. Figure 113 show the results in the form of a histogram with the SPG specification limit.

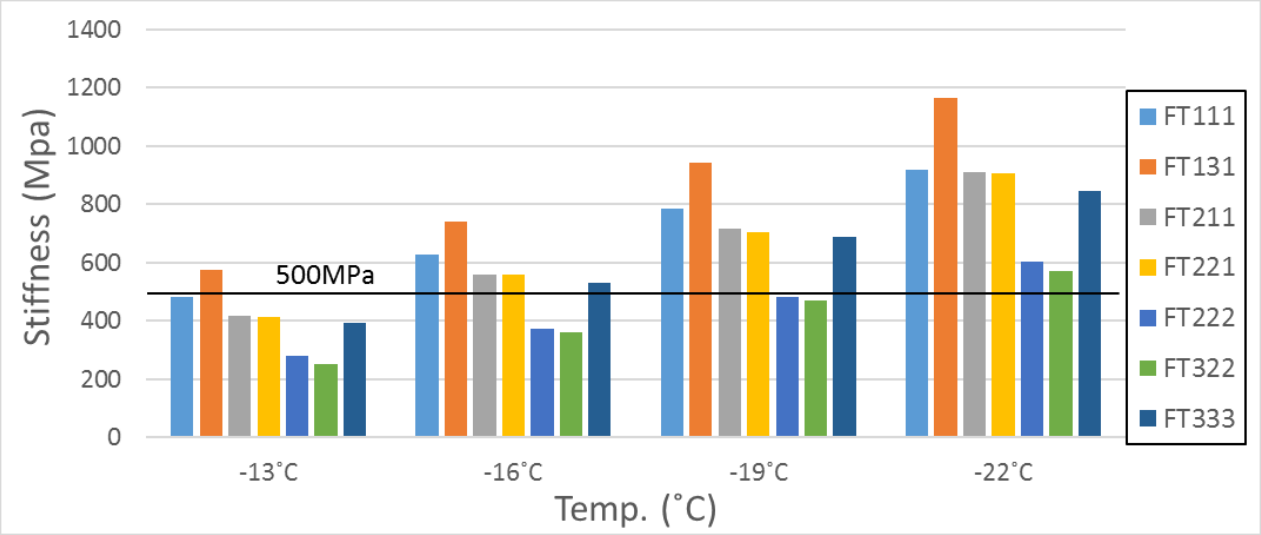

Figure 113: BBR results after 8sec with the SPG specification limit

Figure 113 show that at -13˚C the FT131 binder does not apply to the SPG specifications. The other 6 seal binders apply to the specification at -13˚C. The FT222 and FT322 binders from Tosas in Gauteng indicate the lowest stiffness's at all the required temperatures. These binders are the only ones that satisfy the specification at -16˚C and -19˚C.

The South African Performance Grade Specification for asphalt binders was used to compare the behaviour of the seals in terms of the asphalt specifications and the SPG specification. The South African Performance Grade specification require a binder stiffness of less than 300 MPa after 60sec of testing. The stiffness results from the 7 seal binders at 60sec can be seen in Table 24.

Table 24: Low temperature stiffness's according to the South African Performance Grade specifications

Time 60 sec, Frequency 0.01 Hz, Stiffness(Mpa)					
Binder	Type	PAV1			
		-13˚C	-16˚C	-19˚C	-22˚C
FT111	Unmodified	283.667	406.198	557.296	772.803
FT131	Unmodified	342.939	469.502	636.352	808.747
FT211	Modified (3% SBS)	243.754	351.347	484.619	608.210
FT221	Modified (3% SBS)	232.257	342.317	438.500	606.000
FT222	Modified (3% SBS)	161.044	226.615	310.341	412.318
FT322	Modified (5% SBS)	140.332	215.101	299.292	340.806
FT333	Modified (5% SBS)	231.132	335.273	462.687	603.053

Table 24 show similar low temperature stiffness failures as seen in Table 23 in terms of the seal binders. The only difference between the results by comparing the two specifications with one another in terms of the low temperature results is that the FT222 binder at -19˚C is just outside the South African Performance Grade Specification limit. Figure 114 show the BBR results after 60sec according to the South African Performance Grade Specification.

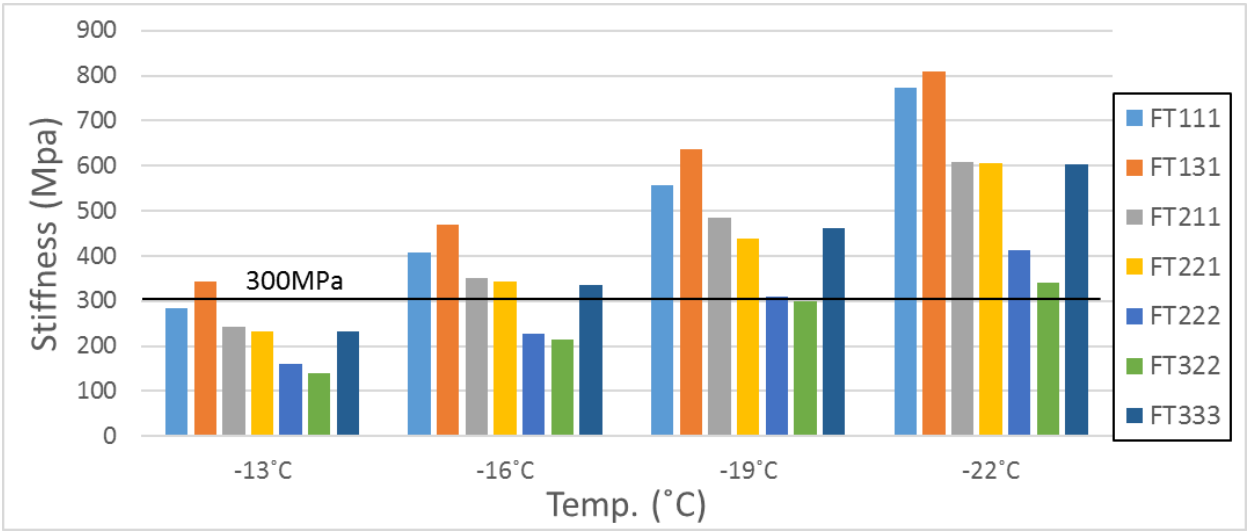

Figure 114: BBR results after 60sec with the South African Performance Grade Specification limit

Figure 114 has a similar form as seen in Figure 113 in terms of the stiffness results of the seal binders. Once again it is the FT222 and FT322 that has the lowest stiffness results at -13˚C and -16˚C. At -19˚C there is a slight difference in the two specifications where the FT222 binder is just outside the limits of the South African Performance Grade Specification.

The m-value of the 7 seal binders was determined according to the SPG specification before Vijaykumar (2012) researh, for the SPG specification after Vijaykumar (2012) reasearch and for the South African Performance Grade specification. The SPG specification after it was modified requires m-values after 8sec at -13˚C, -16˚C-19˚C-22˚C. The limiting m-value for the specification is less than 0.21. Table 25 and Figure 115 show the m-value results of the 7 seal binders according to the SPG specification after Vijaykumar (2012) reasearch.

Table 25: Low temperature m-value according to the SPG specifications after Vijaykumar (2012) reasearch

Time 8 sec, Frequency 0.01 Hz, m-value					
Binder	Type	PAV1			
		-13˚C	-16˚C	-19˚C	-22˚C
FT111	Unmodified	0.219	0.183	0.151	0.126
FT131	Unmodified	0.204	0.176	0.149	0.120
FT211	Modified (3% SBS)	0.219	0.189	0.163	0.143
FT221	Modified (3% SBS)	0.241	0.208	0.175	0.143
FT222	Modified (3% SBS)	0.241	0.202	0.170	0.148
FT322	Modified (5% SBS)	0.247	0.214	0.186	0.165
FT333	Modified (5% SBS)	0.211	0.180	0.152	0.132

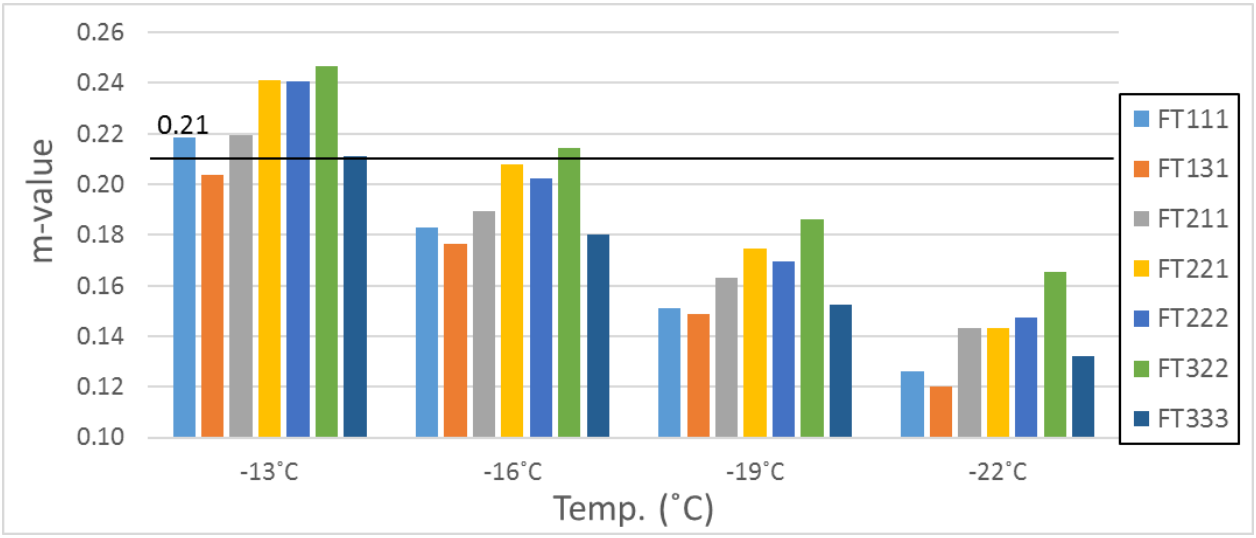

Figure 115: m-value results after 8sec according to the SPG specifications after Vijaykumar (2012) reasearch

After the work done by Vijaykumar (2012) it was suggested to decrease the m-value to 0.21 because most of the seal binders failed to the 0.24 limit of the SPG specification before Vijaykumar (2012) research. Only the FT131 bider fail in the -13˚C region. The FT322 binder is the only binder that satisfy the specification at -16˚C. Table 26 and Figure 116 summarises the m-value results with the limiting values of the South African Performance Grade specification for a m-value greater than 0.3 after 60sec of testing.

Table 26: Low temperature m-value according to the South African Performance Grade specification

Time 60 sec, Frequency 0.01 Hz, m-value					
Binder	Type	PAV1			
		-13˚C	-16˚C	-19˚C	-22˚C
FT111	Unmodified	0.296	0.257	0.221	0.193
FT131	Unmodified	0.282	0.250	0.219	0.193
FT211	Modified (3% SBS)	0.297	0.267	0.239	0.215
FT221	Modified (3% SBS)	0.319	0.281	0.245	0.213
FT222	Modified (3% SBS)	0.308	0.265	0.230	0.209
FT322	Modified (5% SBS)	0.317	0.284	0.252	0.225
FT333	Modified (5% SBS)	0.294	0.254	0.220	0.197

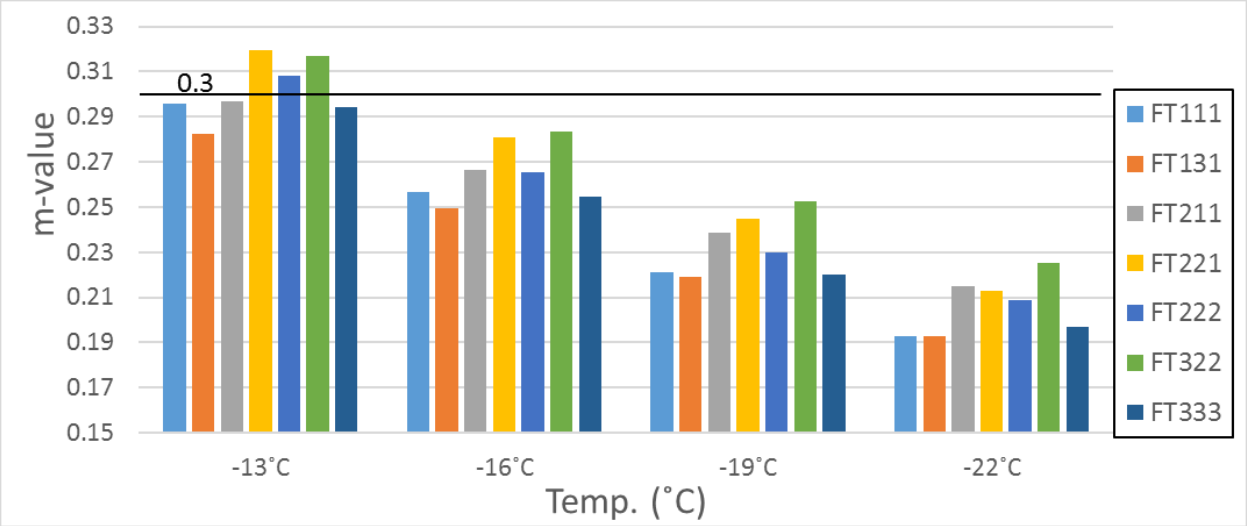

Figure 116: m-value results after 60sec according to the South African Performance Grade specification

The results in Table 26 and Figure 116 show that the FT221, FT222 and FT322 at -13˚C is the only binders that satisfy the South African Performance Grade specification limit for the m-value. By comparing the results of the SPG specification after Vijaykumar (2012) reasearch and the results in Table 26 and Figure 116 the specifications differ. Much more binders apply to the limiting value of the SPG specification after Vijaykumar (2012) reasearch. It was decided to analyse the m-value results for the SPG specification after Vijaykumar (2012) reasearch and compare it to the results above. The m-valuye results according to the SPG specification before the work of Vijaykumar (2012) is shown in Table 27 and Figure 117.

Table 27: Low temperature m-value according to the SPG specifications before Vijaykumar (2012) reasearch

Time 8 sec, Frequency 0.01 Hz, m-value					
Binder	Type	PAV1			
		-12˚C	-18˚C	-24˚C	-30˚C
FT111	Unmodified	0.230	0.159	0.109	0.047
FT131	Unmodified	0.213	0.158	0.101	0.069
FT211	Modified (3% SBS)	0.229	0.170	0.130	0.065
FT221	Modified (3% SBS)	0.252	0.185	0.122	0.066
FT222	Modified (3% SBS)	0.253	0.177	0.133	0.094
FT322	Modified (5% SBS)	0.257	0.193	0.151	0.110
FT333	Modified (5% SBS)	0.222	0.159	0.119	0.070

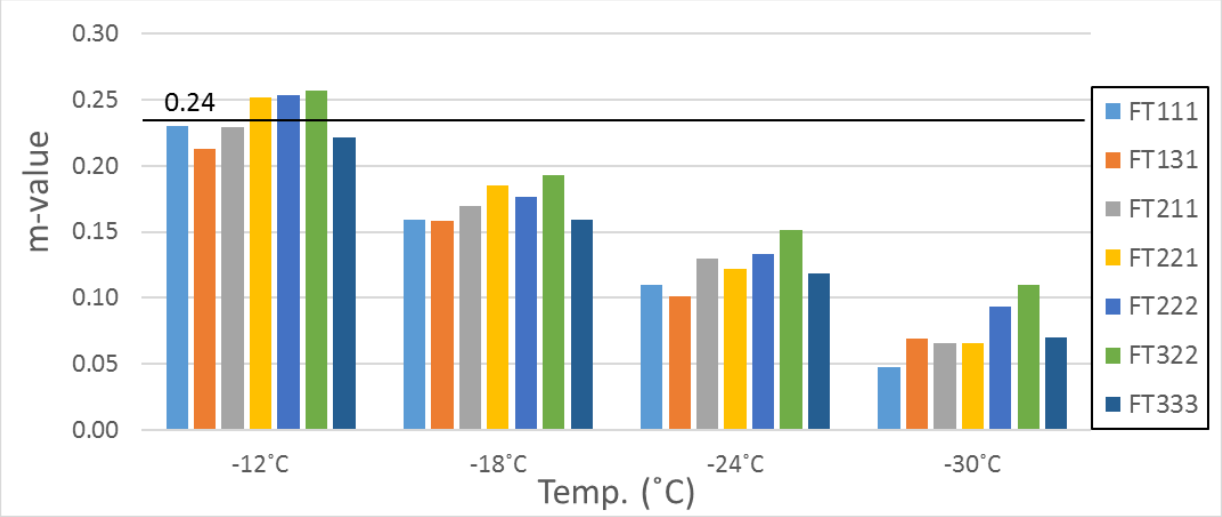

Figure 117: m-value results after 8sec according to the SPG specifications before Vijaykumar (2012) reasearch

The results in Table 27 and Figure 117 is very similar to the results obtained in Table 26 and Figure 116 where the South African Performance Grade specification limits were used. Once again it is only the FT221, FT222 and FT322 binders that satisfy the m-value specification at -13˚C.

6.4 Conclusion

The results of the stiffness for the 7 seal binders indicate that the SPG specification and the South African Performance Grade specification is similar. Although the South African Performance Grade specification is developed for asphalt binders the low temperature results of the seal binders are similar by comparing the limits of both specification.

The m-value results show that the results according to the SPG specification after Vijaykumar (2012) reasearch do not agree with the results according to the South African Performance Grade specification. With this said, the m-values were determined again according to the SPG specification before the work of Vijaykumar (2012) and the results look similar to those according to the South African Performance Grade specification.

6.5 Recommendations

The following recommendations can be made for the specification for surfacing seal binders:

- Focus on high temperature parameters for seals i.e. J_{nr};
- Analyse more than 7 seal binders around the required regions, and
- Do multiple repeats on tests to ensure accuracy.

Chapter 7: Conclusions and recommendations

This study looked at the rheological behaviour of various seal binders and how ageing effects the performance of these binders. The following conclusions were made for each chapter in this document.

7.1 Literature study

Seals in general consist of a mixture between bituminous binder and aggregate where the binder provides the viscoelastic properties of the mixture. Factors such as permanent deformation, cohesive and adhesive failure may be the cause of seal failure. This study discusses the fundamental concepts regarding the characterisation of seal binders.

In practice binder ageing occurs due to a change in temperature and weather conditions. The simulation of binder ageing includes short-term ageing and long-term ageing. The short-term ageing is done with the RTFO device and the long-term ageing with the PAV device.

Typical testing devices for the performance of bituminous binders is the BBR for low temperature testing and the DSR for intermediate to high temperature testing. The modelling of the results from these tests include master curves using the thermorheologically simple behaviour of bitumen. The modelling of master curves includes shift factors and mathematical models. The Kaelble shift factor equation was found to indicate the lowest RMS error for master curves which include low and high temperature data. Mathematical models such as the CA and CAM are most commonly used for analysing the rheological behaviour of bituminous binders. The GL model appears to analyse highly modified binders more accurately in comparison to the CA and CAM models.

After the data was analysed several ageing parameters were used to evaluate the performance of the binders as they aged. Commonly used ageing parameters are the G-R parameter, ΔTc, cross-over frequency, J_{nr} etc.

7.2 Methodology

Eight seal binders were collected from all over South Africa with two unmodified 70/100 binders, three S-E1 binders, two S-E2 binders and one SC-E1 emulsion. The testing was done at Stellenbosch University, Much Asphalt and Colas in the Western Cape. The testing of the binders included BBR and DSR testing at five binder ages i.e. Unaged, RTFO and PAV (20hr, 40hr and 80hr). The testing temperatures for the BBR specimens were -6˚C to -30˚C with increments of 6˚C. The DSR testing temperatures were 10˚C, 15˚C, 25˚C, 35˚C, 45˚C, 60˚C, and 70˚C.

7.3 Results and interpretation

From the analysis of the data obtained, the following is concluded:

<u>The low temperature results</u>

- ΔTc decreases as the age of the seal binders increase;
- The FT222 and FT322 binders showed the lowest ΔTc results for all the binder ages in comparison to the other binders;
- These binders are just inside the ΔTc limit for the South African Performance Grade Specification of -5˚C at the PAV1 state of the binders. The FT222 binder has a ΔTc of -4.8˚C and the FT322 binder -4.7˚C, and
- The FT221 binder had the highest ΔTc value of -3.189˚C at the PAV4 state of the binders.

Cross-over frequency comparison

- The cross-over frequency for each binder decreases as the age of the binders increase;
- At the Unaged and RTFO state the unmodified binders showed much larger cross-over frequency results compared to the modified binders;
- The cross-over frequency results for all the binders at the PAV4 state appears to differ slightly, and
- The stiffness at the cross-over frequency decrease for each binder with their ages as the cross-over frequency decrease with an increase in the age of the binders.

Model comparison

- The CA and CAM models had the lowest RMS error for the unmodified binders at the Unaged and RTFO state;
- The GL and DS had the best fit for the unmodified and modified binders at the Unaged and RTFO sate;
- The RMS error of the CA and CAM models decreases as the age of the modified binders increase. The reason for this statement is that the master curve of the binders flattens off as the binders age, and
- The DS was selected as the model for further analysis due to the model having the best fit for the data range under consideration.

Black space diagrams

- The black space diagram of the unmodified binders converges at the low viscosity and high phase angle of 90˚. This behaviour is expected for unmodified binders as it becomes more viscous as temperature increases;
- The 3% modified binders experience a change in the shape of their black space diagrams at 70˚ and 80˚. This behaviour is mostly in the Unaged and RTFO state of the binders and due to the modifier, that improves the properties of the elastic component in the binder;
- The 5% modified binders experience a change in the shape of their black space diagrams at 60˚ and 70˚. This behaviour shows the impact that 2% of modifier has by comparing the 3% modified results with the 5% modified results.
- The behaviour of black space diagrams for the modified PAV1, PAV2 and PAV4 binders are similar to the unmodified binders due to the curves that flattens off to 90˚. It appears that the particles within the modifier detach and rupture as the binders age.

High temperature results

- The MSCR data showed that the J_{nr} for the unmodified binders decreased as the binders aged while the percentage recovery decreased for the modified binders.
- The AI specifications indicated that at the unaged state all the binders applied to the specifications. As the binders aged the results for the 58˚C, 64˚C and 70˚C started to enter the failure zone.
- At the PAV4 state both the unmodified binders applied to the AI specification at 58˚C while the other binders were completely inside the failure zone.

G-R parameter and R

- The G-R results showed that as the binders age the binders became stiffer with an increase in the complex modulus. At the same time the phase angle decreased which indicated an increase in the properties of the elastic component of the binders. This behaviour contradicts the results for the black space diagrams.

- FT111, FT131, FT211 and FT333 were the only binders that entered the G-R crack initiation limit of 180kPa at their PAV4 state.
- At the PAV4 state the FT211 binder had the highest G-R value of 310.802kPa while the FT221 binder had the lowest G-R value of 37.177kPa.
- The R value correlates well with G-R. The rheological index increase as the age of the binders increases. It appears that a R of 2.1 is a good measure for thermal cracking at seal binders after comparing G-R with R and ΔTc.

Rheological Performance Requirements for Seal binders

The comparison of the South African Performance Grade Specification and the SPG Specification showed that the variation in the limiting values of the specifications appears to be very similar by comparing the results for both limits. It appears that the low temperature seal binder results are similar to those of the asphalt binders according to the analyses of these two specifications.

The high temperature performance of seal binders cannot be compared in a similar way as for the low temperature performance due to a lack of high temperature performance specifications for seal binders. The high temperature performance of the seven seal binders tested in this study appears to indicate acceptable results by analysing the results according to the South African Performance Grade Specification for asphalt binders.

After this study it is hard to say that there has to be a definite difference between the specifications for asphalt binders and seal binders. Although the high temperature performance limits for seal binders are not yet defined it is something to look at in the near future.

All the rheological parameters used in this study to analyse the age-related performance of surfacing seal binders is relevant. Much more research and testing need to be done to conclude if it is necessary to include all the parameters analysed in this study in one specification. Although these parameters give important information regarding each binder property the final decision regarding which parameters have to be included in the specification depends on various South African entities.

7.4 Limitations of this research

As mentioned in Chapter 3, eight seal binders were prepared for testing. The SC-E1 binder is an emulsion that had to be recovered for further testing. The recovery procedure that was followed was unsuccessful. Time was limit and the residue for the recovered emulsion was used. The BBR results were unusable due to the data that did not make any sense. On the other hand, MSCR tests were done on the residue and the results are included in this document.

During the BBR tests the rubber moulds and steel moulds were used. The dimensions of the beams were measured each time before the tests were performed. The dimensions of the beams from the rubber mould appeared to be at the lower boundary of the specifications and the steel moulds at the upper limit. In some cases, the beams did not satisfy the ASTM and the results were unusable. Time was limited, and all the beams could not have been retested with the steel moulds. Only one binder (FT131) was completely retested with the steel moulds.

The devices needed to complete the testing for this study were limited. Three researchers had to use the same equipment and devices which made time limited. Productive schedules had to be conducted for each one to complete his/her research and testing in time.

7.5 Recommendations

- The number of test repeats was minimal and the results for only one repeat is analysed in this document. More accurate results may be obtained by repeating the tests three to five times.
- The amount of seal binders used in this study may be increased for each region. The comparison of the results for each region may then be clearer.
- The ageing parameters used in this study to analyse the age-related properties of each binder do not cover all the existing ageing parameters. More parameters can be analysed to completely understand the behaviour of each binder.
- Analyse high temperature performance limits for seal binders.
- More testing should be done on modified and unmodified seal and asphalt binders to understand the VET behaviour of the binders. The current limiting values can be used as a temporary limit but only for unmodified binders.
- More data needs to be analysed to decide which parameters have to be used to compile a clear set of compliance criteria for the optimal seal binder selection.

References

Abrahams. (2015). *Application of the MMLS3 for evaluating the performance of surfacing seals*. Retrieved from http://scholar.sun.ac.za/bitstream/handle/...1/.../abrahams_towards_2015.pdf

Alatas, T., & Yilmaz, M. (2013). Effects of different polymers on mechanical properties of bituminous binders and hot mixtures. *Construction and Building Materials*, *42*, 161–167. https://doi.org/10.1016/j.conbuildmat.2013.01.027

Anderson, M. (2014). Acknowledgments, (October).

Anderson A, D., Christensen W, D., Bahia U, H., Dongre, R., Sharma G, M., Antle E, C., & Button, J. (1994). *Binder characterization and evaluation. Volume 3: Physical characterization* (Vol. 3). Retrieved from http://onlinepubs.trb.org/onlinepubs/shrp/SHRP-A-369.pdf

Anderson et al. (2008). Historical and Current Rheological Binder Characterization vs. Binder Performance, 1–17.

Anderson et al. (2011a). Evaluation of the Relationship between Asphalt Binder Properties and Non-Load Related Cracking. *Association of Asphalt Paving Technologists*, *80*.

Anderson et al. (2011b). Evaluation of the Relationship between Asphalt Binder Properties and Non-Load Related Cracking, 615–663.

Anton Paar. (2016). The Modular Compact Rheometer Series, 19. https://doi.org/10.1017/CBO9781107415324.004

Asgharzadeh et al. (2013). Evaluation of rheological master curve models for bituminous binders. *Materials and Structures*, *48*, 393–406. https://doi.org/10.1617/s11527-013-0191-5

Asphalt Academy. (2007). *Technical Guideline 1: The use of Bituminous Binders in Road Construction*. *The use of Bituminous Binders in Road Construction* (Vol. Second). Pretoria: Sabita / Asphalt Academy.

Asphalt Institute. (2010). Guidance on the Use of the MSCR Test with the AASHTO M320 Specification, *40511*(December), 2–4.

ASTM D 2872-04. (2004). Standard Test Method for Effect of Heat and Air on a Moving Film of Asphalt (Rolling Thin-Film Oven Test). *Annual Book of ASTM Standards*, (C), 1–6. https://doi.org/10.1520/D2872

ASTM D 6521 - 08. (2008). Standard Practice for Accelerated Aging of Asphalt Binder Using a Pressurized Aging Vessel (PAV). *Www.Astm.Org*, *i*(April), 1–6. https://doi.org/10.1520/D6521-08.Copyright

ASTM D 6648-08. (2012). Standard Test Method for Determining the Flexural Creep Stiffness of Asphalt Binder Using the Bending Beam Rheometer (BBR). *Annual Book of American Society for Testing Materiasl ASTM Standards*, *4*(C), 1–14. https://doi.org/10.1520/D6648-08.2

ASTM D 7175-08. (2013). Standard Test Method for Determining the Rheological Properties of Asphalt Binder Using a Dynamic Shear Rheometer. *Annual Book of American Society for Testing Materiasl ASTM Standards*, (C), 1–16. https://doi.org/10.1520/D7175-08.2

ASTM D 7405. (2012). Standard Test Method for Multiple Stress Creep and Recovery (MSCR) of Asphalt Binder Using a Dynamic Shear Rheometer 1 , 2. *Annual Book of ASTM Standards*, *i*(C), 10–13. https://doi.org/10.1520/D7405-10A.2

Baglieri et al. (2012). SIIV - 5th International Congress - Sustainability of Road Infrastructures Influence of Physical Hardening on the Low-Temperature Properties of Bitumen and Asphalt Mixtures. *Procedia - Social and Behavioral Sciences*, *53*, 504–513.

https://doi.org/10.1016/j.sbspro.2012.09.901

Chhabra. (2010). Non-Newtonian fluids: An introduction. *Rheology of Complex Fluids*, 3–34. https://doi.org/10.1007/978-1-4419-6494-6_1

Christensen. (1992). Chemical-Physical Property Relationship for Asphalt cements and the dispersed polar fluid model, (I), 1279–1291.

Christensen et al. (1992). Interpretation of dynamic mechanical test data for paving grade asphalt cements.

Claxton, M. (1996). *Rheology of bituminous binders : glossary of rheological terms : a practical summary of the most common concepts*. Brussels : European Bitumen Association. Retrieved from http://www.worldcat.org/title/rheology-of-bituminous-binders-glossary-of-rheological-terms-a-practical-summary-of-the-most-common-concepts/oclc/643560378

Clyne, T. R., & Marasteanu, M. O. (2004). Inventory of Properties of Minnesota Certified Asphalt Binders, 102.

Collins. (2006). Ordering and Steric-Hardening in SBS-Modified Bitumen. *Energy & Fuels : An American Chemical Society Journal.*, *20*(3), 1266.

Da Silva et al. (2004). Study of rheological properties of pure and polymer-modified Brazilian asphalt binders. *Journal of Materials Science*, *39*(2), 539–546. https://doi.org/10.1023/B:JMSC.0000011509.84156.3b

Dzwig. (2011). NEN-EN 13074-2.

Farrar et al. (2015). Technical White Paper Determining the Low-Temperature Rheological Properties of Asphalt Binder Using a Dynamic Shear Rheometer (DSR).

Francken, L., & Clauwaert, C. (1987). Characterization and Structural Assessment of Bound Materials for Flexible Road Structures, *1*, 130–144.

Gerber. (2016). *Numerical modelling of performance and failure criteria for surfacing seals*.

Gierhart, D. (2011). Simple Talking Points for Sharing Why Your State Should Be Implementing MSCR.

Gordon, G. V, & Shaw, M. T. (1994). *Computer programs for rheologists*. Munich; New York; Cincinnati: Hanser ; Hanser/Gardner.

Hagos. (2006). 5 Effect of aging on Rheological and Mechanical Characteristics, 159–321.

Hagos, E. (2008). *The effect of aging on binder properties of porous asphalt concrete*. *Delft University of Technology*. Retrieved from http://www.ct.tudelft.nl/fileadmin/Faculteit/CiTG/Over_de_faculteit/Afdelingen/Afdeling_Bouw/-_Secties/Sectie_Weg_en_Railbouwkunde/-_Nieuws/-_Colloquia/doc/presentation_Hagos.pdf

Harrigan, E. T., Leahy, R. B., & Youtcheff, J. S. (1994). *SHRP-A-379 "The SUPERPAVE Mix Design System Manual of Specifications , Test Methods , and Practices." Strategic Highway Research Program*.

Hoyt et al. (2010). Surface performance-grading system to grade chip seal emulsion residues. *Transportation Research Record: Journal of the Transportation Research Board, 2150, 6.*

Hunter, R. N., Self, A., & Read, J. (2015). *The Shell Bitumen Handbook*.

Jacobs, M. M. J. (1995). Crack Growth in Asphalt Mixes.

Kashaya. (2013). Surface run-off behaviour of bitumen emulsions used for the construction of seals, (March).

Lin et al. (2015). Interfacial sciences in unconventional petroleum production: from fundamentals to applications. *Chemical Society Reviews*, *44*(15), 5446–5494. https://doi.org/10.1039/C5CS00102A

Little & Jones. (2003). Chemical and Mechanical Processes of Moisture Damage in Hot-Mix Asphalt Pavements. In L. and Jones (Ed.), *Moisture Sensitivity of Asphalt Pavements* (Vol. http://onl, p. 37). Transportation Research Board.

Lu, X., Sandman, B., & Redelius, P. (2007). Aging Characteristics of Polymer Modified Binders in Porous Asphalt Pavements, (Eapa).

Lu & Isacsson. (1998). Chemical and rheological evaluation of ageing properties of SBS polymer modified bitumens. *Fuel*, *77*(9–10), 961.

Lytton, R. L., Uzan, J., Fernando, E. G., Roque, R., Hiltunen, D., & Stoffels, S. M. (1993). Development and validation of performance prediction models and specifications for asphalt binders and paving mixes. SHRP-A-357, 552.

Macosko, W. (1994). *Rheology Principles, Measurements and Applications*. VCH.

Mainardi & Spada. (2011). Creep, relaxation and viscosity properties for basic fractional models in rheology. *European Physical Journal: Special Topics*, *193*(1), 133–160. https://doi.org/10.1140/epjst/e2011-01387-1

Mastrofini & Scarsella. (2000). Application of rheology to the evaluation of bitumen ageing. *Fuel*. https://doi.org/10.1016/S0016-2361(99)00244-6

Medani, T. O., Tech, M., & Huurman, M. (2003). Constructing the Stiffness Master Curves for Asphaltic Mixes. *Civil Engineering*, (January), 1–21.

Migliori et al. (1999). Correlations between the thermal stress cracking of bituminous mixes and their binders' rheological characteristics. *Eurobitume Workshop on Performance Related Properties for Bituminous Binders*.

Milne. (2004). *Towards a performance related seal design method for bitumen and modified road seal binders*.

Mo. (2010). *Damage development in the adhesive zone and mortar of porous asphalt concrete*. Retrieved from http://resolver.tudelft.nl/uuid:968a9218-3a7d-4ec8-bfe8-156f2916000a#.Vp8J-S6gvvA.mendeley

Mukandila, E. (2016). Investigation of rheological response , cohesion and adhesion fatigue damage of bituminous road seal materials.

Paliukaitė et al. (2014). Evaluation of bitumen fractional composition depending on the crude oil type and production technology. *The 9th International Conference Environmental Engineering*, (May).

Panda et al. (1999). Engineering Properties of EVA-Modified Bitumen Binder for Paving Mixes. *Journal of Materials in Civil Engineering.*, *11*(2), 131.

Partal & Franco. (2010). Non-Newtonian Fluids. *Rheology: Encyclopaedia of Life Support Systems (EOLSS), UNESCO. Eolss, Oxford*, *1*, 96–119.

Pavement Interactive. (2012). Pavement Interactive. Retrieved from http://www.pavementinteractive.org/article/raveling/

Poulikakos, L. D., & Partl, M. N. (2012). A multi-scale fundamental investigation of moisture induced deterioration of porous asphalt concrete. *Construction and Building Materials*, *36*(19500), 1025–1035. https://doi.org/10.1016/j.conbuildmat.2012.04.071

Read & Whiteoak. (2003). *The Shell Bitumen Handbook*. London: Thomas Telford.

Refined Bitumen Association. (2016). Bitumen Manufacture. Retrieved from http://www.bitumenuk.com/bitumen-manufacture.asp

Romberg et al. (1959). Some chemical aspects of the components of asphalt, *4*(2).

Rowe. (1996). *Applcation of the dissipated energy concept to fatigue cracking in asphalt pavements*.

Rowe. (1997). Linear Visco-elastic Binder Properties and Asphalt Pavement Cracking.

Rowe, G. (2014). Interpretation in Rheological Parameters Geoffrey Rowe, Abatech 51st Petersen Asphalt Research Conference July 14-16, 2014 Laramie, Wyoming 1.

Rowe, G. M., Eng, C., & Ph, D. (2014). Interrelationships in Rheology for Asphalt Binder Specifications.

Rowe et al. (2011). Advanced Techniques to Develop Asphalt Master Curves from the Bending Beam Rheometer. *Petroleum and Coal.*, *43*(1), 54–59.

Rowe et al. (2005). Development of a New Method for Assessing Asphalt Binder Durability with Field Validation, *7*(2).

Rowe et al. (2008). A Generalized Logistic Function to describe the Master Curve Stiffness Properties of Binder Mastics and Mixtures. In *45th Petersen Asphalt Research Conference* (pp. 1–28). University of Wyoming Laramie, Wyoming.

Rowe et al. (2017). New methods for assessing rheology data such as Δ Tc and G-R Parameter and their relationship to performance of REOB in asphalt binders and other materials, (April), 1–23.

Rowe, & Sharrock. (2011). Alternate Shift Factor Relationship for Describing Temperature Dependency of Viscoelastic Behavior of Asphalt Materials. *Transportation Research Record: Journal of the Transportation Research Board*, *2207*(1), 125–135. https://doi.org/10.3141/2207-16

Sayegh, G. (1967). Viscoelastic Properties of Bituminous Mixtures, P 614-627.

Shell Bitumen. (1995). *The Shell Bitumen industrial handbook.* Chertsey: Shell Bitumen.

Skoglund, R., & Peltonen, P. (2002). Superpave test methods for asphalt procedure for DSR testing Leif Bakløkk Randi Skoglund Björn Kalman Petri Peltonen.

Somwangthanaroj, A. (2010). Rheology and polymer characterisation. Retrieved from http://pioneer.netserv.chula.ac.th/~sanongn1/rheology.pdf

Standards for Highways. (2008). VOLUME 1 SPECIFICATION FOR HIGHWAY WORKS ROAD PAVEMENTS - BITUMINOUS BOUND MATERIALS, *1*(November).

Sybilski, D., Vanelstraete, A., & Partl, M. N. (2004). Recommendation of RILEM TC 182-PEB on bending beam and rheometer measurements of bituminous binders. *Materials and Structures*, *37*(October 2004), 539–546. https://doi.org/10.1617/14205

Tarrer & Wagh. (1991). *The effect of the physical and chemical characteristics of the aggregate on bonding*. Washington, D.C. Retrieved from http://onlinepubs.trb.org/onlinepubs/shrp/SHRP-91-507.pdf

Technical Guideline 1. (2016). Sabita Technical Guideline :, (January).

TRH 3. (2007). *Design and Construction of Surfacing Seals*. Pretoria: South African National Roads Agency (SANRAL).

Van De Ven. (2001). Rheology of polymer modified bitumen: A comparitive study of three binders and three binders/filler systems Senior Scientist SASOL Oil Sasolburg. *20th South African Transport Conference*, (July), 16–20.

Vijaykumar, A. (2012). Validation of Surface Performance-Graded Specification for Surface Treatment

Binders, (August).

Webb. (2010). *The Seal Coat and Surface Treatment Manual*. Texas: Texas Department of Transportation.

Widyatmoko. (2005). The Viscous to Elastic Transition Temperature and the In Situ Performance of Bituminous and Asphaltic Materials, (December 2015).

Widyatmoko et al. (2002). Ageing Characteristics of Low Penetration Bitumens. *Performance and Durability of Bituminous and Hydraulic Materials in Pavements, ISBN 90 5809 3751*.

Widyatmoko et al. (2004). Mapping Crack Susceptibility of Bituminous Materials with Binder Durability. *Proceedings of the Fifth RILEM International Conference on Cracking in Pavements – Mitigation, Risk Assessment and Prevention*.

Woldekidan, M. F. (2011). *Response Modelling of Bitumen, Bituminous Mastic and Mortar*.

Yusoff. (1997). A Comparative Study of the Influence of Shift Factor Equations on Master Curve Construction, *4*(6), 324–336. https://doi.org/4(6):324-336

Yusoff et al. (2010). Modelling the Linear Viscoelastic Rheological Properties of Unaged Bitumens. *Malaysian Journal of Civil Engineering*, *22*(1), 22–37.

Zieli ski, K. (2008). Effect of styrene-butadiene-styrene content on the adhesion properties of bitumen before and after heat aging. *Canadian Journal of Civil Engineering*, *35*, 454–460.

Zipf, K. (2016). Cookbook for Rheological Models – Asphalt Binders, (May).

Zvirblis et al. (2014). Influence of High RAP on Binder Properties in Hot Mix Asphalt of Northeast.

Annexure A: Strain Sweep (LVE) results

FT111 (70/100 WP)

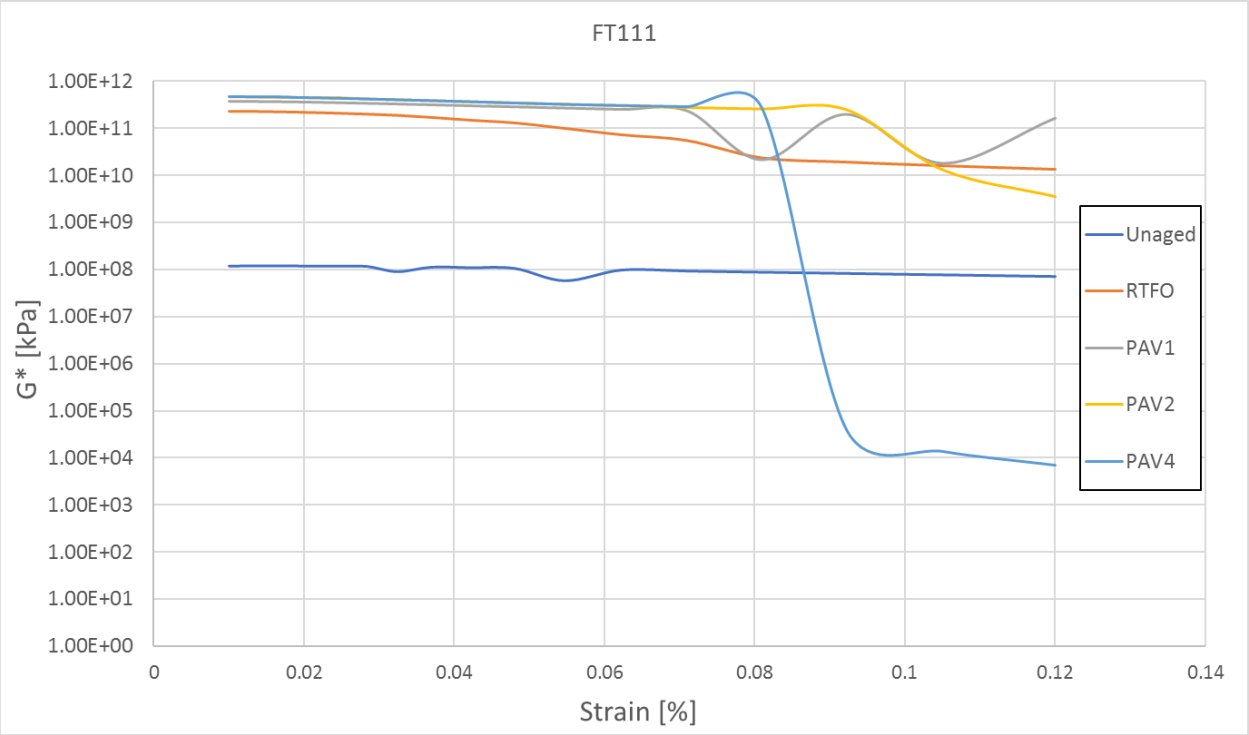

FT131 (70/100 KZN)

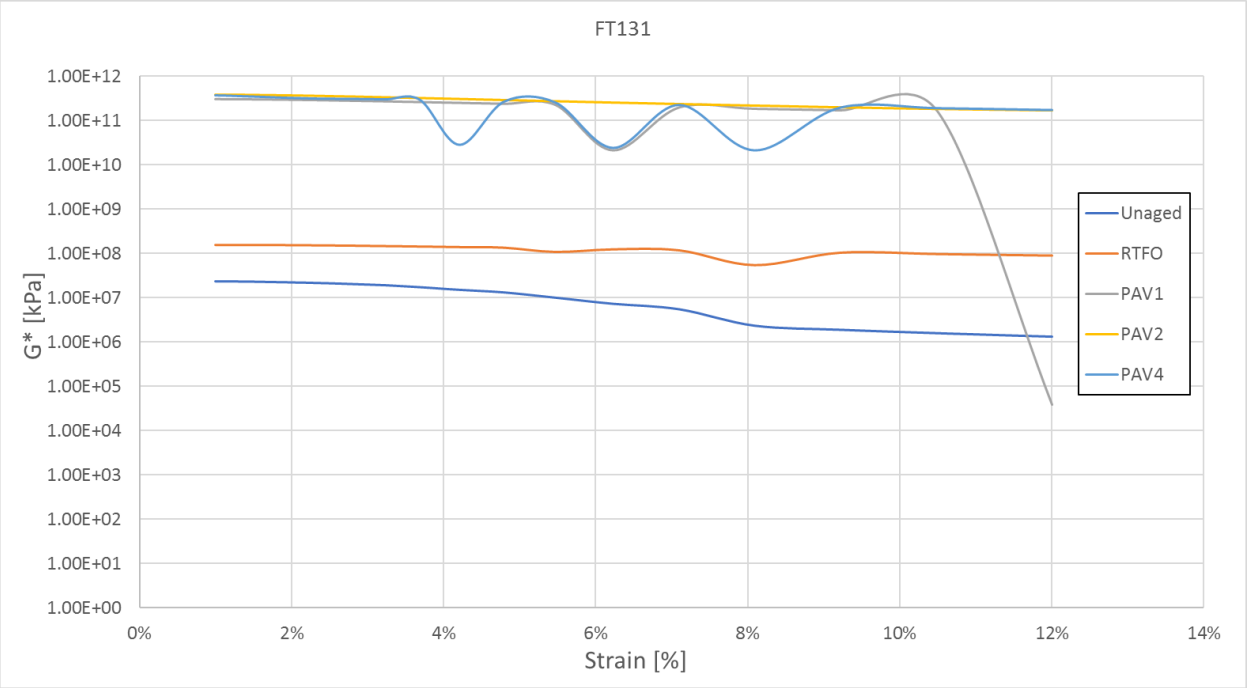

FT211 (S-E1 WP Colas)

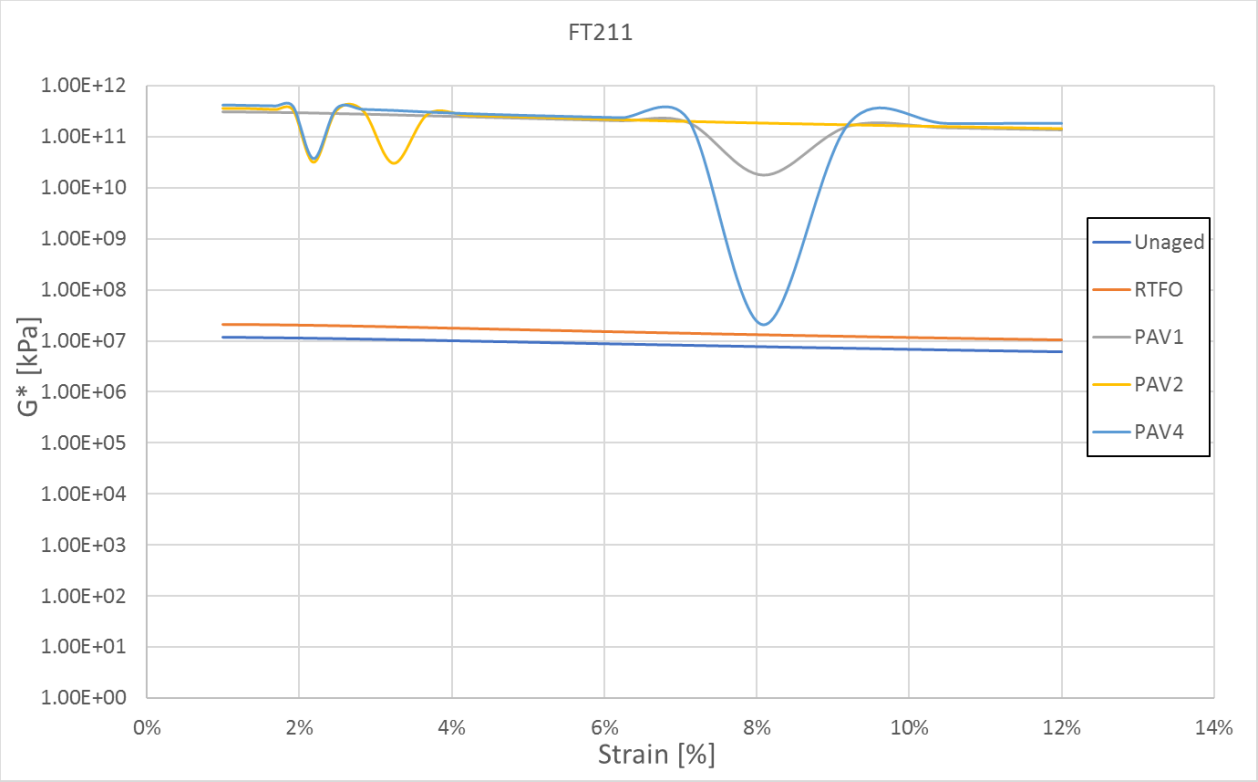

FT221 (S-E1 GP Colas)

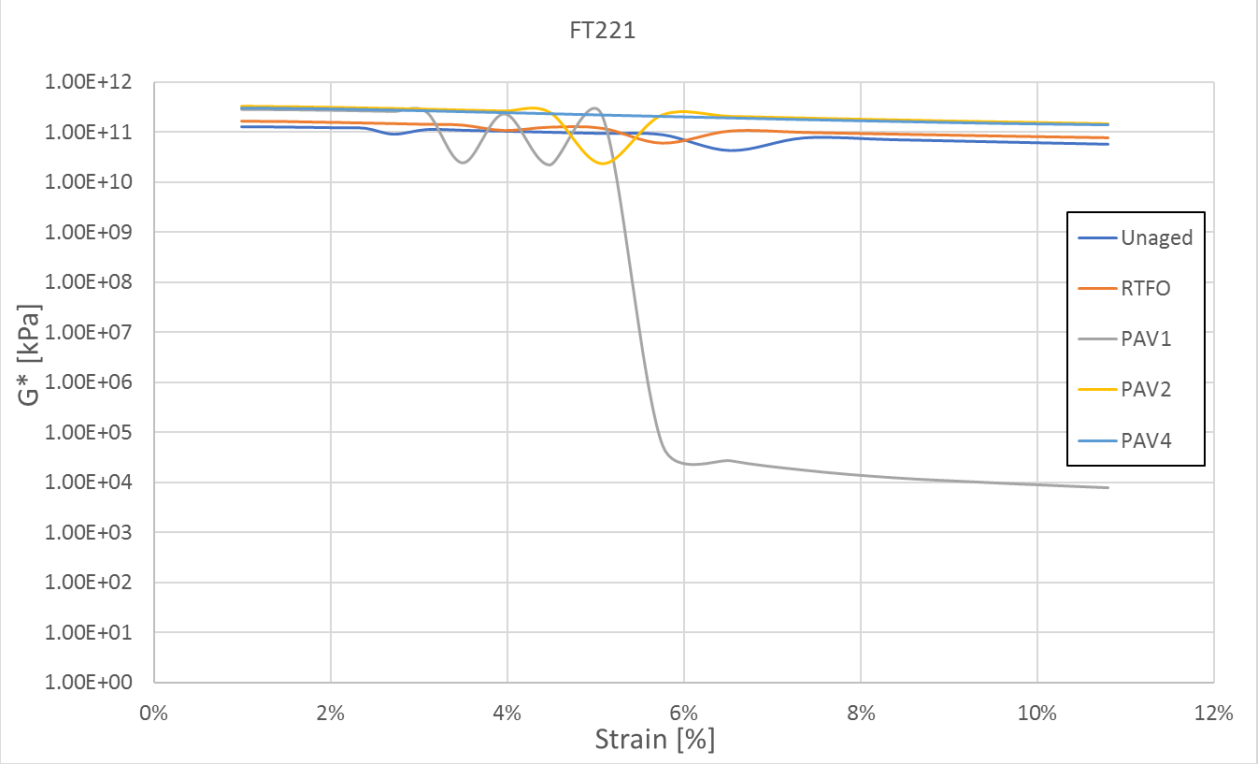

FT222 (S-E1 GP Tosas)

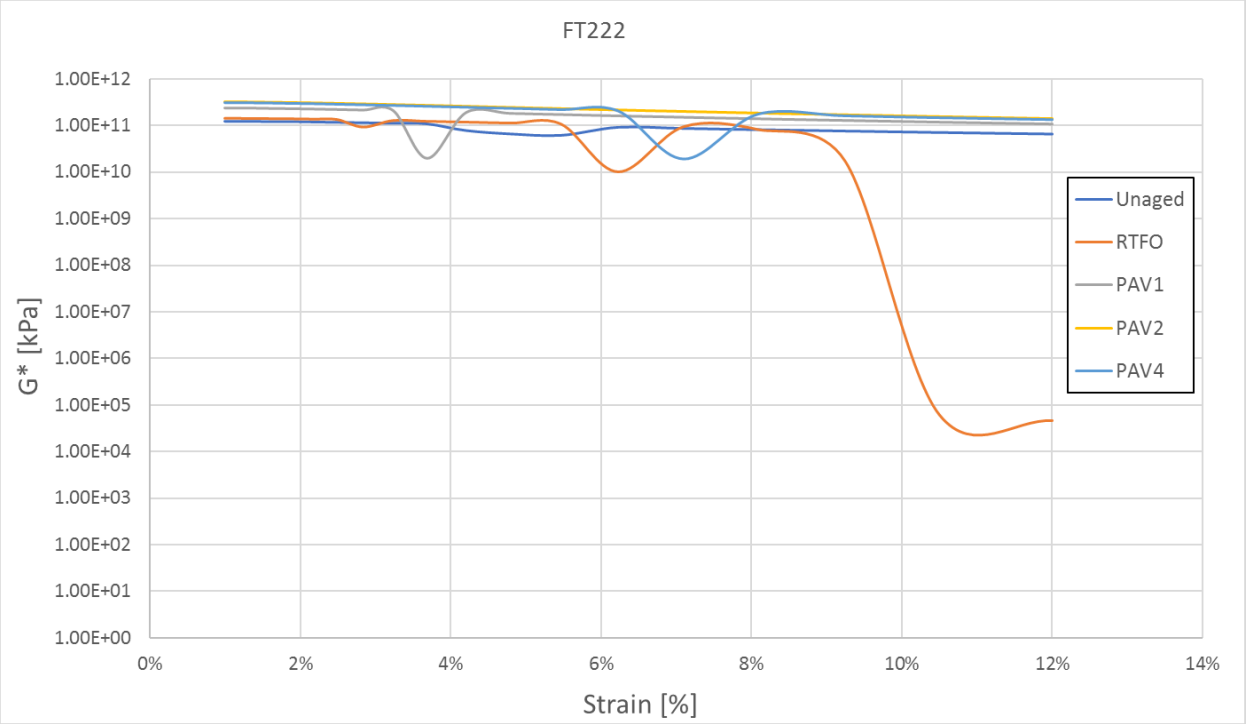

FT322 (S-E2 GP)

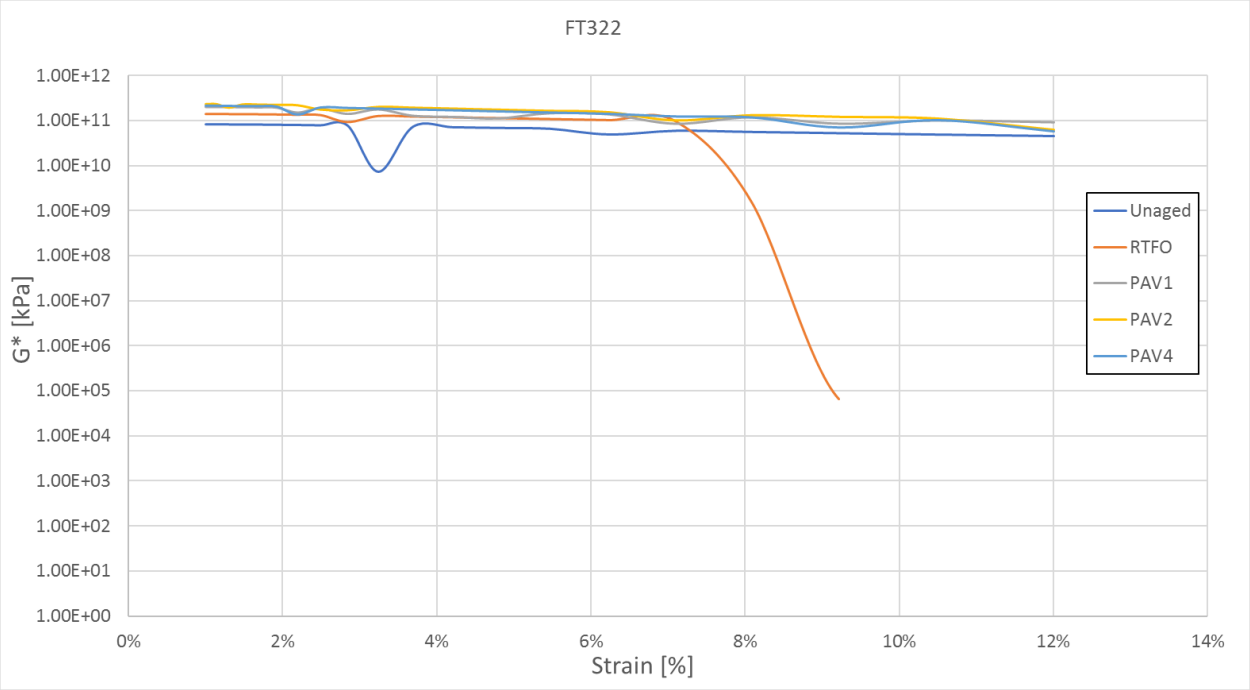

FT333 (S-E2 KZN)

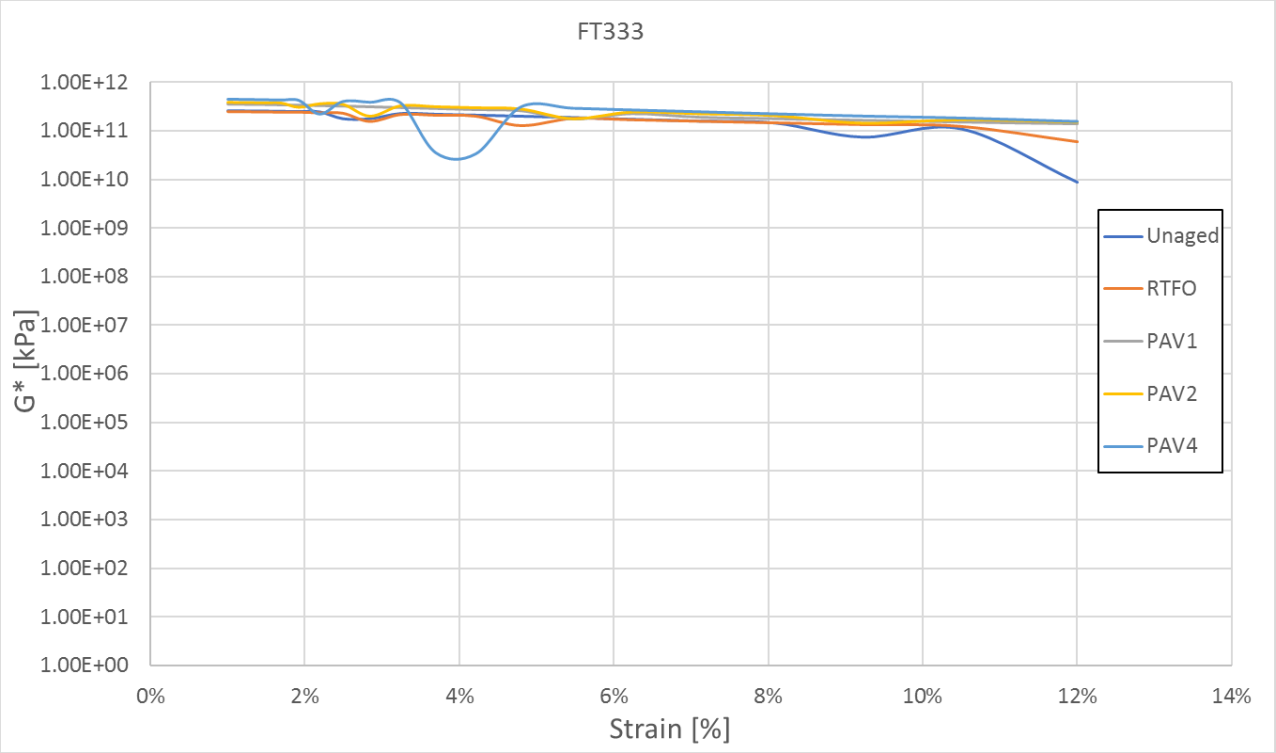

Annexure B: BBR deflection results

FT111 (70/100 WP)

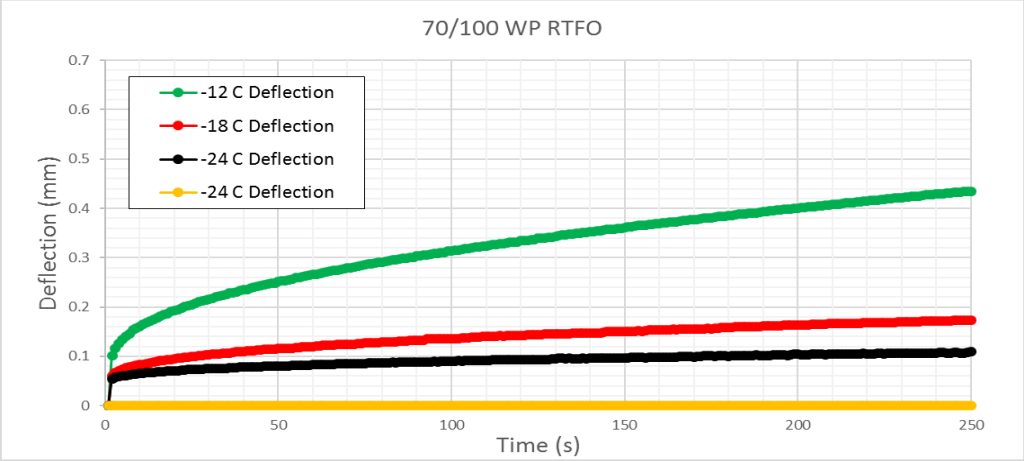

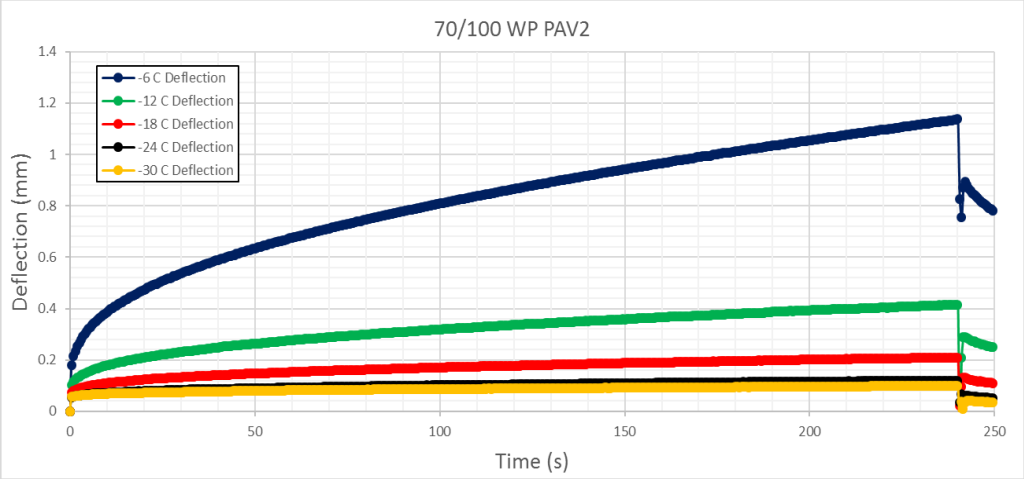

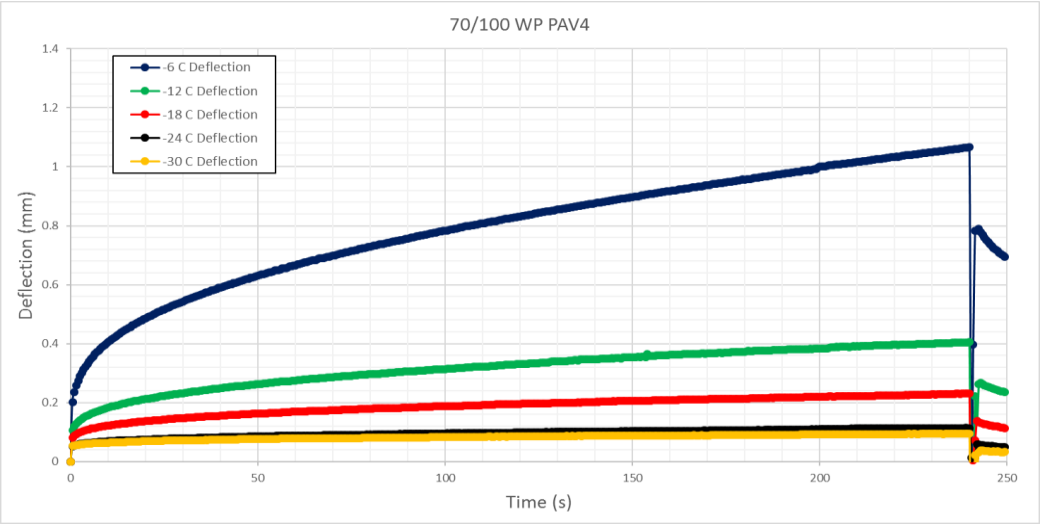

FT131 (70/100 KZN)

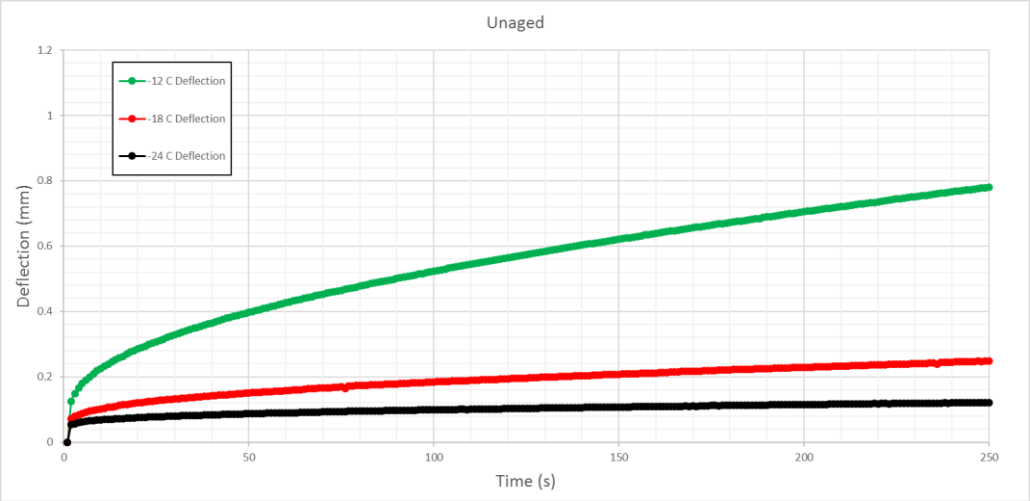

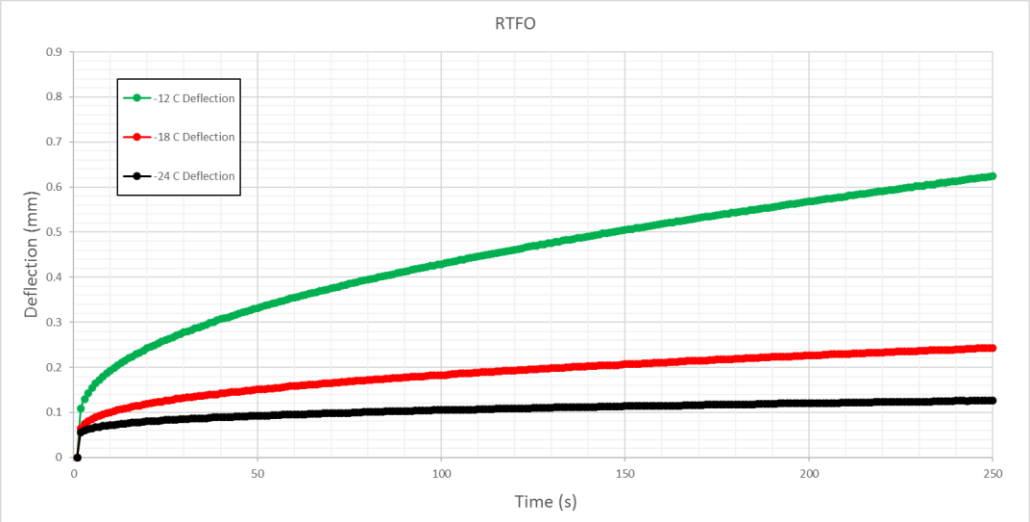

Annexure B: BBR deflection results

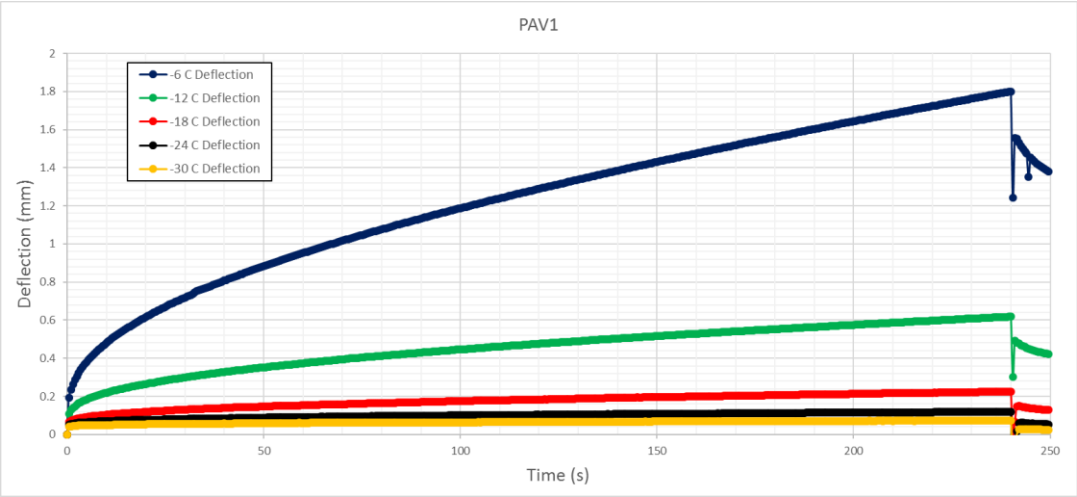

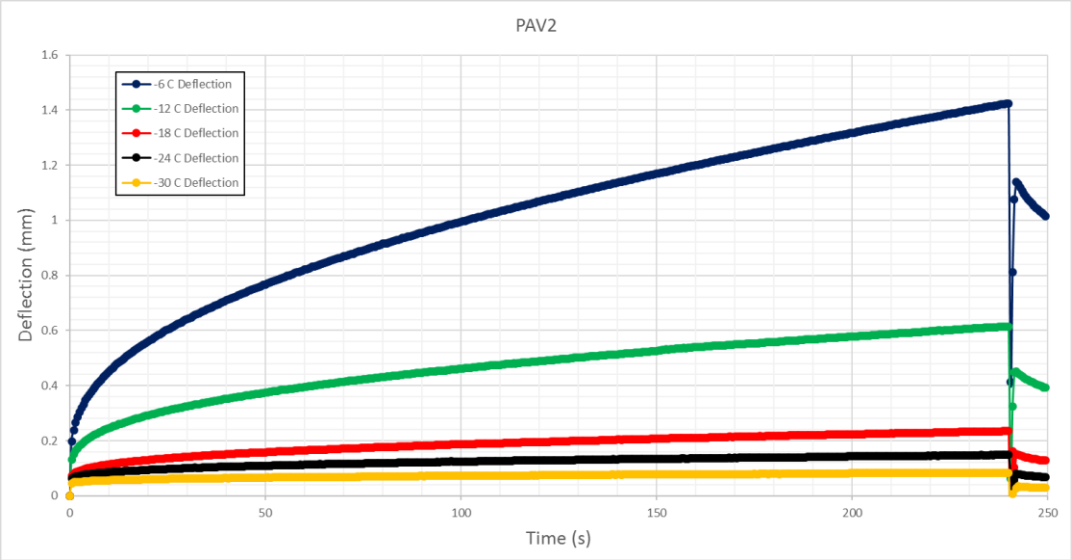

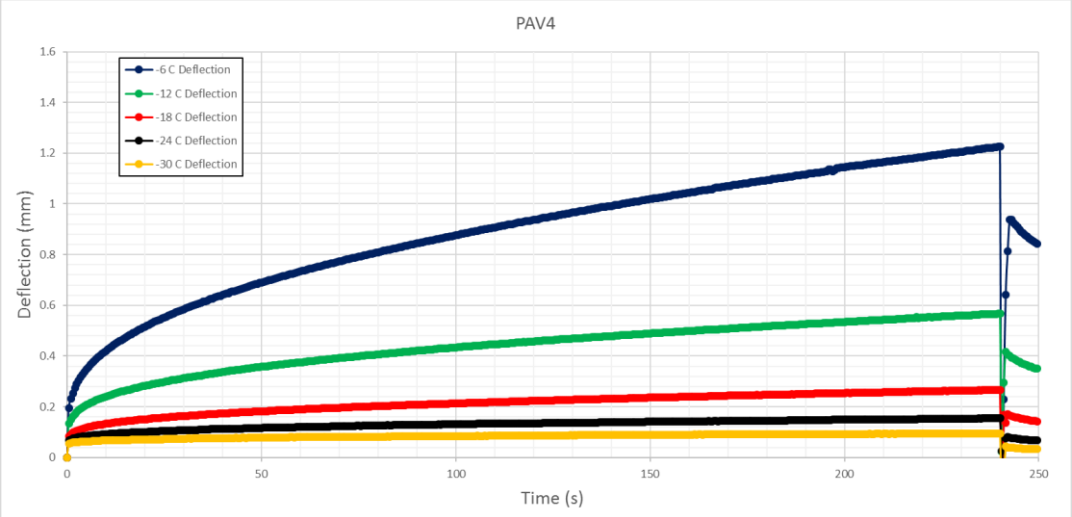

FT211 (S-E1 WP Colas)

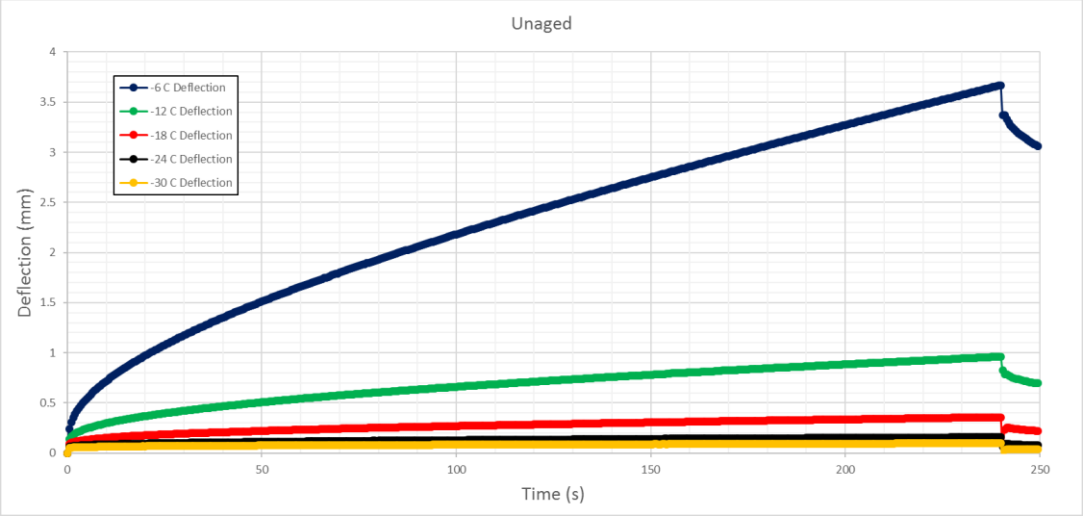

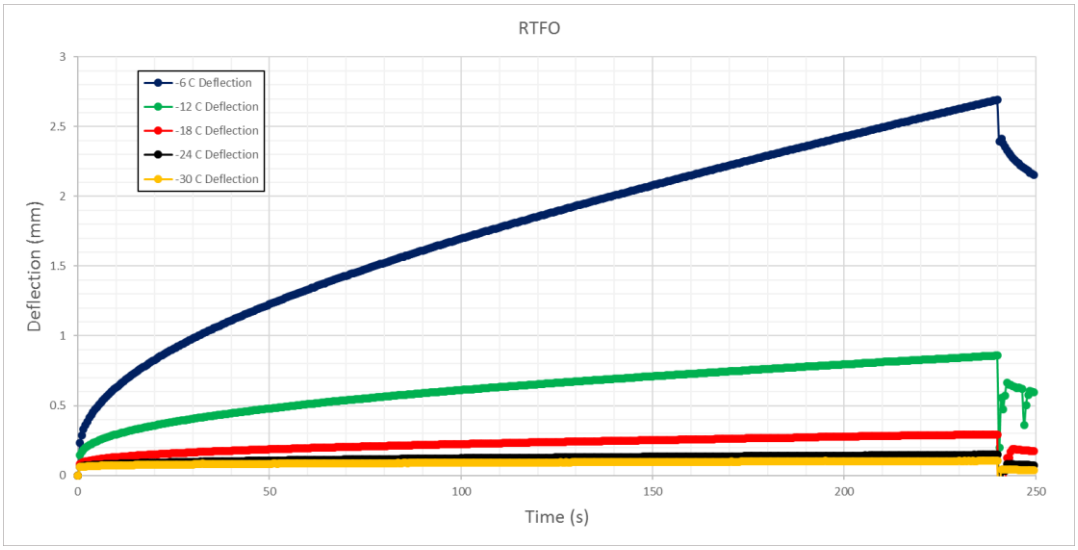

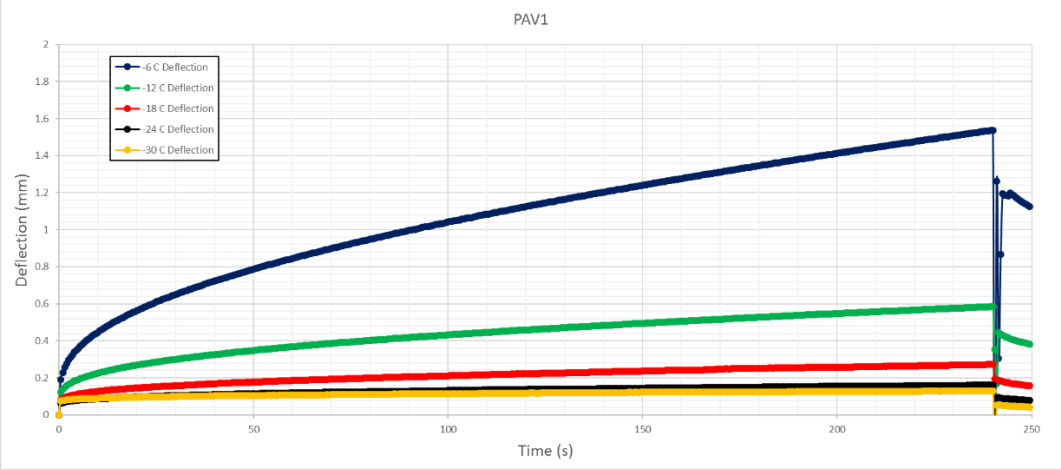

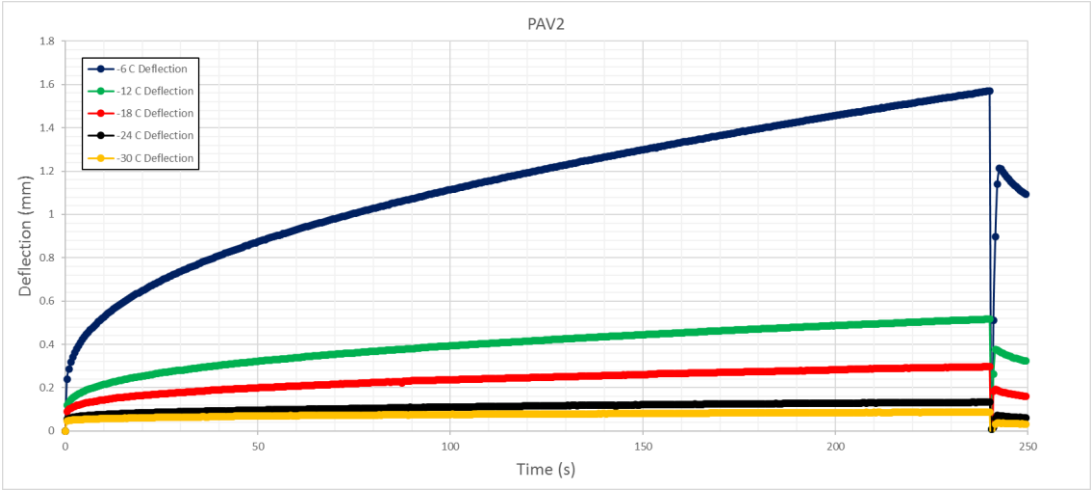

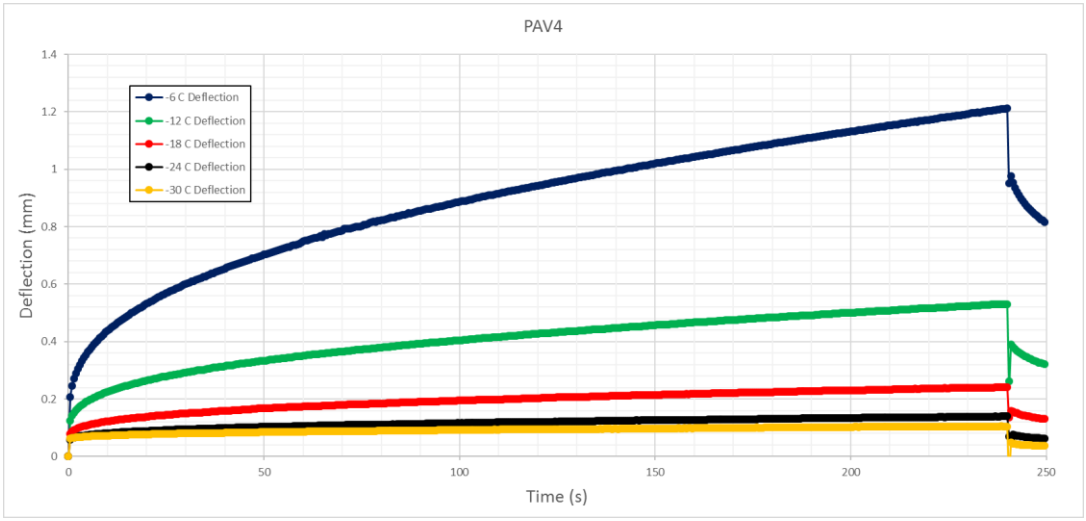

FT221 (S-E1 GP Colas)

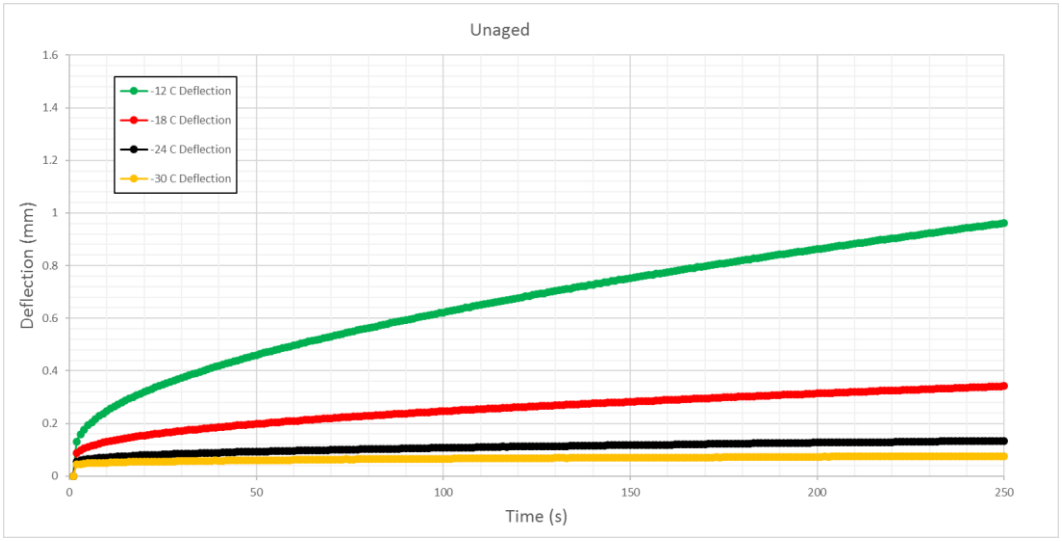

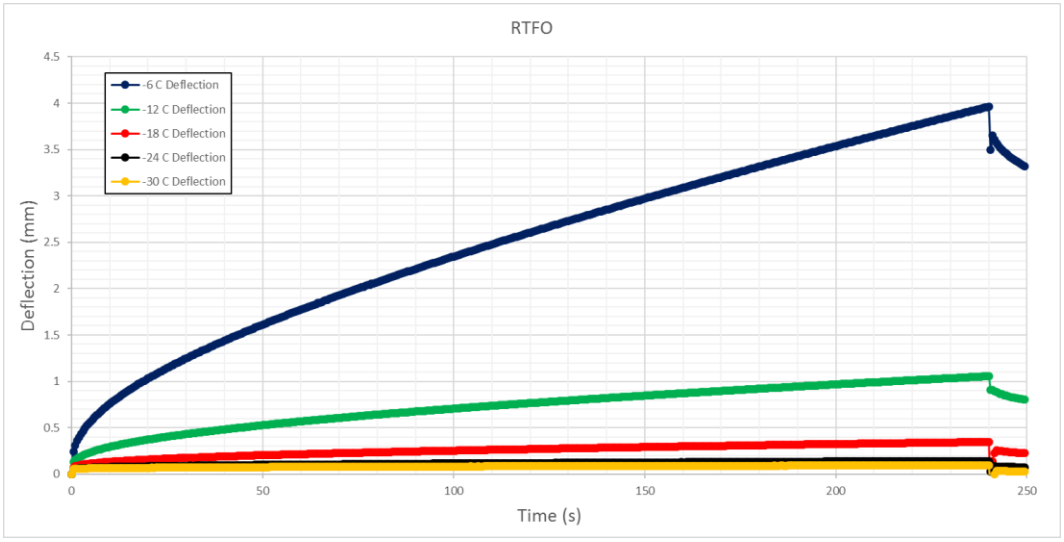

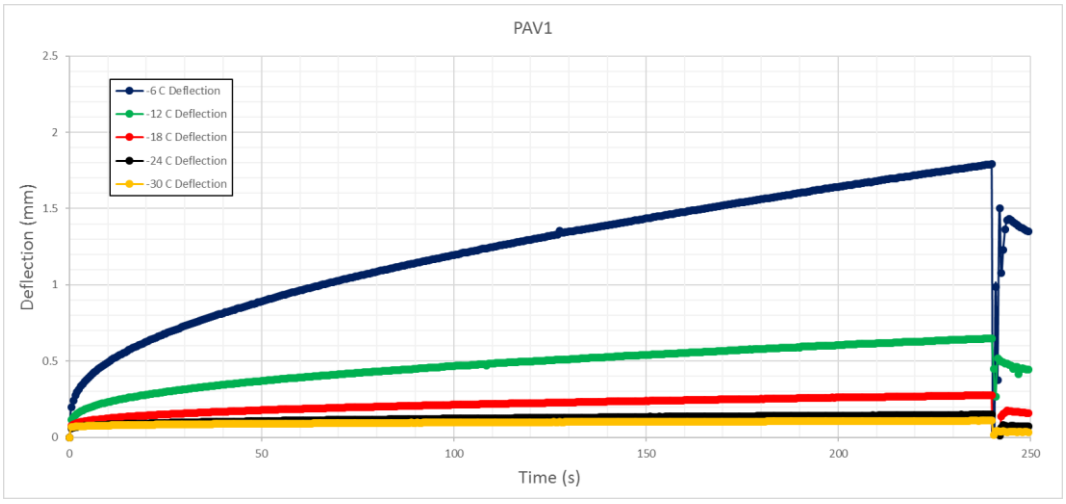

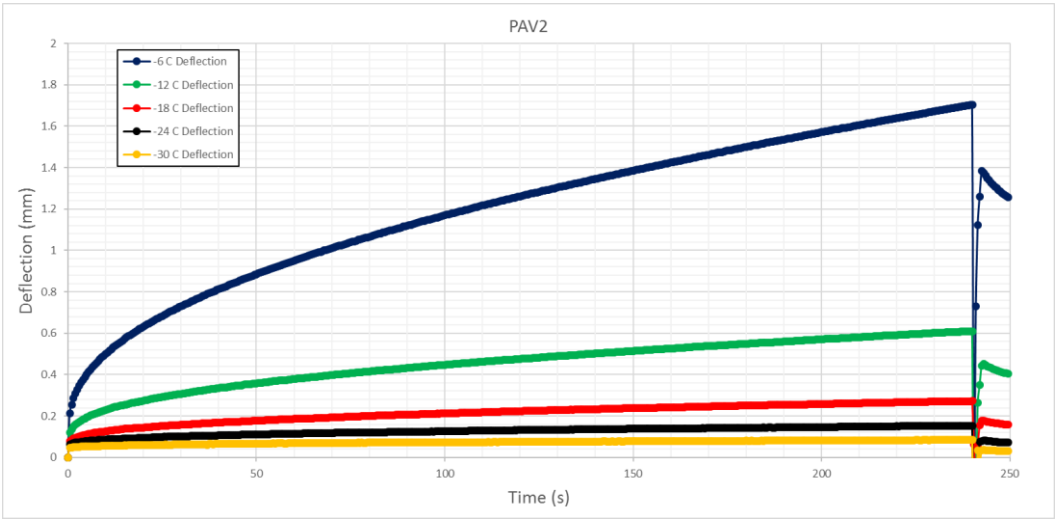

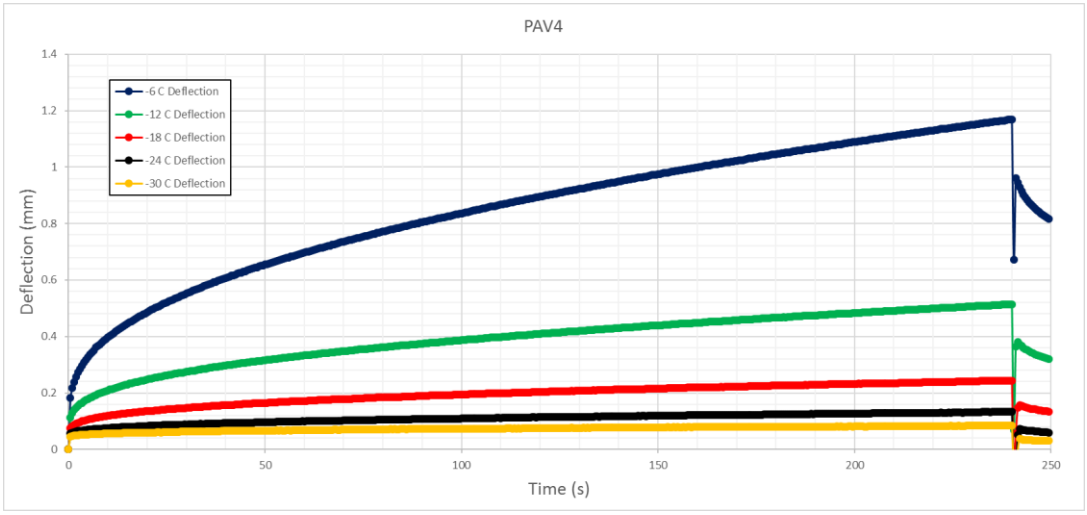

FT222 (S-E1 GP Tosas)

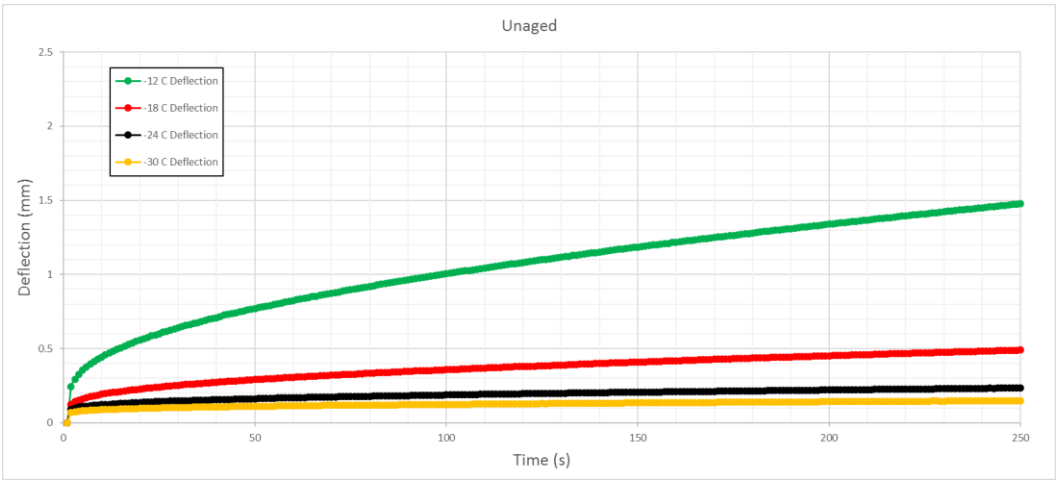

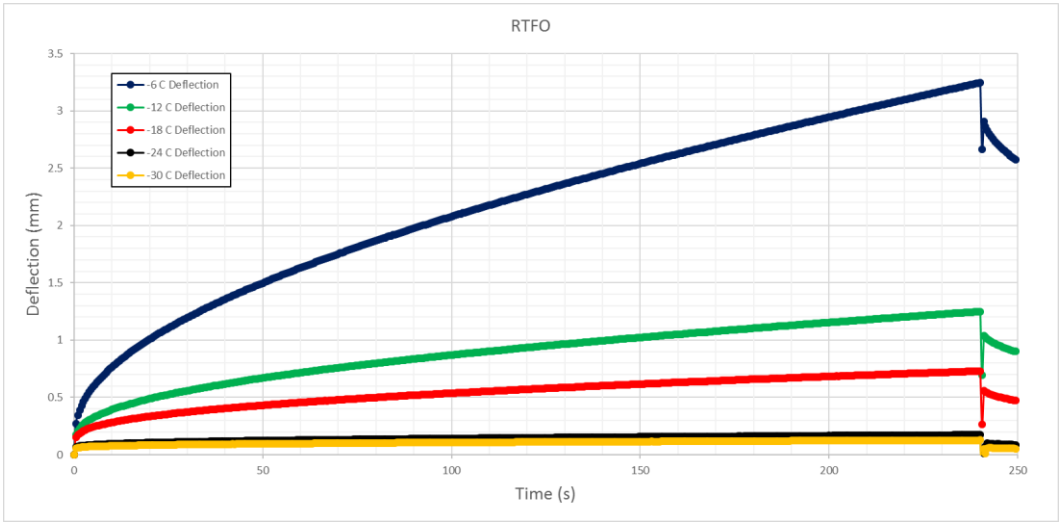

Annexure B: BBR deflection results

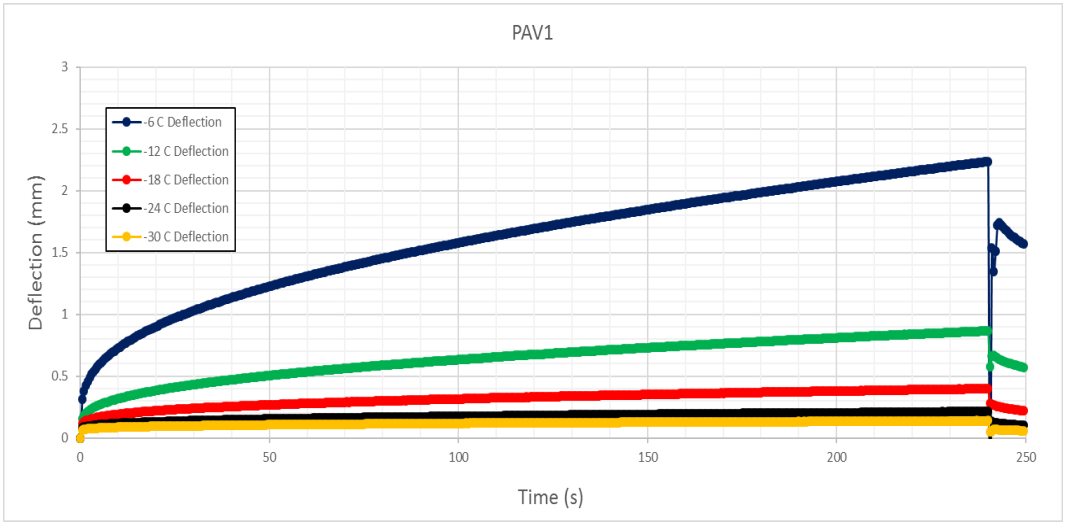

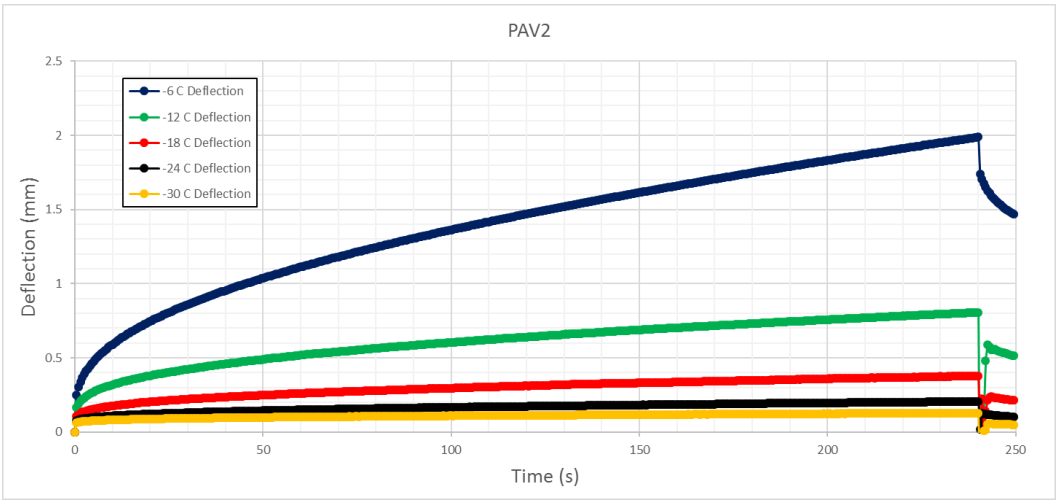

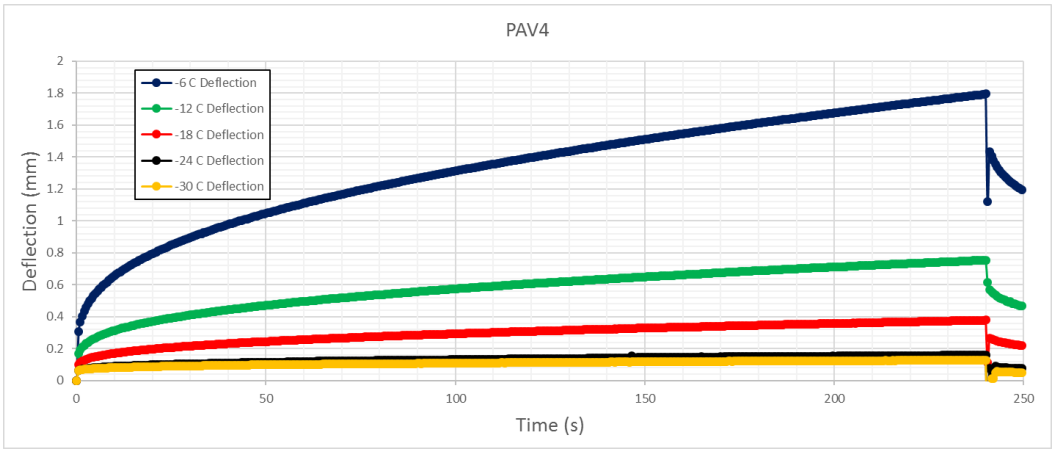

FT322 (S-E2 GP)

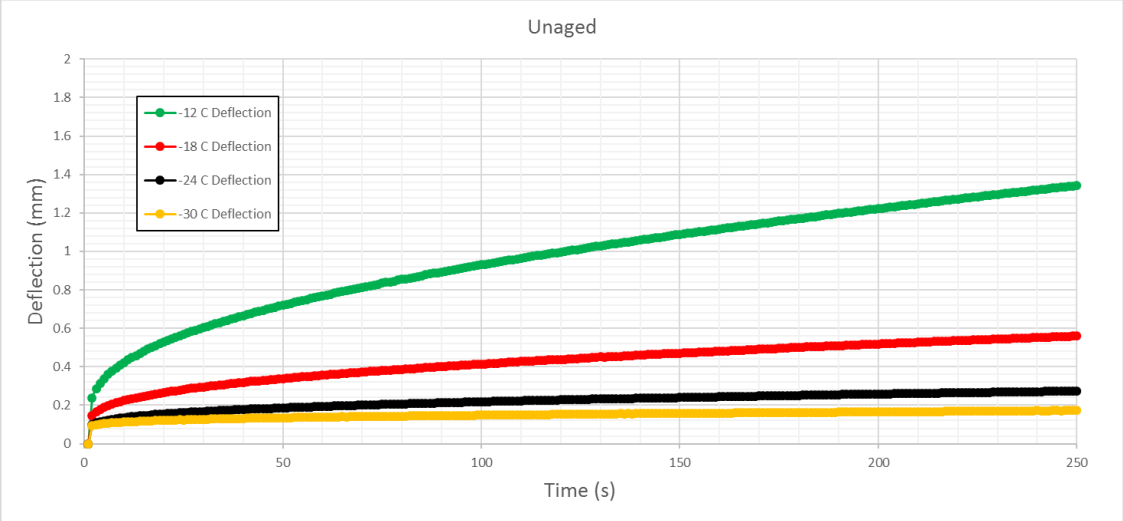

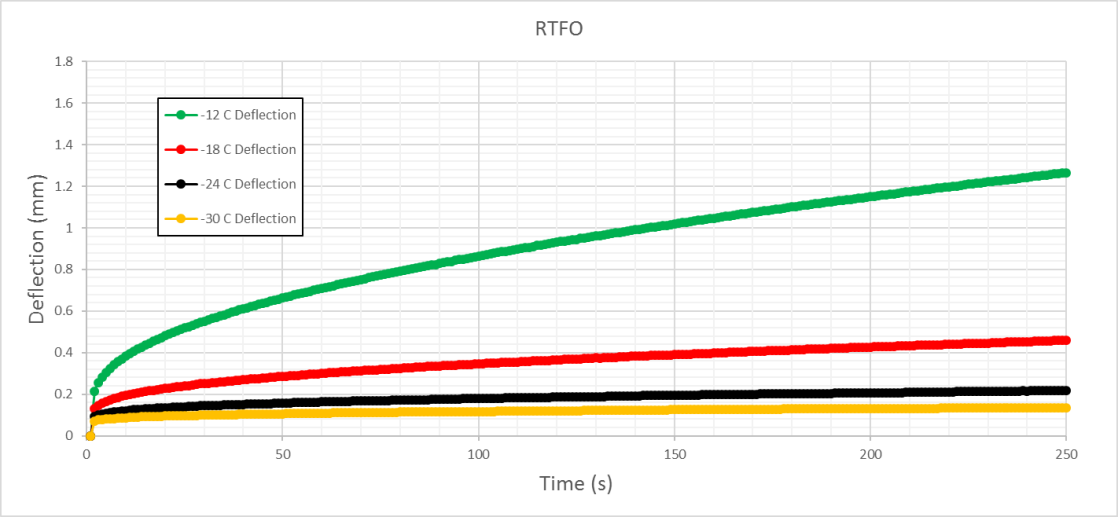

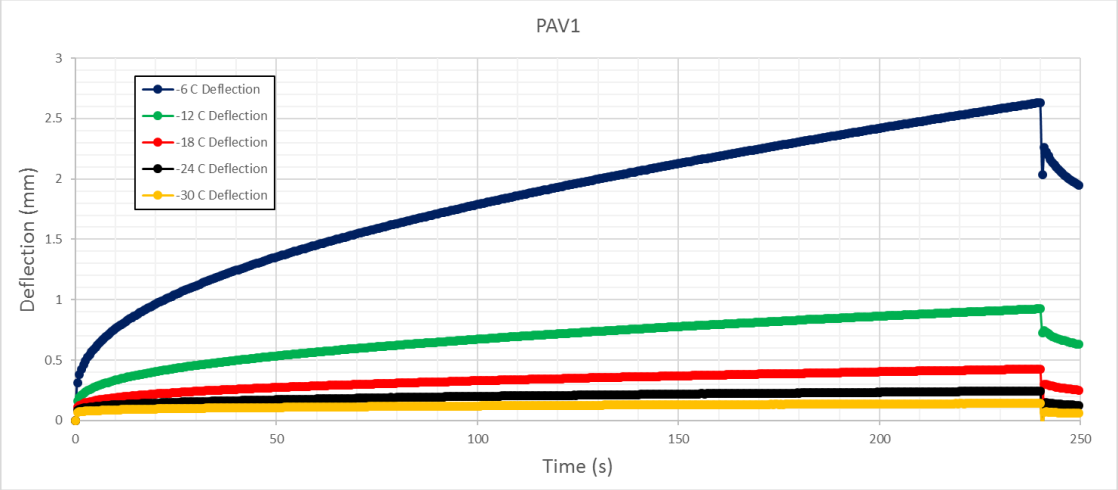

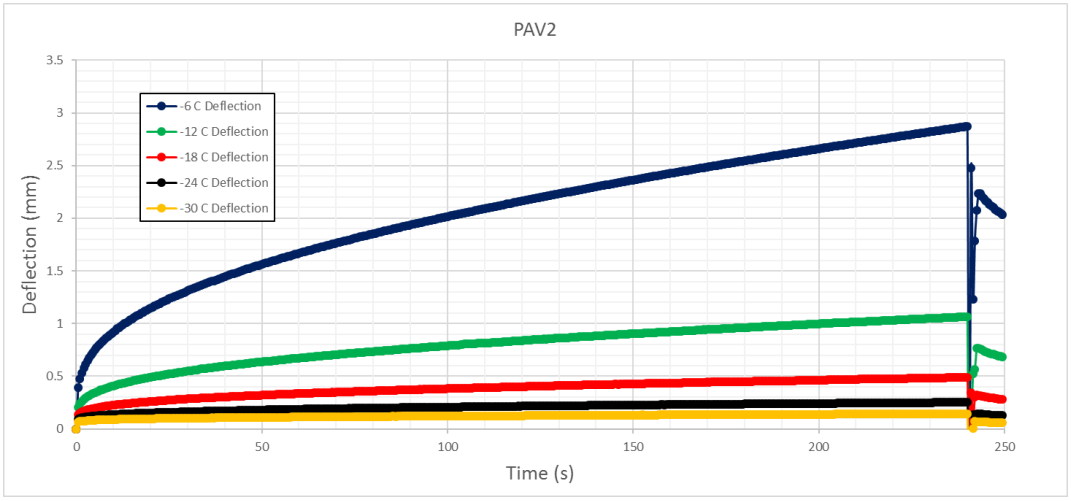

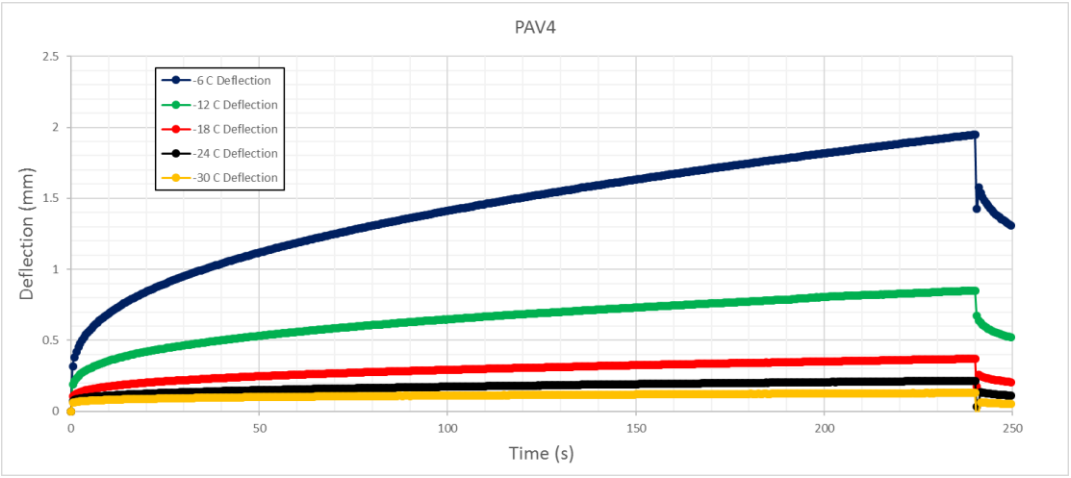

FT333 (S-E2 KZN)

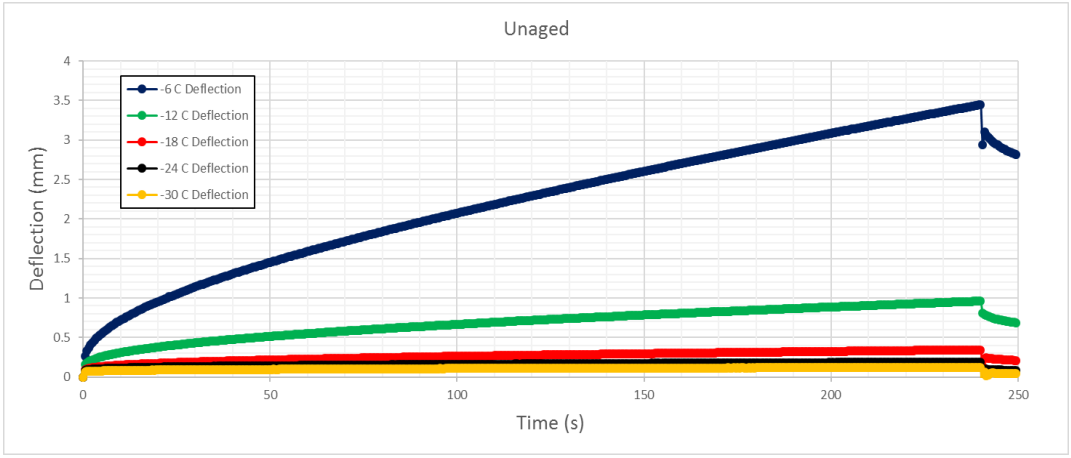

Annexure B: BBR deflection results

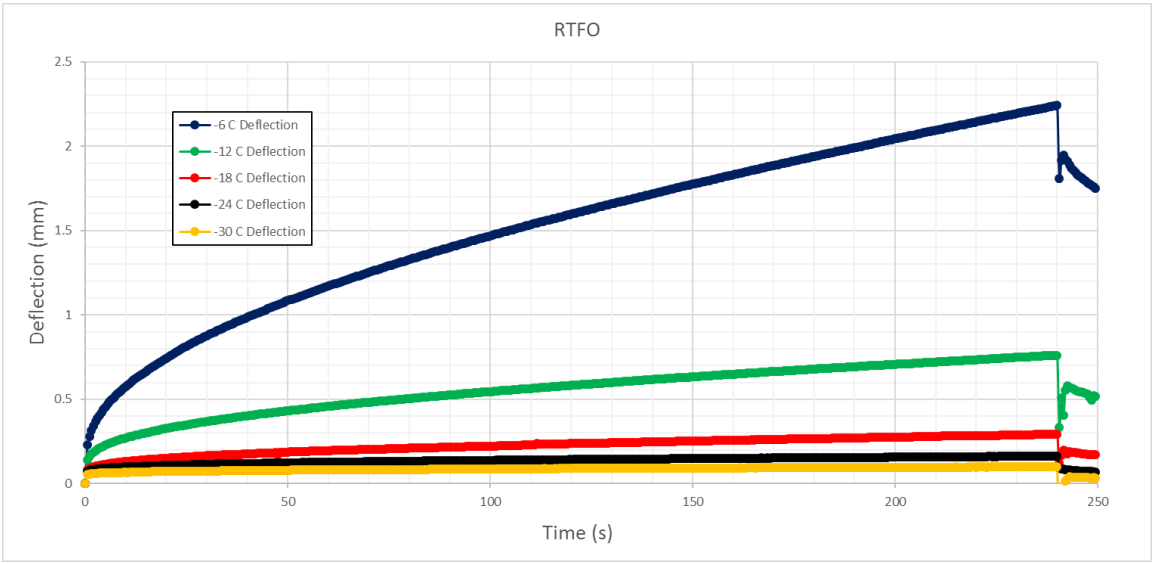

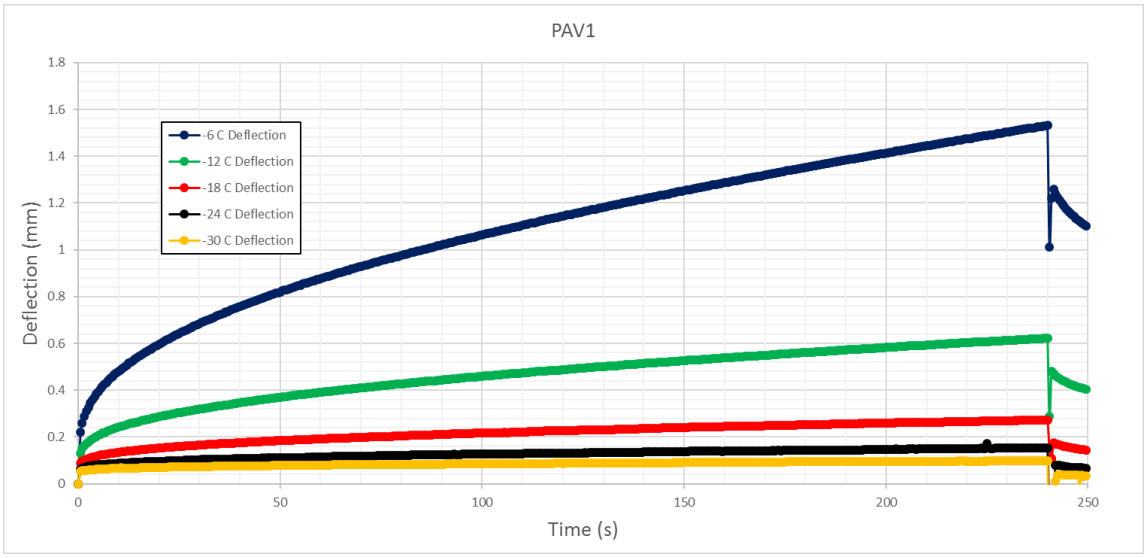

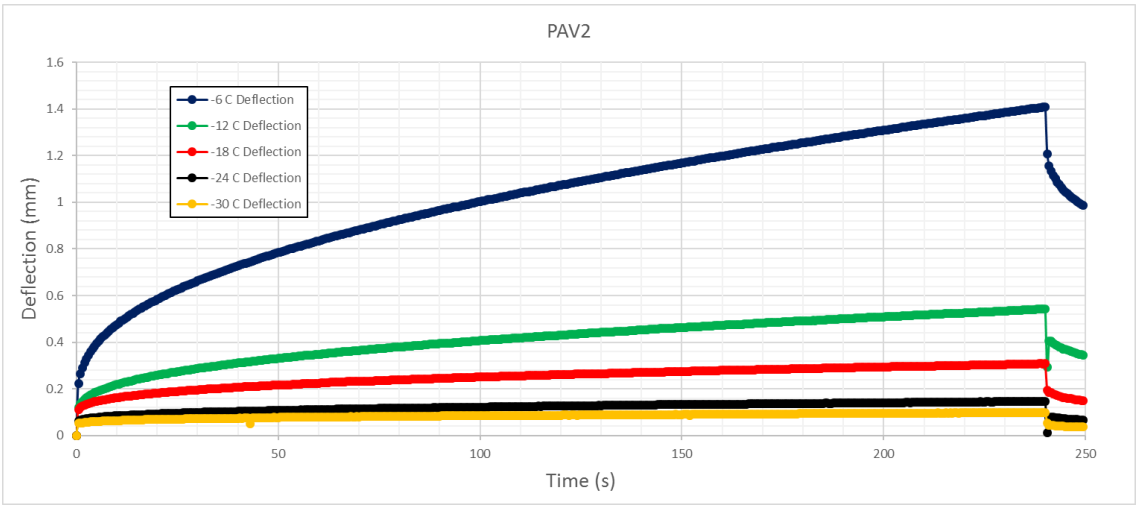

Annexure B: BBR deflection results

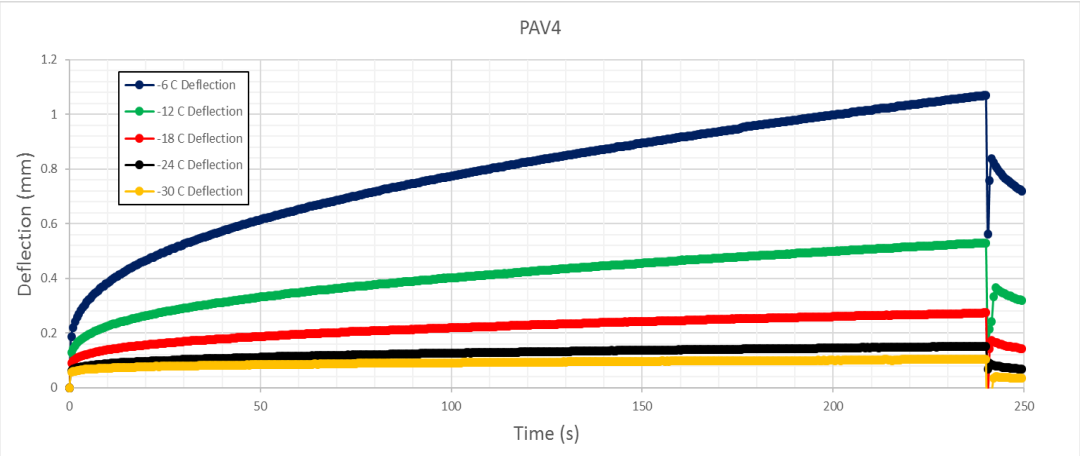

Annexure C: S-value, m-value and ΔTc

FT131 (70/100 KZN)

Unaged		
TEMP (˚C)	S60 (Mpa)	m60
-6	Deflection > 5mm	
-12	140	0.424
-18	409	0.312
-24	772	0.207
-30		
Tc,S	-16.273	
Tc,m	-18.702	
ΔTc	2.429	

RTFO		
TEMP (˚C)	S60 (Mpa)	m60
-6	Deflection > 5mm	
-12	172	0.394
-18	411	0.299
-24	741	0.196
-30		
Tc,S	-15.842	
Tc,m	-17.913	
ΔTc	2.071	

PAV1		
TEMP (˚C)	S60 (Mpa)	m60
-6	83	0.425
-12	212	0.335
-18	519	0.253
-24	871	0.176
-30	1333	0.122
Tc,S	-14.330	
Tc,m	-14.566	
ΔTc	0.235	

PAV2		
TEMP (˚C)	S60 (Mpa)	m60
-6	118	0.347
-12	288	0.271
-18	518	0.210
-24	858	0.166
-30	977	0.126
Tc,S	-12.425	
Tc,m	-9.692	
ΔTc	-2.734	

PAV4		
TEMP (˚C)	S60 (Mpa)	m60
-6	137	0.328
-12	300	0.269
-18	567	0.215
-24	953	0.175
-30	1268	0.130
Tc,S	-11.997	
Tc,m	-5.540	
ΔTc	-6.457	

DATA SUMMARY		
AGE	Tc,S (˚C)	Tc,m (˚C)
Unaged	-16.273	-18.702
RTFO	-15.842	-17.913
PAV1	-14.330	-14.566
PAV2	-12.425	-9.692
PAV4	-11.997	-5.540
AGE	ΔTc (˚C)	
Unaged	2.429	
RTFO	2.071	
PAV1	0.235	
PAV2	-2.734	
PAV4	-6.457	

FT211 (S-E1 WP Colas)

Unaged		
TEMP (˚C)	S60 (Mpa)	m60
-6	48	0.525
-12	148	0.378
-18	343	0.277
-24	690	0.200
-30	1045	0.134
Tc,S	-17.054	
Tc,m	-16.639	
ΔTc	-0.415	

RTFO		
TEMP (˚C)	S60 (Mpa)	m60
-6	59	0.467
-12	154	0.346
-18	405	0.263
-24	721	0.189
-30	942	0.125
Tc,S	-16.134	
Tc,m	-15.332	
ΔTc	-0.802	

PAV1		
TEMP (˚C)	S60 (Mpa)	m60
-6	94	0.398
-12	216	0.307
-18	427	0.247
-24	673	0.200
-30	736	0.118
Tc,S	-14.896	
Tc,m	-12.684	
ΔTc	-2.212	

PAV2		
TEMP (˚C)	S60 (Mpa)	m60
-6	86	0.350
-12	235	0.282
-18	384	0.234
-24	797	0.183
-30	1146	0.142
Tc,S	-14.971	
Tc,m	-10.406	
ΔTc	-4.565	

PAV4		
TEMP (˚C)	S60 (Mpa)	m60
-6	106	0.326
-12	228	0.276
-18	459	0.219
-24	757	0.177
-30	929	0.121
Tc,S	-14.360	
Tc,m	-9.121	
ΔTc	-5.238	

DATA SUMMARY		
AGE	Tc,S (˚C)	Tc,m (˚C)
Unaged	-17.054	-16.639
RTFO	-16.134	-15.332
PAV1	-14.896	-12.684
PAV2	-14.971	-10.406
PAV4	-14.360	-9.121
AGE	ΔTc (˚C)	
Unaged	-0.415	
RTFO	-0.802	
PAV1	-2.212	
PAV2	-4.565	
PAV4	-5.238	

FT221 (S-E1 GP Colas)

Unaged		
TEMP (˚C)	S60 (Mpa)	m60
-6	Deflection > 5mm	
-12	117	0.459
-18	299	0.345
-24	716	0.235
-30	1186	0
Tc,S	-18.025	
Tc,m	-20.448	
ΔTc	2.423	

RTFO		
TEMP (˚C)	S60 (Mpa)	m60
-6	45	0.534
-12	140	0.412
-18	371	0.312
-24	790	0.206
-30	1028	0
Tc,S	-16.692	
Tc,m	-18.673	
ΔTc	1.981	

PAV1		
TEMP (˚C)	S60 (Mpa)	m60
-6	83	0.416
-12	201	0.332
-18	425	0.255
-24	718	0.191
-30	871	0.110
Tc,S	-15.211	
Tc,m	-14.518	
ΔTc	-0.693	

PAV2		
TEMP (˚C)	S60 (Mpa)	m60
-6	84	0.395
-12	211	0.317
-18	429	0.248
-24	689	0.187
-30	1183	0.131
Tc,S	-14.988	
Tc,m	-13.497	
ΔTc	-1.491	

PAV4		
TEMP (˚C)	S60 (Mpa)	m60
-6	114	0.348
-12	239	0.289
-18	464	0.232
-24	809	0.186
-30	1179	0.133
Tc,S	-14.062	
Tc,m	-10.872	
ΔTc	-3.189	

DATA SUMMARY		
AGE	Tc,S (˚C)	Tc,m (˚C)
Unaged	-18.025	-20.448
RTFO	-16.692	-18.673
PAV1	-15.211	-14.518
PAV2	-14.988	-13.497
PAV4	-14.062	-10.872
AGE	ΔTc (˚C)	
Unaged	2.423	
RTFO	1.981	
PAV1	-0.693	
PAV2	-1.491	
PAV4	-3.189	

FT222 (S-E1 GP Tosas)

Unaged		
TEMP (˚C)	S60 (Mpa)	m60
-6	Deflection > 5mm	
-12	59	0.408
-18	228	0.307
-24	609	0.210
-30	904	0.142
Tc,S	-19.673	
Tc,m	-18.410	
ΔTc	-1.264	

RTFO		
TEMP (˚C)	S60 (Mpa)	m60
-6	49	0.463
-12	111	0.370
-18	174	0.308
-24	622	0.195
-30	805	0.161
Tc,S	-20.561	
Tc,m	-18.402	
ΔTc	-2.159	

PAV1		
TEMP (˚C)	S60 (Mpa)	m60
-6	61	0.361
-12	150	0.322
-18	288	0.237
-24	507	0.195
-30	737	0.157
Tc,S	-18.442	
Tc,m	-13.574	
ΔTc	-4.869	

PAV2		
TEMP (˚C)	S60 (Mpa)	m60
-6	71	0.389
-12	153	0.299
-18	306	0.246
-24	537	0.206
-30	793	0.149
Tc,S	-17.835	
Tc,m	-11.901	
ΔTc	-5.934	

PAV4		
TEMP (˚C)	S60 (Mpa)	m60
-6	71	0.323
-12	160	0.282
-18	310	0.257
-24	671	0.189
-30	793	0.149
Tc,S	-17.693	
Tc,m	-9.378	
ΔTc	-8.316	

DATA SUMMARY		
AGE	Tc,S (˚C)	Tc,m (˚C)
Unaged	-19.673	-18.410
RTFO	-20.561	-18.402
PAV1	-18.442	-13.574
PAV2	-17.835	-11.901
PAV4	-17.693	-9.378
AGE	ΔTc (˚C)	
Unaged	-1.264	
RTFO	-2.159	
PAV1	-4.869	
PAV2	-5.934	
PAV4	-8.316	

FT322 (S-E2 GP)

Unaged		
TEMP (˚C)	S60 (Mpa)	m60
-6	Deflection > 5mm	
-12	80	0.388
-18	180	0.315
-24	348	0.241
-30	525	0.153
Tc,S	-22.645	
Tc,m	-19.199	
ΔTc	-3.445	

RTFO		
TEMP (˚C)	S60 (Mpa)	m60
-6	Deflection > 5mm	
-12	85	0.400
-18	215	0.296
-24	428	0.200
-30	662	0.157
Tc,S	-20.905	
Tc,m	-17.780	
ΔTc	-3.125	

PAV1		
TEMP (˚C)	S60 (Mpa)	m60
-6	54	0.398
-12	121	0.328
-18	271	0.261
-24	438	0.208
-30	728	0.156
Tc,S	-19.272	
Tc,m	-14.534	
ΔTc	-4.738	

PAV2		
TEMP (˚C)	S60 (Mpa)	m60
-6	56	0.365
-12	135	0.307
-18	270	0.249
-24	443	0.200
-30	741	0.157
Tc,S	-19.279	
Tc,m	-12.699	
ΔTc	-6.580	

PAV4		
TEMP (˚C)	S60 (Mpa)	m60
-6	67	0.333
-12	143	0.281
-18	308	0.239
-24	514	0.216
-30	781	0.149
Tc,S	-17.790	
Tc,m	-9.787	
ΔTc	-8.003	

DATA SUMMARY		
AGE	Tc,S (˚C)	Tc,m (˚C)
Unaged	-22.645	-19.199
RTFO	-20.905	-17.780
PAV1	-19.272	-14.534
PAV2	-19.279	-12.699
PAV4	-17.790	-9.787
AGE	ΔTc (˚C)	
Unaged	-3.445	
RTFO	-3.125	
PAV1	-4.738	
PAV2	-6.580	
PAV4	-8.003	

FT333 (S-E2 KZN)

Unaged		
TEMP (˚C)	S60 (Mpa)	m60
-6	49.86057	0.507612
-12	146	0.366
-18	348	0.270
-24	547	0.172
-30	823	0.129
Tc,S	-16.977	
Tc,m	-16.126	
ΔTc	-0.852	

RTFO		
TEMP (˚C)	S60 (Mpa)	m60
-6	68.23591	0.437971
-12	174	0.333
-18	408	0.260
-24	626	0.163
-30	982	0.128
Tc,S	-15.827	
Tc,m	-14.712	
ΔTc	-1.115	

PAV1		
TEMP (˚C)	S60 (Mpa)	m60
-6	91	0.372
-12	204	0.307
-18	417	0.228
-24	698	0.181
-30	1005	0.130
Tc,S	-15.229	
Tc,m	-12.556	
ΔTc	-2.673	

PAV2		
TEMP (˚C)	S60 (Mpa)	m60
-6	95	0.349
-12	230	0.292
-18	357	0.208
-24	721	0.177
-30	1017	0.138
Tc,S	-15.609	
Tc,m	-11.151	
ΔTc	-4.457	

PAV4		
TEMP (˚C)	S60 (Mpa)	m60
-6	122	0.330
-12	228	0.276
-18	410	0.221
-24	694	0.175
-30	929	0.120
Tc,S	-14.809	
Tc,m	-9.334	
ΔTc	-5.475	

DATA SUMMARY		
AGE	Tc,S (˚C)	Tc,m (˚C)
Unaged	-16.977	-16.126
RTFO	-15.827	-14.712
PAV1	-15.229	-12.556
PAV2	-15.609	-11.151
PAV4	-14.809	-9.334
AGE	ΔTc (˚C)	
Unaged	-0.852	
RTFO	-1.115	
PAV1	-2.673	
PAV2	-4.457	
PAV4	-5.475	

Annexure D: Stiffness master curves

FT131 (70/100 KZN)

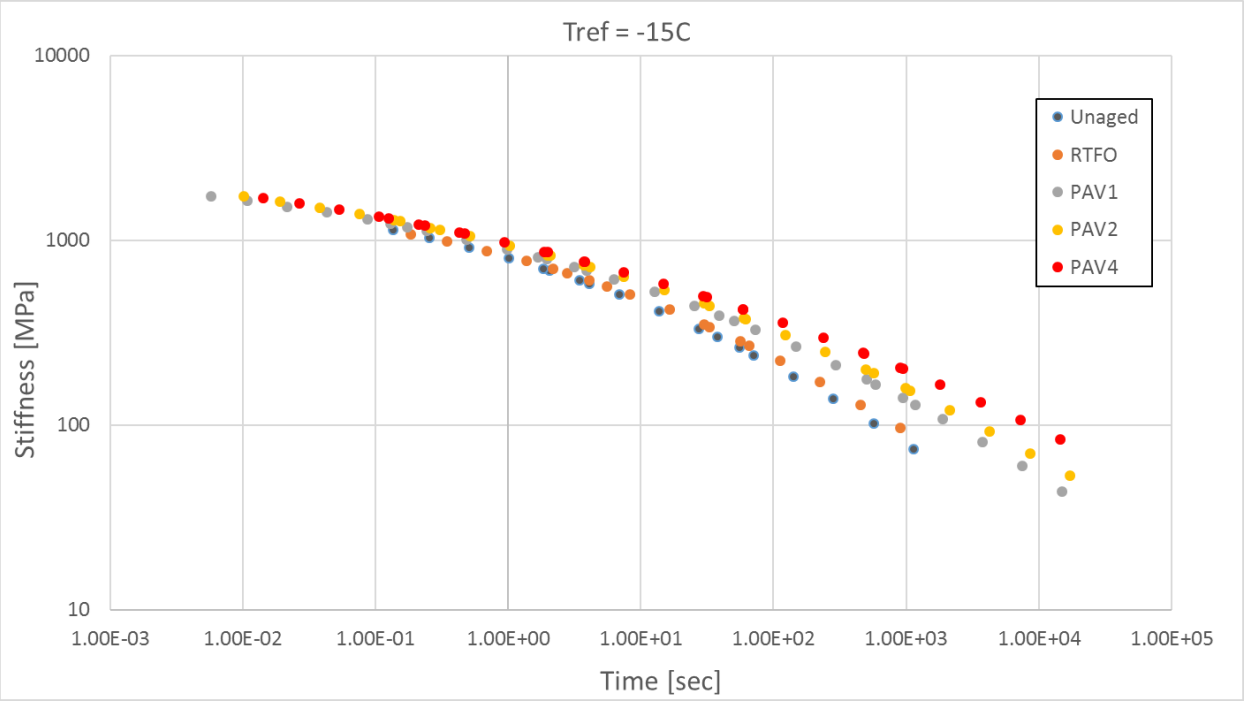

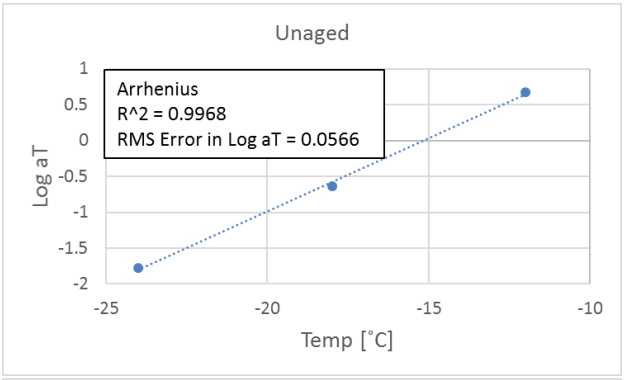

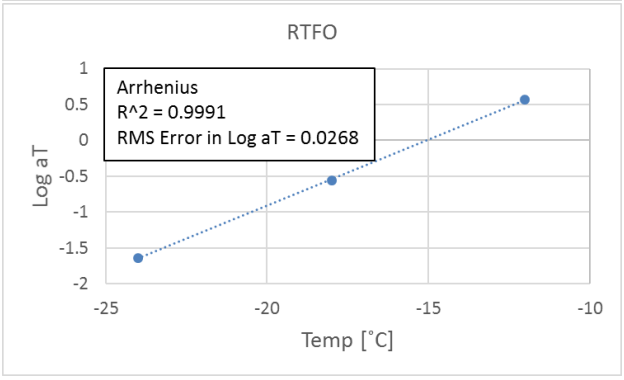

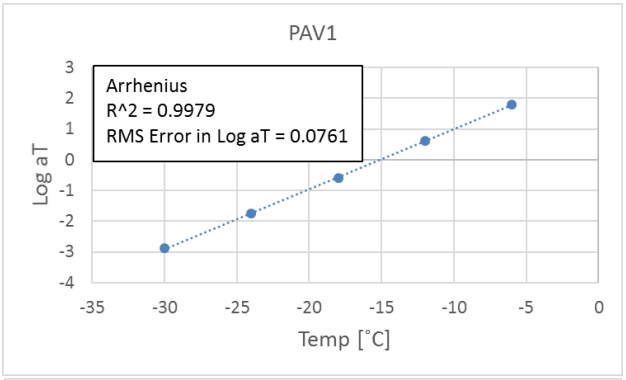

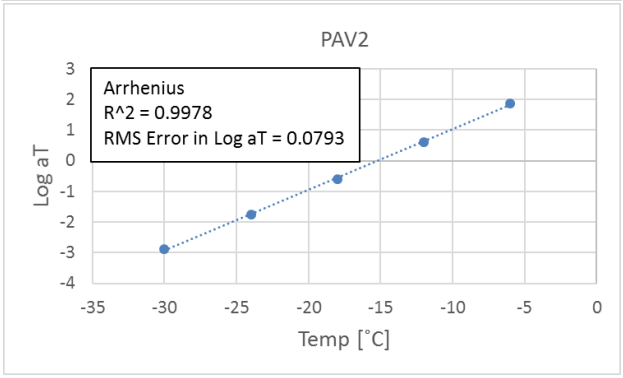

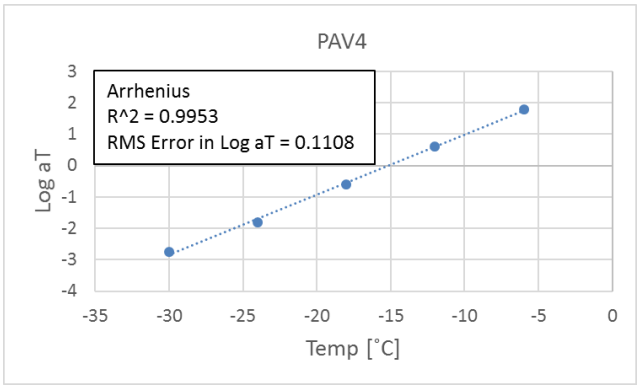

FT211 (S-E1 WP Colas)

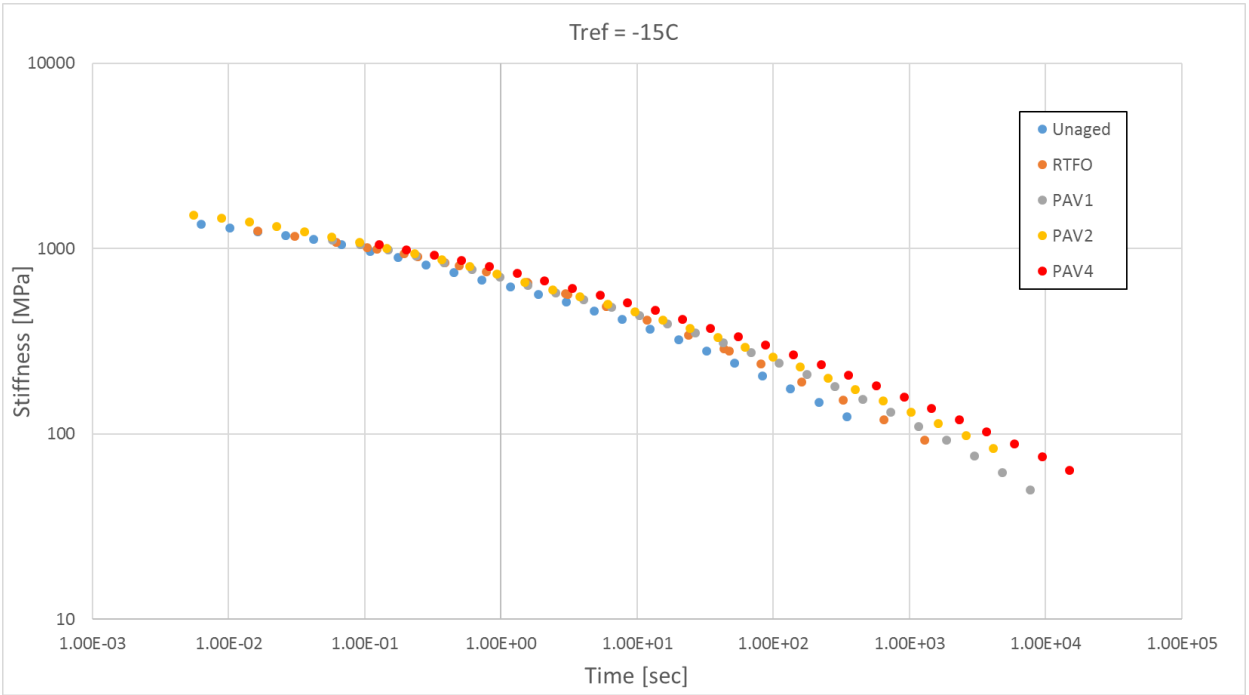

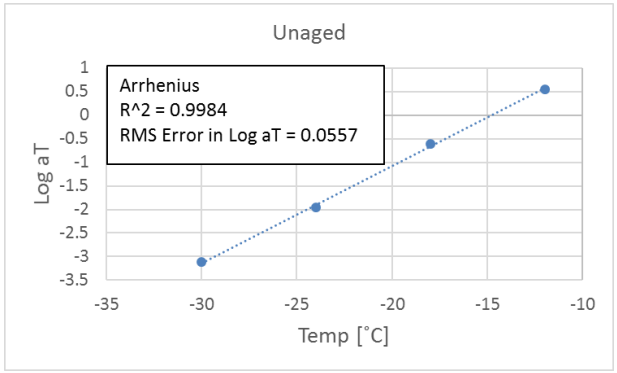

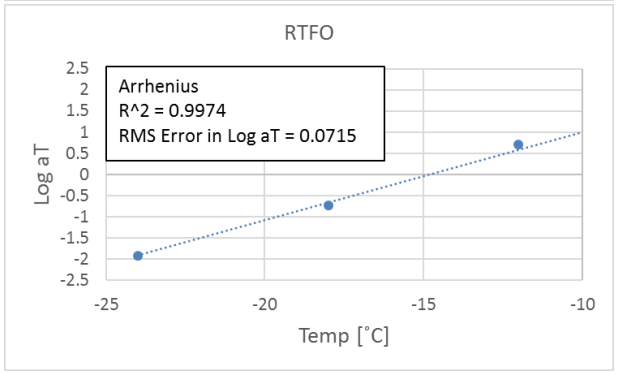

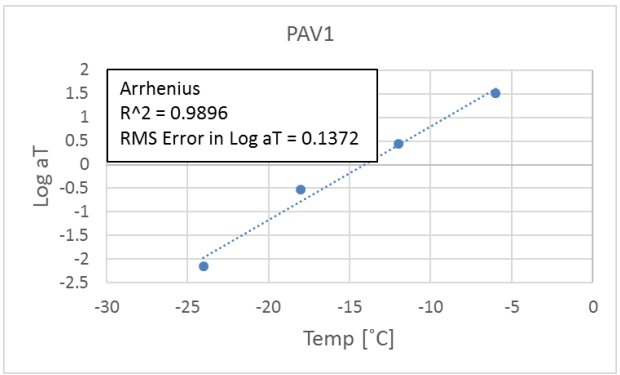

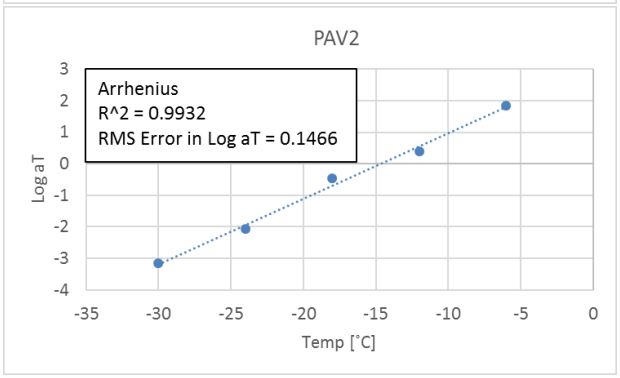

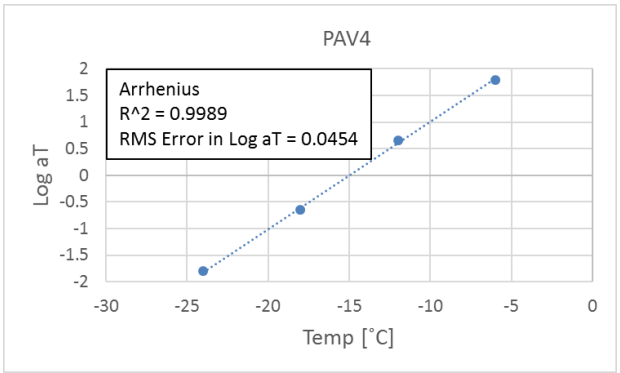

FT221 (S-E1 GP Colas)

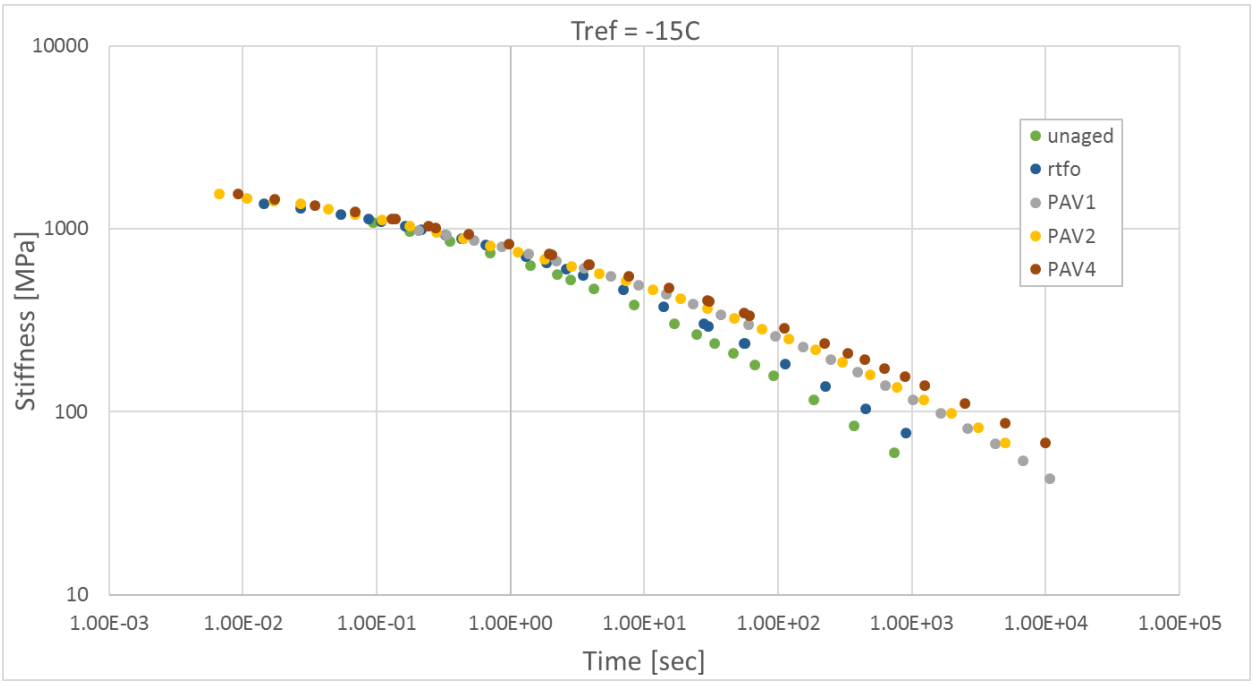

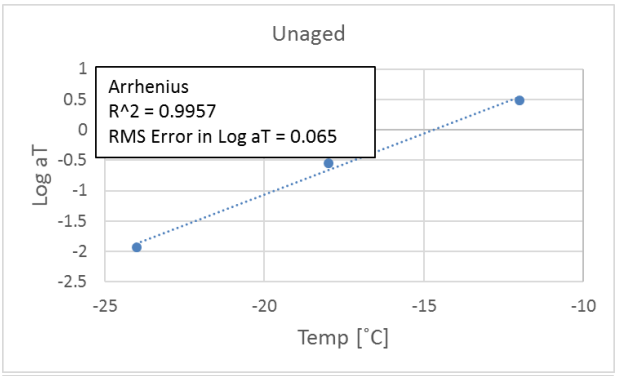

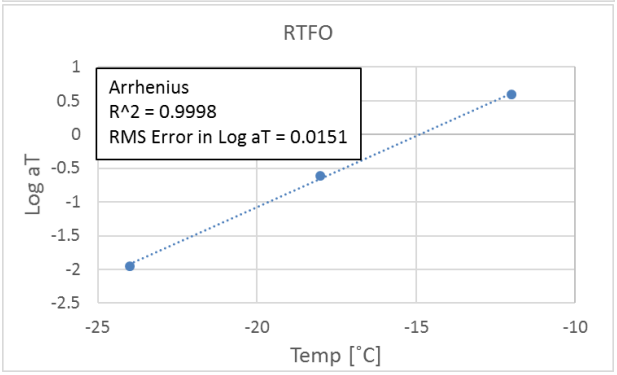

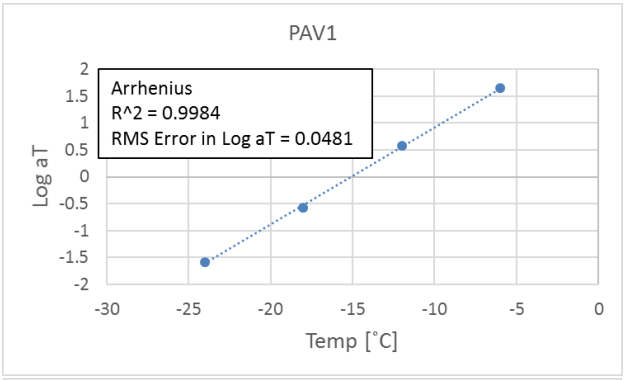

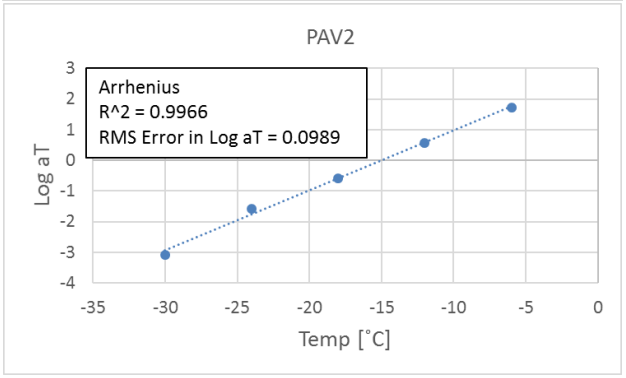

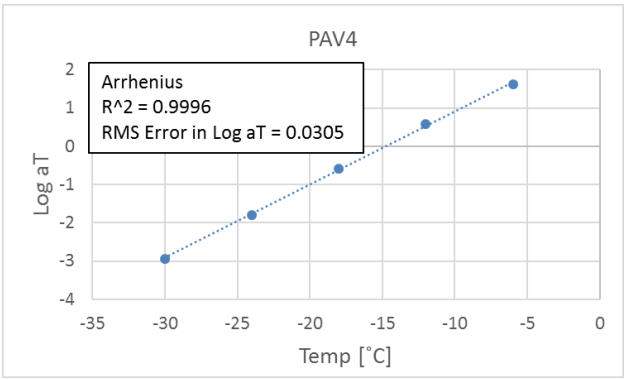

FT222 (S-E1 GP Tosas)

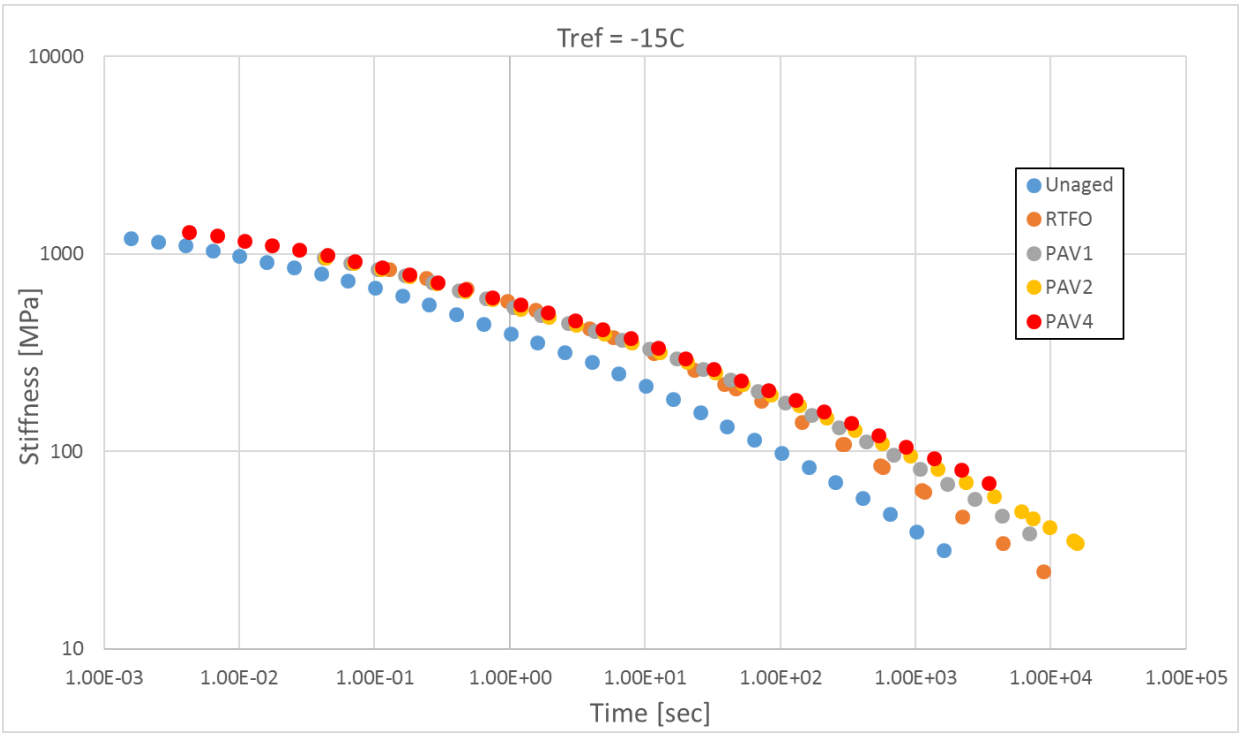

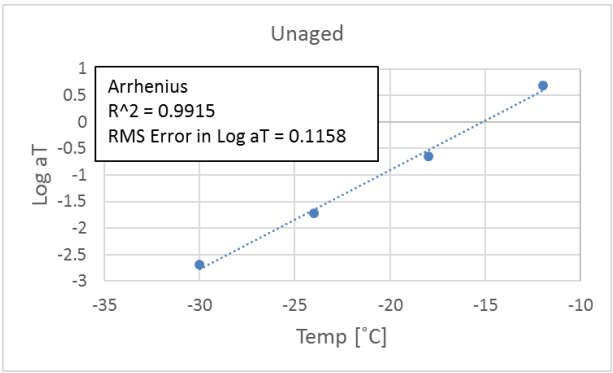

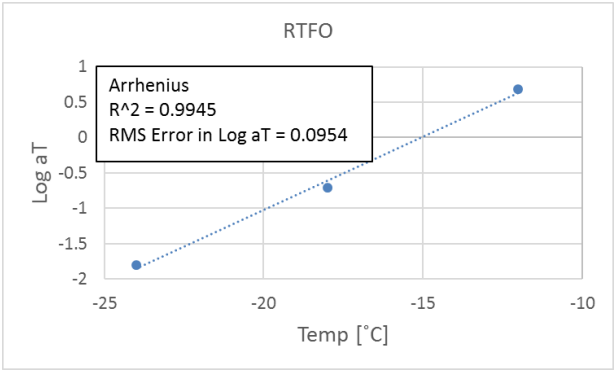

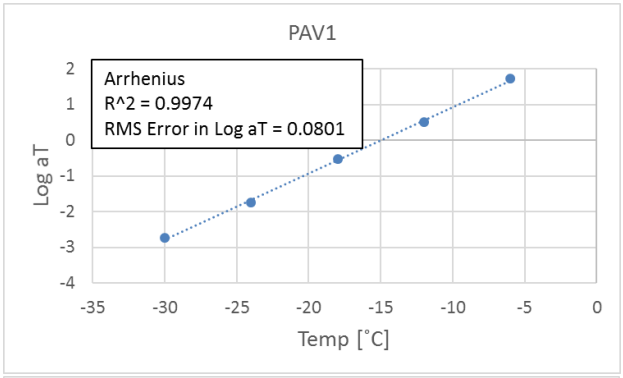

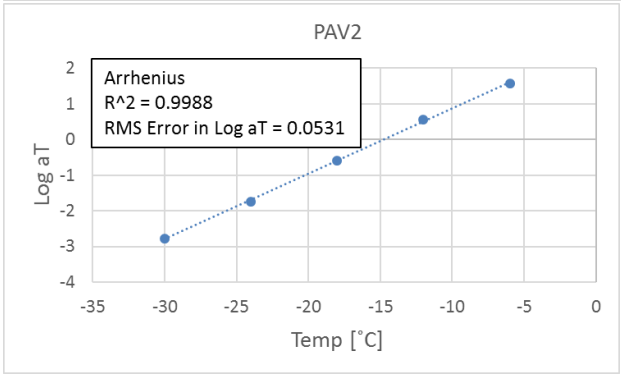

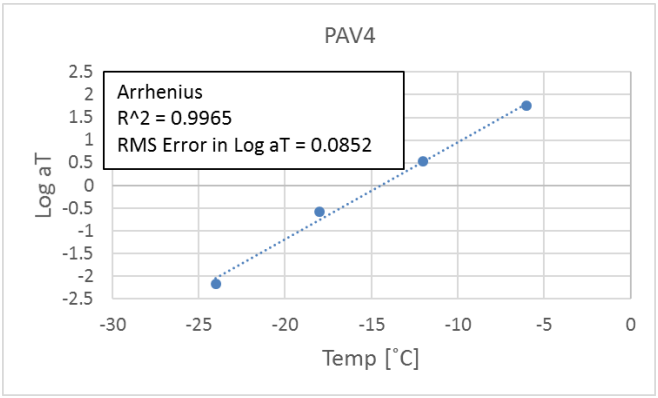

FT322 (S-E2 GP)

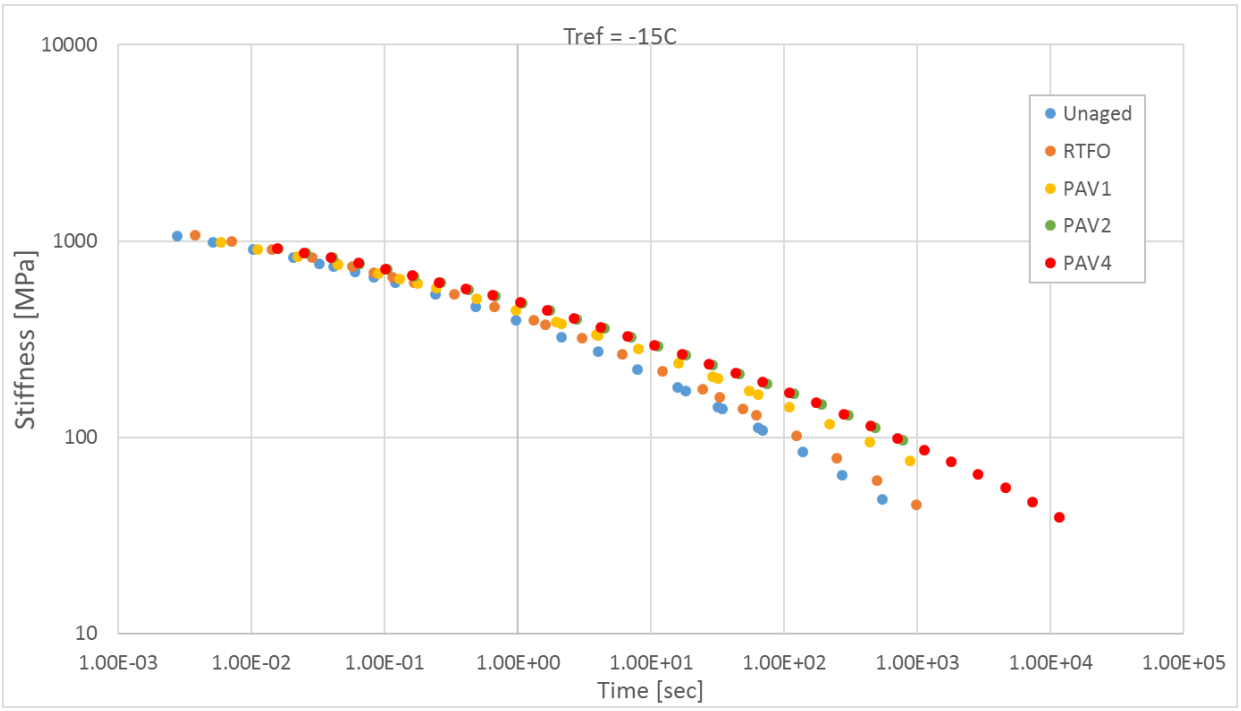

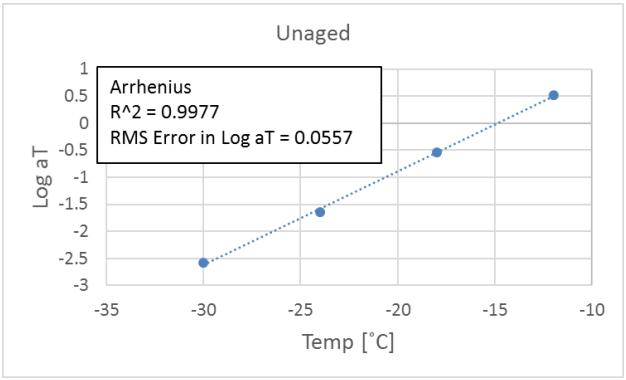

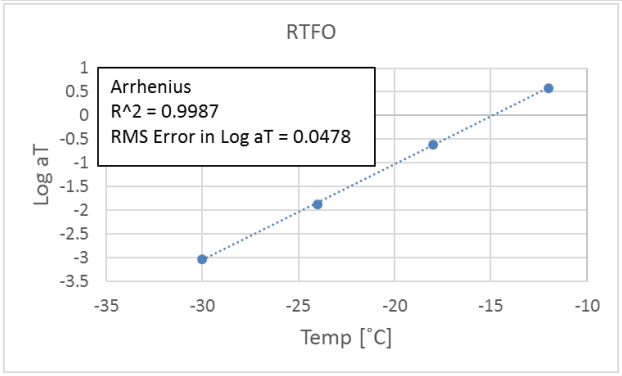

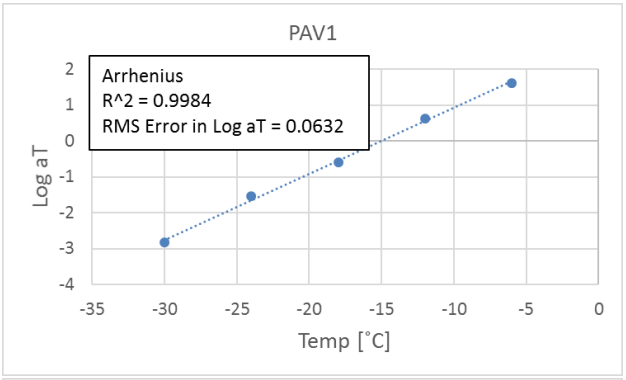

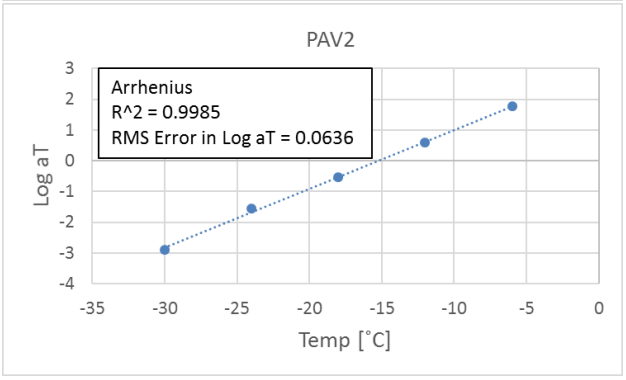

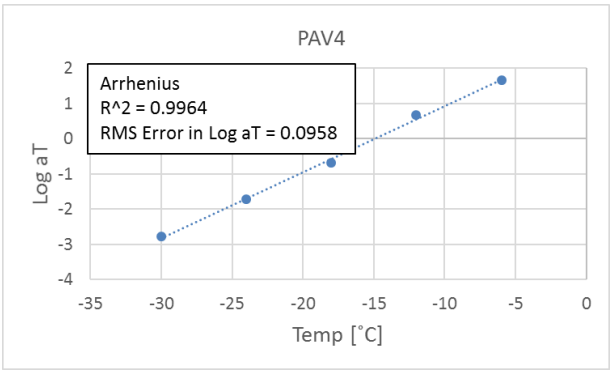

FT333 (S-E2 KZN)

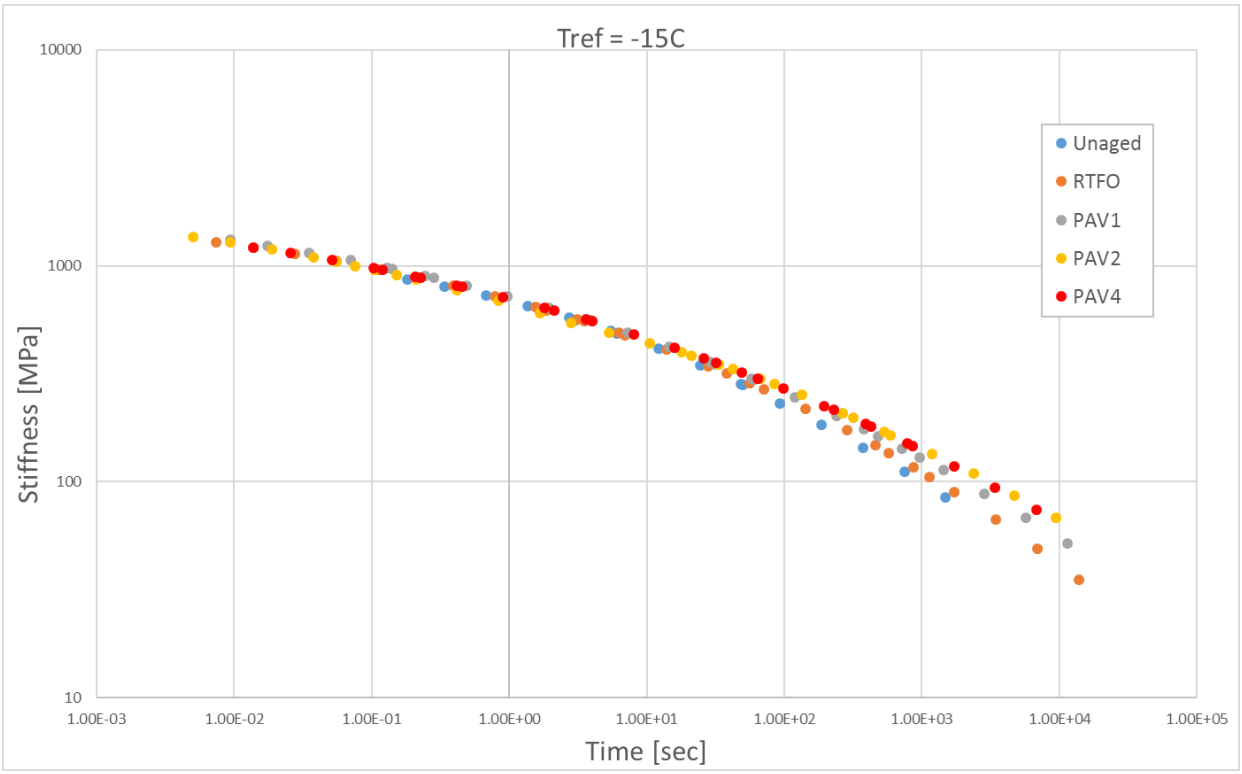

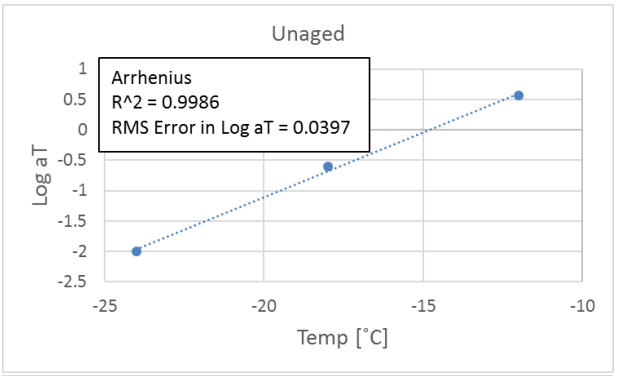

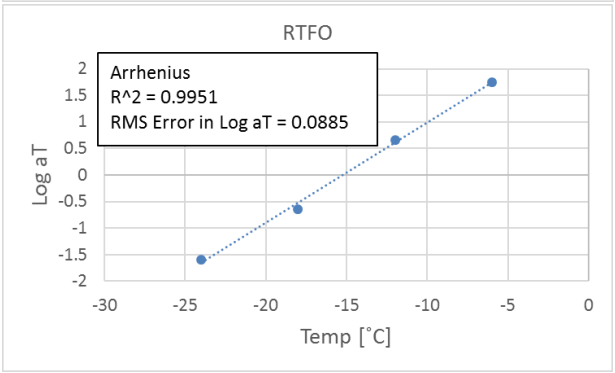

Annexure D: Stiffness master curves

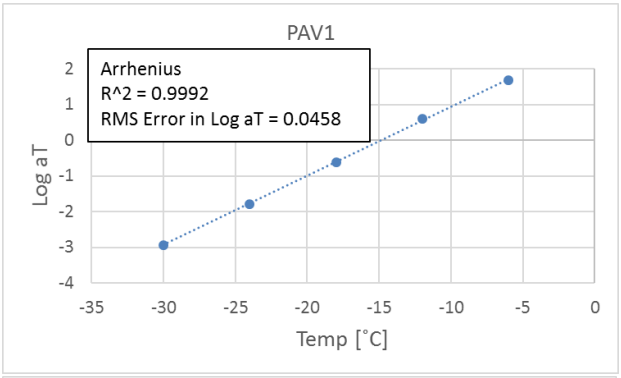

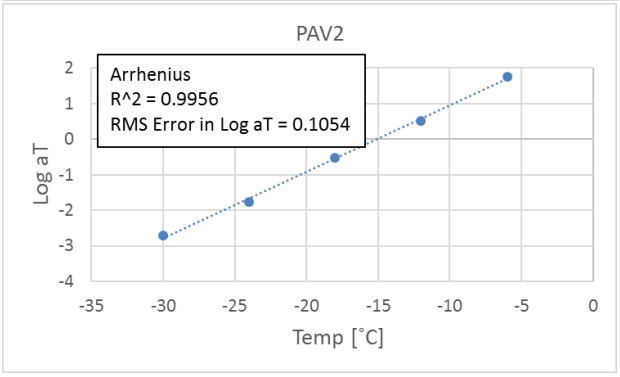

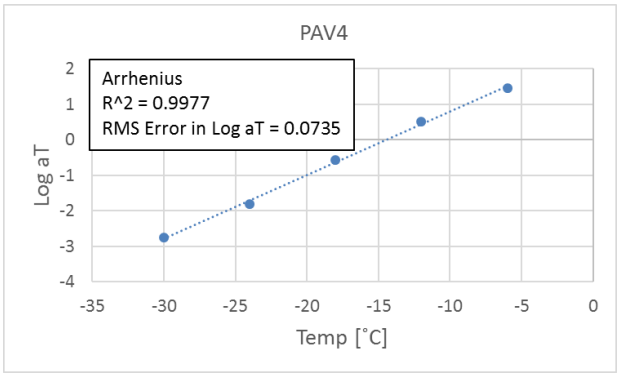

Annexure E: Combined master curves

FT131 (70/100 KZN)

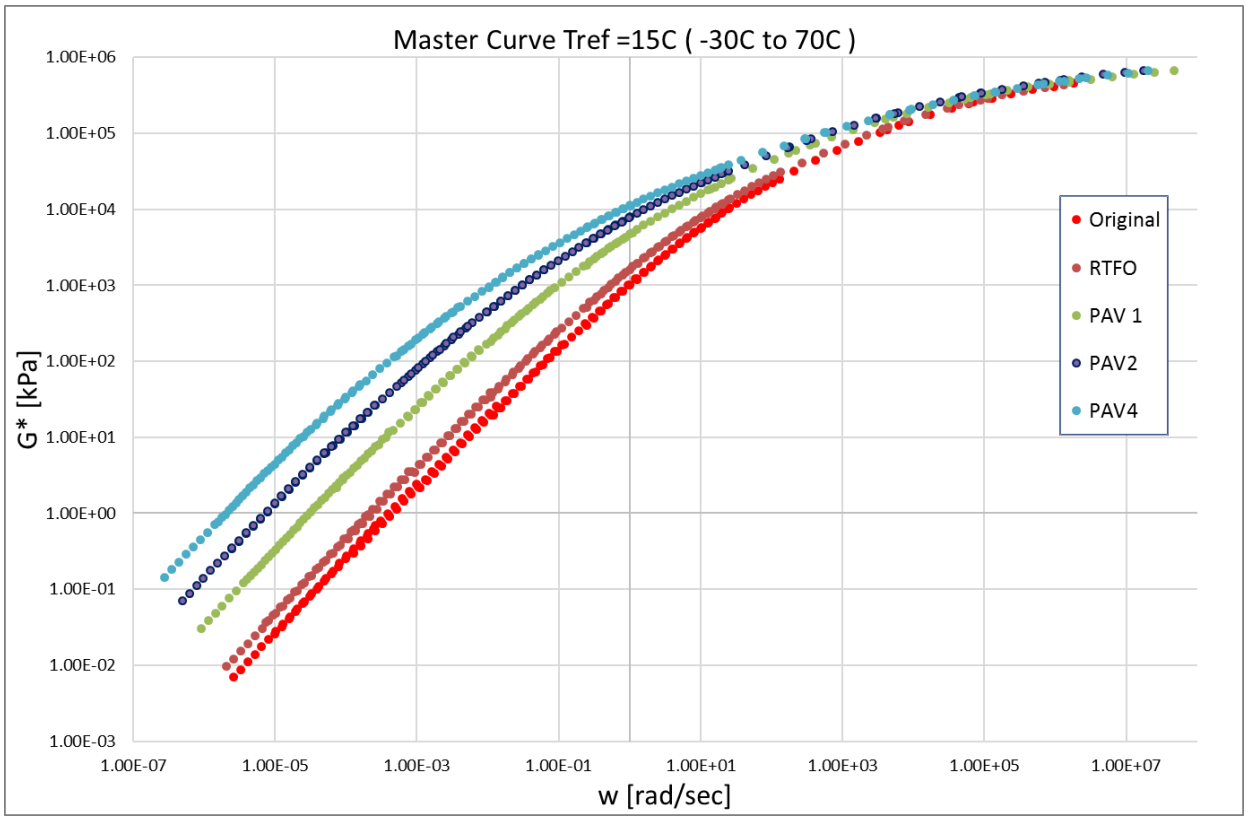

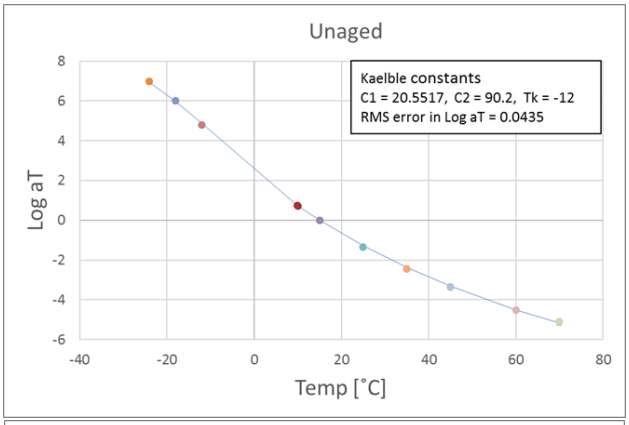

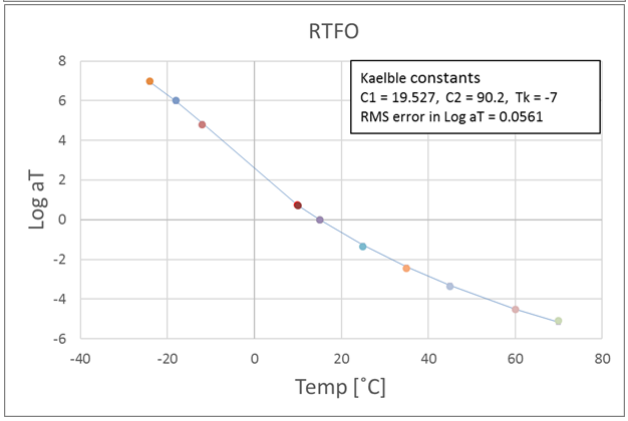

Annexure E: Combined master curves

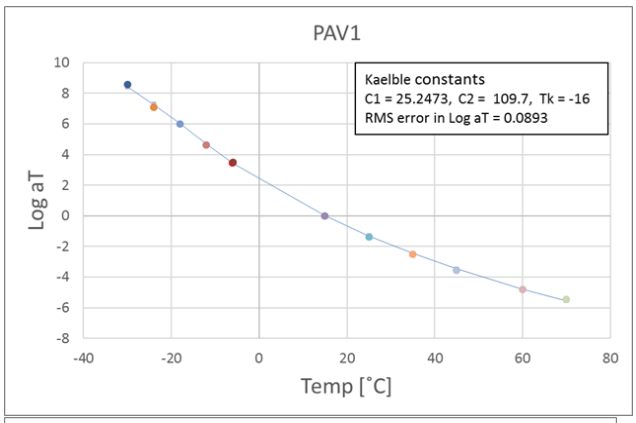

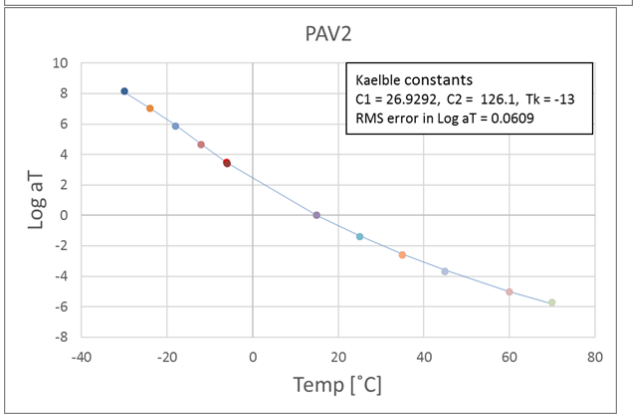

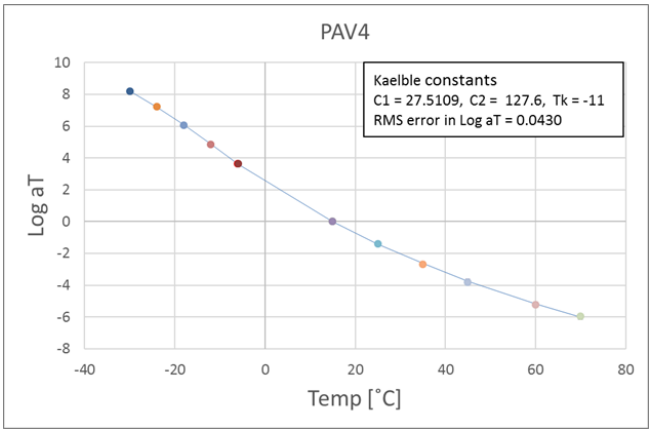

FT211 (S-E1 WP Colas)

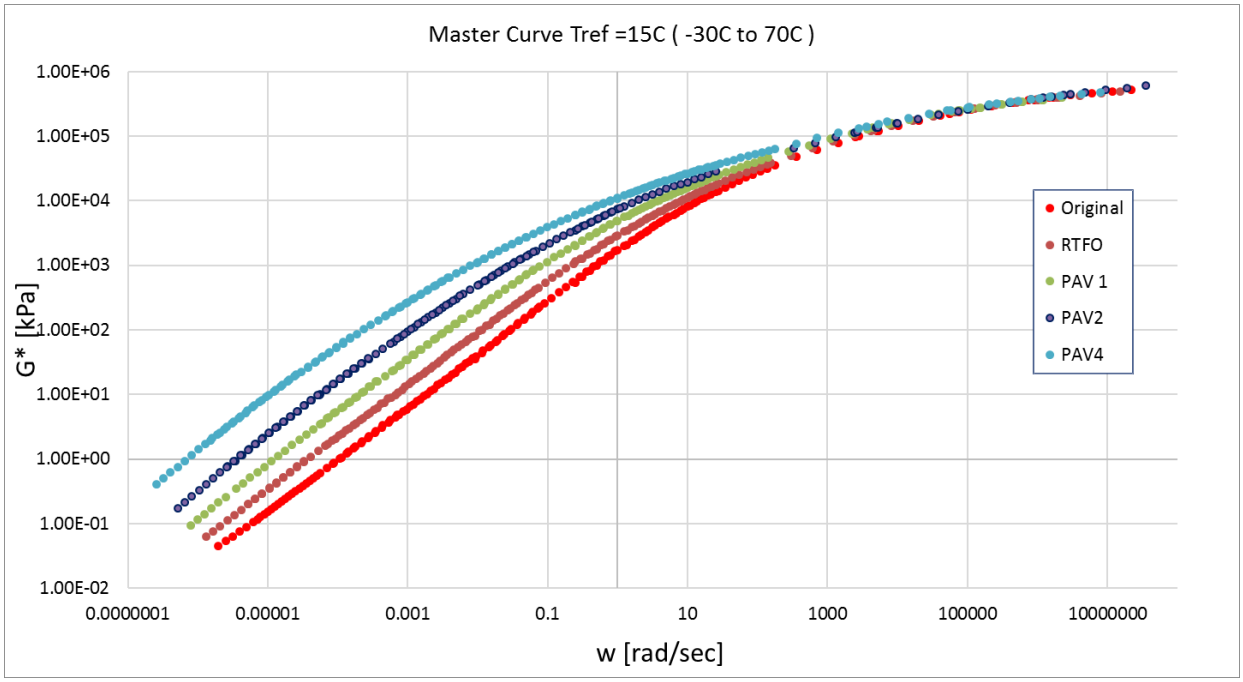

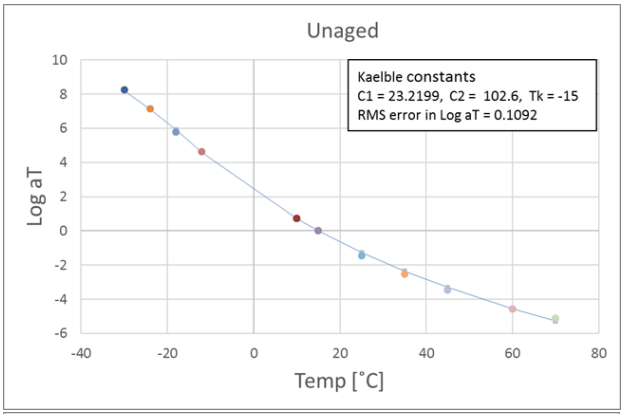

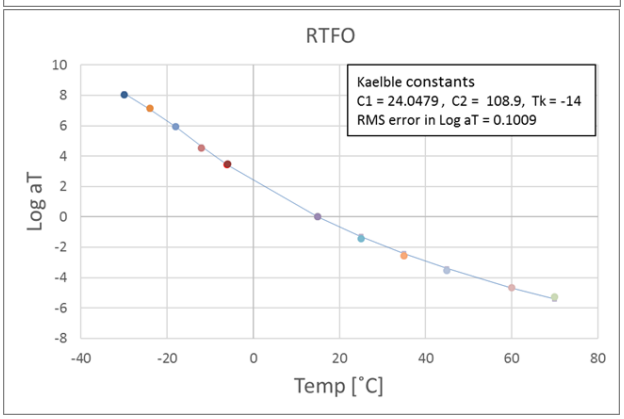

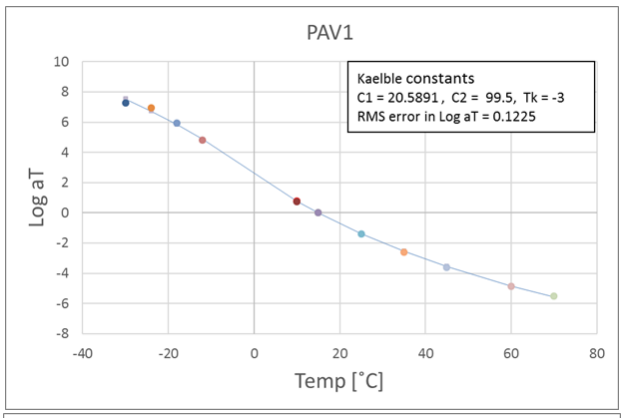

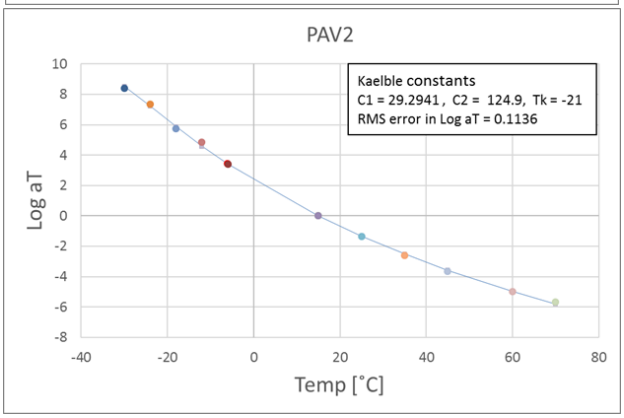

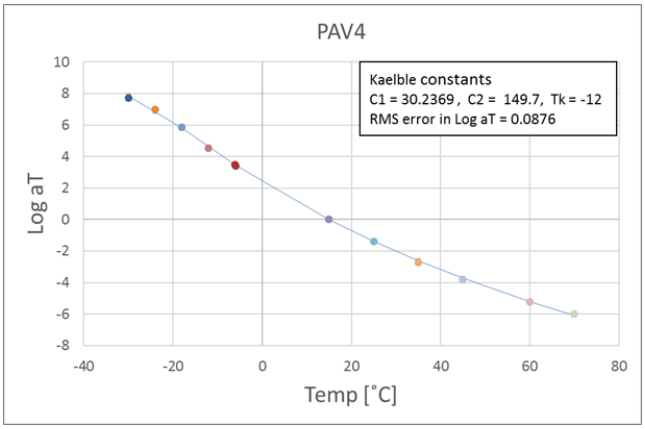

FT221 (S-E1 GP Colas)

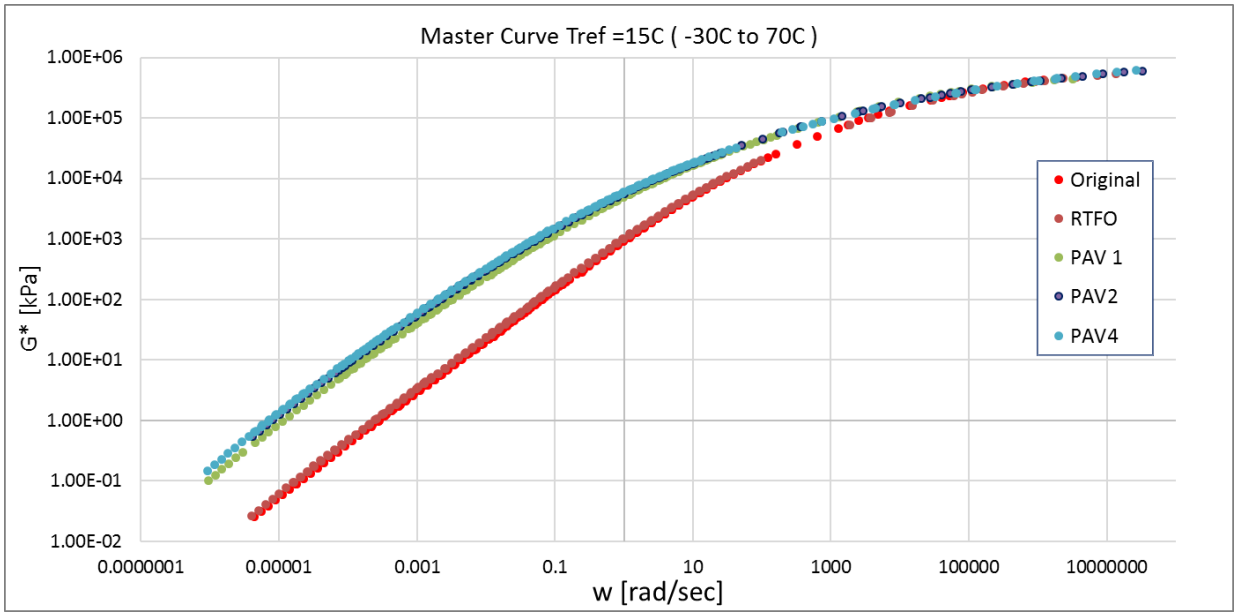

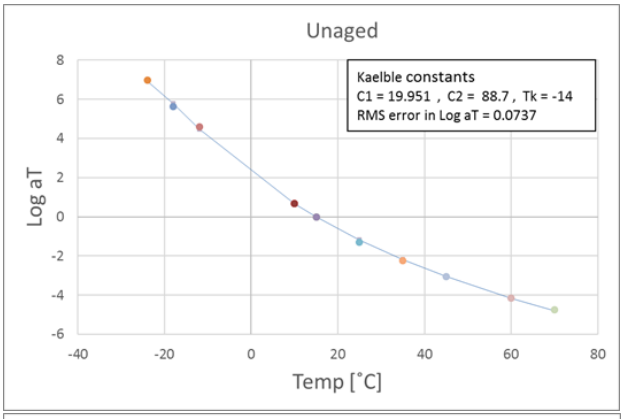

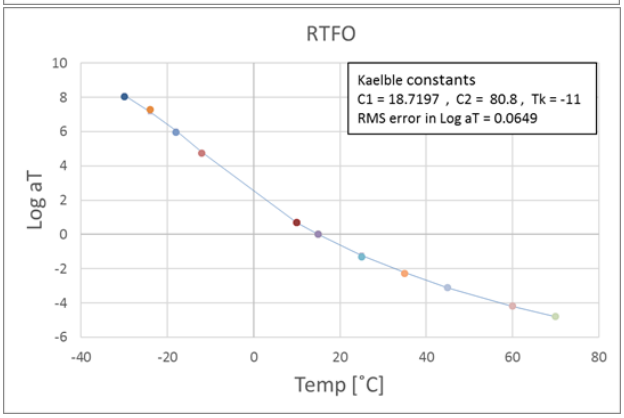

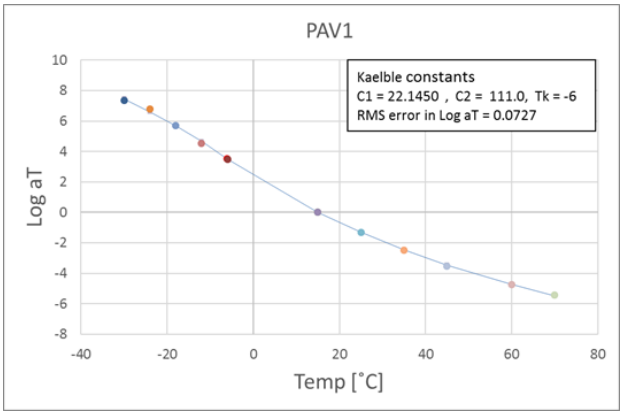

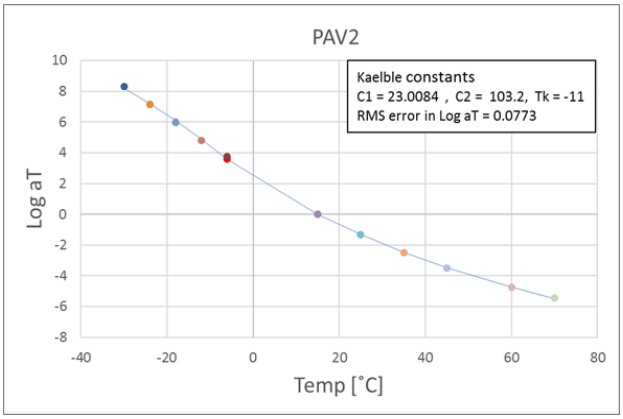

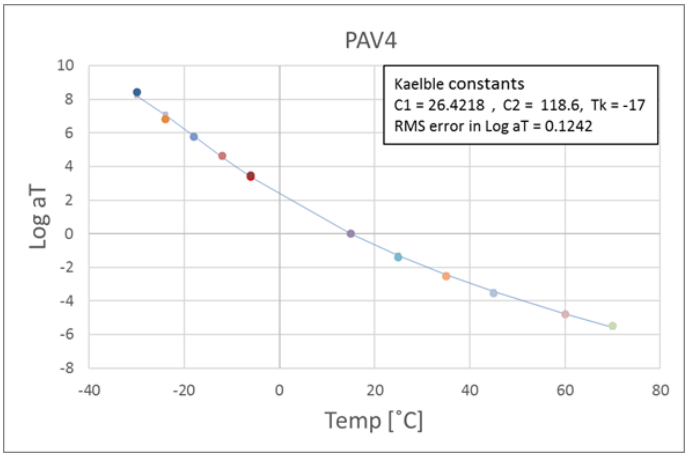

FT222 (S-E1 GP Tosas)

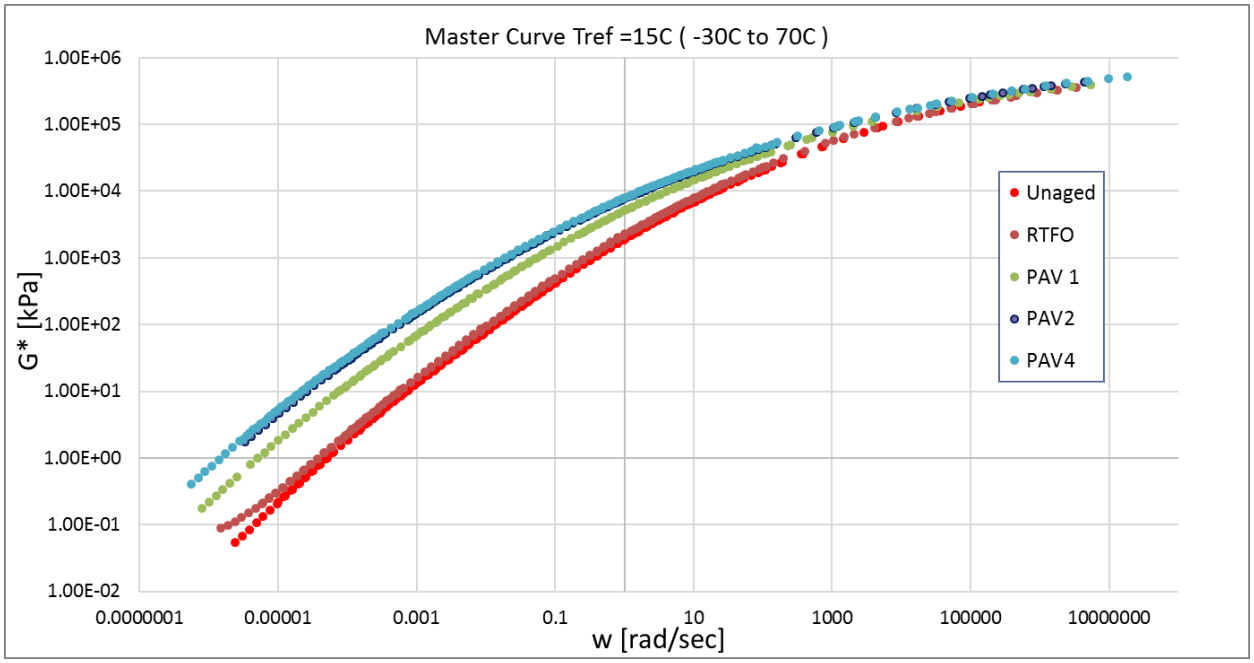

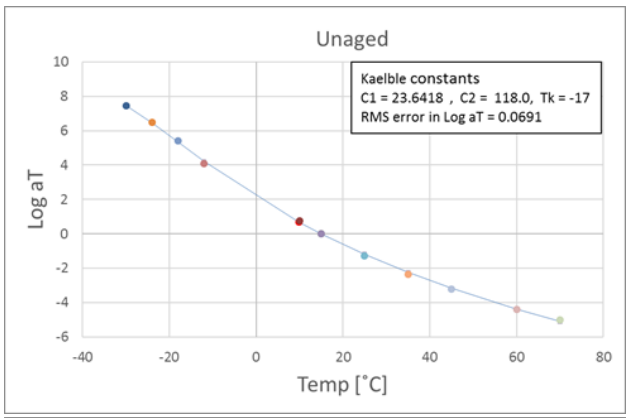

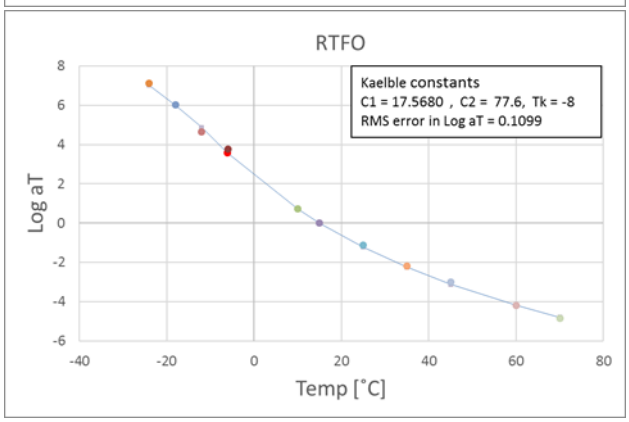

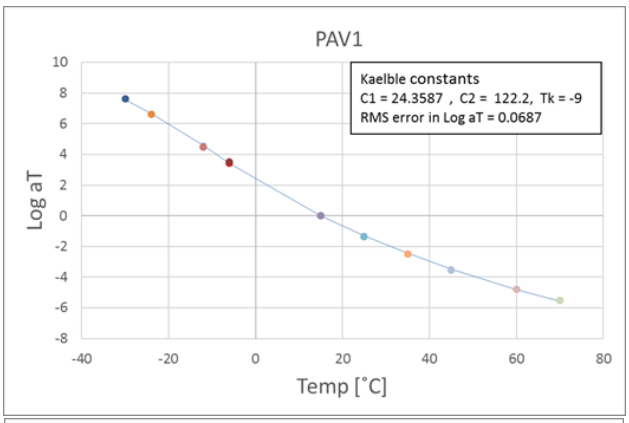

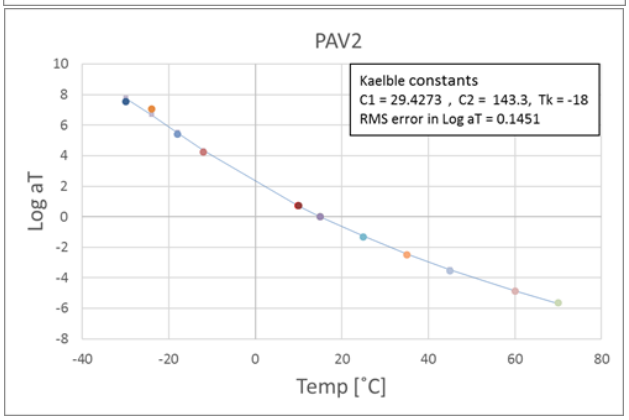

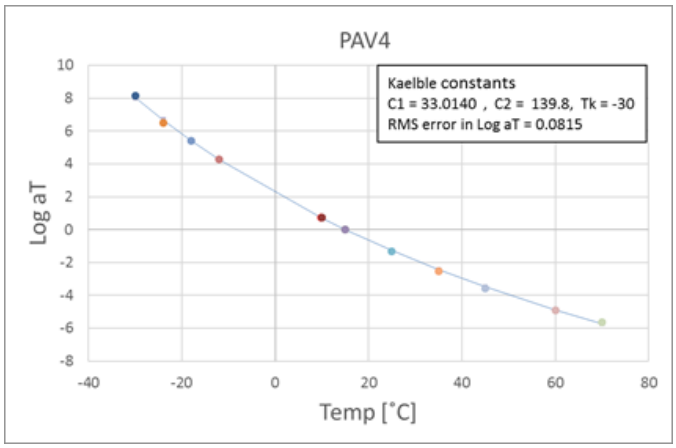

FT322 (S-E2 GP)

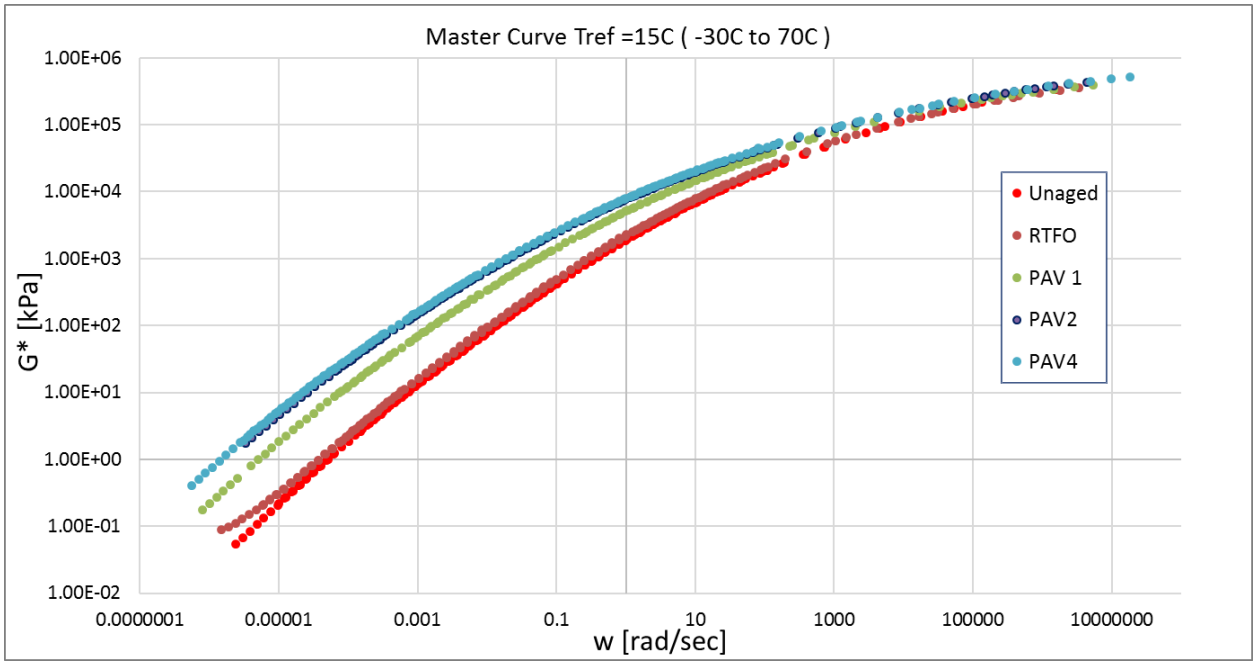

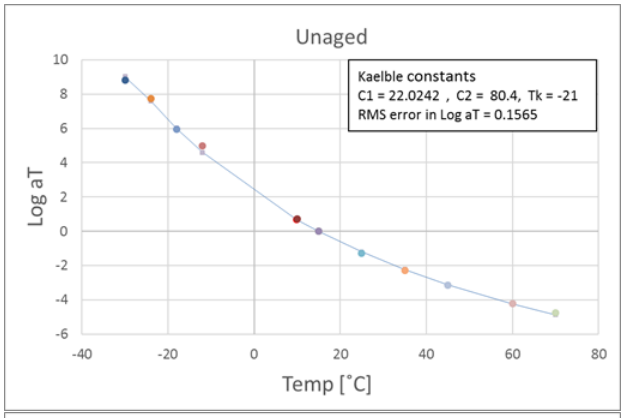

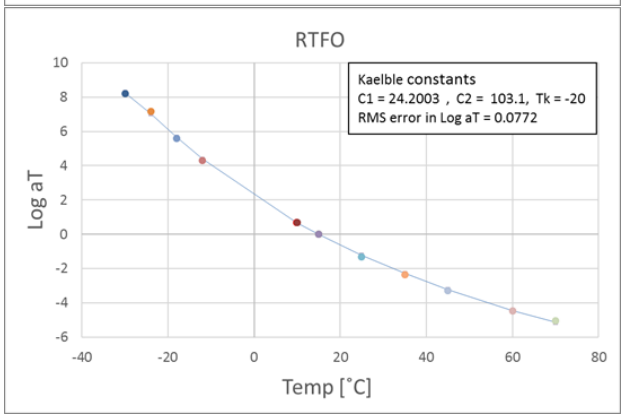

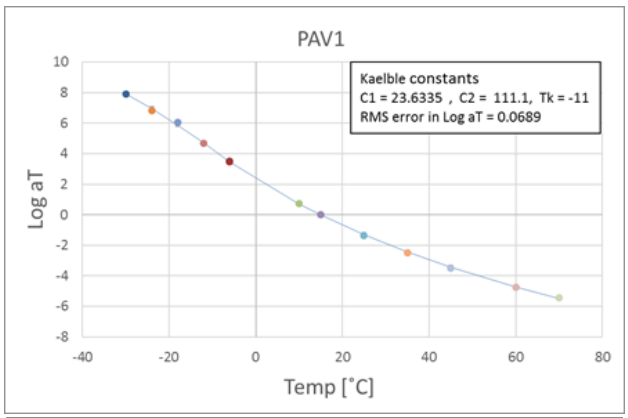

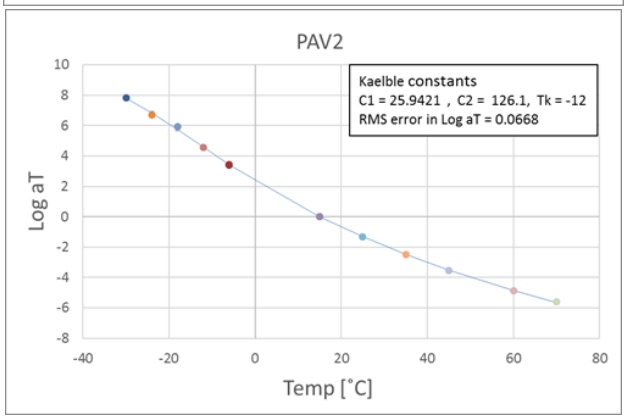

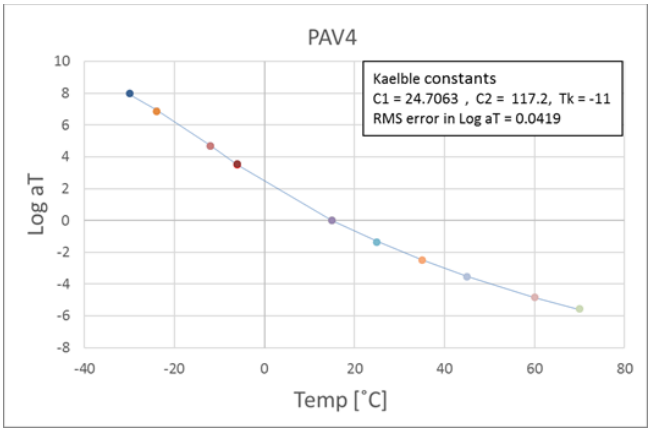

FT333 (S-E2 KZN)

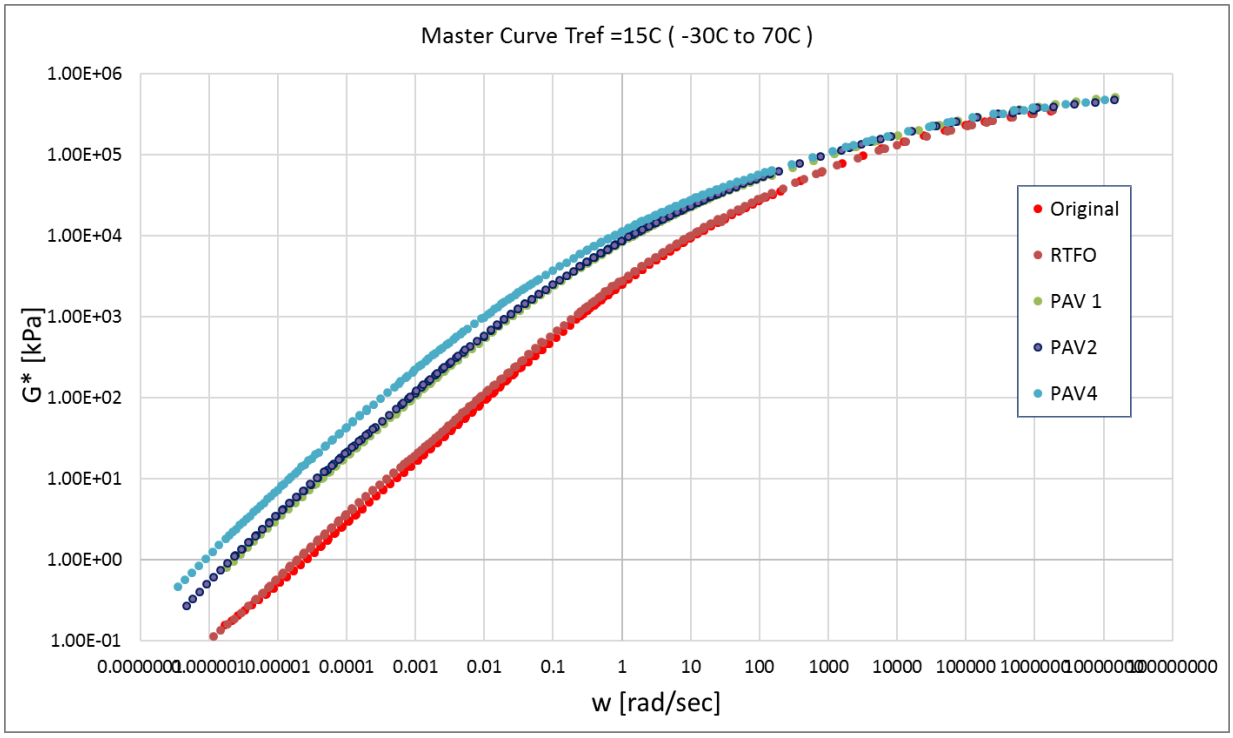

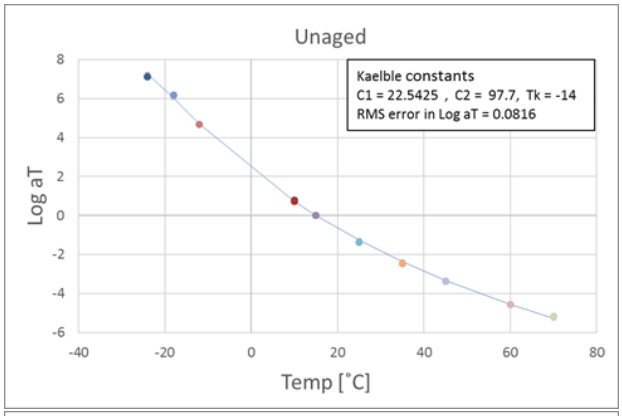

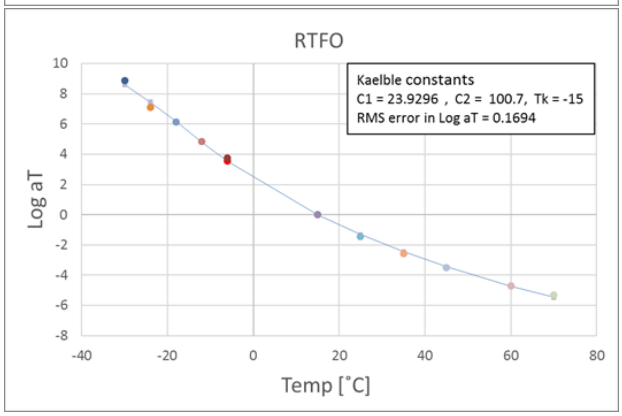

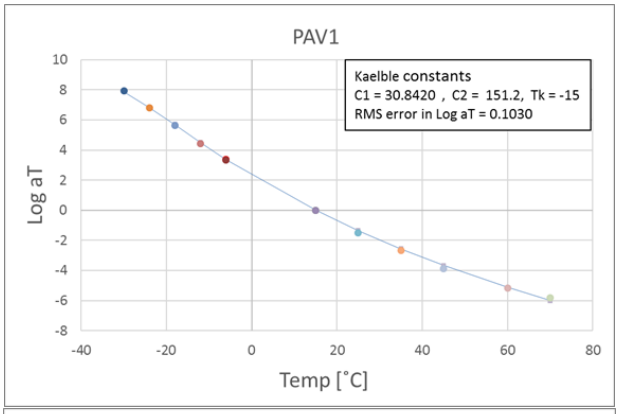

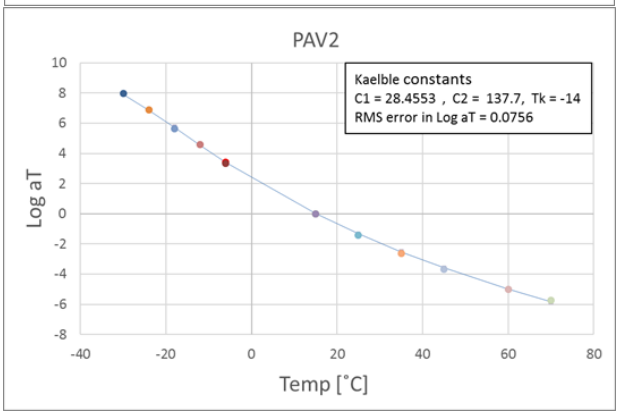

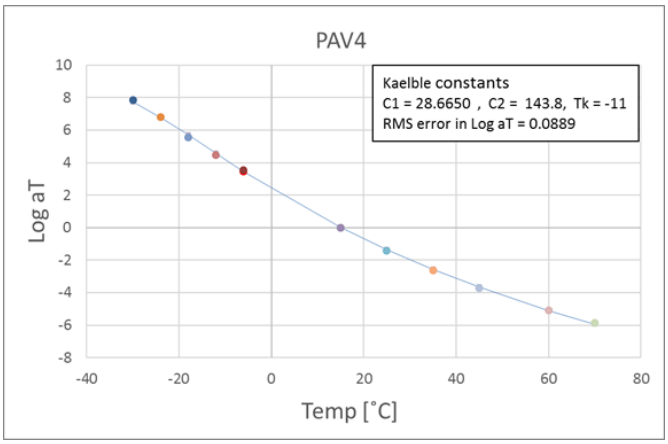

Annexure F: Mathematical model comparison

The shift-factor curves for these master curves is as seen in Annexure E.

FT111 (70/100 WP)

RTFO:

	CA model parameters	
	G*	δ
Go (Pa)	615405150.661	
wo	16.476	16.476
B	0.217	0.228
K	1	1
RMS error (Log)	0.0278	0.0467

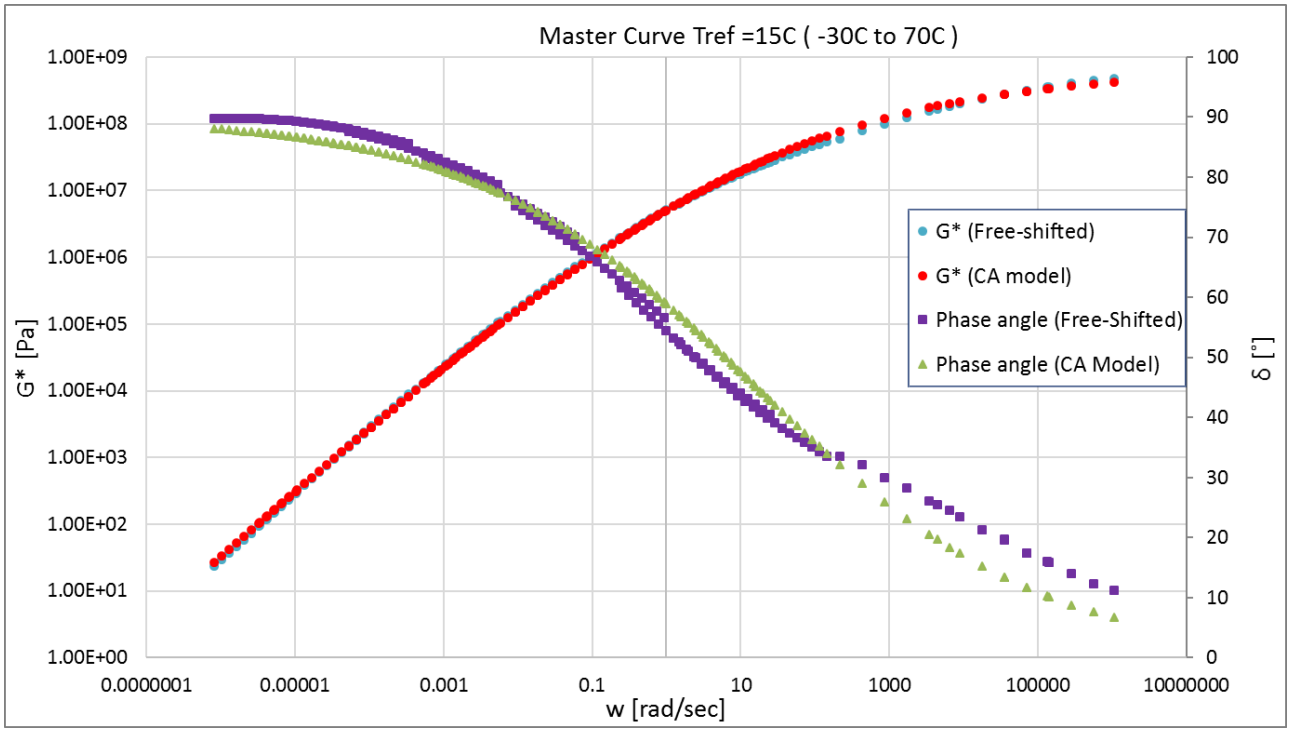

	CAM model parameters	
	G*	δ
Go (Pa)	665104842.275	
wo	16.476	16.476
B	0.212	0.186
K	1.004	1.057
RMS error (Log)	0.0275	0.0374

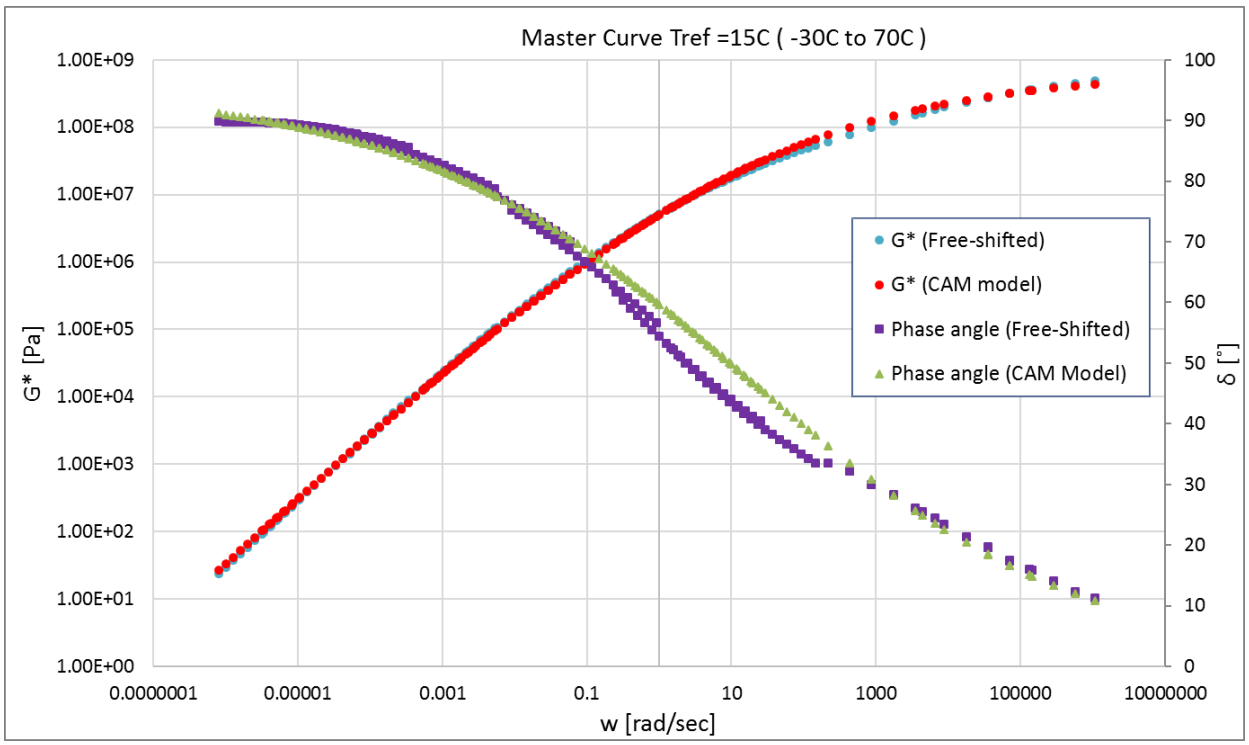

	GL model parameters	
	G*	δ
A	24.730	0.927
B	0.358	0.323
D	-18.710	
M	-5.692	-5.281
T	5.307	3.926
RMS error (Log)	0.0104	0.013

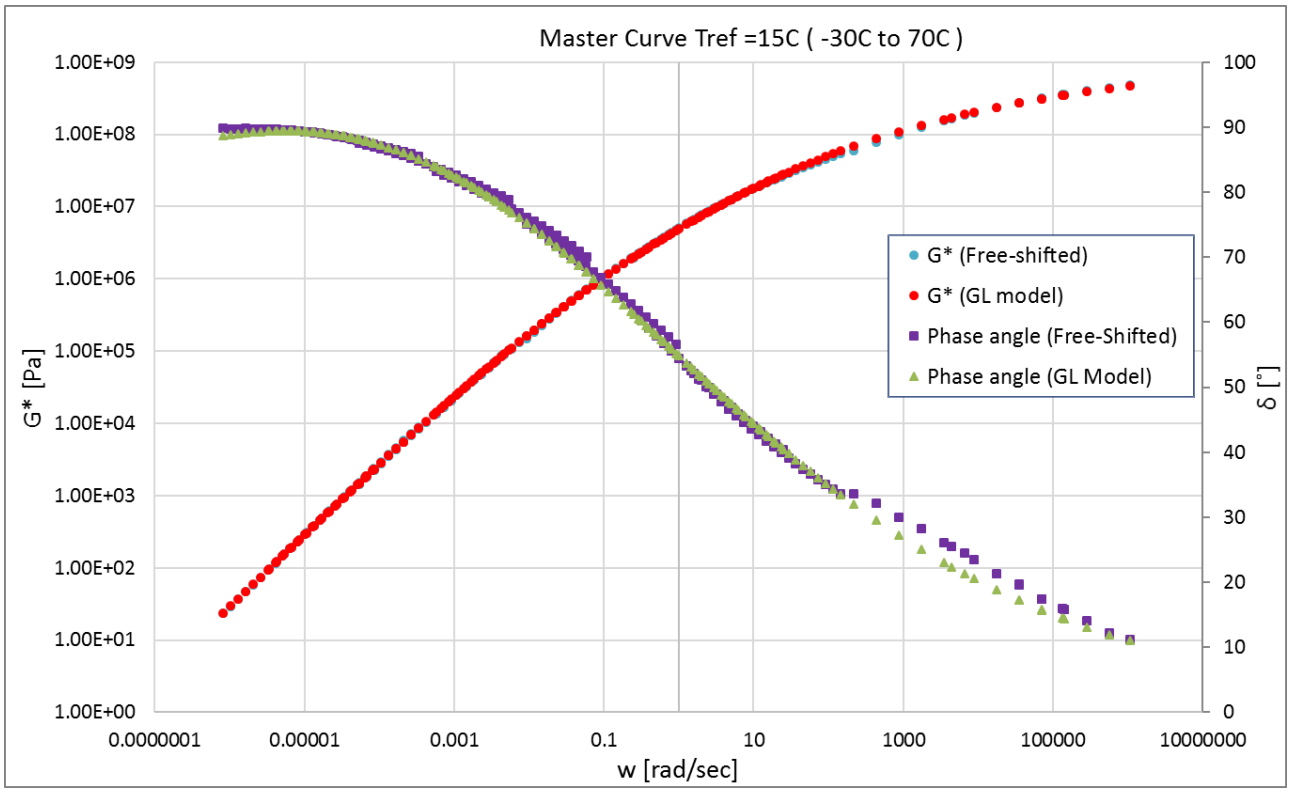

Rhea Discrete spectra		
Mode	gi, pa	li, sec
1	7.15E+04	1.04E-07
2	1.47E+05	1.90E-06
3	1.14E+05	1.42E-05
4	9.54E+04	8.83E-05
5	6.90E+04	5.40E-04
6	3.94E+04	3.74E-03
7	2.16E+04	2.40E-02
8	1.03E+04	1.53E-01
9	3.55E+03	9.00E-01
10	9.74E+02	5.44E+00
11	1.64E+02	3.46E+01
12	2.57E+01	1.93E+02
13	3.11E+00	1.17E+03
14	2.44E-01	7.41E+03
15	4.71E-03	7.38E+04
16	6.31E-05	3.65E+06
17		
18		
19		
20		
21		
22		
RMS error (%)	4.94%	

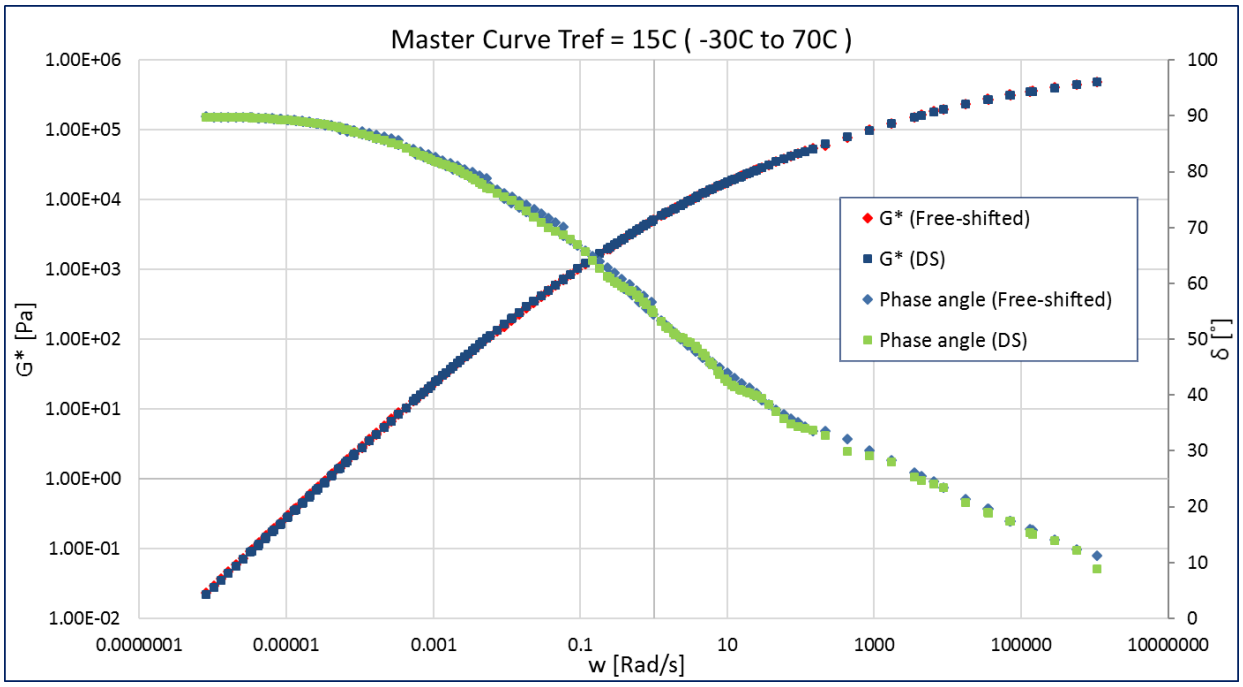

PAV1:

	CA model parameters	
	G*	δ
Go (Pa)	678999976.928	
wo	6.597	6.597
B	0.196	0.206
K	1	1
RMS error (Log)	0.0338	0.0486

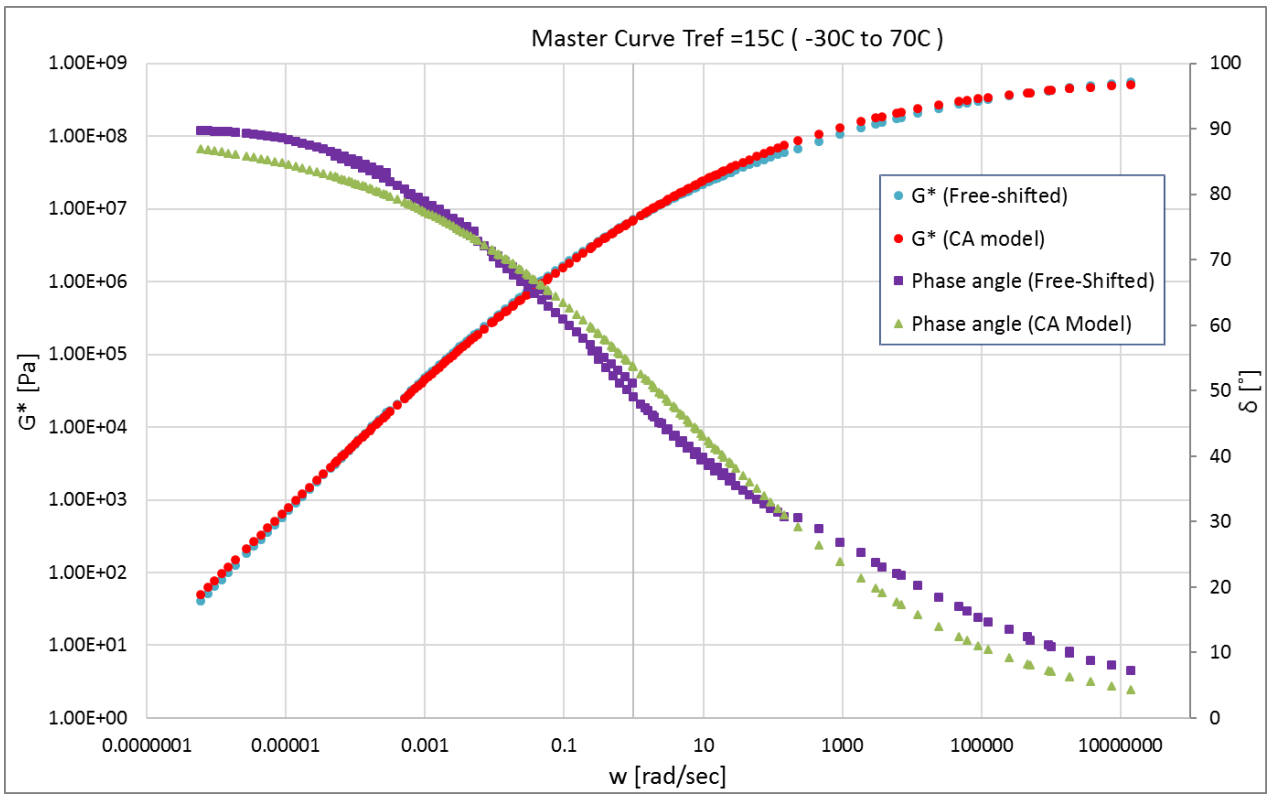

	CAM model parameters	
	G*	δ
Go (Pa)	621545021.971	
wo	6.597	6.597
B	0.199	0.178
K	0.994	1.048
RMS error (Log)	0.0334	0.0455

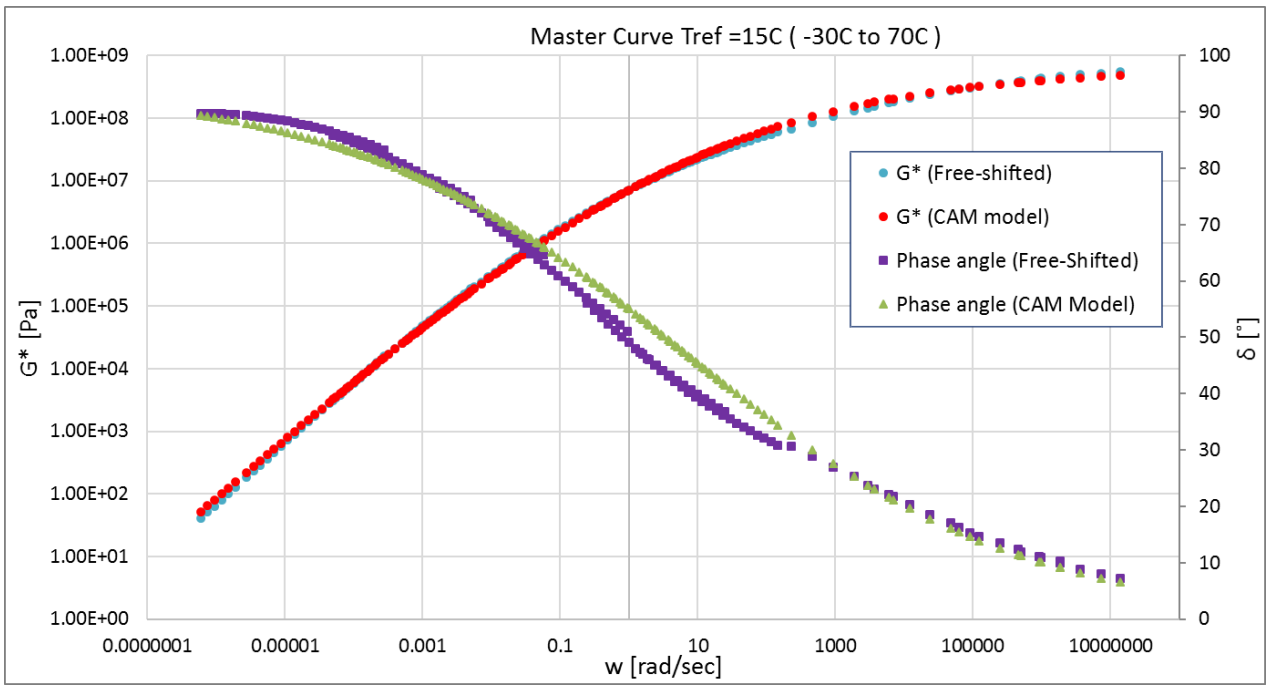

	GL model parameters	
	G*	δ
A	25.662	0.712
B	0.344	0.298
D	-19.696	
M	-6.445	-5.747
T	5.217	3.124
RMS error (Log)	0.0095	0.011

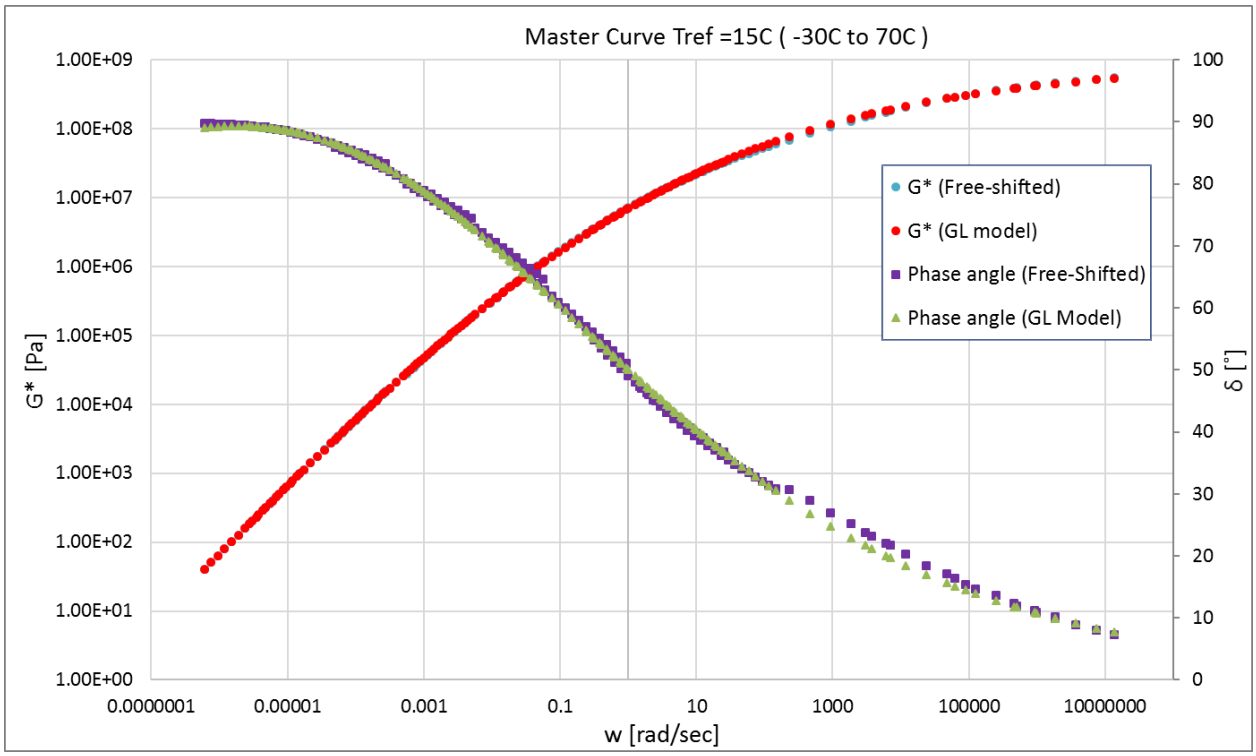

Rhea Discrete spectra		
Mode	gi, pa	li, sec
1	5.35E+04	9.20E-09
2	1.13E+05	1.78E-07
3	9.17E+04	1.23E-06
4	9.07E+04	6.79E-06
5	8.23E+04	3.48E-05
6	7.20E+04	1.78E-04
7	5.36E+04	9.26E-04
8	3.60E+04	4.79E-03
9	2.08E+04	2.55E-02
10	1.20E+04	1.36E-01
11	5.52E+03	7.12E-01
12	1.91E+03	3.81E+00
13	5.44E+02	1.91E+01
14	1.26E+02	1.04E+02
15	2.05E+01	5.70E+02
16	2.90E+00	3.00E+03
17	2.77E-01	1.68E+04
18	8.90E-03	1.43E+05
19	1.15E-04	2.56E+06
20		
21		
22		
RMS error (%)	3.68%	

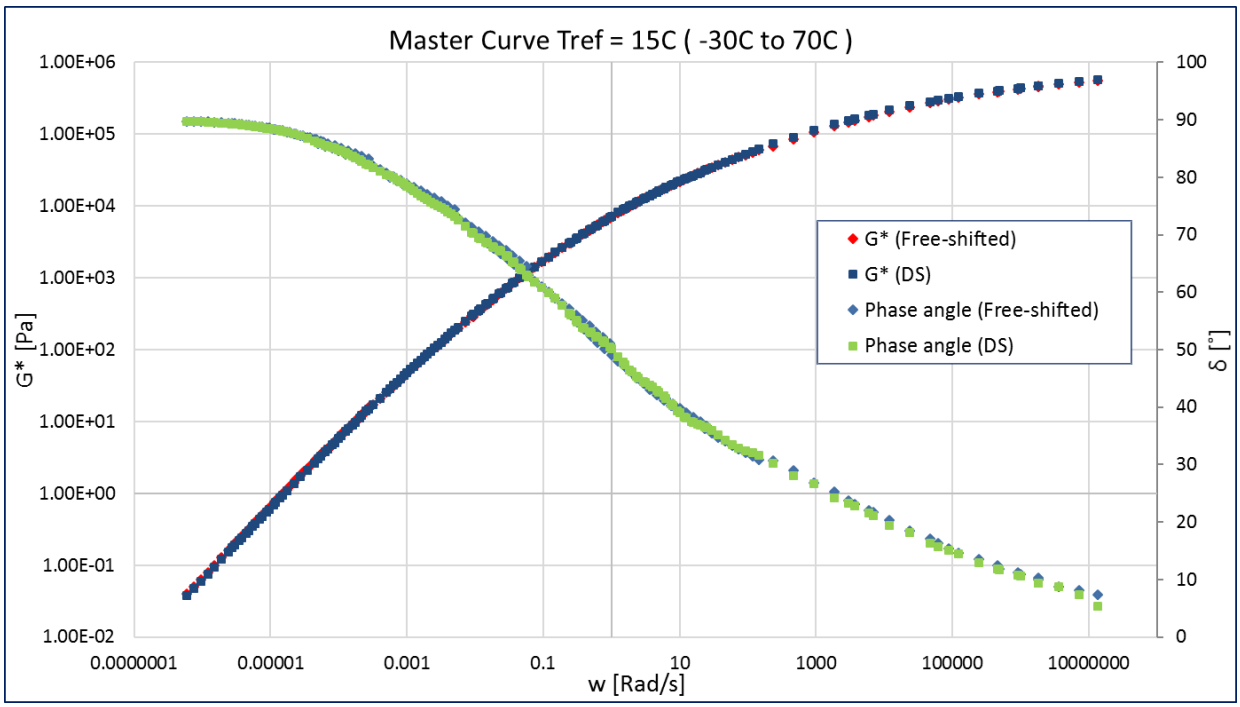

PAV2:

	CA model parameters	
	G*	δ
Go (Pa)	661551863.383	
wo	1.260	1.260
B	0.173	0.186
K	1	1
RMS error (Log)	0.0406	0.0492

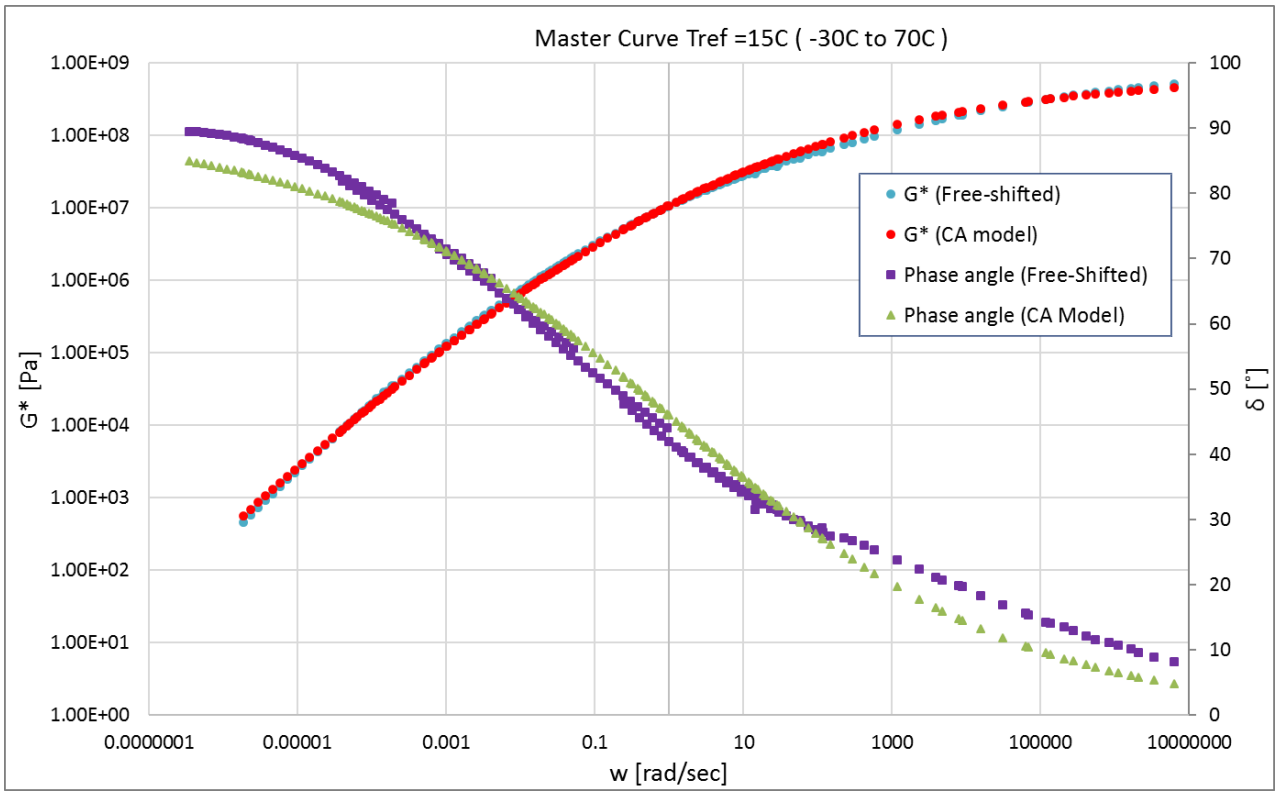

	CAM model parameters	
	G*	δ
Go (Pa)	597794260.482	
wo	1.260	1.260
B	0.176	0.184
K	0.991	1.005
RMS error (Log)	0.0400	0.0491

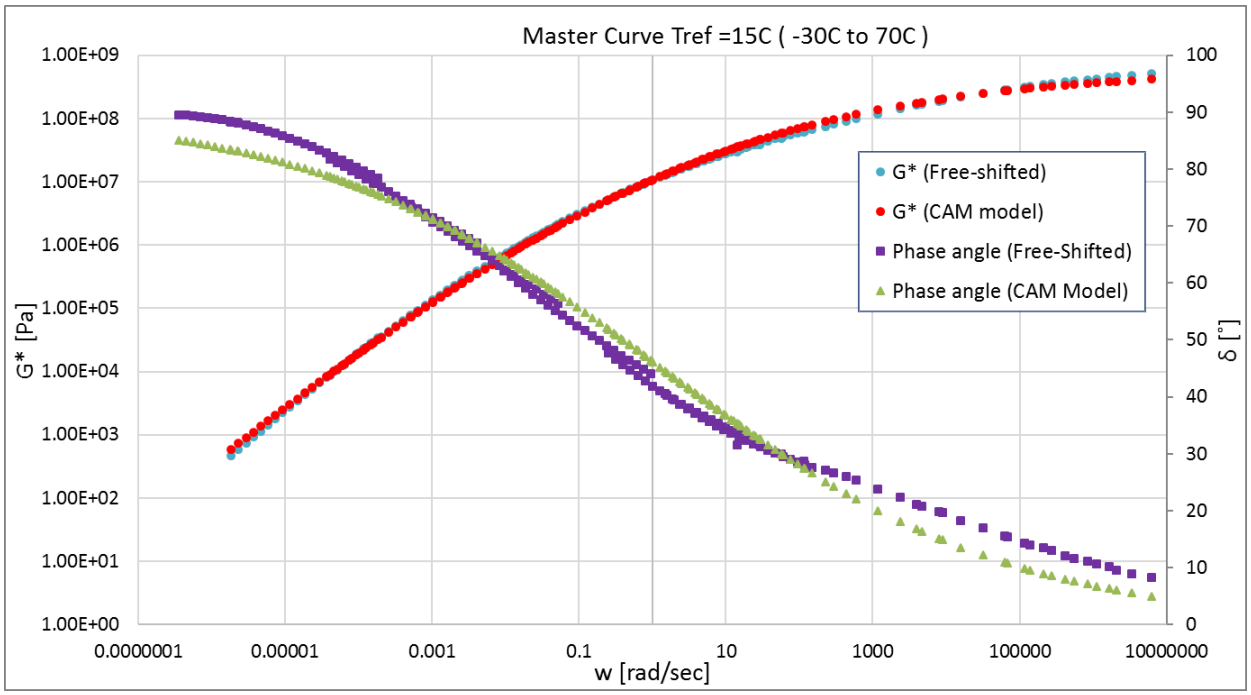

	GL model parameters	
	G*	δ
A	8.806	0.424
B	0.245	0.249
D	-2.656	
M	-5.422	-6.521
T	-0.328	1.784
RMS error (Log)	0.0083	0.010

Annexure F: Mathematical model comparison

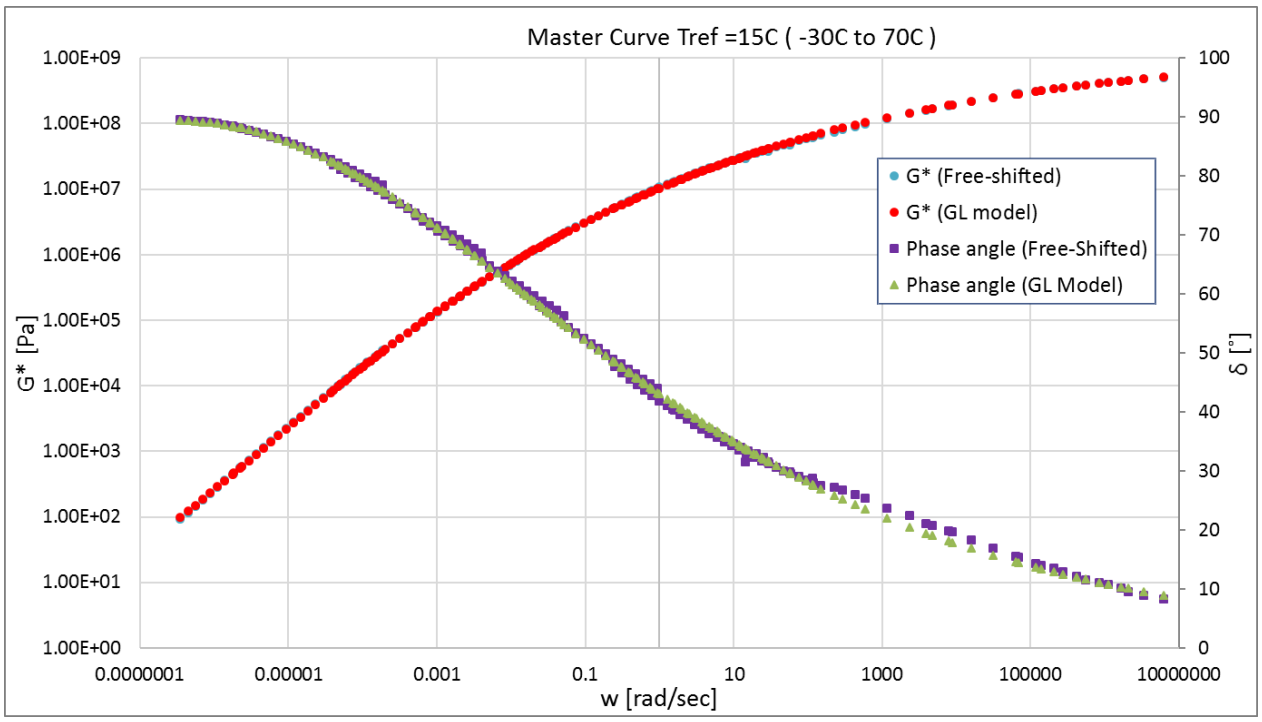

Rhea Discrete spectra		
Mode	gi, pa	li, sec
1	1.10E+05	2.55E-07
2	9.16E+04	1.72E-06
3	9.12E+04	1.05E-05
4	8.06E+04	6.42E-05
5	6.39E+04	3.83E-04
6	4.53E+04	2.29E-03
7	2.81E+04	1.39E-02
8	1.72E+04	8.14E-02
9	9.25E+03	4.51E-01
10	4.25E+03	2.27E+00
11	1.75E+03	1.15E+01
12	5.49E+02	5.95E+01
13	1.51E+02	2.95E+02
14	3.37E+01	1.48E+03
15	6.11E+00	7.18E+03
16	7.68E-01	3.67E+04
17	5.18E-02	2.28E+05
18	4.90E-04	7.74E+06
19		
20		
21		
22		
RMS error (%)	2.96%	

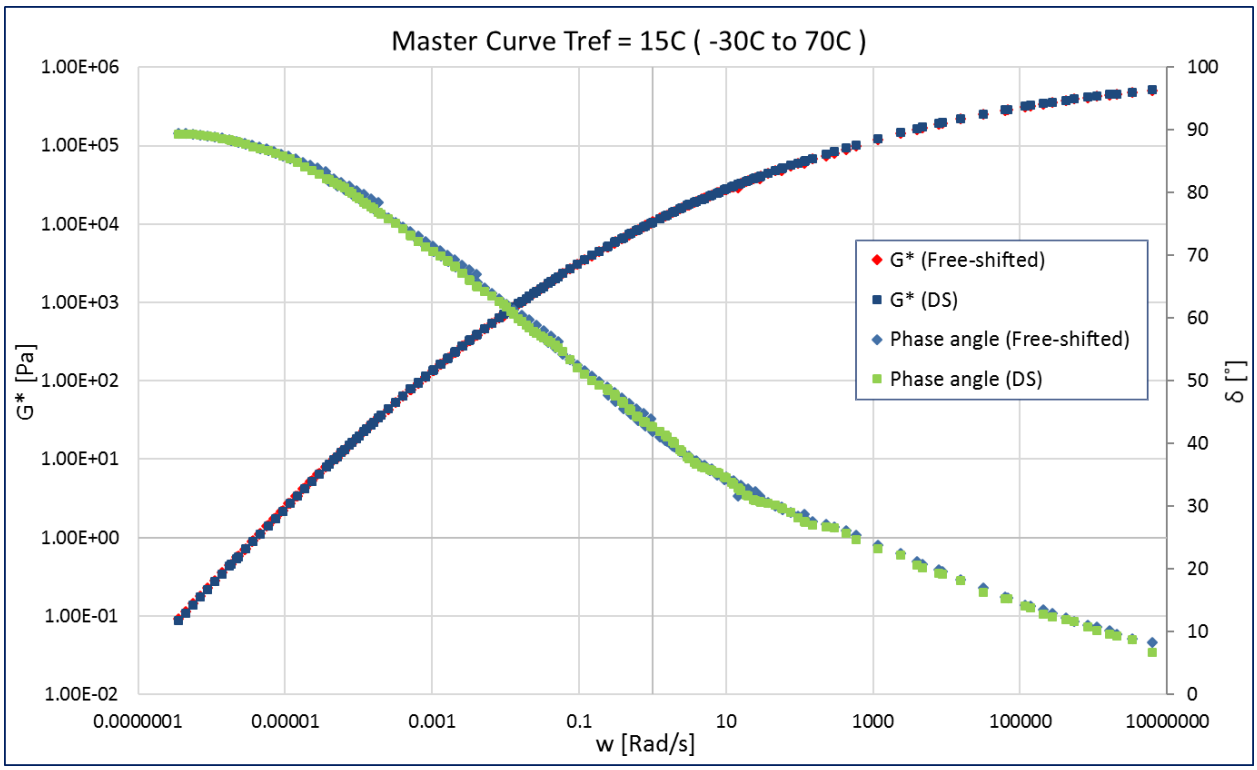

PAV4:

	CA model parameters	
	G*	δ
Go (Pa)	681024697.052	
wo	0.408	0.408
B	0.159	0.173
K	1	1
RMS error (Log)	0.0457	0.0540

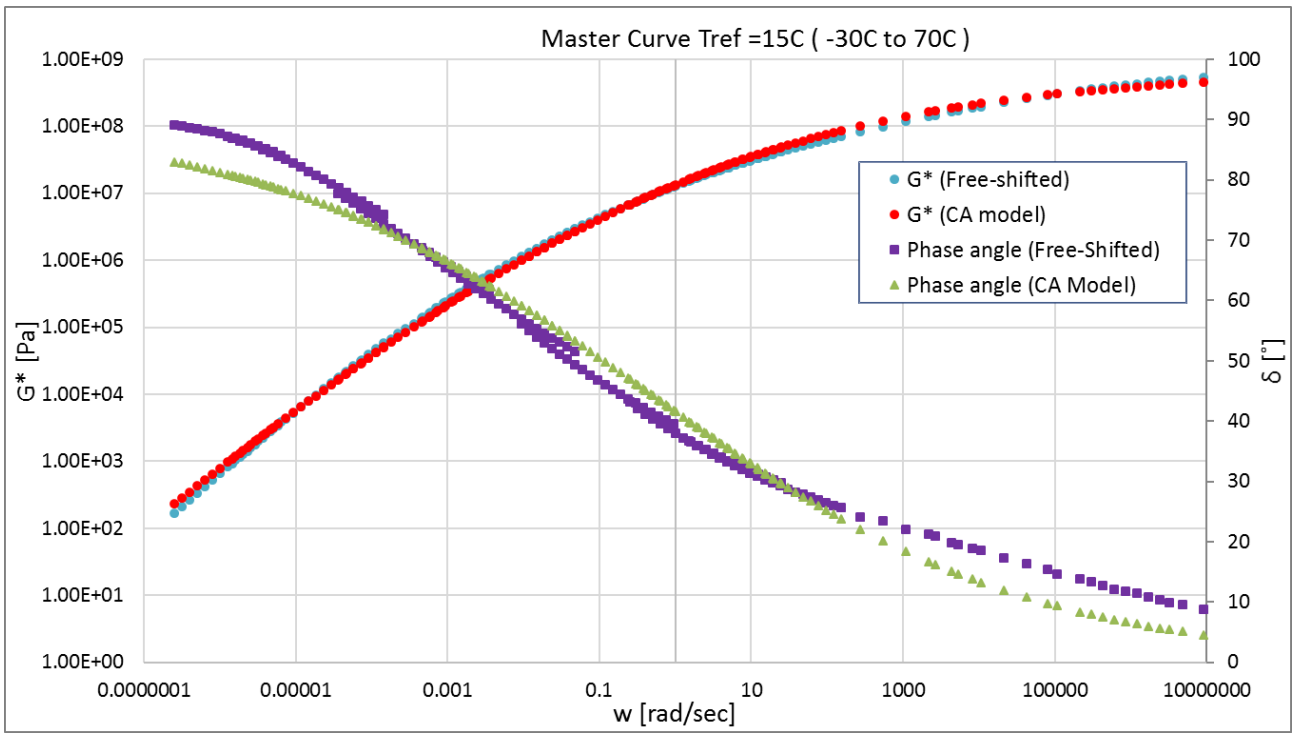

	CAM model parameters	
	G*	δ
Go (Pa)	600026303.827	
wo	0.408	0.408
B	0.162	0.174
K	0.988	0.996
RMS error (Log)	0.0446	0.0540

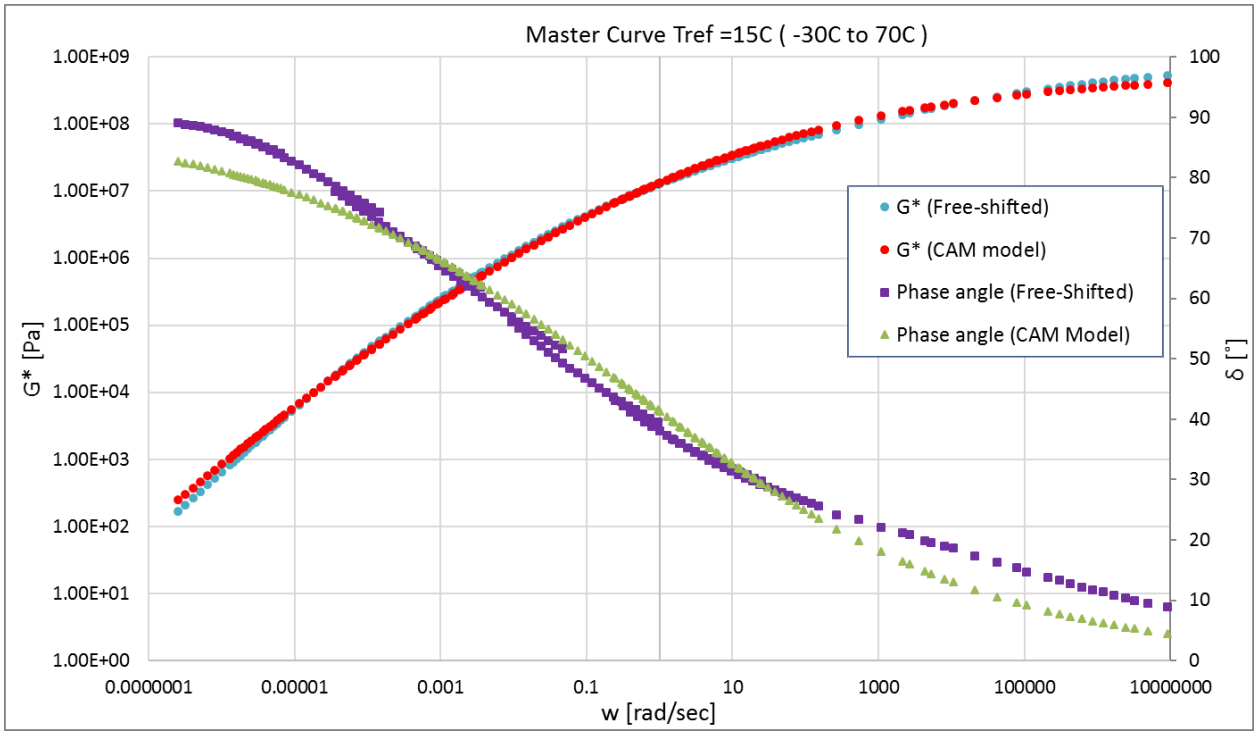

	GL model parameters	
	G*	δ
A	13.152	0.270
B	0.238	0.209
D	-7.022	
M	-7.433	-6.702
T	0.248	0.838
RMS error (Log)	0.0078	0.008

Annexure F: Mathematical model comparison

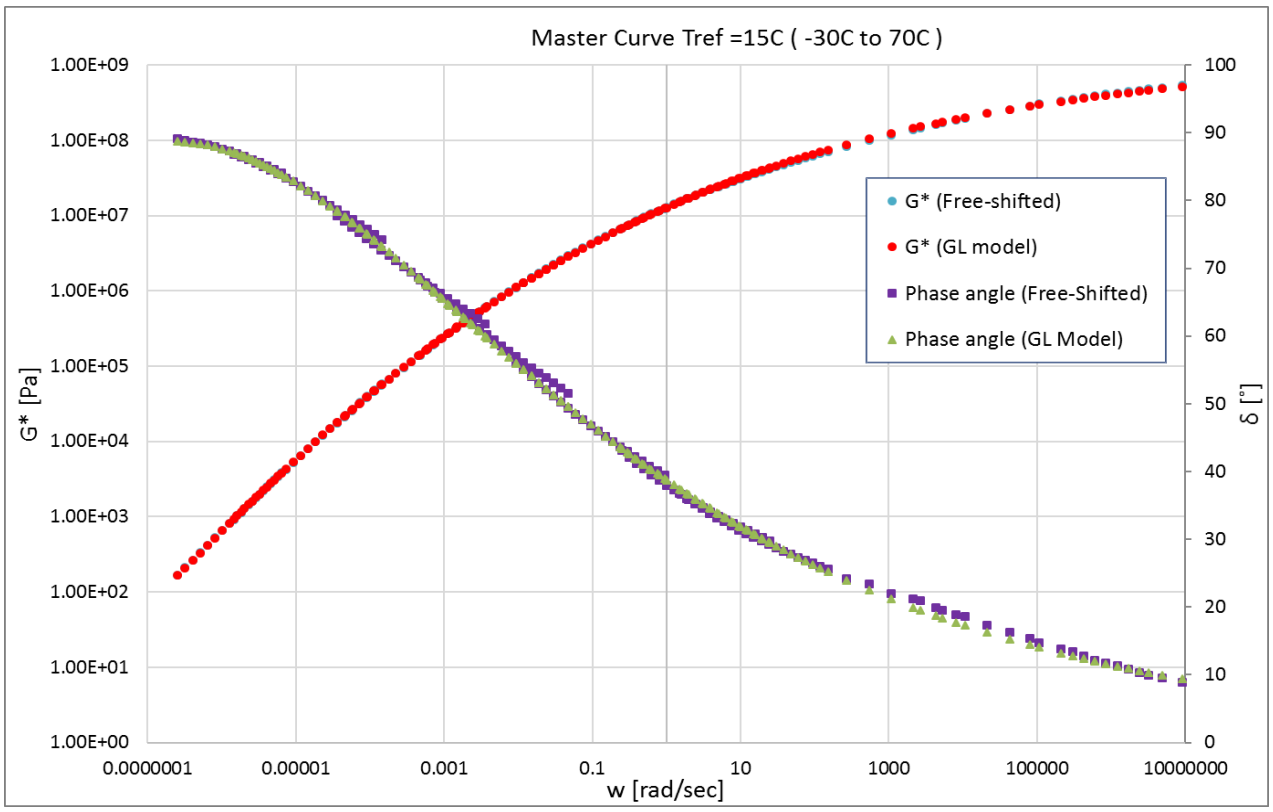

Rhea Discrete spectra		
Mode	gi, pa	li, sec
1	1.38E+05	2.26E-07
2	9.02E+04	1.64E-06
3	7.75E+04	7.98E-06
4	6.78E+04	3.64E-05
5	5.69E+04	1.65E-04
6	4.46E+04	7.58E-04
7	3.32E+04	3.53E-03
8	2.40E+04	1.76E-02
9	1.68E+04	9.07E-02
10	9.78E+03	4.78E-01
11	5.06E+03	2.33E+00
12	2.43E+03	1.17E+01
13	9.21E+02	5.69E+01
14	3.17E+02	2.71E+02
15	8.74E+01	1.38E+03
16	1.95E+01	7.39E+03
17	2.60E+00	4.41E+04
18	1.85E-01	2.94E+05
19	4.87E-03	2.48E+06
20		
21		
22		
RMS error (%)	2.65%	

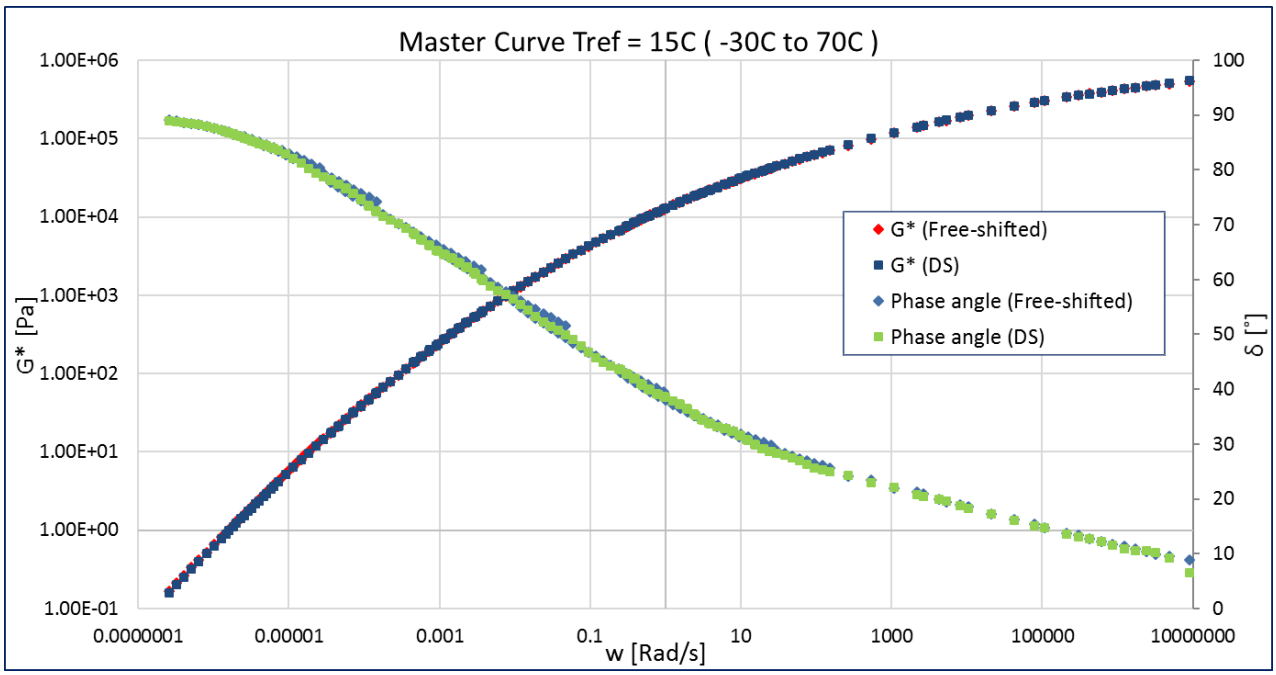

FT131 (70/100 KZN)

Unaged:

	CA model parameters	
	G*	δ
Go (Pa)	746141973.839	
wo	260.227	260.227
B	0.232	0.265
K	1	1
RMS error (Log)	0.0201	0.0259

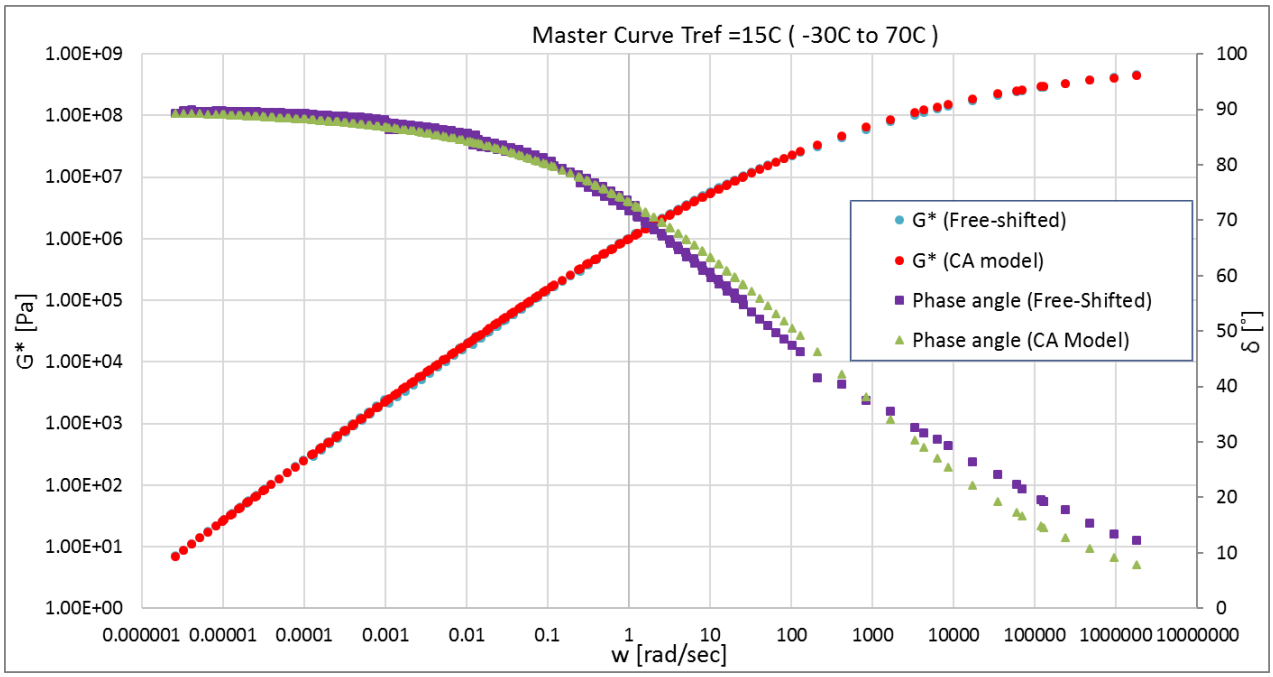

	CAM model parameters	
	G*	δ
Go (Pa)	615522978.401	
wo	260.227	260.227
B	0.247	0.230
K	0.990	1.024
RMS error (Log)	0.0192	0.0192

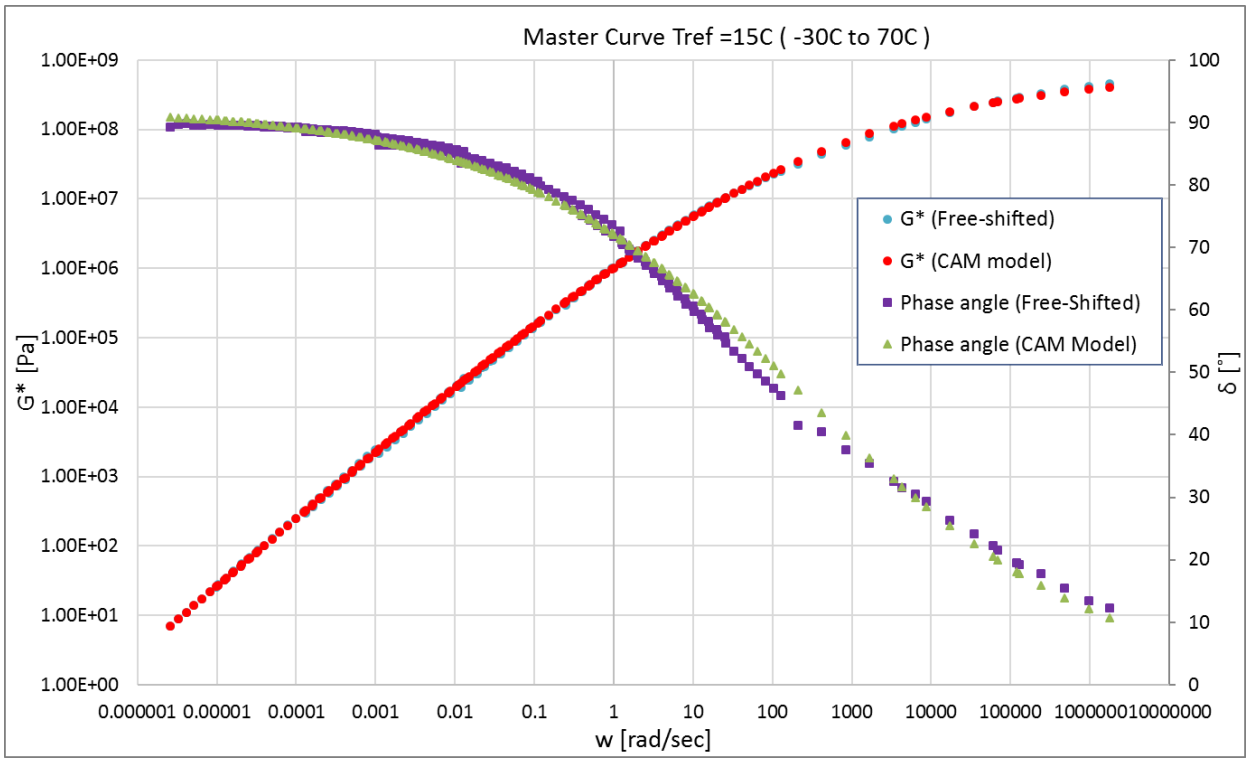

	GL model parameters	
	G*	δ
A	21.512	3.532
B	0.440	0.436
D	-15.540	
M	-3.208	-4.372
T	6.249	14.547
RMS error (Log)	0.0194	0.011

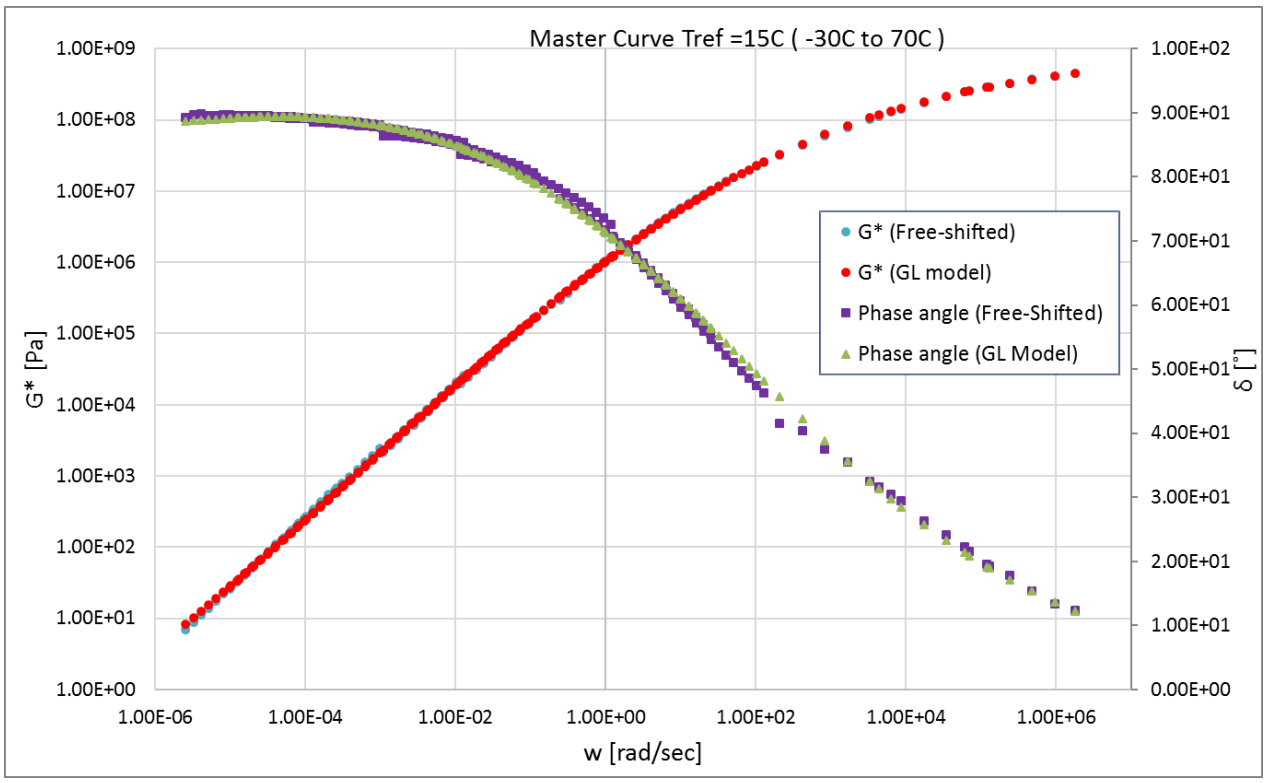

Rhea Discrete spectra		
Mode	gi, pa	li, sec
1	1.33E+05	8.39E-07
2	1.10E+05	4.97E-06
3	8.91E+04	2.39E-05
4	6.88E+04	1.06E-04
5	4.57E+04	4.68E-04
6	2.55E+04	2.17E-03
7	1.36E+04	9.75E-03
8	6.20E+03	5.05E-02
9	1.50E+03	3.41E-01
10	1.33E+02	3.87E+00
11	6.02E+00	5.35E+01
12	1.89E-01	8.64E+02
13	2.75E-03	1.85E+04
14	3.85E-05	4.79E+05
15	1.03E+05	7.47E-08
16		
17		
18		
19		
20		
21		
22		
RMS error (%)	14.31%	

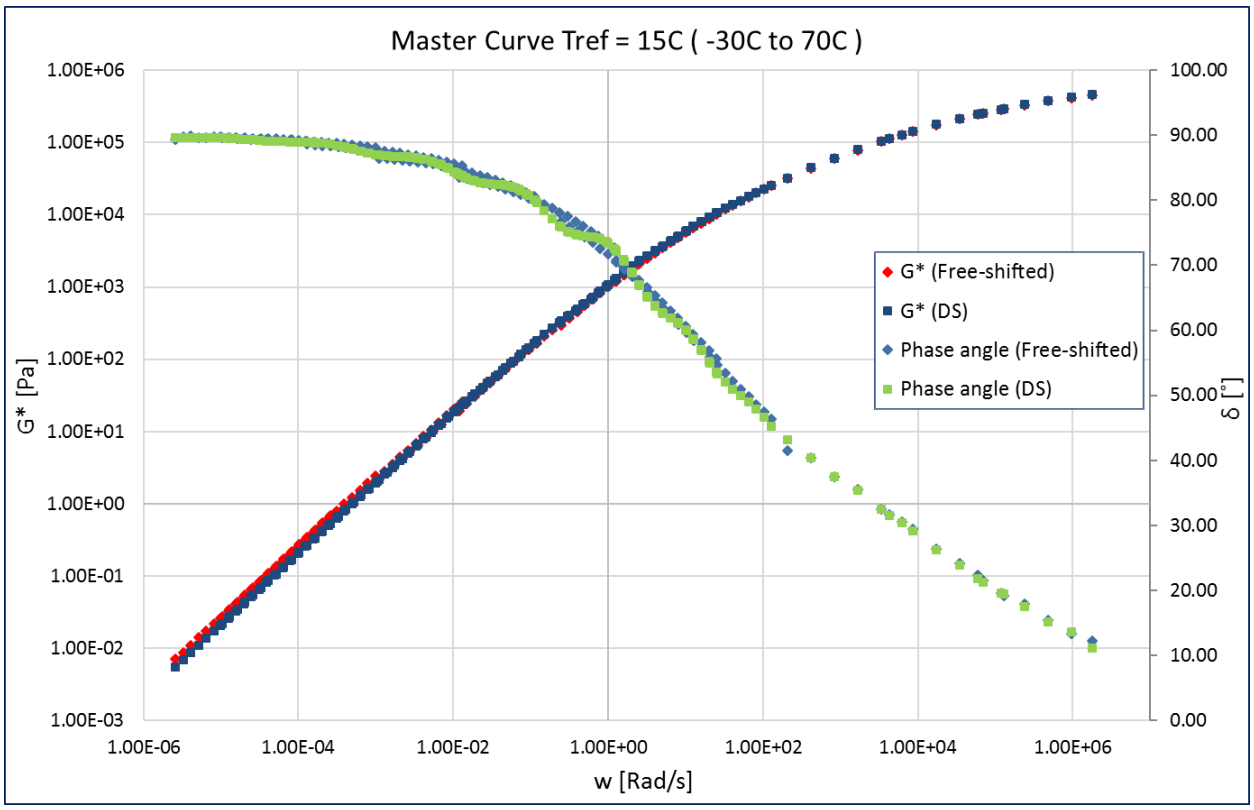

RTFO:

	CA model parameters	
	G*	δ
Go (Pa)	661898993.150	
wo	123.586	123.586
B	0.231	0.244
K	1	1
RMS error (Log)	0.0173	0.0318

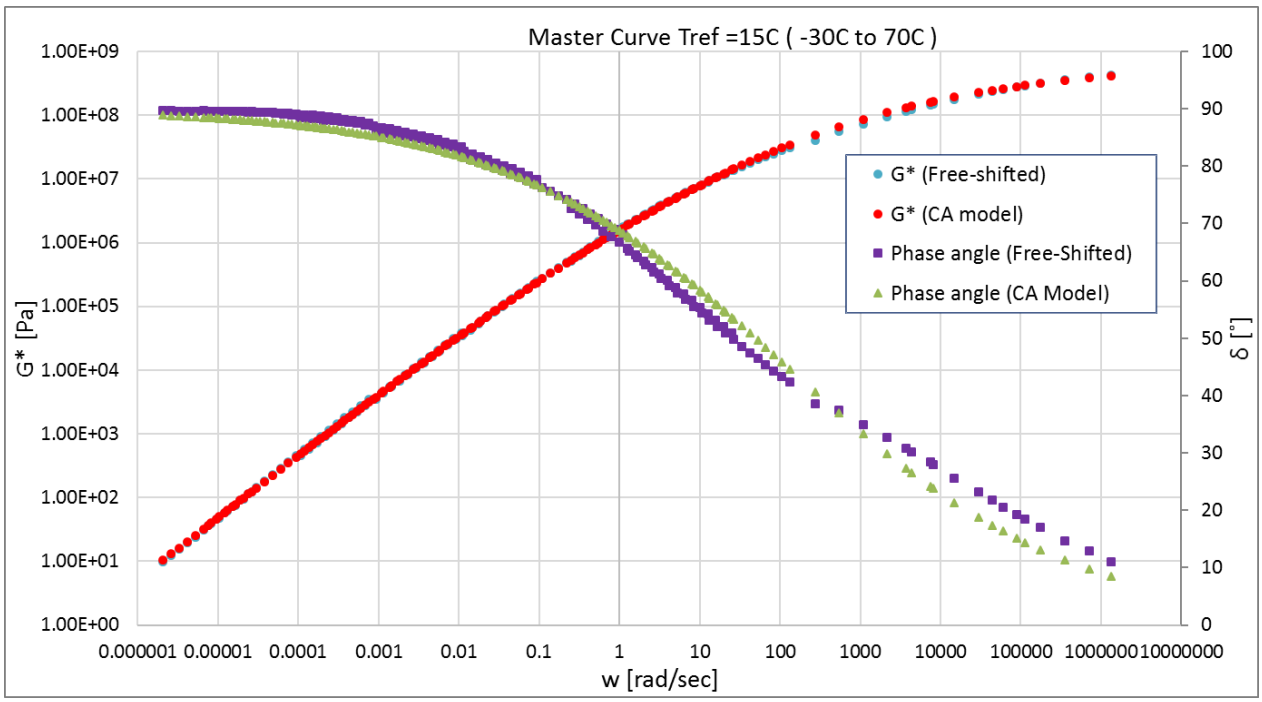

	CAM model parameters	
	G*	δ
Go (Pa)	642078860.111	
wo	123.586	123.586
B	0.233	0.211
K	0.998	1.036
RMS error (Log)	0.0173	0.0215

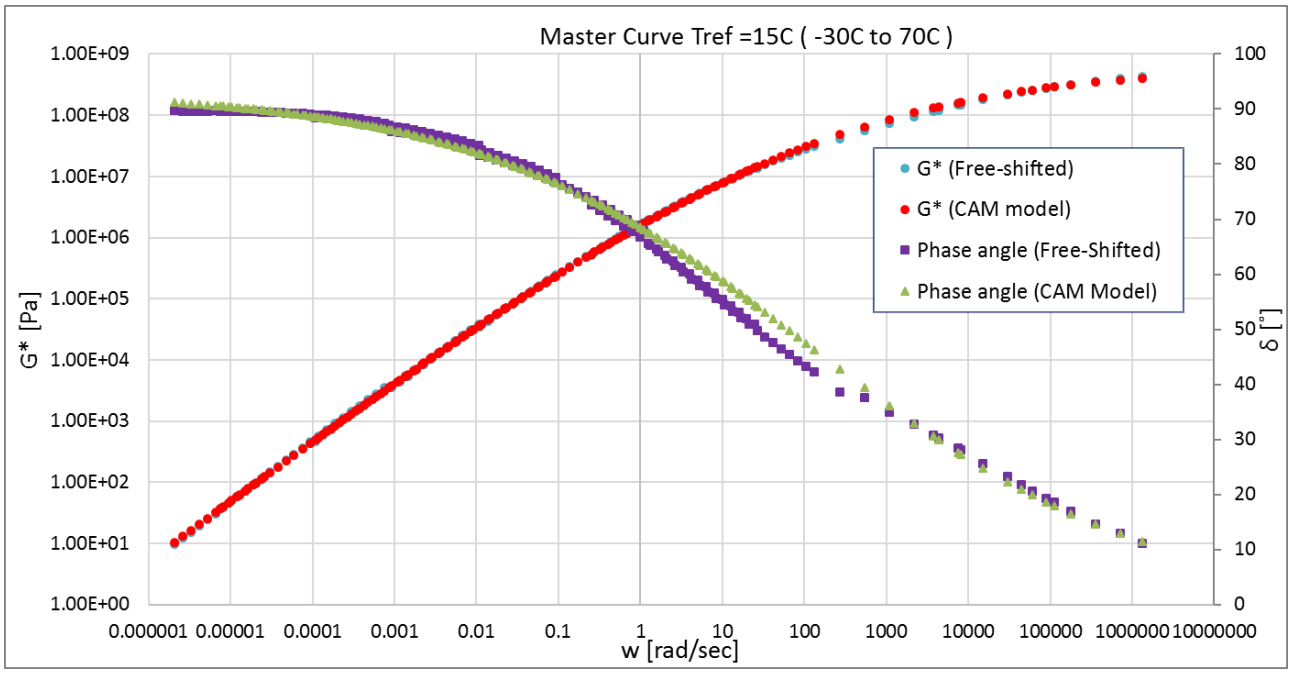

	GL model parameters	
	G*	δ
A	21.585	2.427
B	0.402	0.403
D	-15.588	
M	-3.938	-4.731
T	5.373	10.548
RMS error (Log)	0.0152	0.010

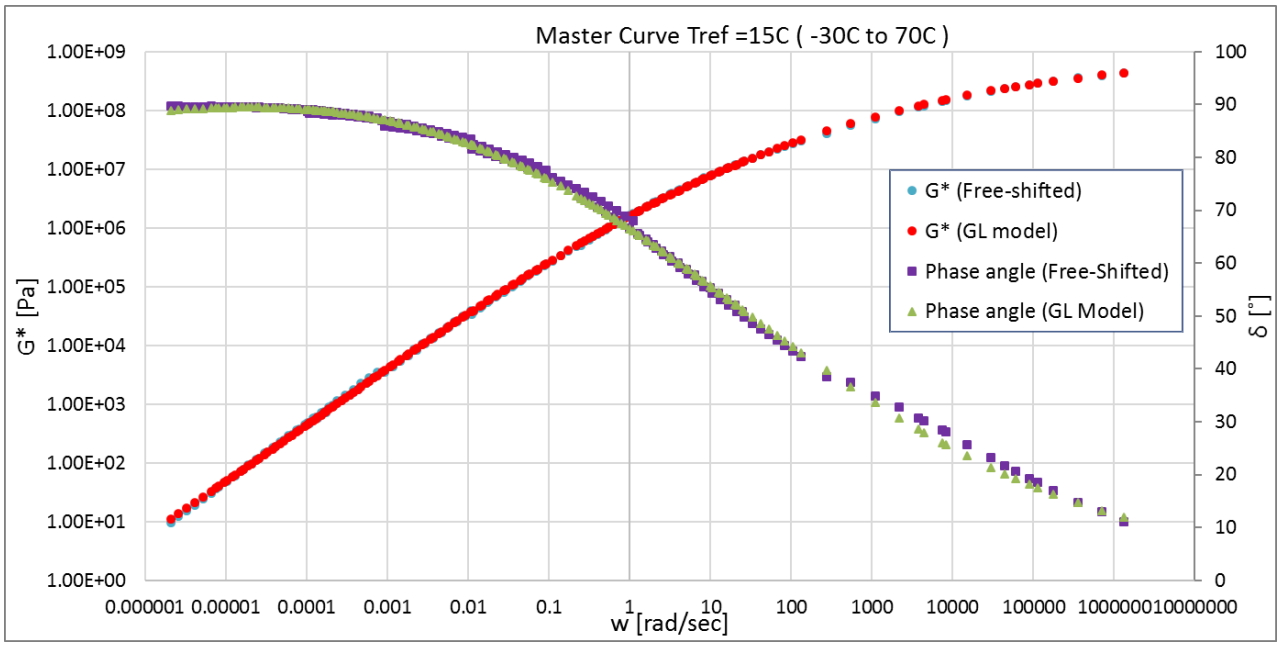

Rhea Discrete spectra		
Mode	gi, pa	li, sec
1	8.63E+04	1.53E-08
2	6.49E+04	1.20E-07
3	9.92E+04	1.06E-06
4	7.72E+04	4.39E-06
5	6.94E+04	1.41E-05
6	6.41E+04	4.46E-05
7	5.22E+04	1.41E-04
8	4.38E+04	4.88E-04
9	2.52E+04	2.01E-03
10	1.44E+04	6.98E-03
11	8.21E+03	2.27E-02
12	4.86E+03	7.95E-02
13	1.91E+03	3.43E-01
14	3.76E+02	1.57E+00
15	1.28E+02	5.19E+00
16	2.37E+01	2.90E+01
17	2.29E+00	2.26E+02
18	8.95E-02	2.36E+03
19	2.21E-03	2.60E+04
20	6.21E-05	1.09E+06
21		
22		
RMS error (%)	9.00%	

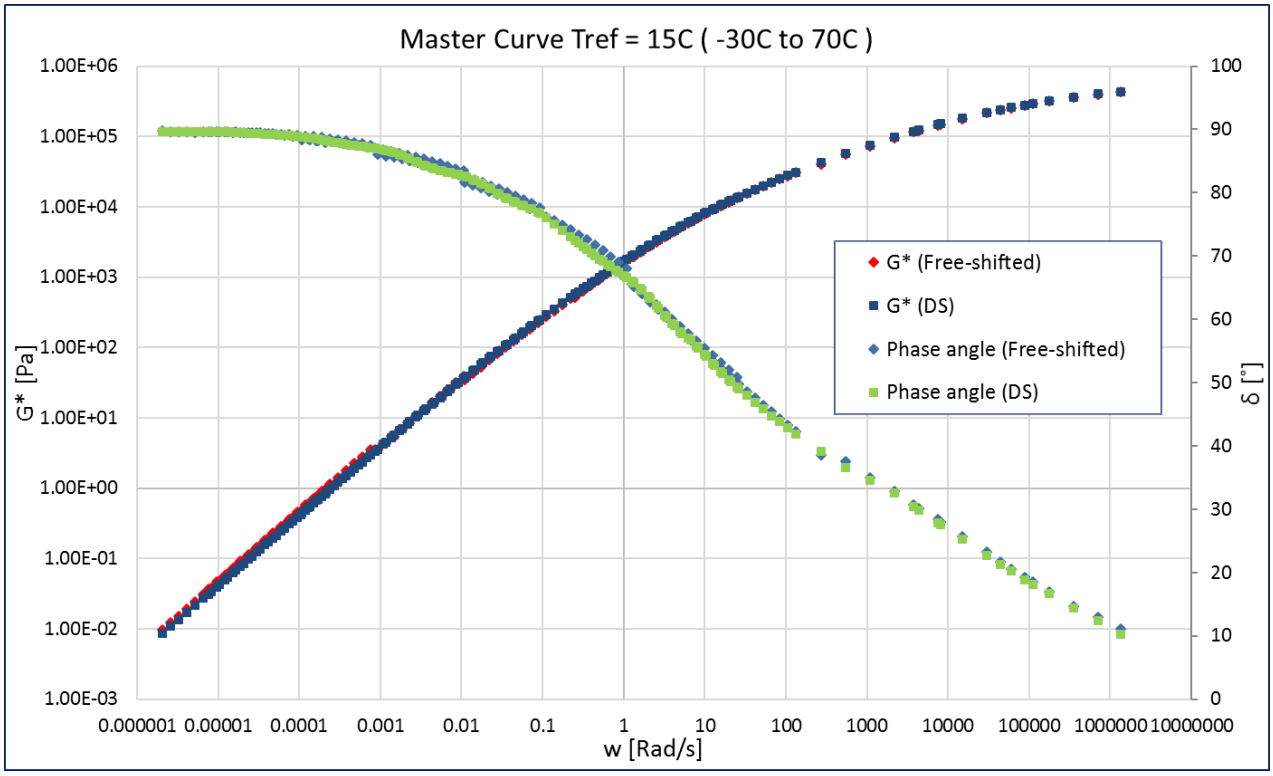

PAV1:

	CA model parameters	
	G*	δ
Go (Pa)	739477041.022	
wo	15.481	15.481
B	0.198	0.204
K	1	1
RMS error (Log)	0.0278	0.0455

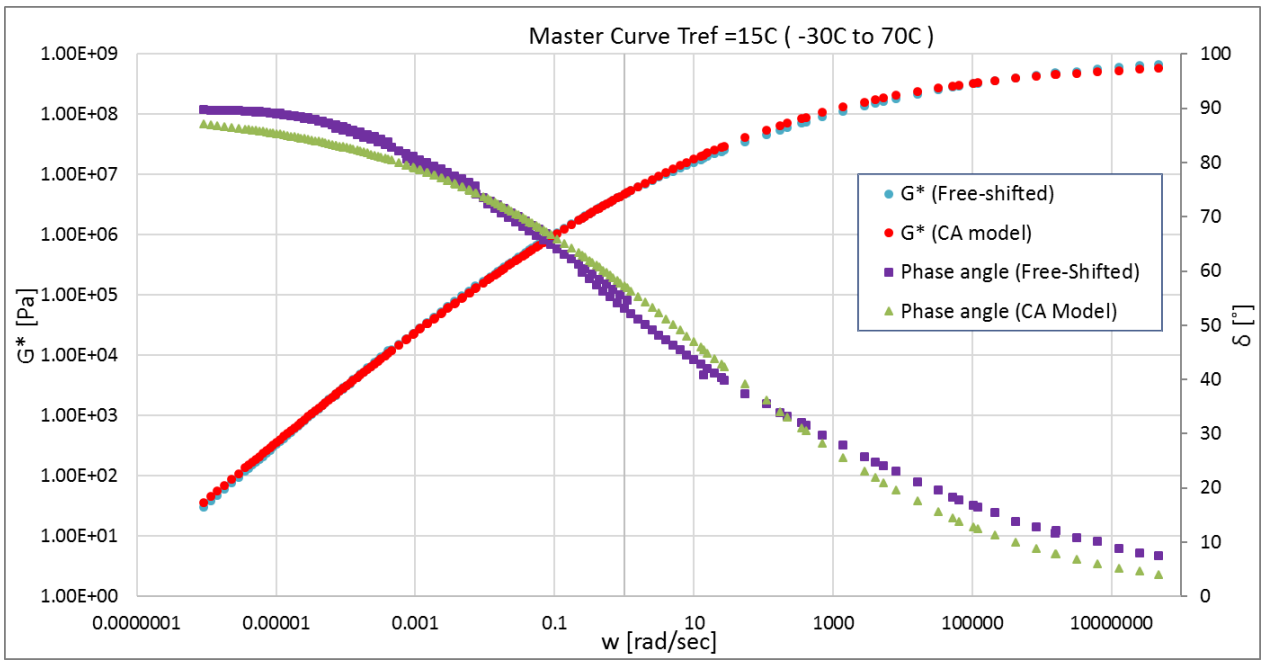

	CAM model parameters	
	G*	δ
Go (Pa)	788765662.947	
wo	15.481	15.481
B	0.195	0.177
K	1.003	1.058
RMS error (Log)	0.0276	0.0352

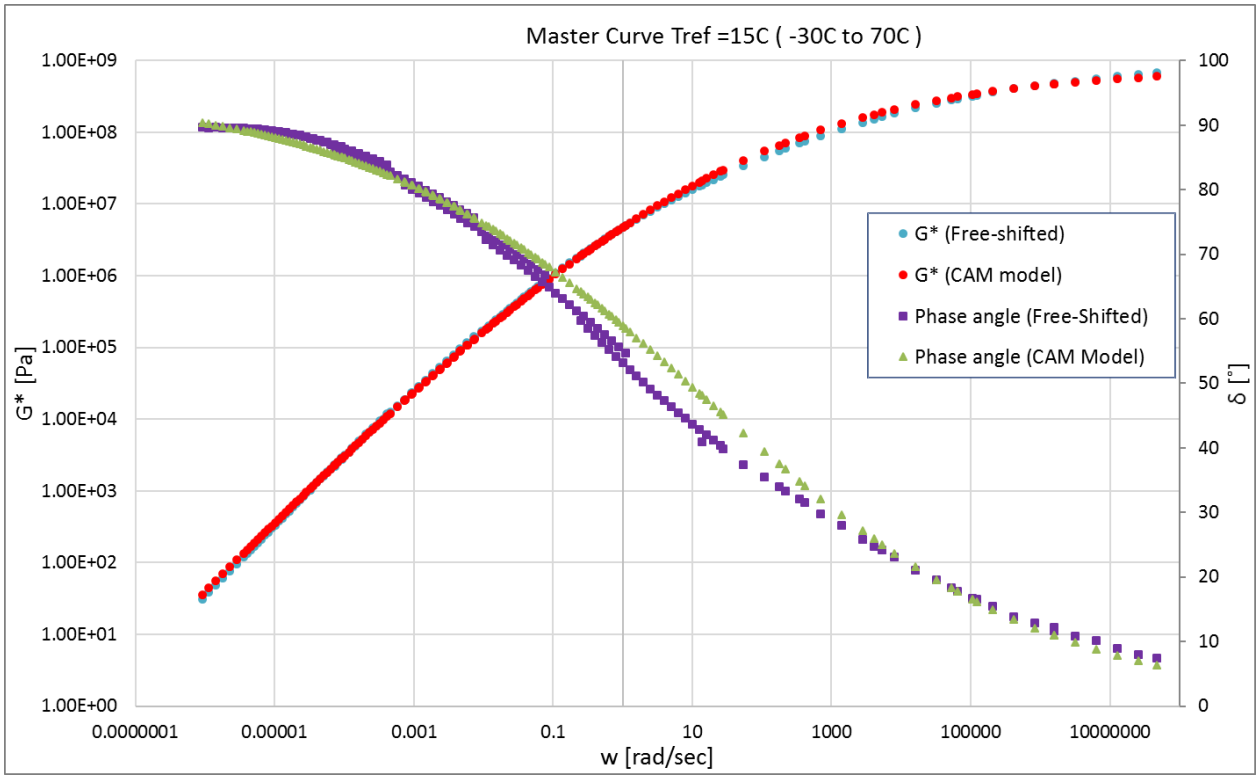

	GL model parameters	
	G*	δ
A	26.674	0.769
B	0.332	0.289
D	-20.595	
M	-6.320	-5.665
T	5.227	3.373
RMS error (Log)	0.0074	0.008

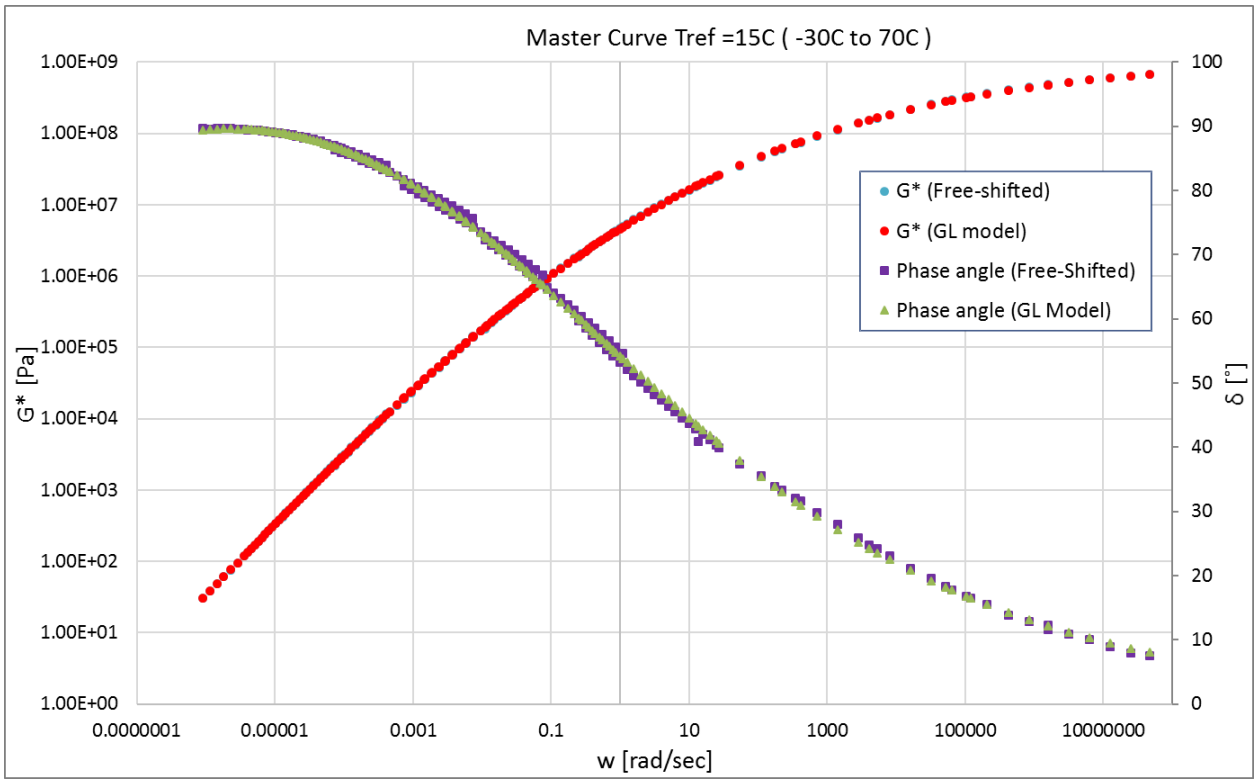

Rhea Discrete spectra		
Mode	gi, pa	li, sec
1	1.47E+05	3.71E-08
2	1.14E+05	2.81E-07
3	1.05E+05	1.54E-06
4	1.11E+05	8.95E-06
5	8.00E+04	4.79E-05
6	6.68E+04	2.24E-04
7	4.48E+04	1.07E-03
8	2.87E+04	4.64E-03
9	1.75E+04	2.10E-02
10	9.29E+03	9.10E-02
11	4.34E+03	4.01E-01
12	1.75E+03	1.63E+00
13	6.57E+02	7.23E+00
14	1.51E+02	4.00E+01
15	2.81E+01	2.15E+02
16	3.93E+00	1.25E+03
17	3.05E-01	8.54E+03
18	4.83E-03	1.13E+05
19	8.04E-05	1.14E+06
20		
21		
22		
RMS error (%)	5.55%	

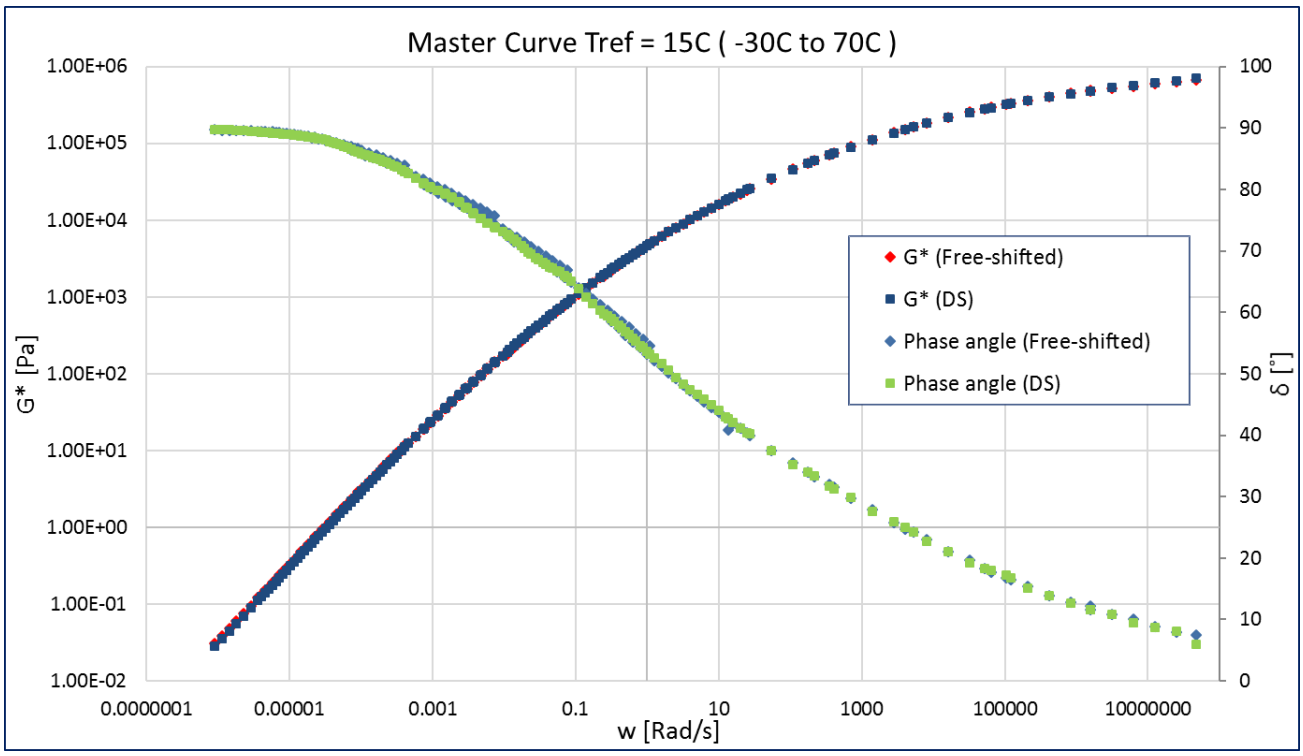

PAV2:

	CA model parameters	
	G*	δ
Go (Pa)	949054484.501	
wo	3.310	3.310
B	0.167	0.177
K	1	1
RMS error (Log)	0.0374	0.0548

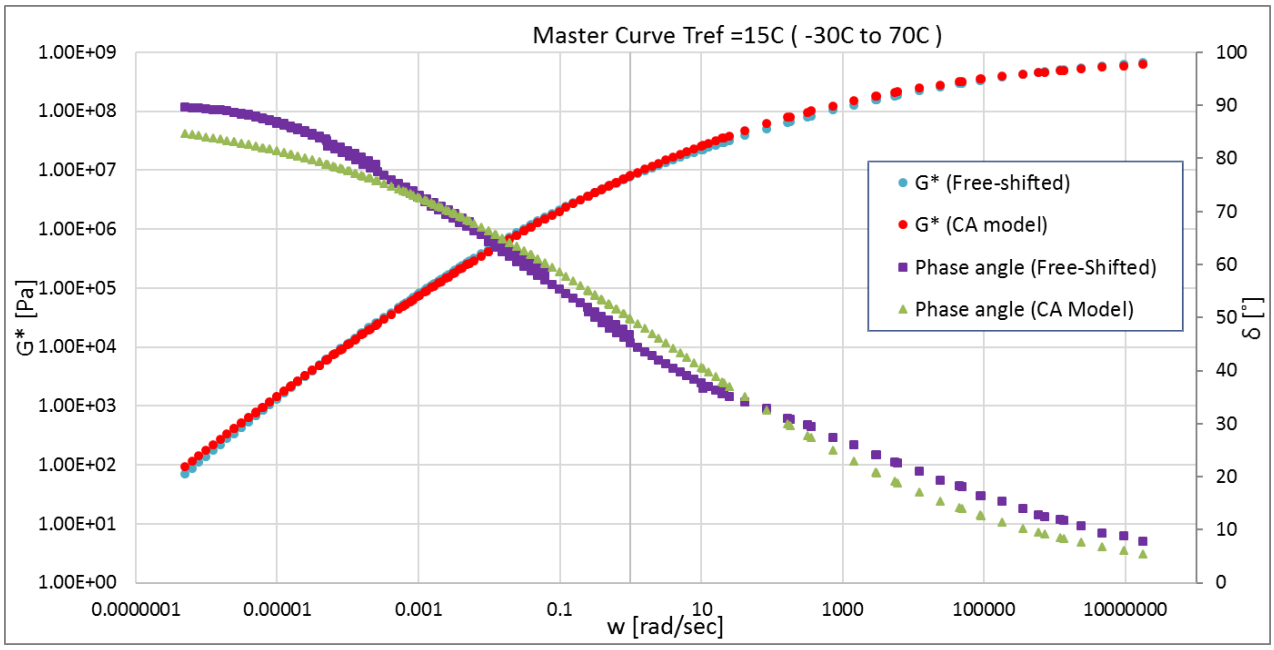

	CAM model parameters	
	G*	δ
Go (Pa)	878460026.567	
wo	3.310	3.310
B	0.170	0.156
K	0.996	1.045
RMS error (Log)	0.0370	0.0505

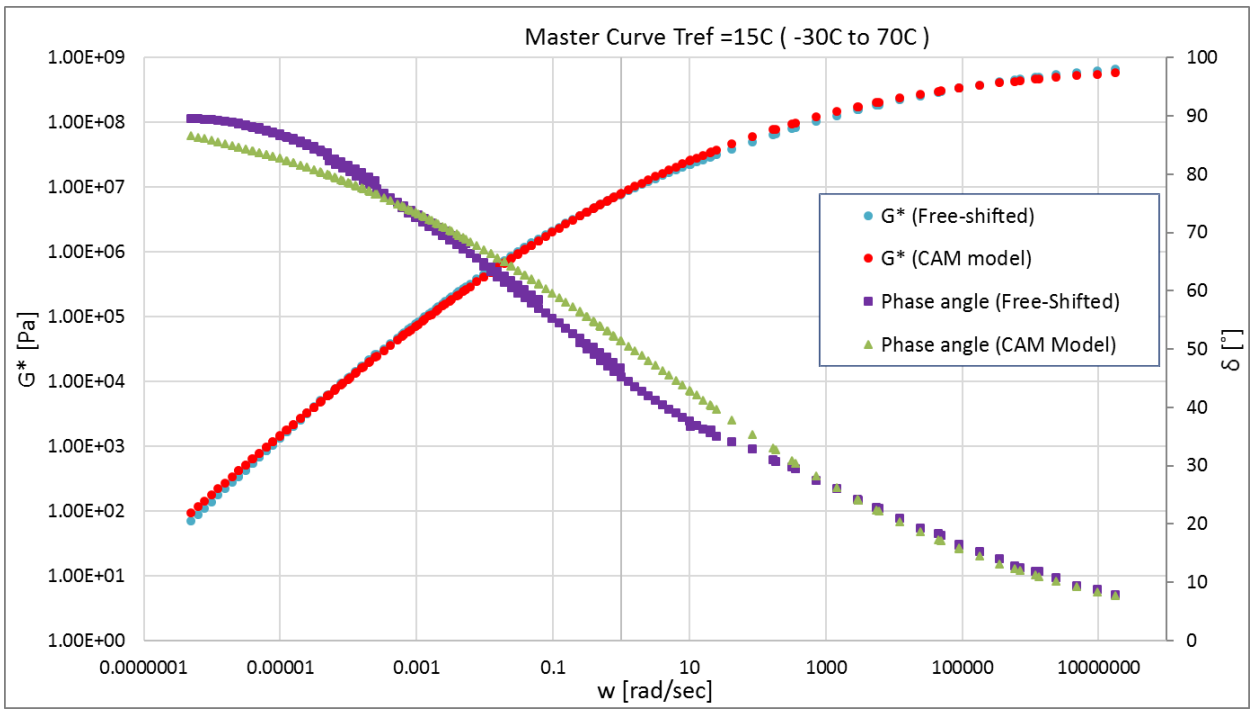

	GL model parameters	
	G*	δ
A	9.494	0.395
B	0.229	0.230
D	-3.117	
M	-5.408	-6.342
T	-0.319	1.514
RMS error (Log)	0.0079	0.009

Annexure F: Mathematical model comparison

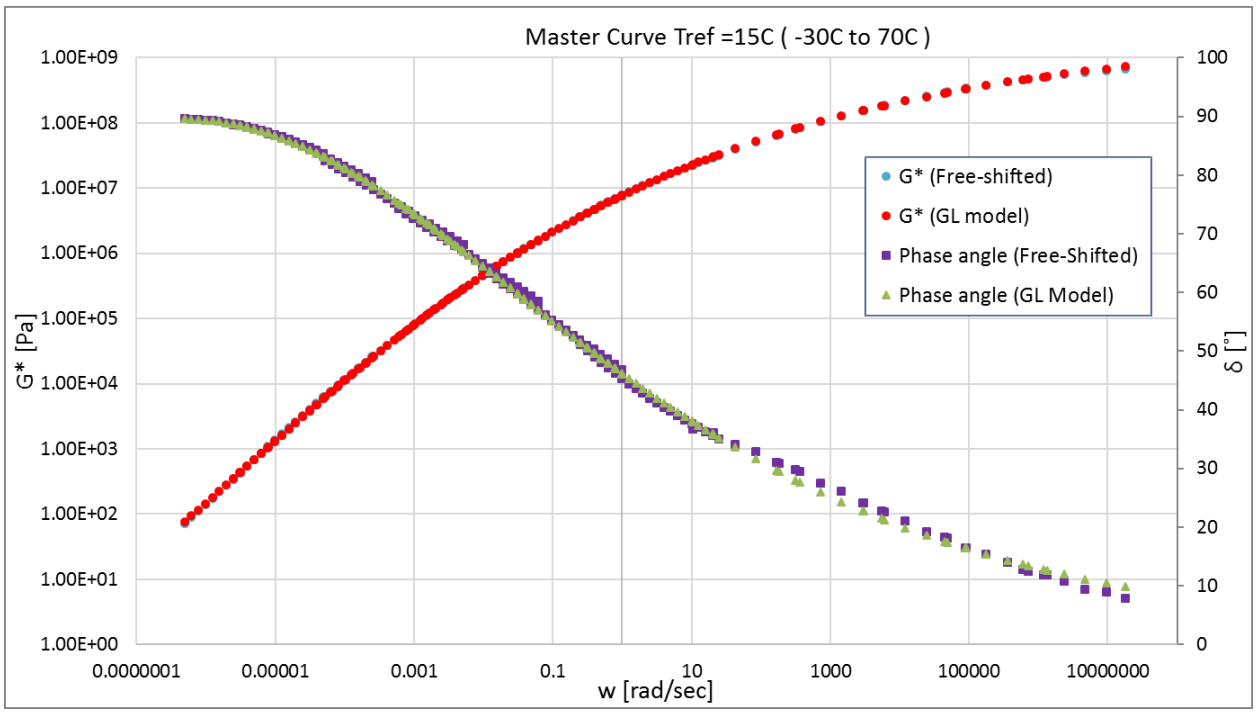

Rhea Discrete spectra		
Mode	gi, pa	li, sec
1	1.49E+05	7.99E-08
2	1.09E+05	5.22E-07
3	1.02E+05	2.52E-06
4	9.85E+04	1.18E-05
5	8.41E+04	5.67E-05
6	6.58E+04	2.63E-04
7	4.72E+04	1.21E-03
8	3.14E+04	5.50E-03
9	1.88E+04	2.58E-02
10	1.10E+04	1.12E-01
11	6.17E+03	5.22E-01
12	2.72E+03	2.31E+00
13	1.15E+03	1.01E+01
14	3.77E+02	4.78E+01
15	1.07E+02	2.23E+02
16	2.47E+01	1.05E+03
17	4.76E+00	5.10E+03
18	5.27E-01	2.75E+04
19	2.85E-02	1.70E+05
20	3.55E-04	1.43E+06
21		
22		
RMS error (%)	2.72%	

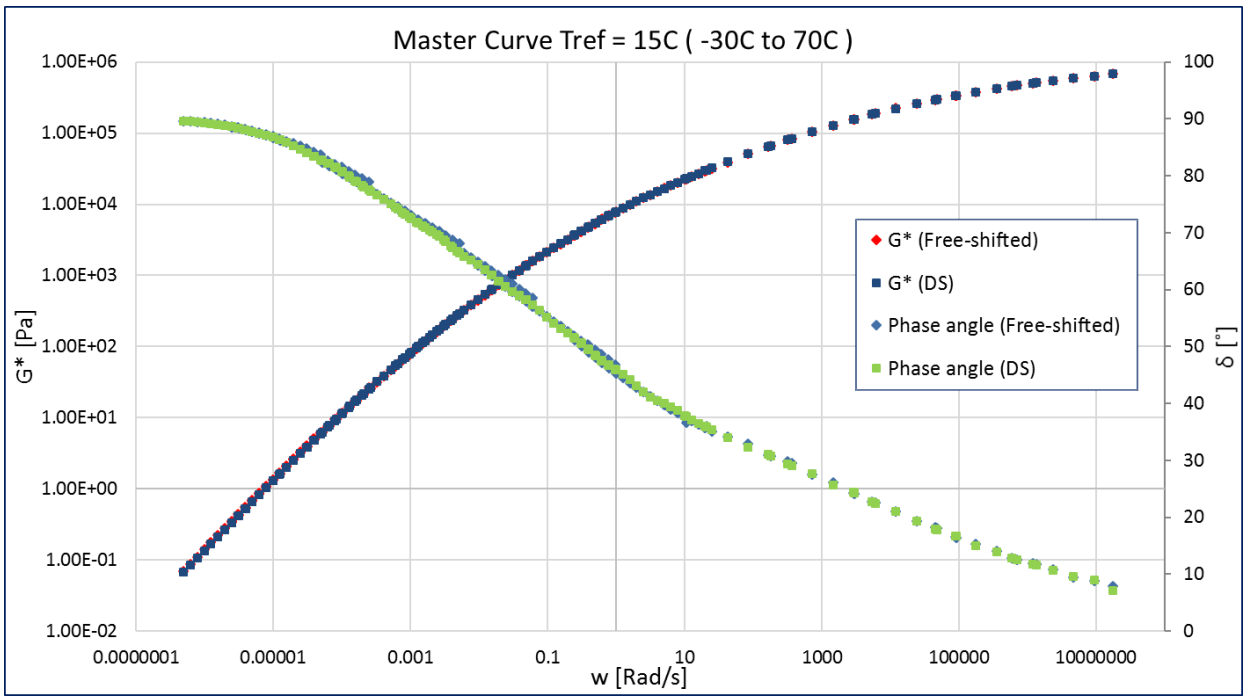

PAV4:

	CA model parameters	
	G*	δ
Go (Pa)	903824176.276	
wo	0.661	0.661
B	0.154	0.164
K	1	1
RMS error (Log)	0.0428	0.0587

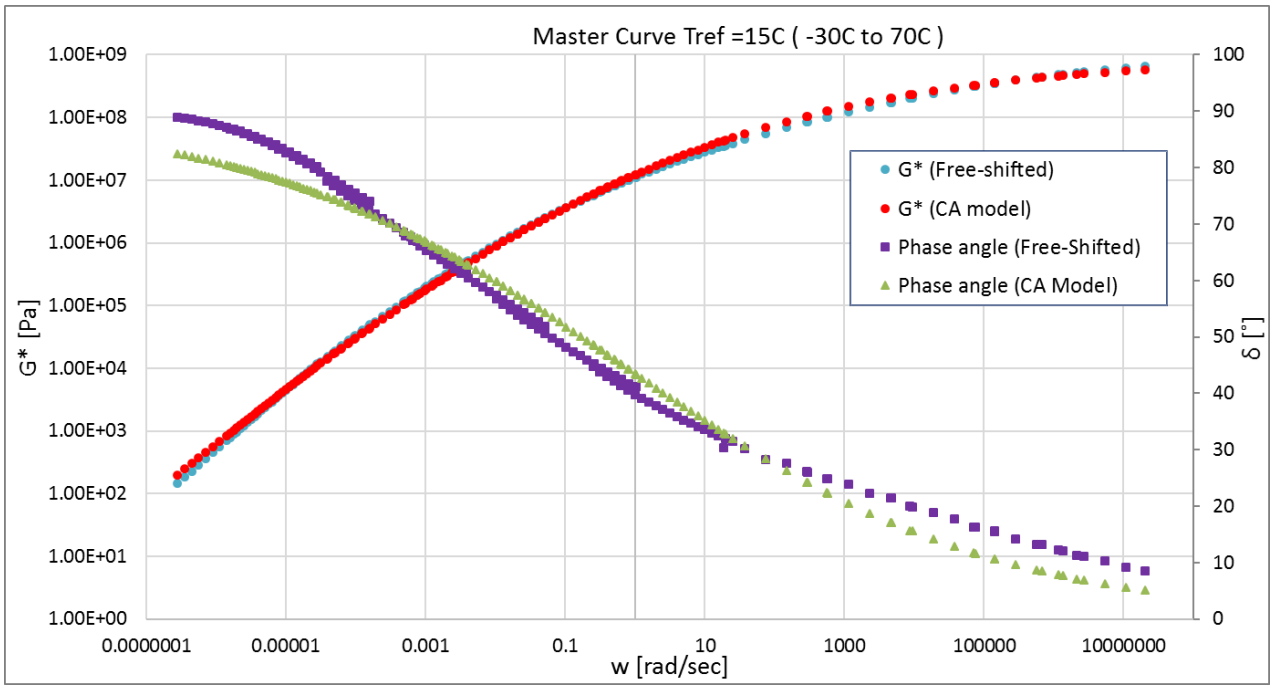

	CAM model parameters	
	G*	δ
Go (Pa)	833496974.903	
wo	0.661	0.661
B	0.155	0.152
K	0.993	1.025
RMS error (Log)	0.0419	0.0582

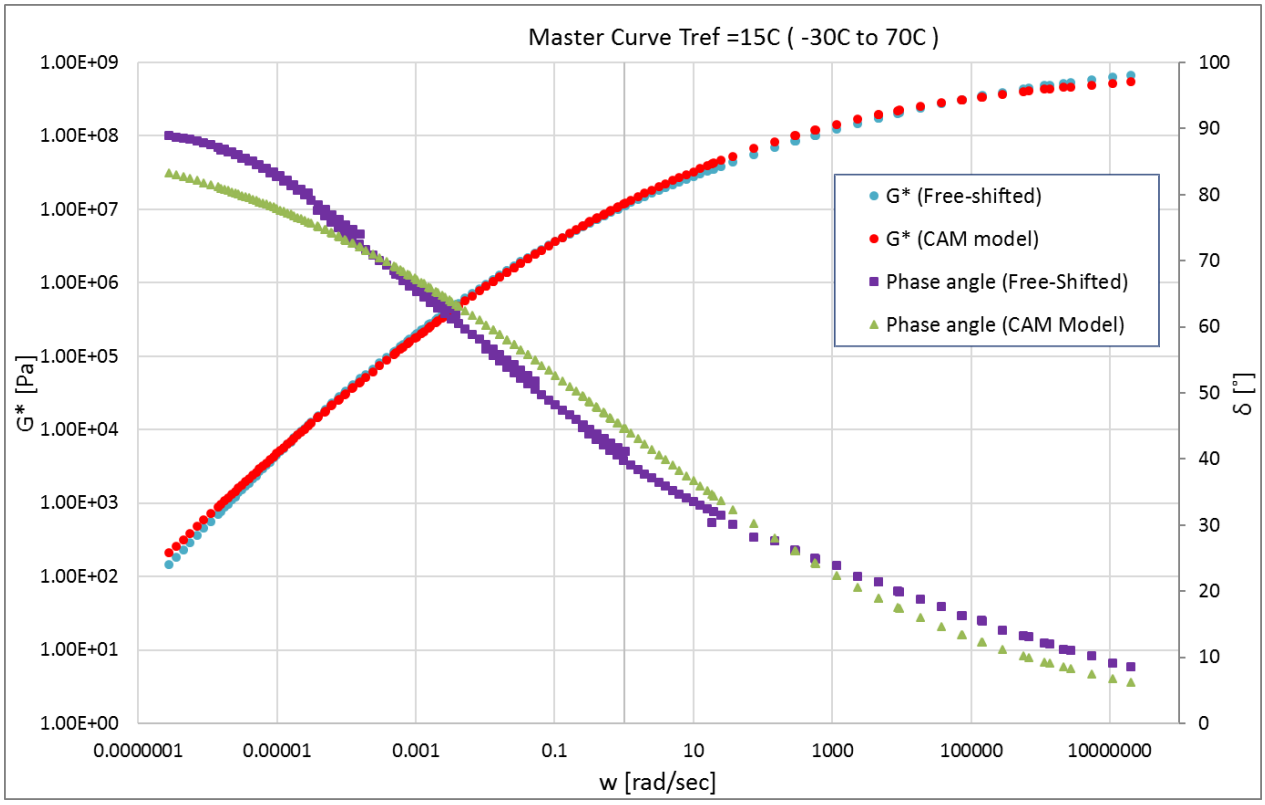

	GL model parameters	
	G*	δ
A	14.152	0.252
B	0.221	0.193
D	-7.834	
M	-7.797	-6.727
T	0.204	0.718
RMS error (Log)	0.0054	0.008

Annexure F: Mathematical model comparison

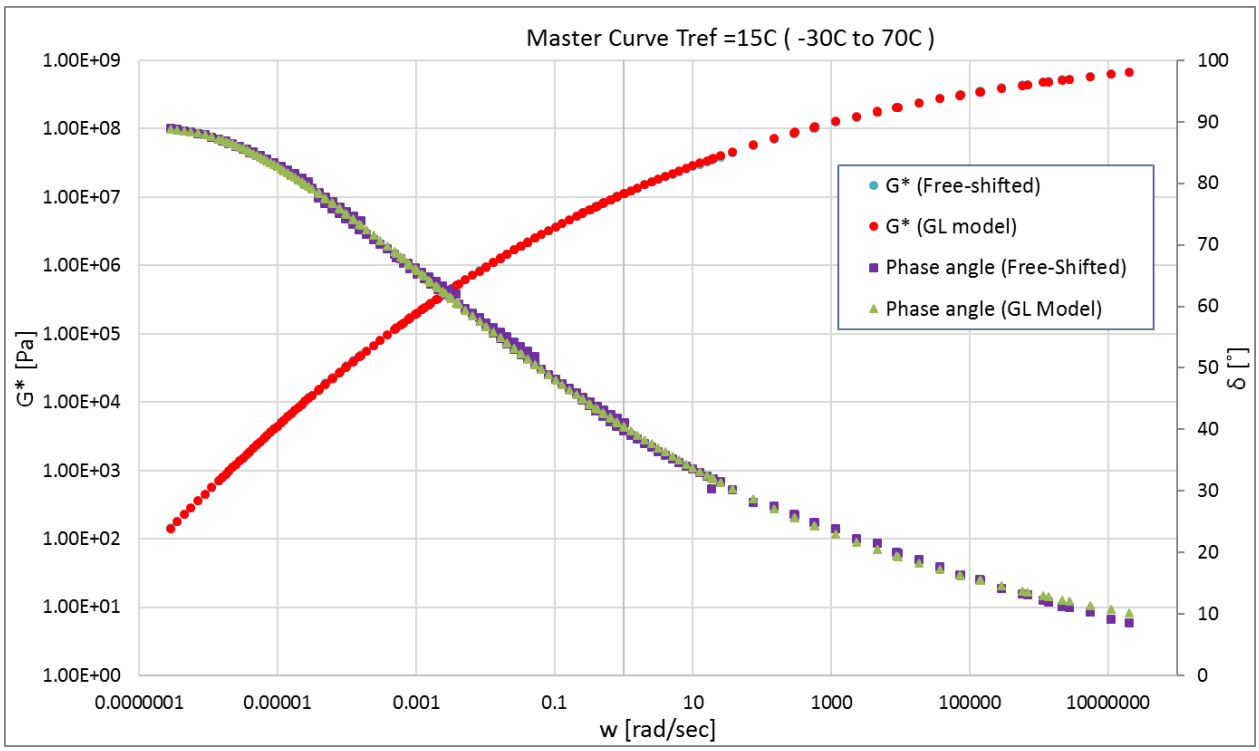

Rhea Discrete spectra		
Mode	gi, pa	li, sec
1	1.56E+05	4.92E-08
2	1.19E+05	3.42E-07
3	1.13E+05	1.99E-06
4	1.03E+05	1.15E-05
5	8.57E+04	6.78E-05
6	6.56E+04	4.10E-04
7	4.51E+04	2.60E-03
8	2.90E+04	1.73E-02
9	1.64E+04	1.14E-01
10	8.65E+03	7.76E-01
11	3.47E+03	5.28E+00
12	1.21E+03	3.39E+01
13	3.44E+02	2.24E+02
14	7.33E+01	1.54E+03
15	1.18E+01	1.08E+04
16	9.45E-01	8.60E+04
17	3.03E-02	6.71E+05
18		
19		
20		
21		
22		
RMS error (%)	4.90%	

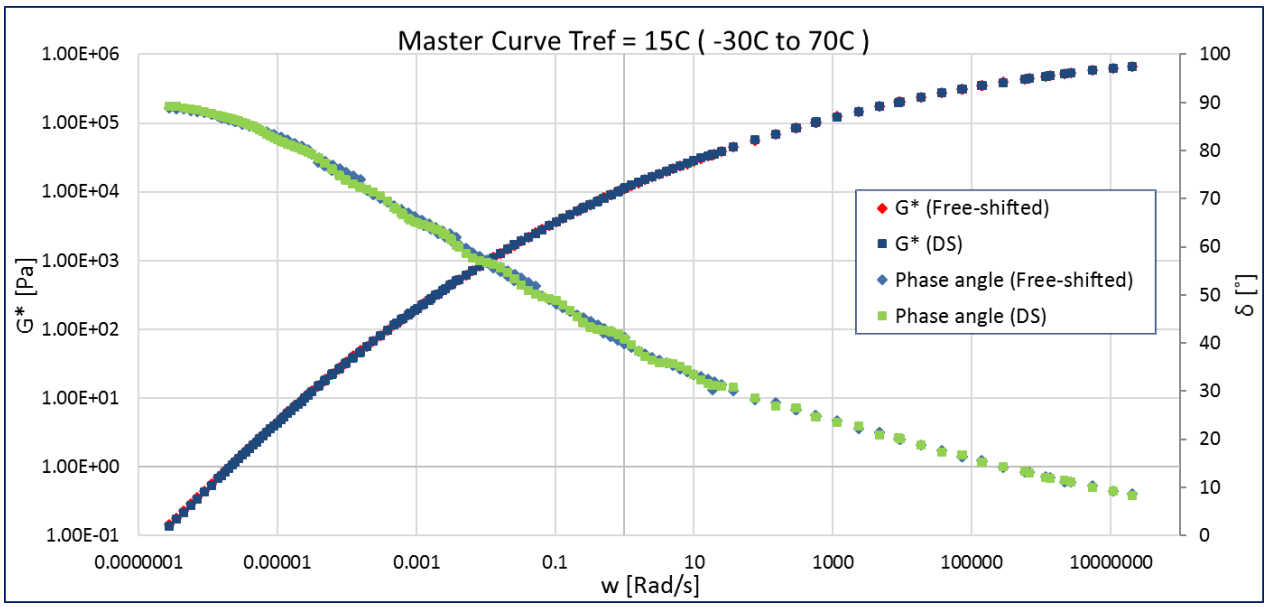

FT211 (S-E1 WP Colas)

Unaged:

	CA model parameters	
	G*	δ
Go (Pa)	628954412.305	
wo	43.260	43.260
B	0.190	0.178
K	1	1
RMS error (Log)	0.0763	0.1000

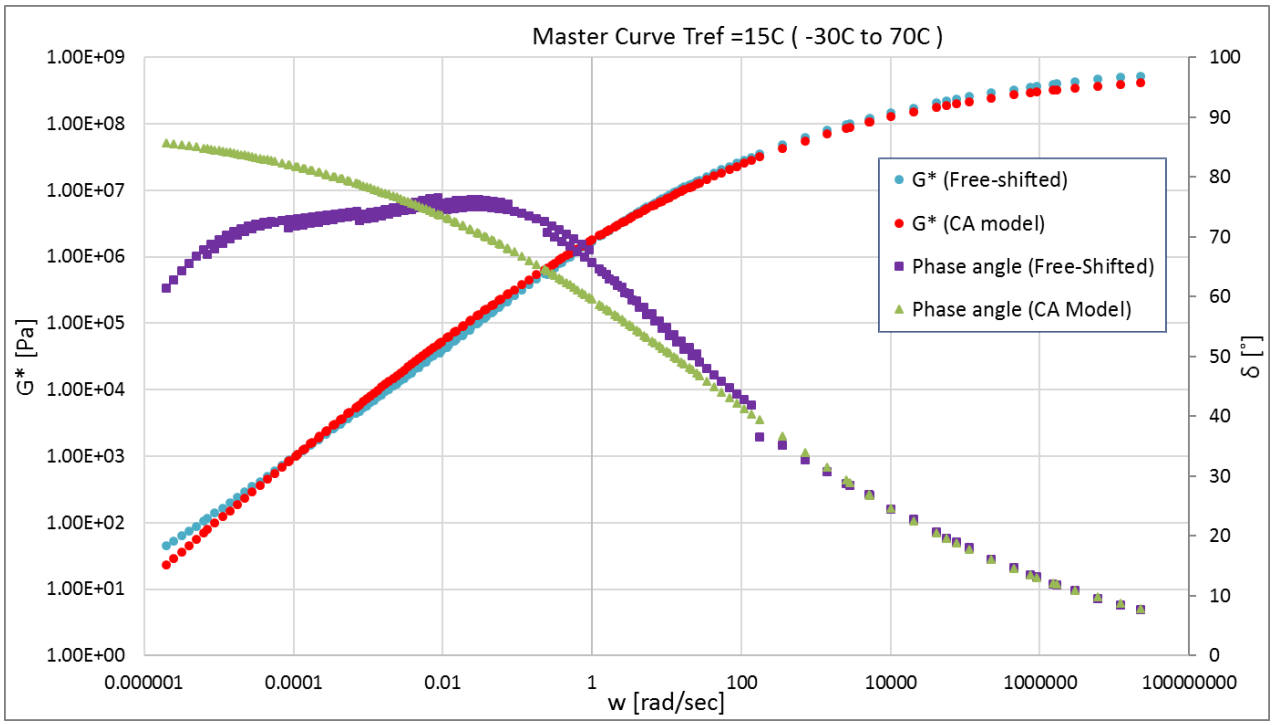

	CAM model parameters	
	G*	δ
Go (Pa)	924813004.757	
wo	43.260	43.260
B	0.177	0.572
K	1.025	0.825
RMS error (Log)	0.0666	0.0828

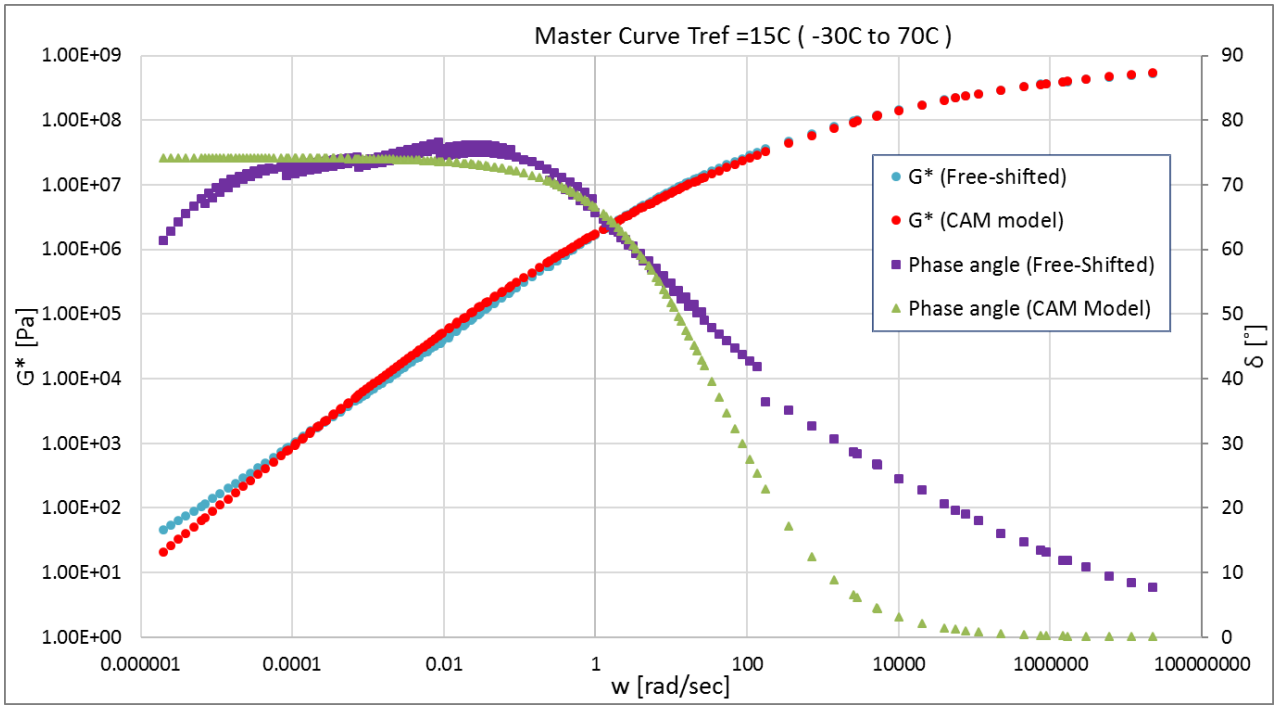

	GL model parameters	
	G*	δ
A	17.013	1.471
B	0.507	0.379
D	-11.217	
M	-2.399	-2.471
T	6.600	3.300
RMS error (Log)	0.0148	0.019

Annexure F: Mathematical model comparison

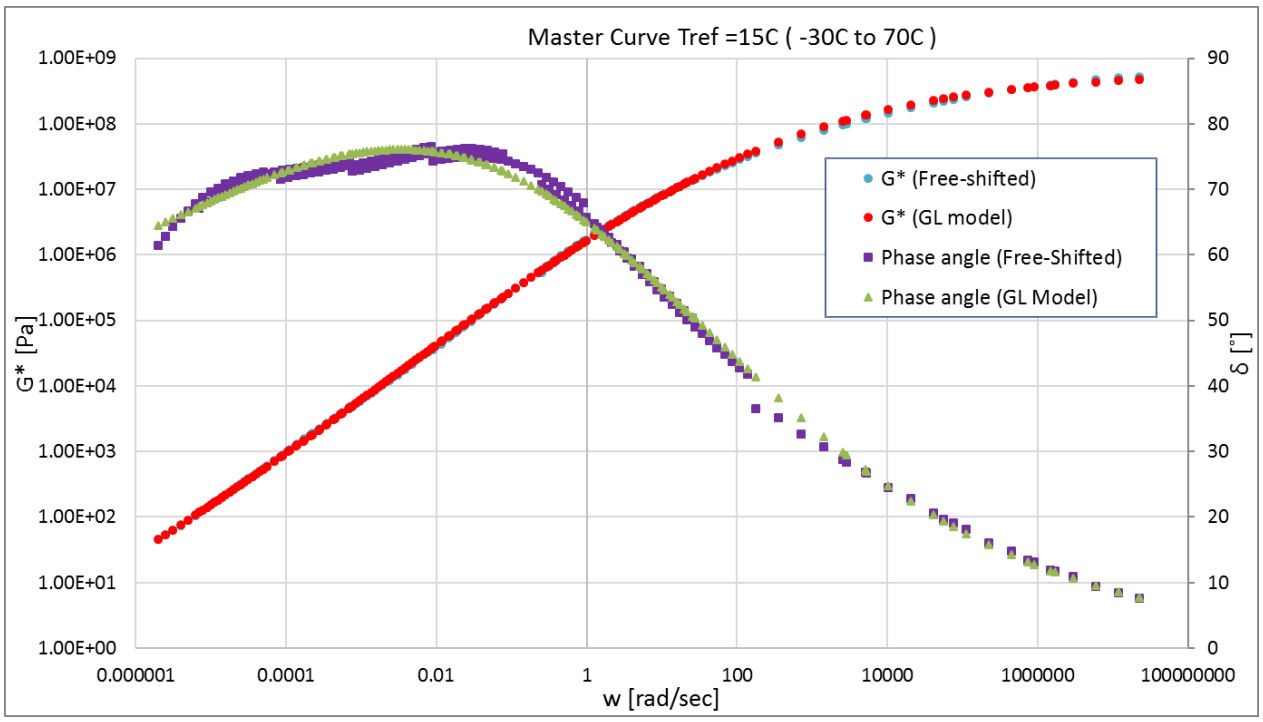

Rhea Discrete spectra		
Mode	gi, pa	li, sec
1	1.15E+05	5.57E-08
2	1.05E+05	4.42E-07
3	1.05E+05	3.05E-06
4	9.34E+04	2.00E-05
5	7.20E+04	1.33E-04
6	4.52E+04	8.91E-04
7	2.42E+04	5.79E-03
8	1.06E+04	3.75E-02
9	3.14E+03	2.24E-01
10	5.35E+02	1.27E+00
11	1.53E+02	6.34E+00
12	2.05E+01	4.70E+01
13	4.70E+00	2.77E+02
14	1.26E+00	1.55E+03
15	3.42E-01	9.70E+03
16	6.74E-02	6.18E+04
17	2.22E-02	3.44E+05
18		
19		
20		
21		
22		
RMS error (%)	3.14%	

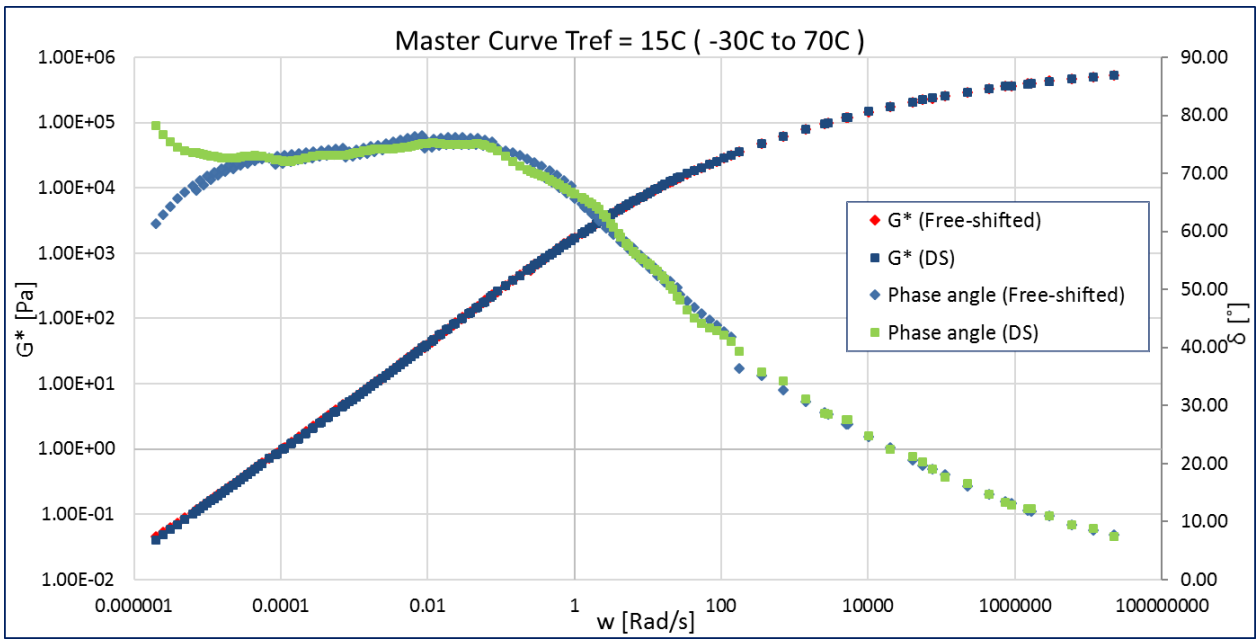

RTFO:

	CA model parameters	
	G*	δ
Go (Pa)	820816300.871	
wo	17.381	17.381
B	0.171	0.166
K	1	1
RMS error (Log)	0.0436	0.0572

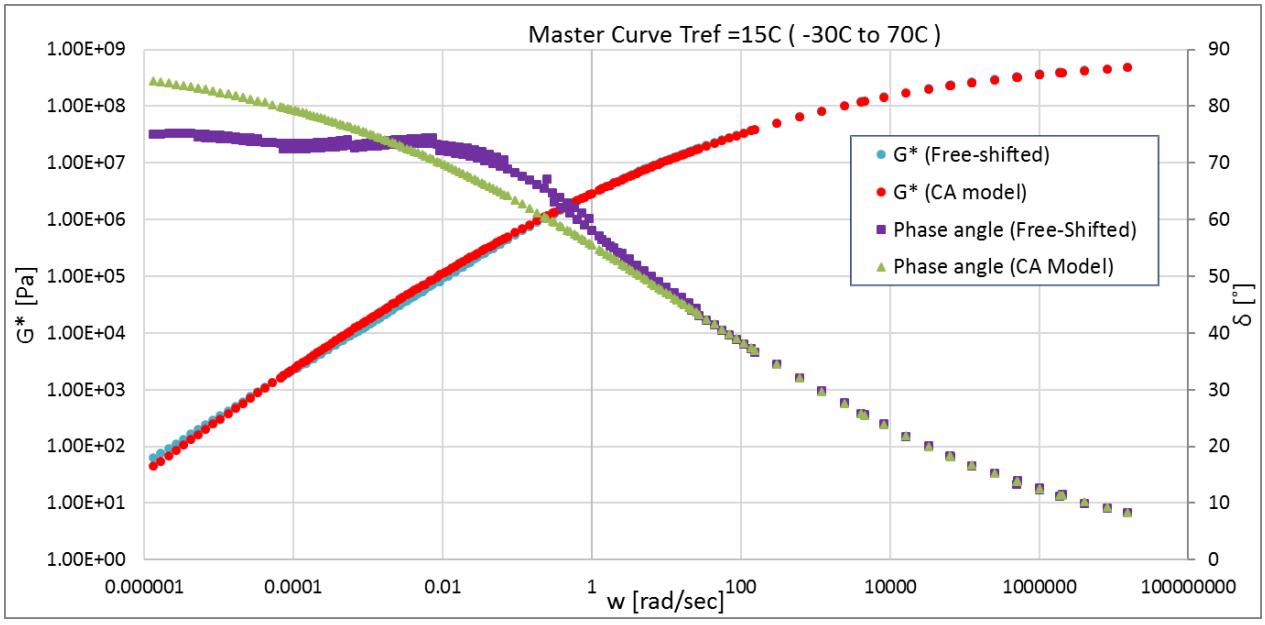

	CAM model parameters	
	G*	δ
Go (Pa)	850983161.824	
wo	17.381	17.381
B	0.171	0.166
K	1.009	0.997
RMS error (Log)	0.0413	0.0571

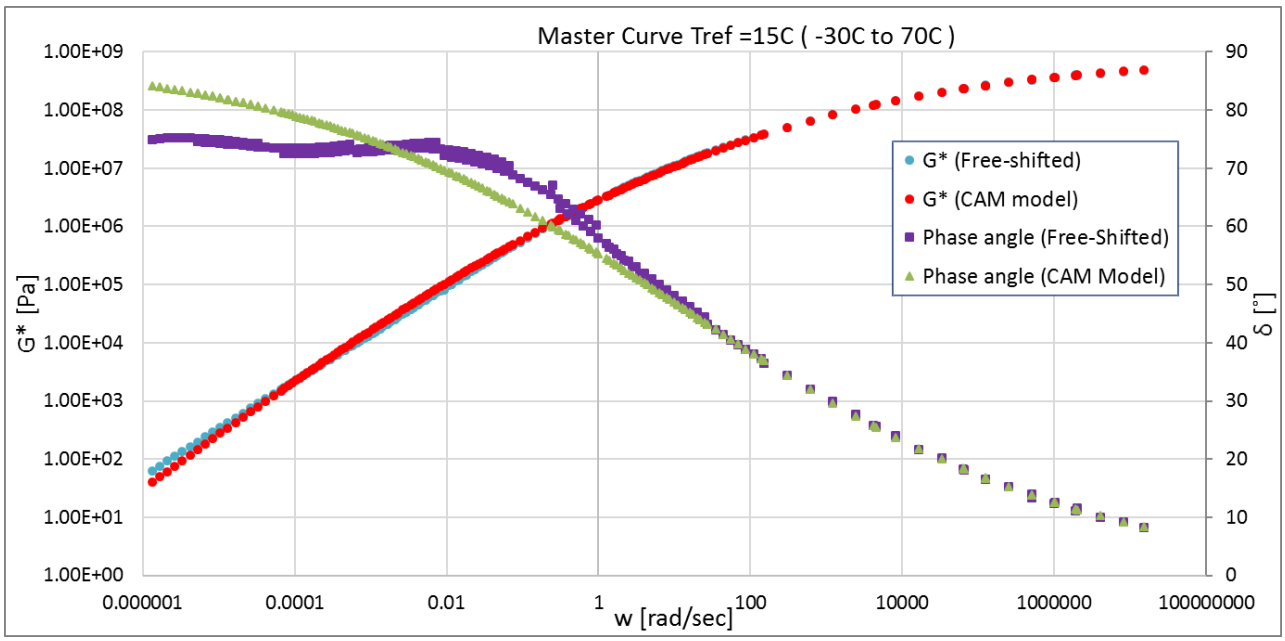

	GL model parameters	
	G*	δ
A	17.674	1.109
B	0.423	0.346
D	-11.827	
M	-3.548	-3.687
T	5.417	3.871
RMS error (Log)	0.0131	0.021

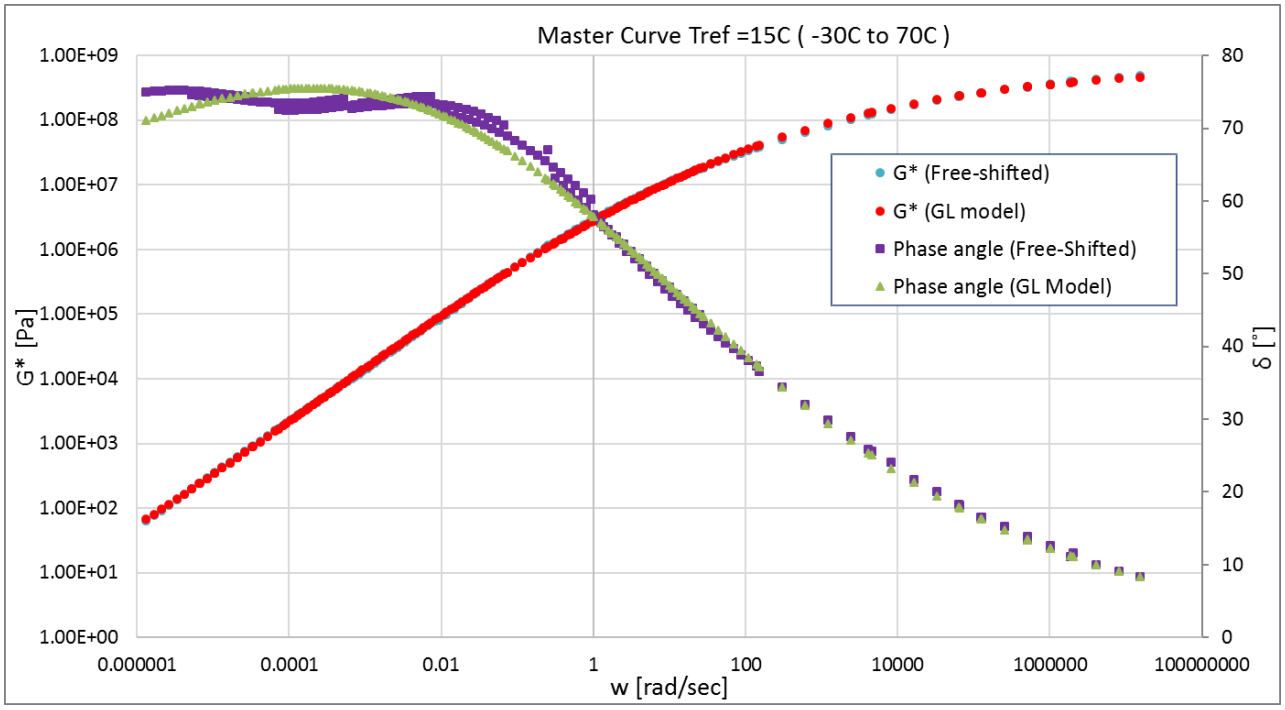

Rhea Discrete spectra		
Mode	gi, pa	li, sec
1	1.13E+05	7.77E-08
2	9.57E+04	5.90E-07
3	9.42E+04	3.85E-06
4	8.49E+04	2.36E-05
5	6.97E+04	1.46E-04
6	4.65E+04	9.07E-04
7	2.63E+04	5.53E-03
8	1.34E+04	3.37E-02
9	5.22E+03	2.11E-01
10	1.35E+03	1.19E+00
11	3.90E+02	6.68E+00
12	5.67E+01	5.37E+01
13	9.89E+00	3.53E+02
14	2.34E+00	2.36E+03
15	5.29E-01	1.48E+04
16	1.10E-01	8.96E+04
17	2.55E-02	5.60E+05
18		
19		
20		
21		
22		
RMS error (%)	2.52%	

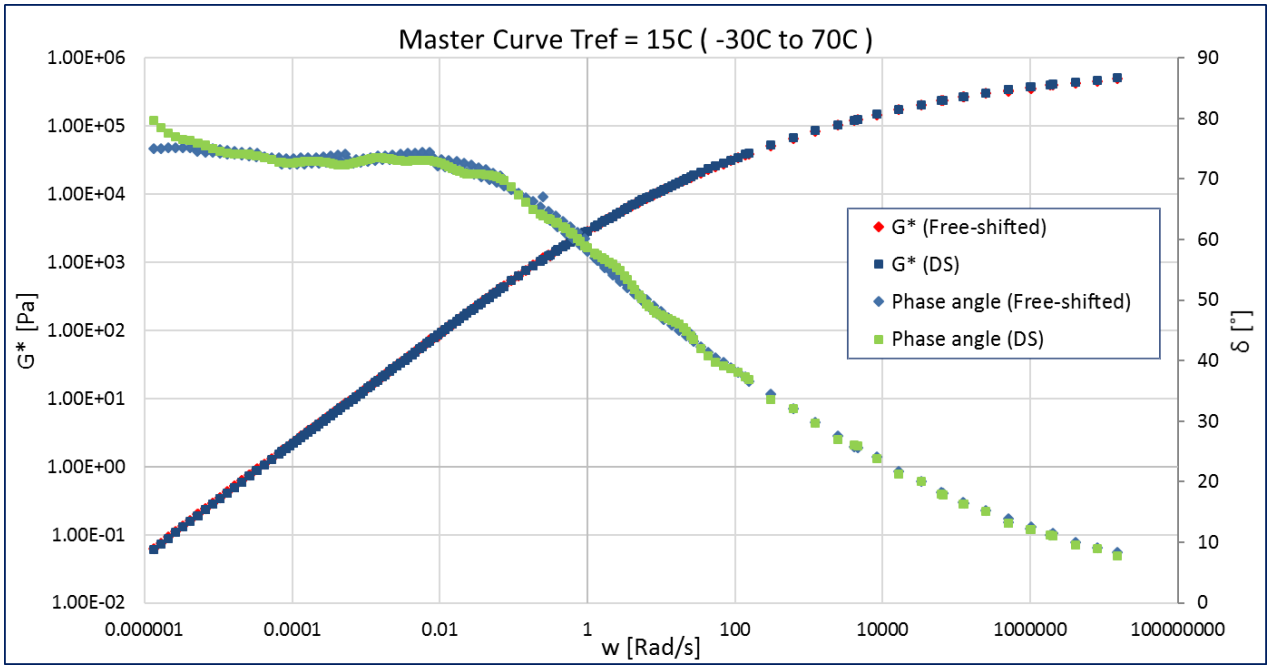

PAV1:

	CA model parameters	
	G*	δ
Go (Pa)	788419961.179	
wo	5.213	5.213
B	0.164	0.160
K	1	1
RMS error (Log)	0.0228	0.0331

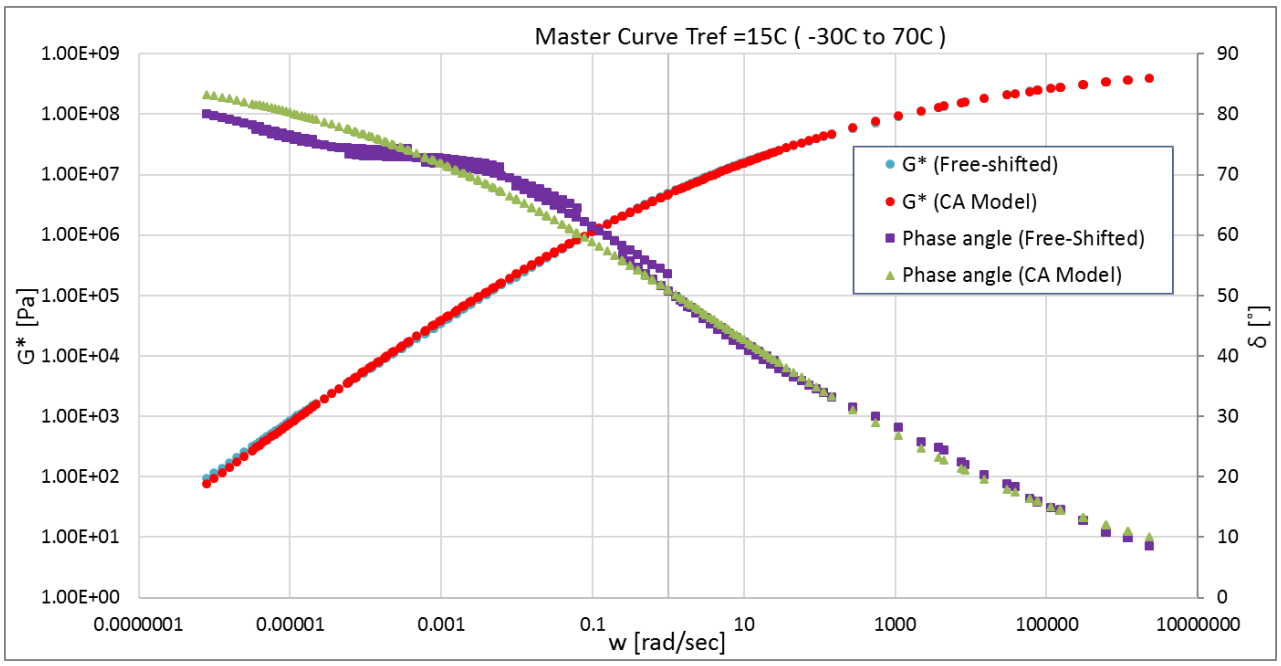

	CAM model parameters	
	G*	δ
Go (Pa)	792824121.237	
wo	5.213	5.213
B	0.164	0.161
K	1.001	0.990
RMS error (Log)	0.0227	0.0321

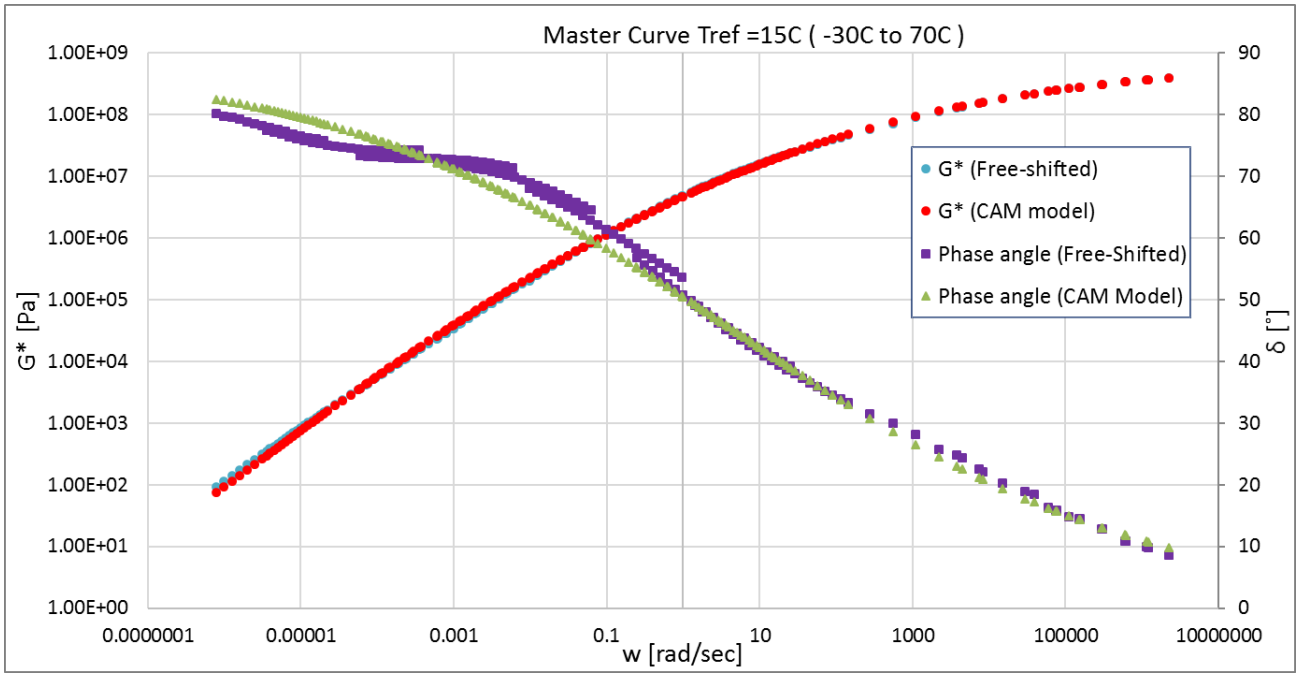

	GL model parameters	
	G*	δ
A	20.903	1.022
B	0.380	0.335
D	-15.034	
M	-4.891	-4.986
T	5.847	4.995
RMS error (Log)	0.0103	0.020

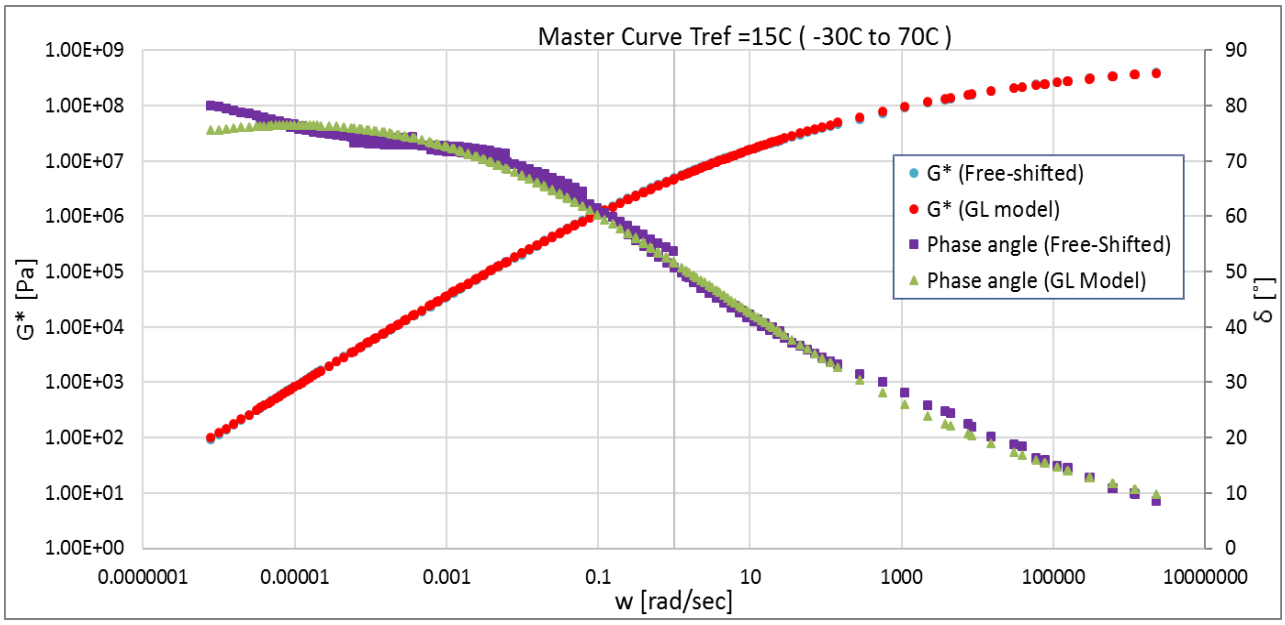

Rhea Discrete spectra		
Mode	gi, pa	li, sec
1	7.19E+04	4.07E-08
2	8.98E+04	1.94E-07
3	7.30E+04	1.73E-06
4	5.87E+04	7.26E-06
5	5.52E+04	2.40E-05
6	5.52E+04	8.69E-05
7	4.78E+04	3.40E-04
8	2.93E+04	1.32E-03
9	2.17E+04	4.64E-03
10	1.53E+04	1.76E-02
11	9.72E+03	7.35E-02
12	5.12E+03	3.16E-01
13	2.10E+03	1.29E+00
14	8.79E+02	5.57E+00
15	2.13E+02	2.06E+01
16	9.88E+01	8.29E+01
17	2.01E+01	3.88E+02
18	6.58E+00	1.81E+03
19	1.70E+00	1.03E+04
20	3.66E-01	6.88E+04
21	5.69E-02	5.96E+05
22	1.38E-03	8.84E+06
RMS error (%)	3.29%	

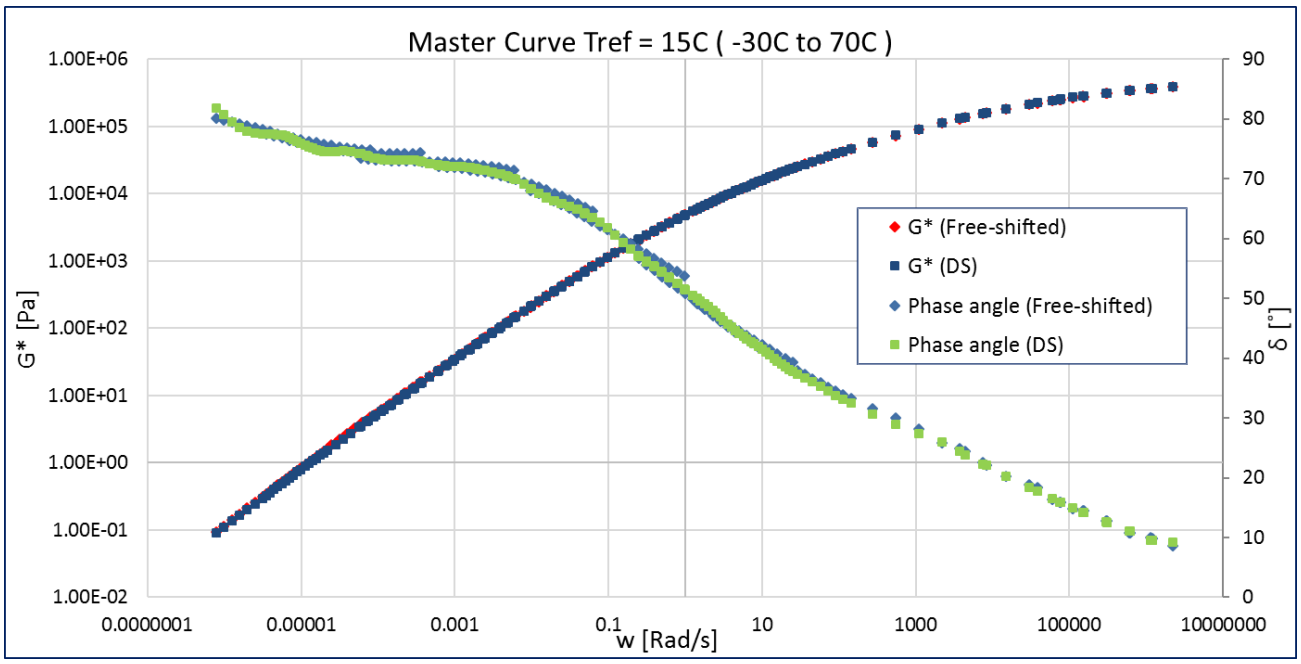

PAV2:

	CA model parameters	
	G*	δ
Go (Pa)	849742715.195	
wo	1.188	1.188
B	0.149	0.154
K	1	1
RMS error (Log)	0.0126	0.0276

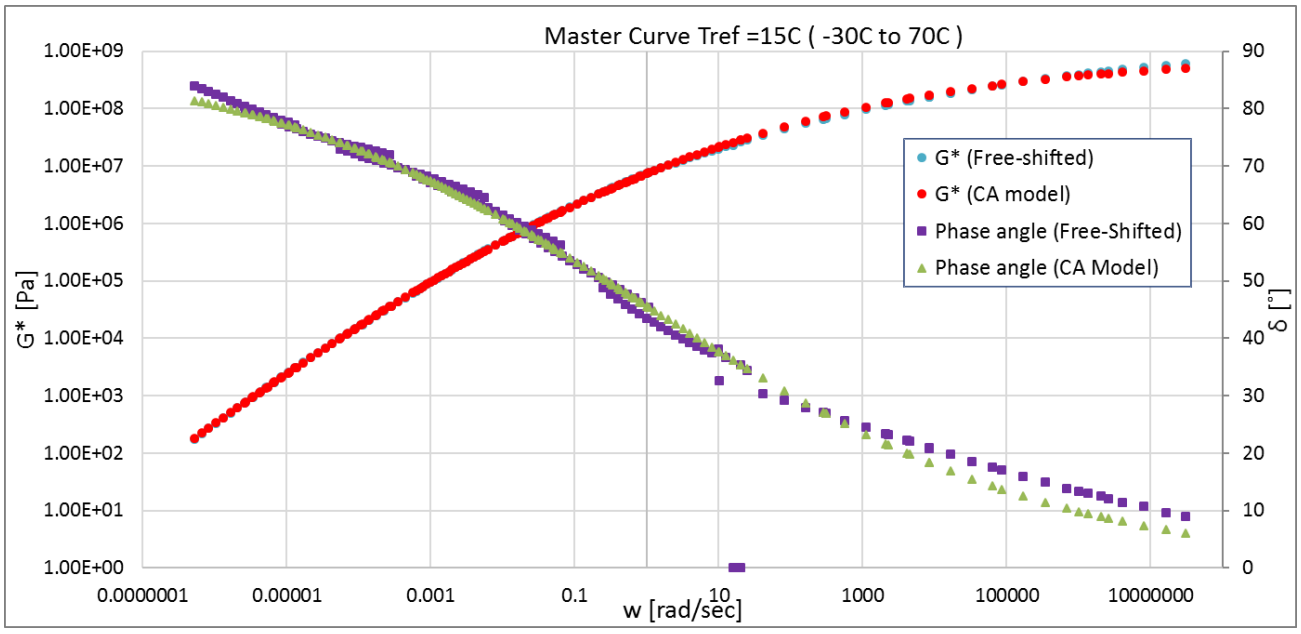

	CAM model parameters	
	G*	δ
Go (Pa)	858288657.369	
wo	1.188	1.188
B	0.149	0.150
K	1.001	1.007
RMS error (Log)	0.0126	0.0275

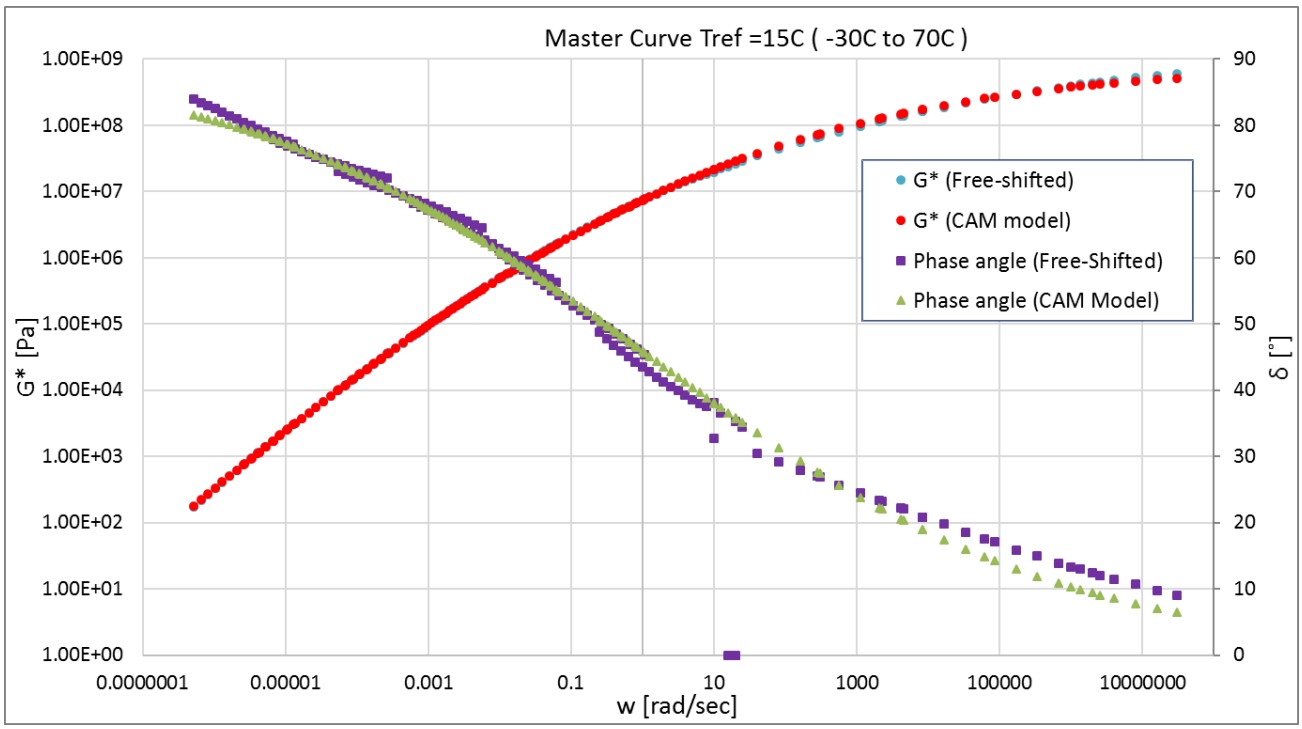

	GL model parameters	
	G*	δ
A	10.653	0.612
B	0.255	0.254
D	-4.509	
M	-5.394	-7.366
T	0.372	3.947
RMS error (Log)	0.0093	0.023

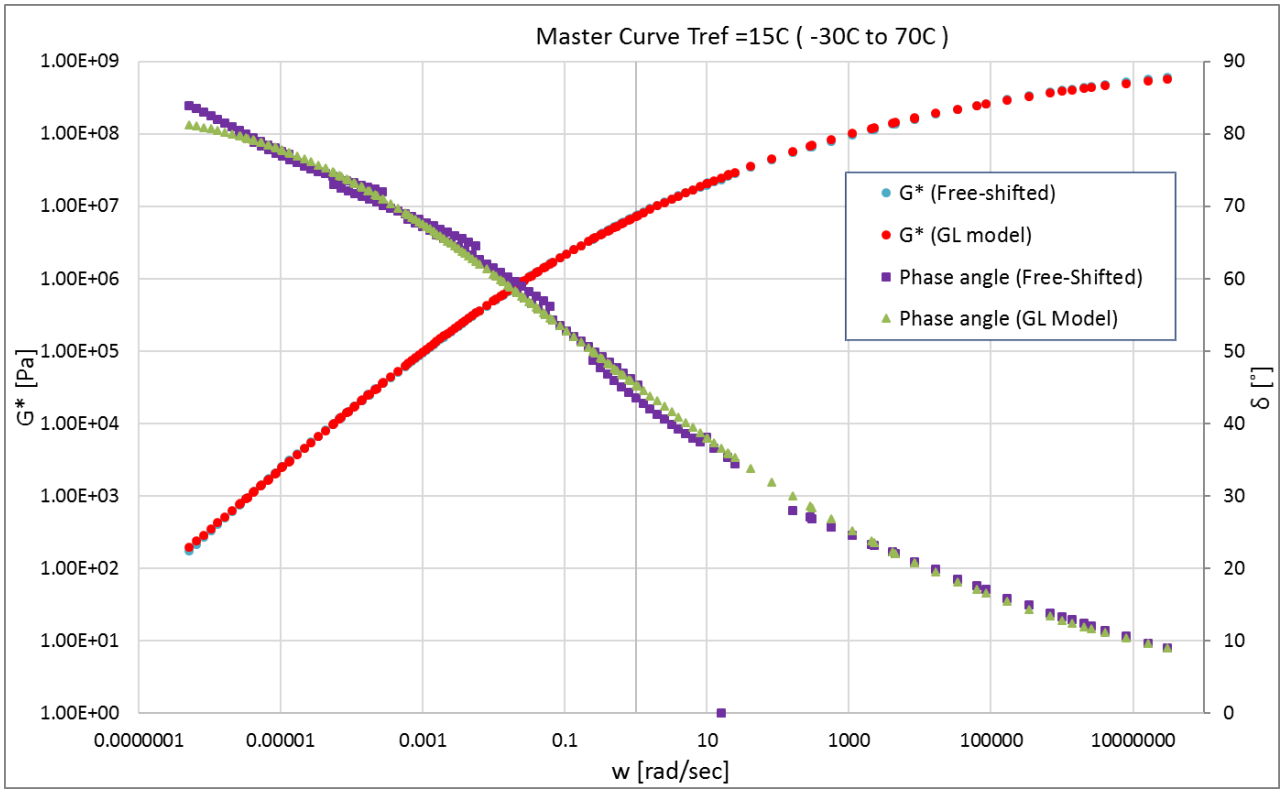

Rhea Discrete spectra		
Mode	gi, pa	li, sec
1	1.50E+05	4.35E-08
2	9.78E+04	2.77E-07
3	8.60E+04	1.26E-06
4	7.85E+04	5.47E-06
5	6.84E+04	2.42E-05
6	5.66E+04	1.10E-04
7	4.39E+04	5.17E-04
8	3.16E+04	2.54E-03
9	2.20E+04	1.34E-02
10	1.32E+04	7.28E-02
11	7.66E+03	4.25E-01
12	2.94E+03	2.67E+00
13	1.02E+03	1.52E+01
14	2.98E+02	9.92E+01
15	6.00E+01	7.27E+02
16	1.15E+01	5.19E+03
17	1.85E+00	4.03E+04
18	2.32E-01	3.14E+05
19	1.53E-02	6.38E+06
20		
21		
22		
RMS error (%)	2.85%	

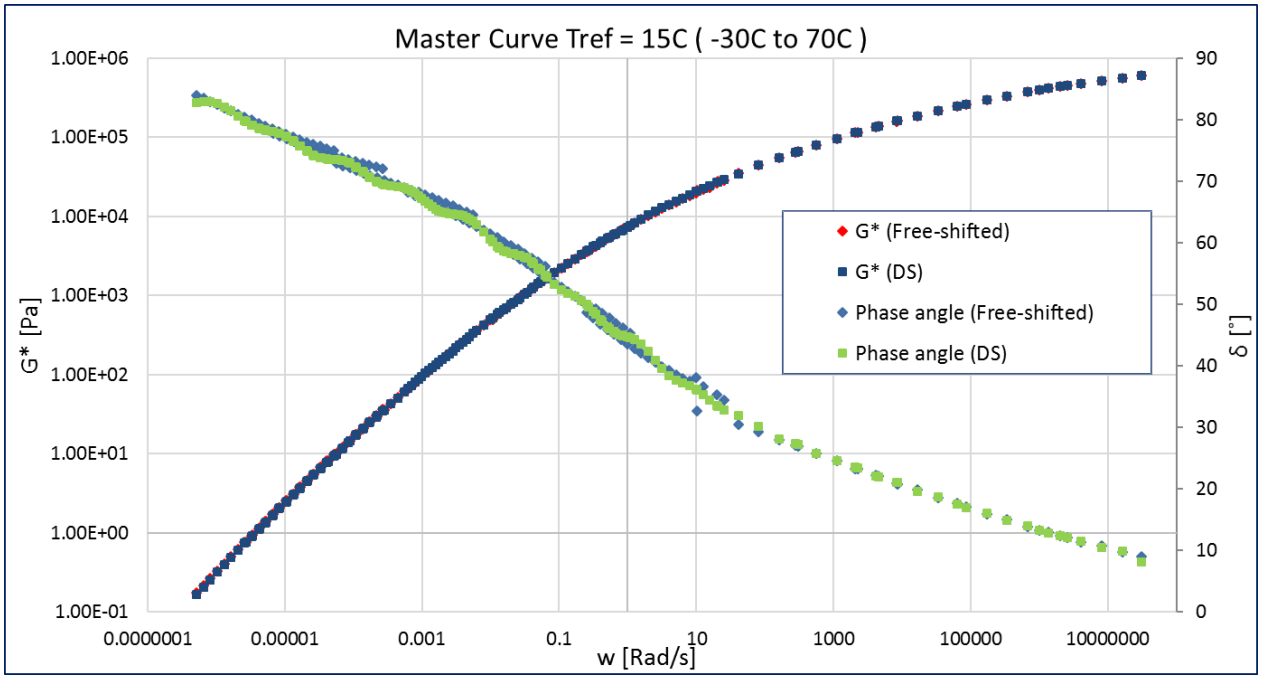

PAV4:

	CA model parameters	
	G*	δ
Go (Pa)	976445730.969	
wo	0.148	0.148
B	0.130	0.136
K	1	1
RMS error (Log)	0.0212	0.0209

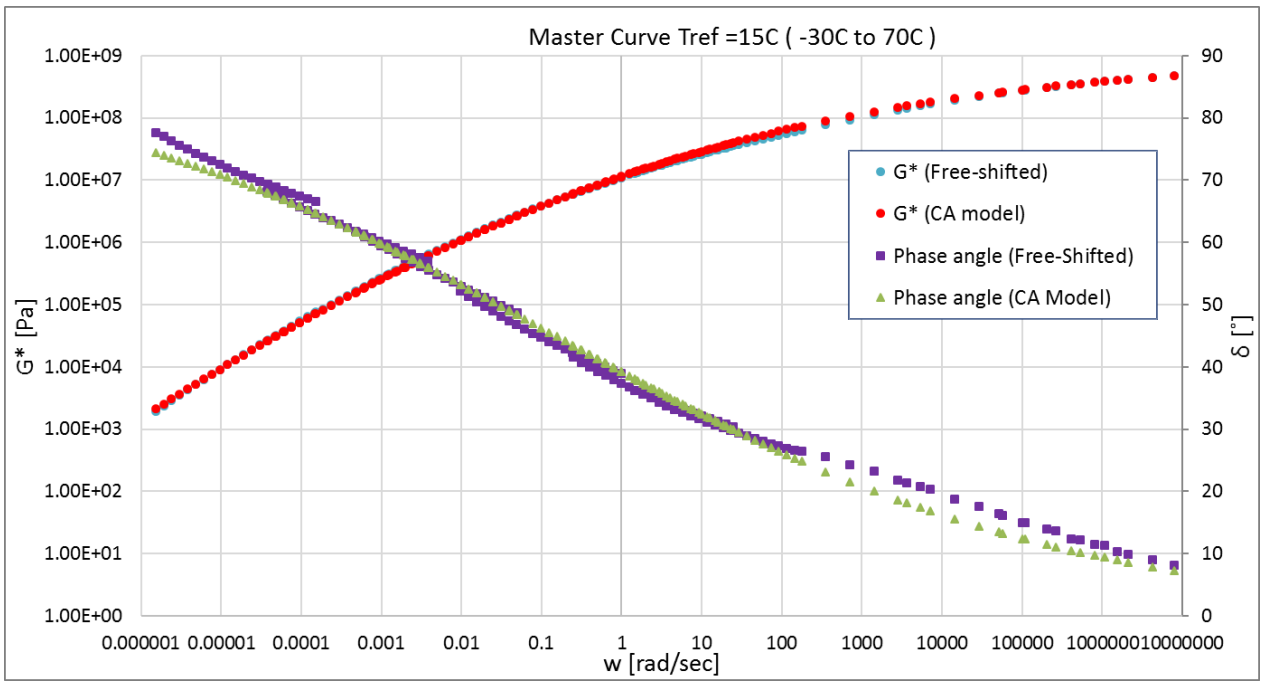

	CAM model parameters	
	G*	δ
Go (Pa)	957446612.132	
wo	0.148	0.148
B	0.129	0.137
K	0.989	0.998
RMS error (Log)	0.0176	0.0209

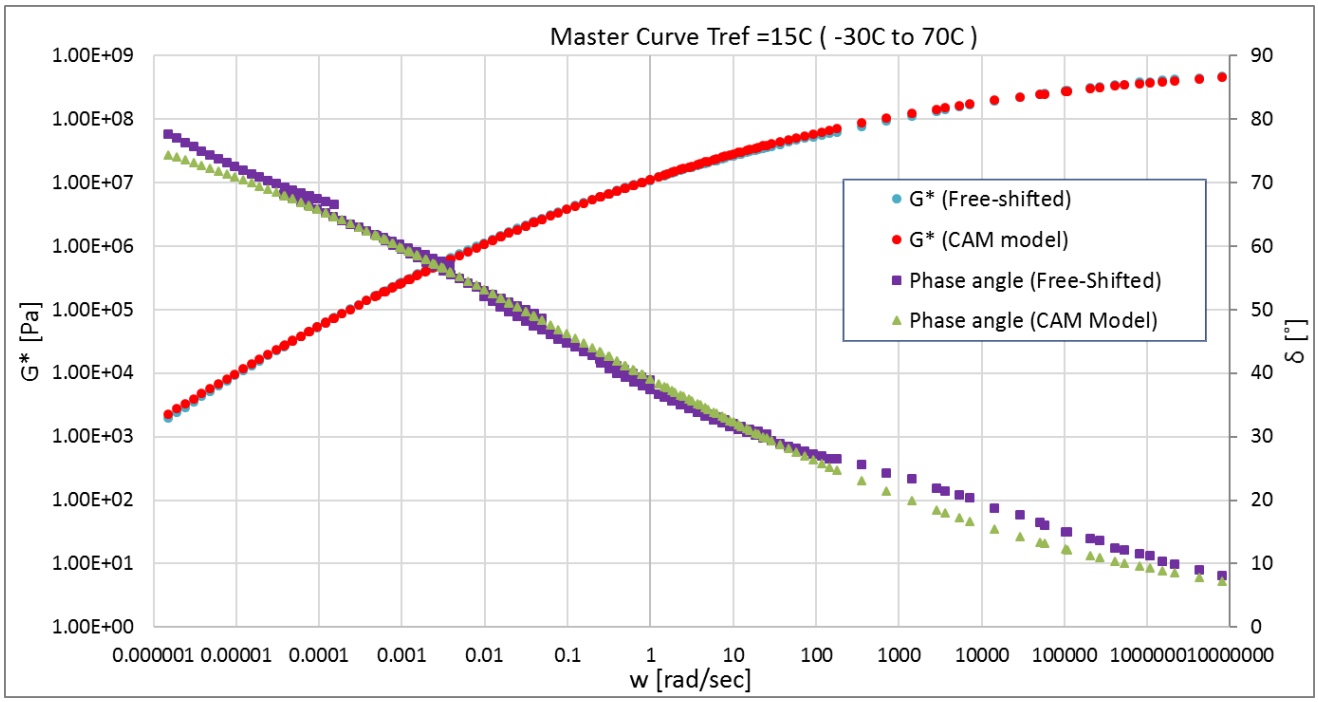

	GL model parameters	
	G*	δ
A	12.660	0.469
B	0.217	0.219
D	-6.431	
M	-7.547	-10.025
T	0.258	3.733
RMS error (Log)	0.0057	0.011

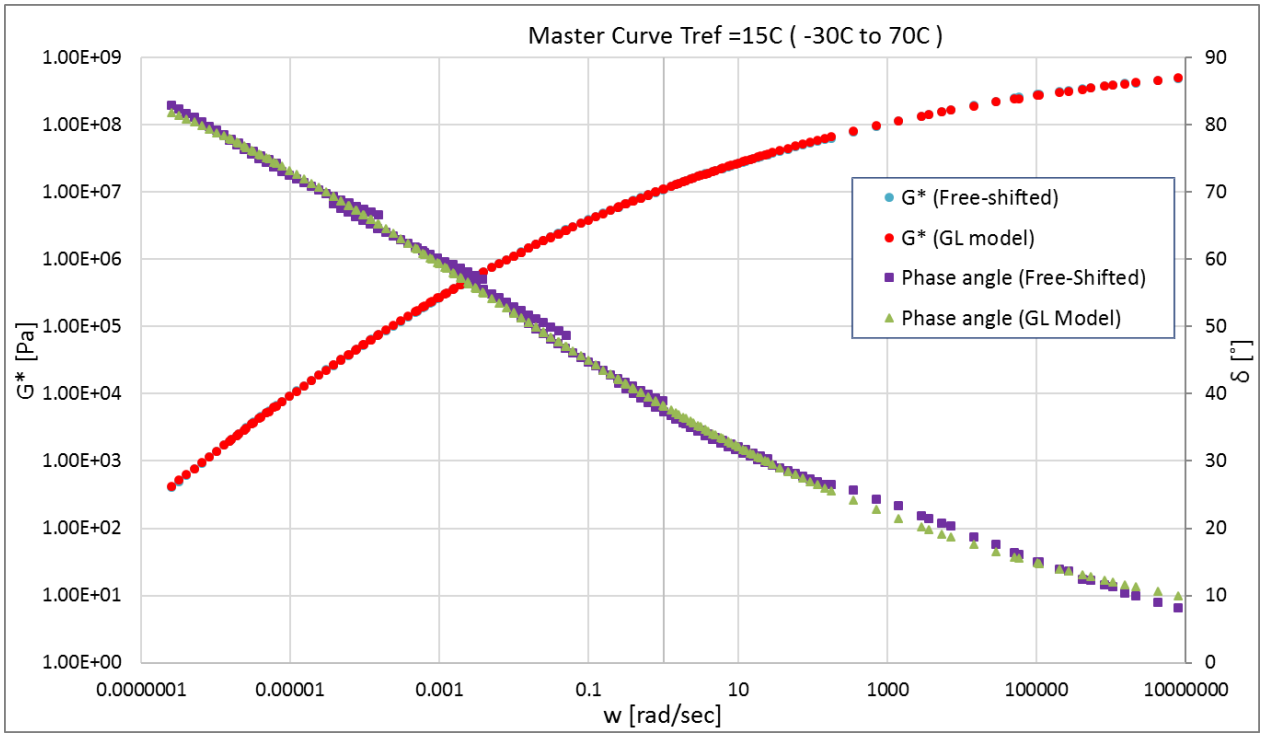

Rhea Discrete spectra		
Mode	gi, pa	li, sec
1	9.45E+04	3.91E-08
2	7.75E+04	2.72E-07
3	7.71E+04	1.36E-06
4	7.48E+04	6.47E-06
5	6.68E+04	2.92E-05
6	5.63E+04	1.29E-04
7	4.43E+04	5.71E-04
8	3.13E+04	2.49E-03
9	2.13E+04	1.05E-02
10	1.42E+04	4.49E-02
11	9.84E+03	1.80E-01
12	6.37E+03	7.81E-01
13	3.35E+03	3.46E+00
14	1.77E+03	1.54E+01
15	7.21E+02	7.04E+01
16	2.88E+02	2.89E+02
17	1.06E+02	1.29E+03
18	3.43E+01	5.64E+03
19	1.02E+01	2.48E+04
20	2.78E+00	1.15E+05
21	5.73E-01	6.30E+05
22	4.76E-02	1.91E+07
RMS error (%)	2.36%	

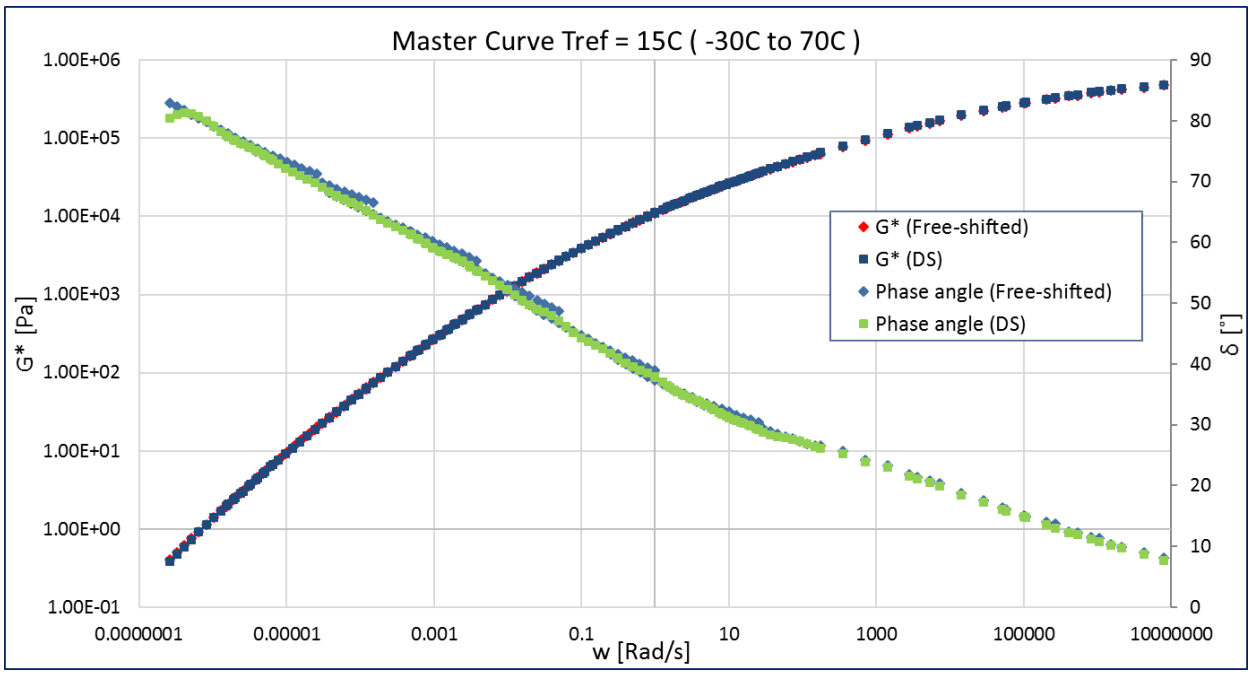

FT221 (S-E1 GP Colas)

Unaged:

	CA model parameters	
	G*	δ
Go (Pa)	1412155736.628	
wo	268.920	268.920
B	0.181	0.185
K	1	1
RMS error (Log)	0.0418	0.0516

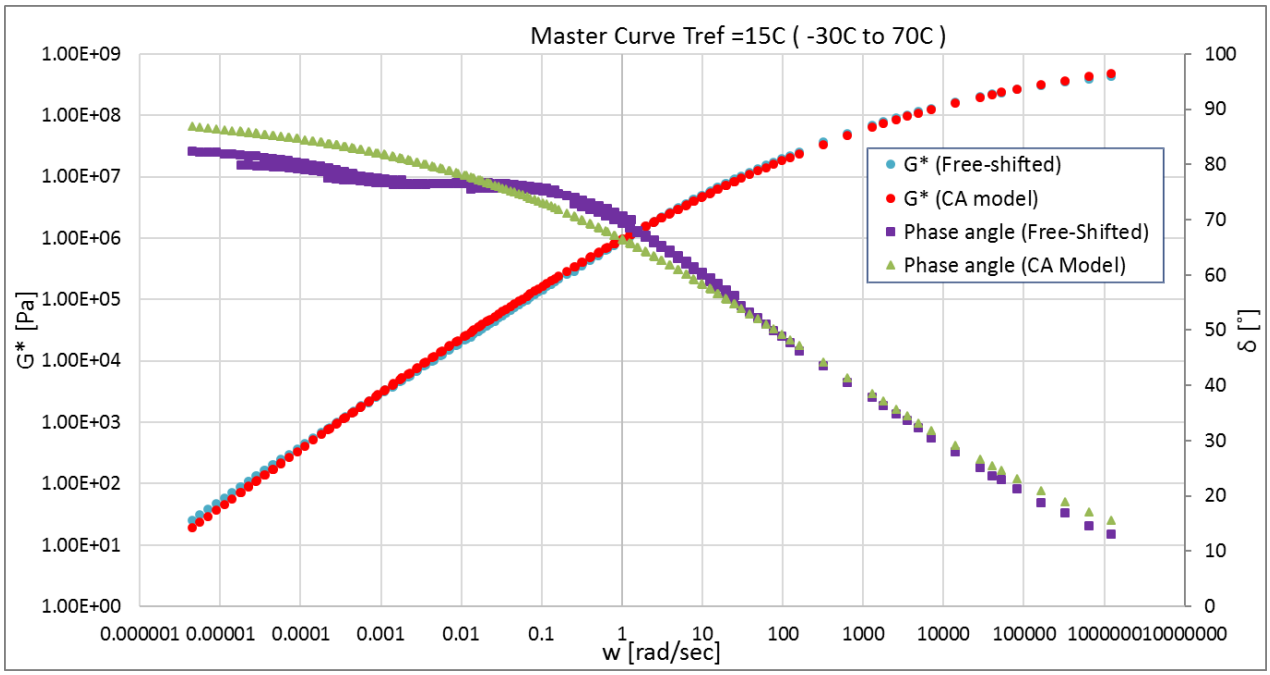

	CAM model parameters	
	G*	δ
Go (Pa)	1133559545.683	
wo	268.920	268.920
B	0.192	0.329
K	0.990	0.891
RMS error (Log)	0.0413	0.0319

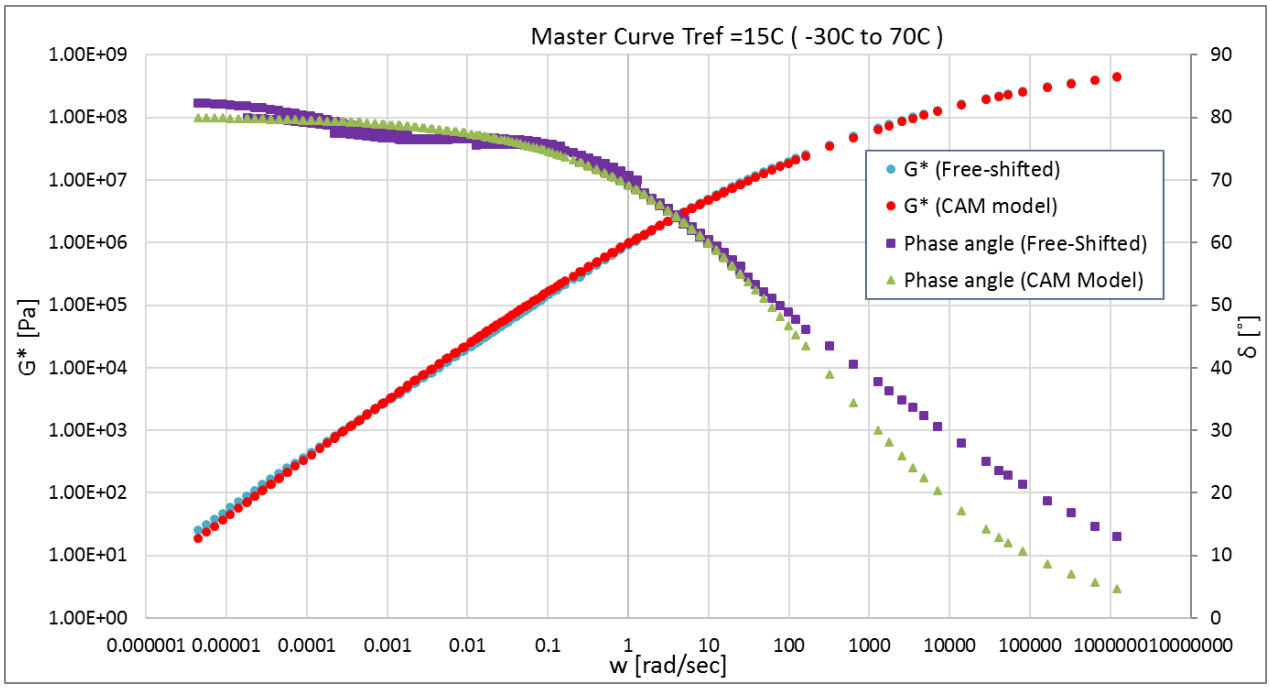

	GL model parameters	
	G*	δ
A	18.510	7.666
B	0.468	0.509
D	-12.557	
M	-2.405	-4.379
T	6.344	37.008
RMS error (Log)	0.0131	0.019

Annexure F: Mathematical model comparison

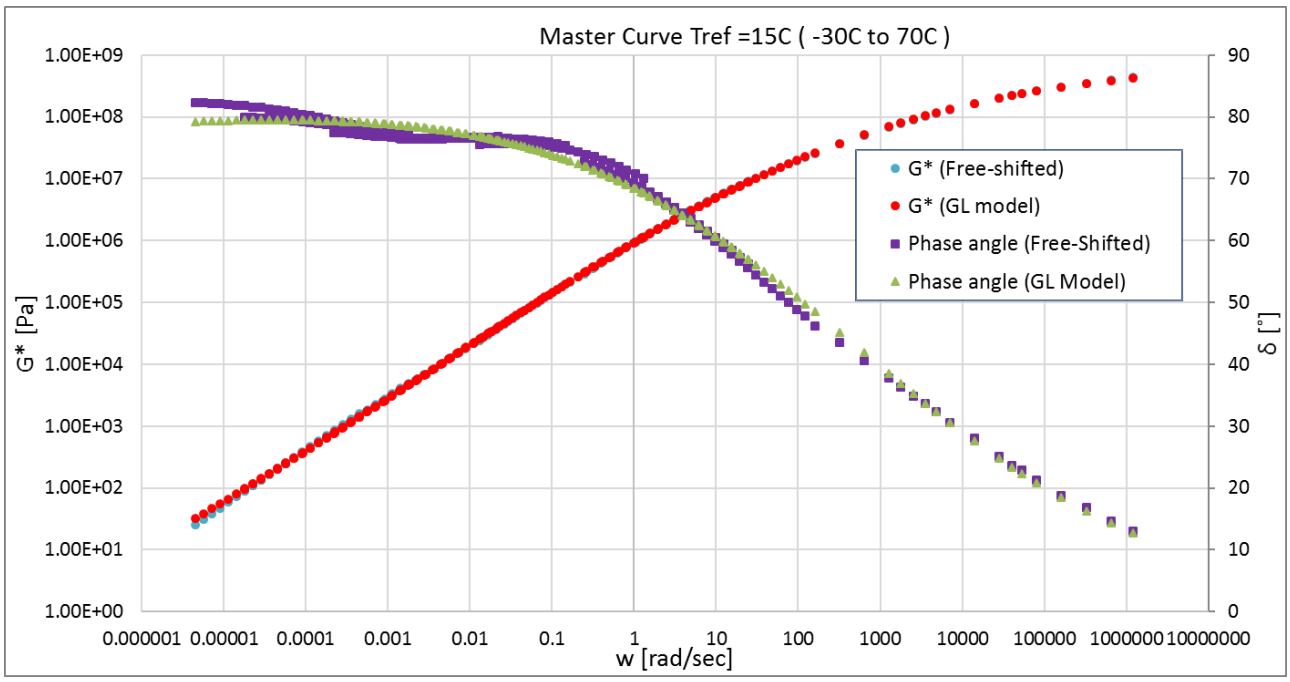

Rhea Discrete spectra		
Mode	gi, pa	li, sec
1	2.02E+05	5.16E-08
2	1.96E+05	3.61E-07
3	1.57E+05	5.27E-06
4	1.13E+05	4.51E-05
5	6.47E+04	3.25E-04
6	2.79E+04	1.93E-03
7	1.20E+04	9.12E-03
8	5.31E+03	4.16E-02
9	1.53E+03	2.76E-01
10	1.68E+02	2.81E+00
11	2.07E+01	1.90E+01
12	4.88E+00	1.08E+02
13	1.06E+00	6.80E+02
14	2.19E-01	4.54E+03
15	2.59E-02	5.44E+04
16	1.70E-04	1.42E+06
17		
18		
19		
20		
21		
22		
RMS error (%)	5.73%	

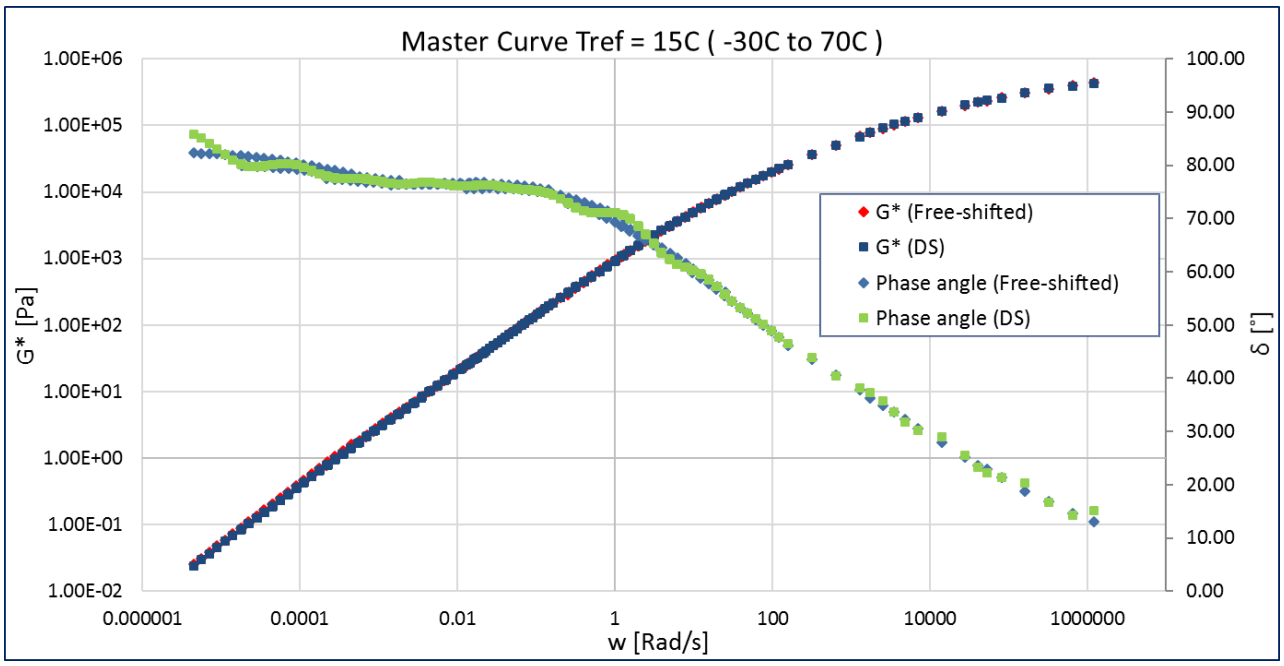

RTFO:

	CA model parameters	
	G*	δ
Go (Pa)	1094617317.336	
wo	186.139	186.139
B	0.187	0.192
K	1	1
RMS error (Log)	0.0388	0.0484

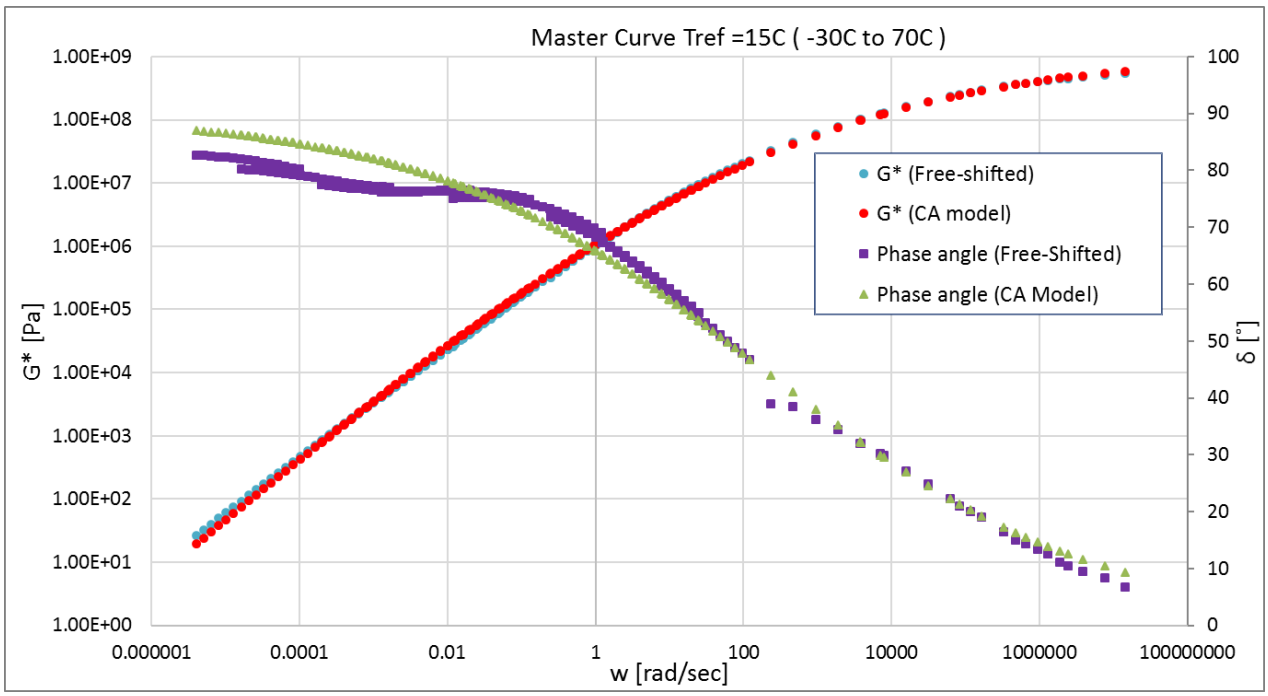

	CAM model parameters	
	G*	δ
Go (Pa)	1527371213.099	
wo	186.139	186.139
B	0.173	0.362
K	1.024	0.886
RMS error (Log)	0.0474	0.0400

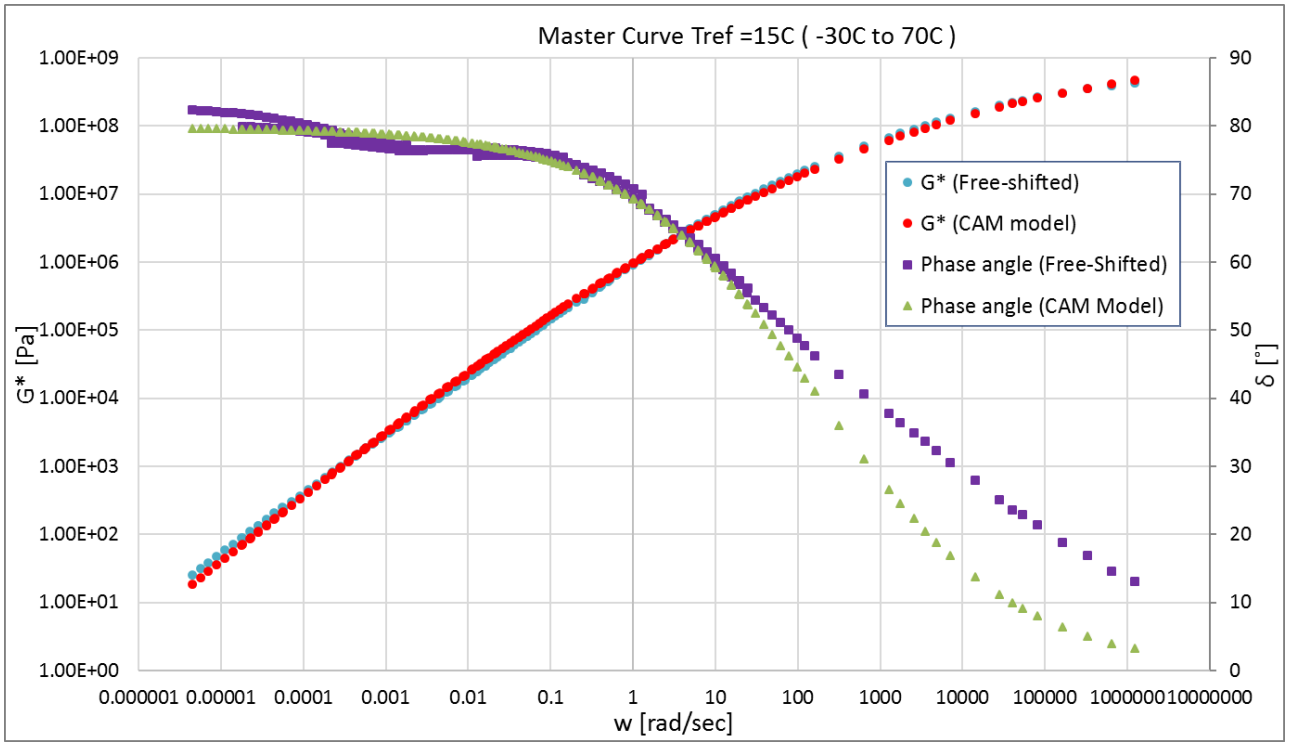

	GL model parameters	
	G*	δ
A	17.511	7.893
B	0.446	0.507
D	-11.553	
M	-2.577	-4.724
T	5.423	41.130
RMS error (Log)	0.0118	0.020

Annexure F: Mathematical model comparison

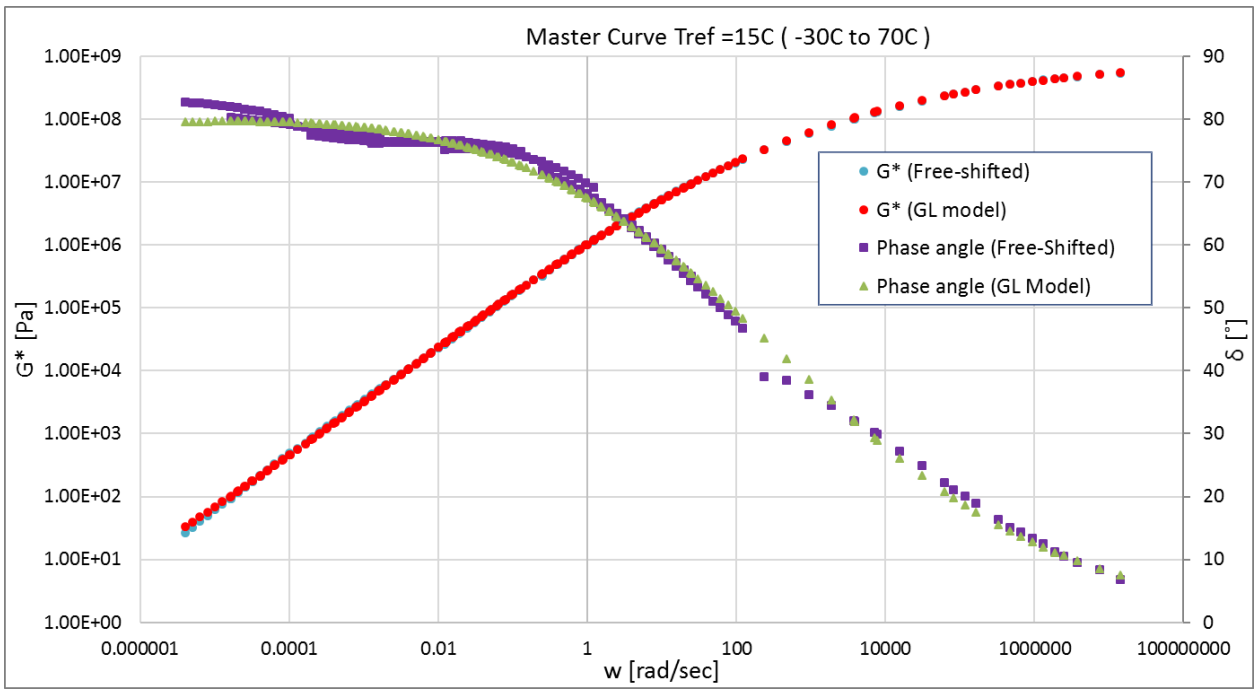

Rhea Discrete spectra		
Mode	gi, pa	li, sec
1	1.98E+05	1.94E-08
2	1.03E+05	3.71E-07
3	9.33E+04	1.84E-06
4	9.01E+04	7.25E-06
5	8.01E+04	2.90E-05
6	6.01E+04	1.20E-04
7	3.95E+04	5.12E-04
8	2.40E+04	2.35E-03
9	1.15E+04	1.09E-02
10	4.99E+03	5.12E-02
11	1.39E+03	2.72E-01
12	2.38E+02	1.40E+00
13	7.79E+01	5.62E+00
14	1.51E+01	3.34E+01
15	3.43E+00	1.84E+02
16	8.36E-01	1.06E+03
17	1.66E-01	6.77E+03
18	2.10E-02	5.45E+04
19	2.61E-03	2.06E+05
20		
21		
22		
RMS error (%)	4.37%	

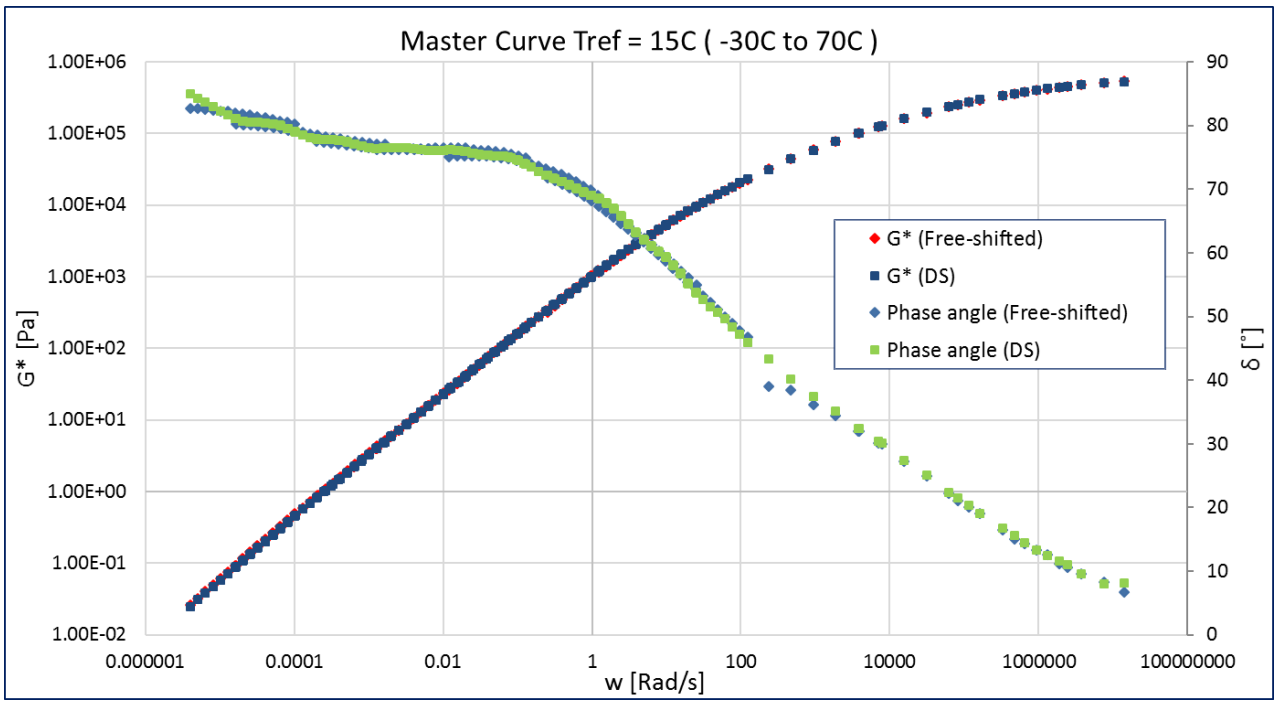

PAV1:

	CA model parameters	
	G*	δ
Go (Pa)	1026392476.627	
wo	5.569	5.569
B	0.156	0.159
K	1	1
RMS error (Log)	0.0111	0.0163

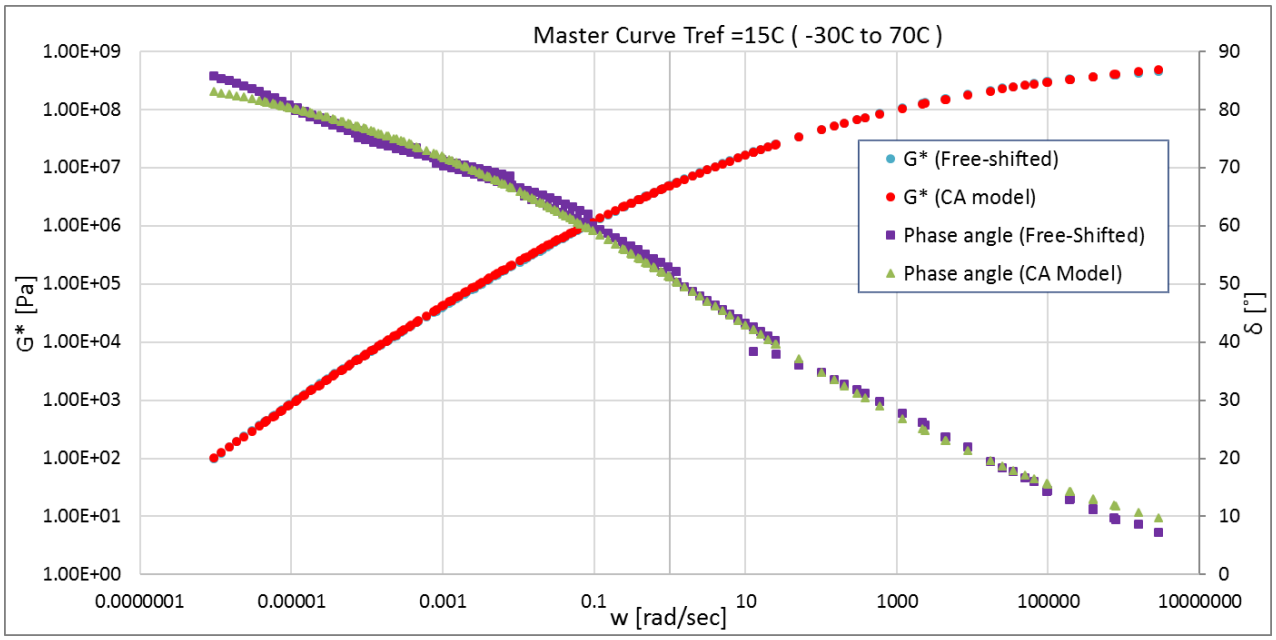

	CAM model parameters	
	G*	δ
Go (Pa)	1104591759.922	
wo	5.569	5.569
B	0.154	0.158
K	1.004	1.003
RMS error (Log)	0.0105	0.0162

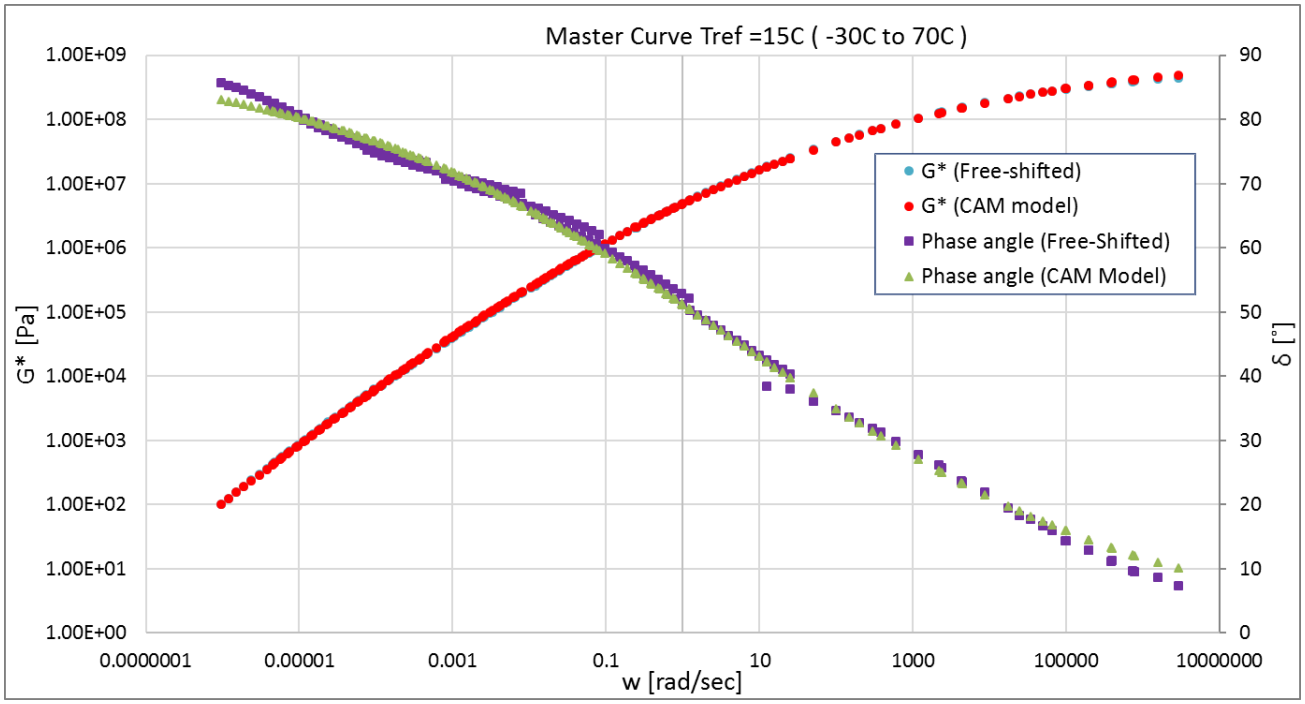

	GL model parameters	
	G*	δ
A	23.784	3.450
B	0.343	0.362
D	-17.742	
M	-5.649	-8.832
T	5.885	31.986
RMS error (Log)	0.0084	0.017

Annexure F: Mathematical model comparison

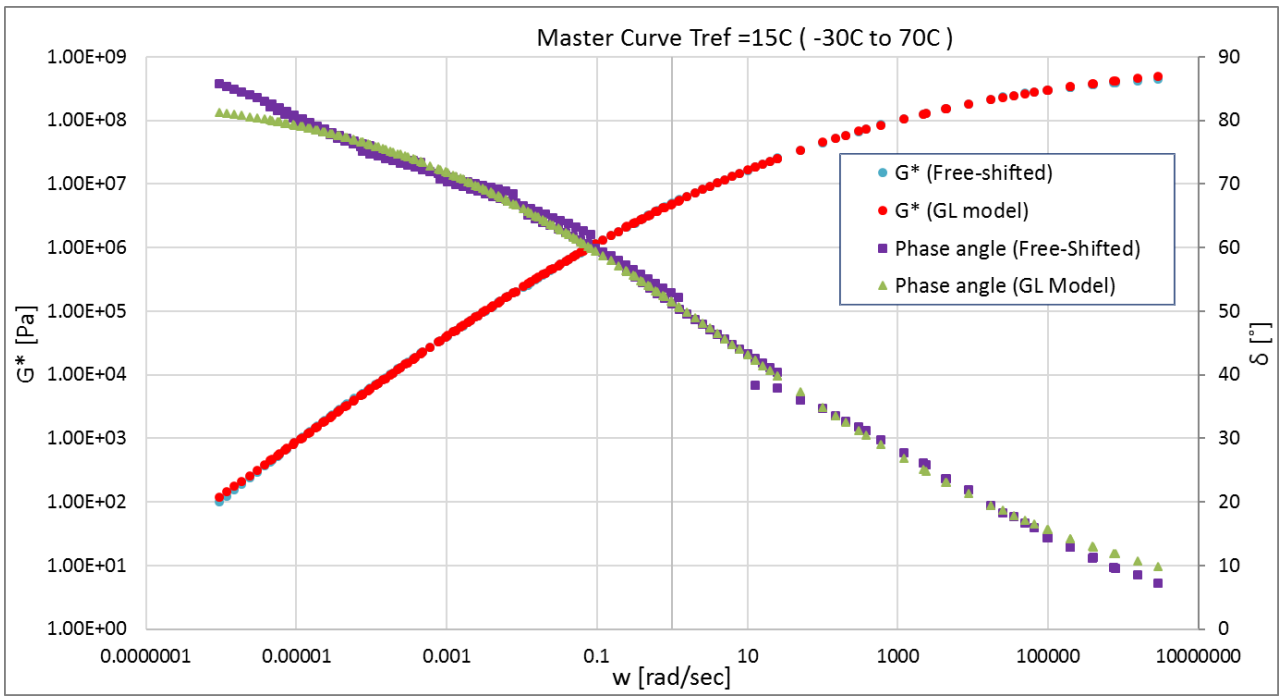

Rhea Discrete spectra		
Mode	gi, pa	li, sec
1	6.15E+04	2.74E-08
2	1.27E+05	1.17E-07
3	8.69E+04	1.70E-06
4	8.41E+04	9.64E-06
5	7.42E+04	4.50E-05
6	6.11E+04	1.93E-04
7	4.59E+04	8.13E-04
8	3.04E+04	3.41E-03
9	1.87E+04	1.45E-02
10	1.07E+04	5.80E-02
11	5.41E+03	2.31E-01
12	2.79E+03	8.48E-01
13	1.17E+03	4.05E+00
14	3.31E+02	1.89E+01
15	1.11E+02	9.37E+01
16	2.46E+01	5.67E+02
17	5.48E+00	3.54E+03
18	8.97E-01	2.49E+04
19	1.11E-01	1.66E+05
20	5.80E-03	4.09E+06
21		
22		
RMS error (%)	2.50%	

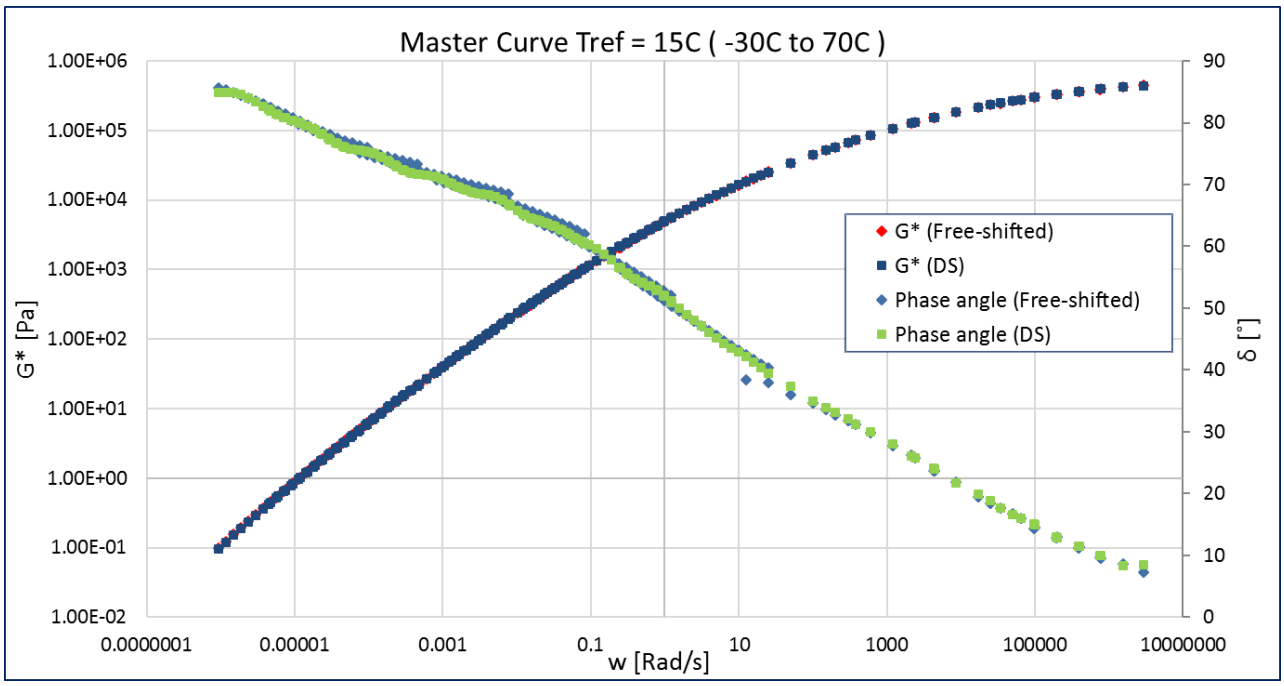

PAV2:

	CA model parameters	
	G*	δ
Go (Pa)	1020169453.095	
wo	3.523	3.523
B	0.152	0.155
K	1	1
RMS error (Log)	0.0066	0.0139

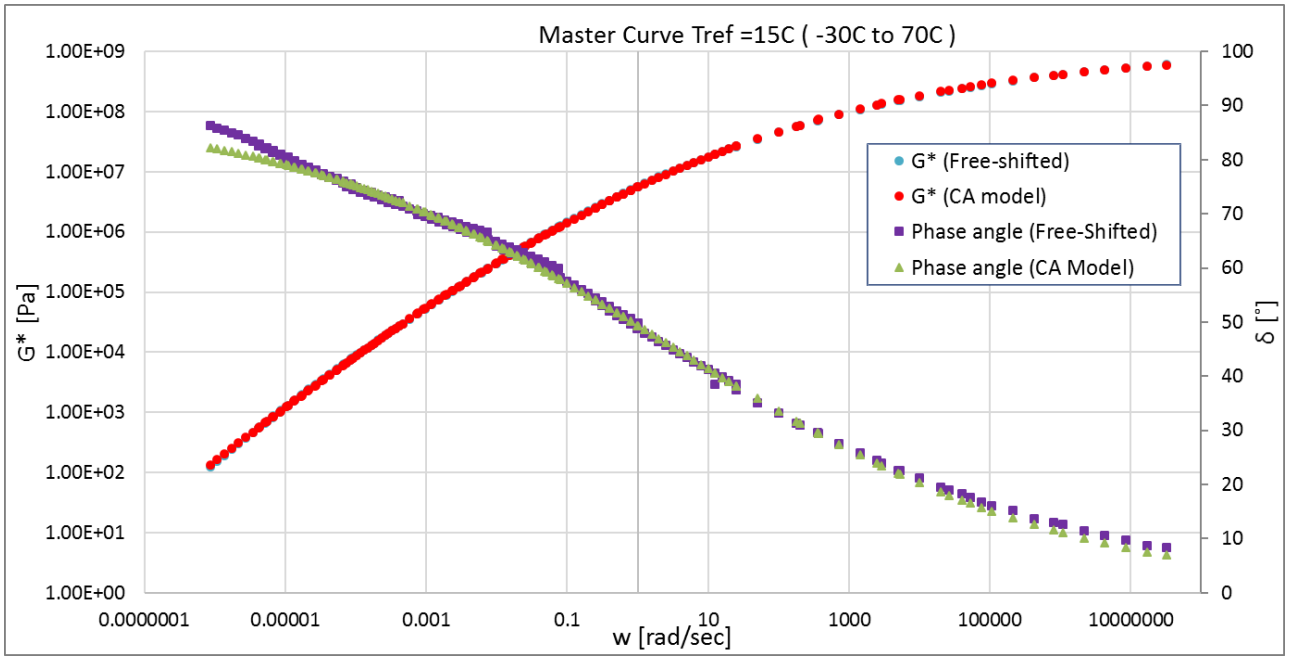

	CAM model parameters	
	G*	δ
Go (Pa)	980863202.834	
wo	3.523	3.523
B	0.153	0.151
K	0.998	1.009
RMS error (Log)	0.0064	0.0131

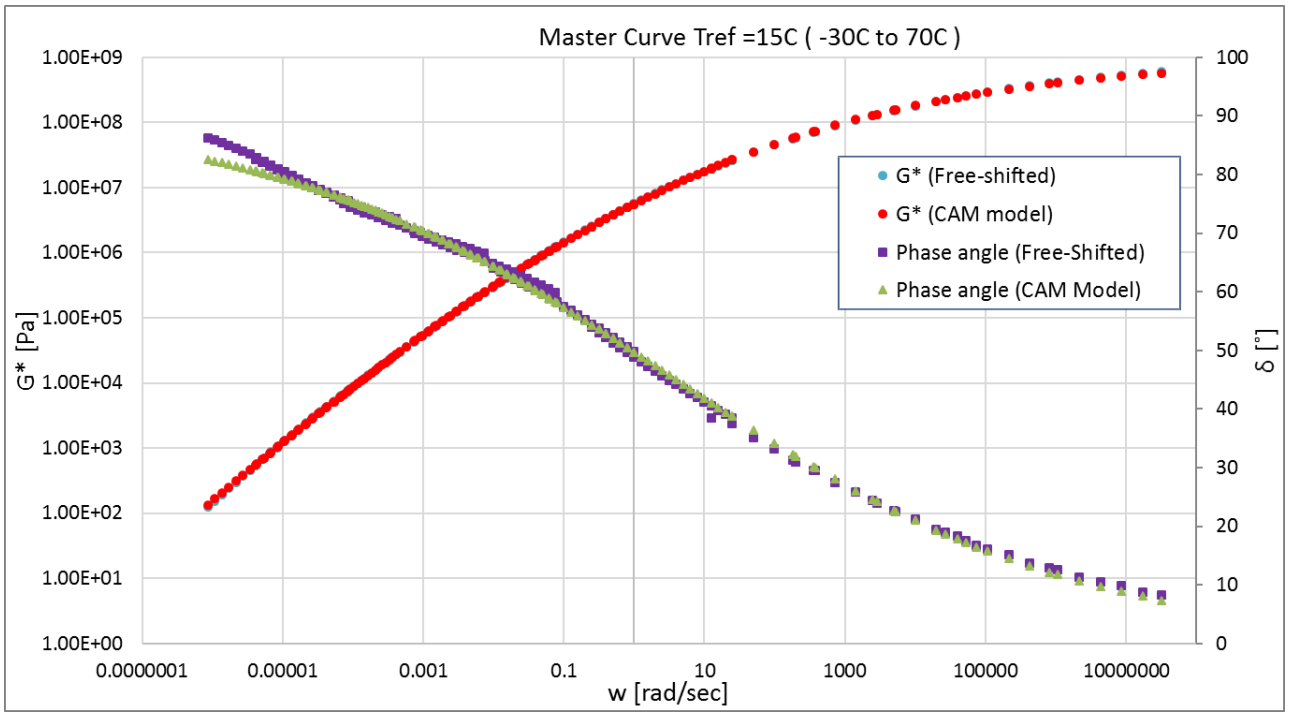

	GL model parameters	
	G*	δ
A	12.103	4.348
B	0.285	0.322
D	-5.966	
M	-4.906	-12.057
T	1.067	51.296
RMS error (Log)	0.0084	0.018

Annexure F: Mathematical model comparison

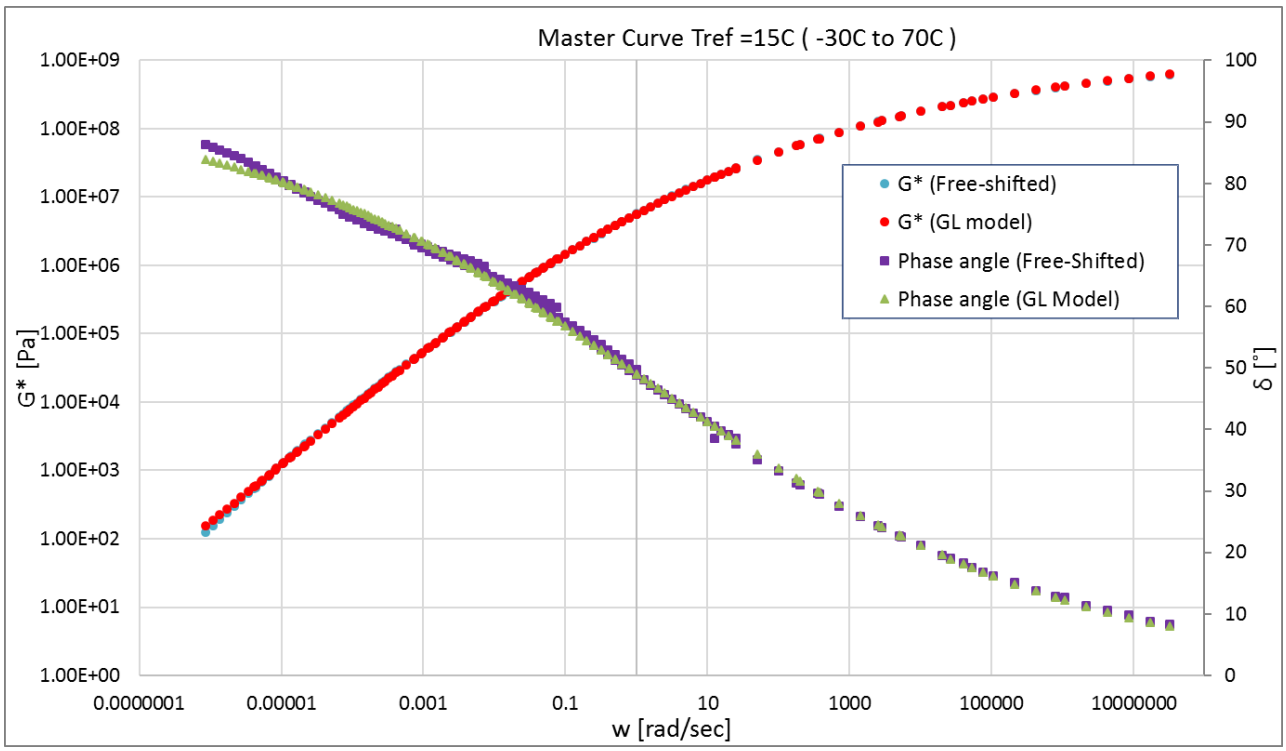

Rhea Discrete spectra		
Mode	gi, pa	li, sec
1	9.85E+04	2.39E-07
2	9.94E+04	1.18E-06
3	1.03E+05	6.88E-06
4	7.49E+04	3.86E-05
5	5.47E+04	1.83E-04
6	4.03E+04	7.94E-04
7	2.75E+04	3.44E-03
8	1.87E+04	1.35E-02
9	1.18E+04	5.42E-02
10	6.35E+03	2.17E-01
11	3.70E+03	8.54E-01
12	1.50E+03	4.52E+00
13	4.34E+02	2.29E+01
14	1.39E+02	1.15E+02
15	3.31E+01	6.60E+02
16	7.90E+00	3.79E+03
17	1.37E+00	2.43E+04
18	1.93E-01	1.49E+05
19	8.60E-03	3.01E+06
20	1.39E+05	4.04E-08
21		
22		
RMS error (%)	2.09%	

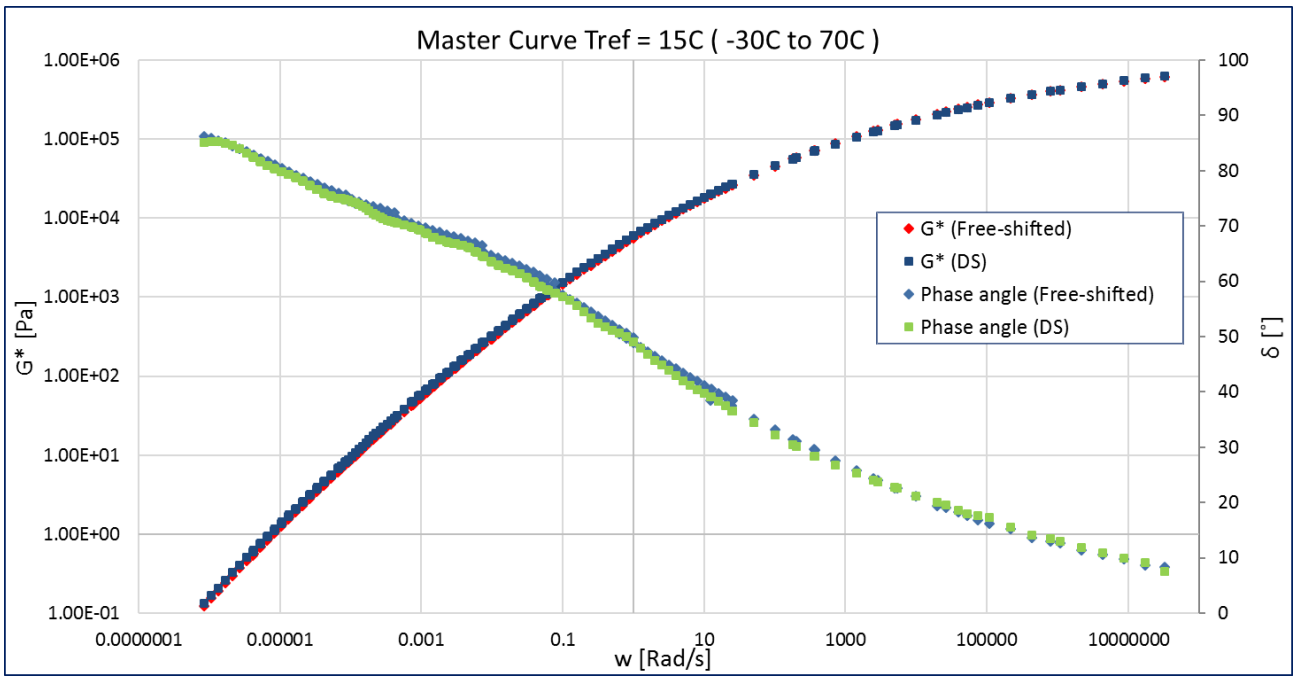

PAV4:

	CA model parameters	
	G*	δ
Go (Pa)	1011864095.070	
wo	3.064	3.064
B	0.152	0.154
K	1	1
RMS error (Log)	0.0090	0.0291

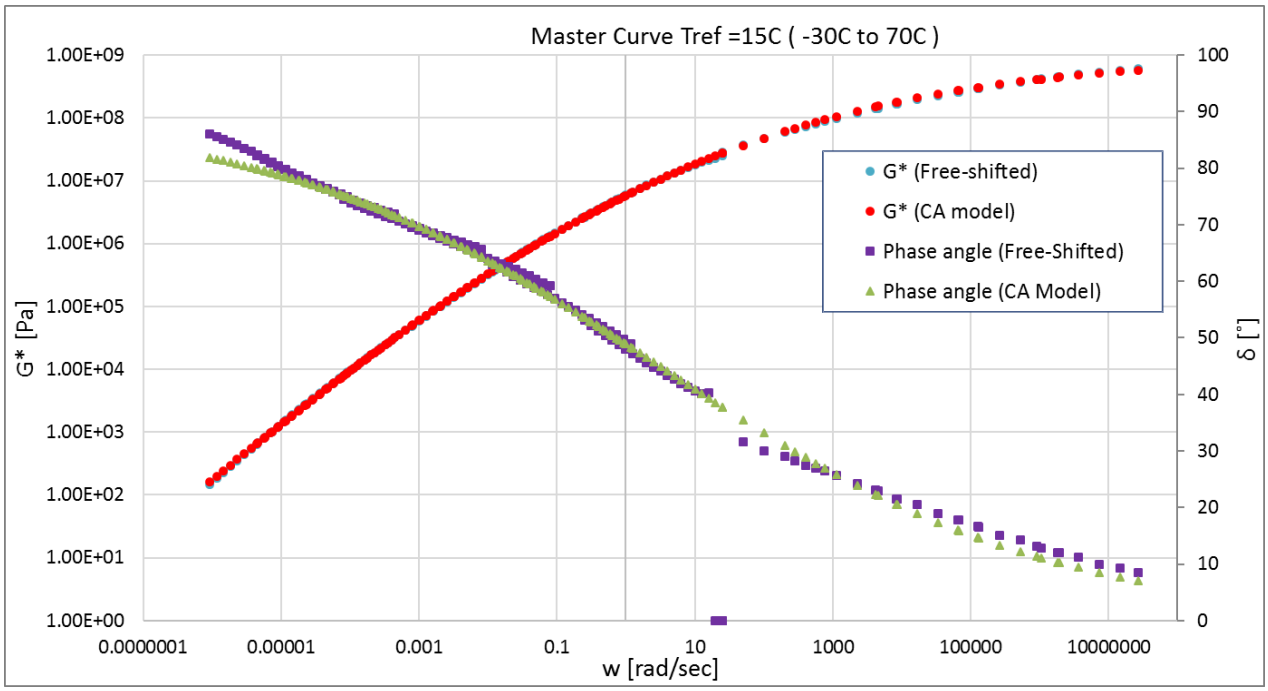

	CAM model parameters	
	G*	δ
Go (Pa)	976578266.114	
wo	3.064	3.064
B	0.152	0.148
K	0.998	1.011
RMS error (Log)	0.0089	0.0283

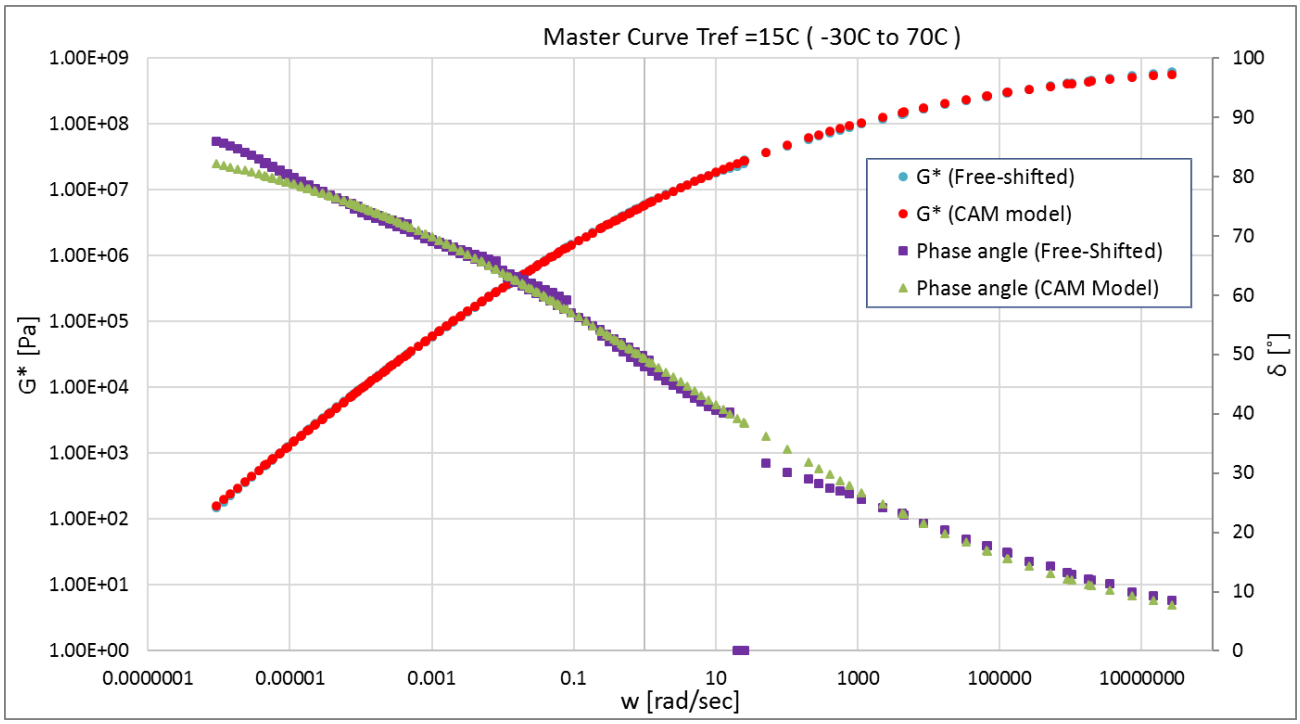

	GL model parameters	
	G*	δ
A	10.233	2.024
B	0.262	0.302
D	-4.036	
M	-4.789	-10.055
T	0.348	19.822
RMS error (Log)	0.0107	0.026

Annexure F: Mathematical model comparison

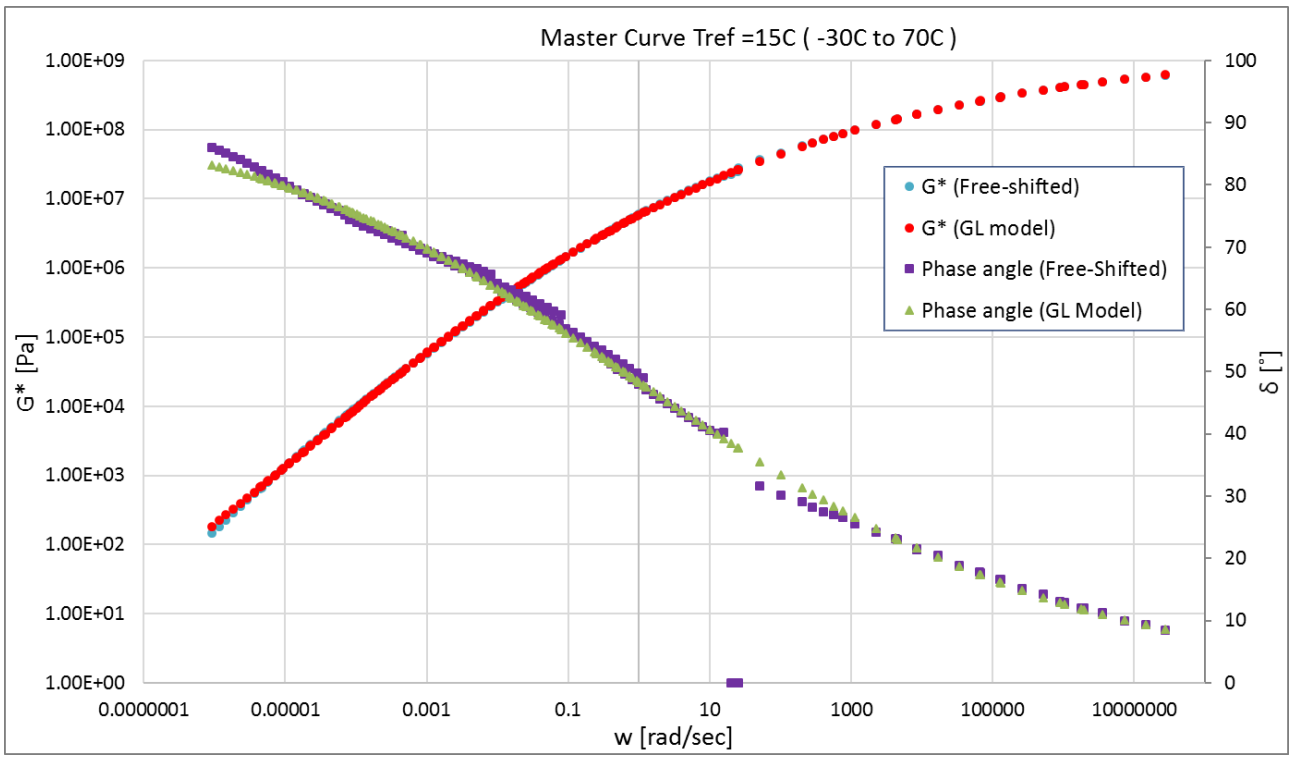

Rhea Discrete spectra		
Mode	gi, pa	li, sec
1	1.32E+05	3.07E-08
2	9.54E+04	1.88E-07
3	9.20E+04	9.24E-07
4	8.54E+04	4.43E-06
5	7.83E+04	2.11E-05
6	6.58E+04	1.04E-04
7	4.98E+04	5.00E-04
8	3.56E+04	2.43E-03
9	2.22E+04	1.19E-02
10	1.26E+04	5.55E-02
11	6.33E+03	2.56E-01
12	2.87E+03	1.11E+00
13	1.20E+03	5.13E+00
14	3.61E+02	2.27E+01
15	1.34E+02	9.37E+01
16	3.93E+01	4.77E+02
17	9.42E+00	3.21E+03
18	1.23E+00	2.52E+04
19	1.51E-01	1.61E+05
20	6.47E-03	3.07E+06
21		
22		
RMS error (%)	2.14%	

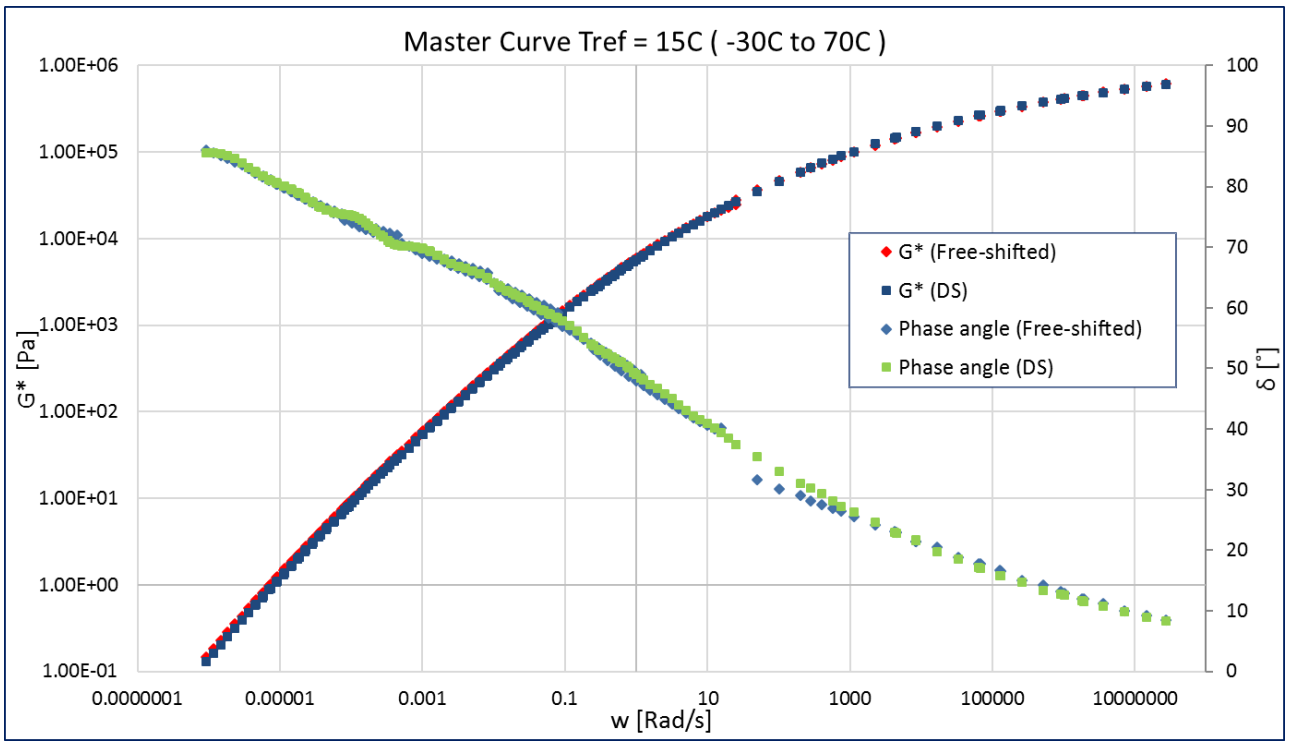

FT222 (S-E1 GP Tosas)

Unaged:

	CA model parameters	
	G*	δ
Go (Pa)	2018331960.808	
wo	25.672	25.672
B	0.137	0.149
K	1	1
RMS error (Log)	0.0264	0.0484

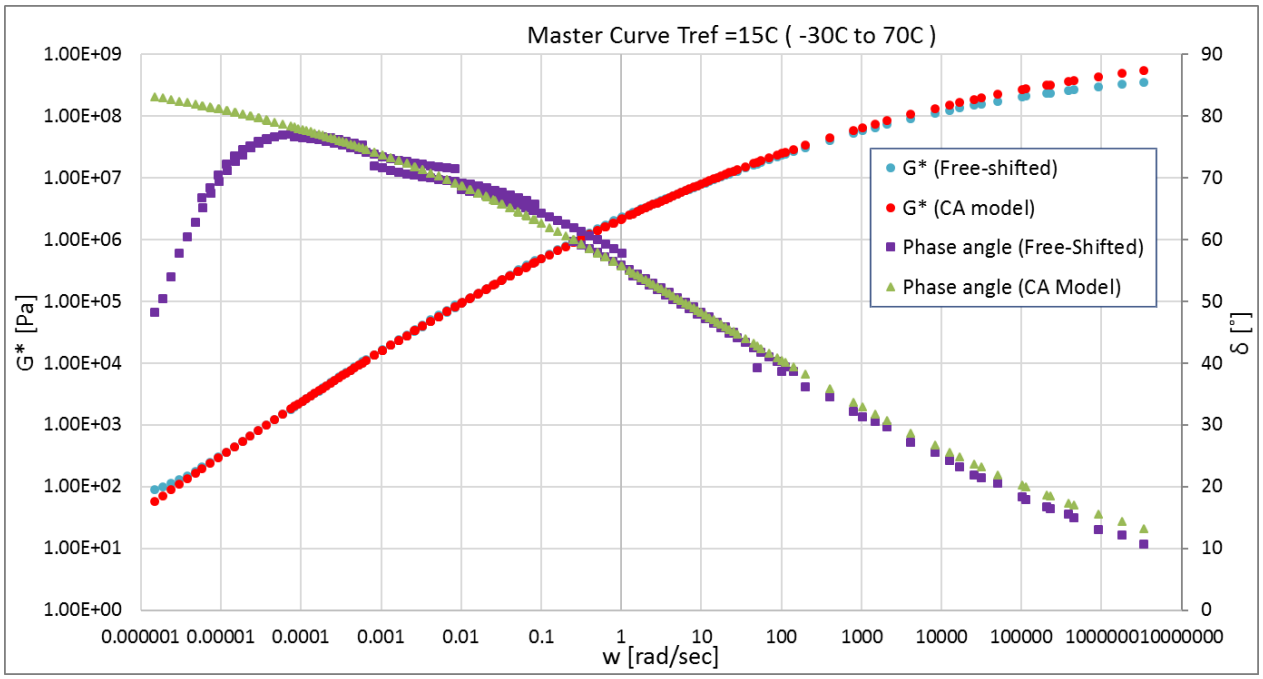

	CAM model parameters	
	G*	δ
Go (Pa)	850332604.242	
wo	25.672	25.672
B	0.159	0.160
K	0.965	0.980
RMS error (Log)	0.0105	0.0441

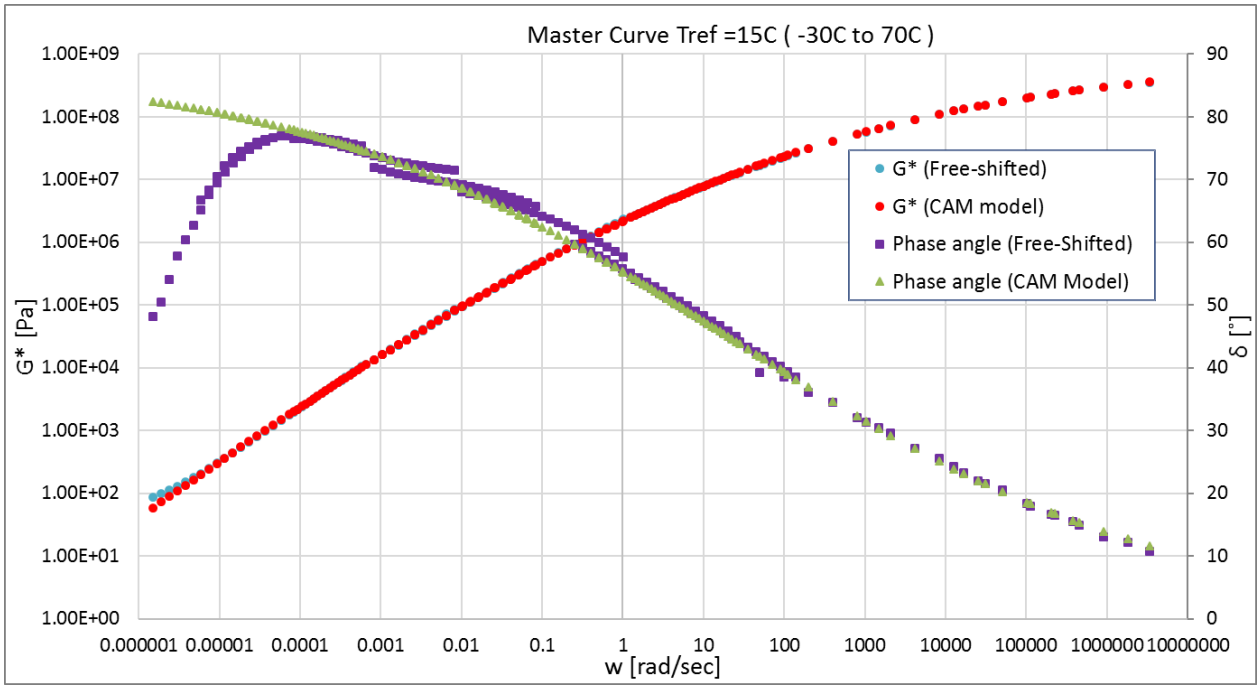

	GL model parameters	
	G*	δ
A	24.398	3.525
B	0.318	0.373
D	-18.365	0.000
M	-5.719	-7.486
T	5.316	28.601
RMS error (Log)	0.0067	0.016

Annexure F: Mathematical model comparison

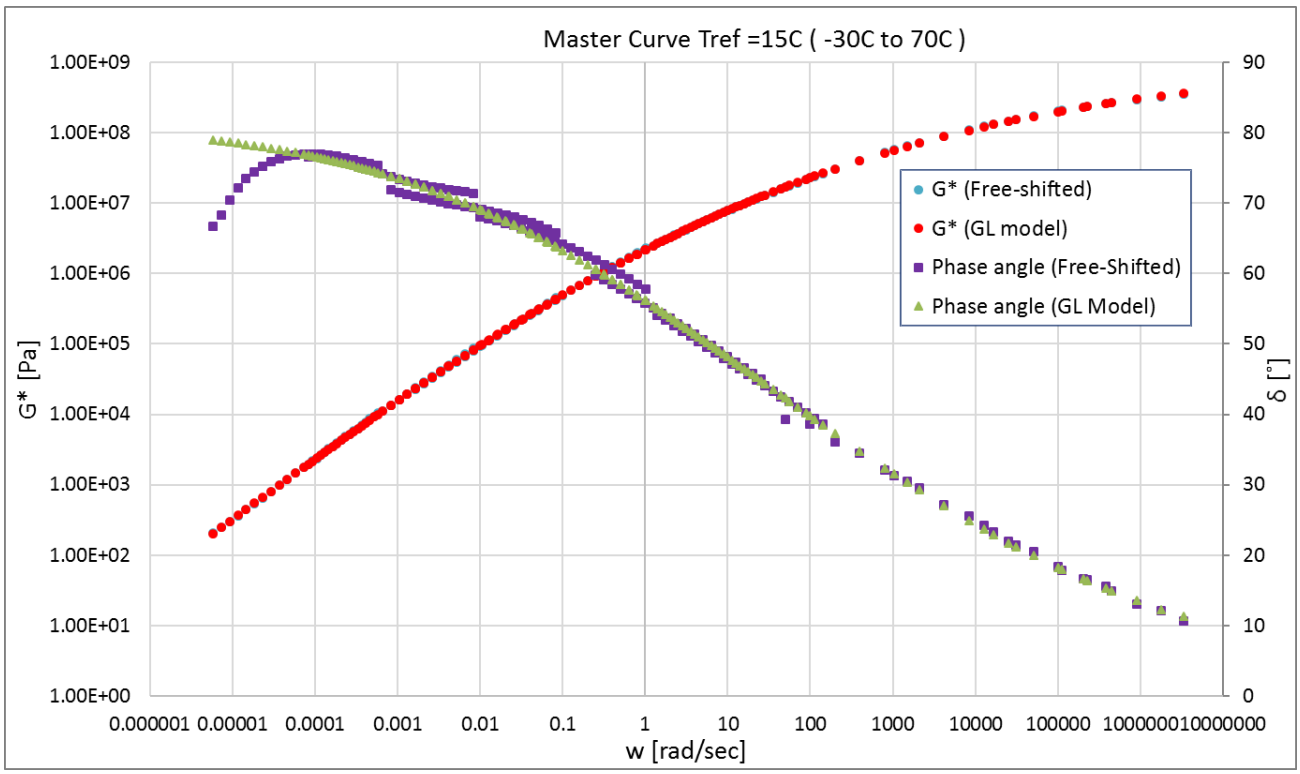

Rhea Discrete spectra		
Mode	gi, pa	li, sec
1	1.05E+05	3.04E-07
2	8.11E+04	2.12E-06
3	7.25E+04	1.24E-05
4	5.78E+04	7.00E-05
5	4.11E+04	3.99E-04
6	2.42E+04	2.29E-03
7	1.26E+04	1.31E-02
8	5.99E+03	7.67E-02
9	2.25E+03	4.69E-01
10	6.38E+02	2.92E+00
11	1.71E+02	1.61E+01
12	3.96E+01	1.11E+02
13	7.74E+00	8.28E+02
14	8.38E-01	9.12E+03
15	8.63E-02	9.46E+04
16	3.28E-02	1.29E+06
17		
18		
19		
20		
21		
22		
RMS error (%)	4.57%	

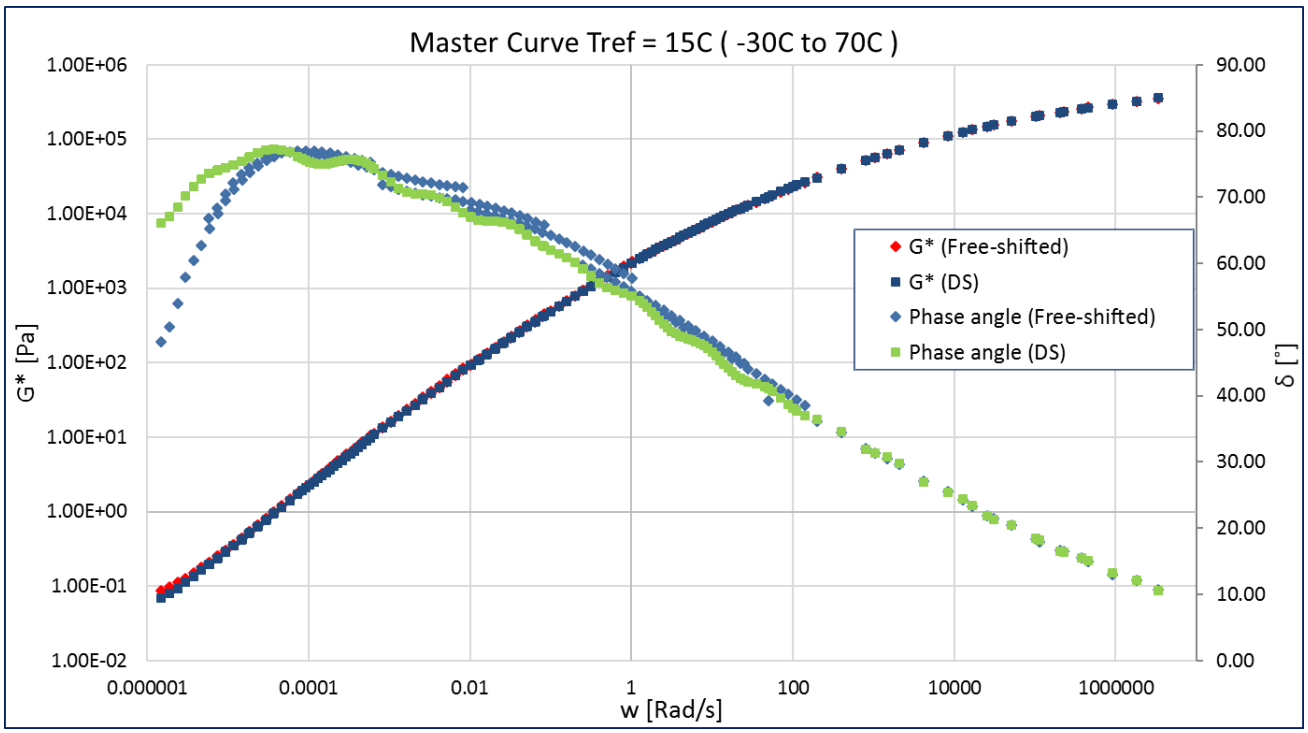

RTFO:

	CA model parameters	
	G*	δ
Go (Pa)	949004842.695	
wo	19.900	19.900
B	0.152	0.164
K	1	1
RMS error (Log)	0.0121	0.0280

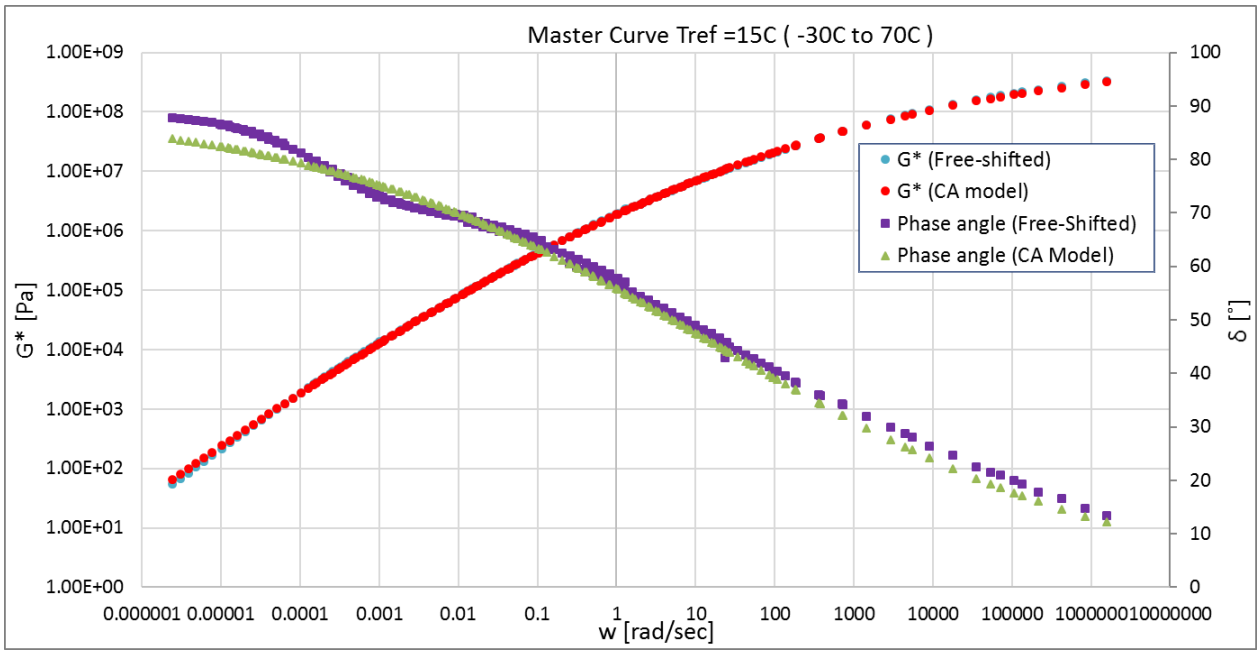

	CAM model parameters	
	G*	δ
Go (Pa)	1088296565.443	
wo	19.900	19.900
B	0.148	0.151
K	1.006	1.027
RMS error (Log)	0.0112	0.0194

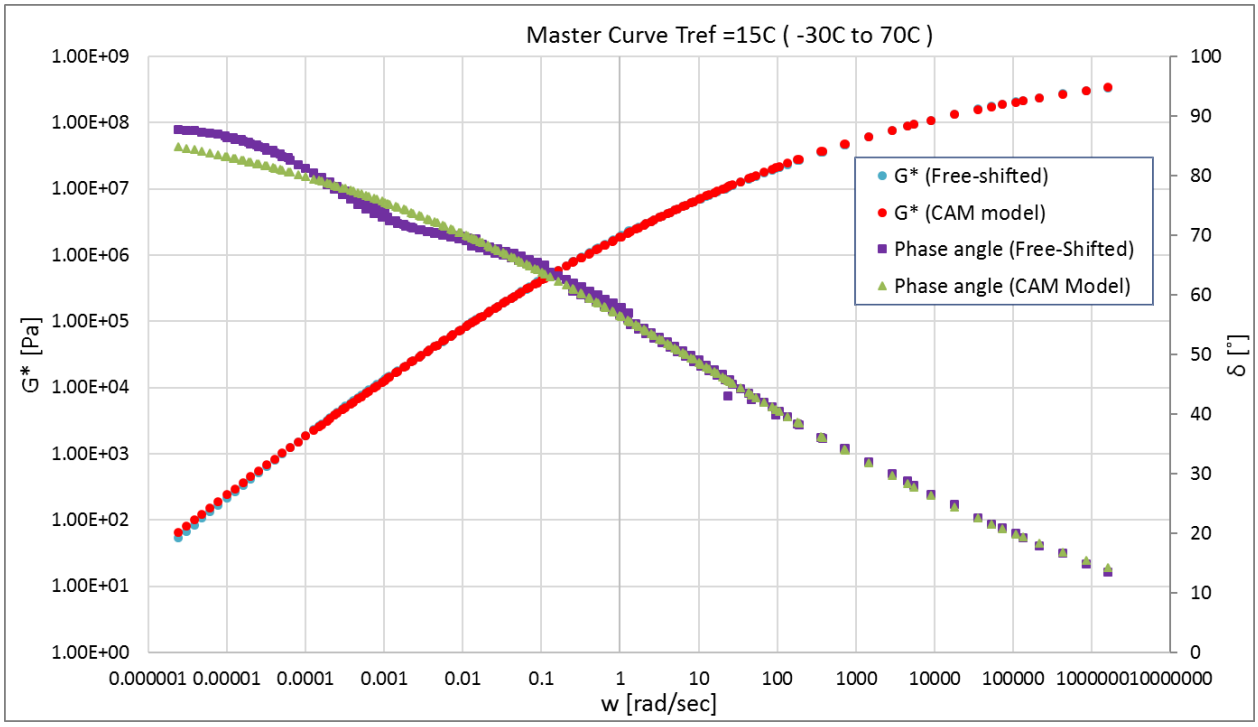

	GL model parameters	
	G*	δ
A	26.400	3.646
B	0.298	0.336
D	-20.242	0.000
M	-6.187	-9.292
T	5.186	34.413
RMS error (Log)	0.0078	0.016

Annexure F: Mathematical model comparison

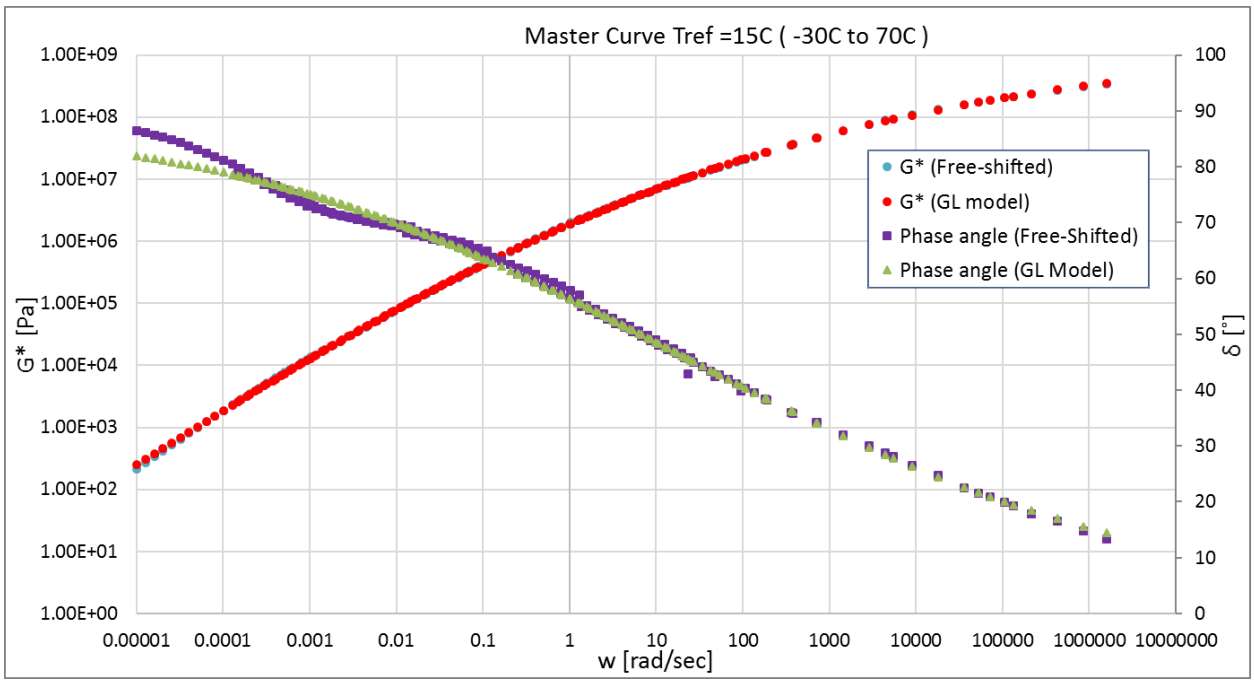

Rhea Discrete spectra		
Mode	gi, pa	li, sec
1	2.93E+05	5.44E-09
2	8.55E+04	1.17E-07
3	8.82E+04	8.06E-07
4	6.58E+04	3.47E-06
5	5.61E+04	1.25E-05
6	4.61E+04	4.32E-05
7	3.71E+04	1.48E-04
8	2.73E+04	5.23E-04
9	1.83E+04	1.87E-03
10	1.16E+04	6.85E-03
11	6.41E+03	2.48E-02
12	3.47E+03	8.78E-02
13	1.84E+03	3.47E-01
14	6.53E+02	1.33E+00
15	3.05E+02	4.80E+00
16	8.69E+01	2.23E+01
17	2.80E+01	1.05E+02
18	6.67E+00	5.21E+02
19	1.14E+00	2.57E+03
20	7.18E-02	1.87E+04
21	1.31E-03	2.89E+06
22		
RMS error (%)	4.42%	

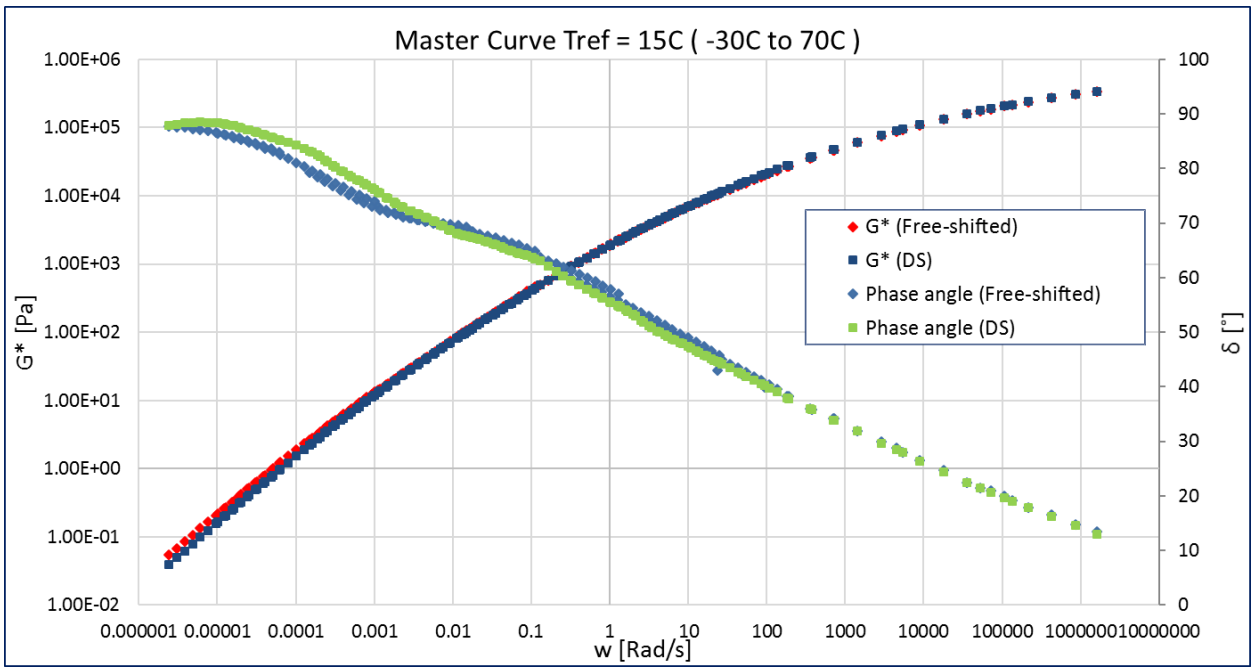

PAV1:

	CA model parameters	
	G*	δ
Go (Pa)	986689807.298	
wo	1.424	1.424
B	0.136	0.140
K	1	1
RMS error (Log)	0.0114	0.0210

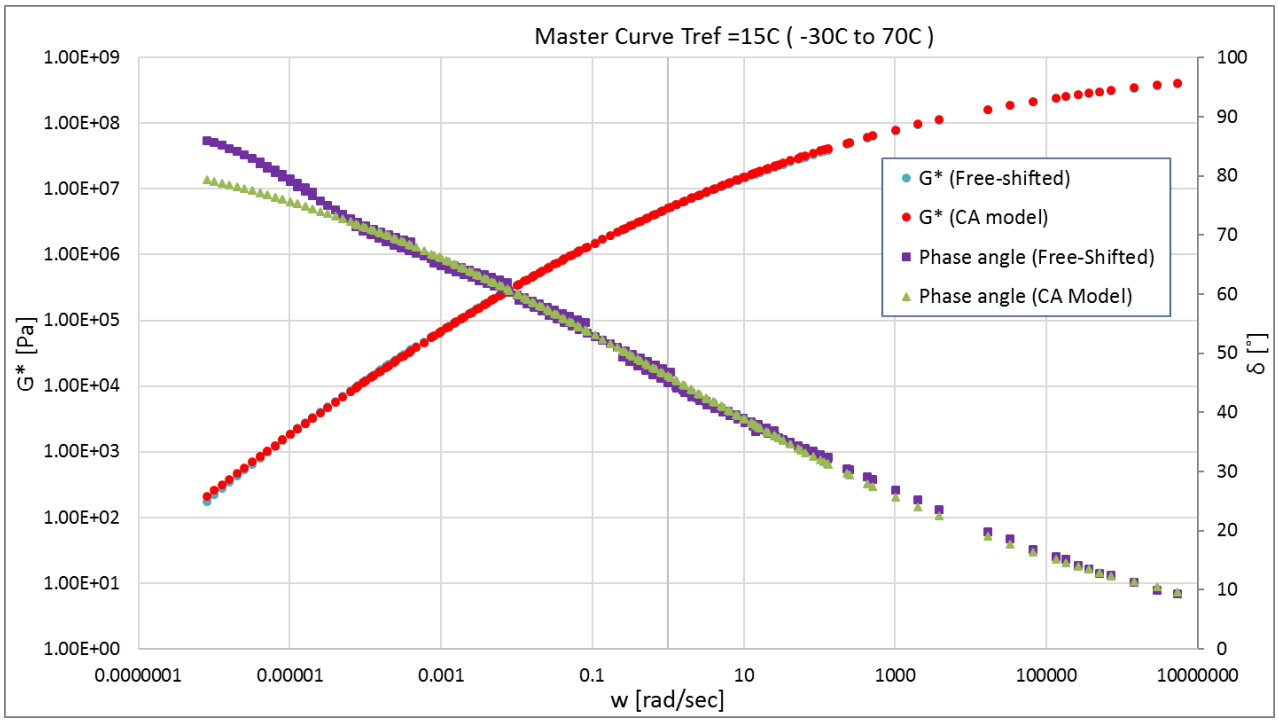

	CAM model parameters	
	G*	δ
Go (Pa)	946833039.774	
wo	1.424	1.424
B	0.136	0.139
K	0.995	1.003
RMS error (Log)	0.0095	0.0208

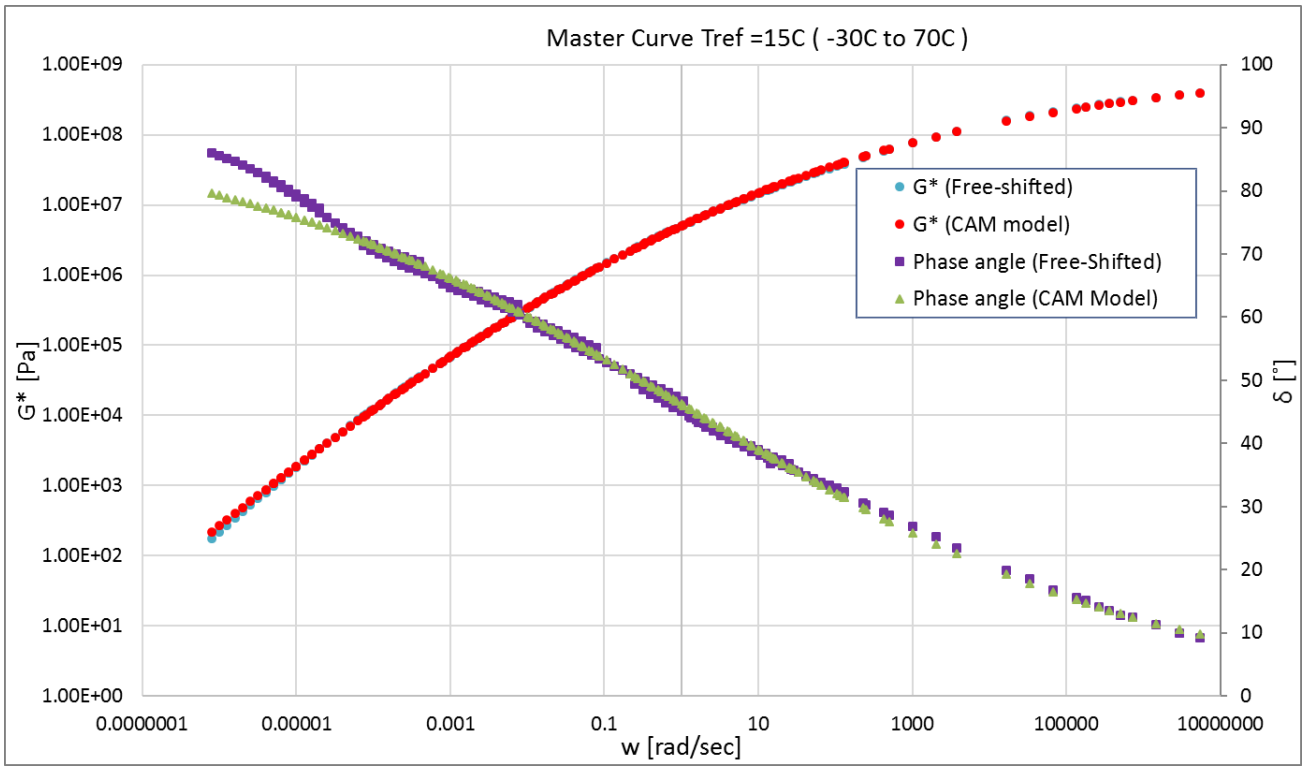

	GL model parameters	
	G*	δ
A	25.388	3.302
B	0.276	0.282
D	-19.312	0.000
M	-7.579	-13.864
T	4.478	43.955
RMS error (Log)	0.0052	0.013

Annexure F: Mathematical model comparison

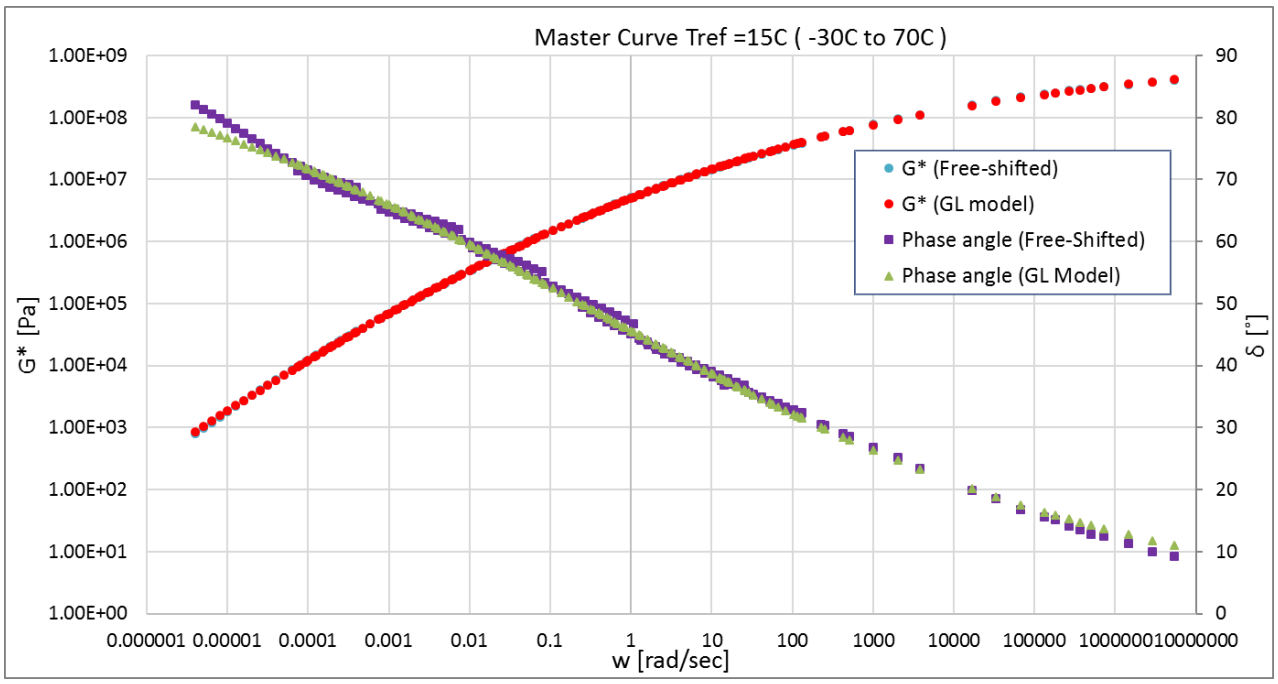

Rhea Discrete spectra		
Mode	gi, pa	li, sec
1	9.13E+04	1.42E-08
2	7.94E+04	8.87E-08
3	7.03E+04	5.82E-07
4	6.63E+04	2.73E-06
5	6.18E+04	1.23E-05
6	5.37E+04	5.34E-05
7	4.36E+04	2.32E-04
8	3.23E+04	1.01E-03
9	2.21E+04	4.45E-03
10	1.39E+04	2.01E-02
11	8.03E+03	9.13E-02
12	4.34E+03	4.37E-01
13	1.90E+03	2.07E+00
14	8.28E+02	9.80E+00
15	2.72E+02	5.04E+01
16	8.74E+01	2.34E+02
17	2.52E+01	1.12E+03
18	8.42E+00	4.85E+03
19	1.93E+00	2.45E+04
20	3.23E-01	1.36E+05
21	1.22E-02	9.27E+06
22		
RMS error (%)	3.08%	

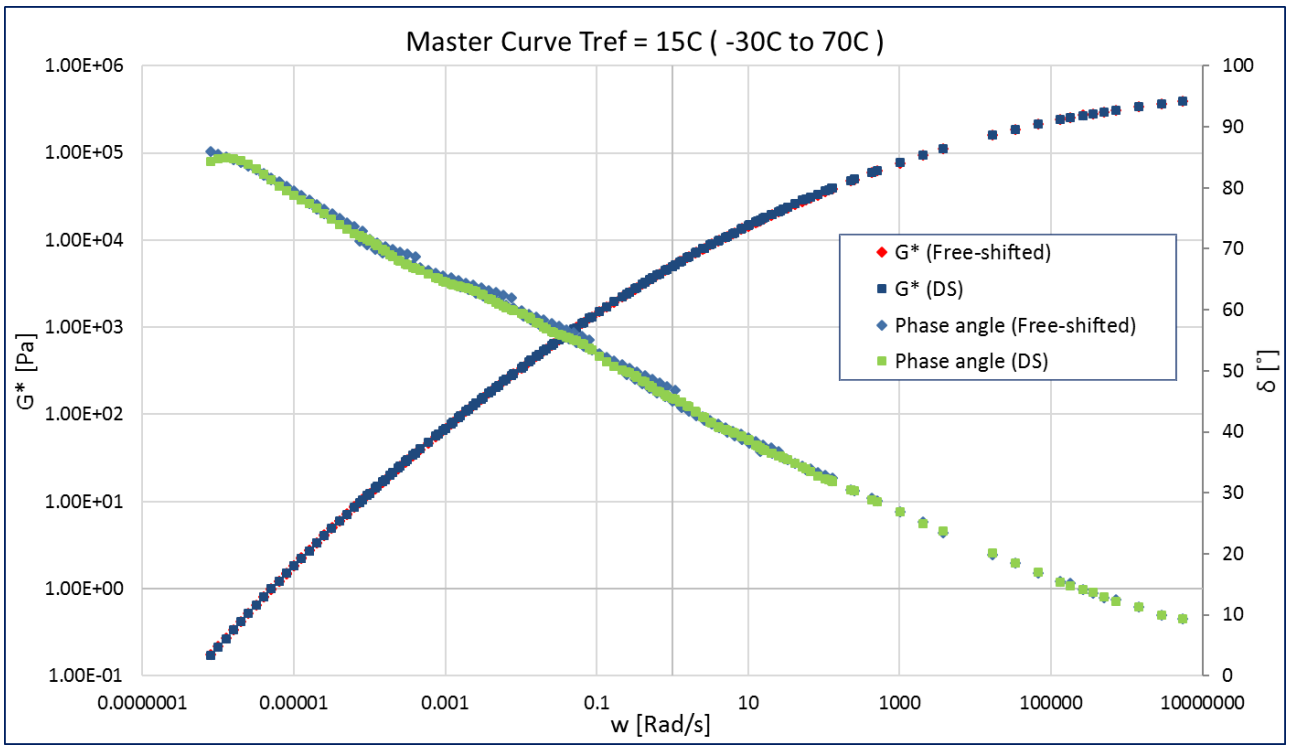

PAV2:

	CA model parameters	
	G*	δ
Go (Pa)	1034531044.257	
wo	0.396	0.396
B	0.129	0.132
K	1	1
RMS error (Log)	0.0188	0.0279

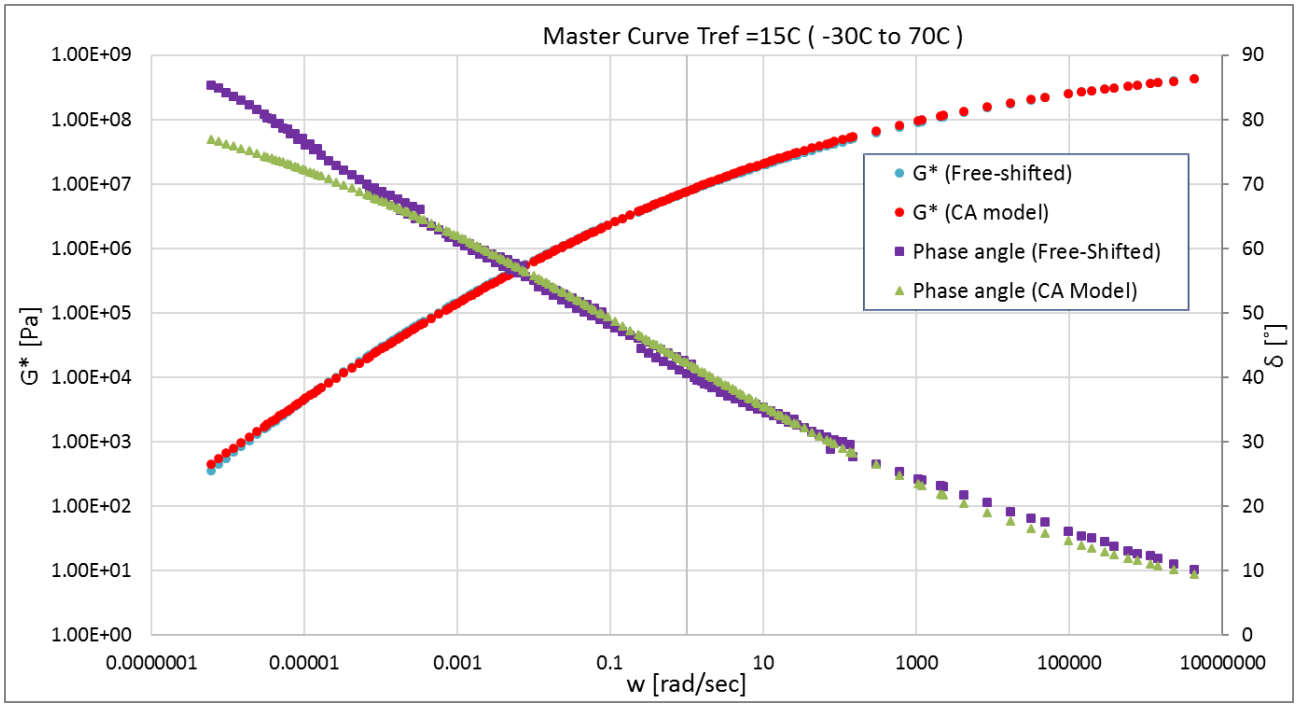

	CAM model parameters	
	G*	δ
Go (Pa)	948251163.325	
wo	0.396	0.396
B	0.130	0.133
K	0.990	0.999
RMS error (Log)	0.0169	0.0279

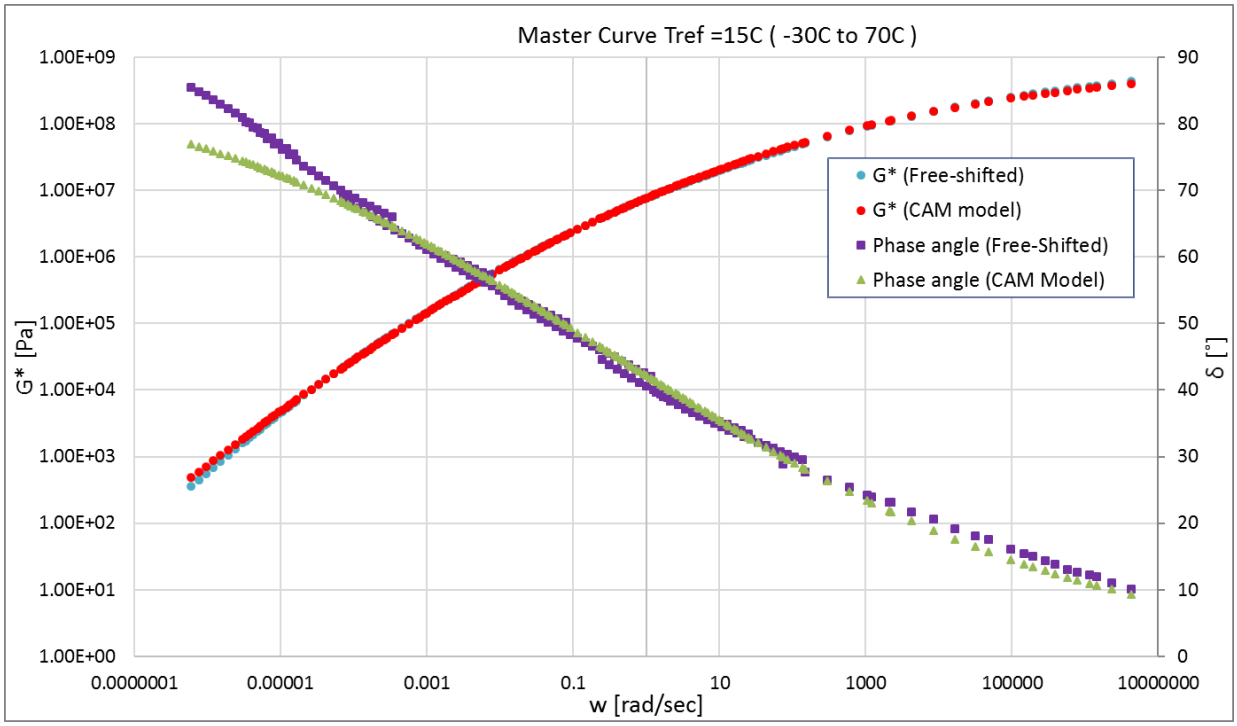

	GL model parameters	
	G*	δ
A	26.157	3.130
B	0.237	0.236
D	-19.948	0.000
M	-9.388	-18.893
T	3.129	46.797
RMS error (Log)	0.0036	0.010

Annexure F: Mathematical model comparison

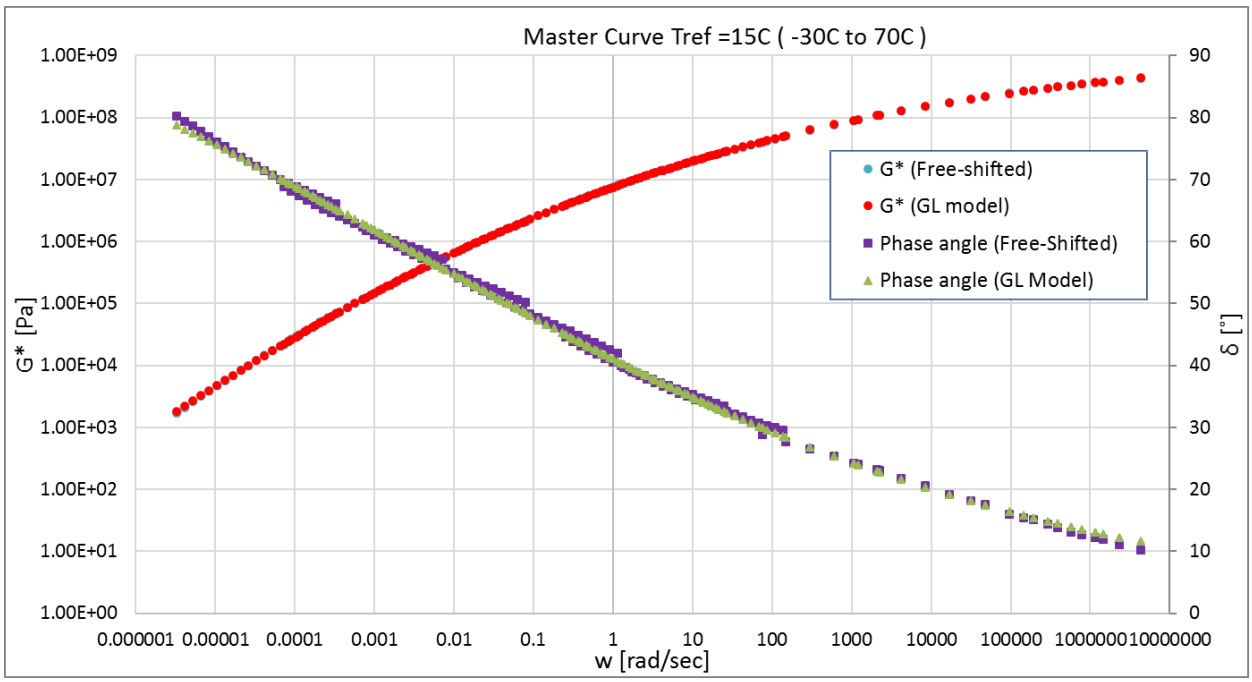

Rhea Discrete spectra		
Mode	gi, pa	li, sec
1	2.12E+05	1.17E-08
2	9.28E+04	2.59E-07
3	6.62E+04	1.16E-06
4	6.25E+04	4.28E-06
5	5.91E+04	1.63E-05
6	5.18E+04	6.52E-05
7	4.23E+04	2.69E-04
8	3.14E+04	1.11E-03
9	2.27E+04	4.45E-03
10	1.59E+04	1.85E-02
11	1.08E+04	8.33E-02
12	5.66E+03	3.67E-01
13	3.13E+03	1.39E+00
14	1.69E+03	5.76E+00
15	7.23E+02	2.31E+01
16	3.29E+02	9.28E+01
17	1.26E+02	3.80E+02
18	4.64E+01	1.65E+03
19	1.48E+01	7.01E+03
20	3.89E+00	3.36E+04
21	7.41E-01	1.83E+05
22	3.11E-02	1.32E+07
RMS error (%)	3.33%	

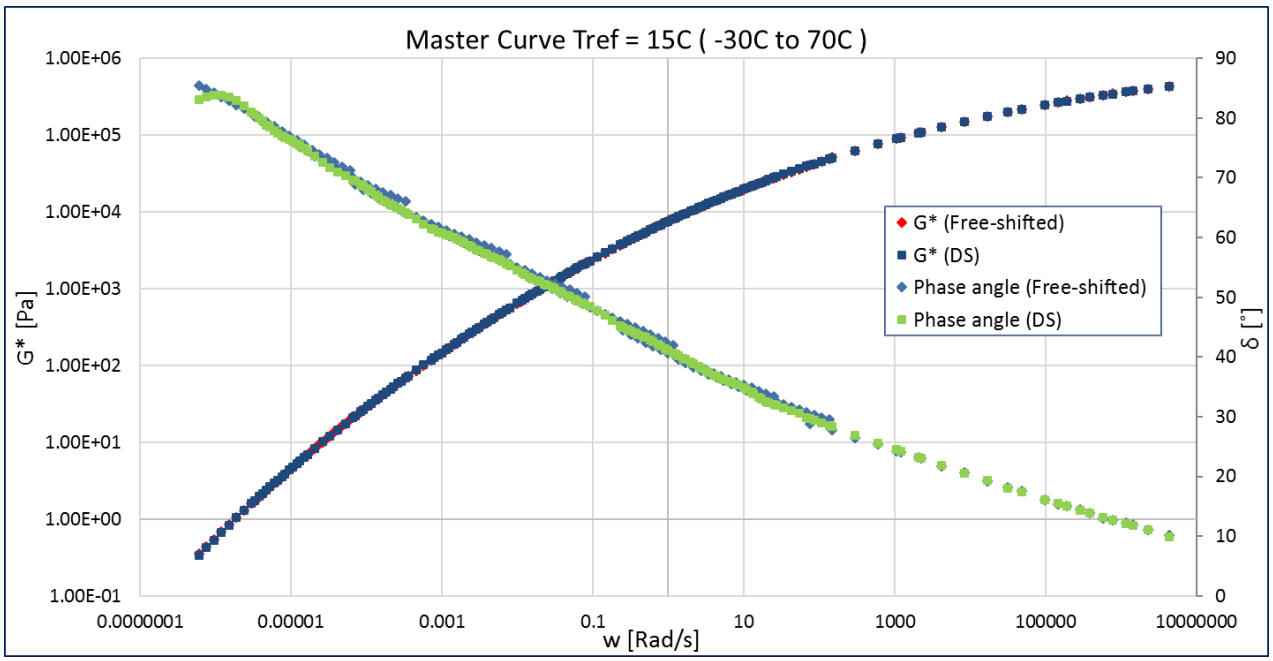

PAV4:

	CA model parameters	
	G*	δ
Go (Pa)	1079548120.883	
wo	0.325	0.325
B	0.127	0.129
K	1	1
RMS error (Log)	0.0161	0.0246

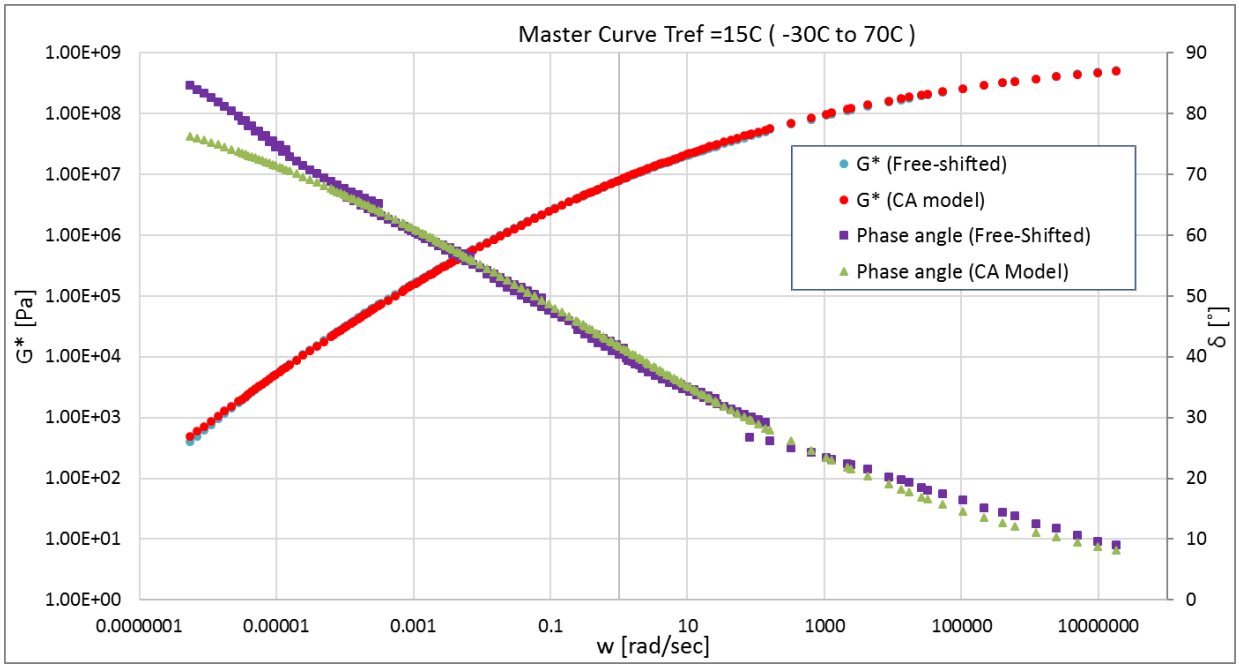

	CAM model parameters	
	G*	δ
Go (Pa)	952488599.546	
wo	0.325	0.325
B	0.129	0.130
K	0.990	0.998
RMS error (Log	0.0134	0.0245

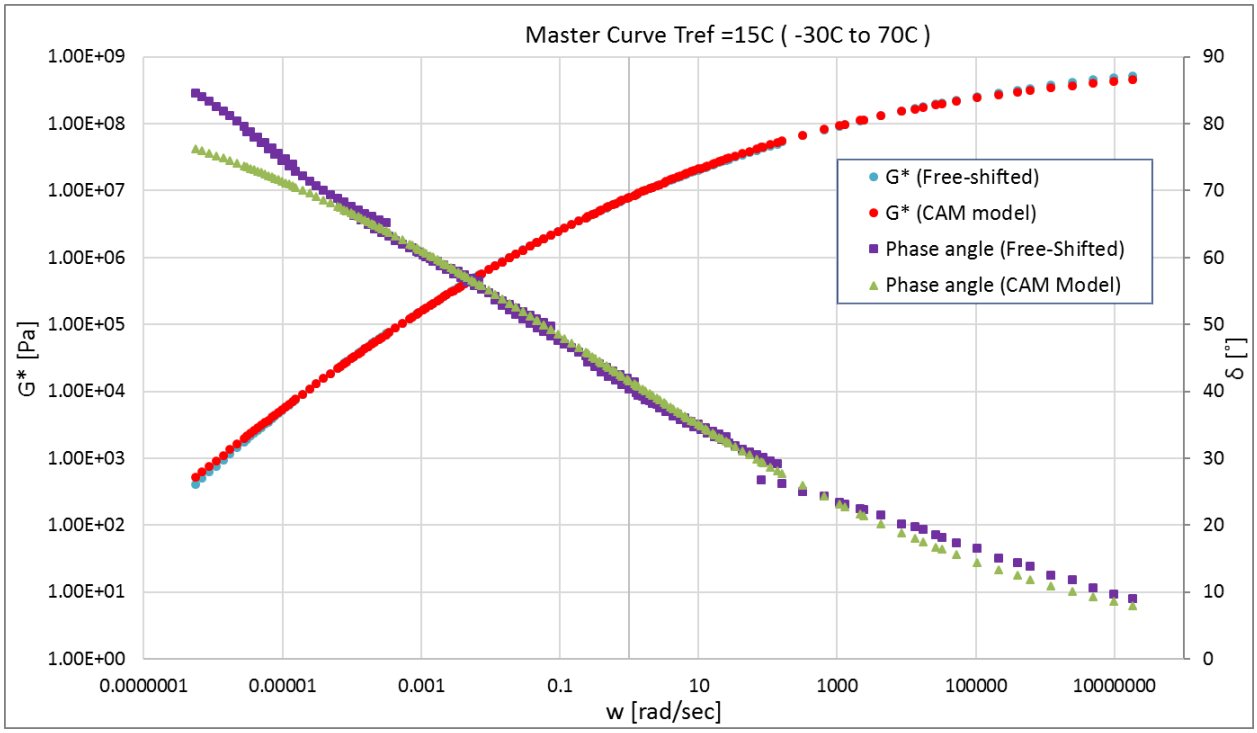

	GL model parameters	
	G*	δ
A	25.113	3.114
B	0.243	0.240
D	-18.933	0.000
M	-9.014	-18.453
T	3.305	47.957
RMS error (Log)	0.0035	0.009

Annexure F: Mathematical model comparison

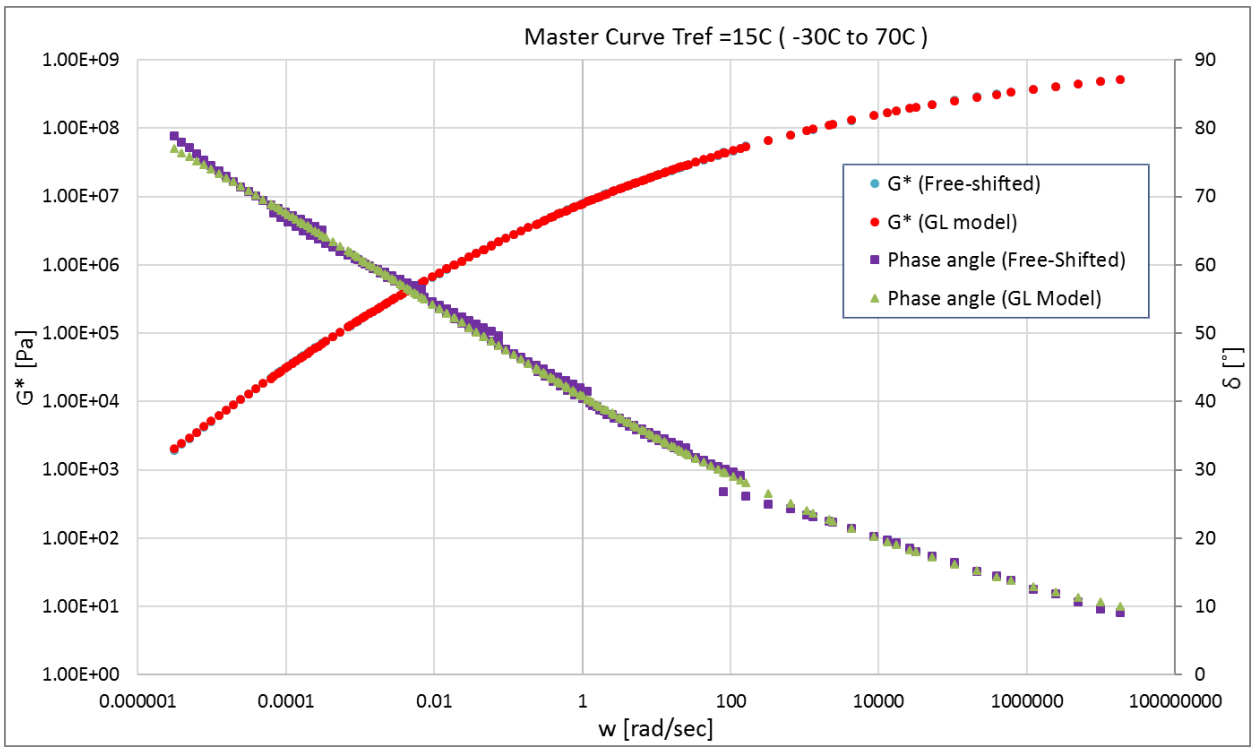

Rhea Discrete spectra		
Mode	gi, pa	li, sec
1	1.15E+05	4.52E-08
2	7.91E+04	2.34E-07
3	7.69E+04	9.86E-07
4	7.16E+04	4.16E-06
5	6.30E+04	1.76E-05
6	5.22E+04	7.41E-05
7	4.06E+04	3.09E-04
8	2.93E+04	1.26E-03
9	2.21E+04	4.84E-03
10	1.59E+04	1.98E-02
11	1.14E+04	9.14E-02
12	5.83E+03	4.37E-01
13	2.96E+03	1.78E+00
14	1.56E+03	7.32E+00
15	6.65E+02	2.99E+01
16	2.99E+02	1.18E+02
17	1.14E+02	4.95E+02
18	4.21E+01	2.20E+03
19	1.29E+01	9.60E+03
20	3.49E+00	4.73E+04
21	6.46E-01	2.53E+05
22	3.55E-02	9.01E+06
RMS error (%)	2.48%	

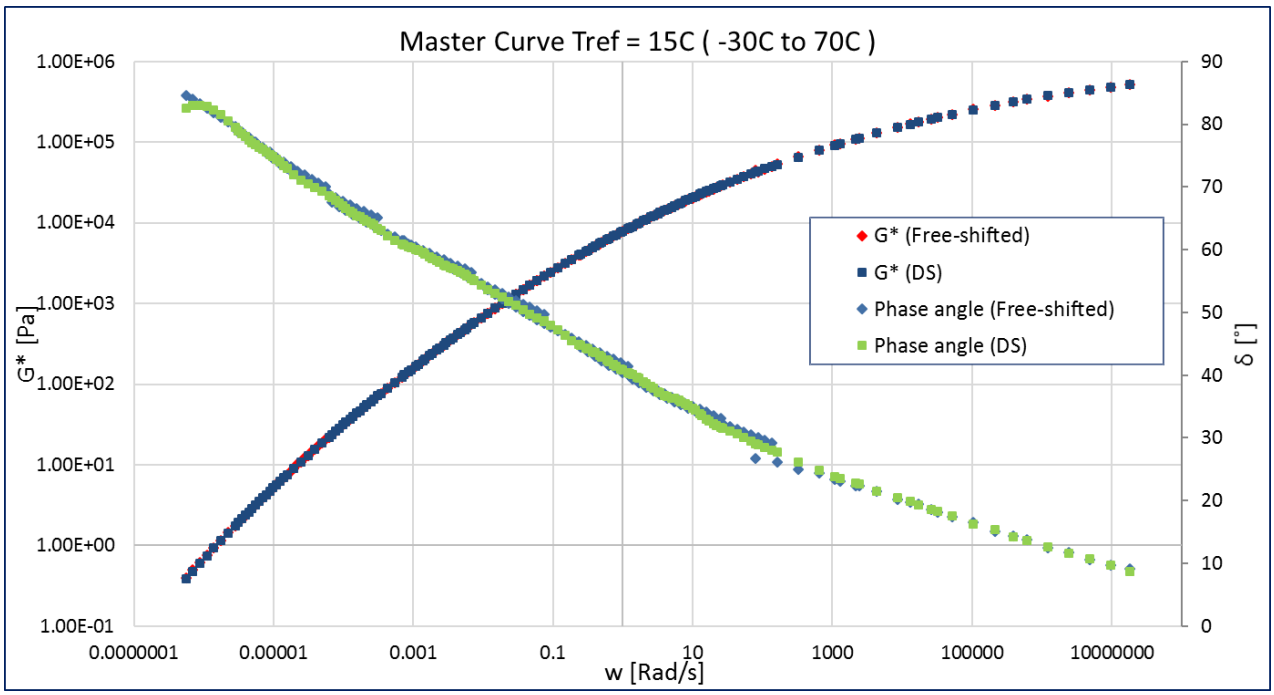

FT322 (S-E2 GP)

Unaged:

	CA model parameters	
	G*	δ
Go (Pa)	18307598713.959	
wo	67.103	67.103
B	0.089	0.070
K	1	1
RMS error (Log)	0.0751	0.1416

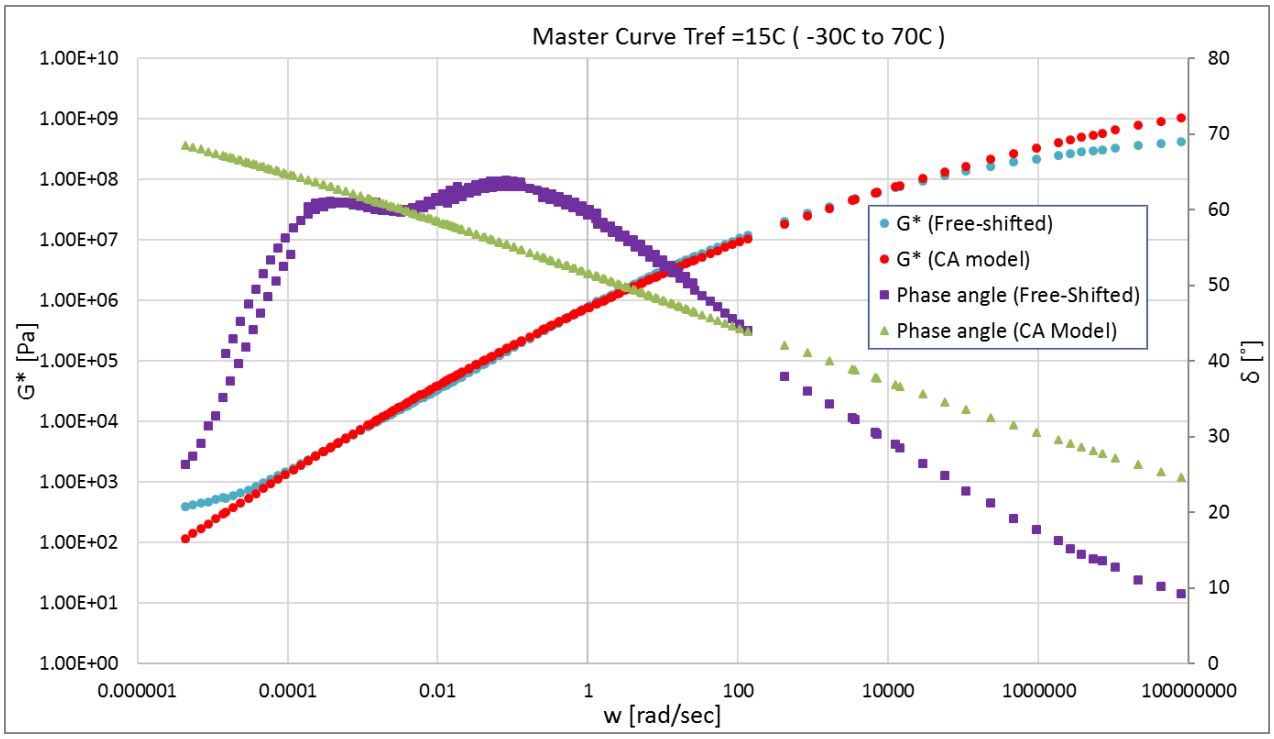

	CAM model parameters	
	G*	δ
Go (Pa)	2674153882.918	
wo	67.103	67.103
B	0.112	0.925
K	0.953	0.676
RMS error (Log)	0.0683	0.1261

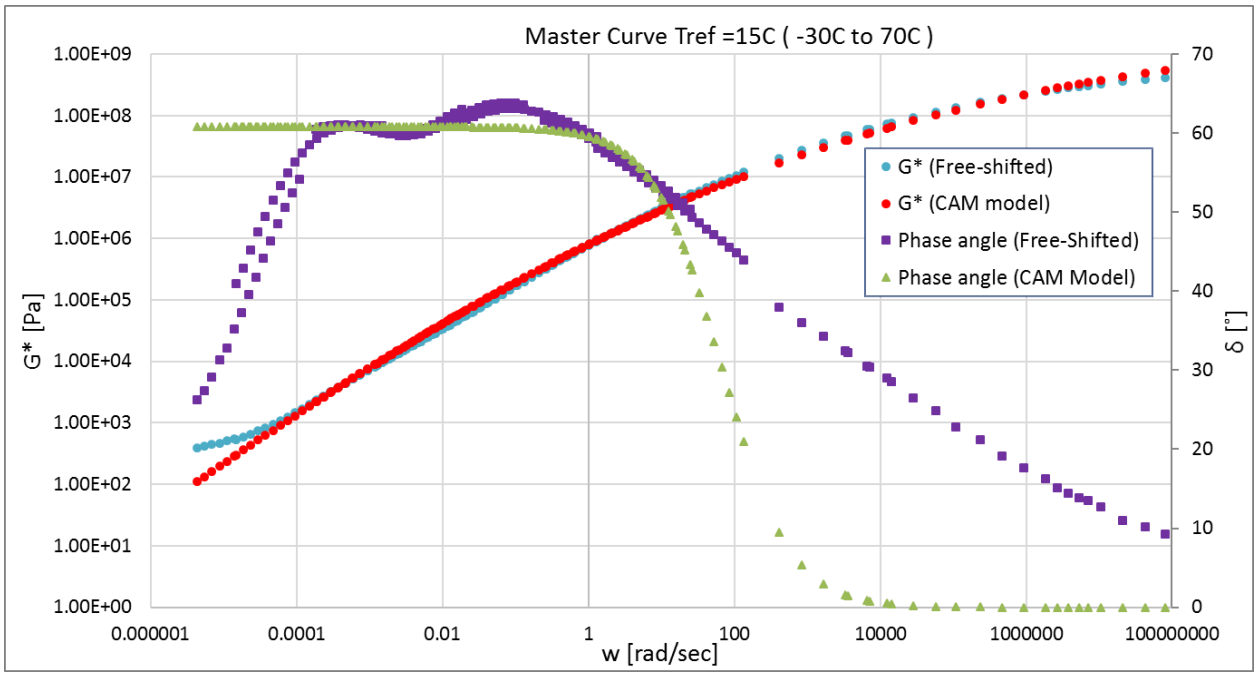

	GL model parameters	
	G*	δ
A	8.584	1.088
B	0.319	0.273
D	-2.578	
M	-1.791	-1.378
T	0.954	1.132
RMS error (Log)	0.0117	0.031

Annexure F: Mathematical model comparison

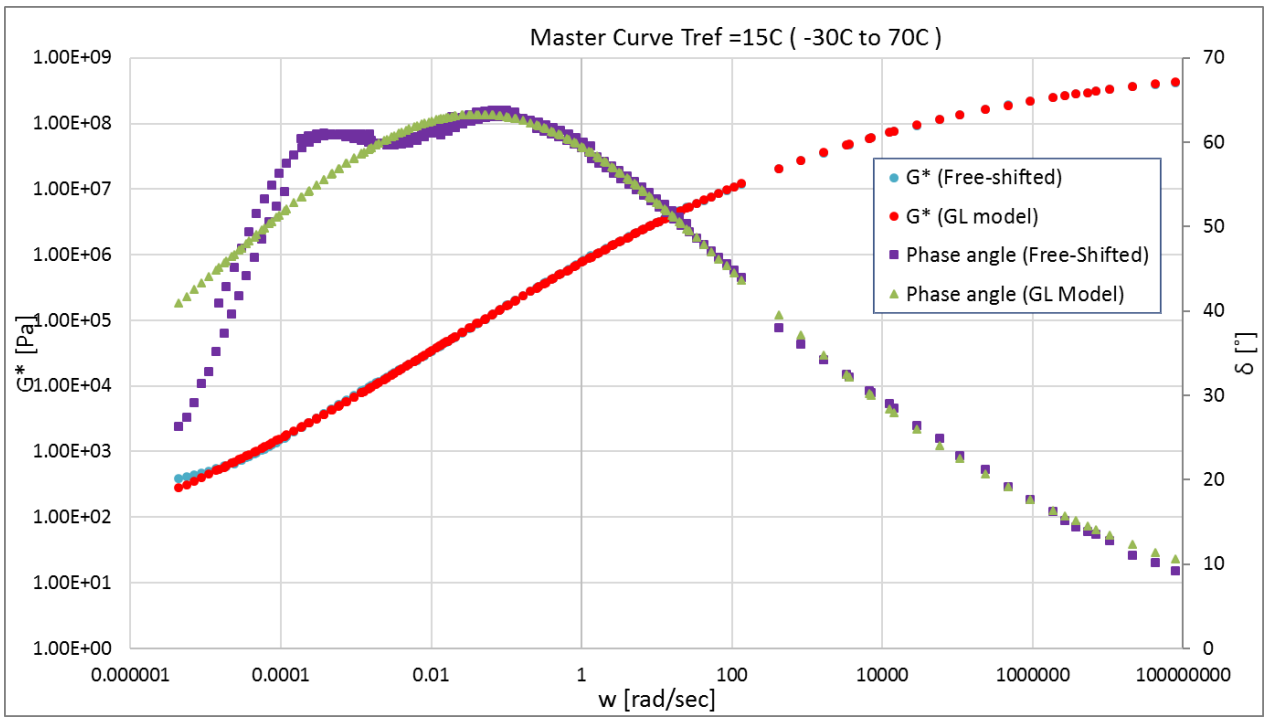

Rhea Discrete spectra		
Mode	gi, pa	li, sec
1	1.13E+05	1.54E-08
2	9.54E+04	1.32E-07
3	8.87E+04	9.89E-07
4	7.01E+04	7.06E-06
5	4.75E+04	4.93E-05
6	2.73E+04	3.29E-04
7	1.39E+04	2.06E-03
8	6.06E+03	1.24E-02
9	2.41E+03	7.30E-02
10	7.76E+02	4.53E-01
11	1.99E+02	3.24E+00
12	4.39E+01	2.13E+01
13	1.29E+01	1.33E+02
14	4.36E+00	6.42E+02
15	1.39E+00	4.27E+03
16	2.89E-01	4.17E+04
17	2.63E-01	9.89E+05
18		
19		
20		
21		
22		
RMS error (%)	3.67%	

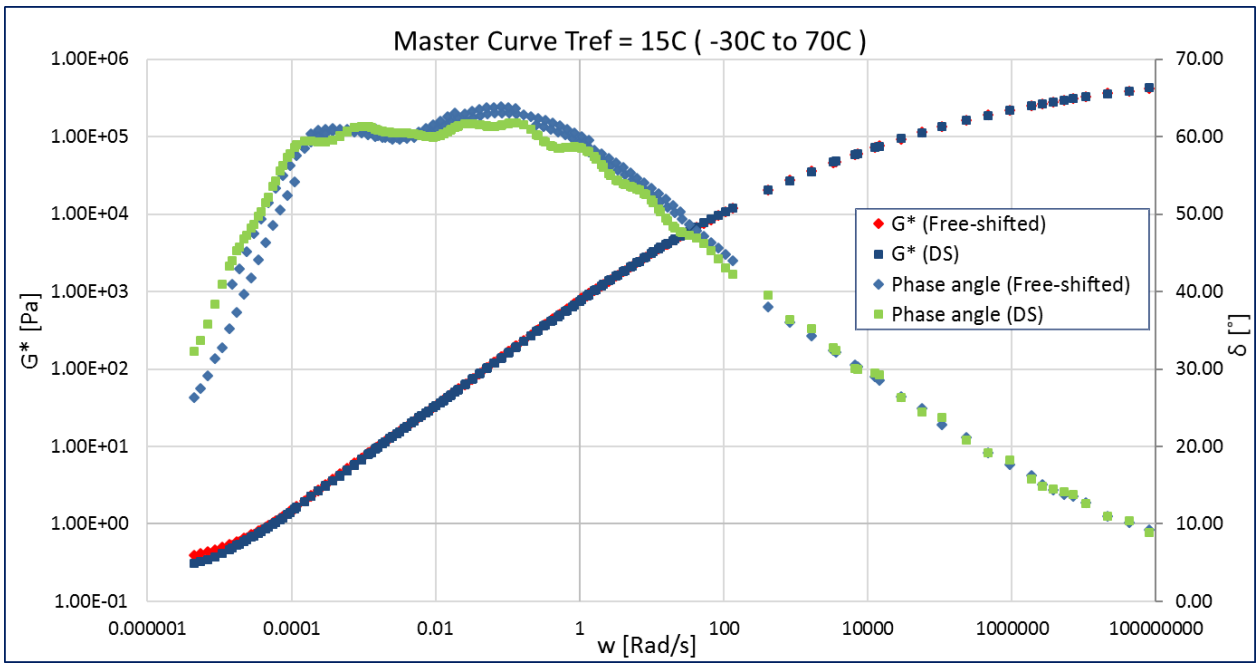

RTFO:

	CA model parameters	
	G*	δ
Go (Pa)	2875083685.940	
wo	15.927	15.927
B	0.118	0.105
K	1	1
RMS error (Log)	0.0369	0.0521

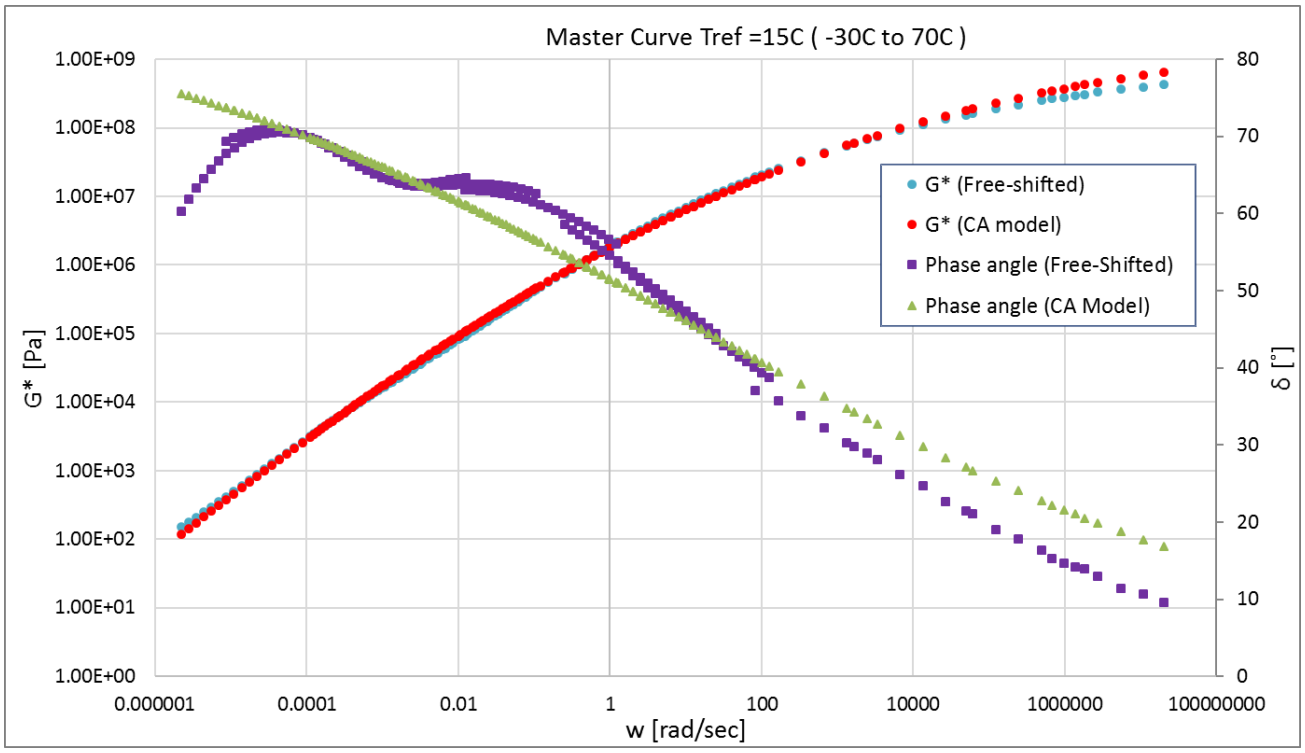

	CAM model parameters	
	G*	δ
Go (Pa)	1320738702.589	
wo	15.927	15.927
B	0.133	0.131
K	0.976	0.942
RMS error (Log)	0.0321	0.0507

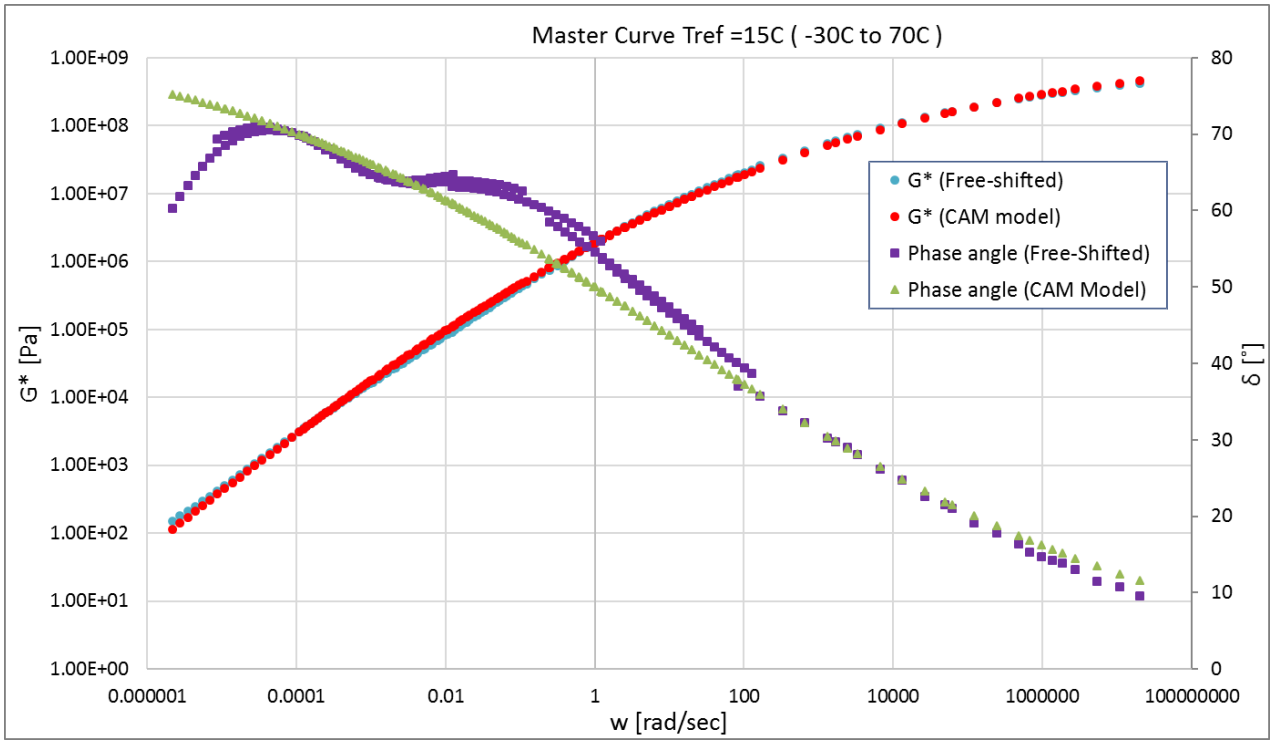

	GL model parameters	
	G*	δ
A	11.374	1.069
B	0.313	0.316
D	-5.362	0.000
M	-3.391	-4.085
T	1.591	4.729
RMS error (Log)	0.0139	0.021

Annexure F: Mathematical model comparison

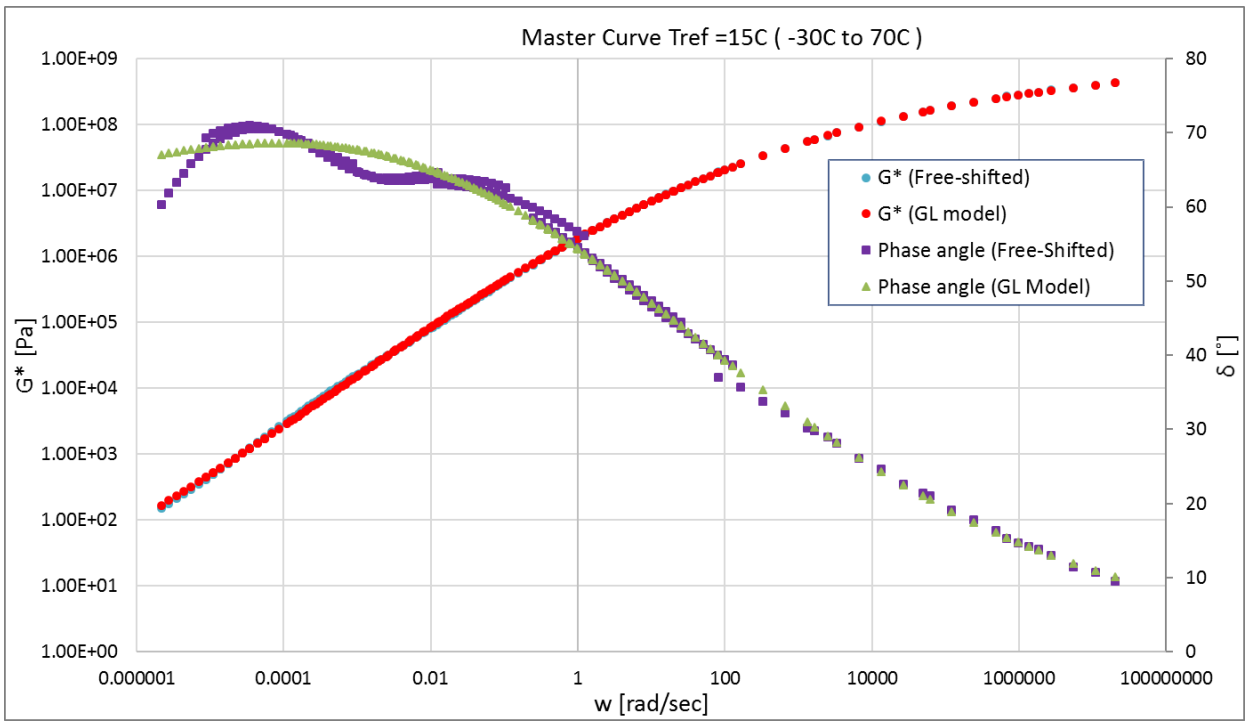

Rhea Discrete spectra		
Mode	gi, pa	li, sec
1	1.14E+05	5.08E-08
2	8.84E+04	3.65E-07
3	8.14E+04	2.22E-06
4	6.88E+04	1.29E-05
5	5.17E+04	7.53E-05
6	3.47E+04	4.36E-04
7	2.10E+04	2.60E-03
8	1.08E+04	1.50E-02
9	4.95E+03	8.88E-02
10	1.78E+03	5.41E-01
11	4.88E+02	3.83E+00
12	1.02E+02	2.59E+01
13	2.75E+01	1.67E+02
14	7.56E+00	1.03E+03
15	1.77E+00	7.02E+03
16	2.46E-01	4.84E+04
17	7.91E-02	2.52E+05
18		
19		
20		
21		
22		
RMS error (%)	2.36%	

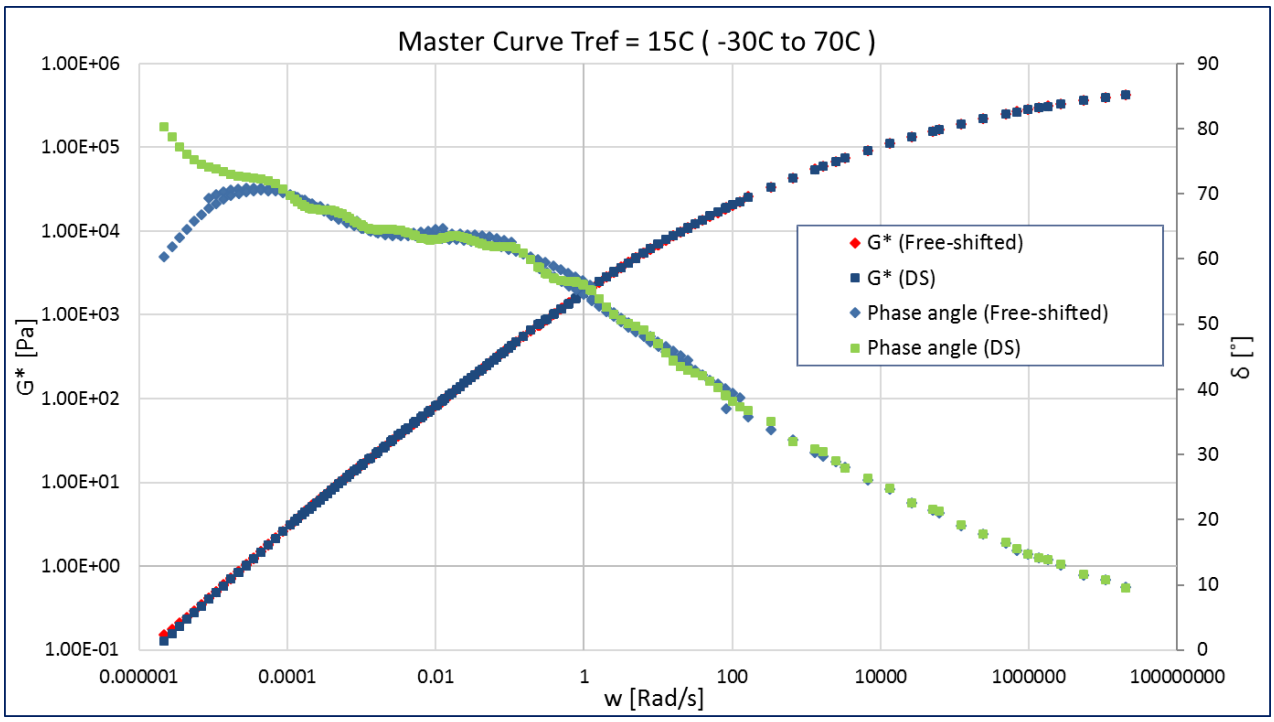

PAV1:

	CA model parameters	
	G*	δ
Go (Pa)	939076674.888	
wo	1.107	1.107
B	0.128	0.130
K	1	1
RMS error (Log)	0.0091	0.0163

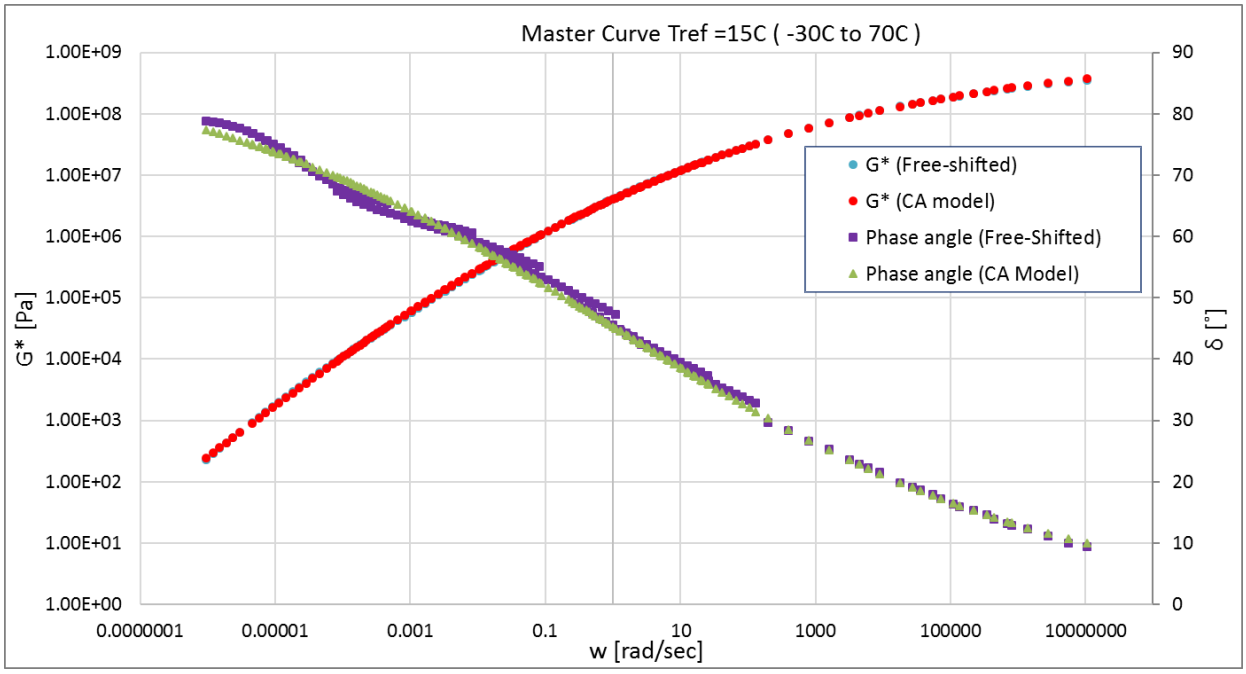

	CAM model parameters	
	G*	δ
Go (Pa)	941731674.505	
wo	1.107	1.107
B	0.128	0.130
K	1.001	1.007
RMS error (Log)	0.0091	0.0152

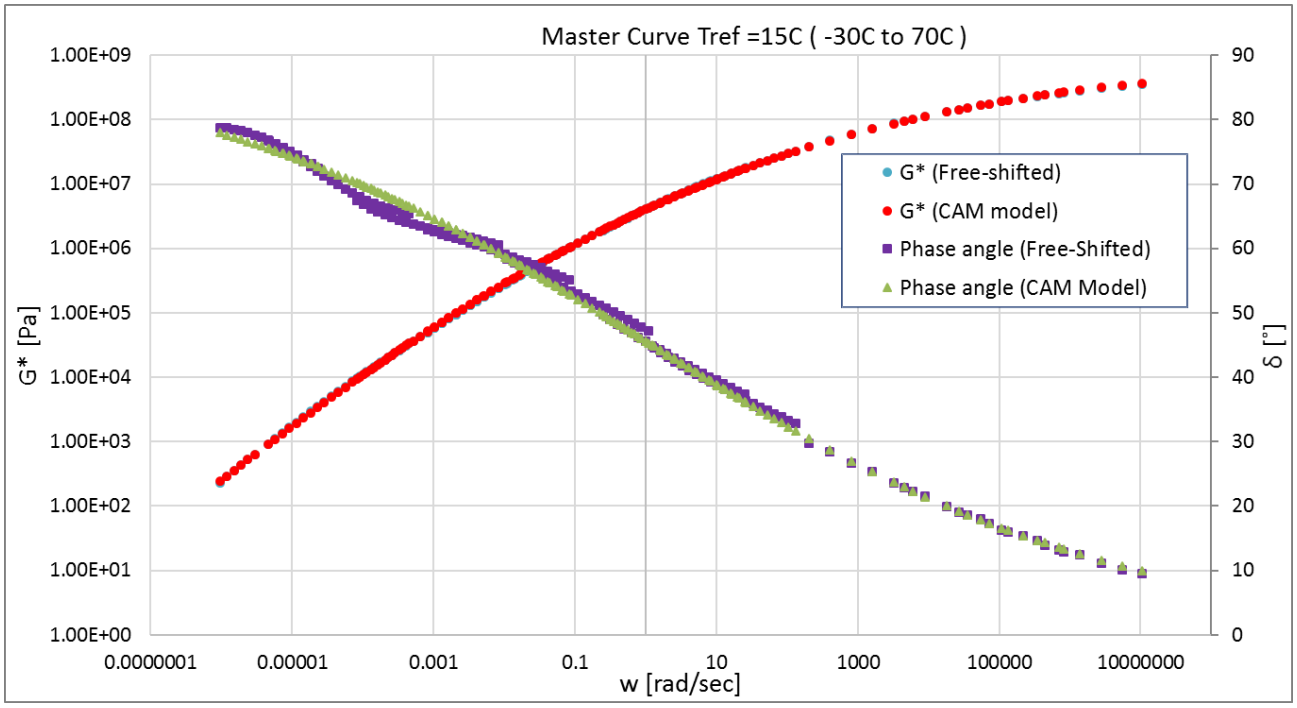

	GL model parameters	
	G*	δ
A	12.727	2.634
B	0.272	0.294
D	-6.722	
M	-5.199	-11.782
T	1.414	32.445
RMS error (Log)	0.0090	0.016

Annexure F: Mathematical model comparison

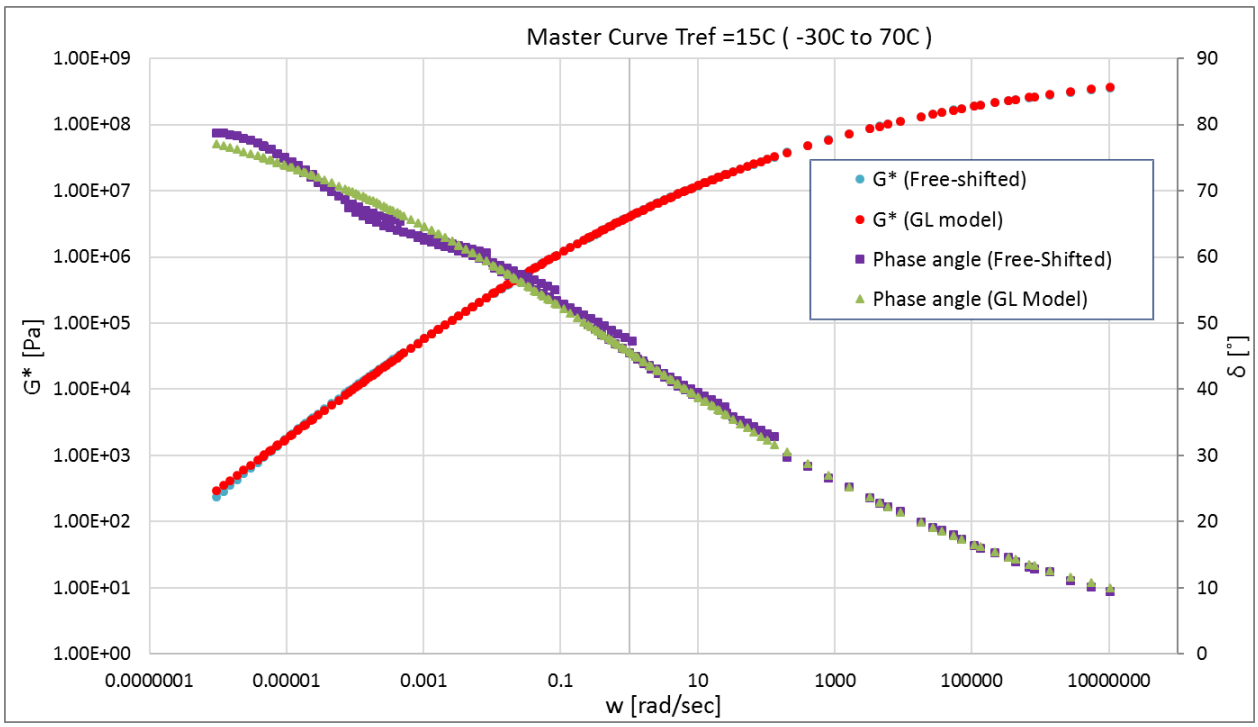

Rhea Discrete spectra		
Mode	gi, pa	li, sec
1	1.08E+05	3.70E-08
2	6.88E+04	3.26E-07
3	6.38E+04	1.79E-06
4	5.79E+04	9.56E-06
5	4.84E+04	4.95E-05
6	3.76E+04	2.54E-04
7	2.68E+04	1.31E-03
8	1.70E+04	6.83E-03
9	1.01E+04	3.36E-02
10	5.72E+03	1.72E-01
11	2.50E+03	8.71E-01
12	1.05E+03	4.42E+00
13	3.61E+02	2.02E+01
14	1.42E+02	9.19E+01
15	4.34E+01	4.54E+02
16	1.47E+01	2.35E+03
17	3.88E+00	1.19E+04
18	8.59E-01	5.52E+04
19	2.10E-01	2.68E+05
20	3.22E-02	3.21E+06
21		
22		
RMS error (%)	1.68%	

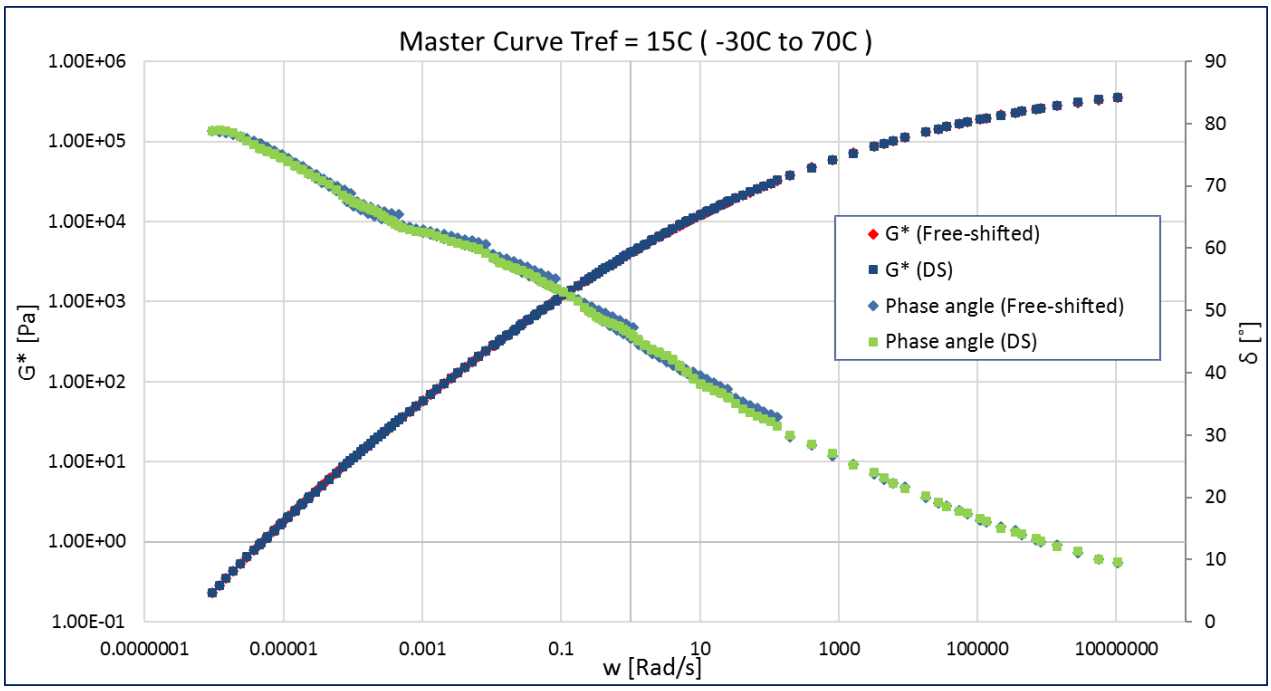

PAV2:

	CA model parameters	
	G*	δ
Go (Pa)	1162413134.333	
wo	0.284	0.284
B	0.115	0.117
K	1	1
RMS error (Log)	0.0099	0.0195

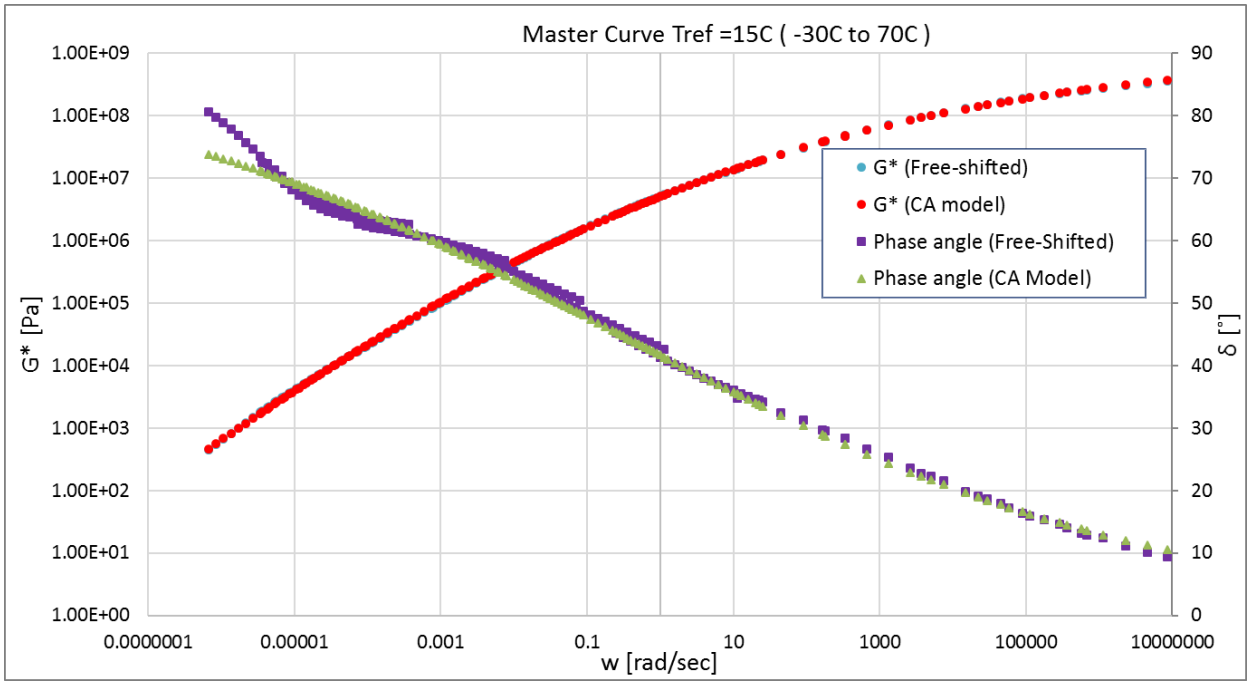

	CAM model parameters	
	G*	δ
Go (Pa)	1163840350.542	
wo	0.284	0.284
B	0.115	0.116
K	1.000	1.011
RMS error (Log)	0.0099	0.0185

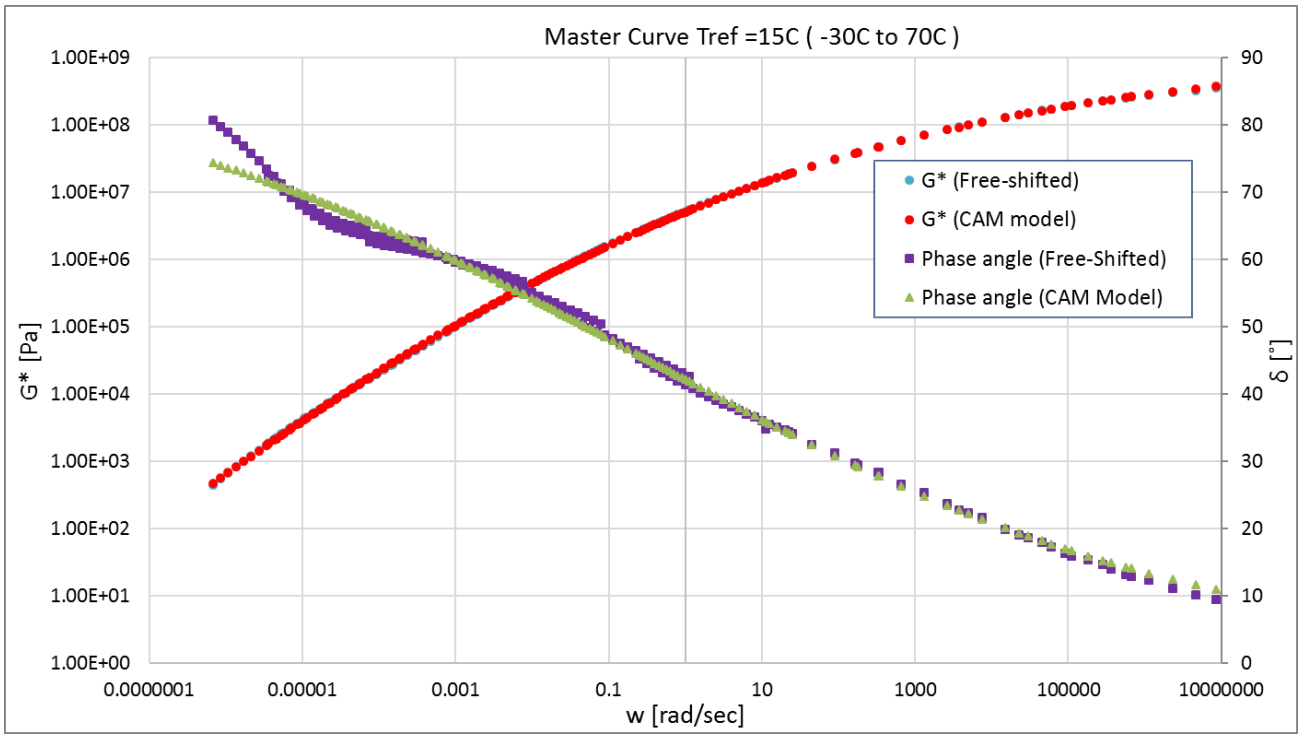

	GL model parameters	
	G*	δ
A	13.029	2.519
B	0.248	0.279
D	-6.953	0.000
M	-5.961	-12.915
T	1.278	35.797
RMS error (Log)	0.0078	0.017

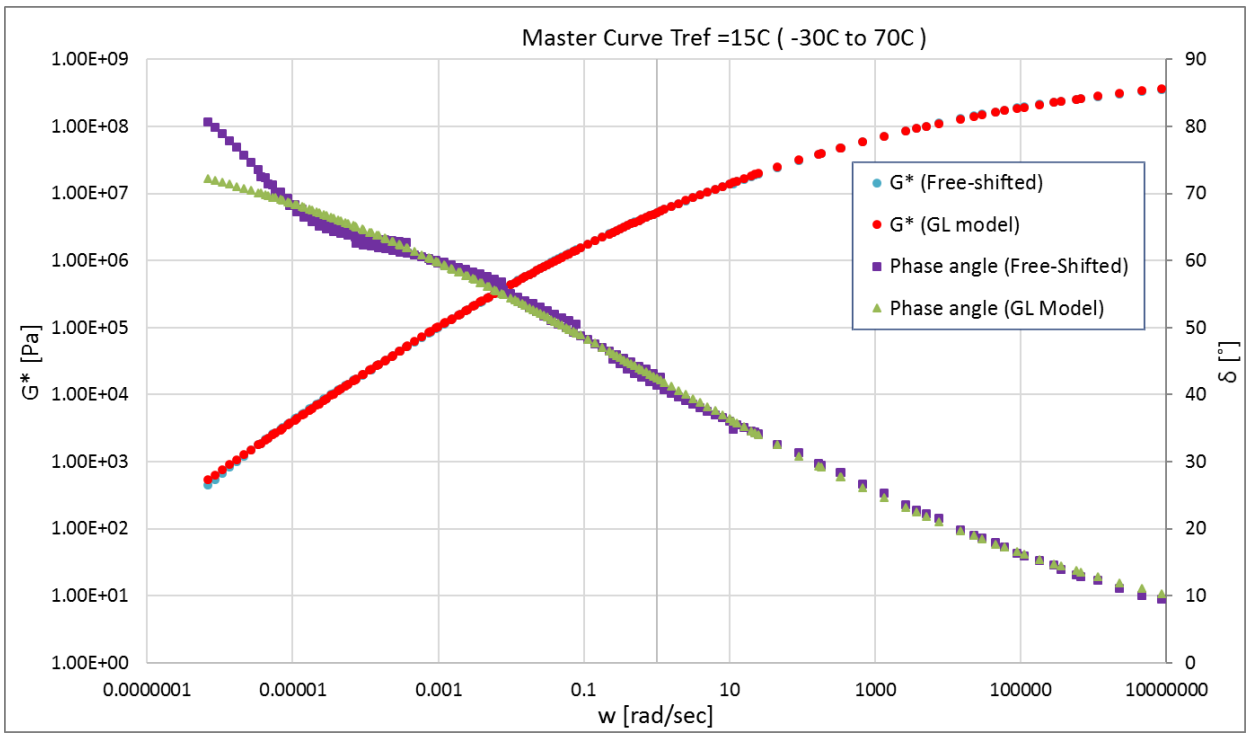

Rhea Discrete spectra		
Mode	gi, pa	li, sec
1	1.35E+05	4.36E-08
2	7.02E+04	5.10E-07
3	6.07E+04	2.70E-06
4	5.44E+04	1.31E-05
5	4.56E+04	6.12E-05
6	3.62E+04	2.81E-04
7	2.66E+04	1.30E-03
8	1.78E+04	5.93E-03
9	1.07E+04	2.62E-02
10	6.60E+03	1.16E-01
11	3.76E+03	5.43E-01
12	1.84E+03	2.34E+00
13	9.53E+02	9.91E+00
14	3.87E+02	4.60E+01
15	1.50E+02	1.83E+02
16	5.97E+01	8.04E+02
17	1.95E+01	3.50E+03
18	7.38E+00	1.28E+04
19	3.46E+00	6.40E+04
20	8.04E-01	3.60E+05
21	9.24E-02	6.11E+06
22		
RMS error (%)	2.13%	

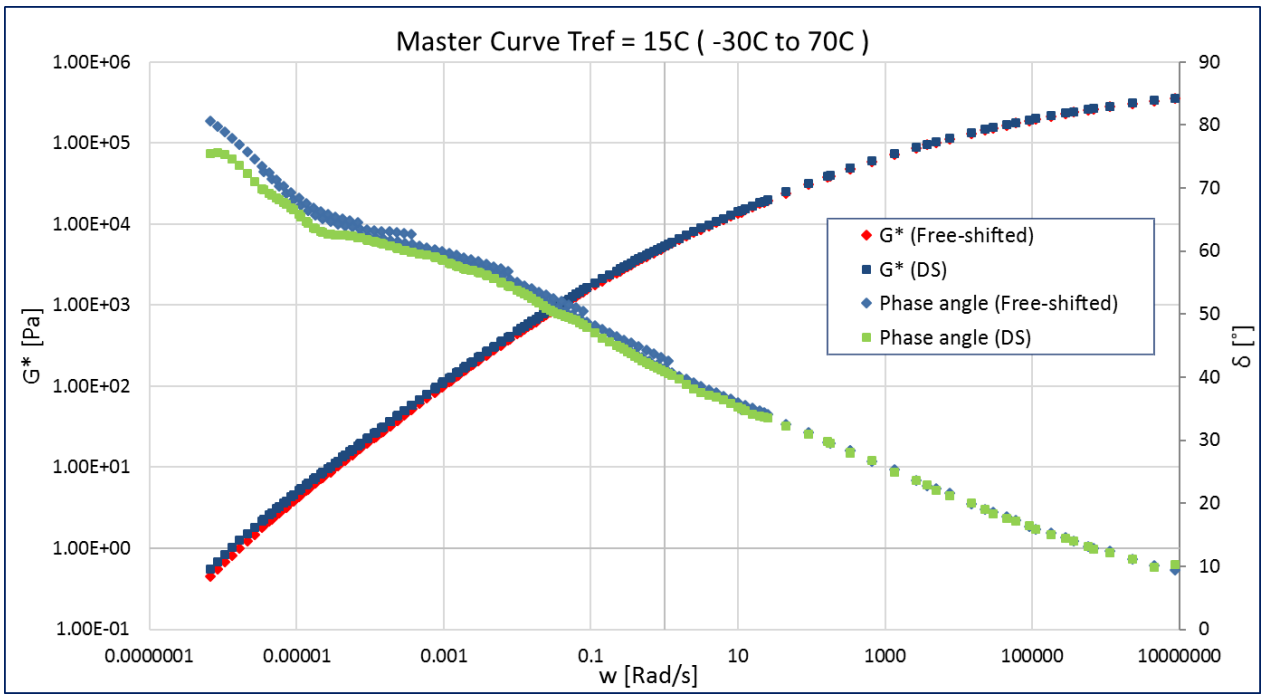

PAV4:

	CA model parameters	
	G*	δ
Go (Pa)	1097331340.830	
wo	0.183	0.183
B	0.113	0.112
K	1	1
RMS error (Log)	0.0117	0.0247

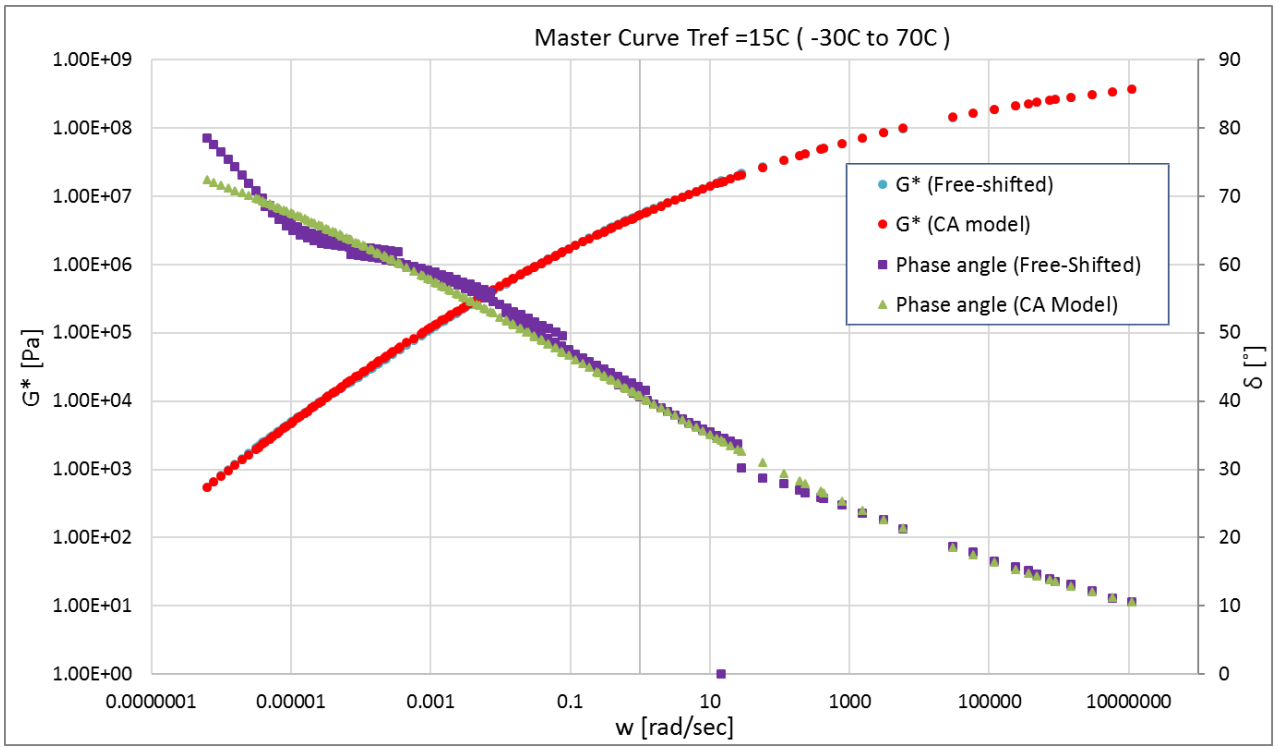

	CAM model parameters	
	G*	δ
Go (Pa)	1094821217.739	
wo	0.183	0.183
B	0.113	0.112
K	1.001	1.012
RMS error (Log)	0.0116	0.0238

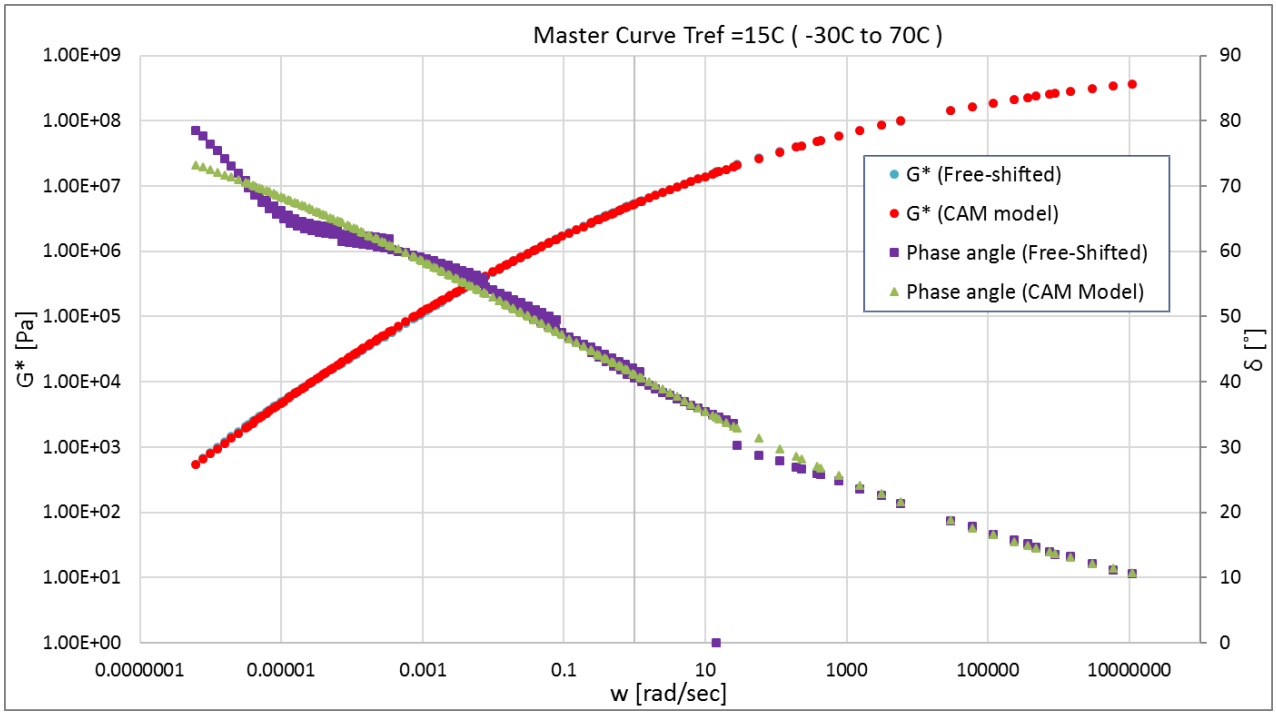

	GL model parameters	
	G*	δ
A	13.034	2.432
B	0.252	0.272
D	-7.009	0.000
M	-5.976	-13.339
T	1.404	36.093
RMS error (Log)	0.0073	0.022

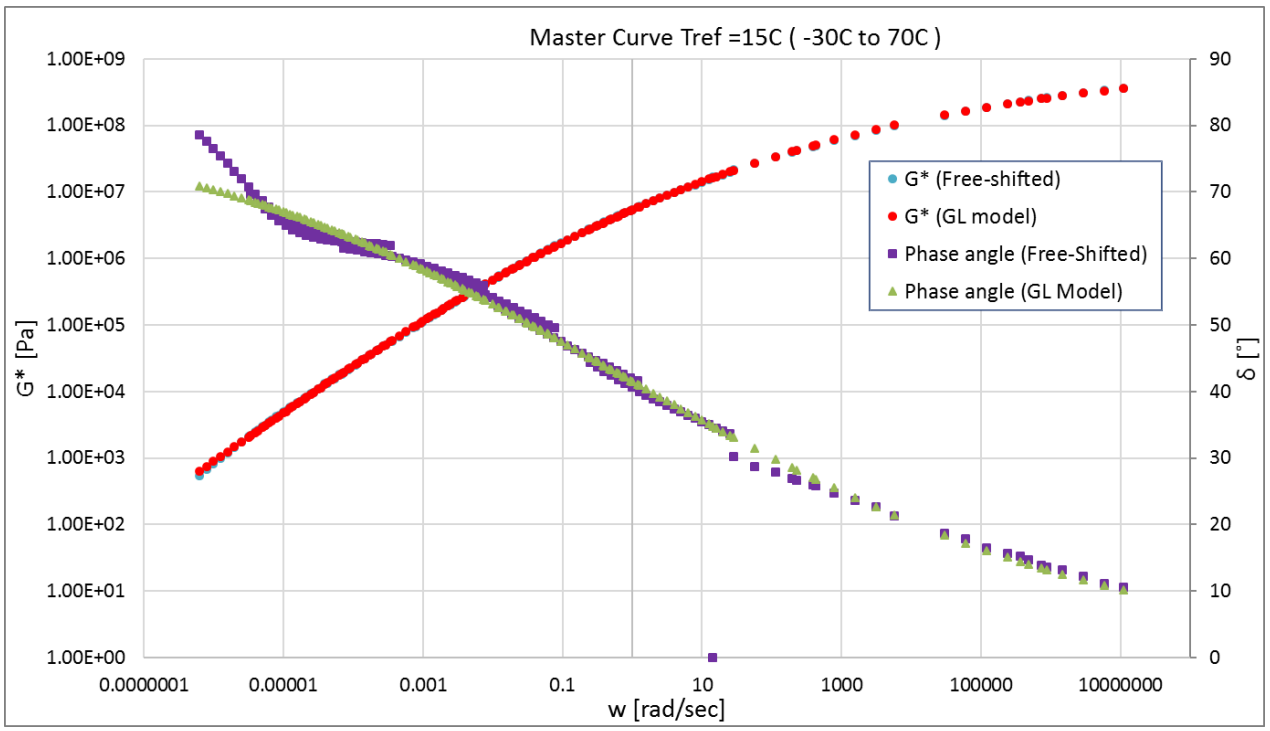

Rhea Discrete spectra		
Mode	gi, pa	li, sec
1	1.07E+05	2.98E-08
2	6.79E+04	1.90E-07
3	6.25E+04	8.87E-07
4	5.63E+04	4.07E-06
5	4.84E+04	1.87E-05
6	3.90E+04	8.62E-05
7	2.97E+04	3.96E-04
8	2.14E+04	1.82E-03
9	1.48E+04	8.64E-03
10	9.32E+03	3.81E-02
11	5.61E+03	1.62E-01
12	3.63E+03	7.20E-01
13	1.66E+03	3.74E+00
14	7.08E+02	1.75E+01
15	2.95E+02	8.84E+01
16	9.09E+01	4.61E+02
17	3.01E+01	2.15E+03
18	1.08E+01	9.99E+03
19	3.75E+00	6.05E+04
20	8.27E-01	3.54E+05
21	9.30E-02	6.05E+06
22		
RMS error (%)	2.24%	

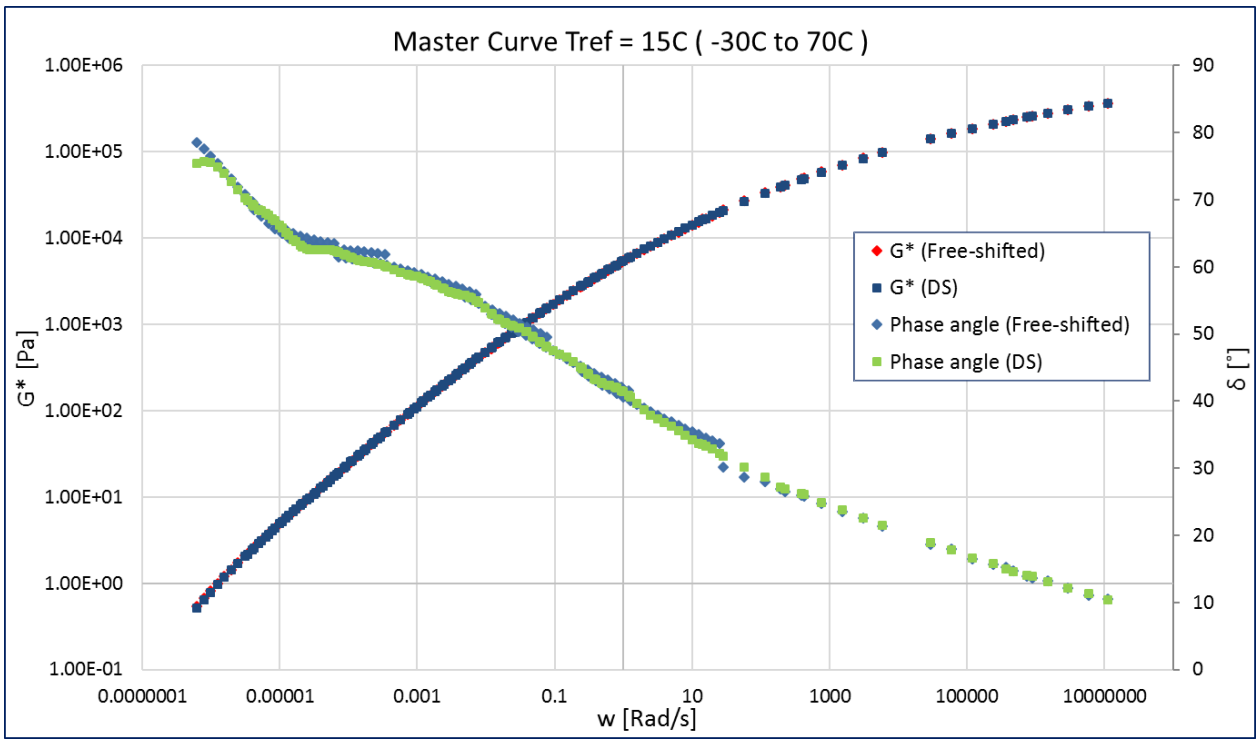

FT333 (S-E2 KZN)

Unaged:

	CA model parameters	
	G*	δ
Go (Pa)	1340823978.257	
wo	15.800	15.800
B	0.145	0.122
K	1	1
RMS error (Log)	0.0482	0.1014

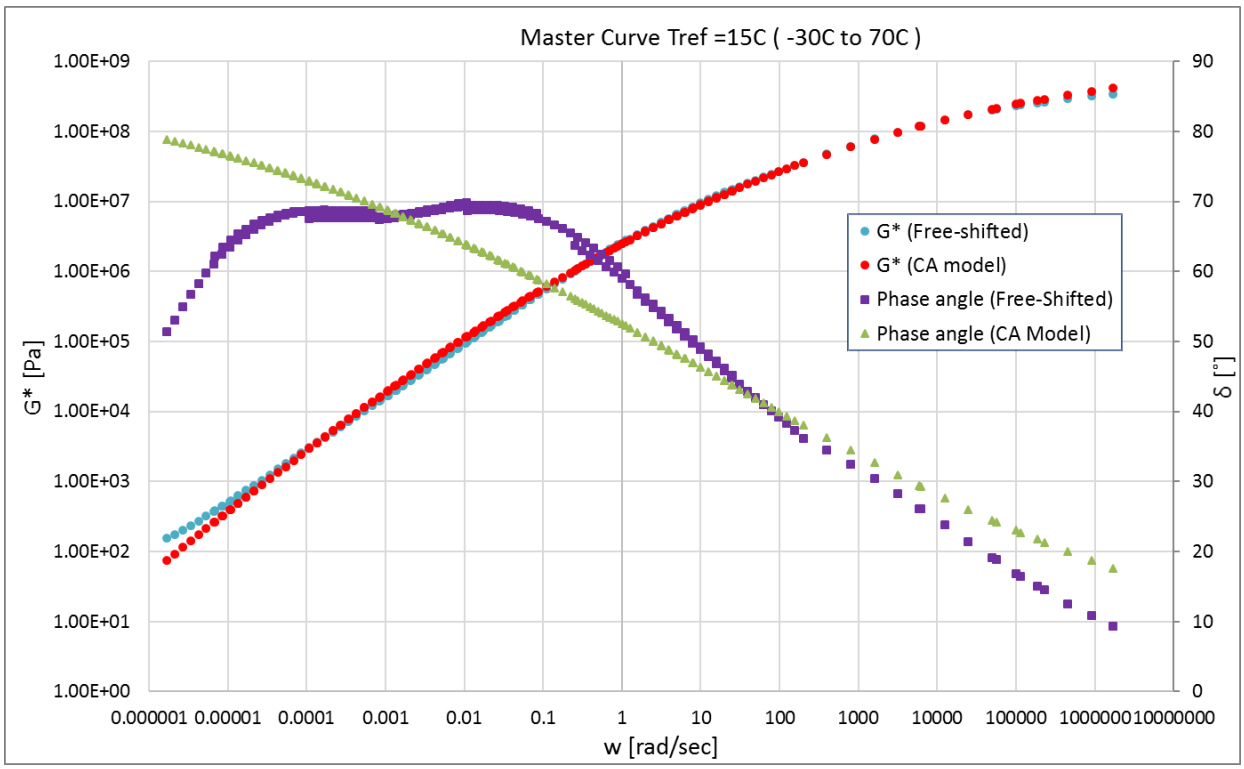

	CAM model parameters	
	G*	δ
Go (Pa)	1169140612.496	
wo	15.800	15.800
B	0.149	0.132
K	0.995	0.983
RMS error (Log)	0.0480	0.1012

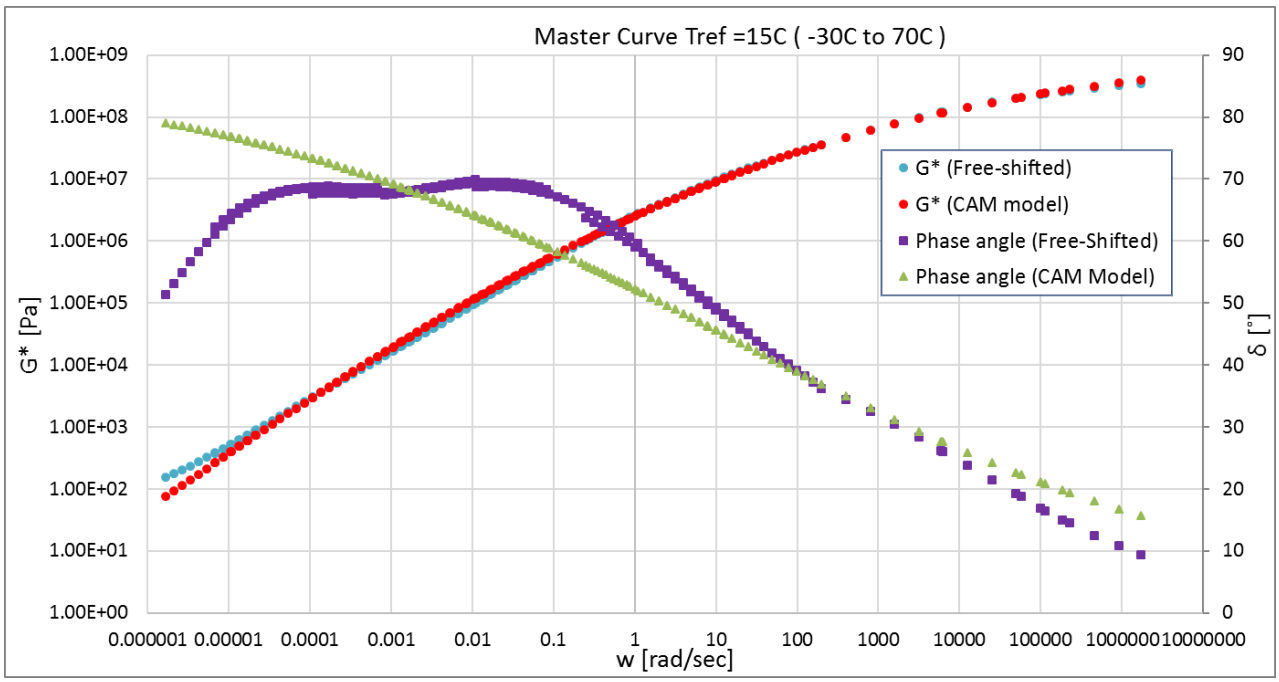

	GL model parameters	
	G*	δ
A	10.795	0.984
B	0.356	0.325
D	-4.856	
M	-2.972	-2.972
T	1.795	2.767
RMS error (Log)	0.0113	0.026

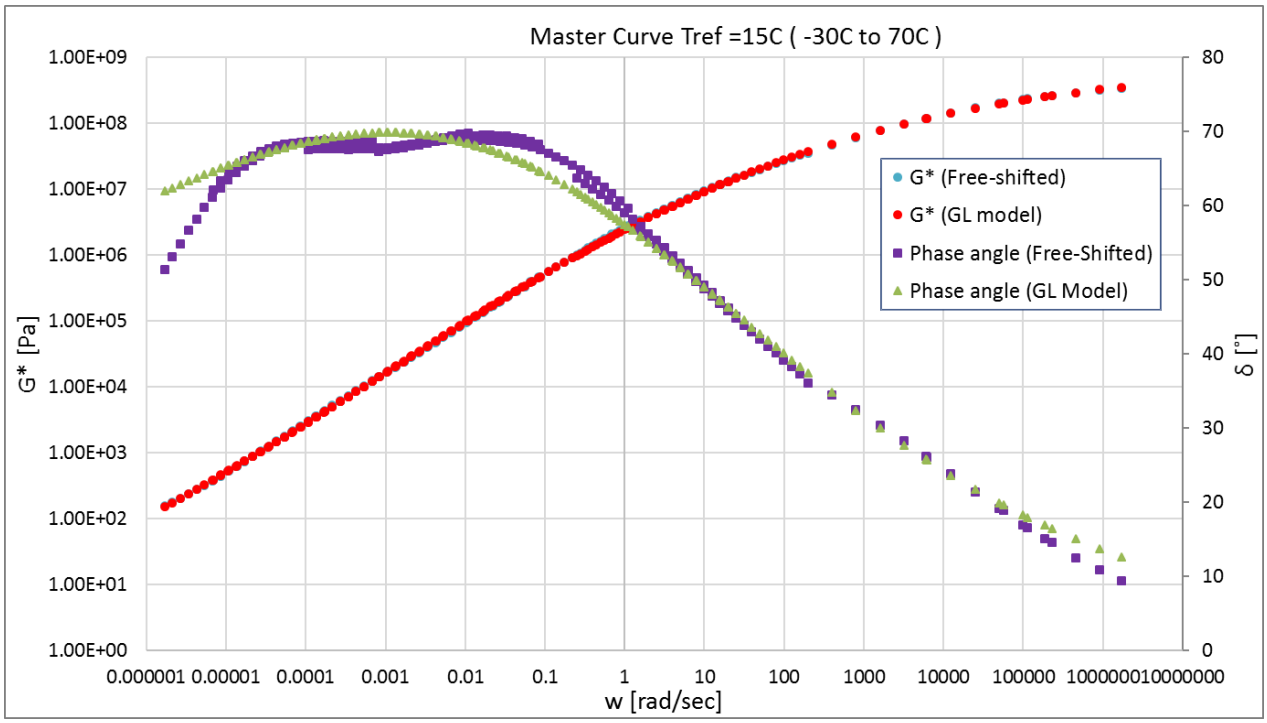

Rhea Discrete spectra		
Mode	gi, pa	li, sec
1	8.33E+04	6.04E-07
2	7.60E+04	3.79E-06
3	7.39E+04	2.02E-05
4	6.19E+04	1.05E-04
5	4.40E+04	5.53E-04
6	2.53E+04	3.32E-03
7	1.31E+04	1.89E-02
8	5.99E+03	1.07E-01
9	2.19E+03	5.93E-01
10	5.75E+02	4.12E+00
11	9.22E+01	2.99E+01
12	2.19E+01	1.86E+02
13	6.04E+00	1.09E+03
14	1.61E+00	7.35E+03
15	2.89E-01	5.47E+04
16	9.01E-02	3.58E+05
17		
18		
19		
20		
21		
22		
RMS error (%)	3.55%	

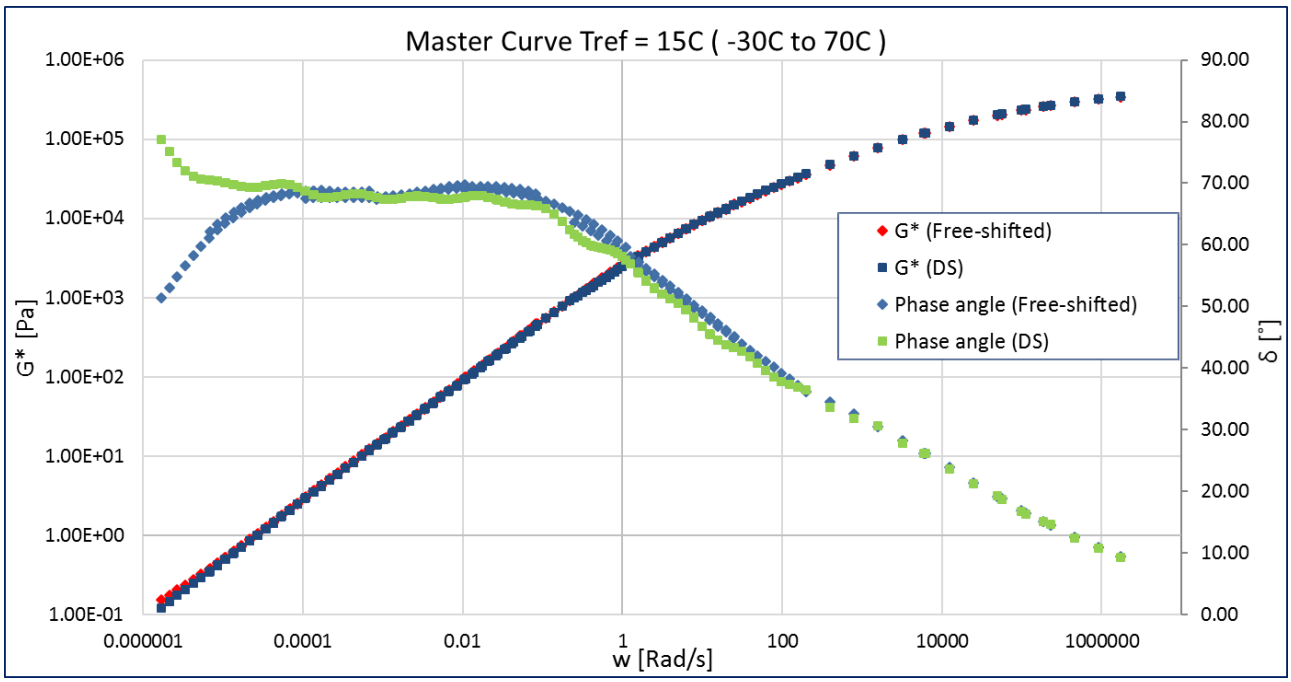

RTFO:

	CA model parameters	
	G*	δ
Go (Pa)	1730808411.575	
wo	12.104	12.104
B	0.135	0.122
K	1	1
RMS error (Log)	0.0422	0.0778

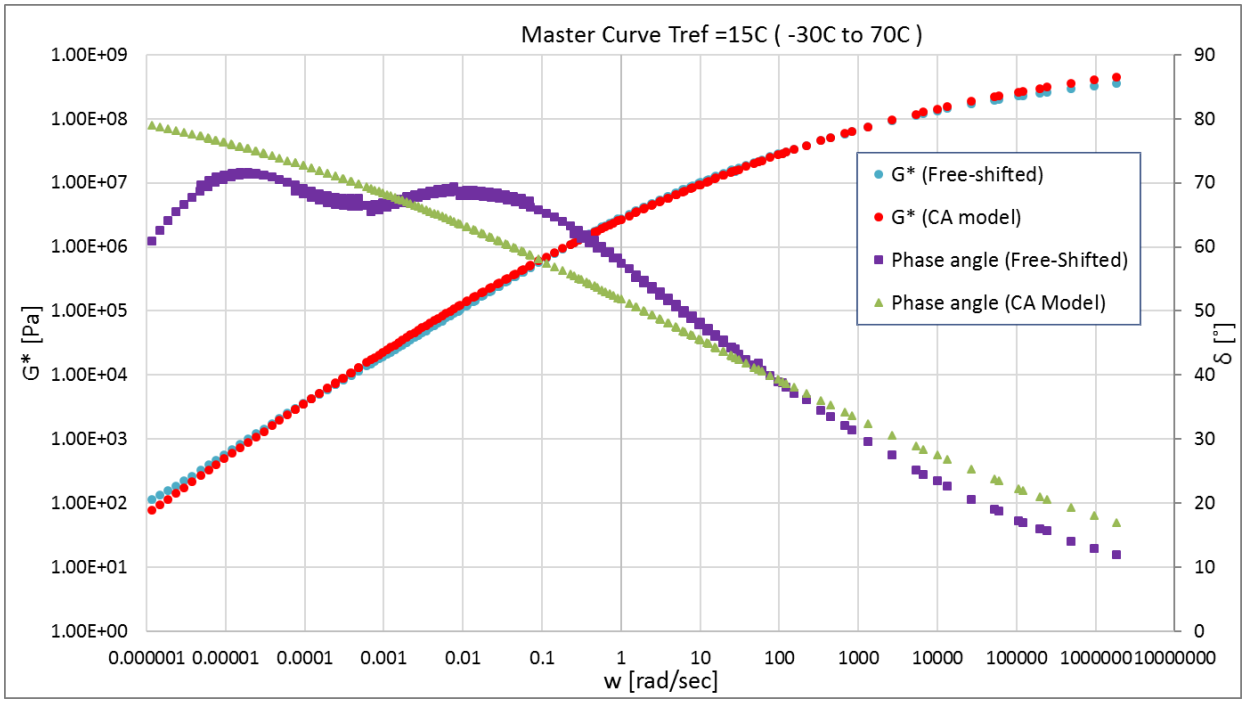

	CAM model parameters	
	G*	δ
Go (Pa)	1151899399.461	
wo	12.104	12.104
B	0.146	0.123
K	0.985	0.998
RMS error (Log)	0.0398	0.0777

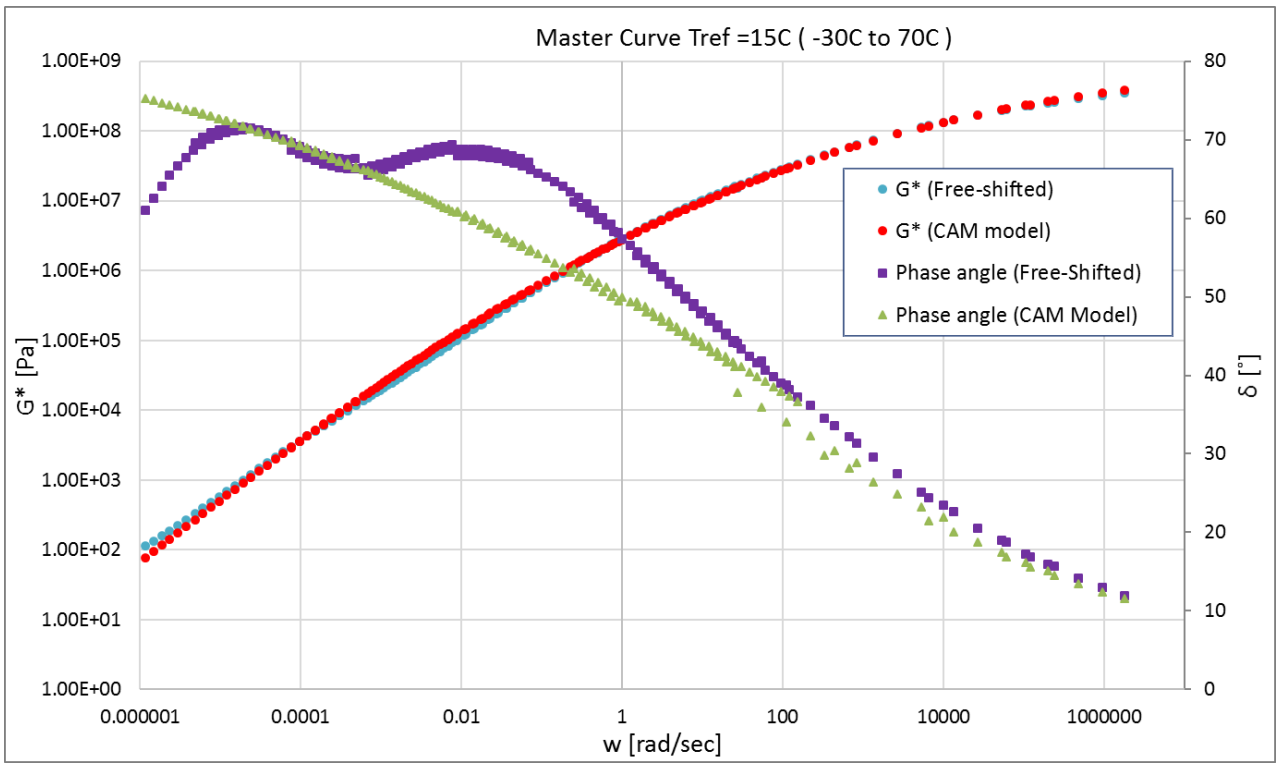

	GL model parameters	
	G*	δ
A	12.351	1.258
B	0.348	0.358
D	-6.411	0.000
M	-3.491	-3.387
T	2.280	4.451
RMS error (Log)	0.0145	0.023

Annexure F: Mathematical model comparison

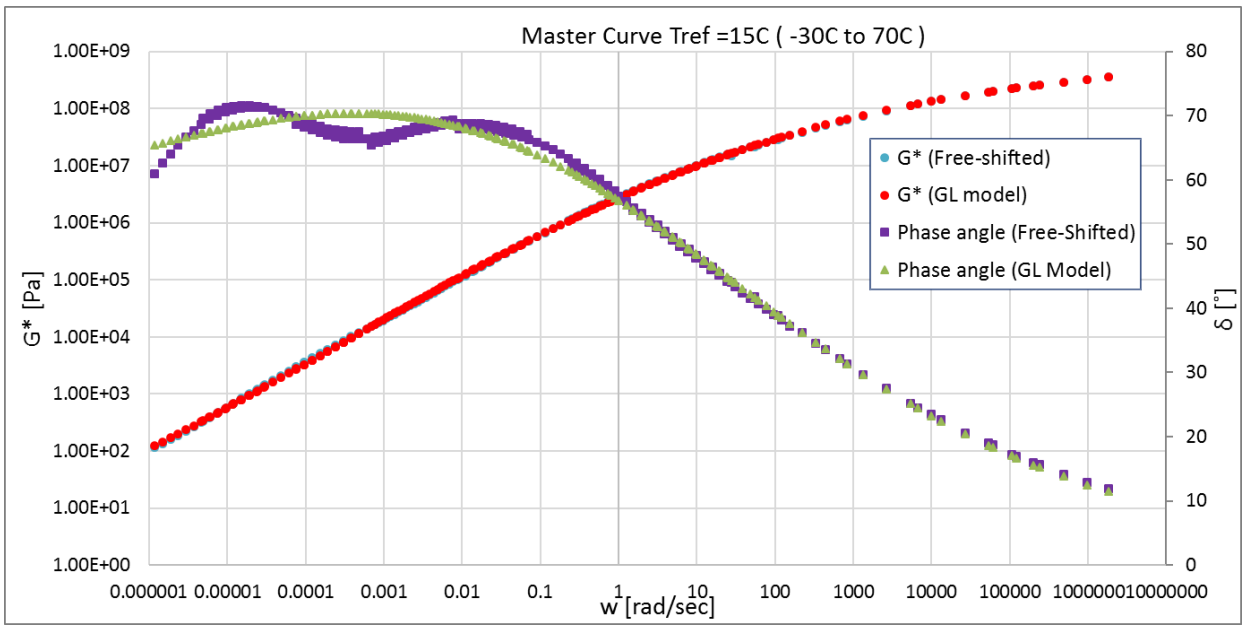

Rhea Discrete spectra		
Mode	gi, pa	li, sec
1	1.04E+05	1.14E-08
2	8.74E+04	8.71E-08
3	8.85E+04	5.76E-07
4	8.27E+04	3.76E-06
5	7.43E+04	2.33E-05
6	6.08E+04	1.43E-04
7	4.22E+04	9.02E-04
8	2.44E+04	5.52E-03
9	1.17E+04	3.30E-02
10	4.67E+03	1.99E-01
11	1.49E+03	1.10E+00
12	4.60E+02	6.57E+00
13	8.09E+01	4.71E+01
14	1.97E+01	2.92E+02
15	5.41E+00	1.82E+03
16	1.57E+00	1.07E+04
17	2.28E-01	7.57E+04
18	6.64E-02	4.18E+05
19		
20		
21		
22		
RMS error (%)	3.65%	

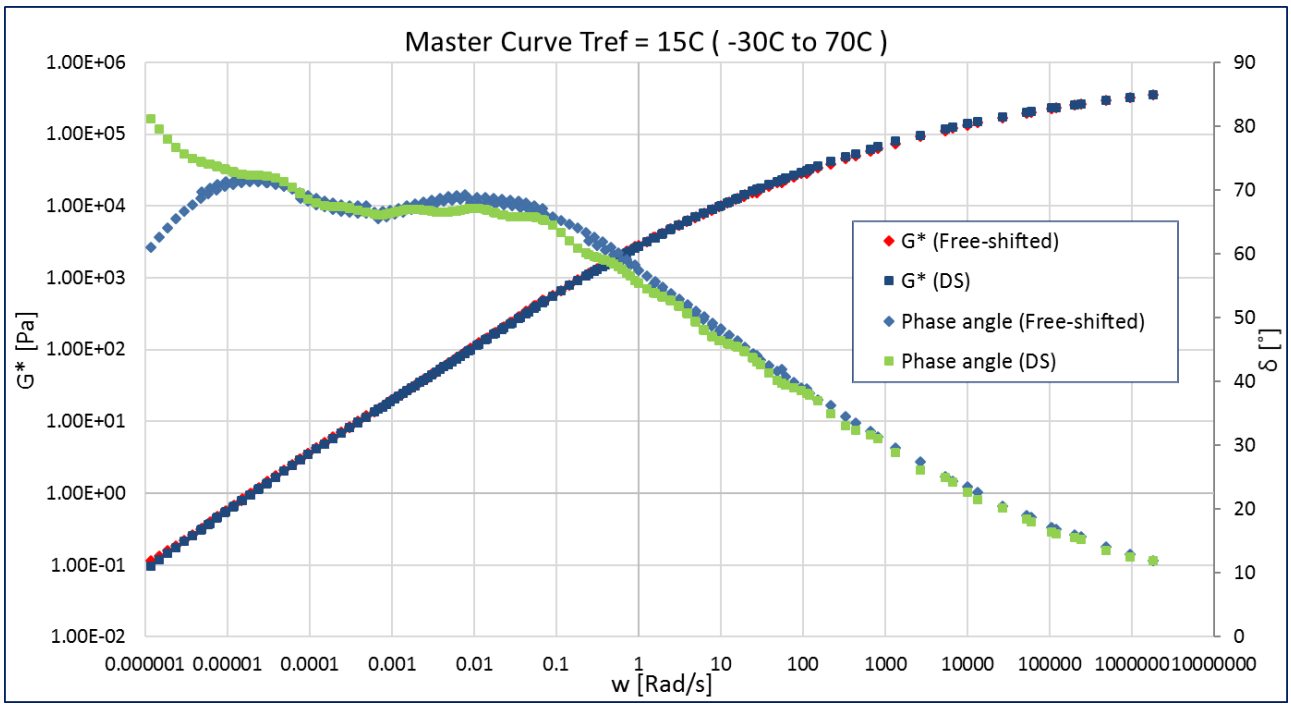

PAV1:

	CA model parameters	
	G*	δ
Go (Pa)	842504244.326	
wo	0.873	0.873
B	0.147	0.137
K	1	1
RMS error (Log)	0.0176	0.0298

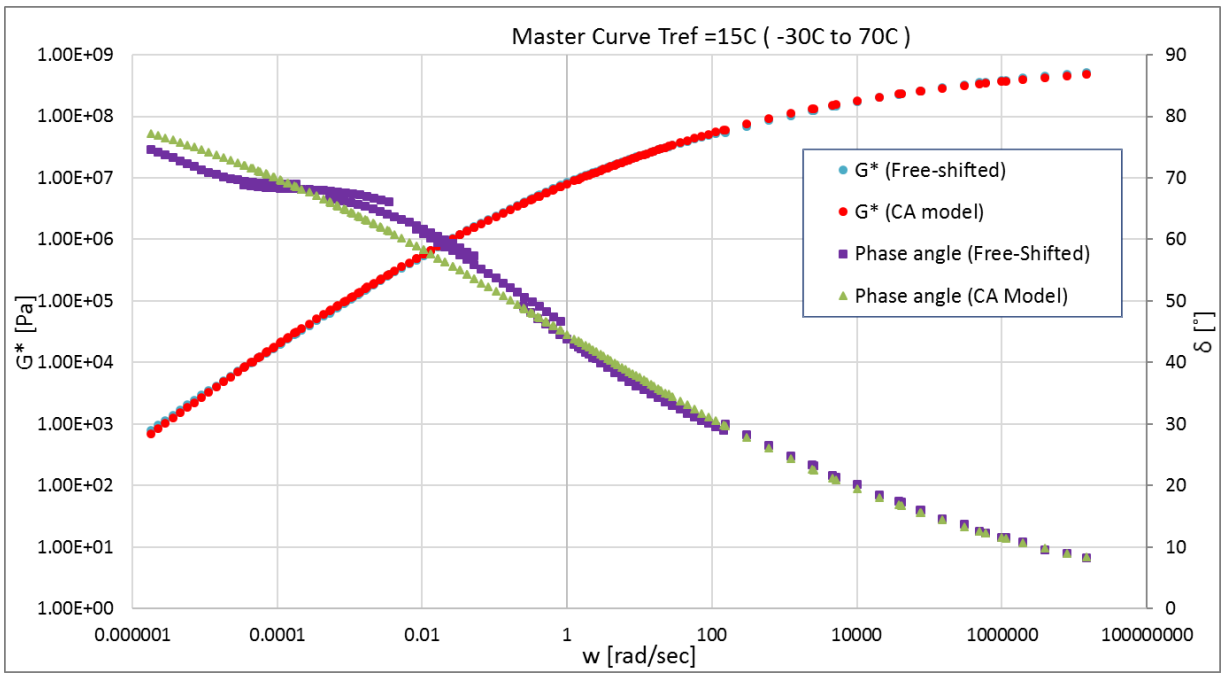

	CAM model parameters	
	G*	δ
Go (Pa)	864173222.975	
wo	0.873	0.873
B	0.146	0.138
K	1.004	0.999
RMS error (Log)	0.0172	0.0298

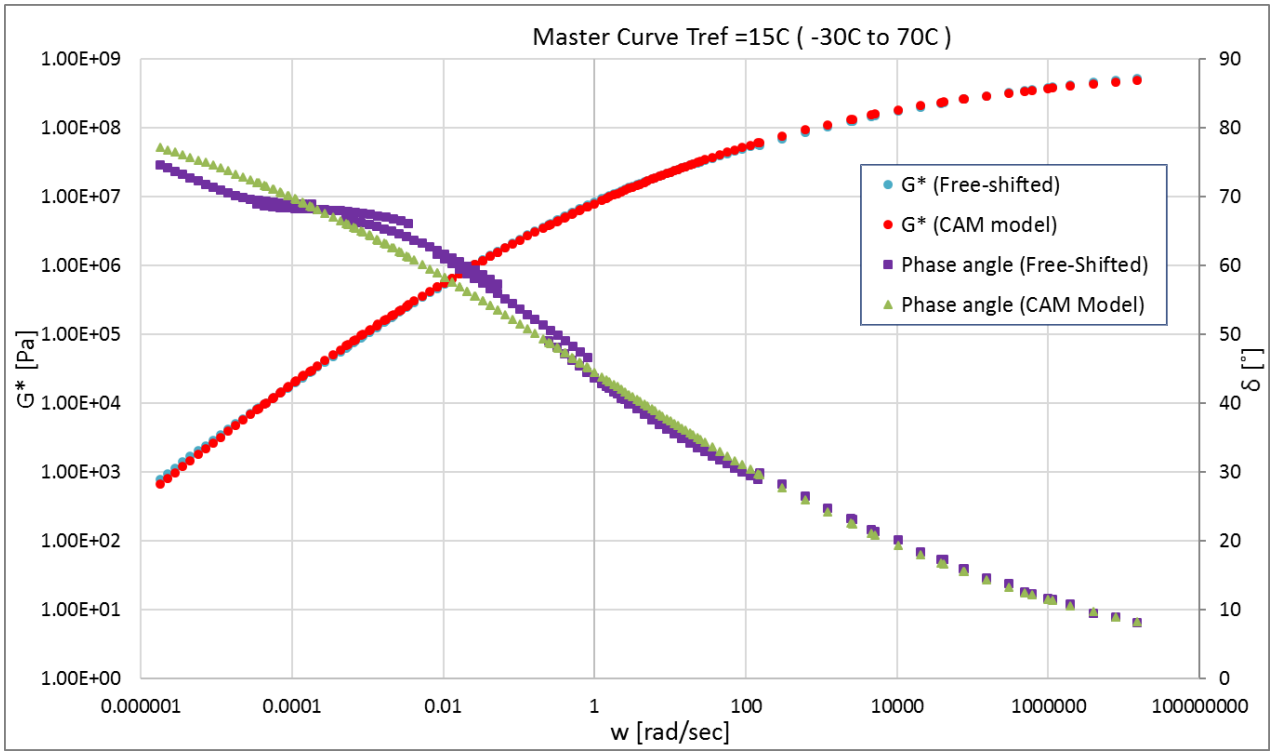

	GL model parameters	
	G*	δ
A	11.396	0.426
B	0.307	0.257
D	-5.431	0.000
M	-4.799	-4.503
T	1.383	1.451
RMS error (Log	0.0105	0.018

Annexure F: Mathematical model comparison

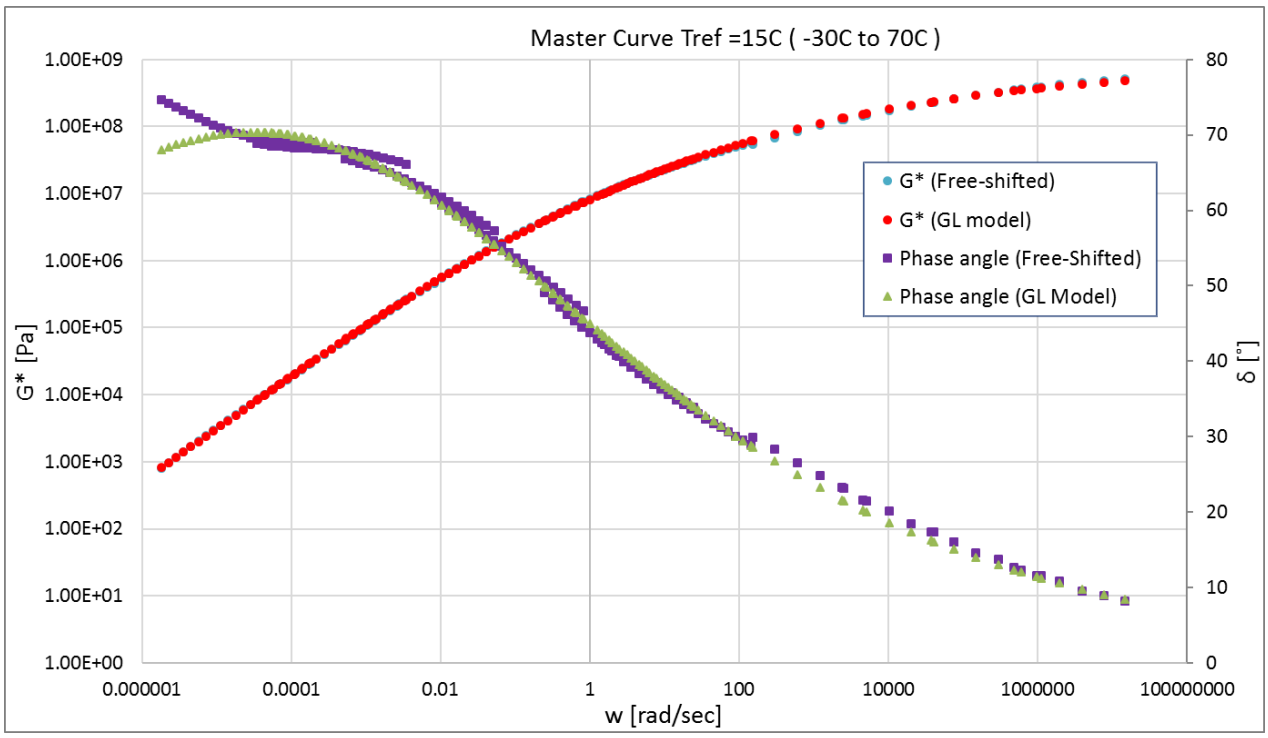

Rhea Discrete spectra		
Mode	gi, pa	li, sec
1	1.12E+05	4.08E-08
2	7.67E+04	2.52E-07
3	7.39E+04	1.10E-06
4	7.06E+04	4.61E-06
5	6.79E+04	1.91E-05
6	5.91E+04	8.12E-05
7	4.93E+04	3.43E-04
8	3.74E+04	1.47E-03
9	2.70E+04	6.20E-03
10	1.78E+04	2.74E-02
11	1.09E+04	1.19E-01
12	6.11E+03	5.41E-01
13	2.83E+03	2.20E+00
14	1.37E+03	9.37E+00
15	4.13E+02	4.00E+01
16	1.82E+02	1.59E+02
17	4.56E+01	8.37E+02
18	1.30E+01	3.85E+03
19	4.19E+00	1.59E+04
20	1.33E+00	6.89E+04
21	3.73E-01	3.14E+05
22	1.04E-01	2.02E+06
RMS error (%)	1.99%	

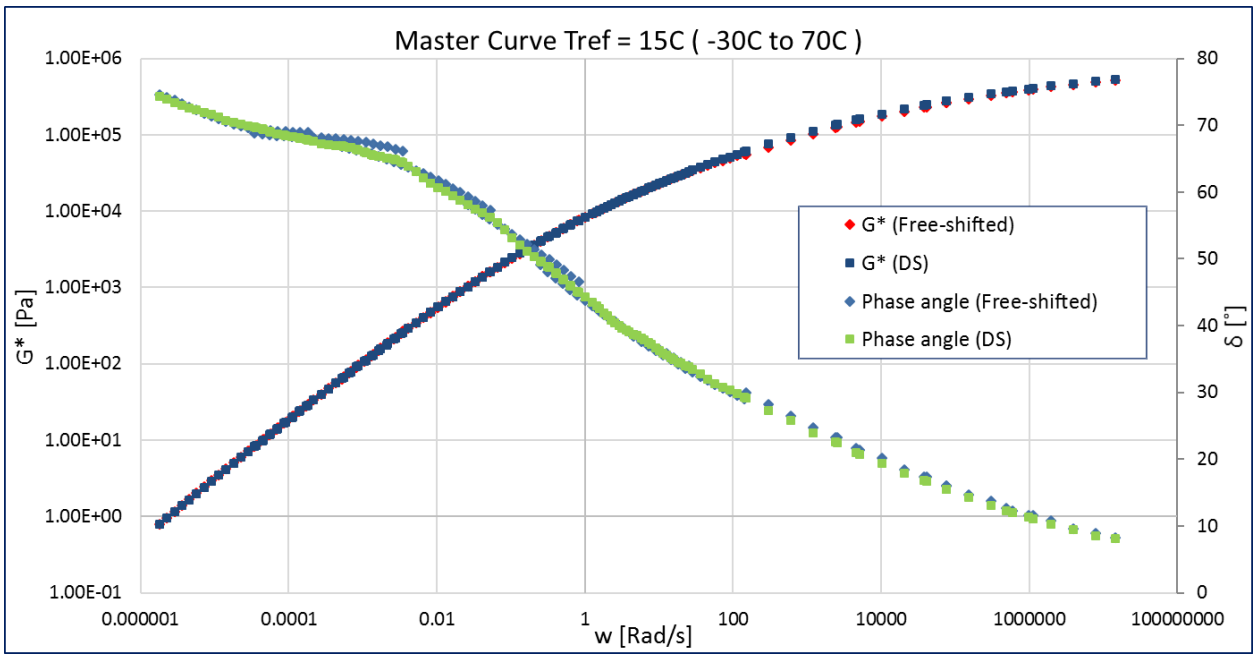

PAV2:

	CA model parameters	
	G*	δ
Go (Pa)	850201766.761	
wo	0.675	0.675
B	0.144	0.140
K	1	1
RMS error (Log)	0.0155	0.0212

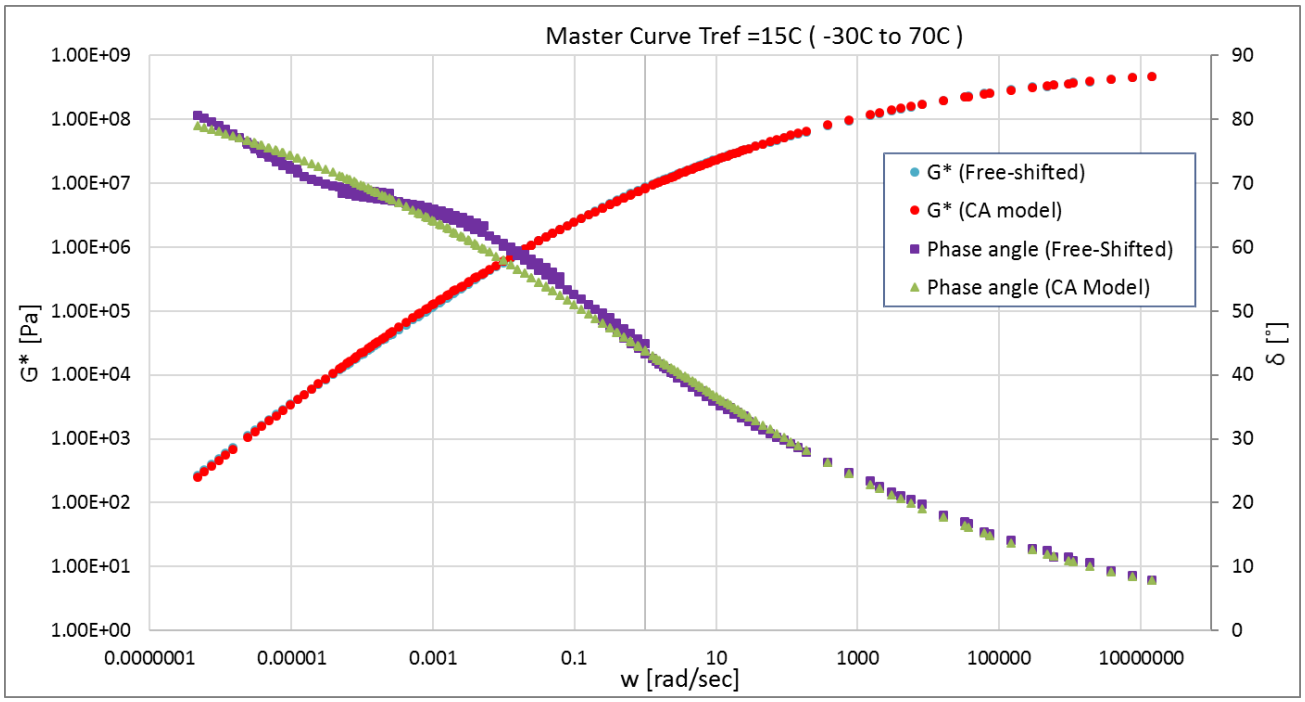

	CAM model parameters	
	G*	δ
Go (Pa)	852490343.224	
wo	0.675	0.675
B	0.144	0.139
K	1.000	1.001
RMS error (Log)	0.0155	0.0212

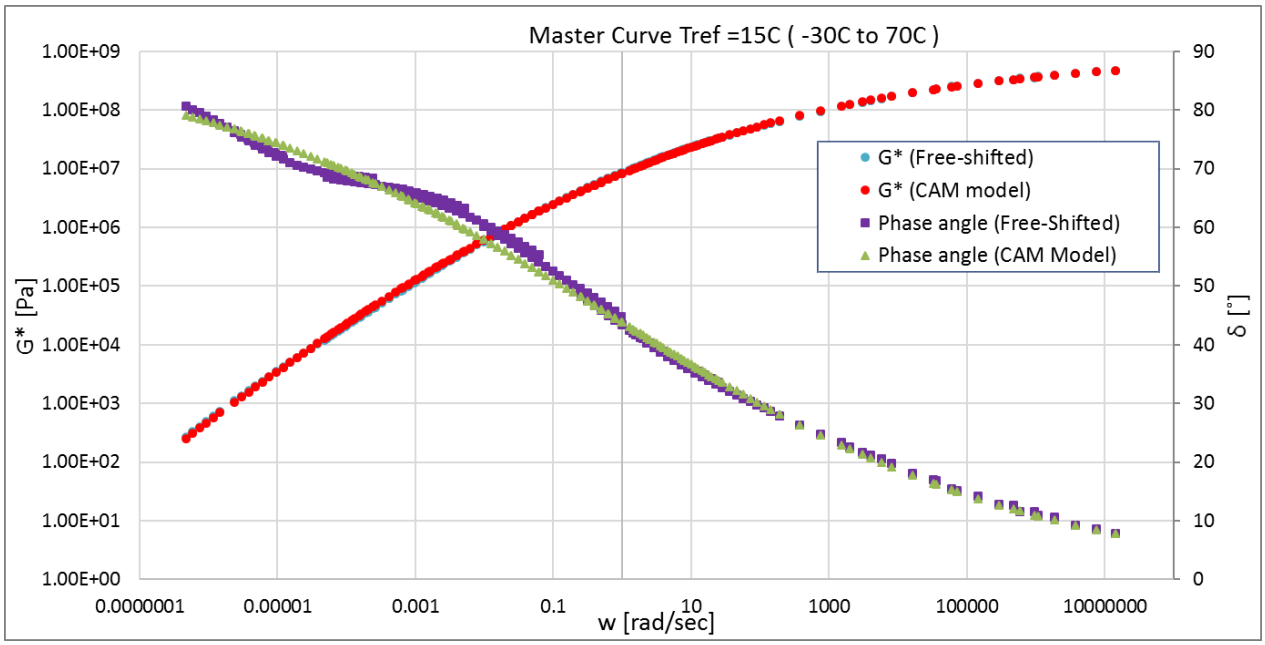

	GL model parameters	
	G*	δ
A	11.152	2.989
B	0.298	0.333
D	-5.183	0.000
M	-4.976	-10.445
T	1.158	33.666
RMS error (Log)	0.0085	0.020

Annexure F: Mathematical model comparison

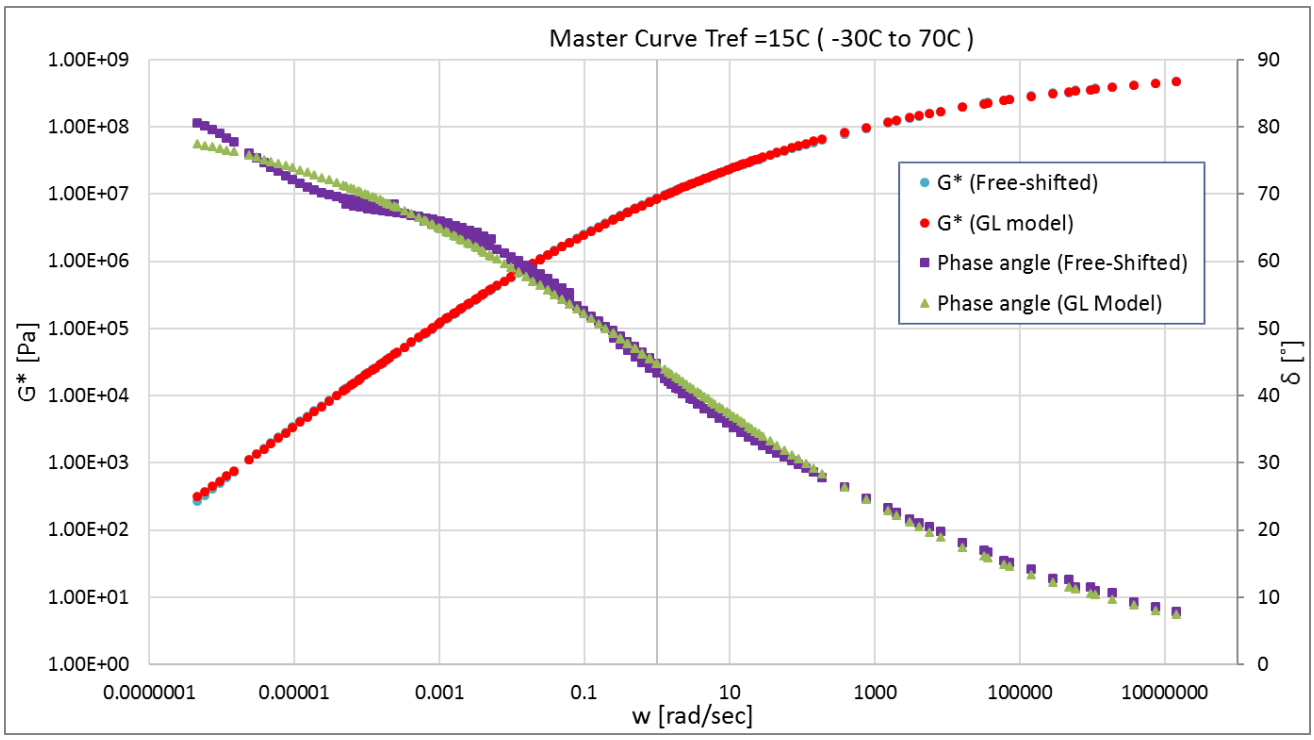

Rhea Discrete spectra		
Mode	gi, pa	li, sec
1	9.68E+04	2.42E-08
2	6.81E+04	1.57E-07
3	6.86E+04	7.17E-07
4	6.85E+04	3.17E-06
5	6.88E+04	1.45E-05
6	6.01E+04	6.61E-05
7	5.11E+04	2.96E-04
8	3.93E+04	1.35E-03
9	2.73E+04	6.14E-03
10	1.87E+04	2.84E-02
11	1.12E+04	1.32E-01
12	6.61E+03	6.48E-01
13	2.77E+03	3.44E+00
14	1.04E+03	1.69E+01
15	3.41E+02	9.73E+01
16	7.73E+01	5.78E+02
17	2.07E+01	3.24E+03
18	5.27E+00	1.73E+04
19	1.39E+00	1.00E+05
20	2.24E-01	6.32E+05
21	2.38E-02	7.62E+06
22		
RMS error (%)	1.71%	

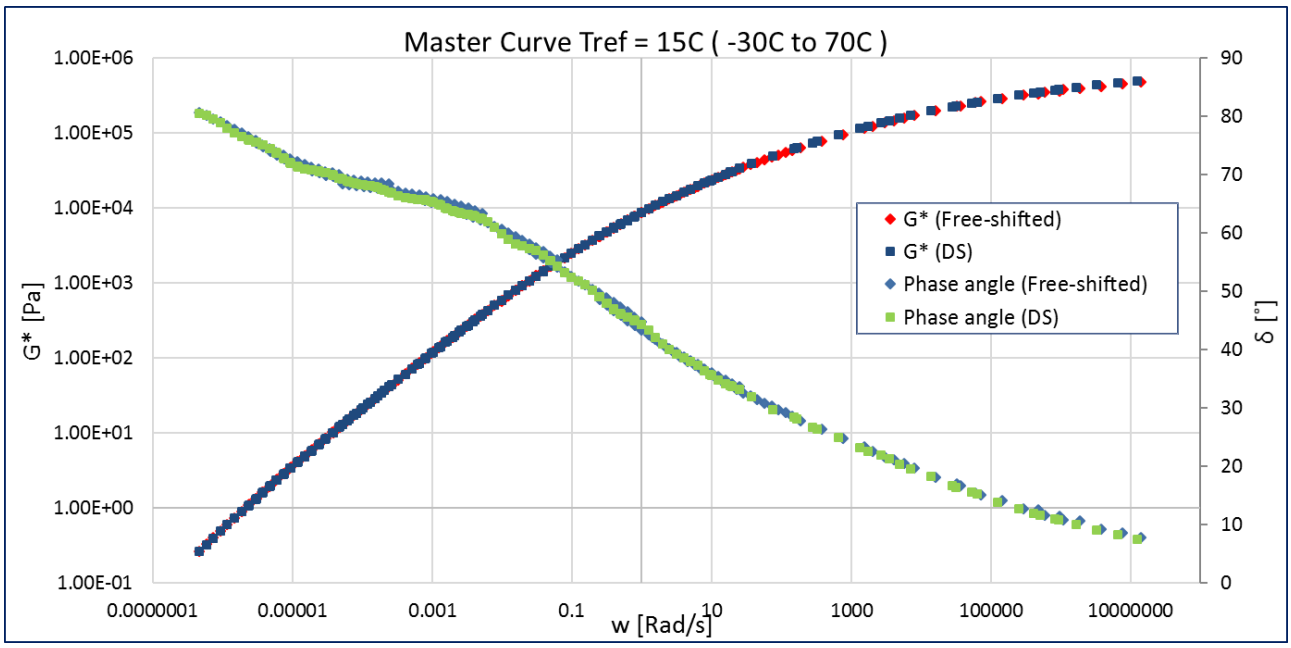

PAV4:

	CA model parameters	
	G*	δ
Go (Pa)	848619214.453	
wo	0.224	0.224
B	0.138	0.140
K	1	1
RMS error (Log)	0.0105	0.0155

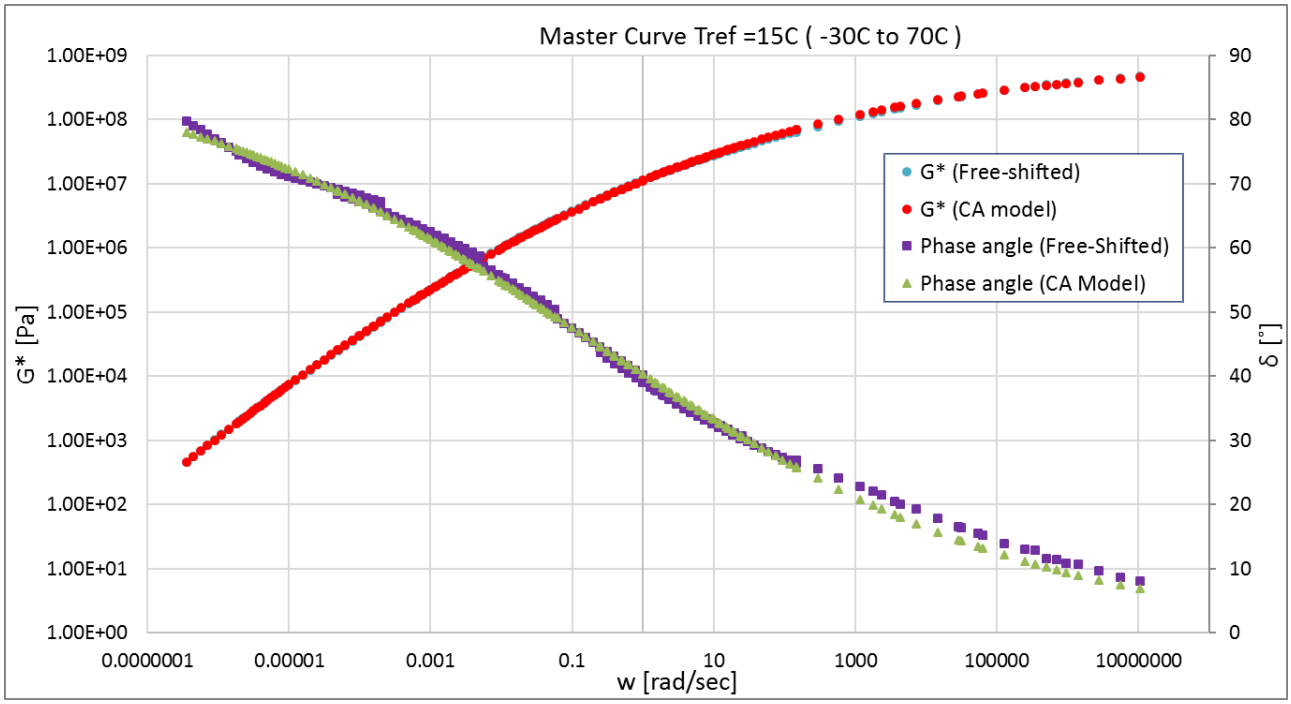

	CAM model parameters	
	G*	δ
Go (Pa)	828379676.931	
wo	0.224	0.224
B	0.138	0.140
K	0.998	1.001
RMS error (Log)	0.0103	0.0155

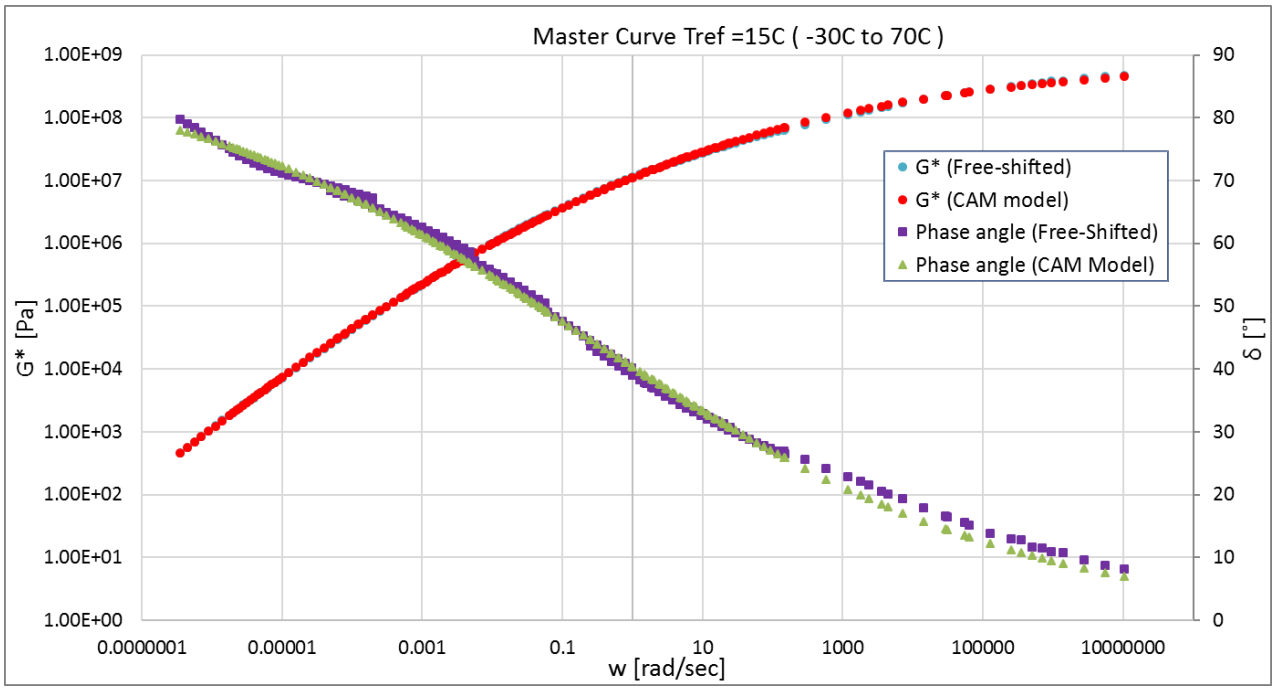

	GL model parameters	
	G*	δ
A	13.221	2.855
B	0.269	0.306
D	-7.196	0.000
M	-6.389	-12.602
T	1.269	36.543
RMS error (Log)	0.0068	0.015

Annexure F: Mathematical model comparison

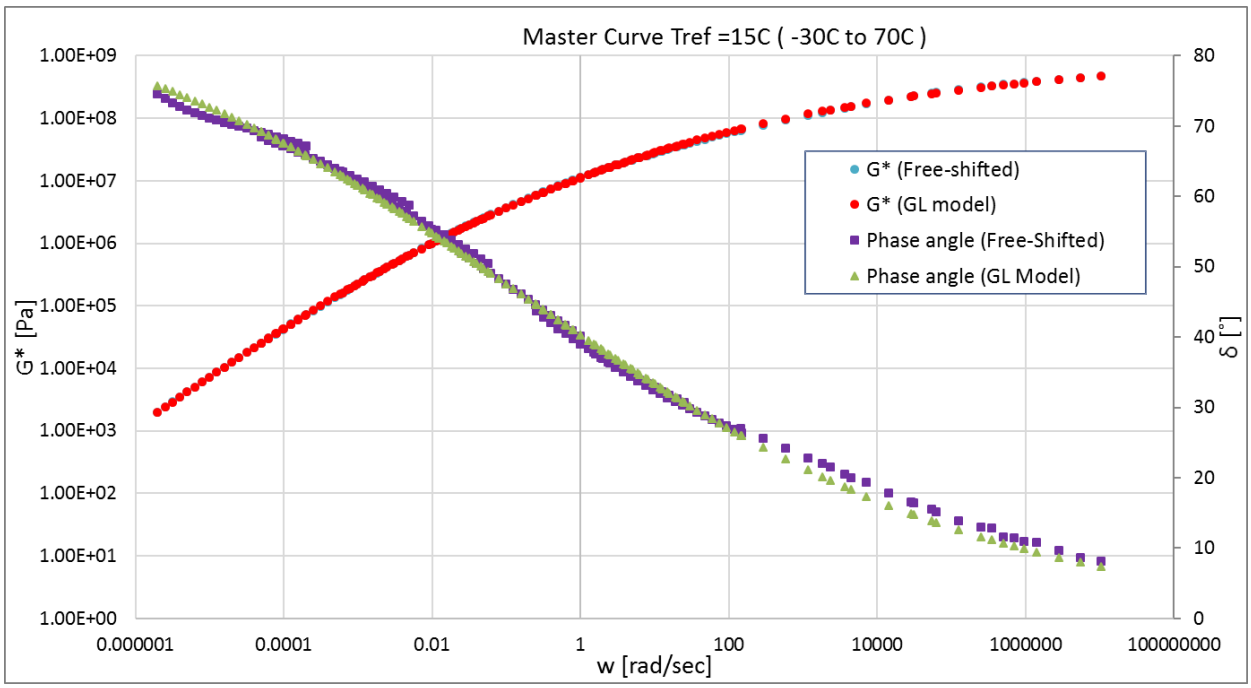

Rhea Discrete spectra		
Mode	gi, pa	li, sec
1	2.52E+05	7.69E-09
2	7.91E+04	1.39E-07
3	6.93E+04	6.90E-07
4	6.81E+04	3.01E-06
5	6.72E+04	1.33E-05
6	5.95E+04	5.82E-05
7	5.06E+04	2.50E-04
8	3.99E+04	1.08E-03
9	3.01E+04	4.62E-03
10	2.05E+04	2.03E-02
11	1.37E+04	8.77E-02
12	8.06E+03	3.86E-01
13	4.75E+03	1.48E+00
14	2.56E+03	6.18E+00
15	1.18E+03	2.58E+01
16	4.91E+02	1.22E+02
17	1.48E+02	6.14E+02
18	4.55E+01	2.96E+03
19	1.23E+01	1.67E+04
20	2.81E+00	1.07E+05
21	5.03E-01	6.85E+05
22	6.62E-02	7.76E+06
RMS error (%)	1.72%	

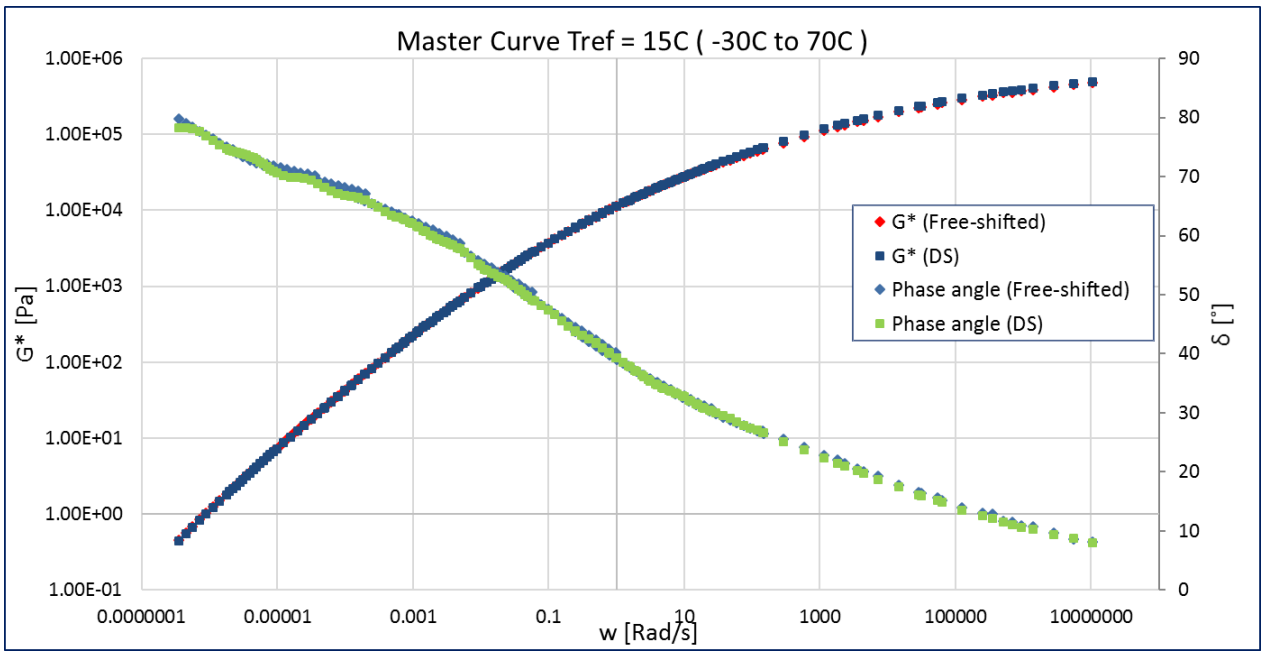

Annexure G: Black space diagrams

FT221 (S-E1 GP Colas)

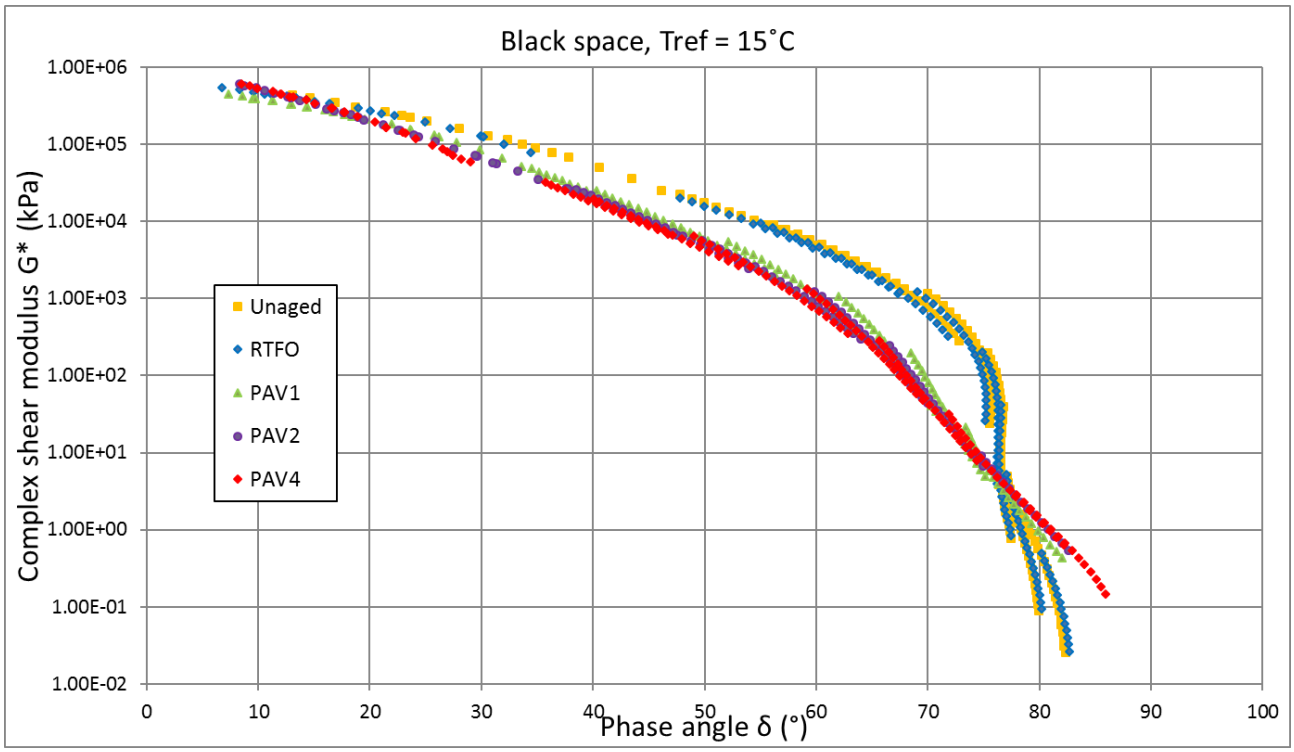

FT222 (S-E1 GP Tosas)

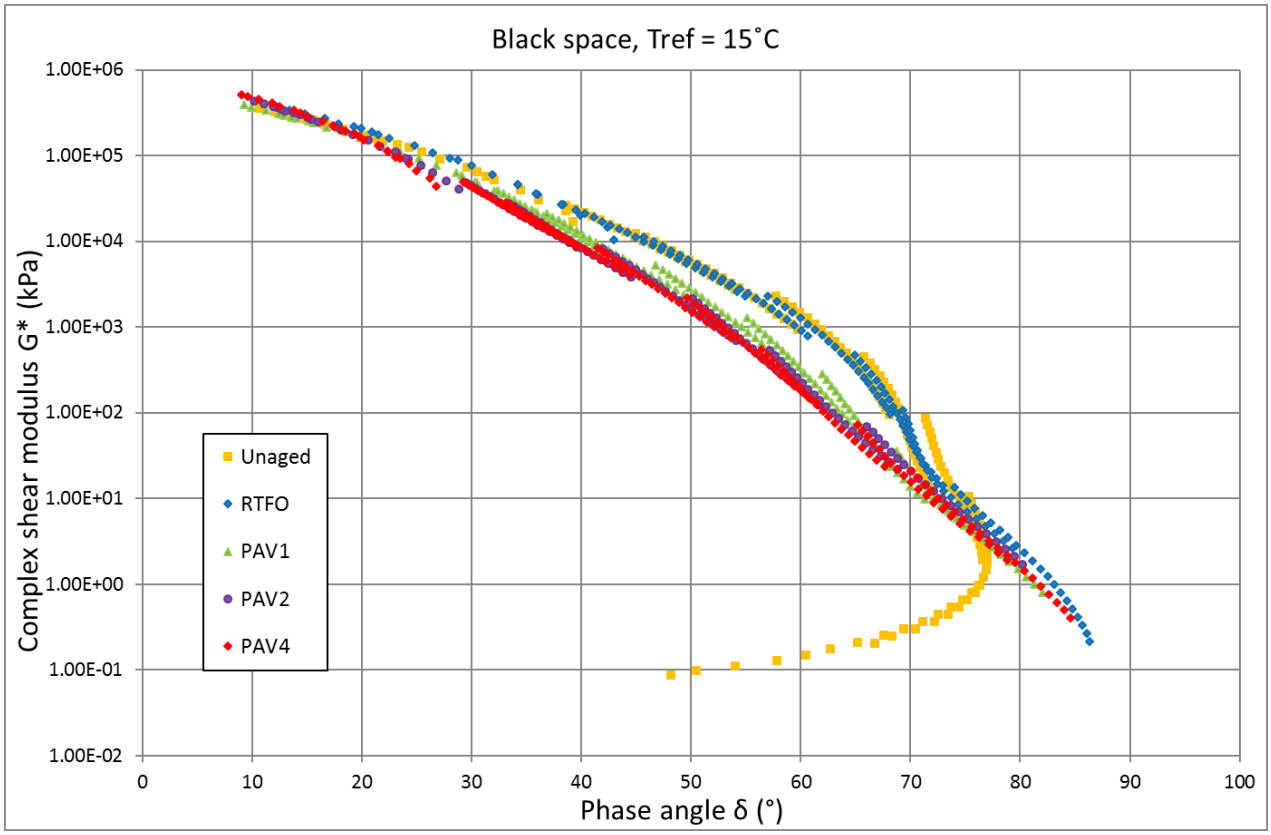

Annexure H: Creep and recovery results

SC-E1 WP Colas

		0.1kPa		3.2kPa	
	Tmax (°C)	JNR (1/kPa)	Recovery (%)	JNR (1/kPa)	Recovery (%)
Unaged	58	0.819	101.508	0.088	90.278
	64	0.000	110.652	0.174	89.868
	70	0.000	111.920	0.223	91.290
RTFO	58	0.809	76.315	0.158	72.880
	64	0.197	80.092	0.425	60.300
	70	0.238	87.067	0.792	60.053
PAV1	58	0.699	64.360	0.168	55.894
	64	0.322	56.223	0.468	40.256
	70	0.721	54.373	1.155	33.804
PAV2	58	0.277	56.191	0.063	51.600
	64	0.187	43.953	0.225	34.366
	70	0.525	32.400	0.674	19.123
PAV4	58	0.039	80.575	0.007	77.489
	64	0.032	64.372	0.036	59.459
	70	0.120	45.791	0.138	38.175

0.1kPa

		Unaged	RTFO	PAV1	PAV2	PAV4
FT111 (58˚C)	Jnr (1/kPa)	4.776	1.912	0.779	0.279	0.145
	Recovery (%)	0.000	1.500	3.831	11.051	18.839
FT131 (58˚C)	Jnr (1/kPa)	3.315	2.659	1.081	0.355	0.161
	Recovery (%)	3.377	1.913	3.220	9.646	18.776
FT211 (58˚C)	Jnr (1/kPa)	0.014	0.273	0.224	0.127	0.043
	Recovery (%)	99.110	66.701	59.466	48.734	57.278
FT221 (58˚C)	Jnr (1/kPa)	1.677	0.707	0.276	0.167	0.212
	Recovery (%)	37.355	38.661	37.580	38.210	35.946
FT222 (58˚C)	Jnr (1/kPa)	0.100	0.093	0.110	0.046	0.057
	Recovery (%)	117.139	120.835	49.045	52.549	48.145
FT322 (58˚C)	Jnr (1/kPa)	0.107	0.162	0.071	0.019	0.024
	Recovery (%)	122.085	70.961	65.721	82.513	78.912
FT333 (58˚C)	Jnr (1/kPa)	0.021	0.035	0.057	0.059	0.032
	Recovery (%)	103.466	93.816	76.346	64.732	67.754

		Unaged	RTFO	PAV1	PAV2	PAV4
FT111 (64˚C)	Jnr (1/kPa)	10.680	4.594	1.475	0.812	0.434
	Recovery (%)	0.000	0.000	21.631	5.309	9.836
FT131 (64˚C)	Jnr (1/kPa)	8.362	6.506	2.799	1.028	0.482
	Recovery (%)	0.000	0.517	0.608	4.344	9.714
FT211 (64˚C)	Jnr (1/kPa)	0.013	0.671	0.606	0.351	0.133
	Recovery (%)	100.437	60.999	52.387	37.931	44.625
FT221 (64˚C)	Jnr (1/kPa)	3.613	1.545	0.656	0.430	0.572
	Recovery (%)	27.699	31.877	29.729	28.340	26.160
FT222 (64˚C)	Jnr (1/kPa)	0.077	0.071	0.337	0.142	0.177
	Recovery (%)	94.297	109.585	34.041	37.709	33.719
FT322 (64˚C)	Jnr (1/kPa)	0.181	0.211	0.182	0.064	0.080
	Recovery (%)	126.807	79.726	59.512	70.651	66.972
FT333 (64˚C)	Jnr (1/kPa)	0.066	0.065	0.182	0.176	0.099
	Recovery (%)	105.854	94.028	64.883	54.697	57.684

		Unaged	RTFO	PAV1	PAV2	PAV4
FT111 (70˚C)	Jnr (1/kPa)	22.653	9.923	4.749	2.072	1.177
	Recovery (%)	0.000	0.000	0.000	1.669	4.573
FT131 (70˚C)	Jnr (1/kPa)	20.538	15.478	6.722	2.603	1.290
	Recovery (%)	0.000	0.000	0.000	1.144	4.627
FT211 (70˚C)	Jnr (1/kPa)	0.001	1.663	1.446	0.935	0.385
	Recovery (%)	100.014	52.311	42.635	28.207	31.820
FT221 (70˚C)	Jnr (1/kPa)	8.326	3.635	1.642	1.110	1.371
	Recovery (%)	15.711	23.061	19.916	20.284	17.932
FT222 (70˚C)	Jnr (1/kPa)	0.124	4.718	0.889	0.419	0.495
	Recovery (%)	93.942	2.194	24.350	23.986	21.503
FT322 (70˚C)	Jnr (1/kPa)	0.288	0.464	0.504	0.239	0.274
	Recovery (%)	121.787	76.289	47.489	49.137	46.689
FT333 (70˚C)	Jnr (1/kPa)	0.111	0.105	0.211	0.548	0.278
	Recovery (%)	105.358	95.133	80.252	36.409	47.220

3.2kPa

		Unaged	RTFO	PAV1	PAV2	PAV4
FT111 (64˚C)	Jnr (1/kPa)	11.45	4.903	2.000	0.868	0.463
	Recovery (%)	0.00	0.000	3.464	1.640	5.387
FT131 (64˚C)	Jnr (1/kPa)	9.733	7.652	3.060	1.123	0.524
	Recovery (%)	0.000	0.000	0.000	1.046	5.045
FT211 (64˚C)	Jnr (1/kPa)	1.387	1.149	0.931	0.454	0.161
	Recovery (%)	50.883	35.462	29.624	22.265	33.449
FT221 (64˚C)	Jnr (1/kPa)	5.617	2.322	0.880	0.546	0.734
	Recovery (%)	2.408	9.877	12.971	14.648	11.903
FT222 (64˚C)	Jnr (1/kPa)	1.540	0.772	0.428	0.166	0.206
	Recovery (%)	25.408	30.148	22.225	29.267	24.868
FT322 (64˚C)	Jnr (1/kPa)	0.335	0.896	0.314	0.100	0.125
	Recovery (%)	71.759	32.783	35.937	56.730	52.050
FT333 (64˚C)	Jnr (1/kPa)	0.592	0.614	0.340	0.260	0.129
	Recovery (%)	56.704	51.617	40.801	37.327	47.281